LOAN DOCUMENT

PHOTOGRAPH THIS SHEET

AD-A252 129

DTIC ACCESSION NUMBER

LEVEL

1

INVENTORY

Proceedings of the 16th Annual Gravity Gradiometry Conference

DOCUMENT IDENTIFICATION

10 - 11 Feb 88

DISTRIBUTION STATEMENT A

Approved for public release;
Distribution Unlimited

DISTRIBUTION STATEMENT

ACCESSION FOR

NTIS GRA&I

DTIC TRAC

UNANNOUNCED

JUSTIFICATION

BY

DISTRIBUTION/

AVAILABILITY CODES

DISTRIBUTION	AVAILABILITY AND/OR SPECIAL
A-1	

DISTRIBUTION STAMP

DTIC
ELECTE
JUN 2 4 1992
S C D

DATE ACCESSIONED

DATE RETURNED

92 6 23 040

DATE RECEIVED IN DTIC

92-16508

REGISTERED OR CERTIFIED NUMBER

PHOTOGRAPH THIS SHEET AND RETURN TO DTIC-FDAC

DTIC FORM 70A JUN 90

DOCUMENT PROCESSING SHEET

PREVIOUS EDITIONS MAY BE USED UNTIL STOCK IS EXHAUSTED.

LOAN DOCUMENT

HANDLE WITH CARE

16th GRAVITY GRADIOMETRY CONFERENCE
10-11 FEBRUARY 1988

SPONSORED BY:
AIR FORCE GEOPHYSICS LABORATORY
EARTH SCIENCES DIVISION

Proceedings

of the

Sixteenth Annual Gravity Gradiometry Conference

United States Air Force Academy
Colorado Springs, Colorado

Approved for public release; distribution unlimited.

Compiled By:

Capt Vishnu V. Nevrekar, USAF
Earth Sciences Division
USAF Geophysics Laboratory
Hanscom AFB, MA 01731

16th GRAVITY GRADIOMETRY CONFERENCE
10-11 FEBRUARY 1988

SPONSORED BY:
AIR FORCE GEOPHYSICS LABORATORY
EARTH SCIENCES DIVISION

ABOUT THE GRAVITY GRADIOMETRY CONFERENCE.....

The First Gravity Gradiometry Conference was held at the Air Force Cambridge Research Laboratory (AFCRL, now AFGL) in 1973. Its purpose was to provide a forum to evaluate and compare the efforts of three vendors (Charles Stark Draper Lab, Hughes Research Lab and Bell Aerospace Textron) in still-emerging areas of gravity gradiometry. About 15 people attended, most of them from the companies mentioned above or the Terrestrial Sciences Division at AFCRL. In contrast, the 1988 Conference had a guest list of 60 plus attendees, with participation from academia (foreign and domestic), private industry and government. The papers presented were not restricted to gradiometry alone. Indeed, the scope of this annual event has broadened considerably since 1973.

Gradiometry reached a major milestone in 1988 with the delivery of the Gravity Gradiometer Survey System (GGSS) to DMA. This one-of-a-kind, moving base gravity gradiometer was manufactured for DMA by Bell Aerospace Textron of Buffalo, NY under AFGL management. That the GGSS is an operational system today is a splendid testimonial to the foresight and effort of the scientists and engineers who got together for that very first Conference in 1973! For further historical perspective, we've included the attendance list and agenda from the 1978 Conference on the next few pages. Some of the key players are still in the game today!

The Geodesy and Gravity Branch of the Earth Sciences Division of the Air Force Geophysics Laboratory (AFGL), Hanscom AFB, Massachusetts, has always organized the Conference. With the exception of the first two conferences, all the others have been held at the US Air Force Academy in Colorado Springs, Colorado. In 1989, however, the venue is likely to shift to the AFGL Conference Center at Hanscom AFB. While prior conferences have been held around the second week in February, the 1989 Conference will be sometime in the month of April. We will provide more information on these changes in future mailings.

If you are not already on our mailing list and would like to attend the 1989 Conference, or if you have any questions, please write to:

Ms Claire Marcotte
AFGL/LW
Hanscom AFB, Bedford, MA 01731
USA

Copies of conference proceedings for prior years are not available. Also, we appreciate any comments or suggestions you may have regarding this document.

6th MOVING BASE GRADIOMETER REVIEW

United States Air Force Academy
Colorado Springs, Colorado

28 February - 1 March 1978

AGENDA

28 February 1978

0800-0900	Registration - Fairchild Hall
0900-0930	Introduction and Welcome Administrative Announcements Opening Remarks
0930-1200	Review of Gradiometer Developments - Charles Stark Draper Labs
1200-1330	Lunch
1330-1600	Review of Gradiometer Developments - Hughes Research Labs Discussion on the Hughes Presentation
1600-1630	Electronic Cooling of the Hughes Rotating Gravity Gradiometer - Dr. Robert Forward

1 March 1978

0900-1200	Review of Gradiometer Developments - Bell Aerospace Textron Discussion on the Bell Presentation
1200-1330	Lunch
1330-1600	DoD Executive Session

GRAVITY GRADIOMETER

28 Feb - 1 Mar 78

NAME	ORGANIZATION	TELEPHONE NUMBER
ED GORIN	BELL AEROSPACE TEXTRON	714-884-6027
ERNIE METZGER	BELL AEROSPACE TEXTRON	716-297-1000
CLIVE AFFLECK	BELL AEROSPACE TEXTRON	716-297-1000
AARON J, COPELAND	BELL AEROSPACE TEXTRON	716-297-1000
HUGH M. NEESON	BELL AEROSPACE TEXTRON	716-297-1000
G.F. MARTIN	DEFENSE MAPPING AGENCY	202-254-4472
DALE L. LANDIS	THE ANALYTIC SCIENCES CORP	617-944-6850 x273
KEVIN TAIT	THE ANALYTIC SCIENCES CORP	617-944-6850 x273
WARREN HELLER	THE ANALYTIC SCIENCES CORP	617-944-6850 x273
WILLIAM J. BEST	AIR FORCE OFFICE OF SCIENTIFIC RESEARCH	202-767-5011
CAPT D.E. WHEELER	SAMSO/MNNG	714-382-5476
BERNARD CHOVITZ	NOAA/NOS	301-443-8531
DONALD H. ECKHARDT	AIR FORCE GEOPHYSICS LAB	617-861-3486
LTC ED DOBKOWSKI	AIR FORCE GEOPHYSICS LAB	AV 478-3606
STANLEY SIEGEL	SPERRY SYSTEMS MGT	516-574-1260
MARVIN MOLNY	SPERRY SYSTEMS MGT	516-574-1567
BILL WHITESELL	6585TH TEST GP HOLLOMAN AFB	AV 349-2231
RUDY LIST	SPERRY SYSTEMS MGT	516-LR4-2495
WILLIAM PASSARELLI	SPERRY SYSTEMS MGT	516-LR-4-2553
WALTER FELDMEN	SPERRY SYSTEMS MGT	516-LR-4-1567
HENRY ZIEGLER	SPERRY SYSTEMS MGT	516-574-2320
PIO BIZZIGOTTI	SPERRY SYSTEMS MGT	516-574-1654
WALTER A. GALLIE	HQ AFSC/DLS	AV 858-2364
RAYMOND A. NASH	TASC	617-944-6850
RICHARD J. ANDERLE	NSWC	703-663-8159
SHIGEO OKUBO	OKUBO INST	303-598-0842
BILL SIMMONS	USAF-FJSRL	303-472-3502
KENNETH POTOCKI	JOHNS HOPKINS/APP PHYS LAB	301-953-7100
TOM CRISS	JOHNS HOPKINS/APL	301-953-7100
EDWARD ROOT	USA ENGR TOPO LAB	703-664-2834
MICHAEL J. HADFIELD	HONEYWELL, INC.	813-531-4611 x2789
M.D. BACON	FJSRL	303-472-3120

Encl 2

J.A. COOK	AFGL	617-861-5495
DONALD O. JOHNSON	C.S. DRAPER LAB	617-258-1362
MILTON B. TRAGESER	C.S. DRAPER LAB	617-258-1329
DAVID J. COLLINS	NAVY/SSPO	202-697-5314
JEROME R. KATZ	SSPO	202-697-4307
BERNARD EPSTEIN	SSPOTR	516-574-3453
DR. ROBERT L. FORWARD	HUGHES RESEARCH LABS	213-456-6411
CHARLES B. AMES	HUGHES AIRCRAFT	213-670-1515
OWEN W. WILLIAMS	HQ DMA	202-254-4451
ROBERT M. PERRY	LACOSTE AND ROMBERG CO	512-453-0821
DEWEY R. HENDERSON	ROCKWELL INTERNATIONAL	714-632-1451
DOUGLAS G. DETHLEFSEN	ORCKWELL INTERNATIONAL	714-632-2971
JAMES E. FALLER	JILA-NBS	303-499-1000 x3463
JAMES A. HAMMON	AFGL	617-861-2760
DOUGLAS A. REKENTHALER	DMA	AC 202-254-4455 AV 294-663-8247
TED SIMS	NSWC	703-663-8247
DAN DEBRA	STANFORD UNIV	415-497-3388
RON NEWLON	HUGHES	213-670-1515
RICHARD B. CLARK	HUGHES	213-670-1515 x1552
AVERIL B. CHATFIELD	GEODYNAMICS CORP	805-687-7747
LYNDON L. SHELDON	GEODETIC SURVEY	AV 481-2901
B. LOUIS DECKER	DMA AEROSPACE CENTER	AV 698-4606 AC 314-268-4606
ROBERT W. BALLEW	DMA AEROSPACE CENTER	AV 698-4606
JEROME J. KURKOWSKI	DMA TOPOGRAPHIC CENTER	202-227-2755
HUGH T. WILSON	HUGHES	213-670-1515 x 1107

16th GRAVITY GRADIOMETRY CONFERENCE
10-11 FEBRUARY 1988

SPONSORED BY:
AIR FORCE GEOPHYSICS LABORATORY
EARTH SCIENCES DIVISION

ABOUT THESE PROCEEDINGS.....

This document contains every paper that was presented at the 1988 Conference. In addition, I have included two papers that were on the agenda but were not presented at the Conference because of clearance problems at that time. They have since been cleared, and can be found at the very end of this document.

Every paper is preceded by an abstract in a standard format. Some papers also have the original abstract included. Further, you may recall the Q&A session we had at the end of each presentation. In cases where a technical interchange did take place, the questions and answers are documented at the end of each pertinent paper. Every paper did not have a Q&A session, and I have included all Q&A sheets that were handed to me at the end of each talk. Except for a few minor editorial changes, the information on these sheets has not been altered. Obviously, these sheets are as "good" as the inputs provided.

I had said I would try to complete and mail these proceedings two to three months after the Conference. Well, it's been seven months, and by the time you receive this document, it will have been eight months. Still, consider the following:

(1) The 1986 Proceedings were distributed at the 1987 Conference (1 year later).

(2) The 1987 Proceedings were mailed out in December 1987 (10 months later).

(3) This year's compilation arrives 8 months after the Conference.

If that isn't progress, I don't know what is!

In closing, I think I have done a thorough job of collecting and checking all the information for these proceedings. Errors will occur, however, and while I will entertain any comments and criticisms on this issue, these proceedings will stand as published.

Thank you for your participation and support.

Captain Vishnu V. Nevrekar
Earth Sciences Division
USAF Geophysics Laboratory
Hanscom AFB, MA 01731

September 1988

16th GRAVITY GRADIOMETRY CONFERENCE
10-11 FEBRUARY 1988

SPONSORED BY:
AIR FORCE GEOPHYSICS LABORATORY
EARTH SCIENCES DIVISION

ACKNOWLEDGMENTS

We'd like to recognize the efforts of some outstanding individuals without whose hard work the Conference could not have been a success.

As always, Ms Nancy Gass from the Directorate of Protocol of the USAF Academy gave us masterful support by handling all the conference arrangements, including hotel accomodation for the attendees, transportation for the Conference and tour, luncheons during the Conference and the "mixers" later in the evening. We are indeed fortunate to have been associated with a superb organizer like Ms Gass over the years. Also, we appreciate the support of the bus drivers from the Academy motor pool.

Next, we thank all the speakers for taking the time to compile and present their papers for the benefit of the Conference attendees. As in the past, the broad mix and high quality of topics went a long way towards making the Conference a stimulating scientific forum.

Finally, we thank Col J.R. Kidd, Commander, AFGL, Dr Donald H. Eckhardt, Director, Earth Sciences Division and Dr Thomas P. Rooney, Chief, Geodesy and Gravity Branch, without whose support and guidance this Conference could not have been held.

16th GRAVITY GRADIOMETRY CONFERENCE
10-11 FEBRUARY 1988

SPONSORED BY:
AIR FORCE GEOPHYSICS LABORATORY
EARTH SCIENCES DIVISION

Alphabetical Listing of Conference Participants

Name	Organization
Don Benson	Dynamics Research Corporation
*John Brozena	Naval Research Laboratory
B. Wayne Castleman	Honeywell, Inc
B. Louis Decker	Defense Mapping Agency
Ed Dinter	Bell Aerospace Textron
Mark Dransfield	University of Western Australia (AUS)
Cyril Edwards	University of Western Australia (AUS)
Harry Emrick	Colorado Geospace
James Fix	Teledyne Geotech
Rene Forsberg	Geodetic Institute (DENMARK)
J. D. Franson	Johns Hopkins Applied Physics Lab
*David Gleason	USAF Geophysics Laboratory
John Goodkind	University of California, San Diego
John Graham	Defense Mapping Agency
*Andrew Grierson	Bell Aerospace Textron
Richard Hansen	Colorado School of Mines
Chris Harrison	Geodynamics Corporation

* Denotes Speaker at Conference

16th GRAVITY GRADIOMETRY CONFERENCE
10-11 FEBRUARY 1988

SPONSORED BY:
AIR FORCE GEOPHYSICS LABORATORY
EARTH SCIENCES DIVISION

Name	Organization
*Warren Heller	The Analytic Sciences Corporation
Boyd Holsapple	USAF Wright Avionics Laboratory
James Huddle	Litton, Inc
Gene Jackson	McDonnell Douglas, Inc
Chris Jekeli	USAF Geophysics Laboratory
Albert Jircitano	Bell Aerospace Textron
J. Edward Jones	USAF Intelligence Service
Andrew Lazarewicz	USAF Geophysics Laboratory
*Jurn-Sun Leung	University of Maryland
James McCullough	US Geological Survey Crawford Lab
Ernest Metzger	Bell Aerospace Textron
*Capt Warner Miller	USAF Weapons Laboratory
Marvin Molny	UNISYS Corporation
Capt Vishnu Nevrekar	USAF Geophysics Laboratory
*Ho Jung Paik	University of Maryland
*Louis Pfohl	Bell Aerospace Textron
*Jean-Paul Richard	University of Maryland
*Anestis Romaides	USAF Geophysics Laboratory
Thomas Rooney	USAF Geophysics Laboratory

* Denotes Speaker at Conference

16th GRAVITY GRADIOMETRY CONFERENCE
10-11 FEBRUARY 1988

SPONSORED BY:
AIR FORCE GEOPHYSICS LABORATORY
EARTH SCIENCES DIVISION

Name	Organization
Alton Schultz	AMOCO Production Company
Ted Sims	Naval Surface Weapons Center
*David Sonnabend	CALTECH/Jet Propulsion Laboratory
*Pierre Touboul	O.N.E.R.A. (FRANCE)
Milton Trageser	Charles Stark Draper Laboratory, Inc
Peter Ugincius	Naval Surface Weapons Center
*Triveni Upadhyay	Mayflower Communications, Inc
Herbert Valliant	LaCoste and Romberg Gravity Meters, Inc
Robert Valska	Defense Mapping Agency
Frank van Kann	University of Western Australia (AUS)
*Donald Vasco	USAF Geophysics Laboratory
Richard Wold	TerraSense, Inc
*Robert Ziegler	Defense Mapping Agency
Alan Zorn	Dynamics Research Corporation
Paul Zucker	Johns Hopkins Applied Physics Lab

* Denotes Speaker at Conference

16th GRAVITY GRADIOMETRY CONFERENCE
10-11 FEBRUARY 1988

SPONSORED BY:
AIR FORCE GEOPHYSICS LABORATORY
EARTH SCIENCES DIVISION

CONFERENCE AGENDA

Tuesday, 9 February

1900 - 2200 - Informal Reception - Hilton Inn
Early Registration for Conference

Wednesday, 10 February

0730 - Buses depart Hilton Inn for Fairchild Hall

0815 - Registration - Third Floor, Fairchild Hall (South End)

0845 - Welcome/Introduction - Capt Vishnu Nevrekar

0850 - Presentation by Mr Lou Pfohl of Bell Aerospace Textron.

"Program Review: Gravity Gradiometer Survey System"

0925 - Presentation by Mr Andrew Grierson of Bell Aerospace Textron.

'Suppression of Motion Sensitivity in Bell Aerospace Gravity Gradiometer Survey System"

0952 - Presentation by Mr Dave Gleason of AFGL Earth Sciences Division.

"An Initial Look at 54 Tracks of Airborne Data from the Gravity Gradiometer Survey System"

1020 - Administrative Details - Break

1042 - Presentation by Dr Warren Heller of TASC.

"GGSS Airborne Data Reduction Results"

1115 - Presentation by Mr Robert Ziegler of DMA Systems Center.

"The Wings of Gradiometry"

1140 - Administrative Details

1145 - Buses depart Fairchild Hall for USAFA Officers' Club

1200 - Lunch at USAFA Officers' Club

1245 - Buses depart USAFA Officers' Club for Fairchild Hall

16th GRAVITY GRADIOMETRY CONFERENCE
10-11 FEBRUARY 1988

SPONSORED BY:
AIR FORCE GEOPHYSICS LABORATORY
EARTH SCIENCES DIVISION

1300 - Set Up VCR, Slide Projector

1310 - Presentation by Dr Donald Vasco of AFGL Earth Sciences Division.

"Linear Inversion of Gravity and Gravity Gradiometry:
A Tale of Two Operators"

1330 - Presentation by Mr John Brozena of Naval Research Laboratory.

"The Airborne Gravity Measurement Program
at the Naval Research Laboratory"

1350 - Presentation by Mr Anestis Romaides of AFGL Earth Sciences Division.

"A Detection of Non-Newtonian Gravity"

1425 - Administrative Details - Break

1450 - Administrative Details

1455 - Presentation by Dr Triveni Upadhyay of Mayflower Communications, Inc.

"STS-GPS Tracking for Anomalous Gravitation Estimation (STAGE)"

1530 - Presentation by Dr Ho Jung Paik of the University of Maryland.

"Three-Axis Superconducting Gravity Gradiometer-Progress Report"

1630 - Administrative Details

1635 - Buses depart Fairchild Hall for Hilton Inn

1730 - Reception - Hilton Inn

Thursday, 11 February

0730 - Depart Hilton Inn for Fairchild Hall

0815 - Administrative Details

0830 - Presentation by Mr Pierre Touboul of ONERA, France.

"The GRADIO Spaceborne Gravity Gradiometer:
Development and Accomodation"

16th GRAVITY GRADIOMETRY CONFERENCE
10-11 FEBRUARY 1988

SPONSORED BY:
AIR FORCE GEOPHYSICS LABORATORY
EARTH SCIENCES DIVISION

0900 - Presentation by Dr Jurn-Sun Leung of the University of Maryland.

"Global Gravity Survey and Precision Gravity Experiments by an Earth-Orbiting Gravity Gradiometer"

0935 - Presentation by Dr Jean-Paul Richard of the University of Maryland.

"Laser Instrumentation for Gravity Measurements in Space"

1000 - Administrative Details - Break

1025 - Administrative Details

1030 - Presentation by Dr David Sonnabend of Jet Propulsion Laboratory.

"Magnetic Isolation - An Update"

1050 - Presentation by Capt Warner Miller of Air Force Weapons Laboratory.

"From Geodetic Triangulation to Space-Time Geodesy"

1125 - Administrative Details - Closing Remarks
Vacate Conference Room

1145 - Buses depart Fairchild Hall for USAFA Officers' Club

Form 2 Groups: Bus I - Those on Academy Tour
Bus II- Those not on Tour

12CO - Lunch at Officers' Club

1315 - Bus I - Tour of USAF Academy
Bus II - Departs for Hilton Inn

1400 - Bus II arrives at Hilton Inn

1530 - Bus I - Tour of USAF Academy ends.
Return to Hilton Inn

1600 - Bus I arrives at Hilton Inn - End of Conference.

16th GRAVITY GRADIOMETRY CONFERENCE
10-11 FEBRUARY 1988

SPONSORED BY:
AIR FORCE GEOPHYSICS LABORATORY
EARTH SCIENCES DIVISION

List of Papers

1. *Mr. Louis L. Pfohl, Bell Aerospace Textron

   "Program Review: Gravity Gradiometer Survey System"

2. *Mr. Andrew D. Grierson, Bell Aerospace Textron

   "Suppression of Motion Sensitivity in Bell Aerospace Gravity Gradiometer Survey System"

3. *Mr. David M. Gleason, Air Force Geophysics Laboratory

   "An Initial Look at 54 Tracks of Airborne Data from the Gravity Gradiometer Survey System"

4. *Dr. W. G. Heller, The Analytic Sciences Corporation
   Dr. S. J. Brzezowski, The Analytic Sciences Corporation
   Dr. J. D. Goldstein, The Analytic Sciences Corporation
   Dr. J. V. White, The Analytic Sciences Corporation

   "GGSS Airborne Data Reduction Results"

5. *Mr. Robert E. Ziegler, Defense Mapping Agency Systems Center

   "The Wings of Gradiometry"

6. *Dr. Donald W. Vasco, Air Force Geophysics Laboratory

   "Linear Inversion of Gravity and Gravity Gradiometry: A Tale of Two Operators"

7. *Mr. John M. Brozena, Naval Research Laboratory

   "The Airborne Gravity Measurement Program at the Naval Research Laboratory"

* Denotes Speaker at Conference

16th GRAVITY GRADIOMETRY CONFERENCE
10-11 FEBRUARY 1988

SPONSORED BY:
AIR FORCE GEOPHYSICS LABORATORY
EARTH SCIENCES DIVISION

8. *Mr. Anestis J. Romaides, Air Force Geophysics Laboratory
Dr. Christopher Jekeli, Air Force Geophysics Laboratory

"A Detection of Non-Newtonian Gravity"

9. *Dr. Triveni N. Upadhyay, Mayflower Communications Company, Inc.
Dr. Duncan B. Cox, Jr., Mayflower Communications Company, Inc.
Dr. Christopher Jekeli, Air Force Geophysics Laboratory

"STS-GPS Tracking for Anomalous Gravitation Estimation (STAGE)"

10. Dr. M.V. Moody, University of Maryland
Dr. Q. Kong, University of Maryland
*Dr. Ho Jung Paik, University of Maryland
Mr. J.W. Parke, University of Maryland

"Three-Axis Superconducting Gravity Gradiometer: Progress Report"

11. Dr. A. Bernard, ONERA (Office National d'Etudes et de Recherches Aerospatiales), France
*Mr. Pierre Touboul, ONERA, France

"The GRADIO Spaceborne Gravity Gradiometer: Development and Accomodation"

12. Dr. Ho Jung Paik, University of Maryland
*Dr. Jurn-Sun Leung, University of Maryland
Dr. Samuel H. Morgan, Marshall Space Flight Center
Dr. Joseph Parker, Marshall Space Flight Center

"Global Gravity Survey and Precision Gravity Experiments by an Earth-Orbiting Gravity Gradiometer"

13. *Dr. Jean-Paul Richard, University of Maryland

"Laser Instrumentation for Gravity Measurements in Space"

* Denotes Speaker at Conference

14. Mr. A. Miguel San Martin, Jet Propulsion Laboratory
*Dr. D. Sonnabend, Jet Propulsion Laboratory

"Magnetic Isolation - An Update"

15. *Dr. Warner A. Miller, Air Force Weapons Laboratory

"From Geodetic Triangulation to Spacetime Geodesy"

* Denotes Speaker at Conference

PROGRAM REVIEW: GRAVITY GRADIOMETER SURVEY SYSTEM

by

Lou Pfohl

Bell Aerospace Textron
P.O. Box 1
Buffalo, NY 14240

Airborne and land mobile gravity gradient surveys were conducted in mid-western Oklahoma in the Spring of 1987 by Bell Aerospace under contract to the Air Force Geophysics Laboratory (Hanscom AFB) with funding from the Defense Mapping Agency. Survey experiences are recounted including field operation problems and accomplishments. The collected gravity gradient data were returned to Bell for post-mission data reduction which included data filtering, compensation, and integration into gravity disturbance vector solutions. Preliminary assessment of airborne data quality and the data reduction process is discussed.

MOVING BASE GRAVITY GRADIOMETER REVIEW

Gravity Gradiometer Survey System (GGSS) Program Review

AIR FORCE ACADEMY

Report No. 6501-927223 ● FEBRUARY 10/11, 1988

Bell Aerospace TEXTRON
Division of Textron Inc.

Gravity Gradiometer Survey System

- PROGRAM OVERVIEW.
- AIRBORNE SURVEY EXPERIENCE.
- LAND SURVEY EXPERIENCE.
- PRELIMINARY ASSESSMENT OF SURVEY DATA.

GGSS Program Overview

- CONTRACT AWARDED IN 1983 TO BELL AEROSPACE TEXTRON FROM THE AIR FORCE GEOPHYSICAL LABORATORY UNDER DIRECTIVE AND FUNDING FROM THE DEFENSE MAPPING AGENCY (HQ-WASH, DC)..

Objective

PRODUCE A GRAVITY SURVEYING TOOL CAPABLE OF FAST, ECONOMIAL,AIRBORNE AND LAND-MOBILE GRAVITY GRADIENT DATA COLLECTION WHICH, WITH OFF-LINE DATA REDUCTION, YIELDS GRAVITY DISTURBANCE VECTOR SOLUTIONS ACCURATE TO 1 MILLIGAL RMS ANAMOLY AND 0.2 ARC SECONDS RMS VERTICAL DEFECTION.

GGSS Workscope Highlights

- DESIGN AND FABRICATE SYSTEM HARDWARE USING EXISTING NAVY ADM/GSS EQUIPMENT DESIGNS WITH MODIFICATIONS AND ADDITIONS REQUIRED TO SUPPORT THE GGSS OBJECTIVES.

- PROCURE D.G. MV-10000 COMPUTER AND UTILIZE FOR POST-MISSION ALGORITHM DEVELOPMENT AND POST-MISSION DATA REDUCTION.

- INSTALL, INTEGRATE, AND TEST GGSS IN LAND VEHICLE AND AIRCRAFT.

- PLAN AND CONDUCT AIRBORNE AND LAND-MOBILE SURVEYS TO COLLECT GRAVITY GRADIENT DATA IN MID-WEST OKLAHOMA.

- REDUCE DATA POST-MISSION. PROVIDE FOR DATA FILTERING MOTION COMPENSATION, AND INTEGRATING INTO DISTURBANCE VECTOR SOLUTION.

GGSS Equipment

1. EXISTING ADM DESIGN "CARRY-OVERS"
   - GRAVITY GRADIOMETER INSTRUMENTS (GGI'S).
   - GGI CONTROL ELECTRONICS.
   - 3 AXIS PLATFORM.
   - PLATFORM STABILIZATION ELECTRONICS.

2. NEW OR MODIFIED EQUIPMENTS
   - PLATFORM ENCLOSURE.
   - IMBEDDED COMPUTER (ROLM MSE/14).
   - UNINTERRUPTABLE POWER SUPPLY.
   - GPS RECEIVER/ATOMIC CLOCK.
   - DATA RECORDING & MONITORING EQUIPMENT.
   - REVCON LAND VEHICLE.
   - AIRCRAFT (GFE).
   - AIRCRAFT INTERFACES.
   - MV-10000 COMPUTER (OFF-LINE DATA REDUCTION).
   - REAL TIME & OFF-LINE COMPUTER PROGRAMS.

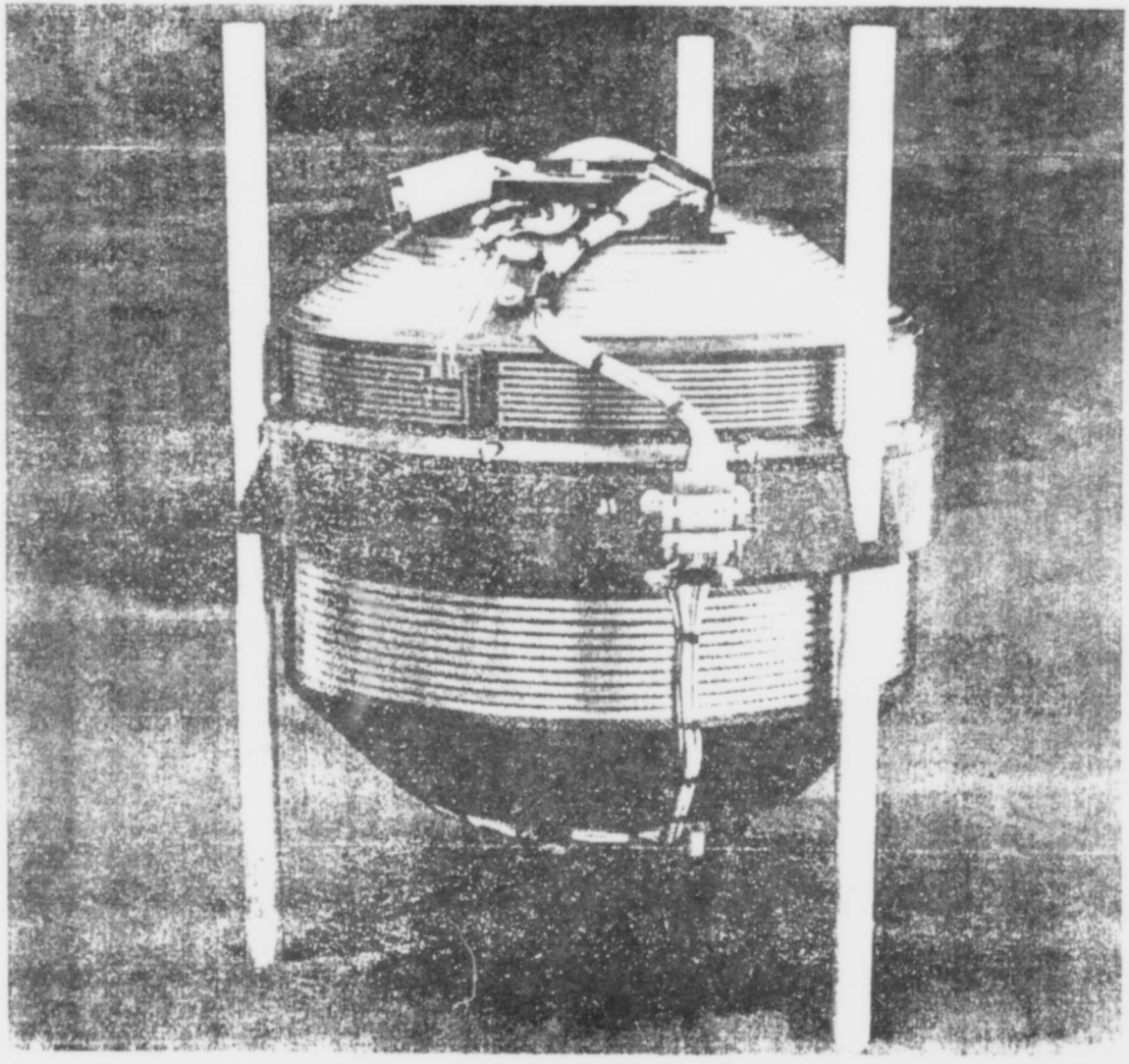

Bell Aerospace TEXTRON

Gravity Gradiometer Instrument

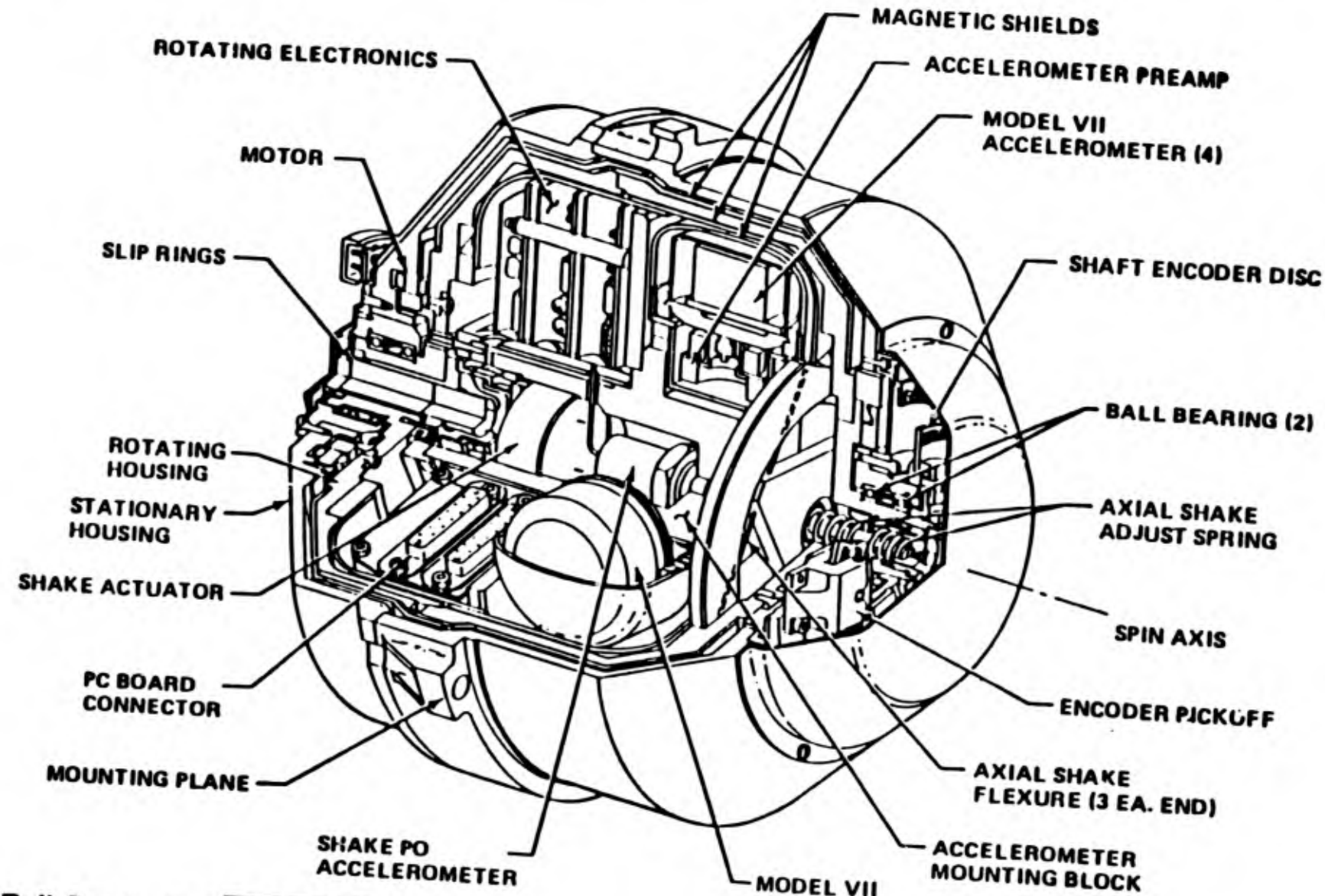

Bell Aerospace TEXTRON

GGI Instrument Block

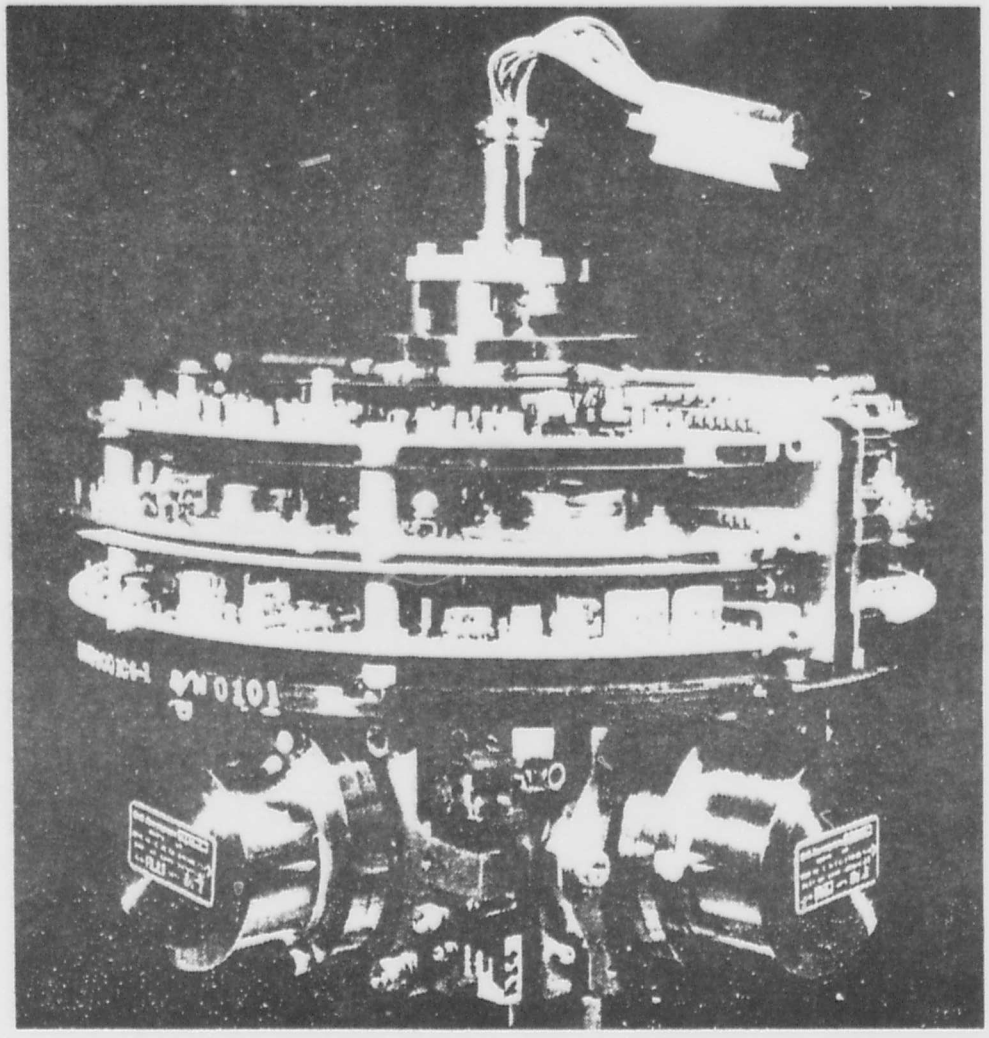

Bell Aerospace TEXTRON

Platform Cutaway Drawing

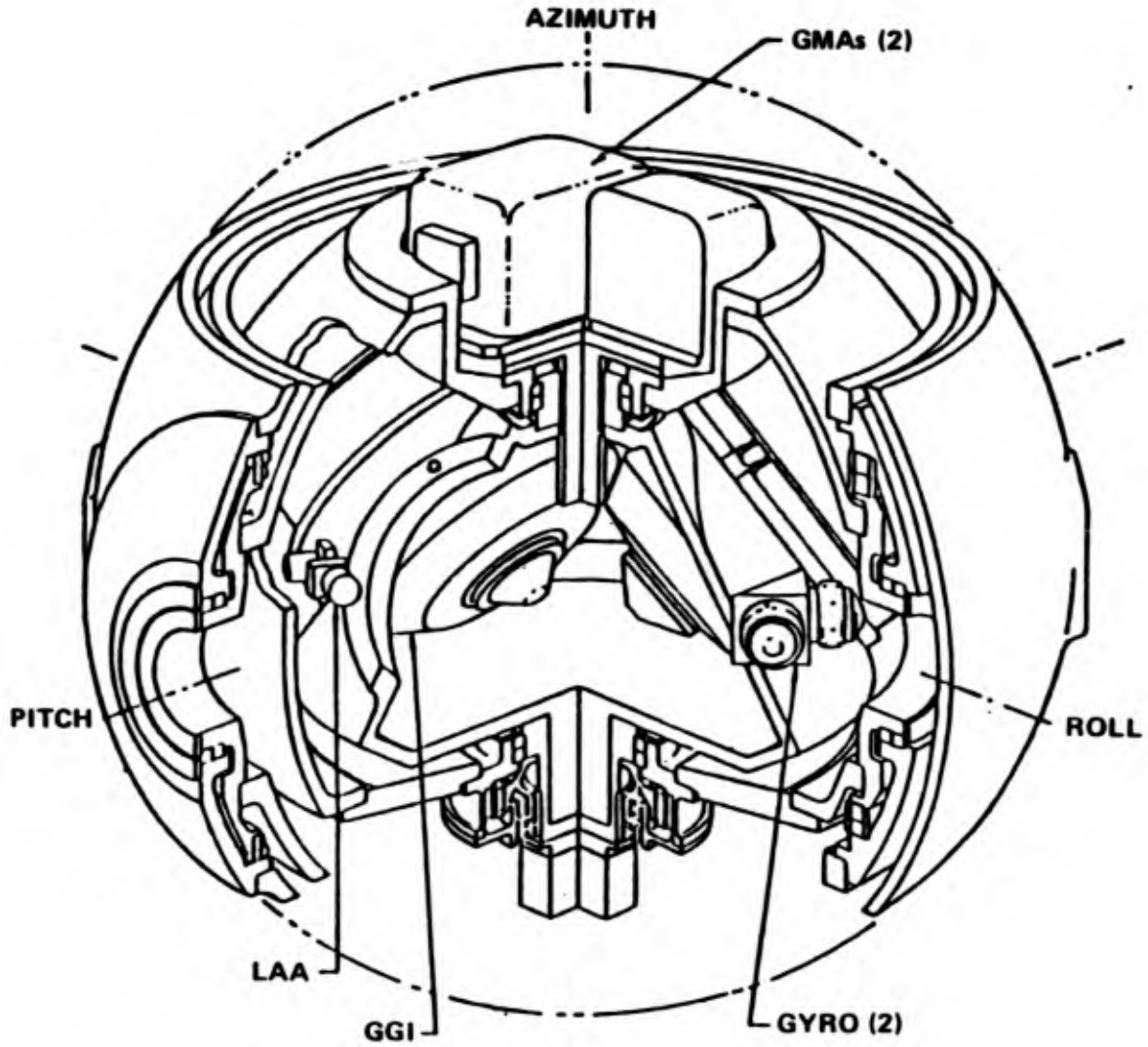

Orientation Of GGIs

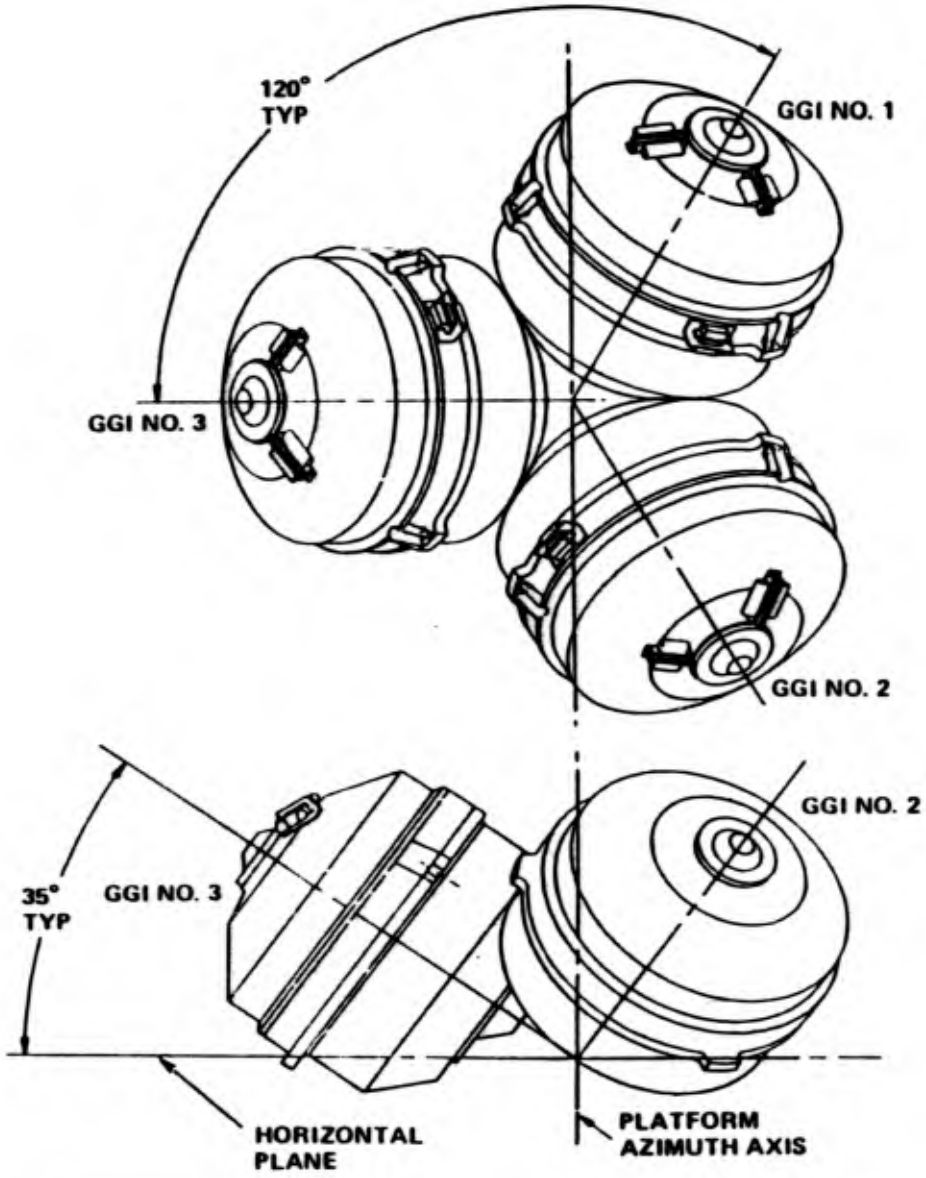

Stable Platform

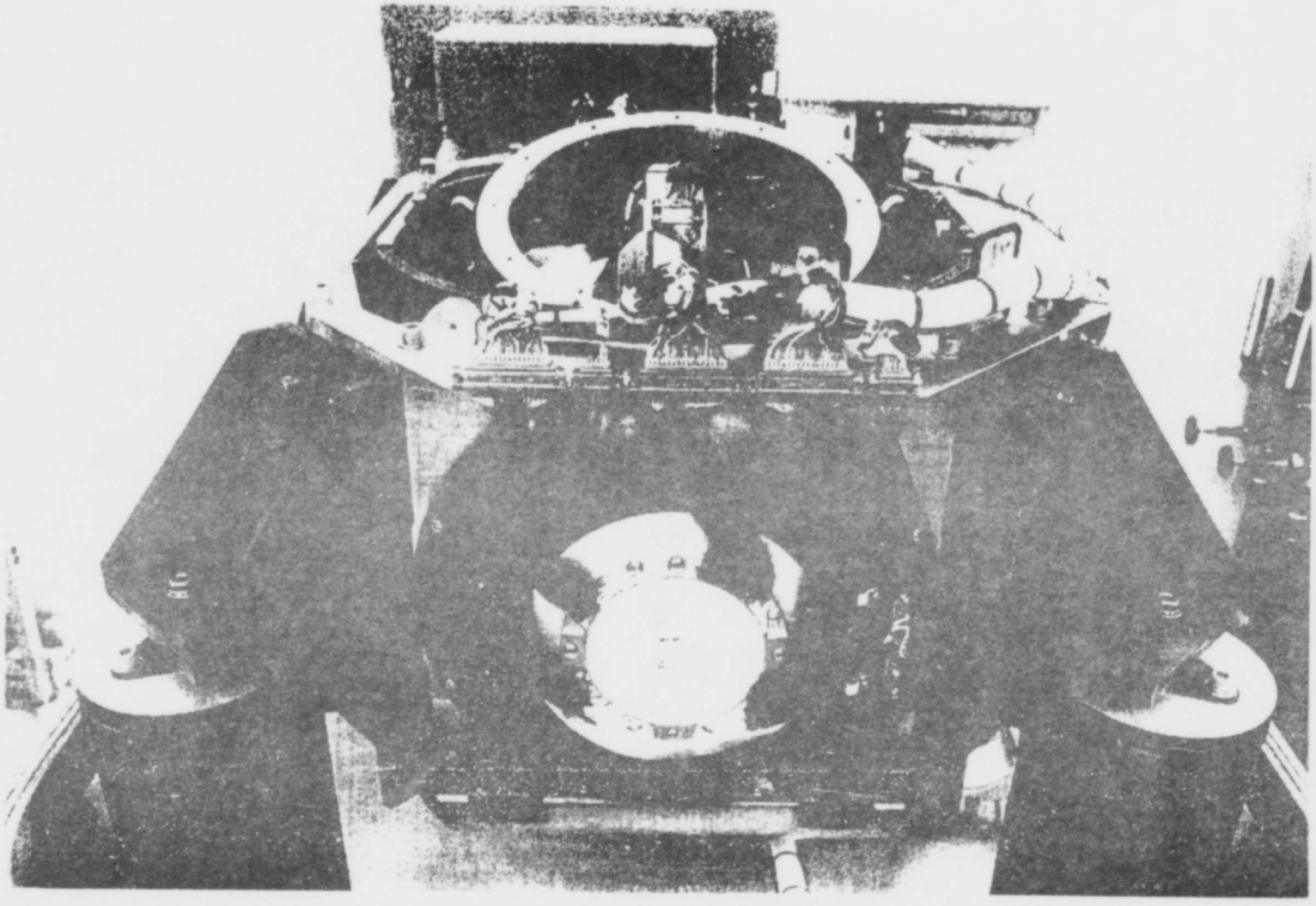

GGSS System

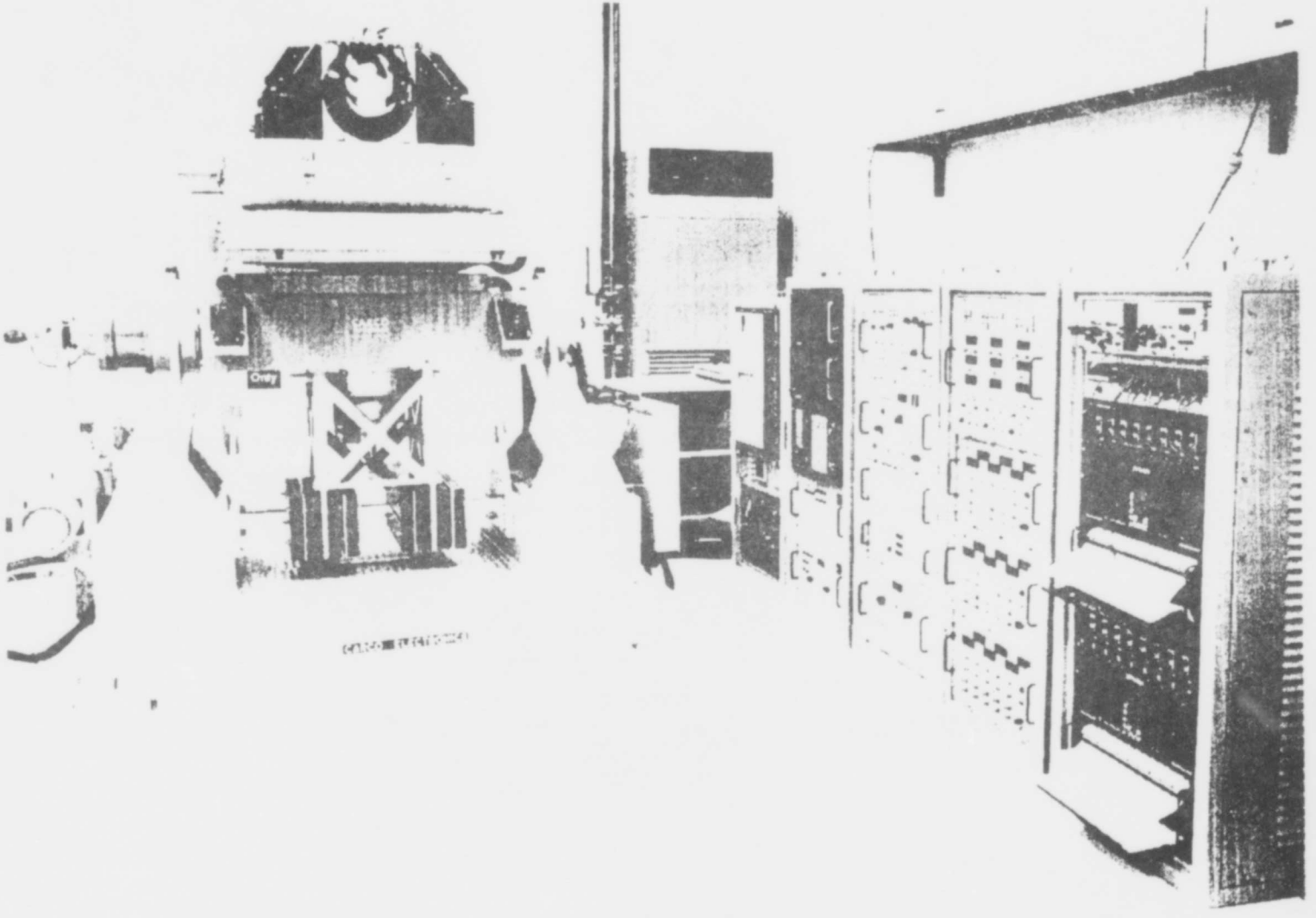

Bell Aerospace TEXTRON

GGSS-Land Vehicle Installation

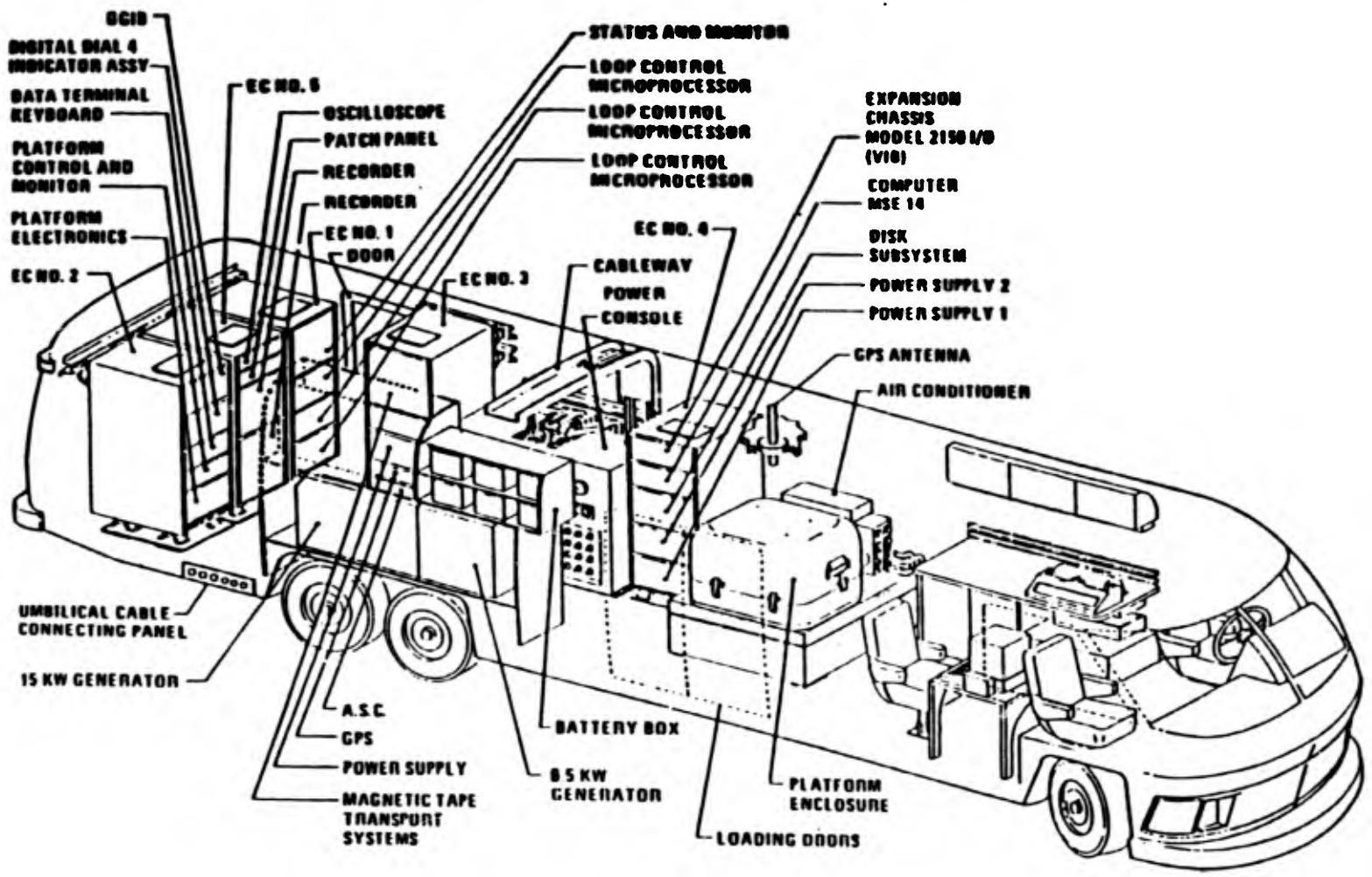

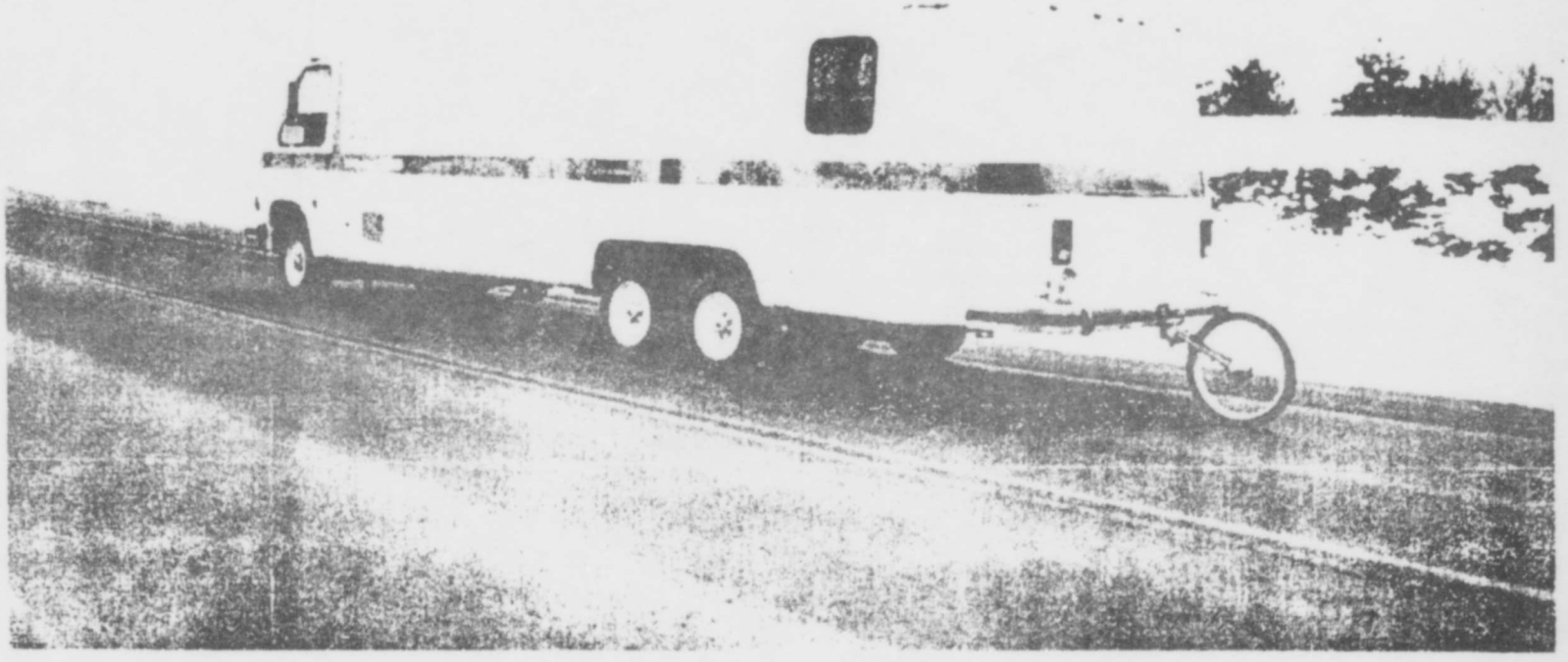

Bell Aerospace TEXTRON

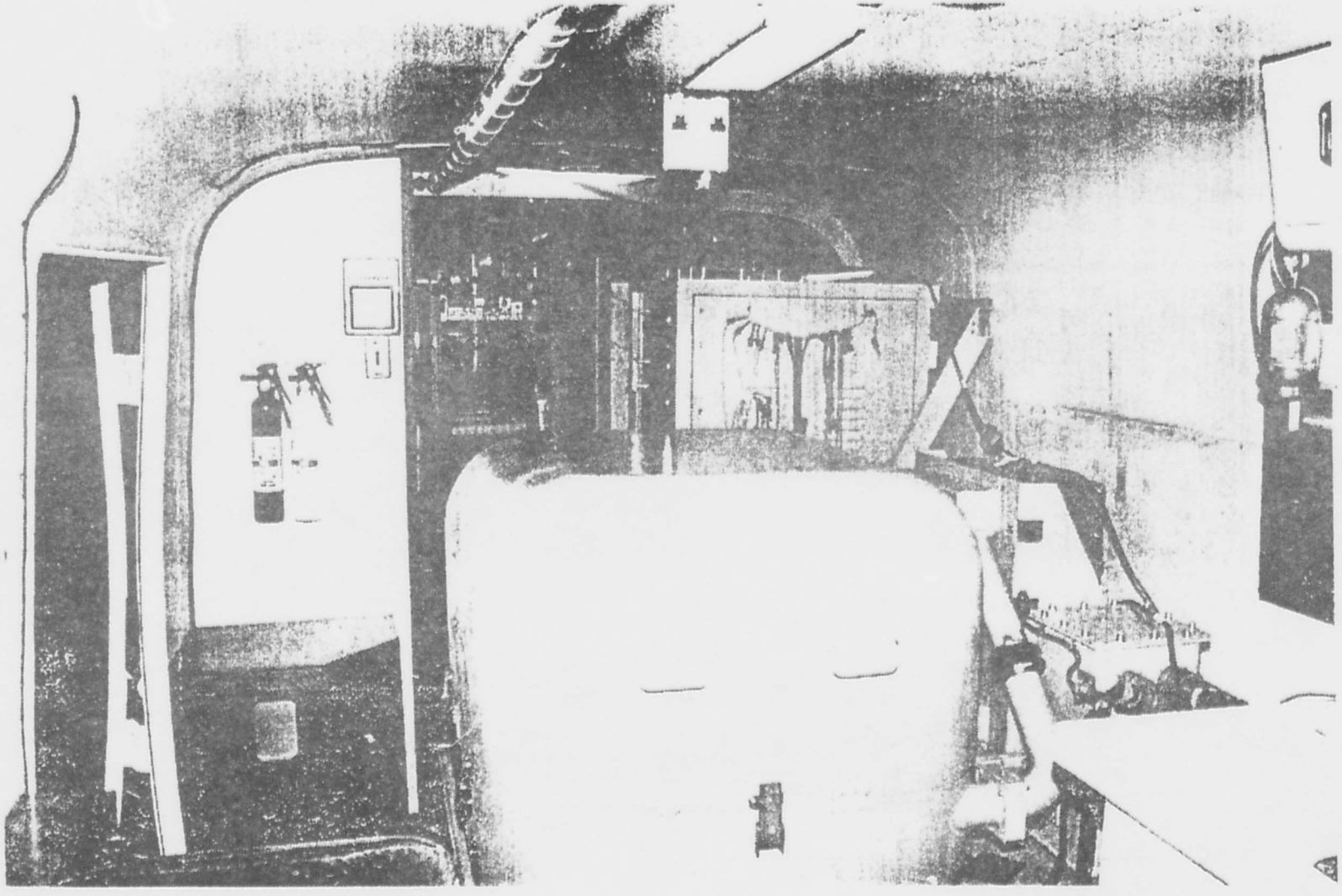

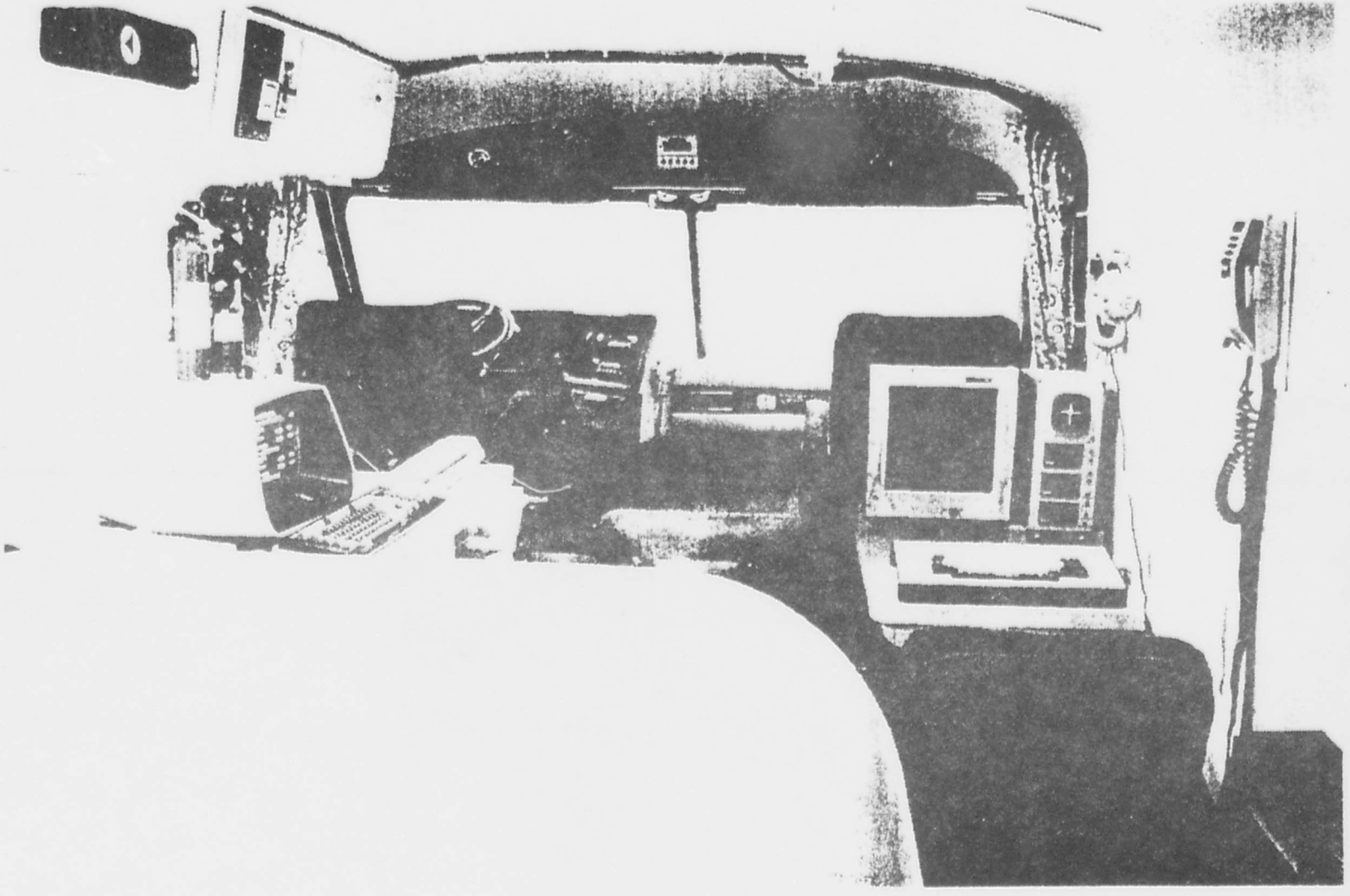

C130 Installation

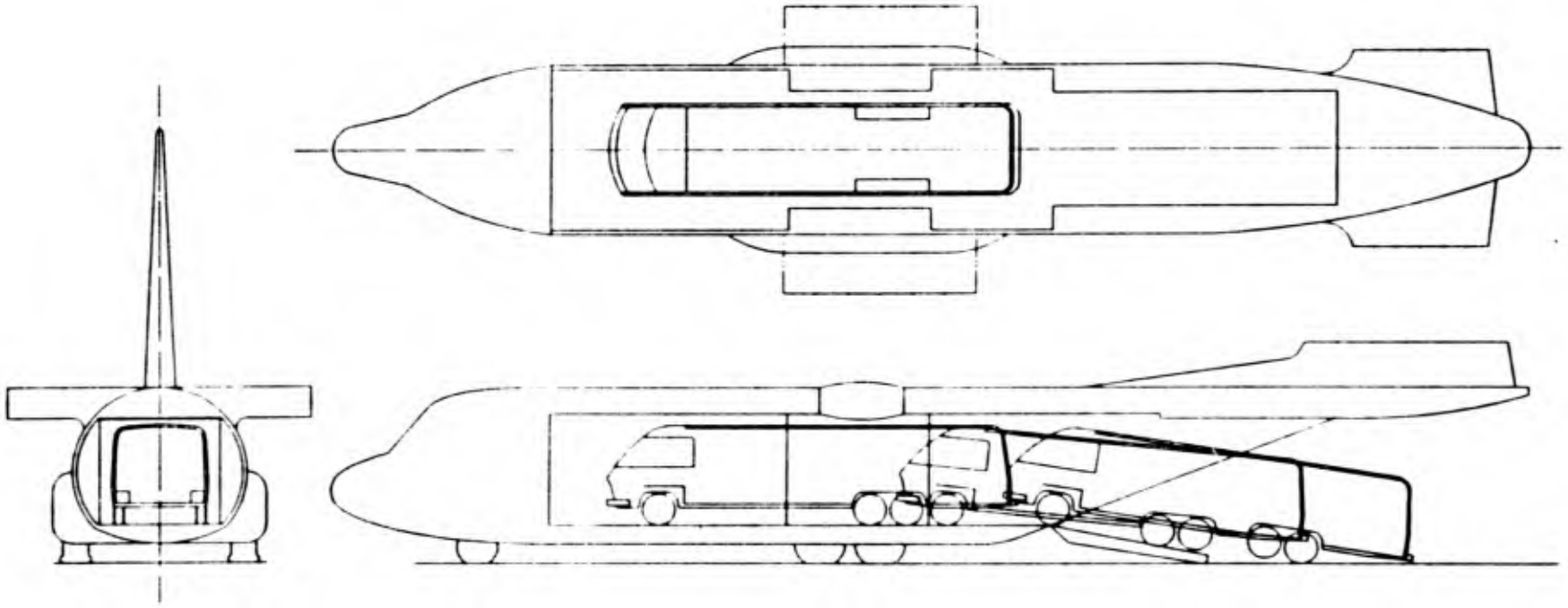

GGSS

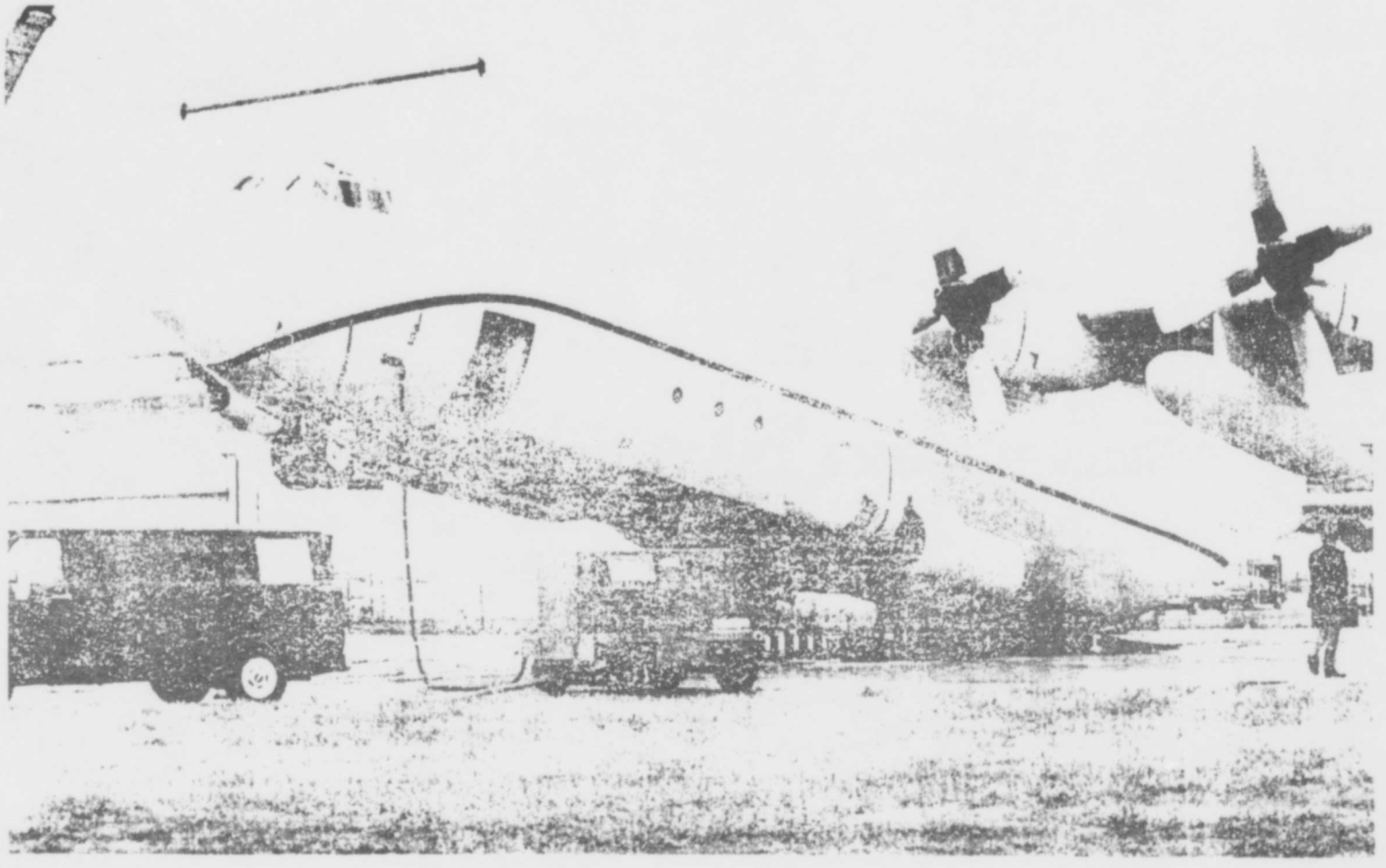

Bell Aerospace TEXTRON

AIRBORNE SURVEY EXPERIENCE

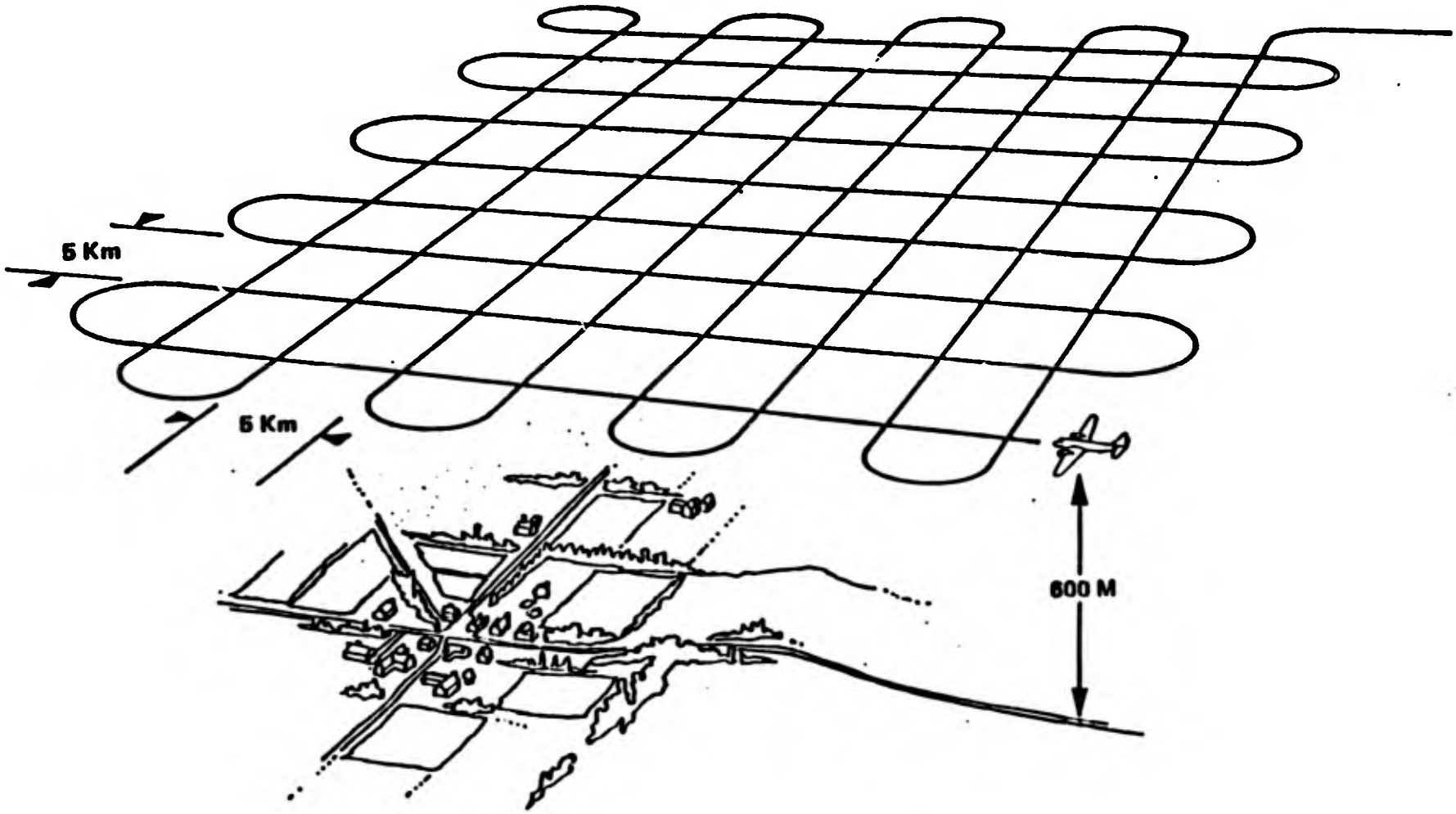
5 Km
5 Km
600 M

AIRBORNE SURVEY EXPERIENCE

- ARRIVED CLINTON-SHERMAN AIRPORT 4 APRIL 87.
- CONDUCTED 31 FLIGHTS BETWEEN 5 APRIL AND 20 MAY.
- WITH 121 LEGS FLOWN (OF 128 PLANNED) SYSTEM GROUNDED FOR 1 WEEK DUE TO WEATHER; AIRBORNE SURVEY TERMINATED.
- APPROXIMATELY 75 MAG TAPES OF DATA SENT BACK TO BELL FOR PROCESSING.
- BETWEEN 5 APRIL AND 20 MAY (46 DAYS).
  - 6 DAYS, LOST DUE TO WEATHER.
  - 5 DAYS, AIRCRAFT UNAVAILABLE.
  - 4 DAYS, GGSS EQUIPMENT DOWN.
  - 19 DAYS (19 FLIGHTS), COMPROMISED BY GPS OUTAGES.
  - 12 DAYS (12 FLIGHTS), ACCORDING TO PLAN.

FIELD EVALUATION - AIRBORNE SURVEY

- INCONSISTANT GPS PERFORMANCE A CONSTANT HEADACHE.
- AIRCRAFT SUPPORT.
  - PILOTS & CREW COOPERATIVE AND EFFICIENT.
  - GOOD FLIGHT CONTROL CHARACTERISTICS FROM C-130/GGSS.
  - OF 5 LOST DAYS, 3 DUE TO ENGINE FAILURE, 1 DUE TO INSTRUMENTATION, 1 DUE TO AIRBORNE COLLISON WITH LARGE BIRD.
  - AIRCRAFT INTERIOR AIR EXCESSIVELY HOT, CAUSED CONTINUOUS VAN AIR CONDITIONER PROBLEMS.
- GGSS EQUIPMENT FAILURES
  - 3 DAYS LOST DUE TO U.P.S OUTPUT STAGE FAILURE.
  - 1 DAY LOST DUE TO ROLM COMPUTER FAILURE (POWER SUPPLY BOARD).
  - EXCESSIVE NOISE IN GGI NO 2 SLIP RING, INTERMITTANT FAILURE; REPLACED SLIP RING ON 10 MAY.

LAND SURVEY EXPERIENCE

GRAVITY GRADIOMETER ground vehicle survey area
Ground Vehicle Cont. Pts.
(positions subject to change)
Grnd. Vechicle Test Course
MILES
10
5
0
LAWTON
CLINTON
ELK CITY
I-40
US-62
US 62
US 183
Wichata Mountain Wildlife Refuge
Clinton Sherman Airfield
Bell Aerospace
TEXTRON

Land Survey Experience

- OVER 500 KM OF ROAD COVERED.
- 25 MPH TO 30 MPH TYPICAL SPEEDS.
- USED 5TH WHEEL NAV-AID & KFP UPDATES (NO GPS).
- MOST ROAD SURFACES IN GOOD CONDITION.
- VAN REAR SUSPENSION POOR AT ANY SPEED AND OVER MOST ROAD CONDITIONS. (FRONT SUSPENSION EXCELLENT).
- ALL 3 COURSES COVERED WITH SINGLE TRAVERSE PER EACH COURSE. TIE POINT SURVEYS BEGUN WHEN GGI SPEED CONTROL FAILURES AND TAPE DRIVE STICTION PROBLEMS PREVENTED FURTHER OFF-SITE OPERATIONS.

Preliminary Assessment Of Airborne Survey Collected Data Set

- GPS OUTAGES CAUSED PLATFORM ANGULAR MOTION TRANSIENTS WHICH SEVERELY CONTAMINATED LARGE PORTIONS OF GGI GRADIENT OUTPUTS.

- NUMBER OF GPS PERFORMANCE DEGRADATION EVENTS OR OUTAGES FOUND (BY POST-MISSION ANALYSIS OF NAVIGATION DATA) TO BE HIGHER THAN DETECTED BY FIELD OPERATIONS.

- HIGHER NUMBER OF INTERMITTANT SLIP RING NOISE EVENTS ALSO FOUND BY POST-MISSION ANALYSIS.

- ONLY 30 OF APPROXIMATELY 120 LEGS FLOWN CONTAINED SUFFICIENTLY CLEAN GRADIENT DATA TO PROCESS WITH NOMINALLY PLANNED STAGE 1 FILTERING & COMPENSATION TECHNIQUES. MORE ADVANCED DATA RECOVERY METHODS COULD OBTAIN PERHAPS 75% OF THE REMAINING UNUSED DATA.

Airborne Data Evaluation

- SPARSITY OF CLEAN GRADIENT DATA PRECLUDED EFFECTIVED USE OF STAGE 2 (TRACK-CROSSING ADJUSTMENT AND INTEGRATION) ALGORITHM.

- BELL PERFORMED ALONG-TRACK INTEGRATION OF EACH OF 30 AIRBORNE TRACKS BUT DOES NOT POSSESS APPROPRIATE TRUTH DATA FOR "SINGLE-TRACK" PERFORMANCE EVALUATION.

- STAGE 1 OUTPUT (FILTERED & COMPENSATED GRADIENT DATA AND POSITION DATA) HAS BEEN SENT TO DMA FOR EVALUATION.

- NOTE: GRADIENT DATA OF SUFFICIENT QUALITY TO PRODUCE A DISTURBANCE VECTOR SOLUTION OF 1 MILLIGAL RMS ERROR WHEN PROCESSED THRU THE TRACK CROSSING ADJUSTMENT ALGORITHM WILL YIELD APPROXIMATELY 10 MILLGAL RMS ERROR ON A "SINGLE-TRACK" PROCESSING BASIS. (JEKELI, 1984, "ANALYSIS OF AIRBORNE GGSS ACCURACY.")

North Gravity Disturbance Vector
Over Oakiahoma Texas Panhandle (Bakers Peak)

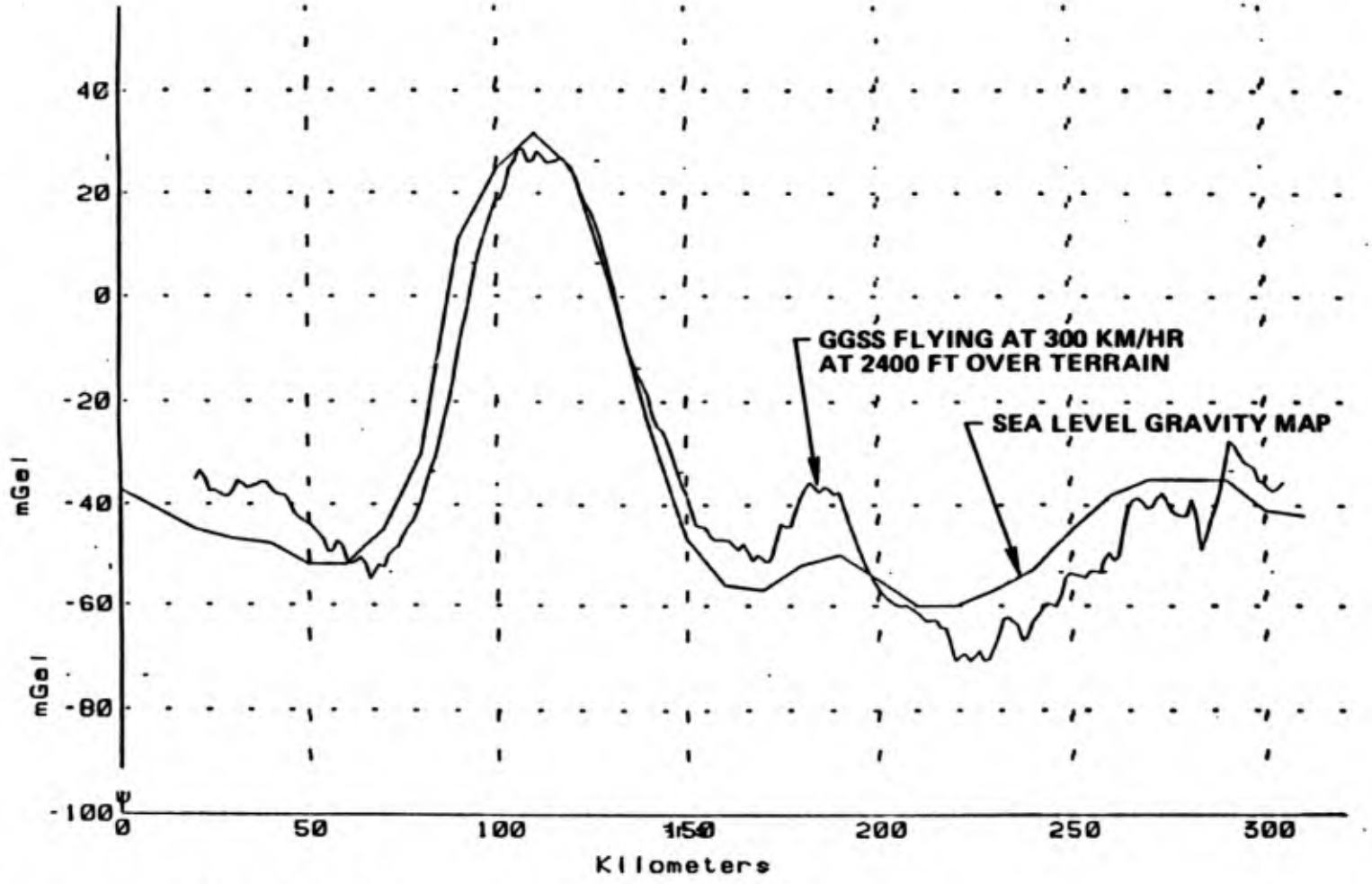

Bell Aerospace TEXTRON

16th GRAVITY GRADIOMETRY CONFERENCE
10-11 FEBRUARY 1988

SPONSORED BY:
AIR FORCE GEOPHYSICS LABORATORY
EARTH SCIENCES DIVISION

TITLE OF PAPER: Program Review: Gravity Gradiometer Survey System

SPEAKER: Lou Pfohl

QUESTIONS AND COMMENTS:

1. Comment: Dave Sonnabend

   I think an operator in the van about 1.5 meters from the instrument would contribute close to 1.0 E of signal.

   Response:

   This was carefully considered. Either the operator sat further away or restricted his movements.

2. Question: Chris Hansen

   What is the state of processing of data taken on the road tests?

   Response:

   Stage 1 processing. We will go into Stage 2 - integration to disturbances - shortly. It should be ready to be sent out to DMA by the end of the month.

SUPPRESSION OF MOTION SENSITIVITY IN BELL AEROSPACE GRAVITY GRADIOMETER SURVEY SYSTEM

by

Andrew D. Grierson

Bell Aerospace Textron
P.O. Box 1
Buffalo, NY 14240

Performance of a Gravity Gradiometer Survey System mounted in a moving vehicle is, in part, dependent upon the presence of motion-induced errors in the measured gradients. The physical origins of these effects and their characteristic signatures in the Bell Aerospace design of a rotating gradiometer are summarized.

In the Bell Aerospace GGSS, motion errors are suppressed by a combination of real-time and post-mission compensations. Some of the most important compensations are those for residual linear acceleration sensitivities. A detailed description is given of post-mission techniques by which linear acceleration sensitivities are identified and their effects removed from the recorded gradient signal.

MOVING BASE GRAVITY GRADIOMETER REVIEW

Gravity Gradiometer Survey System (GGSS)
Suppression of Motion Sensitivity

AIR FORCE ACADEMY

Report No. 6501-927224 • FEBRUARY 10/11, 1988

Bell Aerospace TEXTRON
Division of Textron Inc.

"SUPPRESSION OF MOTION SENSITIVITY IN BELL AEROSPACE GRAVITY GRADIOMETER SURVEY SYSTEM"

PRESENTER: ANDREW D. GRIERSON, BELL AEROSPACE TEXTRON

ABSTRACT

PERFORMANCE OF A GRAVITY GRADIOMETER SURVEY SYSTEM MOUNTED IN A MOVING VEHICLE IS, IN PART, DEPENDENT UPON THE PRESENCE OF MOTION-INDUCED ERRORS IN THE MEASURED GRADIENTS. THE PHYSICAL ORIGINS OF THESE EFFECTS AND THEIR CHARACTERISTIC SIGNATURES IN THE BELL AEROSPACE DESIGN OF ROTATING GRADIOMETER ARE SUMMARIZED.

IN THE BELL AEROSPACE GGSS, MOTION ERRORS ARE SUPPRESSED BY A COMBINATION OF REAL-TIME AND POST-MISSION COMPENSATIONS. SOME OF THE MOST IMPORTANT COMPENSATIONS ARE THOSE FOR RESIDUAL LINEAR ACCELERATION SENSITIVITIES. A DETAILED DESCRIPTION IS GIVEN OF POST-MISSION TECHNIQUES BY WHICH LINEAR ACCELERATION SENSITIVITIES ARE IDENTIFIED AND THEIR EFFECTS REMOVED FROM THE RECORDED GRADIENT SIGNAL.

GRADIOMETER FOR MOVING VEHICLE

IN ADDITION TO REDUCTION OF STATIONARY INSTRUMENT NOISE (E.G. THERMAL NOISE) TO AN ACCEPTABLE LEVEL, EFFECTS ASSOCIATED WITH MOTION MUST BE CONSIDERED.

- DETERMINISTIC MOTION GRADIENTS (E.G VEHICLE AND INSTRUMENT SELF-GRADIENT, CENTRIPETAL GRADIENT) MUST BE REMOVED ACCURATELY.

- BASIC DESIGN SHOULD MINIMISE CONTRIBUTION OF ERRORS DUE TO MOTION.

- RESIDUAL MOTION ERRORS SHOULD BE CAPABLE OF COMPENSATION OR CALIBRATION TO THE GREATEST EXTENT POSSIBLE, EITHER ON-LINE OR POST-MISSION.

Bell Gravity Gradient Instrument (GGI) Principles

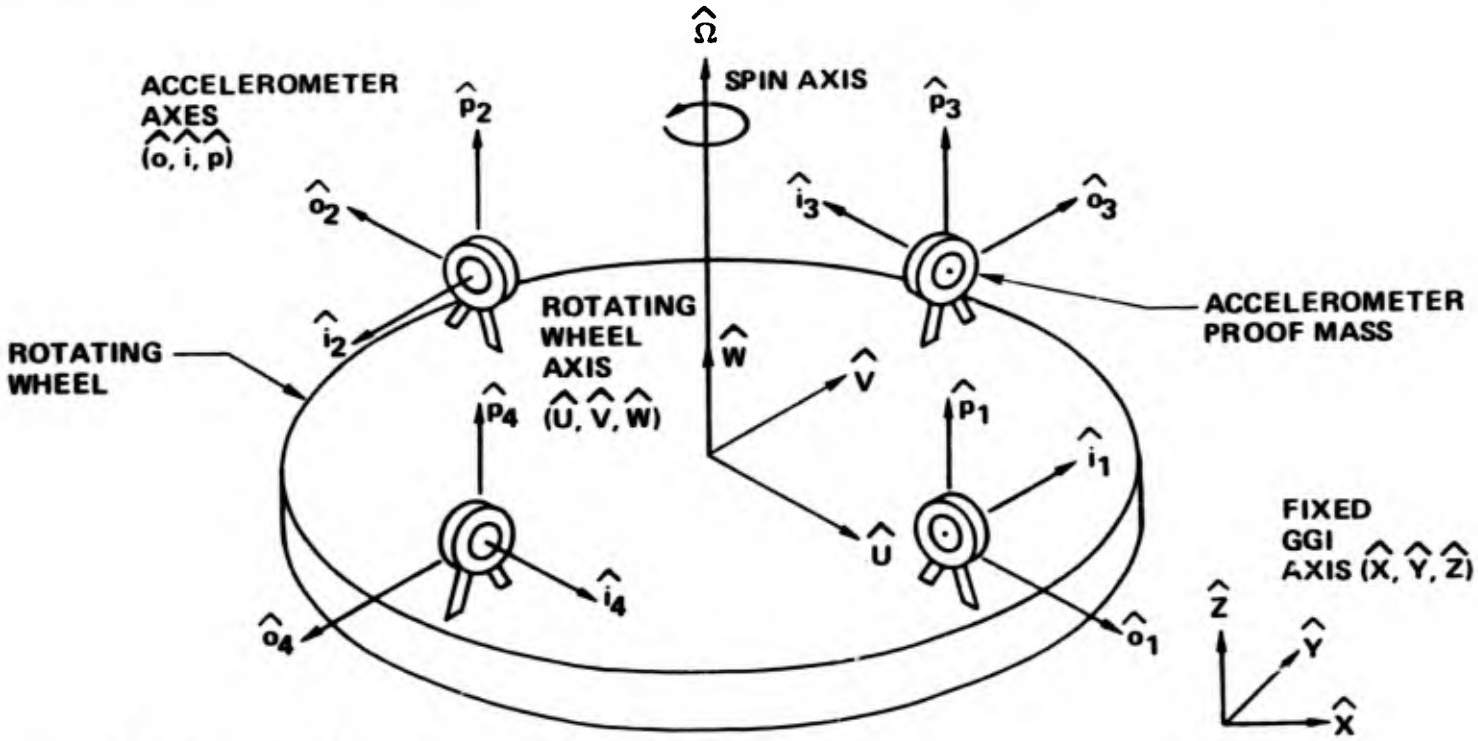

- WHEEL ROTATION PERIOD IS 4 SECONDS
- ACCELERATIONS a_m ARE SENSED ALONG INPUT AXES i_m
- GRADIENT (W) OUTPUT IS

$$(a_1 + a_2) - (a_3 + a_4) = (W_{yy} - W_{xx}) \sin 2\Omega t + 2 W_{xy} \cos 2\Omega t$$

- GRADIENTS ARE EXTRACTED BY SYNCHRONOUS DEMODULATION
- LINEAR ACCELERATIONS CANCEL
- SOME ERRORS ARE MODULATED AT DIFFERENT FREQUENCIES FROM GRADIENT

PRINCIPAL ERROR SOURCES ASSOCIATED WITH MOTION

- CENTRIPETAL GRADIENTS
  DETERMINISTIC WHEN ROTATION RATES ARE KNOWN ACCURATELY.

- SELF-GRADIENTS
  MASS STRUCTURE OF VEHICLE AND GRADIOMETER ASSEMBLY CAN BE CALIBRATED. THEN THIS IS DETERMINISTIC WHEN ATTITUDE IS KNOWN.

- ACCELEROMETER ERRORS
  ε_G SCALE FACTOR MISMATCH
  MISALIGNMENT
  INTERNAL DISTORTION

IN A 1_G ENVIRONMENT, TO MEASURE TO 1 EOTVOS OVER 10CM REQUIRES SCALE FACTOR AND MISALIGNMENT ERRORS BETTER THAN 1 PART IN 10^{11}.

UNCORRECTED ACCELEROMETERS MAY GIVE 1 PART IN 10^5.

ACCELEROMETER ERRORS MAY BE REPRESENTED AS SENSITIVITY COEFFICIENTS TO ACCELERATIONS ALONG THE OUTPUT, INPUT AND PENDULOUS AXES ($\hat{o}$, $\hat{i}$, $\hat{p}$) AND THEIR SECOND ORDER PRODUCTS. THUS EACH ACCELEROMETER (m) HAS 9 COEFFICIENTS:

$$K_O^m,\ K_I^m,\ K_P^m,\ K_{OO}^m,\ K_{OI}^m,\ K_{PP}^m,\ K_{OP}^m,\ K_{II}^m,\ K_{IP}^m,\ K_{PP}^m$$

GGI SENSITIVITY COEFFICIENTS TO ACCELERATIONS AT THE CENTER OF THE WHEEL IN ROTATING WHEEL COORDINATES ($\hat{u}$, $\hat{v}$, $\hat{w}$) ARE COMBINATIONS OF THE COEFFICIENTS FOR THE FOUR ACCELEROMETERS AND THE WHEEL'S CENTRIPETAL ACCELERATION ($\Omega^2 R$).

$$K_u = K_O^1 - K_O^2 + K_I^3 - K_I^4 + \Omega^2 R\ (2K_{OO}^1 - 2K_{OO}^2 + K_{OI}^3 - K_{OI}^4)$$

$$K_v = K_I^1 - K_I^2 - K_O^3 + K_O^4 + \Omega^2 R\ (K_{OI}^1 - K_{OI}^2 - 2K_{OO}^3 + 2K_{OO}^4)$$

$$K_w = K_P^1 + K_P^2 - K_P^3 - K_P^4 + \Omega^2 R\ (K_{OP}^1 + K_{OP}^2 - K_{OP}^3 - K_{OP}^4)$$

$$K_{uu} = K_{OO}^1 + K_{OO}^2 - K_{II}^3 - K_{II}^4$$

$$K_{vv} = K_{II}^1 + K_{II}^2 - K_{OO}^3 - K_{OO}^4$$

$$K_{uv} = K_{OI}^1 + K_{OI}^2 + K_{OI}^3 + K_{OI}^4$$

$$K_{uw} = K_{OP}^1 - K_{OP}^2 + K_{IP}^3 - K_{IP}^4$$

$$K_{vw} = K_{IP}^1 - K_{IP}^2 - K_{OP}^3 + K_{IP}^4$$

$$K_{ww} = K_{PP}^1 + K_{PP}^2 - K_{PP}^3 - K_{PP}^4$$

ACCELERATIONS IN NON-ROTATING GGI COORDINATES ($\hat{x}$, $\hat{y}$, $\hat{z}$), MOUNTED AT UMBRELLA ATTITUDE (SPIN AXIS 35.26° TO HORIZONTAL) ALL HAVE AN EQUAL COMPONENT OF GRAVITY PLUS A VARIABLE MOTION COMPONENT (a_x, a_y, a_z). TRANSFORMING THESE ACCELERATIONS INTO ROTATING WHEEL FRAME AND LINEARIZING GIVES THE FIRST ORDER DOMINANT OUTPUTS, AT VARIOUS HARMONICS OF WHEEL RATE, WHICH ARE PRODUCED BY THE SENSITIVITY COEFFICIENTS.

$$K_u = a_x \cos \Omega t + a_y \sin \Omega t$$

$$K_v = -a_x \sin \Omega t + a_y \cos \Omega t$$

$$K_w = a_z$$

$$K_{uu} - K_{vv} = (a_x - a_y) \cos 2\Omega t + (a_x + a_y) \sin 2\Omega t$$

$$K_{uu} + K_{vv} = a_x + a_y$$

$$K_{uv} = -(a_x - a_y) \sin 2\Omega t + (a_x + a_y) \cos 2\Omega t$$

$$K_{uw} = (a_x + a_z) \cos \Omega t + (a_y + a_z) \sin \Omega t$$

$$K_{vw} = -(a_x + a_z) \sin \Omega t + (a_y + a_z) \cos \Omega t$$

$$K_{ww} = a_z$$

BOTH ON-LINE AND POST-MISSION COMPENSATIONS ARE APPLIED.

ON-LINE

TO KEEP THE OUTPUT SIGNAL WITHIN REASONABLE LIMITS, DEMODULATION AT WHEEL RATE IS PERFORMED AND THE OUTPUTS USED TO DRIVE SCALE-FACTOR ADJUSTMENT COILS IN THE ACCELEROMETERS.

POST-MISSION

CORRELATION OF MODULATED ACCELERATION PRODUCTS WITH GGI OUTPUT IS USED TO IDENTIFY SENSITIVITY COEFFICIENTS.

On-Line Compensation And Recording

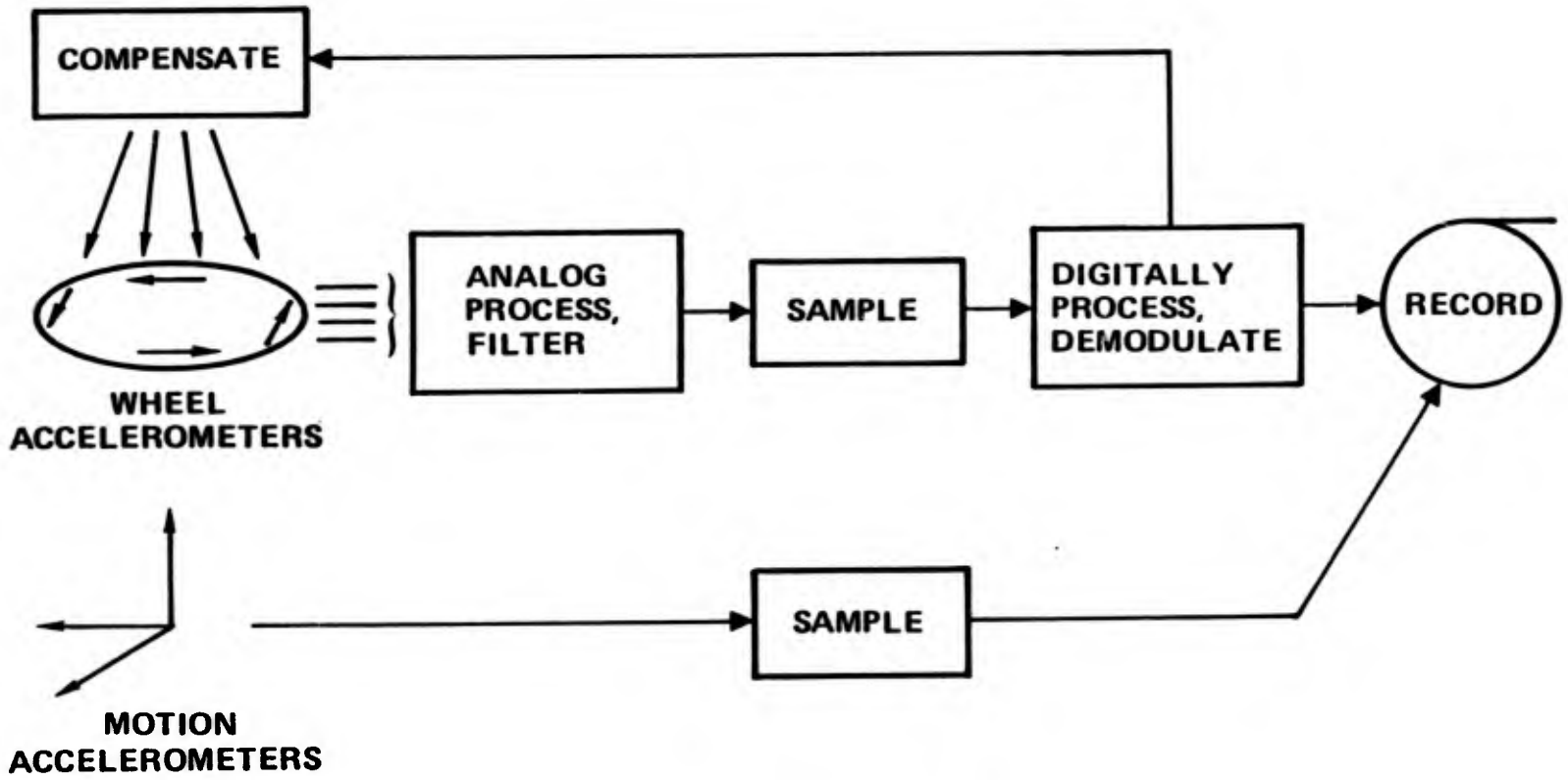

Typical Airborne GGI Output Spectrum

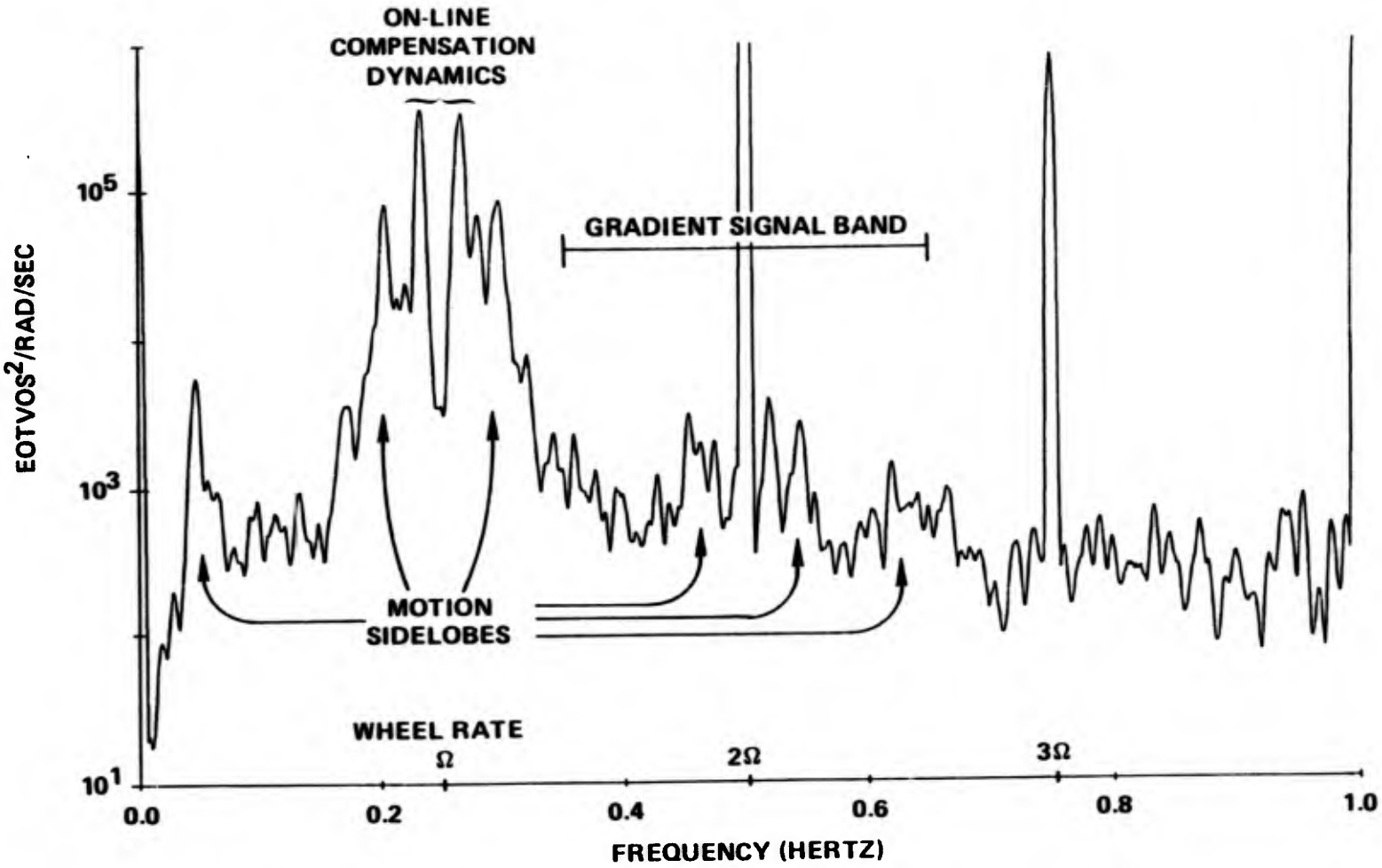

Bell Aerospace TEXTRON

CONSIDERATIONS FOR POST-MISSION CALIBRATION

- COEFFICIENTS MUST BE STABLE OVER THE PERIOD USED FOR ESTIMATION AND COMPENSATION (ε_G BETWEEN MISSIONS).
- SIGNAL AND OTHER INTERFERENCE MUST BE UNCORRELATED WITH MOTION EFFECTS.
- x, y AND z ACCELERATIONS MUST BE DISTINCT IF COEFFICIENTS ARE TO BE SEPARABLE. CAROUSELLING MAY BE USEFUL IN ACHIEVING THIS.
- OUTPUT SPECTRUM INDICATES THAT A COMPLETE MODEL OF THE GGI WOULD BE DIFFICULT.
- IN ORDER TO SEPARATE CERTAIN COEFFICIENTS THE ESTIMATION MUST BE SENSITIVE TO THE PHASE OF MODULATION.
- SOME UNMODELLED DYNAMICS IN GGI SAMPLES MUST BE PERMITTED IN THE ESTIMATION PROCESS.

ESTIMATION PRINCIPLES

- IN ORDER TO BE ABLE TO SELECT THOSE FREQUENCY RANGES WHERE ACCELERATION SENSITIVITY IS DOMINANT, COEFFICIENTS ARE ESTIMATED IN THE FREQUENCY DOMAIN.

- PHASE INFORMATION IS RETAINED IN THE REAL AND IMAGINARY PARTS OF THE TRANSFORMS.

- SINCE THE GGI OUTPUT CONTAINS A LINEAR COMBINATION OF ACCELERATION PRODUCTS IN WHEEL COORDINATES AS DETERMINED BY THE SENSITIVITY COEFFICIENTS, THE FOURIER TRANSFORM OF GGI OUTPUT CONTAINS THE SAME LINEAR COMBINATION OF ACCELERATION PRODUCT TRANSFORMS.

- TO ESTIMATE UNKNOWN DYNAMICS, A SET OF WEIGHTS FOR A RANGE OF TIME ADVANCES AND DELAYS ARE ESTIMATED FOR EACH COEFFICIENT. THUS A TRANSFER FUNCTION IS APPROXIMATED BY THE TRANSFORM OF A TIME WINDOW OF WEIGHTS.

Post-Mission Calibration Process

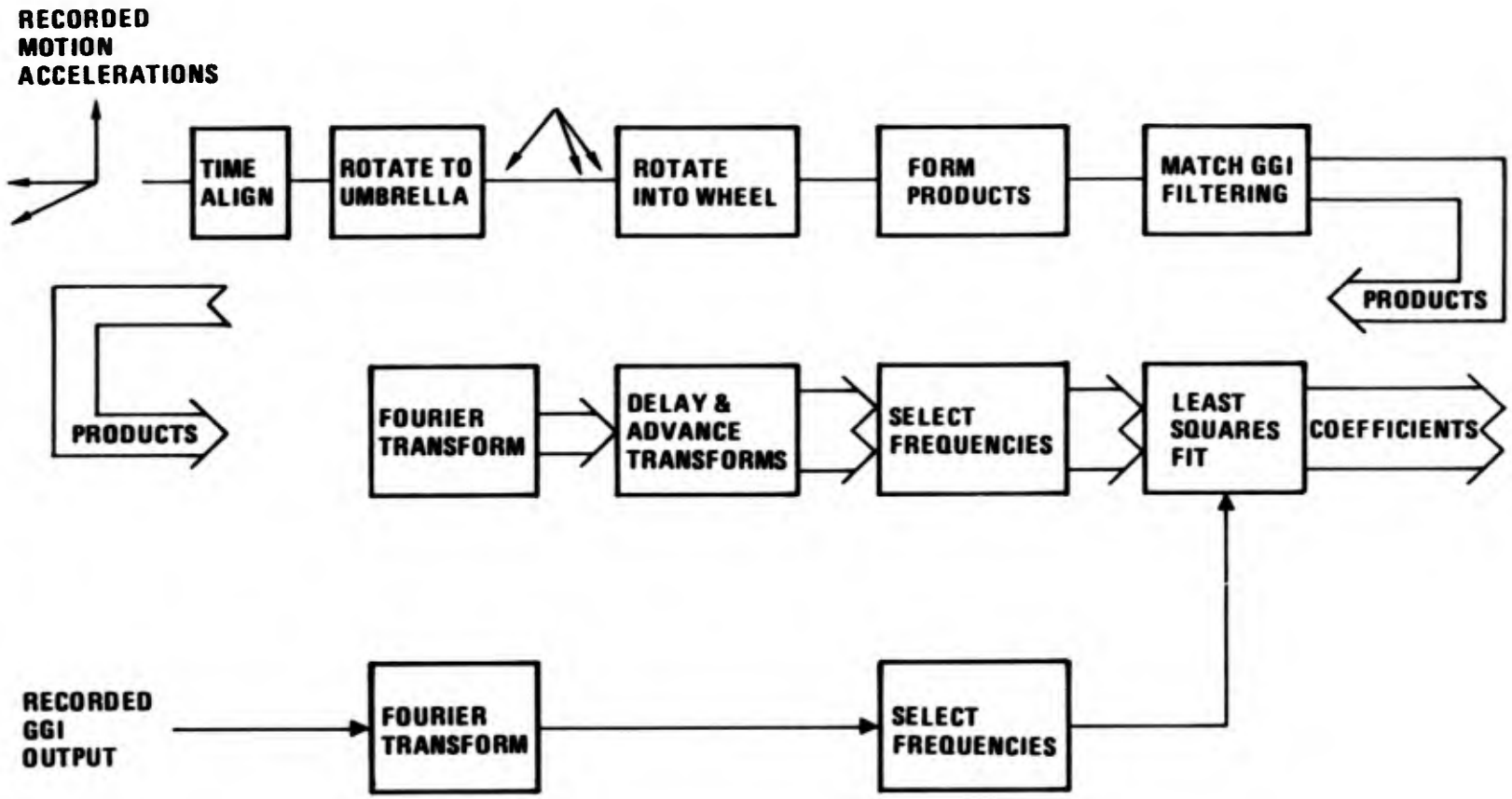

CALIBRATION PROCEDURE - 1

- RECORDED MOTION ACCELERATIONS ARE COMPENSATED FOR SAMPLING TIME SYNCHRONIZATION WITH GGI OUTPUTS AND THEN CONVERTED INTO ROTATING WHEEL COORDINATES.

- SECOND ORDER PRODUCTS ARE FORMED.

- ACCELERATIONS AND PRODUCTS ARE DIGITALLY FILTERED TO MATCH GGI ELECTRONICS. (BANDPASS FILTER).

- FOURIER TRANSFORMS ARE TAKEN OF ALL FILTERED ACCELERATIONS AND PRODUCTS AND OF GGI OUTPUT.

- FOR EACH ACCELERATION PRODUCT TRANSFORM A SET OF FURTHER TRANSFORMS IS CREATED FOR A RANGE OF ADVANCED OR DELAYED SAMPLES BY MULTIPLYING BY $E^{\pm JWNT}$ WHERE T IS SAMPLE SPACING AND $\pm N$ IS THE NUMBER OF SAMPLES ADVANCED OR DELAYED.

Transform Of Filtered Acceleration Product $A_u^2 - A_v^2$

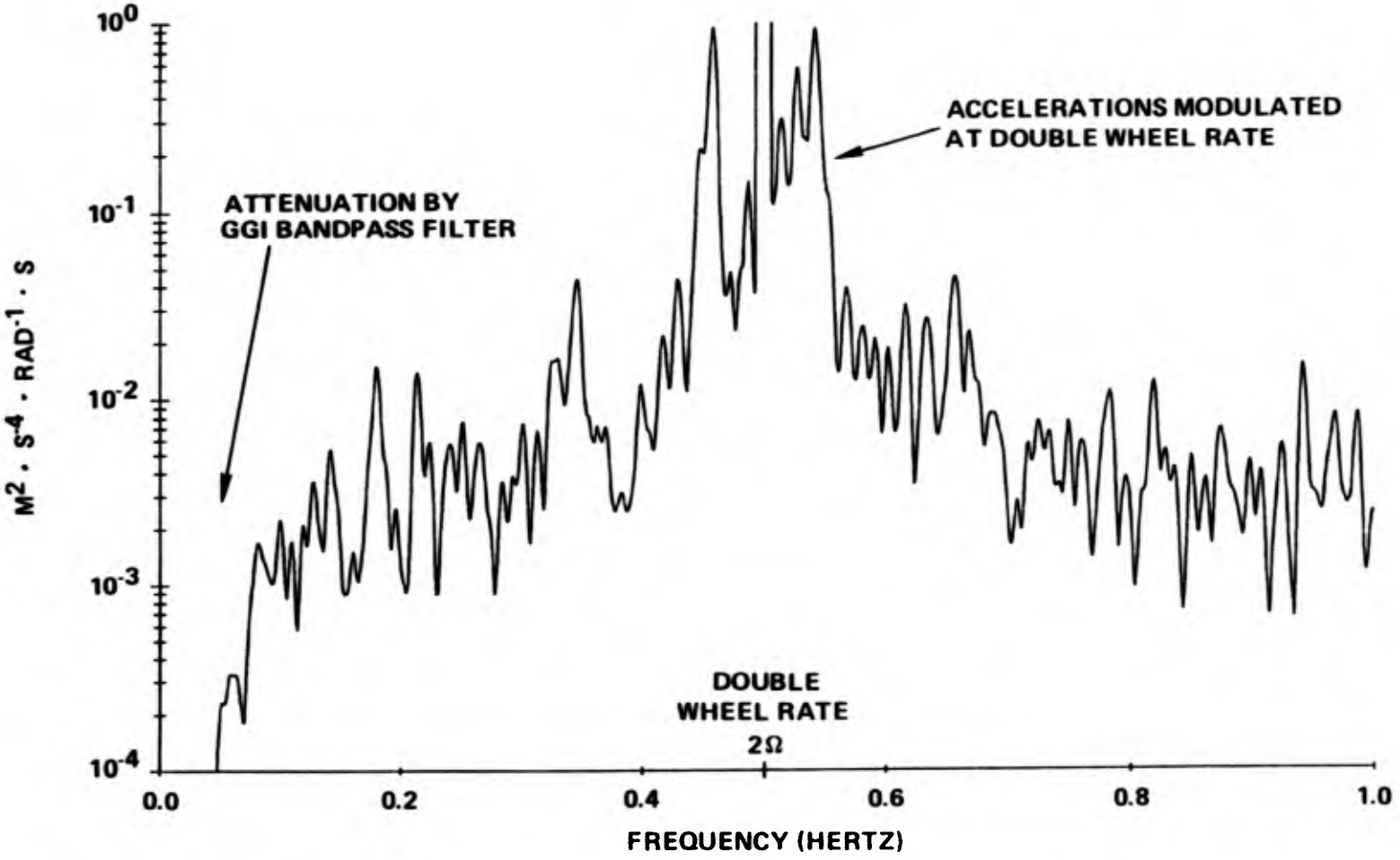

Transform Of Filtered Acceleration Product $A_u^2+A_v^2$

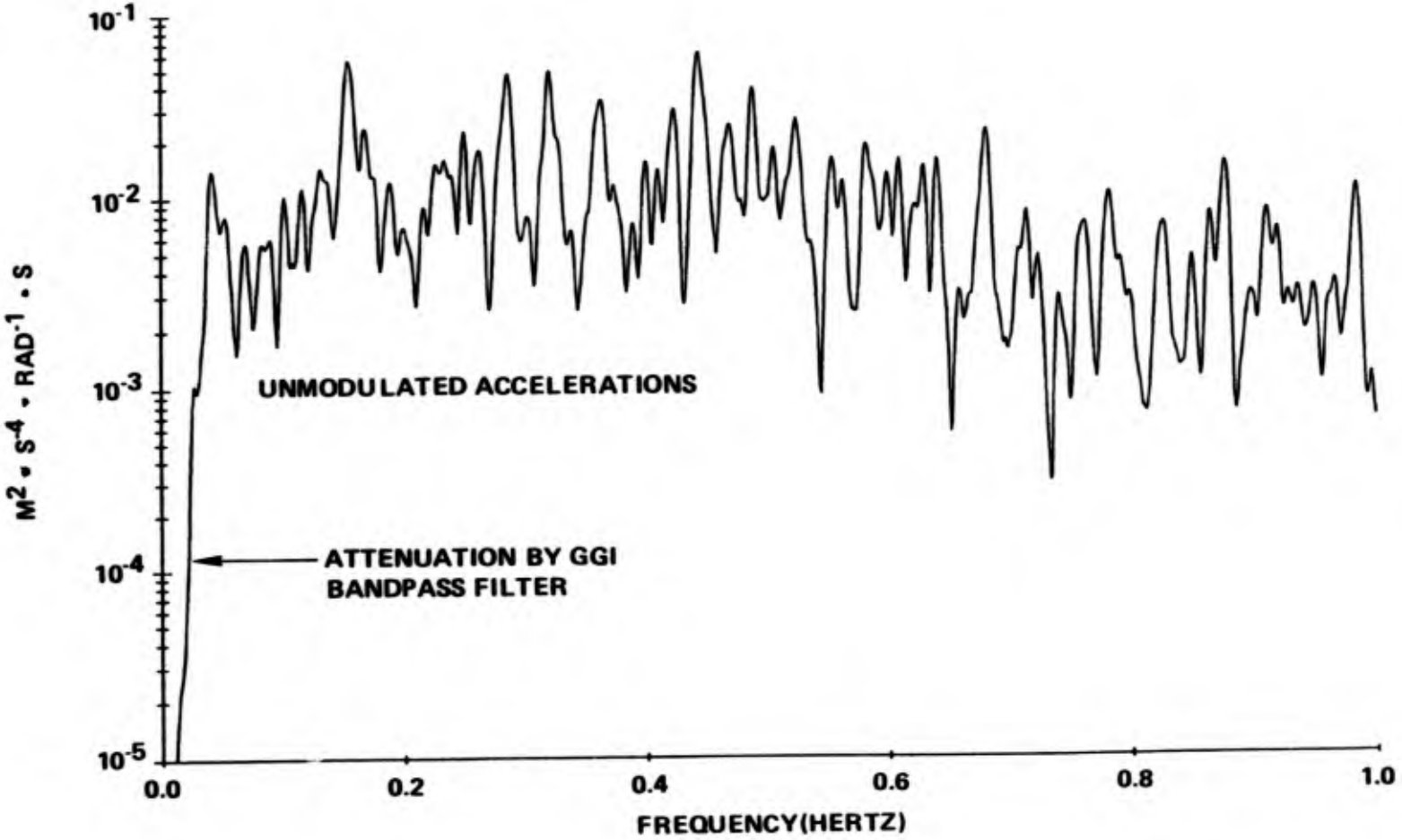

Transform Of Filtered Acceleration Product Au Aw

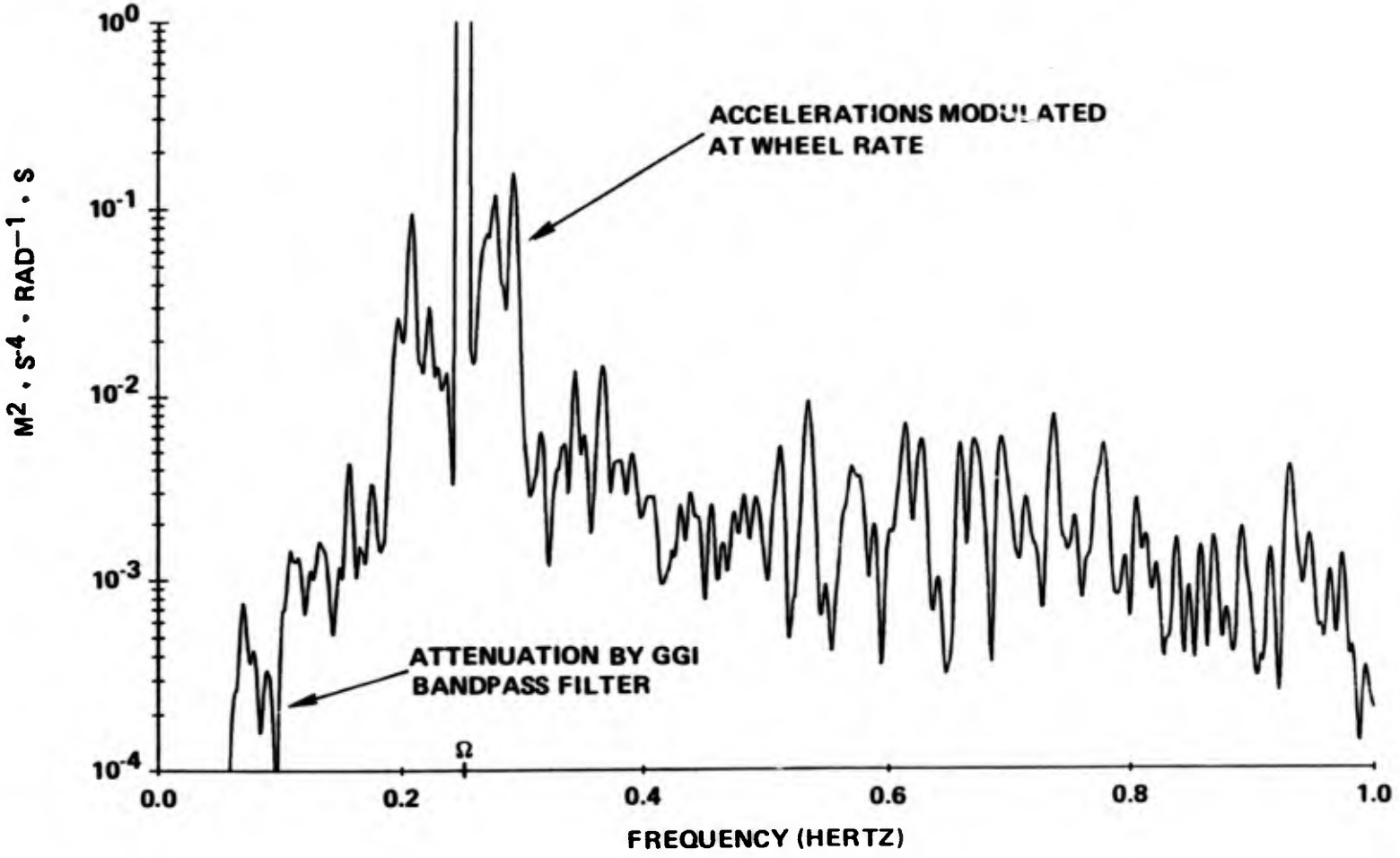

CALIBRATION PROCEDURE - 2

- A LEAST SQUARES REDUCTION IS FORMED USING THOSE FREQUENCY BANDS OF THE TRANSFORMS WHERE ACCELERATION SENSITIVITY IS IMPORTANT.

- CONSTRAINTS ARE APPLIED TO CONTROL THE AMPLIFICATION OF HIGH FREQUENCY NOISE.

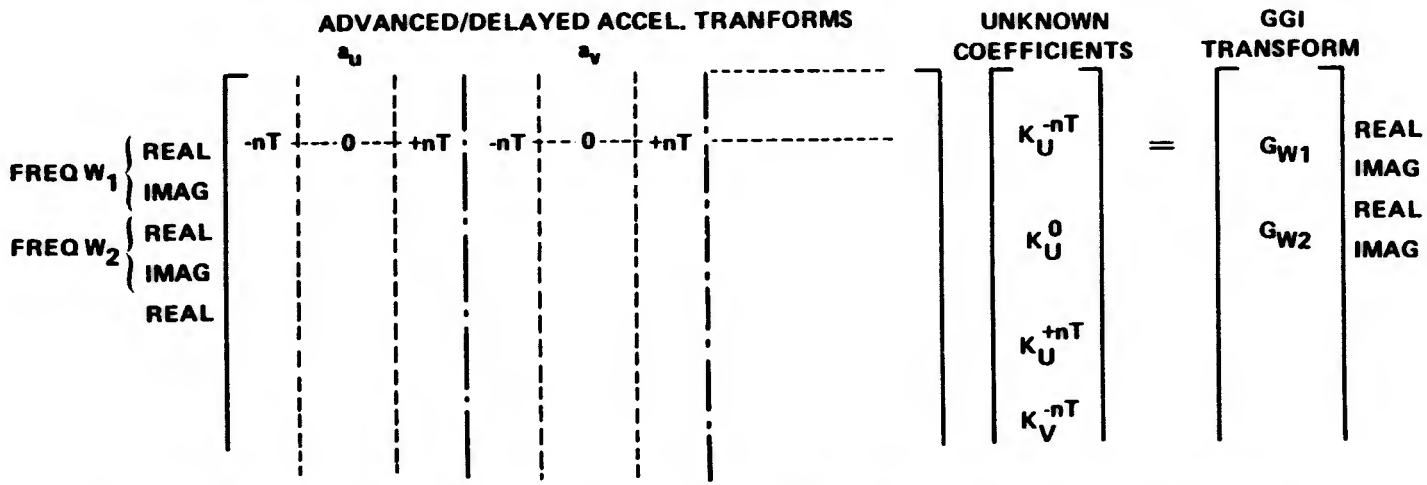

- COEFFICIENTS ESTIMATED IN THE FREQUENCY DOMAIN ARE APPLIED TO ADVANCED AND DELAYED ACCELERATION PRODUCTS IN THE TIME DOMAIN TO OBTAIN A TIME SEQUENCE OF GGI COMPENSATION.

Improvement In GGI Output Transform

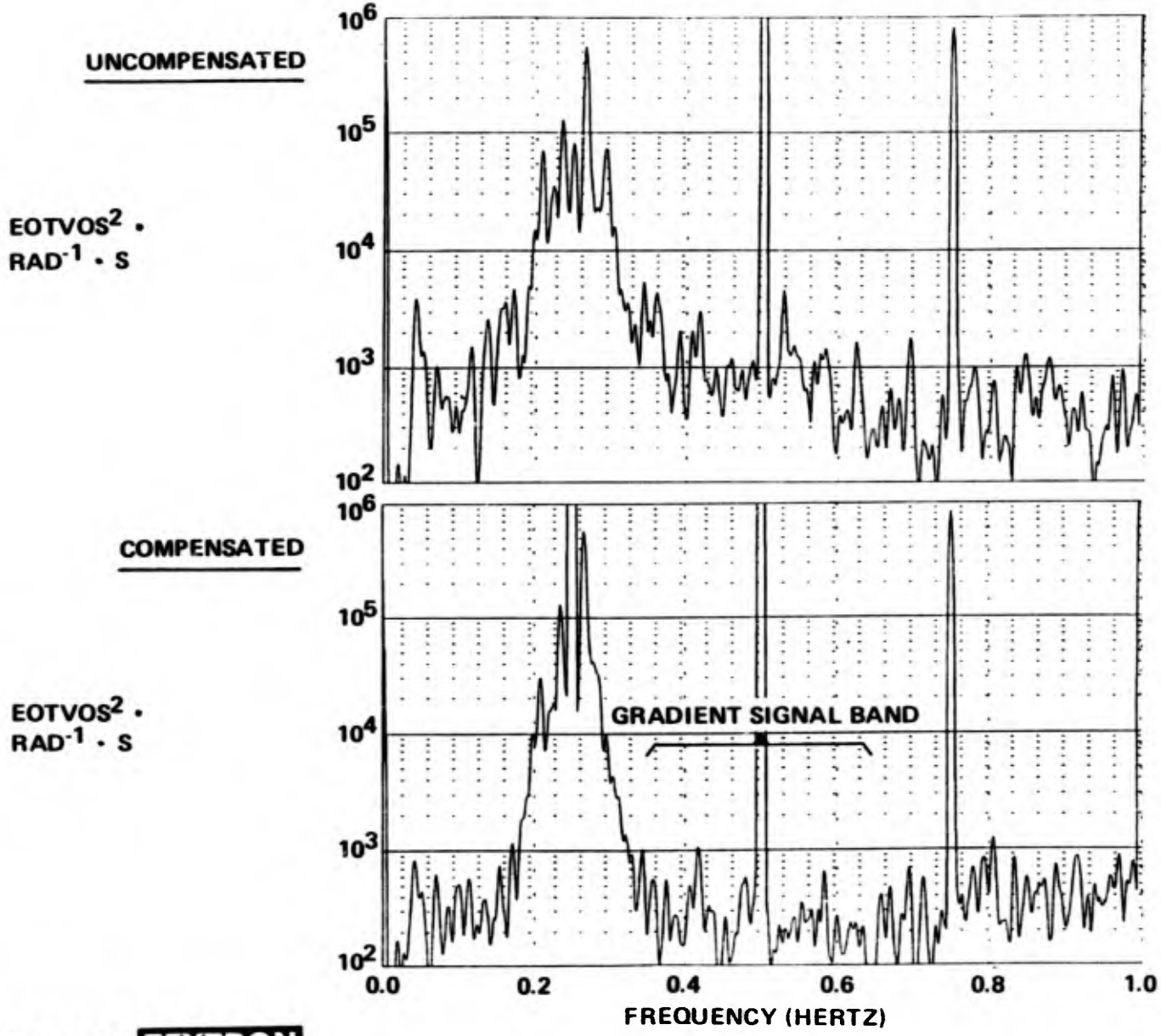

Improvement In Demodulated Gradient

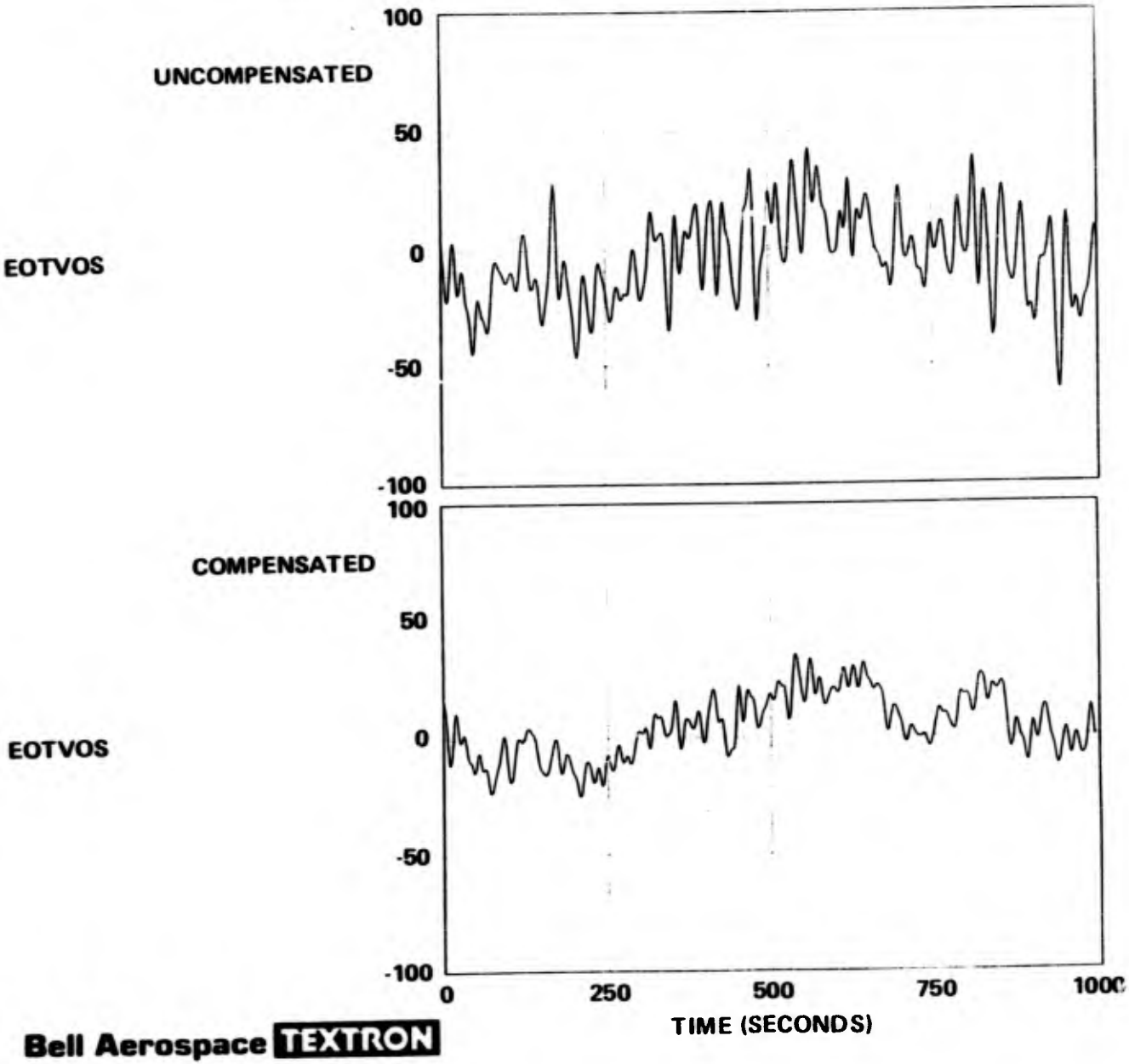

Bell Aerospace TEXTRON

16th GRAVITY GRADIOMETRY CONFERENCE
10-11 FEBRUARY 1988

SPONSORED BY:
AIR FORCE GEOPHYSICS LABORATORY
EARTH SCIENCES DIVISION

TITLE OF PAPER: Suppression of Motion Sensitivity in Bell Aerospace Gravity Gradiometer Survey System

SPEAKER: Andrew Grierson

QUESTIONS AND COMMENTS:

1. Question: John Goodkind

   What was the stability of the coefficients from your least squares fit from day to day?

   Response:

   There is drift when starting up cold and drift from day to day.

2. Question: Alan Zorn

   Your method for post-mission compensation assumes that the GGI rotor is a rigid body. Do you have any feel for possible effects of bending of the GGI rotor? The reason this may be important is because you are differencing accelerations.

   Response:

   It is possible, but the effect is probably small. Our design accounts for this effect - the GGIs are built on a beryllium base. Furthermore, low-frequency earth gradients are easily separated from such high frequency effects.

AN INITIAL LOOK AT 54 TRACKS OF AIRBORNE DATA FROM THE GRAVITY GRADIOMETER SURVEY SYSTEM

by

David M. Gleason

Earth Sciences Division
Air Force Geophysics Laboratory
Hanscom AFB, Bedford MA 01731

In August 1987, Bell Aerospace supplied the Air Force Geophysics Laboratory with a data set consisting of six instrument-framed airborne gravity gradients along 30 north-south and 24 east-west flight tracks over the Texas/Oklahoma survey site. The along-track observations were made every one second in time and approximately every 111 meters in distance. An initial series of data processing steps was performed followed by the appropriate line integrations along single profiles to produce surface gravity disturbance component profiles. Tie points were placed at each profile endpoint. The predicted disturbance components were then compared to "truth-based" values related to a given set of 1' by 1' surface mean gravity anomaly values. Letting the tie point distance range between 120 km and 280 km resulted in the RMS value of the differences between predicted and "truth-based" T_{DOWN}, T_{EAST} and T_{NORTH} components range between 3.5 and 6.8 mgals along certain tracks.

FIGURE 1.

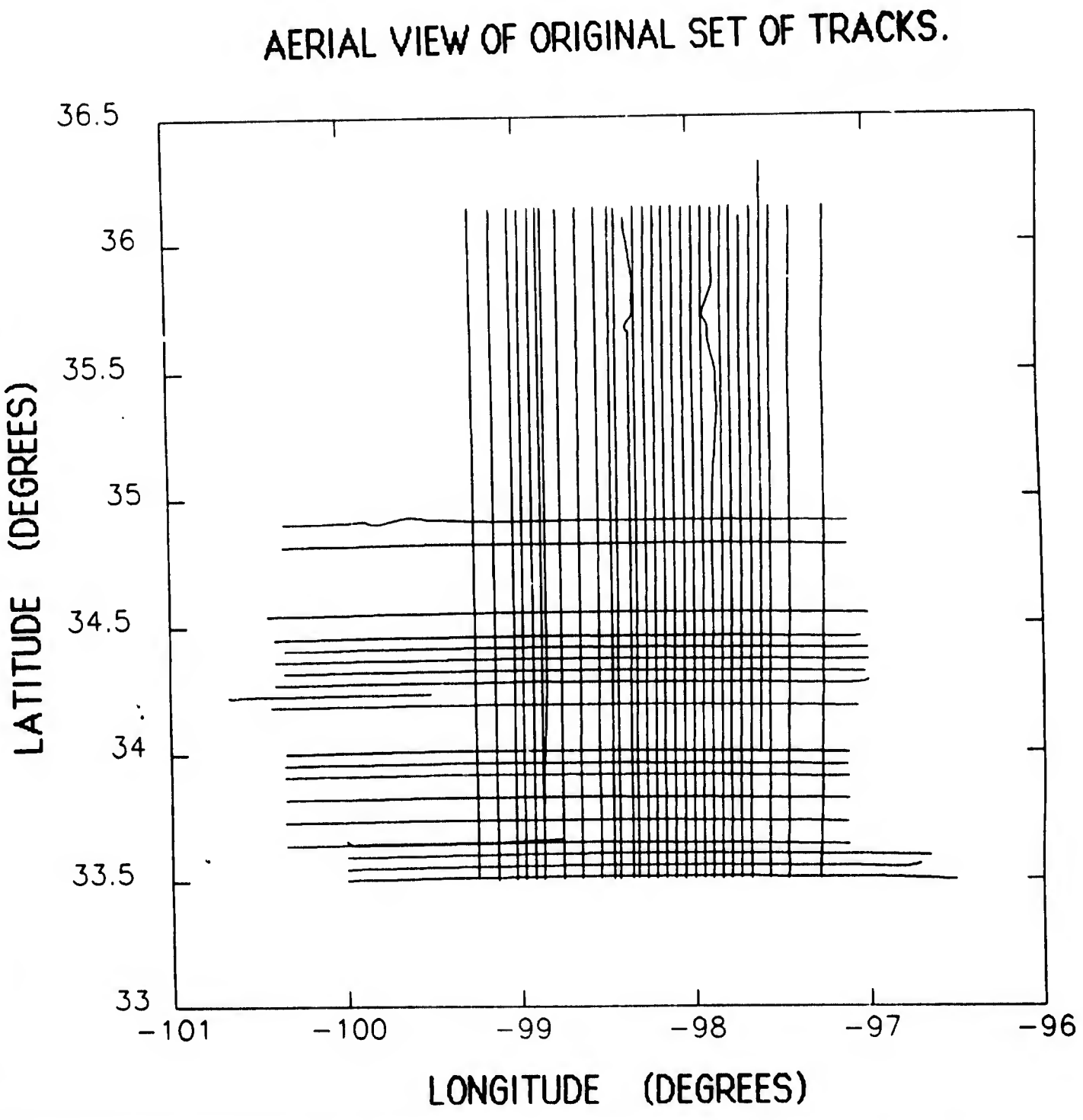
AERIAL VIEW OF ORIGINAL SET OF TRACKS.
36.5
36
35.5
35
34.5
34
33.5
33
LATITUDE (DEGREES)
-101
-100
-99
-98
-97
-96
LONGITUDE (DEGREES)

FIGURE 2.

AERIAL VIEW OF TRACKS AFTER PLATFORM ACCELERATION EDITING.

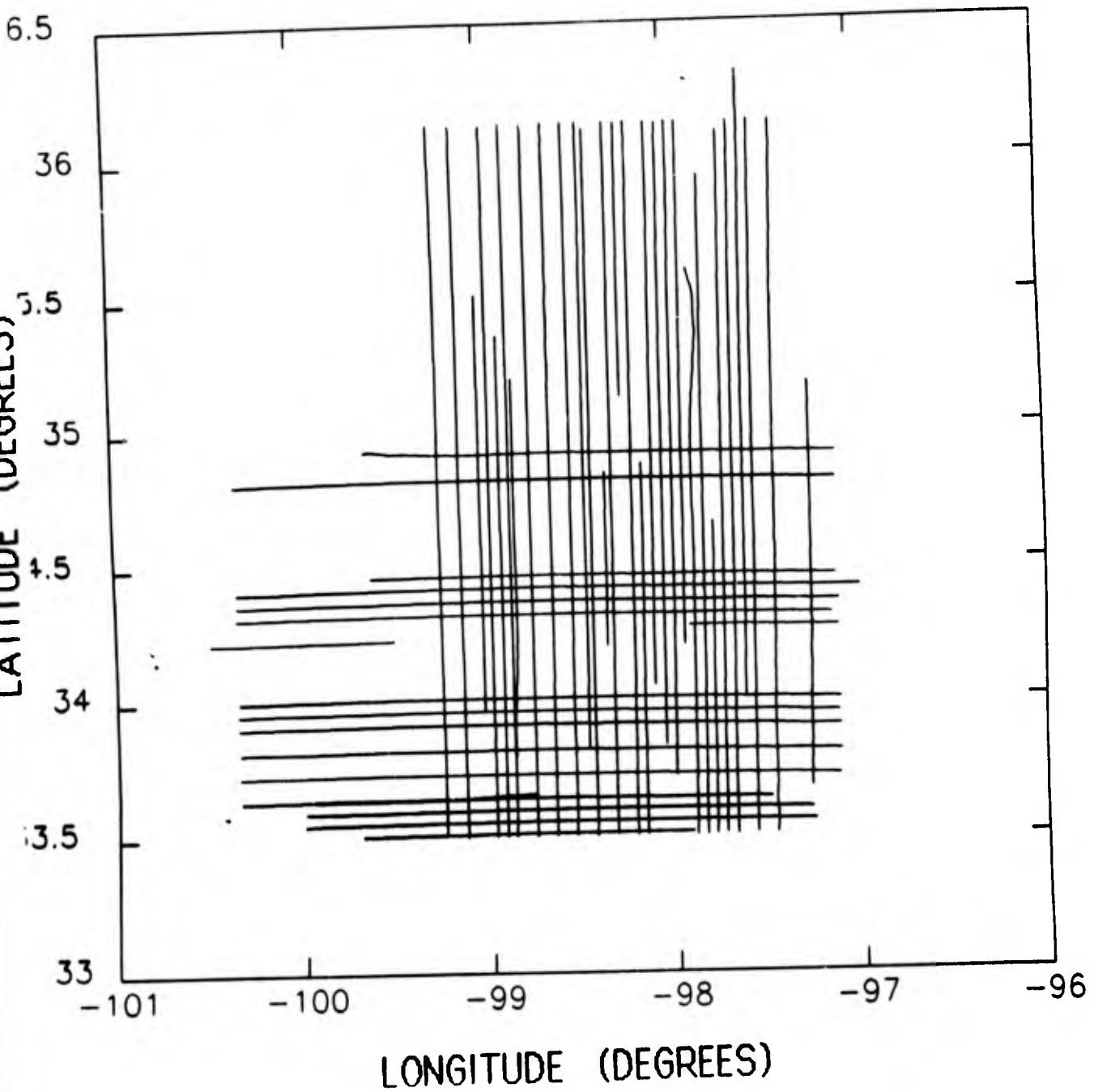

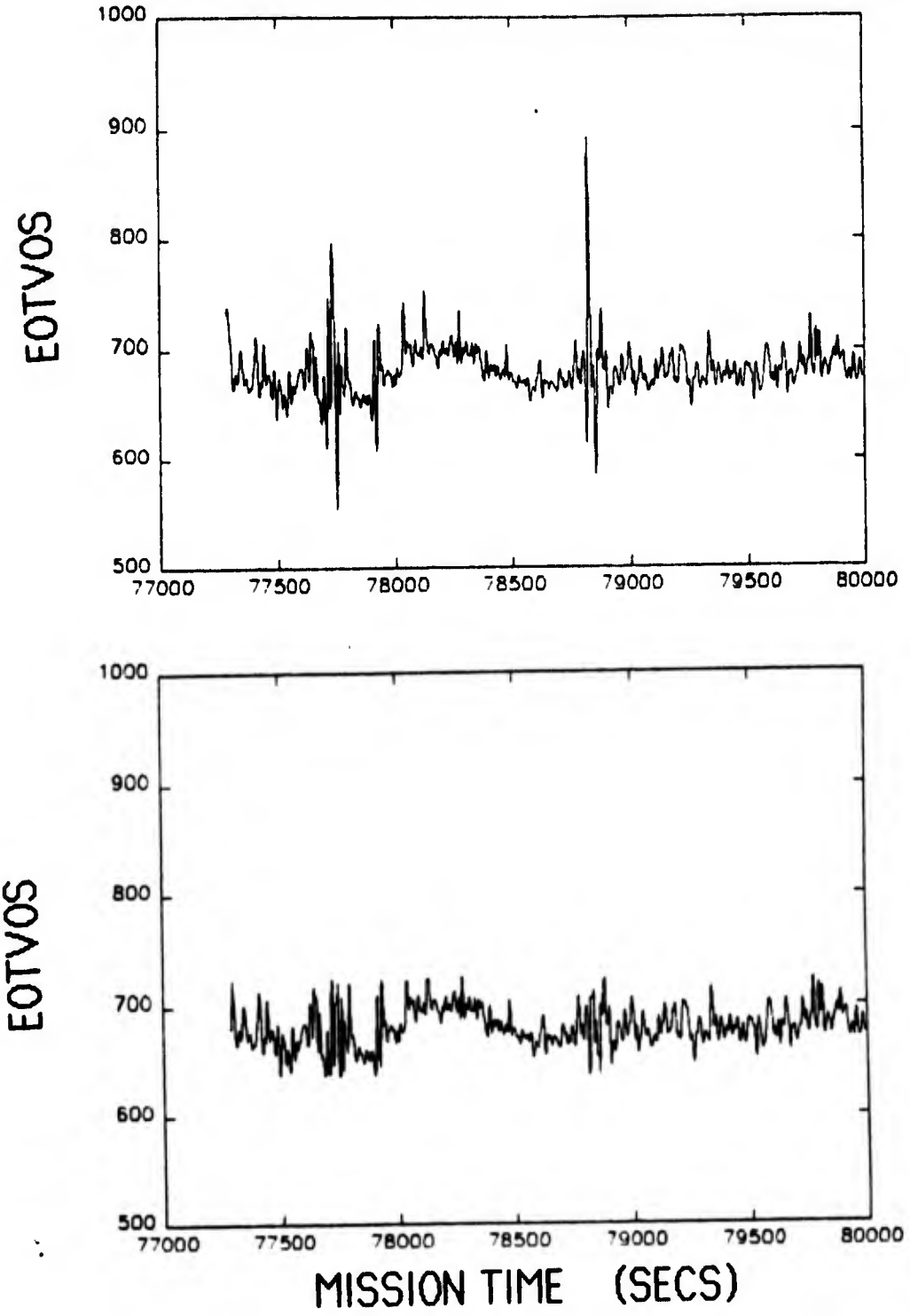

FIGURE 3.

TYPICAL INSTRUMENT-FRAMED GRADIENT PROFILE BEFORE AND AFTER DESPIKING.

TABLE 1.

RANGE OF VALUES OF WGS84 ELLIPSOID REFERENCE FIELD GRADIENTS, IN LOCAL (N,E,D) SYSTEM. (ASSUMING FLIGHT ALTITUDE OF 1 KM)

Gradient	Min. Val	Max. Val	Avg. Val
U_{NN}	-1541 E	-1536 E	-1540 E
$U_{NE} = U_{EN}$	-5 E	5 E	0 E
$U_{ND} = U_{DN}$	-129 E	147 E	9 E
U_{EE}	-1542 E	-1535 E	-1540 E
$U_{ED} = U_{DE}$	-145 E	152 E	3 E
U_{DD}	3069 E	3081 E	3077 E

NOTE: (N,E,D)-FRAMED REFERENCE VALUES WERE TRANSFORMED TO THE INSTRUMENT-FRAMED SYSTEM.

THE BEST-FIT LINE WAS THEN REMOVED FROM EACH GRADIENT PROFILE AS A FIRST-SHOT REMOVAL OF UNWANTED BIASES AND TRENDS.

FIGURE 4.

LEGEND :

CURVE A : AMPLITUDE SPECTRUM OF TYPICAL EDITED,DESPIKED,DETRENDED INSTRUMENT-FRAMED GRADIENT PROFILE.

CURVE B : RESPONSE OF LOWPASS FILTER.

CURVE C : AMPLITUDE SPECTRUM OF CURVE A AFTER BEING FILTERED.

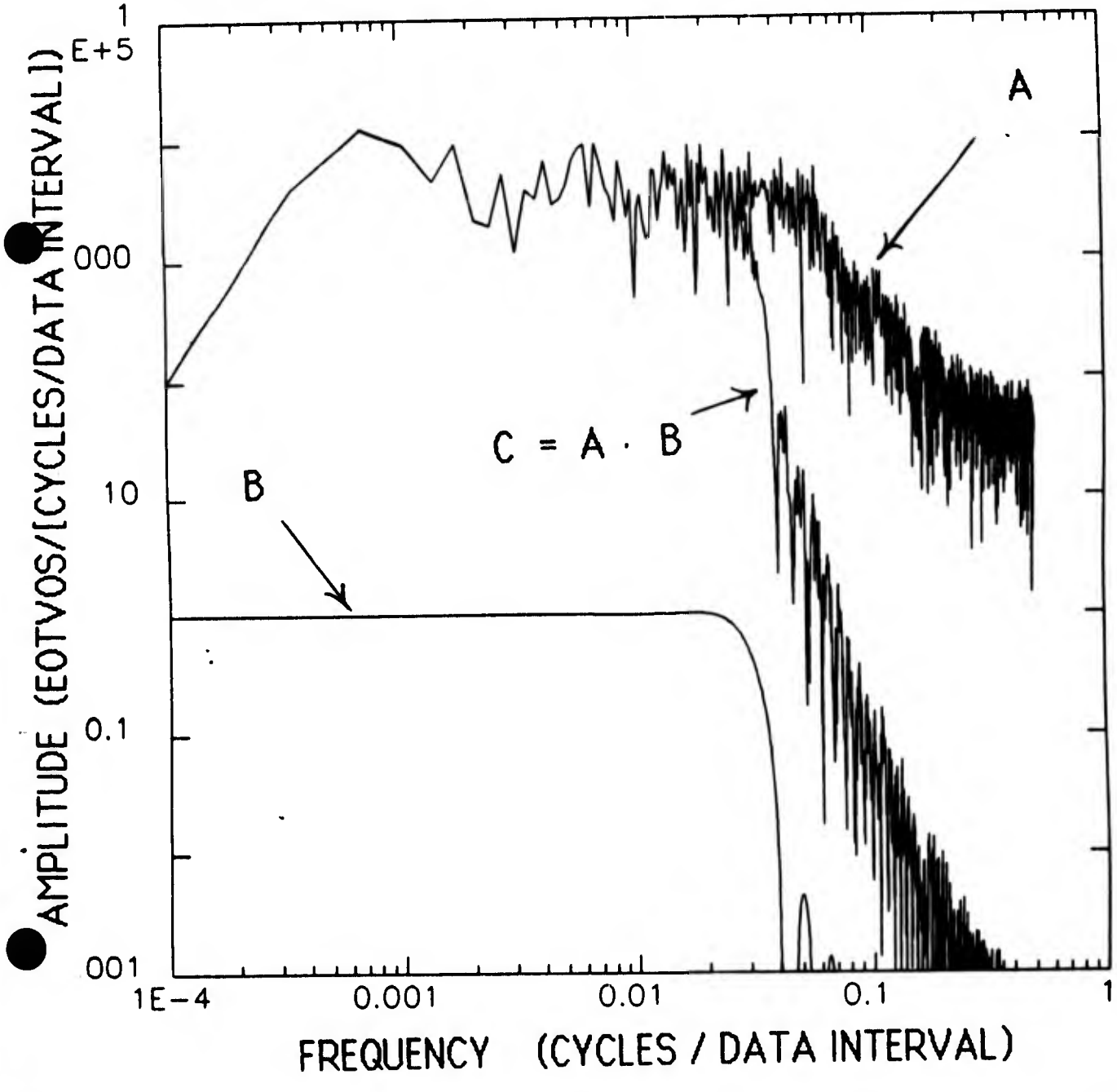

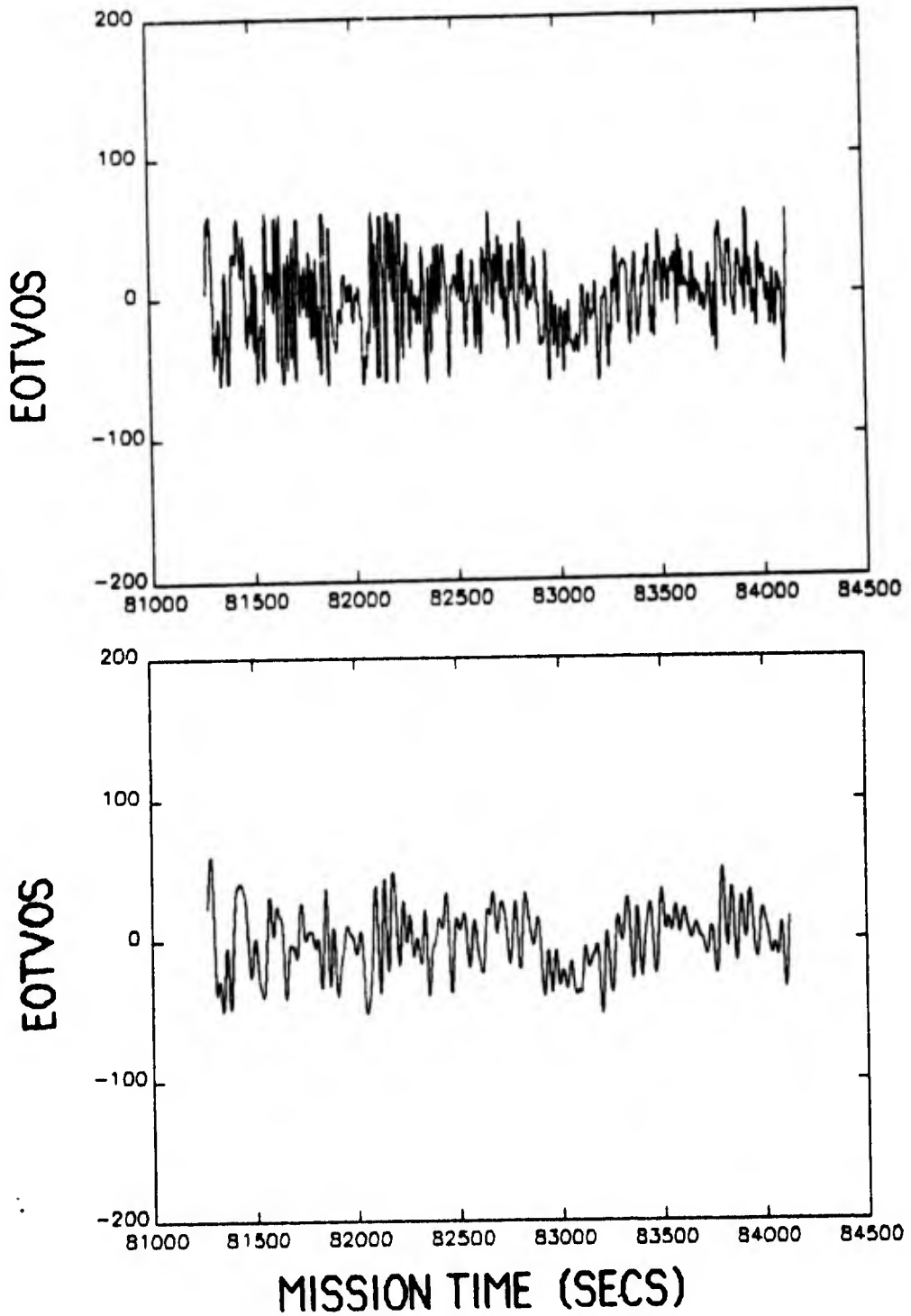

FIGURE 5.

TYPICAL EDITED, DESPIKED, DETRENDED INSTURMENT-FRAMED GRADIENT PROFILE BEFORE AND AFTER FILTERING.

Table 2.

PRE/POST Adjustment Overall RMS Values of the Track Crossing Differences, Measured in EOTVOS.

	GGI INSTRUMENT NUMBER		
	1	2	3
INLINE	20.4/17.7	67.3/60.5	17.0/15.6
CROSS	23.1/20.2	42.3/37.9	15.0/12.4

A total of 40 tracks and 279 track crossings were involved in each of the 6 adjustments.

Since the aircraft altitude is assumed to be constant, i.e. $\Delta D = 0$, the applicable line integrations are simply

$$T_N = \sum_i [\, T_{NN}(i)\Delta N(i) + T_{NE}(i)\Delta E(i) \,]$$

$$T_E = \sum_i [\, T_{NE}(i)\Delta N(i) + T_{EE}(i)\Delta E(i) \,]$$

$$T_D = \sum_i [\, T_{ND}(i)\Delta N(i) + T_{ED}(i)\Delta Ei) \,]$$

The T_D components <u>at altitude</u> can be approximately downward continued to the ground via

$$T_D(\text{ground}) \cong T_D(\text{at altitude}) + T_{DD}(\text{at altitude}) \cdot \Delta h$$

FIGURE 6.

PREDICTED VS. TRUE T_D (GROUND) VALUES ALONG NORTH-SOUTH PROFILE APPROX 280 KM LONG.

$RMS_{(DIFFERENCES)}$ = 6.8 MGALS

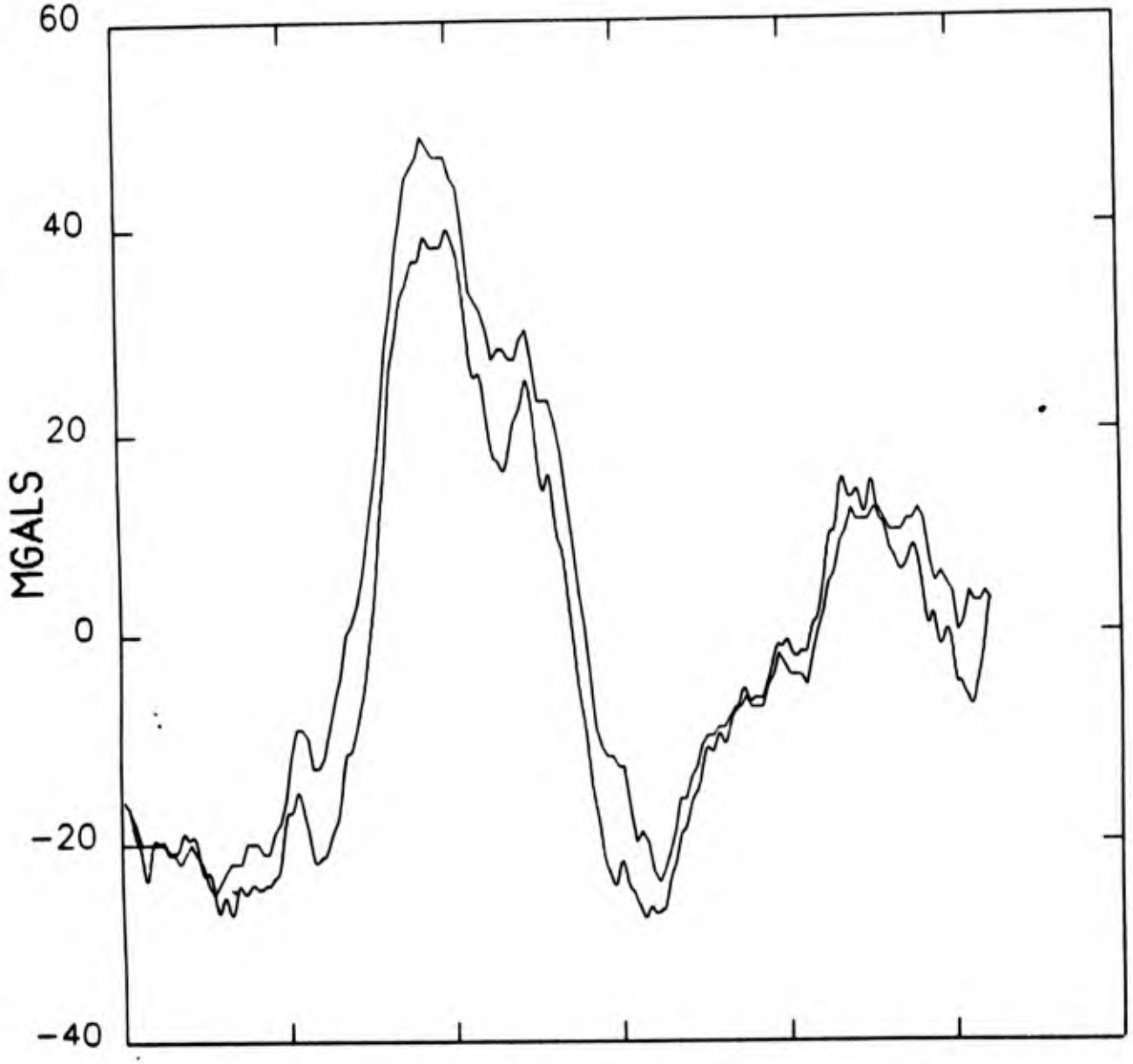

NOTE: TIE POINTS USED AT BOTH ENDPOINTS.

FIGURE 7.

PREDICTED VS. TRUE T_D (GROUND) VALUES ALONG NORTH-SOUTH PROFILE APPROX 180 KM LONG.

$RMS_{(DIFFERENCES)}$ = 3.8 MGALS

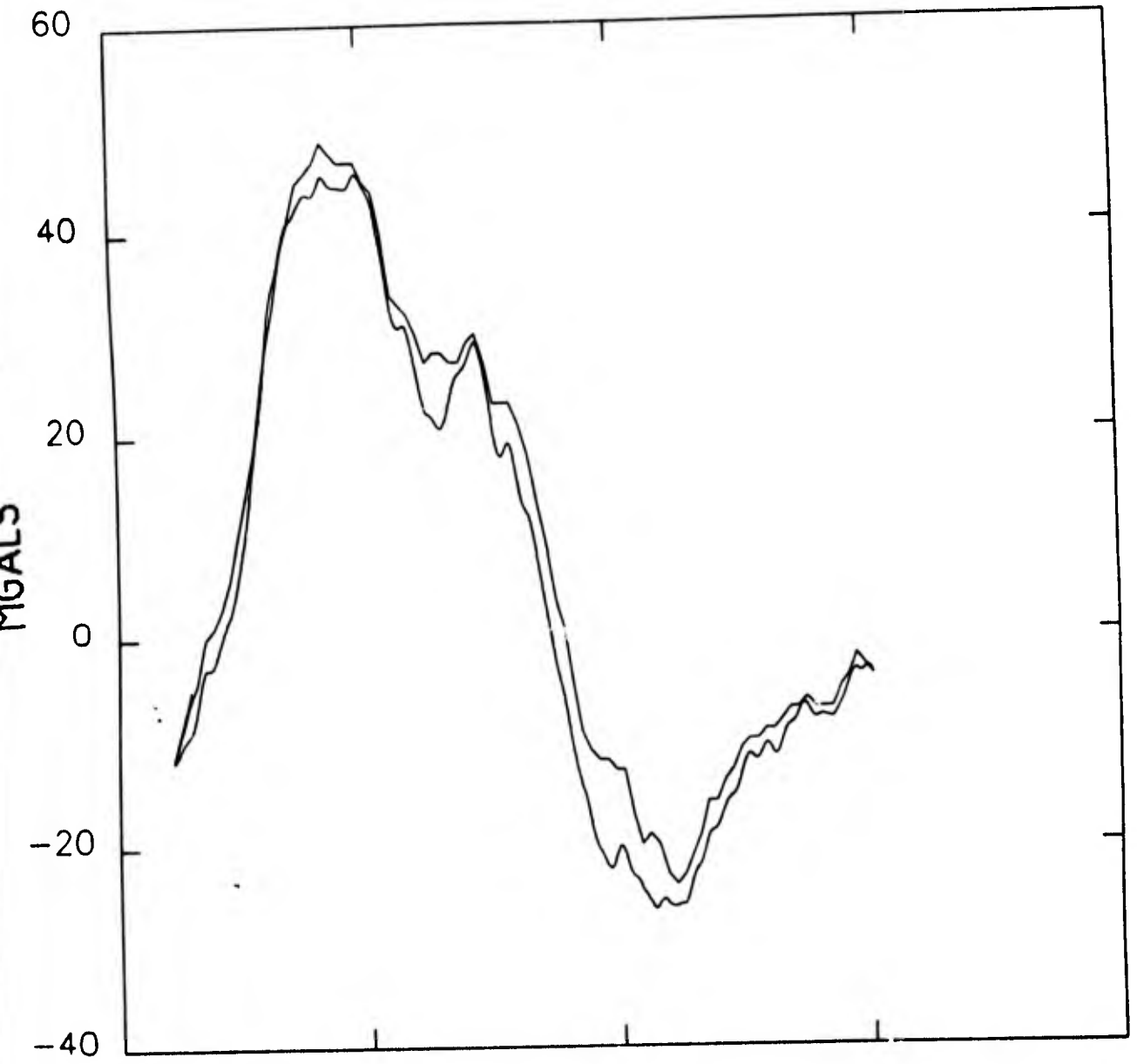

NOTE: TIE POINTS USED AT BOTH ENDPOINTS.

FIGURE 8.

PREDICTED VS. TRUE T_D (GROUND) VALUES ALONG NORTH-SOUTH PROFILE APPROX 120 KM LONG.

$RMS_{(DIFFERENCES)}$ = 3.5 MGALS

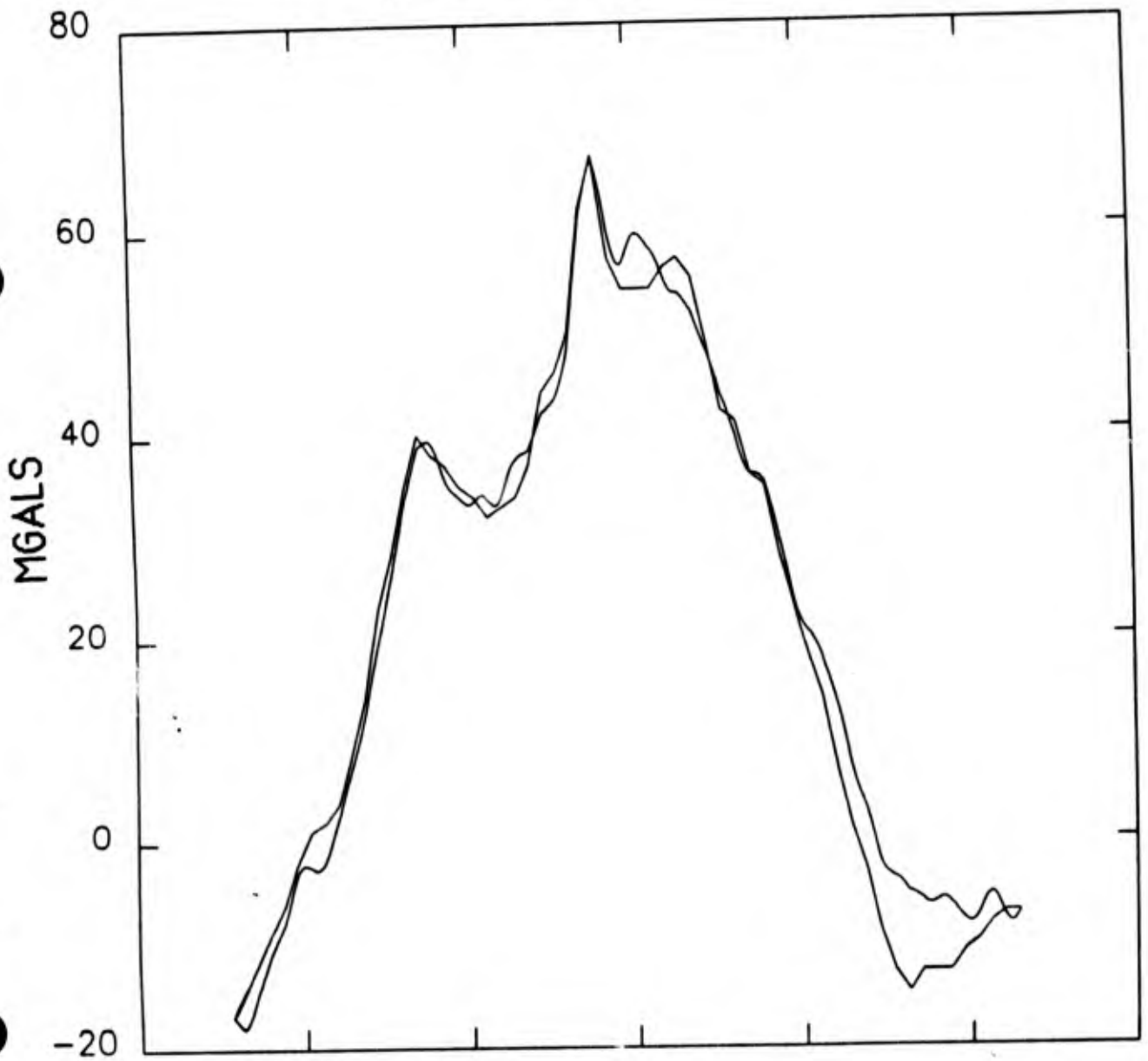

NOTE: TIE POINTS USED AT BOTH ENDPOINTS.

FIGURE 9.

PREDICTED VS. TRUTH-BASED T_N VALUES ALONG NORTH-SOUTH PROFILE APPROX 120 KM LONG.

$RMS_{(DIFFERENCES)}$ = 4.1 MGALS

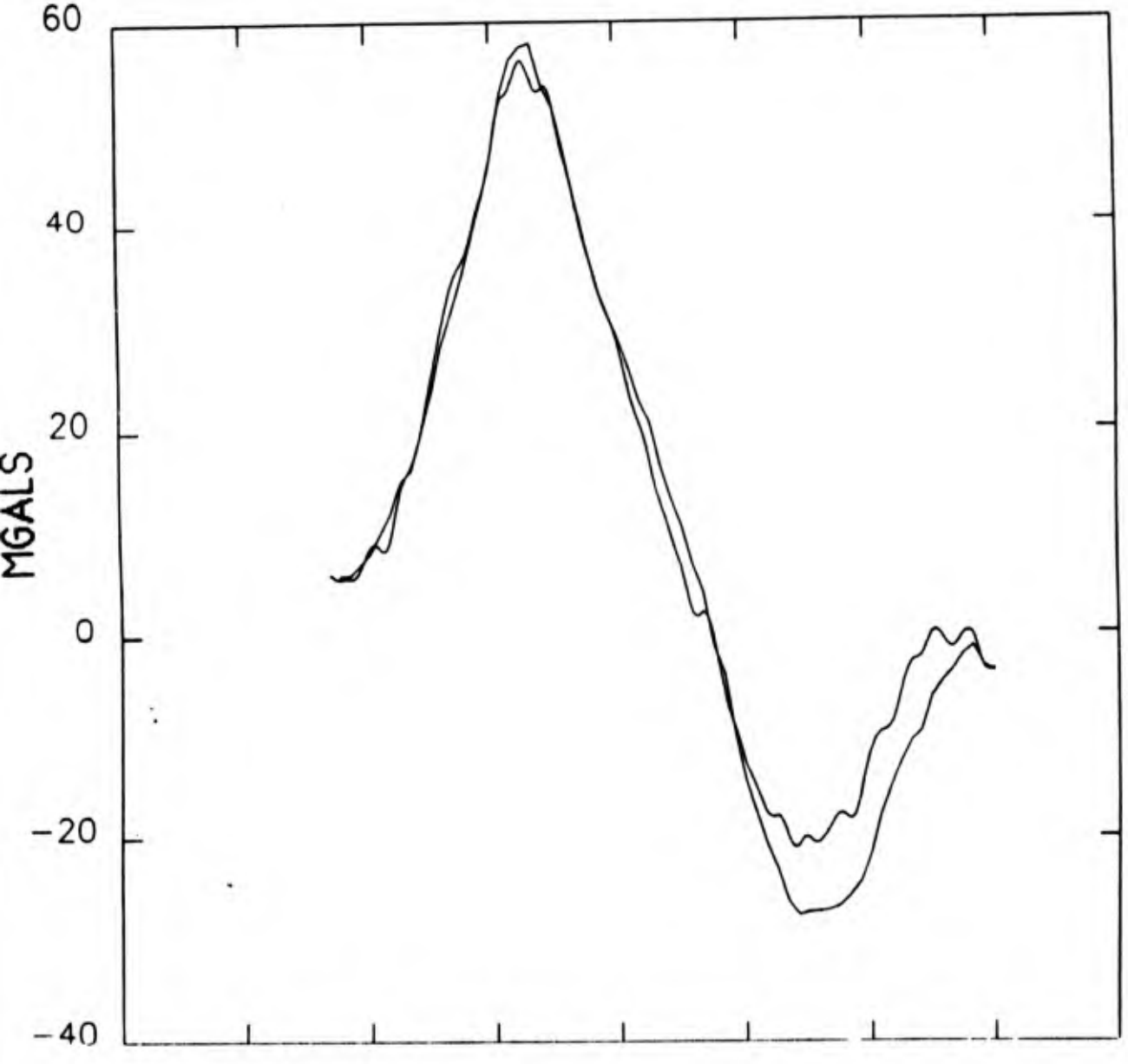

NOTE: TIE POINTS USED AT BOTH ENDPOINTS.

FIGURE 10 .

PREDICTED VS. TRUTH-BASED T_E VALUES ALONG NORTH-SOUTH PROFILE APPROX 200 KM LONG.

$RMS_{(DIFFERENCES)}$ = 5.9 MGALS

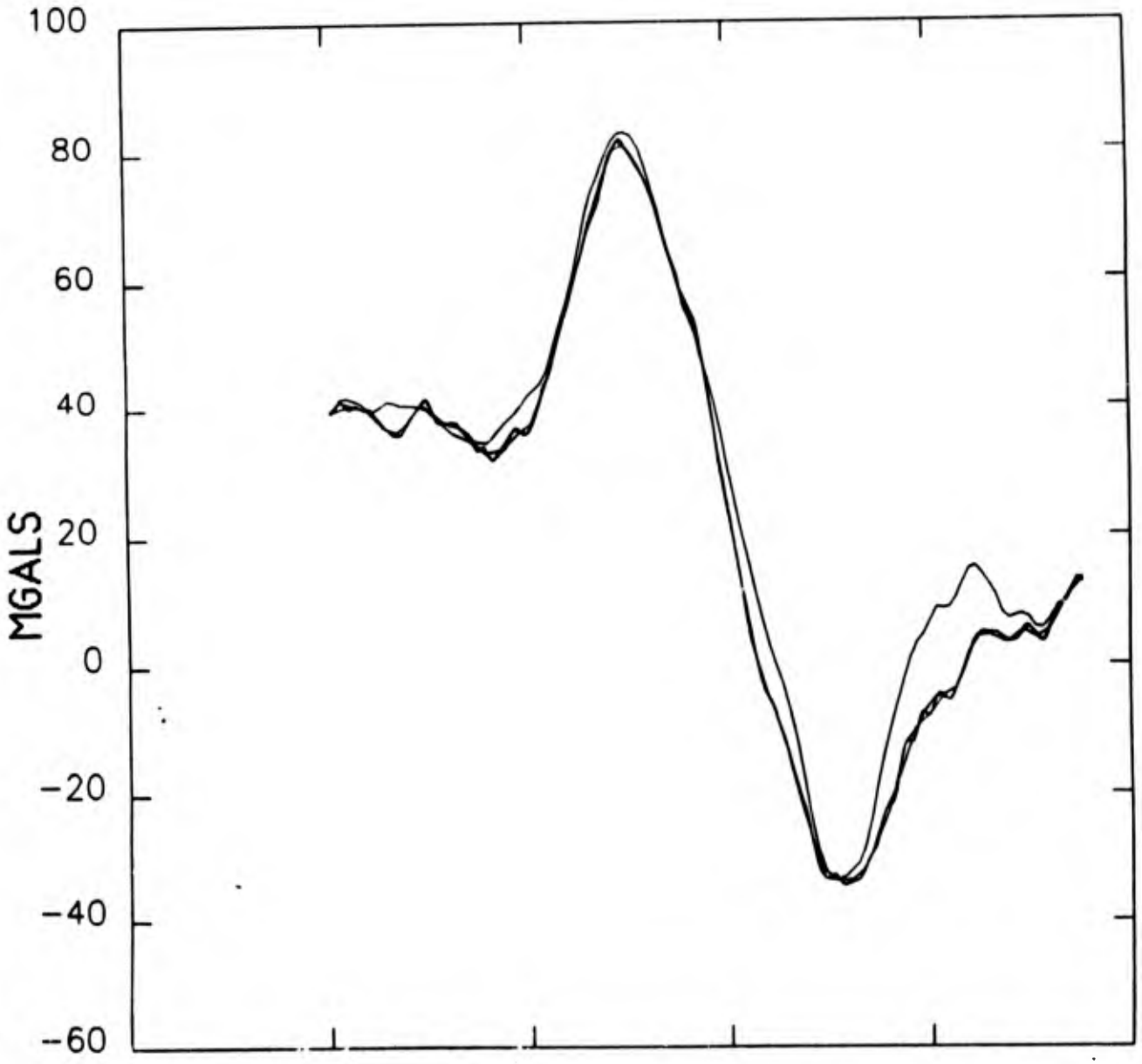

NOTE: TIE POINTS USED AT BOTH ENDPOINTS.

CONCLUDING REMARKS:

ALONG CERTAIN TRACKS THE INSTRUMENT FOLLOWED THE GRAVITY SIGNAL REMARKABLY WELL.

IF AND WHEN A SECOND AIRBORNE SURVEY IS ATTEMPTED, PERHAPS AN EMPHASIS SHOULD BE PLACED ON SHORT AND REPETITIVE FLIGHT PATHS TO

A) ESTABLISH THE INSTRUMENT'S PRECISION AND REPEATABILITY LEVEL

B) MASTER THE LOGISTICAL AND ENGINEERING PROBLEMS ENCOUNTERED OVER MANY TRACKS OF ITS INITIAL VOYAGE.

16th GRAVITY GRADIOMETRY CONFERENCE
10-11 FEBRUARY 1988

SPONSORED BY:
AIR FORCE GEOPHYSICS LABORATORY
EARTH SCIENCES DIVISION

TITLE OF PAPER: An Initial Look at 54 Tracks of Airborne Data from the Gravity Gradiometer Survey System

SPEAKER: Dave Gleason

QUESTIONS AND COMMENTS:

1. Question: John Brozena

   What was the overall rms error statistics for all 54 tracks grouped together?

   Response:

   It was not done.

2. Question: Andrew Grierson

   Did your attempts at dcwnward continuation produce a significant difference in the results?

   Response:

   I tried various heights but found that the optimum height varied from track to track. Therefore, I used fixed processing at 1 km height.

3. Comment: Ernest Metzger

   The main problem with poor tracks was the slow platform recovery after a GPS outage. This has been improved since.

4. Comment: Alan Zorn

   Regarding your observation of spikes in the GGI data, we have seen similar spikes in ADM data at sea. We found they had nothing to do with the GGIs, but were due to azimuth control which induced angular rates.

5. Comment: Chris Jekeli

   GGI #2 's problem is not evident in discrepancies between truth T_z data along EW tracks and integrated gradients since the cross (and in-line) outputs of GGI #2 do not enter into the integration.

GGSS AIRBORNE TEST DATA REDUCTION RESULTS

by

S. J. Brzezowski
J. D. Goldstein
W. G. Heller
J. V. White

The Analytic Sciences Corporation
55 Walkers Brook Drive
Reading, MA 01867

The rotating accelerometer gravity gradiometer survey system (GGSS) has successfuly gathered gravity gradients aloft during flights conducted at the Clinton-Sherman test range between 3 April 1987 and 26 May 1987. The range is located near Oklahoma City, Oklahoma. At TASC, the Bell-demodulated and environmentally-compensated instrument outputs have been intensively analyzed for both signal and error content. Single track-by-track analysis indicates rms cross gradient recovery errors ranging from 8.6 E to 17.5 E at a resolution of 0.9 km for eleven selected tracks. The corresponding white noise floor of the cross gradients in N, E, D coordinates ranged from 623 E^2/Hz to 2550 E^2/Hz. Further analysis indicates that the vertical gravity disturbance along the best tracks can be recovered to about 5.0 mgal rms error for tie points over 200 km apart. To reduce rms error to 1.0 mgal, tie point spacing closer to 20 km is required. More recent analysis, which treates multiple tracks of data simultaneously, indicates that a factor of two reduction in the rms gravity disturbance estimation error is still attainable prior to completion of the GGSS data analysis effort.

SP-5362-7

GRAVITY GRADIOMETER SURVEY SYSTEM (GGSS) AIRBORNE TEST DATA REDUCTION RESULTS

10 February 1988

Prepared for:

Sixteenth Moving Base Gravity Gradiometer Review
United States Air Force Academy
Colorado 80840

Prepared by:

S.J. Brzezowski
J.D. Goldstein
W.G. Heller
J.V. White

THE ANALYTIC SCIENCES CORPORATION
55 Walkers Brook Drive
Reading, Massachusetts 01867

SIXTEENTH ANNUAL GRAVITY GRADIOMETRY CONFERENCE
ABSTRACT - GGSS Airborne Data Reduction Results

The rotating accelerometer gravity gradiometer survey system (GGSS) has successfully gathered gravity gradients aloft during flights conducted at the Clinton-Sherman, Oklahoma test range between 3 April 1987 and 26 May 1987. At TASC, the Bell-demodulated and environmentally-compensated instrument outputs have been intensively analyzed for both signal and error content. Single track-by-track analysis indicated rms cross gradient recovery errors ranging from 6.6 E to 14.6 E at a resolution of 0.9 km for 19 selected tracks. The corresponding white noise floor of the cross gradients in N, E, D coordinates ranged from 200 E^2/Hz to 1700 E^2/Hz (double-sided). Further analysis indicated that the vertical gravity disturbance along the best tracks can be recovered to about 5.0 mgal rms error for tiepoints over 200 km apart. When the tiepoint spacing (rms tiepoint error = 2 mgal rms) is reduced to lengths on the order of 90 km, the accuracy of the gradiometer-derived estimates reaches 2 to 4 mgal rms.

The template algorithm for estimating gravity disturbance components from multitrack gradient data was applied using 13 tracks of data in the southeastern portion of the test area. The Clinton-Sherman AWN Statistical Gravity model, data-derived error models for the GGSS data and the rms uncertainty of the tiepoint values were also incorporated. Gradient biases along each track were explicitly included in the error model. Results of estimating the GGSS-derived vertical disturbance at all track crossings, and comparing with surface truth data indicated rms error in the gradiometer estimates of vertical gravity disturbance to be 2 to 3 mgal. This accuracy agreed well with the predicted errors based on the template estimator covariance equations.

BACKGROUND

G-08490
02/06/88

- **GGSS AIRBORNE TESTING CONDUCTED AT CLINTON-SHERMAN, OKLAHOMA AREA IN SPRING, 1987**

- **AREA WAS SELECTED FOR BENIGN GRAVITY FIELD BEHAVIOR AND MODEST SIGNATURE (31 mgal, 22E rms)**

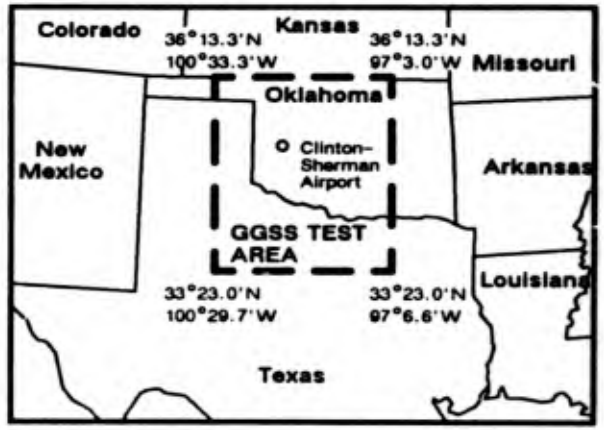

- **C-130 AIRCRAFT FLIGHT REGIME (nominal)**

Altitude	= 1000 m
Speed	= 400 km/hr
Track Spacing	= 5 km
Track Length	= 315 km
Area Spanned	= 315 km x 315 km

- **DATA PROCESSING BY BELL (stage I)**

  Organization Into Standard Format
  Demodulation (0.5 Hz carrier, half bandwidth - 0.12Hz)
  Compensation (self-gradients, accelerations)

- **DATA RECEIVED BY TASC**

  11 Tracks, 8 July 1987
  56 Tracks (includes original 11 reprocessed), 12 August 1987

TASC

DATA DESCRIPTION

G-08491
02/06/88

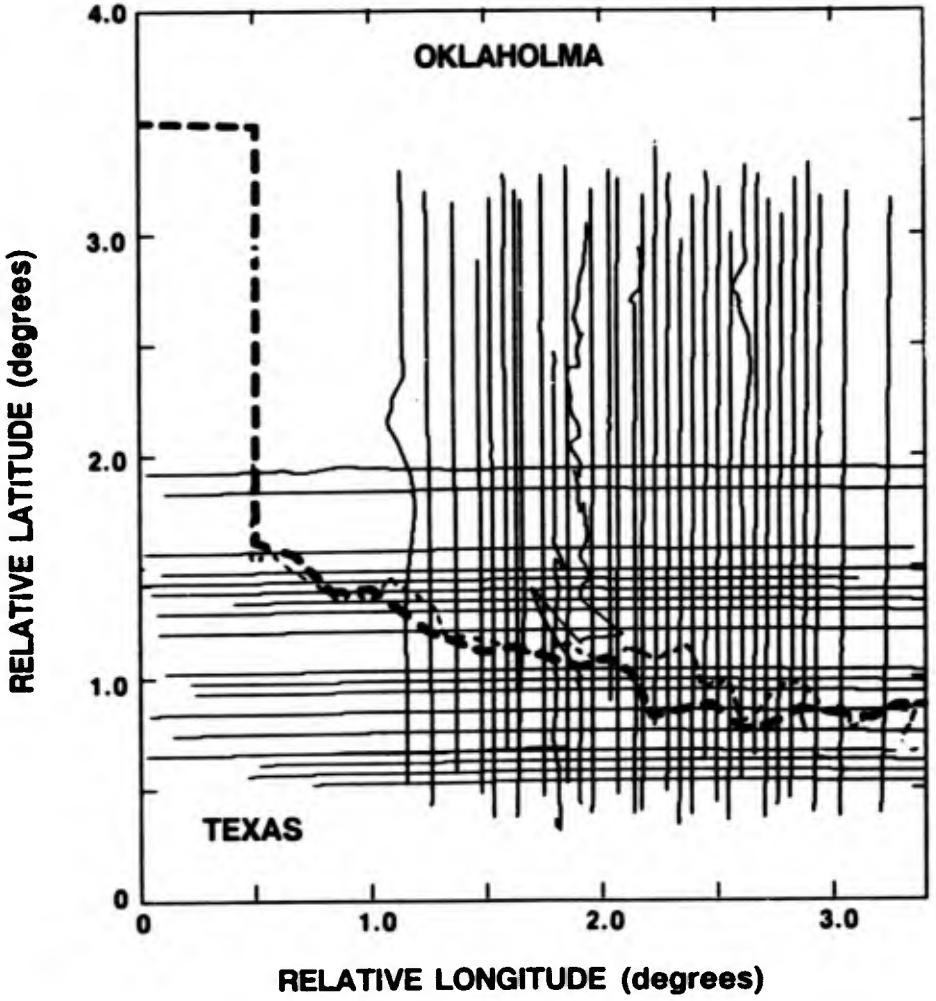

- 33 N–S TRACKS
- 23 E–W TRACKS (5 OUTSIDE OF TEST AREA)
- INCLINE AND CROSS GRADIENTS FOR EACH INSTRUMENT OF TRIAL
- GPS AND GPS–AIDED INERTIAL LATITUDE AND LOGITUDE
- PLATFORM ACCELERATION IN ALL THREE AXES
- HEADING
- DATA RATE IS ONE SAMPLE PER SECOND
- QUICK REVIEW OF ALL 56 TRACKS INDICATES NEED EDIT FOR:
  - Loss of Gradiometer Instrument Output
  - Erratic Flighrt Trajectory
  - Excessive Noise
  - Spike Contact

TASC

TRACKS ANALYZED

G-08492
02/06/88

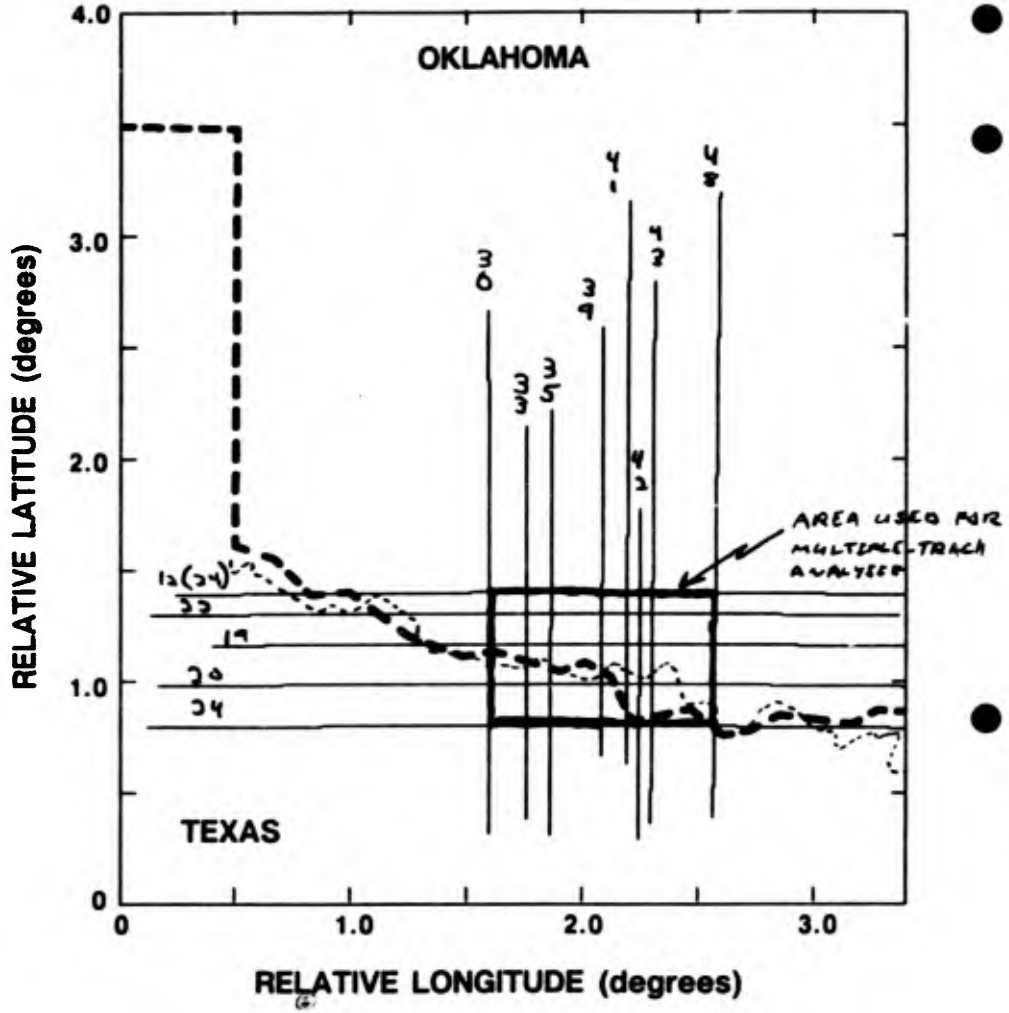

- **19 TRACKS SELECTED FROM EDITED DATA SET (35 TRACKS) FOR FURTHER ANALYSIS**
- **PREPARATION FOR SINGLE TRACK/KALMAN SMOOTHER ANALYSIS**
  - Identification And Removal Of Bad Sections At Track Ends
  - Spikes Removed
  - Sample Mean Removed
  - Transformation From Instrument Frame To N, E, D, Frame
  - 8:1 Decimation* (To 0.88 km/Sample)
  - Gradient Psd Estimation
  - Relevant Cross Gradient Input Is T_{uz} Where u is "ALONG-TRACK"
- **PREPARATION FOR MULTITRACK ANALYSIS (TEMPLATE ALGORITHM)**
  - Eliminate Tracks Having Identifiable Problems And Poor Estimates
  - Clip Tracks Beyond Uppermost Rectangular Border
  - Invert Data Order To Account For East (North) Track Data Acquisition In Opposite Sense As On West (South) Tracks

*DATE BANDWIDTH DETERMINED TO BE 1.1 cy/km (6 db Point)

TASC
THE ANALYTIC SCIENCES CORPORATION

TYPICAL DATA OUTPUT FROM ONE GRAVITY GRADIOMETER INSTRUMENT (GGI) CHANNEL

G-08497
02/06/88

GGI NUMBER 2, EAST TRACK NO. 20,
INLINE GRADIENT

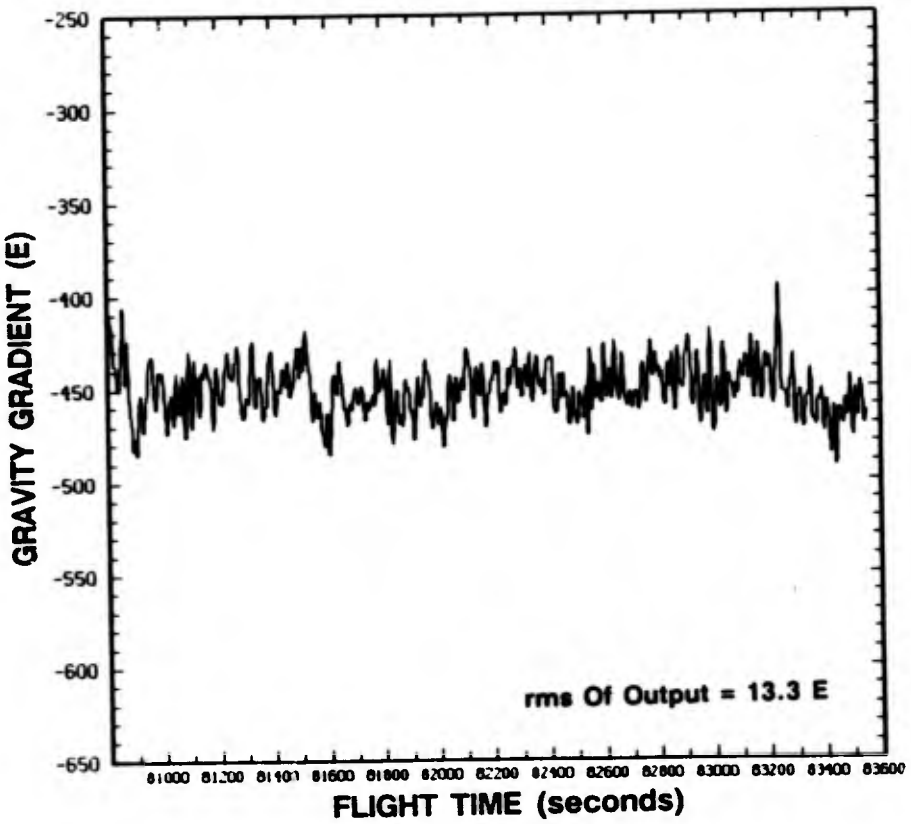

GGI NUMBER 2, WEST TRACK NO. 25,
INLINE GRADIENT

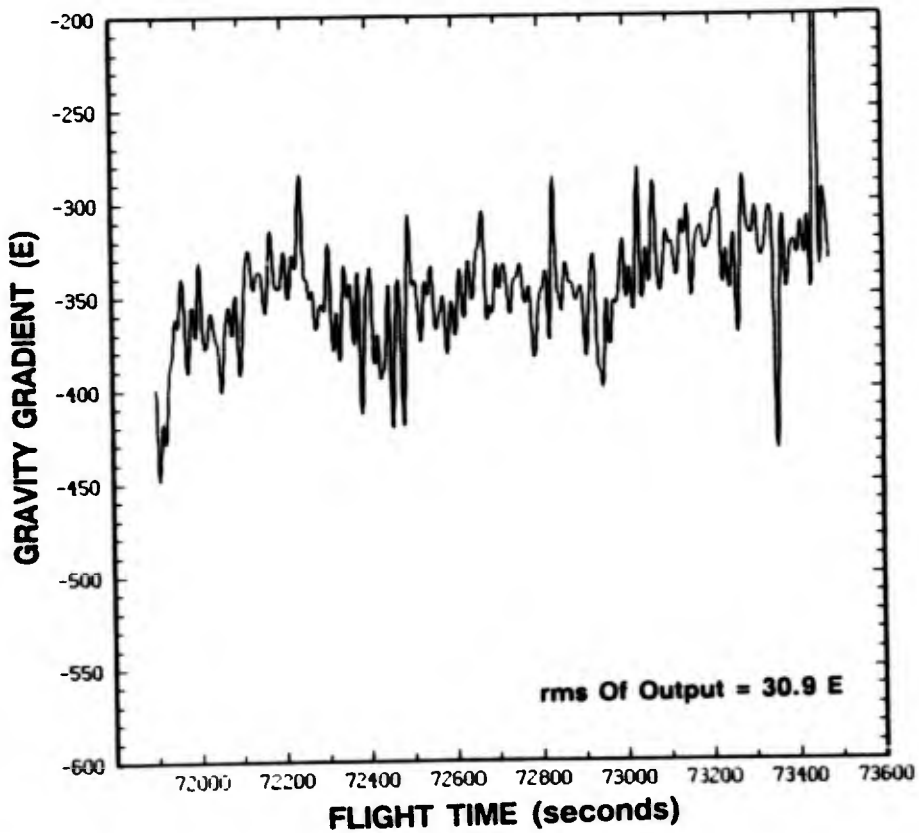

TASC

T-00863

ESTIMATED WHITE NOISE FLOOR OF MEASURED GRADIENTS IN N,E,D FRAME

Level of T_{ED} (E^2/Hz)

BELL N-S TRACK NUMBER	PSD FLOOR LEVEL OF T_{ND} (E^2/Hz)	RMS ERROR* (E)
30	1700	14.6
31	400	7.1
33	800	10.0
35	600	8.7
39	400	7.1
41	1000	11.2
42	900	10.6
43	900	10.6
47	1600	14.1
48	800	10.0

BELL E-W TRACK NUMBER	PSD FLOOR LEVEL OF T_{ED} (E^2/Hz)	RMS ERROR* (E)
10	1000	11.2
12	400	7.1
12 (24)	1000	11.2
18	700	9.4
19	1700	14.6
20	350	6.6
22	200	9.4
25	1700	14.6
27	650	9.0

*ONE SAMPLE EVERY 8 secs FOR RESOLUTION 0F 0.9 km (@ 400 km/hr AIRCRAFT SPEED)

TASC

ERROR MODELS

- GGSS WHITE NOISE FLOOR (DIFFERENT VALUE FOR EACH TRACK) AS IDENTIFIED FROM PSDs
- GRADIENT BIAS UNCERTAINTY BASED ON TRACK LENGTH AND 7-SHELL NORTH TEXAS AWN GRAVITY MODEL
- 2 mgal rms (UNCORRELATED) UNCERTAINTY FOR EACH TIEPOINT
- NO RED NOISE, SCALE FACTOR ERROR OR NAVIGATION ERROR

TASC

T-04766

TRUTH DATA

- TRUTH DATA SET IS 5' x 5' MEAN GRAVITY DISTURBANCE COMPONENTS AT EARTH'S SURFACE

- VERTICAL COMPONENT INTERPOLATED USING 9-POINT BILINEAR SMOOTHER TO PROVIDE:
  - SURFACE TIEPOINT VALUES CENTERED AT APPROPRIATE TRACK ENDPOINTS
  - SURFACE MEAN GRAVITY DISTURBANCES ALONG EACH TRACK (FOR COMPARISON WITH GGSS-DERIVED ESTIMATES)

TASC

SINGLE TRACK GRAVITY DISTURBANCE ESTIMATES FOR TWO GOOD TRACKS

G-08498
02/06/88

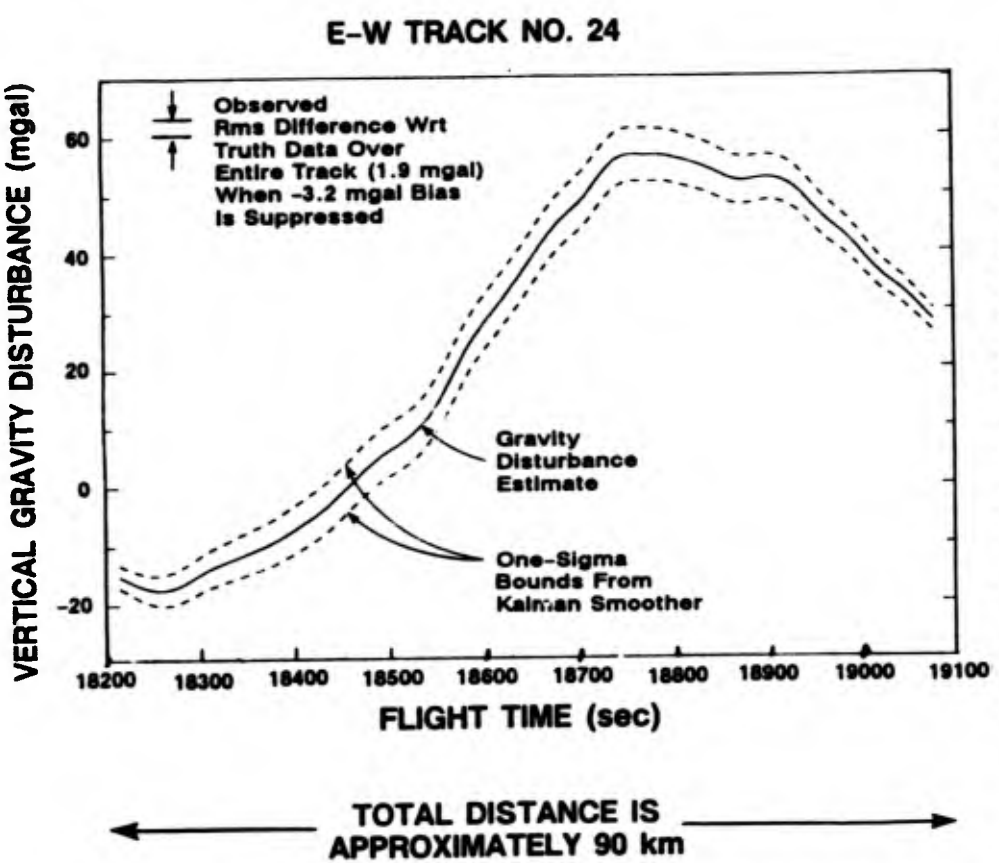

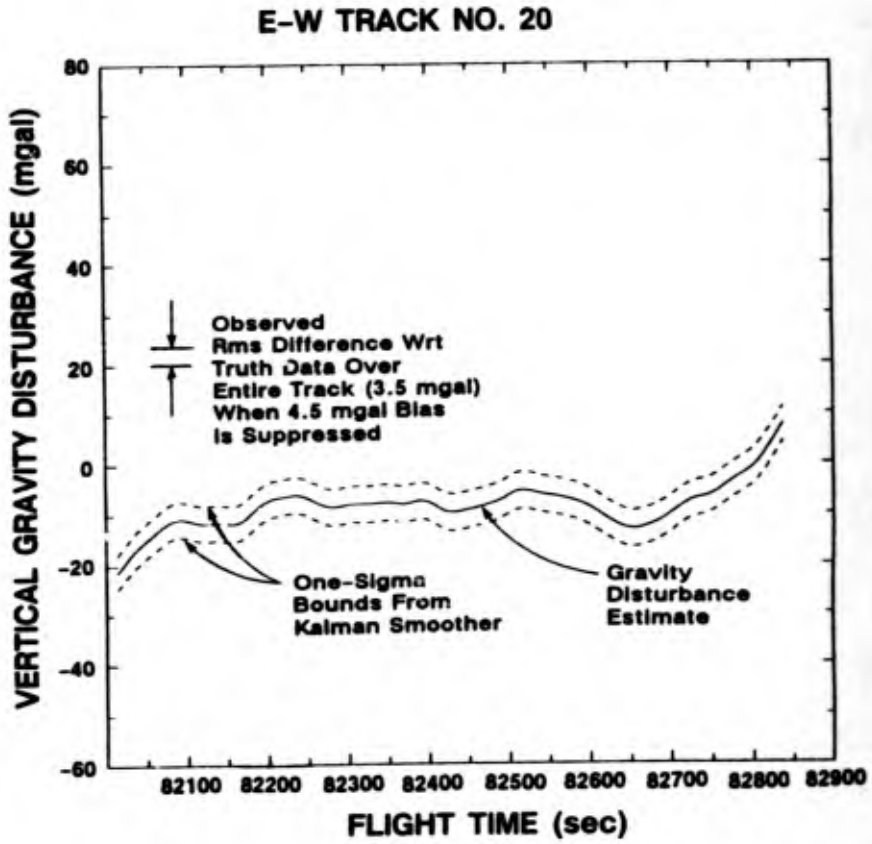

TOTAL DISTANCE IS APPROXIMATELY 90 km

OBSERVATIONS:

- GOOD ABILITY OF GRADIOMETER TO MEASURE GRAVITY FIELD
- MODEST ABILITY TO IDENTIFY TRACK BIASES WITHOUT FULL NETWORK SOLUTION

TASC

T-04767

TEMPLATE METHOD FOR MULTITRACK GRADIOMETER DATA REDUCTION

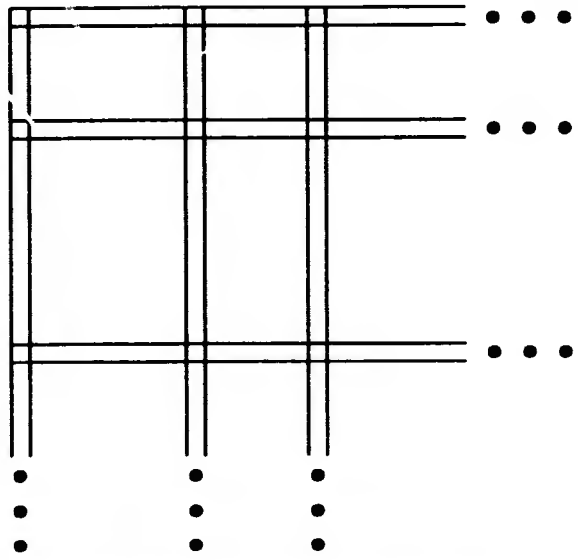

TEMPLATE FORMULATION USED FOR DATA REDUCTION

- MEAN (5' x 5') GRAVITY DISTURBANCE ESTIMATED AT ALL TRACK CROSSINGS
- MEAN GRAVITY DISTURBANCES AT ALL TRACK CROSSINGS
- MEAN GRADIENT ALONG EACH LINK BETWEEN TRACK CROSSINGS IS AN ESTIMATOR STATE
- LINK WIDTH IS 100 m
- TIEPOINTS LIMITED TO OUTER BOUNDARY
- COVARIANCES AMONG ALL LINKS REPRESENTED ANALYTICALLY USING AWN MODEL
- NOTE THAT TEMPLATE ESTIMATOR REDUCES TO NETWORK METHOD WHEN GRAVITY FIELD IS ASSUMED TO BE UNCORRELATED AND MEASUREMENT ERRORS ARE WHITE NOISE

OBSERVATION: DATA FROM OPEN-ENDED OR UNCONNECTED LINKS CAN BE USED IN THE ESTIMATION BUT DO NOT CONTRIBUTE SIGNIFICANTLY TO OUTPUT ACCURACY

TASC
THE ANALYTIC SCIENCES CORPORATION

GRAVITY DISTURBANCE ESTIMATES FROM GRADIENTS ALONG 13 TRACKS

CASE I – TIE POINTS AT ENDS OF EACH TRACK

G-08495
02/06/88

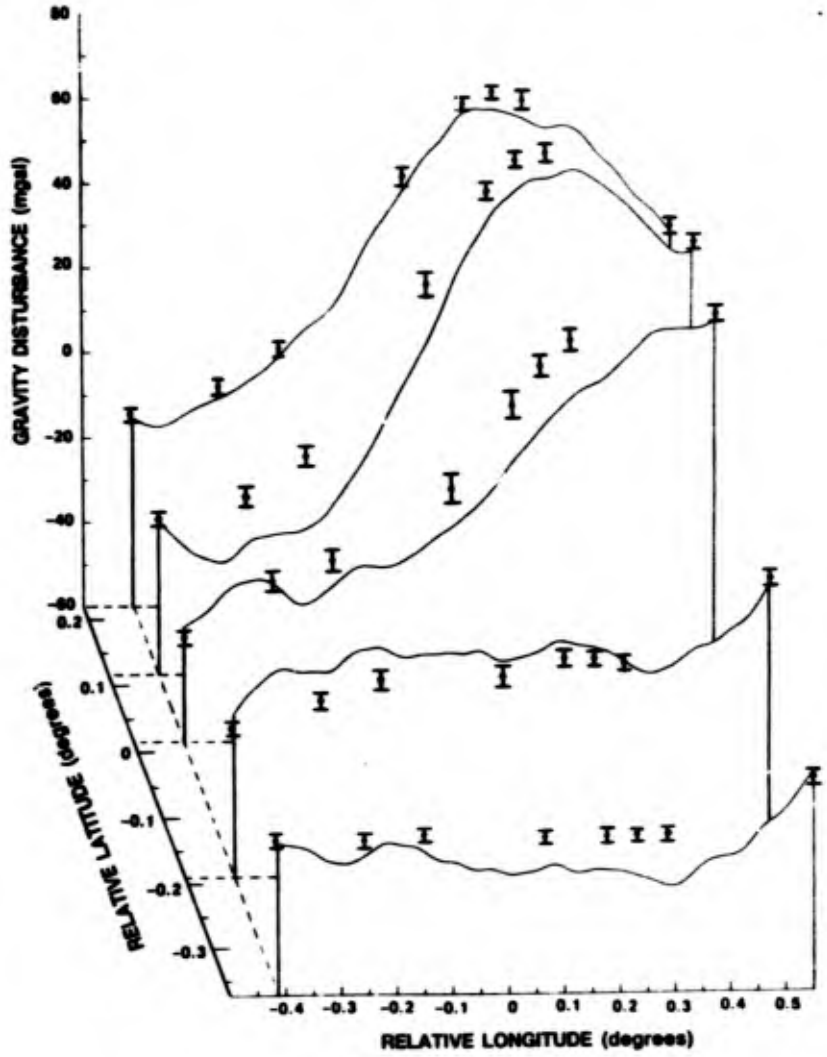

TASC

GGSS / TRUTH DATA RESIDUAL ERROR CONTOURS

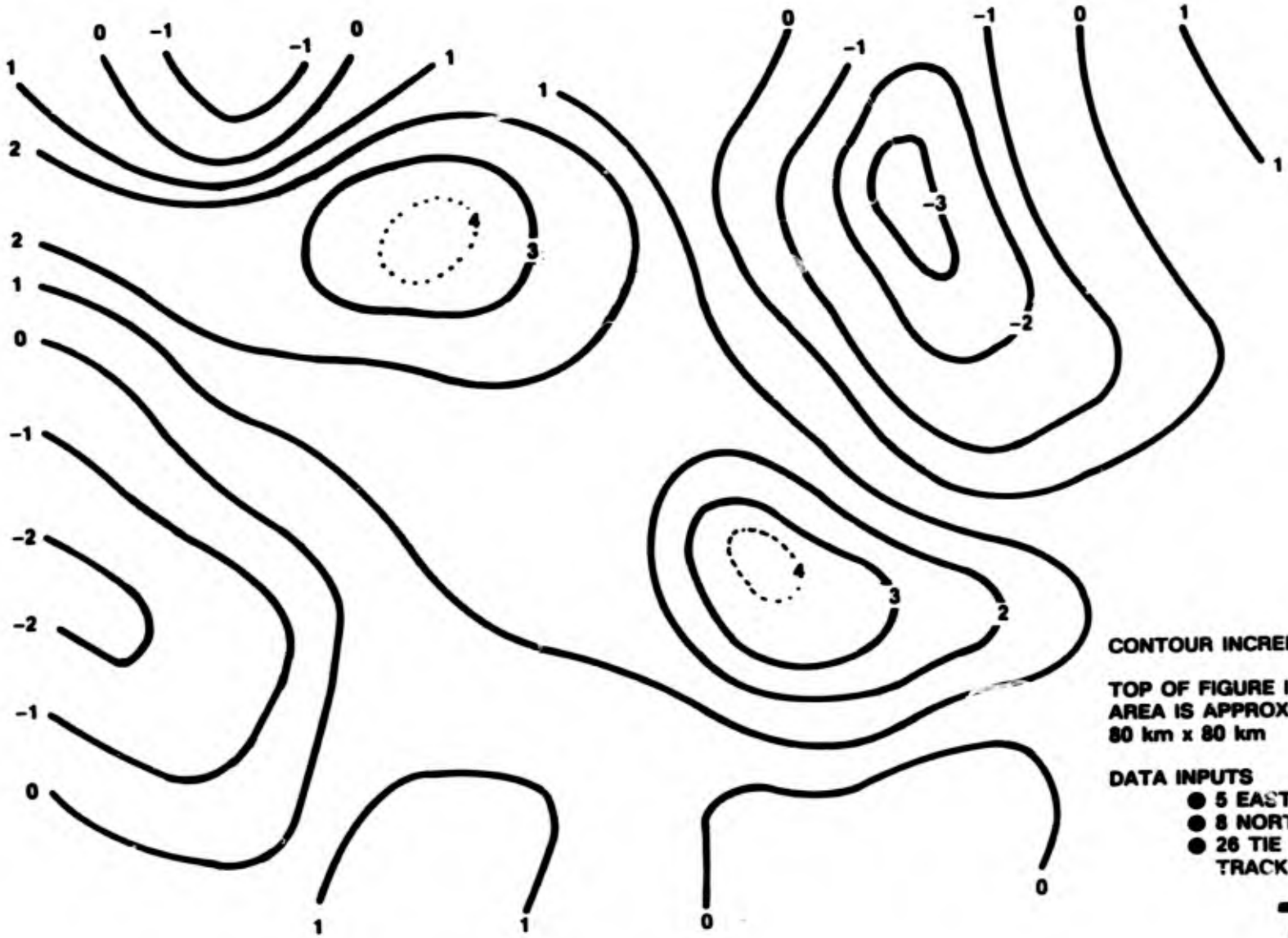

GRAVITY DISTURBANCE ESTIMATES FROM GRADIENTS ALONG 13 TRACKS

CASE II – TIE POINTS AT CENTERS OF BOUNDRY TRACKS ONLY

G-08496
02/06/88

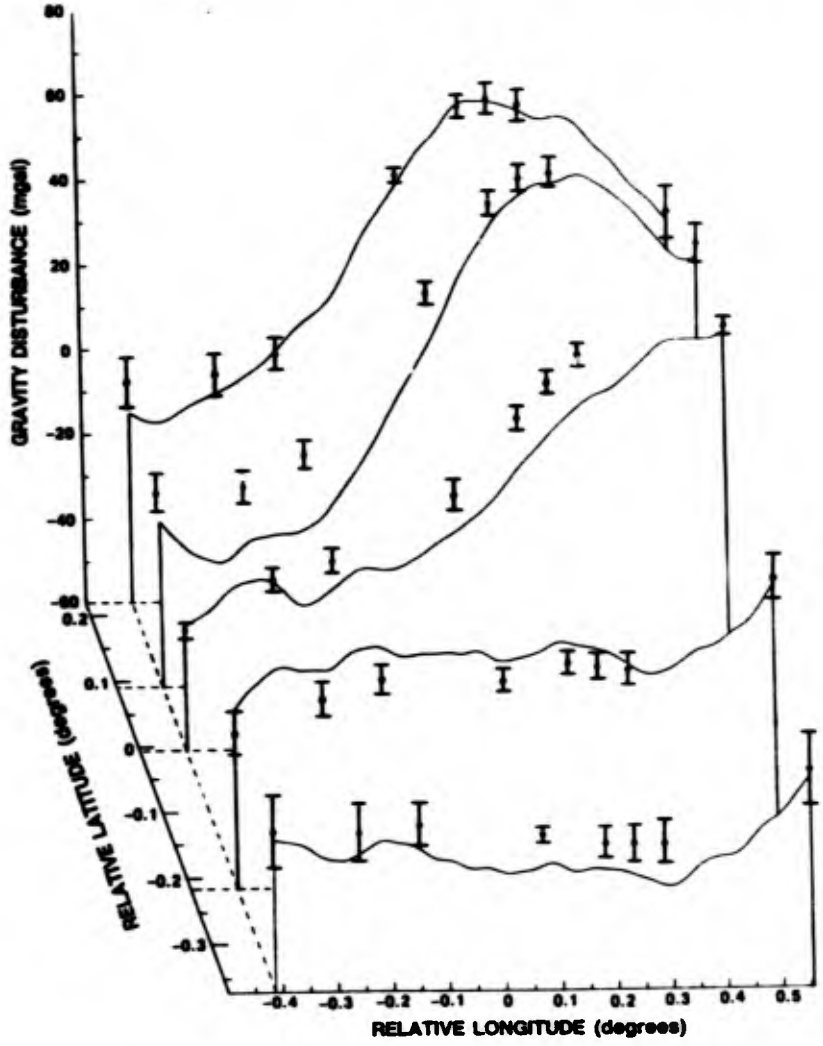

TASC

RESIDUAL ERRORS FROM 13 TRACK ESTIMATES OF VERTICAL GRAVITY DISTURBANCE

CASE II – TIE POINTS CENTERS OF BOUNDRY TRACKS ONLY

G-08494
02/06/88

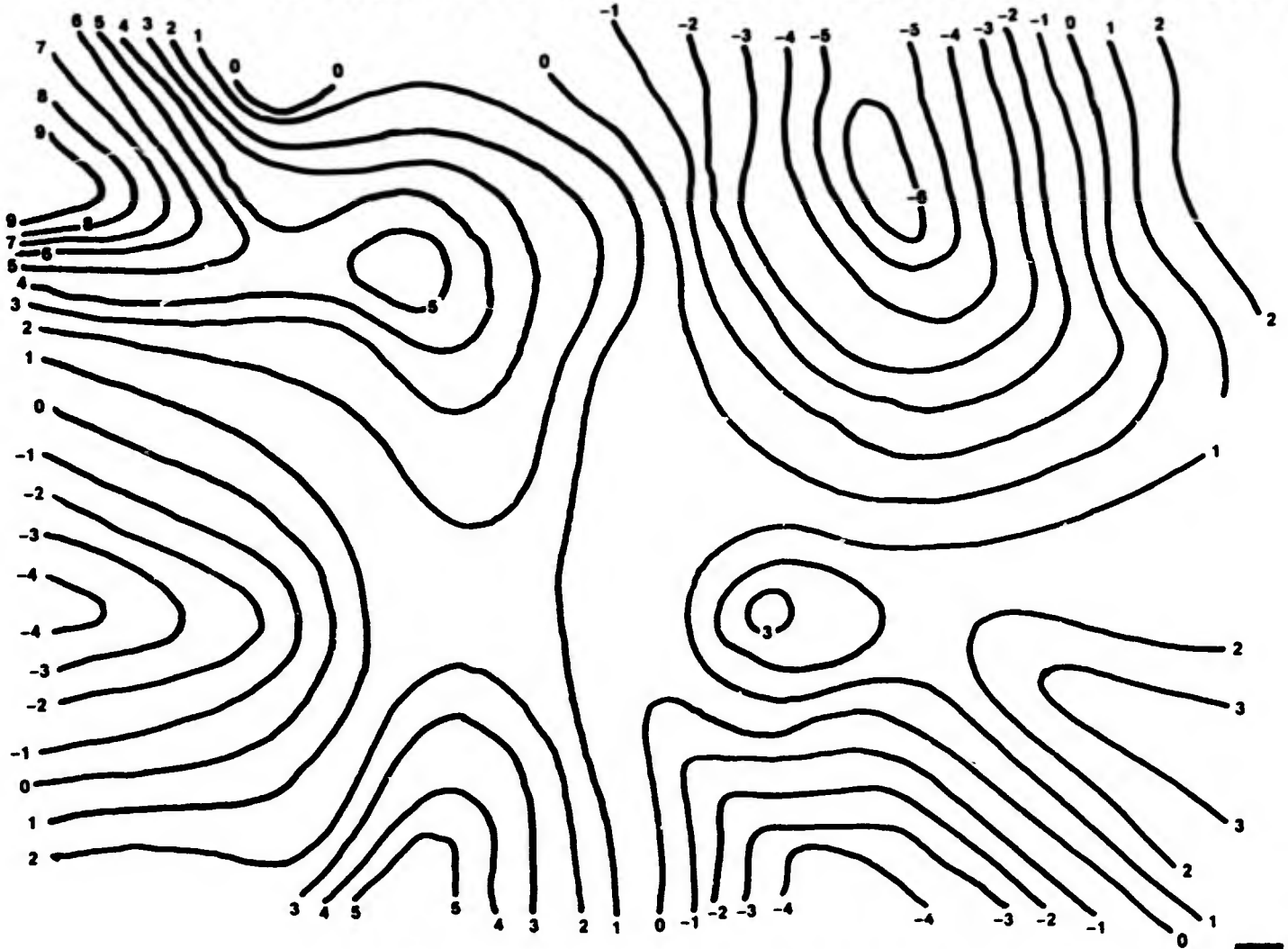

NOTE: NORTH IS NOT AT TOP OF PAGE

TASC
THE ANALYTIC SCIENCES CORPORATION

SUMMARY

- 13 TRACKS OF AIRBORNE GGSS DATA, SITUATED IN REASONABLE PROXIMITY, WERE PROCESSED INTO ESTIMATES OF VERTICAL GRAVITY DISTURBANCES
- ESTIMATES WERE FORMULATED AS 5' x 5' MEANS AND COMPARED WITH 5' x 5' MEAN TRUTH VALUES CENTERED AT EACH ESTIMATION POINT
- SUMMARY OF COMPARISON STATISTICS (40 ESTIMATION POINTS) PRESENTED IN TABLE BELOW:

	rms ERROR, ALL POINTS (mgal)		rms ERROR, NON-TIE POINTS ONLY (mgal)		WORST CASE ACTUAL ERROR (mgal)
	PREDICTED	ACTUAL	PREDICTED	ACTUAL	
CASE I – TIE POINTS AT ENDS OF EACH TRACK	1.93	1.64	2.33	2.16	3.72
CASE II – TIE POINTS AT CENTERS OF BOUNDARY TRACKS ONLY	4.34	3.27	4.53	3.44	8.77

TASC

T-04768

CONCLUSIONS

- TEST DATA SET REQUIRED CONSIDERABLE WINNOWING TO FIND SUITABLE GROUP OF TRACKS WITH APPROPRIATE SPACING AND EXTENT
- MULTITRACK ANALYSIS OF SELECTED TRACKS DEMONSTRATES GRAVITY DISTURBANCE ESTIMATION ACCURACY AT TWO mgal LEVEL
- PRESCREENING IS REQUIRED TO REALIZE FULL POTENTIAL OF CLINTON/SHERMAN TEST DATA
- FUTURE DATA REDUCTION WILL BE AMENABLE TO AUTOMATION
- GGSS AIRBORNE TEST PROGRAM MUST BE VIEWED AS A SUCCESS

TASC

16th GRAVITY GRADIOMETRY CONFERENCE
10-11 FEBRUARY 1988

SPONSORED BY:
AIR FORCE GEOPHYSICS LABORATORY
EARTH SCIENCES DIVISION

TITLE OF PAPER: GGSS Airborne Test Data Reduction Results

SPEAKER: Warren Heller

QUESTIONS AND COMMENTS:

1. Question: Don Benson

   What was the accuracy of the 5' x 5' truth model?

   Response:

   I don't really know, but the filter model has a covariance model. 2.0 mgal rms was used.

2. Comment: Don Benson

   Part of the accuracy between truth and estimates would include rms truth error.

   Response:

   Yes, indicating that the GGSS is really a good system.

3. Question: Rene Forsberg

   Am I correct in understanding you had around 100 states in the "template filter"? Could you give me an estimate of the computing time involved?

   Response:

   Yes, the largest solution had somewhat more than 100 states. The computation load was mainly due to evaluation of the covariances, which contain complicated expressions (Bessel functions, etc). Computation time on a super mini-computer was on the order of magnitude of 45 mins, with the inversion taking only a few minutes.

THE WINGS OF GRADIOMETRY

by

Robert E. Ziegler

Defense Mapping Agency Systems Center
McLean, Virginia

The Defense Mapping Agency procured a modified Hercules C-130 aircraft through competitive contracting to support the test and evaluation of the Gravity Gradiometer Survey System (GGSS). The history and experiences of this project are related.

AIRCRAFT REQUIREMENTS

- HOST GGSS
  - MOTOR HOME 19,000 POUNDS 33 FEET
  - POWER
  - SIGNALS
- GLOBAL FLIGHT CAPABILITY
  - POLAR ICE CAPS
  - EQUATORIAL RAIN FORESTS

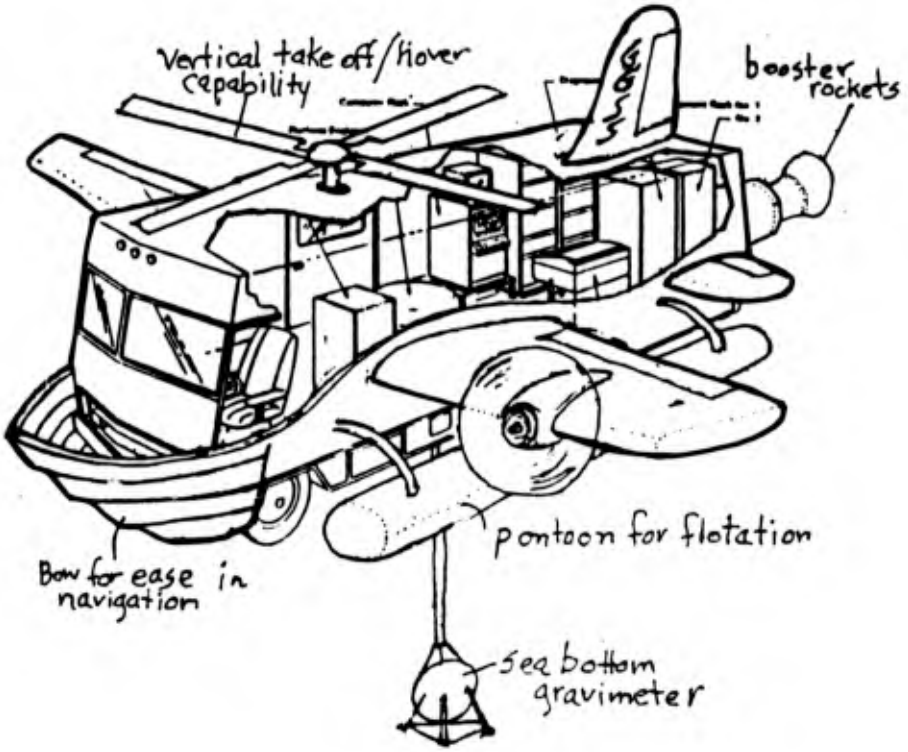
Vertical take off/Hover capability
booster rockets
pontoon for flotation
Bow for ease in navigation
sea bottom gravimeter

AIRCRAFT STANDARDS

- FLIGHT & GROUND CREW CERTIFICATION
- MAINTENANCE STANDARDS
- NAVIGATION AIDS & COMMUNICATIONS
  - DUAL REDUNDANCY
  - RADIO ALTIMETER
  - WEATHER RADAR
  - TWO INERTIAL NAVIGATORS

AIRCRAFT MODIFICATIONS *

- GGSS POWER SUPPLY
  - AIRCRAFT
  - GPU
  - VARIETY OF GROUND SOURCES
  - EMERGENCY SHUTOFF (2)

- GGSS SIGNALS TO AIRCRAFT
  - AUTO PILOT
  - FOUR-AXIS ATTITUDE
  - WAYPOINT DISPLAY
  - BATTERY VENT

- AIRCRAFT SIGNALS TO GGSS
  - FUEL LEVEL
  - BAROMETRIC SENSOR
  - GPS ANTENNA
  - VOICE COMMUNICATION

* SUBJECT TO FAA CERTIFICATION

GRAVITY GRADIOMETER SURVEY SYSTEM

AIRCRAFT CONTRACT

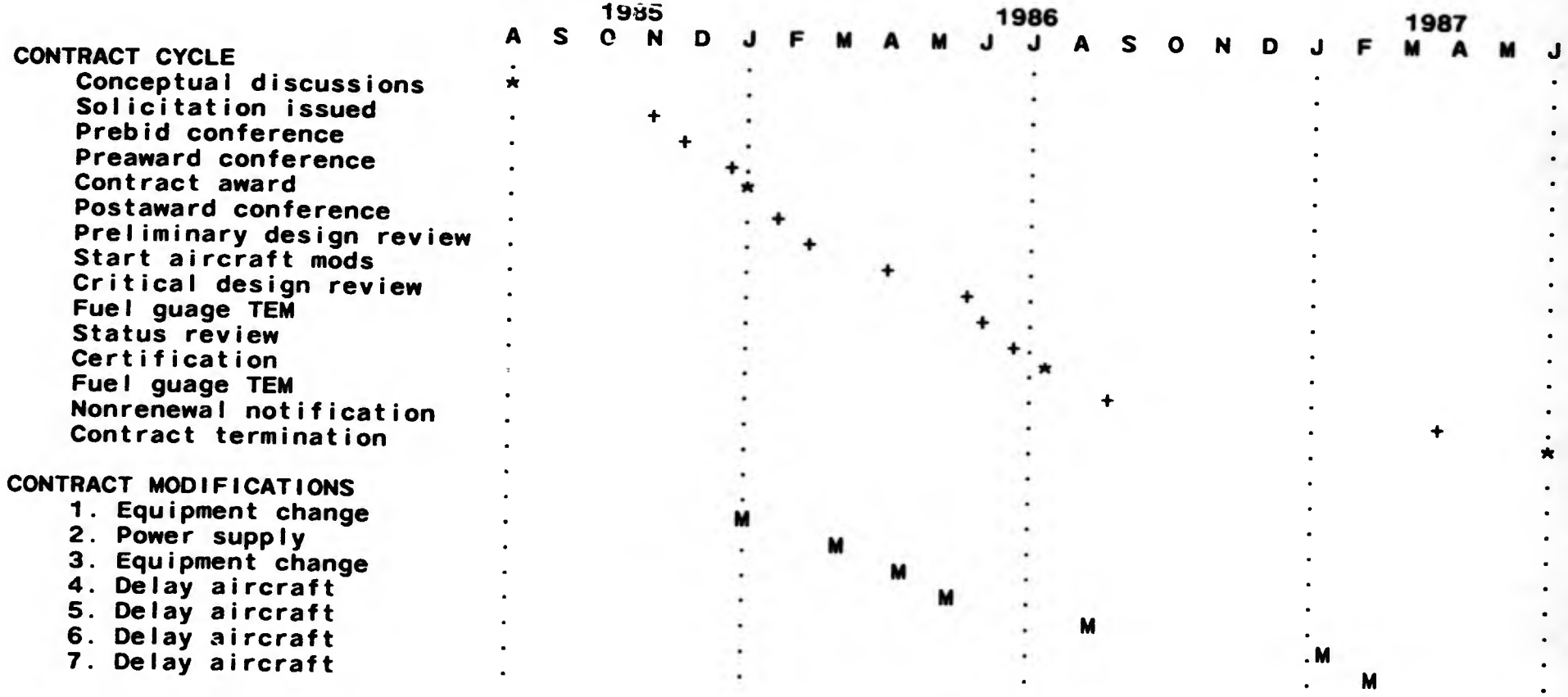

AIRCRAFT CONTRACT EXPENDITURE PROFILE BY BILLING DATE

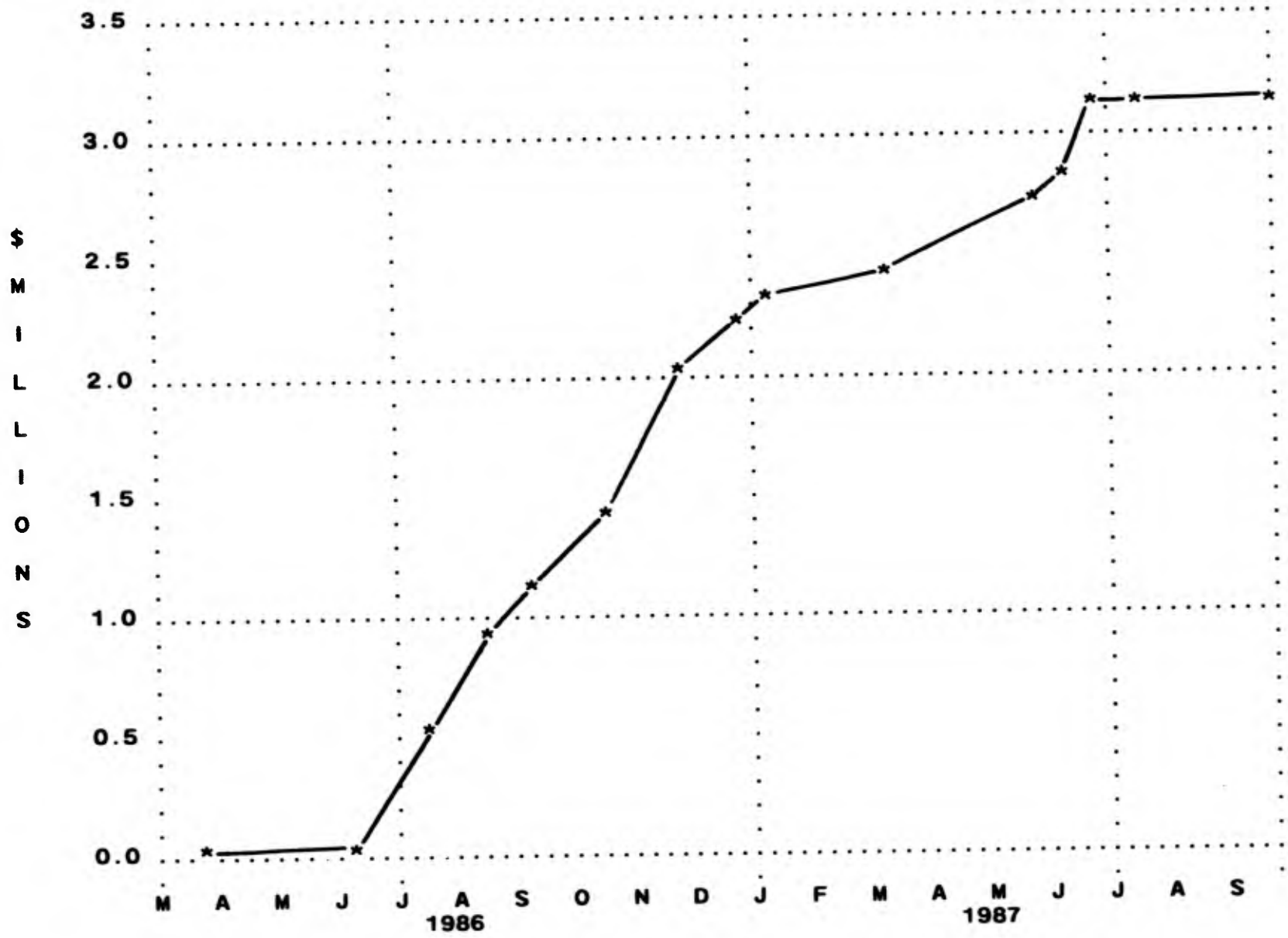

CONTRACT SUMMARY

LENGTH	17	MONTHS
AVAILABILITY	205	DAYS
FLIGHT TIME	263	HOURS
FUEL	184,100	GALLONS

COST SUMMARY

MODIFICATIONS, ETC	$1,328,000
FLIGHT TIME	332,000
FUEL	186,000
AVAILABILITY	1,291,000
TOTAL	3,137,000

LINEAR INVERSION OF GRAVITY AND GRAVITY GRADIOMETRY: A TALE OF TWO OPERATORS

by

Donald W. Vasco

Earth Sciences Division
Air Force Geophysics Laboratory
Hanscom AFB, MA 01731

Gravity gradiometry represents a new potential field data set. This new data may better constrain the density structure in the earth. Using singular value (spectral) decomposition of the gravity and gravity gradient operators, I compare the model parameter resolution and model parameter variance of two synthetic data sets. It is found that gravity gradients do indeed improve the resolution and result in smaller density variances when compared to the vertical component of gravity. This improvement is greatly reduced as depth increases however. The density resolution and variance were computed for a subset of tracks from the airborne gravity gradient system. The resolution of the density is not adaquate below the second layer. Furthermore, the variance of the density values is rather large.

Resolution and Variance Operators of Gravity and Gravity Gradiometry

D. W. Vasco

Earth Sciences Division

Air Force Geophysics Laboratory

Hanscom AFB MA 01731-5000

Abstract

Gravity gradiometry represents a new potential field data set which may better constrain the density structure of the Earth. Using singular value (spectral) decomposition of the gravity and gravity gradient kernels the model parameter resolution and model parameter variance of the two data types are compared using a recently acquired collection of airborne gradient measurments from Bell Aerospace Textron's Gravity Gradient Survey System (GGSS). The GGSS was flown over a portion of south-western Oklahoma, where the gravitational anomaly from the buried Wichita basement rocks is over 60 milligals. The corresponding maximum vertical gravity gradient was found to be 46.2 Eötvös. The problem is cast as a linear inverse problem with the subsurface discretized into a number of blocks each of which may contain a different density value. In order to reduce the non-uniqueness a smoothness criteria is introduced. For the linear inversion the resolution of the density is not adaquate below the second layer (20 km). Furthermore, for a gravity gradient error of 10 E, the estimated error of the actual gradient observations for a resolution of 0.9 km, the maximum error of the density values is 0.1

grams per cubic centimeter. It lies below the second layer in the depth range 20 to 30 km.

Introduction

In recent years there has been rapid progress in the development of gravity gradiometry (Jekeli 1987). For example, a three-axis superconducting gravity gradiometer is being developed which has a fundamental sensitivity of $2.0 \times 10^{-4} E/Hz^{1/2}$ (Moody et. al. 1987). Particularly exciting is the recently tested Gravity Gradiometer Survey System (GGSS) which has airborne capabilities (Metzger and Pfohl 1987, Eckhardt 1986). Simply put, the GGSS consists of pairs of closely spaced accelerometers. The difference between accelerometers in a given pair determines a gradient. Two such pairs in mutually orthogonal directions constitutes a gravity gradient instrument (GGI). The heart of the GGSS consists of three orthogonally mounted GGIs (Figure 1). With this configuration one may determine the six gravity gradient tensor elements. The whole device is mounted on a platform isolated by a system of three gimbals. Two gyroscopes and three accelerometers feedback to the gimbals to stabilize the system. The total apparatus, including accompanying electronics, is installed in a moble van. This van may be driven into a C-130 transport airplane for airborne surveys. In this mode the gravity gradiometer has the ability to revolutionize the gathering of potential field data The full gravity gradient tensor may be determined rapidly, using dense sampling, over large regions of inaccessible, rough, or densely vegatated terrain. For a more detailed discussion of the GGSS

the reader should consult the review article by Jekeli (1988).

During the interval April 3, 1987 to May 26, 1987 the GGSS was flown in south-western Oklahoma. The intent was to fly the instrument over 5.0 km evenly spaced north-south and east-west tracks. The flight path was to be primarily controlled by an auto-pilot with positioning information from the Global Positioning System (GPS). However, due to poor weather, GPS unreliability, plane downtime and instrument downtime, this could not be accomplished. The GGSS flew 30 north-south and 24 east-west tracks, taking measurements every second in time or every 111 meters in distance at a speed of 400.0 km/hr. The data from the 54 tracks flown are not of uniform quality. There was a problem with platform accelerations for some measurements. In addition, one of the GGIs did not function properly for portions of the survey. Because of this the data had to be edited to remove those tracks or portions of tracks containing tainted data. This was done by examining the output from the platform accelerometers for large accelerations. From this subset of data spurious spikes were removed and the reference gradient field of the WGS84 ellipsoid at the elevation of the flight track (estimated to be 1 km) was subtracted as was the mean gradient field. After this, the data were filtered using a 65 term Hamming lowpass filter (Hamming 1977). The resultant vertical gradient components for the set of edited and filtered tracks is shown in Figure 2. The gravity gradient field is

measured in Eötvös: 10^{-6} mgal/cm. Contours of the regional vertical gravity field are also presented in the figure. There is clearly a coherent signal present in these data which mirrors the vertical gravity field in the region.

The gravity and gradient anomaly apparent in Figure 2 is the signiture of the Wichita providence basement rocks (Ham et. al. 1964). These rocks, exposed to the east in the Wichita mountains, consists of ryolites, granites and gabbro aging from 500 to 550 million years old (Ham et. al. 1964). The basement rocks are overlain by a section of Cambro-Ordovician age composed of sandstone, shale, limestone and conglomerate (Widess and Taylor 1959). The average constrast between these two groups lies in the range 0.3-0.6 gm/cm^3. The maximum gravitational anomaly is over 60.0 milligals. This signal is well above the standard errors of the gravity means (2.0-8.0 mgal) and the estimated standard errors of the gradiometer as discussed in the following paragraph.

Because the GGSS is still under development the data quality is not yet optimal and some problems remain. It is important to have an estimate of the errors which are apparent in the data (Figure 2). Analysis by others (Brzezowski et al. 1988) have provided errors of 6.6 to 14.6 E, at a resolution of 0.9 km, for a subset of 19 tracks of the 54 tracks flown. For this work a standard error of 10 E was used, which was close to values from an earlier study (TASC 1987). This early study

concentrated on 11 tracks: north-south tracks 39, 41, 42, 43, 44, 45 and the east-west tracks 27, 25, 24, 22, 19. Post-adjustment residual track crossing differences were 8.6, 9.5, 11.5, 9.6, 8.8, and 8.4 E for the six GGI components. This is much less than the maximum vertical gradient anomaly of 46.2 E observed on track 41 (Figure 2). Figures 3a-f display the data used in this study. The eight tracks overlap considerably with the set examined by TASC (1987). In addition to random errors, some biases may be present in the data which are not yet accounted for.

Given the data set mentioned above, it is appropriate to consider how the gravity gradiometry data differs from conventional vertical gravity data. Do the six gradiometer components contain more information than the vertical component of gravity? How does gradiometry data constrain the density structure of the subsurface? To answer these questions I will consider the inverse problem of determining the subsurface density distribution from potential field data. In particular the model parameter resolution and model parameter variance will be contrasted for the two data sets: vertical gravity and gravity gradiometry. I consider both the linear problem of estimating the density distribution as well as the non-linear problem of determining boundary perturbations for constant density bodies. Because linear problems are amenable to direct calculation of model parameter resolution and variance I linearize the non-linear problem to deal with such questions.

The Formulation

First, consider the linear problem of estimating the subsurface density distribution from potential field data measured at the Earth's surface. The inverse gravity problem has been treated by numerous authors (Al-Chalabi 1971, Green 1975, Vigneresse 1977) and is among the oldest inverse problems in geophysics. The main obstacle in the linear inversion of potential field data is an inherent non-uniqueness that manifests itself in the well known Equivalent Layer theorem. By means of Green's theorem one may show that any gravity anomaly can be explained by a density distribution on a single thin layer (Skeels 1947, Roy 1962). To help circumvent the ambiguity of the linear inversion one must either introduce inequality constraints, such as non-negativity conditions, or minimize some non-linear functional defined over the model space. Frequently in the past, the funtional to be minimized was the total of the squared density perturbations. If this is applied without recourse to an initial model it has the unfortunate property of producing the largest density values nearest to the stations. Instead, I use a smoothness criteria which will be described below. Inequality constraints, when physically appropriate, can be very effective in riding the problem of non-uniqueness (Vigneresse 1977). First, I consider the formulation of the linear problem and the reduction of the problem to a linear system of equations.

For the unconstrained problem the bounds of integration do not depend on the model parameters, hence, the components of gravity and the components of the gravity gradient, $u_{kj}(\mathbf{x})$, are linearly related to the density distribution $\rho(\xi)$,

$$u_{kj}(\mathbf{x}) = \int\int\int \rho(\xi)\, G_{kj}(\mathbf{x}, \xi)\, dV(\xi)\,. \tag{1}$$

The components of $\mathbf{x}$ are the station coordinates $(x_1, x_2, x_3) = (x, y, z)$ and the components of ξ are the source coordinates. The distance between the observation and the source point is $r = \sqrt{(x_1 - \xi_1)^2 + (x_2 - \xi_2)^2 + (x_3 - \xi_3)^3}$. The index k indicates the potential component, j indicates the coordinate to be differentiated, if j is zero than there is no differentiation. The kernel for the vertical component of gravity, $G_{30}(\mathbf{x}, \xi)$ is given by:

$$\frac{-z}{r^3}.$$

For the cross gravity gradients, $k \neq j$, the kernel is

$$\frac{3(x_k - \xi_k)(x_j - \xi_j)}{r^5}.$$

And, the kernel for the diagonal elements of the gradient tensor $G_{kk}(\mathbf{x}, \xi)$ is,

$$\frac{3(x_k - \xi_k)^2 - r^2}{r^5}.$$

Note the faster decay of the gravity gradient kernels with distance from the source. Thus, gradient data will be less sensitive to the longer wavelengths of the gravity field. This characteristic will show up in the resolution matrices derived below.

The above equation may be discretized by expanding the density distribution, in a series of N orthogonal basis functions $\Omega_n(\xi), n = 1, 2, \ldots N$,

$$\rho(\xi) = \sum_{n=1}^{N} c_n \Omega_n(\xi) \tag{2}$$

In what follows the rectangular constant basis functions will be used,

$$\Omega_n(\xi) = \begin{array}{ll} 1 & if \xi \; in \; R_n \\ 0 & if \xi \; not \; in \; R_n \end{array}$$

where R_n is a region of the subsurface. Essentially, the subsurface has been subdivided into a number of rectangular prisms and R_n is the nth prism. Substituting equation (2) into equation (1) and changing the order of summation and integration results in a system of I linear equations, I being the total number of components at all stations,

$$u_i(\mathbf{x}) = \sum_{n=1}^{N} c_n A_{in} \tag{3}$$

with i an index denoting the station and component type. The matrix A_{in} is given by the integral

$$A_{in} = \int\int\int G_i \Omega_n(\xi) \, dV(\xi).$$

For the gravity gradients, $T_{ij}(\mathbf{x}, \xi)$, this integral may be evaluated analytically for the rectangular basis functions (Forsberg (1984), see the Appendix). The coefficients, c_n are weighting factors for the elements of A_{in} and, when the rectangular

constant basis functions are used, can be thought of as the average density of the nth prism. They are the unknown model parameters which will be determined by the potential field data. Once the equations are discretized in this manner we are left with the linear system $\mathbf{u} = \mathbf{Ac}$.

One of the most used techniques in geophysics for the solution of possiblely inconsistent and non-unique linear equations is the generalized inverse (Menke 1984). It follows from the singular value decomposition of $\mathbf{A}$, the coefficient or operator matrix

$$\mathbf{A} = \mathbf{U}\Lambda\mathbf{V}^{\mathrm{T}}. \tag{4}$$

The matrix $\mathbf{A}$ is represented as the product of $\mathbf{U}$, an $I \times p$ column-orthogonal matrix, Λ, a $p \times p$ diagonal matrix of singular values, and the transpose of $\mathbf{V}$, a $p \times N$ row-orthonormal matrix. The index p represents the number of singular values, elements of Λ, used to represent the solution. This number must be less than or equal to the minimum of I and N. The generalized inverse is written in terms of the singular value decomposition

$$\mathbf{A}^{-1} = \mathbf{V}\Lambda^{-1}\mathbf{U}^{\mathrm{T}}$$

and the estimate of the solution to equation (3) is given as

$$\hat{\mathbf{c}} = \mathbf{V}\Lambda^{-1}\mathbf{U}^{\mathrm{T}}\mathbf{u}.$$

The resolution matrix, that is the matrix $\mathbf{R}$ which relates the estimates of the parameters, $\hat{\mathbf{c}}$, to their true values, $\mathbf{c}$,

$$\hat{\mathbf{c}} = \mathbf{R}\mathbf{c}$$

is readily written in terms of the singular value decomposition,

$$\mathbf{R} = \mathbf{V}\mathbf{V}^{\mathbf{T}}. \tag{5}$$

The covariance matrix of the model parameters, $\mathbf{C}_{cc}$, which represents an estimate of the error in the solution, can be related to the data covariance matrix, $\mathbf{C}_{uu}$,

$$\mathbf{C}_{cc} = \mathbf{V}\mathbf{\Lambda}^{-1}\mathbf{U}^{T}\mathbf{C}_{uu}\mathbf{U}\mathbf{\Lambda}^{-1}\mathbf{V}^{T}. \tag{6}$$

These are all the mathematical tools needed to compare the resolution and variance of the model parameters when the different data sets are considered. The parameter estimates, $\hat{\mathbf{c}}$, the resolution matrix, and the covariance matrix all depend on the number of singular values used, p. The relative size of the singular values will be used to determine how many of such values to keep.

As mentioned previously, one difficulty of the linear approach in a fundamental non-uniqueness in potential field data. One way around this problem is to define a non-linear functional to be minimized or maximized over the space of possible models. The generalized inverse given above returns the solution which minimizes

the residuals and sets all components of $\mathbf{c}$ incompatible with the data to zero. If the residual vector is defined by $\mathbf{e} = \mathbf{u} - \mathbf{Ac}$, then the generalized inverse can be thought of as the solution that minimizes,

$$\mathbf{e}^T\mathbf{e} + \mathbf{c}^T\mathbf{c} \tag{7}$$

i.e. the "minimum norm solution". If no initial model is introduced, the density distribution will concentrate near the stations. Another approach is to find the smoothest model which minimizes the misfit to the data. Then, there is no preferential distribution of density near the surface. This can be done by minimizing a functional of the form,

$$\mathbf{e}^T\mathbf{e} + \mathbf{c}^T\mathbf{Wc}. \tag{8}$$

The weighting matrix $\mathbf{W}$ is a product of two banded matrices $\mathbf{D}$ in which the ith row is given by $[\ldots 1\ -2\ 1\ldots]$, with the leading 1 in the ith column. With this weighting matrix the last term in equation (8) represents the square of the second difference between model parameters, a numerical approximation to the square of the Laplacian of the model $\nabla^2\mathbf{c}$, the model curvature. By a suitable transformation the functional given in equation (8) can be put into the form of equation (7). This transformation is based on the singular value decomposition of the squared

Laplacian matrix **W** (Menke 1984),

$$\mathbf{W} = \mathbf{U}_W \mathbf{\Lambda}_W \mathbf{U}_W^T.$$

The variables and parameters become

$$\mathbf{c}\prime = \mathbf{\Lambda}_W^{1/2} \mathbf{U}_W^T \mathbf{c} \tag{9}$$

$$\mathbf{A}\prime = \mathbf{A}\mathbf{U}_W \mathbf{\Lambda}_W^{-1/2}. \tag{10}$$

In the transformed coordinates the generalized inverse will give the desired solution.

The above techniques may be applied to data gathered by the gravity gradiometer, the vertical component is shown in Figure 2. These data were sampled every fifty points resulting in the data set shown in Figures 3a-f. The region extends over a much larger north-south range, 165.0 km, than it does in the east-west direction, 40.0 km. The distribution of the six gravity gradient tensor elements display coherency between tracks and reflect the regional gravity field also shown in these figures. This is especially clear if the vertical derivative of the vertical component, T_{zz}, is considered (Figure 3f). The subsurface of the region in this figure was broken up into four layers, each 10 km thick. Each layer was then divided into twenty-five blocks, five on a side. The dimensions of each block are 33.0 km north-south by 8.0 km east-west. The density of each block is an unknown parameter to be determined from the data.

The station distribution in Figure 3 can be used to generate the coefficient matrices, A_{in}, for a set of vertical gravity and gravity gradient tensor data. Because a smoothness criteria is being used in the inversion, the matrices are transformed as in equation (10). The singular value decomposition of the transformed matrices (equation 4) may now be performed. The first parameters of interest are the singular values of the gravity and gradient operators contained in the respective $\mathbf{\Lambda}$ matrices. The elements of these diagonal matrices indicate the sensitivity of the data to the parameters, the density distribution. In each matrix the singular values fall off rapidly from their respective maximum values, becoming essentially zero after the first layer. There is a slightly higher rate of decrease for the gradient data which is due to the greater decay of the gradient field with distance. From this figure it is clear that the data are not very sensitive to density perturbations below the first layer. In computing the resolution and covariance matrices it is necessary to choose a cutoff for the singular values. That is, a value below which the singular values are set to zero to eliminate vectors associated with them from entering into the matrices. There is a tradeoff between the resolution and variance which hinges on the singular value cutoff. If more singular values are retained the resolution improves while the variance grows larger. In what follows a relative cutoff of 1000 was chosen. That is, any singular values less than 1/1000 th of the maximum value

was set to zero. Other values were tried but this number seemed to yield a balance between the resolution and variance.

Using equation (5) the resolution matrices can be constructed for the two operators. They are presented in Figure 4. The more closely that these matrices approximate an identity matrix, the less the averaging and the better resolved is the "true" density. The first thing to note is the amount of averaging occuring in the gravity resolution operator. Even in the uppermost layer each blocks density is an average over most other blocks. This is not the case with the corresponding gradient resolution resolution. Here, blocks of the deeper layers are averages over blocks but there is very little averaging occuring between blocks in the uppermost layer. Below the second layer the resolution of the gradiometer is very poor. The resolution of the deeper density values is poorer for the gradiometry data than for the gravity. These are again consequences of the higher fall off of gravity gradients with distance, producing higher lateral resolution within the upper layer but lower overall resolution at depth.

If an estimate of the data covariances is obtained, equation (6) can be used to map these values into model parameter covariances. The errors on the one minute means have been computed from point values within the one minute by one minute area, but the gradiometer is still a prototype and its error budget is

not well determined. As mentioned earlier, the value of 10.0 E derived from an earlier study, was chosen as an average error. These values for the standard errors produce a signal to noise ratio of roughly 5:1 for the data in the test area. The resulting covariance matrices are shown in Figure 5. The gradient data seem to have a lower overall parameter covariance. In the first layer the variances are very small. They seem adaquate for a inversion of the present gradient data set if only the two uppermost layers are considered.

The linear approach has highlighted some differences between the resolution and variance of subsurface density estimates for vertical gravity and gravity gradiometry. It is also clear that both gravity and gradiometry are not adaquate for many-layered density models unless additional constraints are availible. Because of this, the non-linear problem of determining perturbations to boundaries between constant density bodies will be taken up in the next section.

Discussion and Conclusions

The airborne gravity gradiometer is likely to become an important instrument for gathering gravitational field data. Its ability to gather a large set of densely spaced data quickly over any terrain surpasses conventional methods. The data set from southern Oklahoma is an example of a GGSS data set. Six airborne gravity gradients were observed approximately every 111 meters along 30 north-south and

24 east-west flight lines. The longest north-south tracks used in this study were more than 160 km in length and attempted track spacing was 5 km.

When a linear inversion of the data is analyzed from the perspective of resolution and variance the results are mixed. These data have better resolution of near surface density features than traditional vertical gravity. However, at depths greater than 20 km the resolution of density is not adaquate in the discretization used. The standard error of the density distribution is adaquate to determine density perturbations greater than 0.06 gm/cm^3 above 20 km in depth. Below this depth the density variance can be as great as 0.1 gm/cm^3. This is less than the expected density constrast of 0.3 to 0.6 gm/cm^3, but the resolution below 20 km is not adaquate.

The GGSS is indeed a viable system for determining regional gravity anomalies. In the future, as it is improved, it could provide detailed local gravity field data useful for exploration work. For now, it is a useful tool for the exploration of remote, thickly vegetated areas, and rugged terrain. It may also prove valuable for offshore regional surveys. Its routine use should only be a matter of time.

Acknowledgements

I wish to acknowledge the valuable assistance of David Gleason who edited, removed the regional field, and filtered the GGSS data. Research sponsored by the Air Force Geophysics Laboratory, United States Air Force, under Contract F19628-86-C-0224. The United States Government is authorized to reproduce and distribute reprints for governmental purposes notwithstanding any copy notation hereon.

References

Al-Chalabi, M., 1971, Some studies relating to the nonuniqueness in gravity and magnetic inverse problems: Geophysics, 36, 835-855.

Burkhard, N. and D. D. Jackson, 1976, Application of stabilized linear inverse theory to gravity data: J. of Geophys. Res., 81, 1513-1518.

Brzezowski, S. J., J. D. Goldstein, W. G. Heller, J. V. White, 1988, Gravity Gradiometer Survey System (GGSS) airborne test data reduction results: TASC report SP-5362-7 TASC, Reading MA.

Eckhardt, D. H., 1986, Isomorphic geodetic and electrical networks: an application to the analysis of airborne gravity gradiometer survey data: Geophysics, 51, 2145-2155.

Forsberg, R., 1984, A study of terrain reductions, density anomalies and geophysical inversion methods in gravity field modelling: Report 355, Department of Geodetic Science and Surveying, Ohio State University, Columbus, Ohio.

Green, W. R., 1975, Inversion of gravity profiles by use of a Backus- Gilbert approach: Geophysics, 40, 763-772.

Ham, W., R. Denison, and C. Merritt, 1964, Basement rocks and structural evolution of southern Oklahoma, Oklahoma Geol. Survey Bull, 95.

Hamming, R. W., 1977, Digital Filters: New Jersey, Prentice-Hall, Inc.

Jekeli, C., 1987, New instrumentation techniques in geodesy: Rev. Geophys., 25, 889.

Jekeli, C., 1988, The Gravity Gradiometer Survey System (GGSS): EOS, Transactions, American Geophysical Society , 69, 8, 105.

Lawson, C. L. and R. J. Hanson, 1974, Solving Least Squares Problems, Prentice-Hall, Englewood Cliffs, N. J.

Menke, W., 1984, Geophysical Data Analysis: Discrete Inverse Theory: Orlando FL, Academic Press.

Metzger, E. H., L. L. Pfohl, 1987, Bell Aerospace Gravity Gradiometer Survey System (GGSS) program review: Proceedings of the Fifteenth Annual Gravity Gradiometry Conference, U. S. Air Force Academy, Colorado Springs, CO.

Moody, M. V., H. A. Chan, Q. Kong, H. J. Paik, and J. W. Parke, 1987, Development of a three-axis superconducting gravity gradiometer and a six-axis superconducting accelerometer: Proceedings of the Fifteenth Annual Gravity Gradiometry Conference, U. S. Air Force Academy, Colorado Springs, CO.

Nagy, P., 1966, The gravitational attraction of a right rectangular prism, Geophysics, 31, 362.

Roy, A., 1962, Ambiguity in geophysical interpretation: Geophysics, 27, 90-99.

Skeels, D. C., 1947, Ambiguity in gravity interpretation: Geophysics, 12, 43-56.

Talwani, M., J. Lamar Worzel, and M. Landisman, 1959, Rapid gravity computations for two dimensional bodies with applications to the Mendocino submarine fracture

zone, J. Geophys. Res., 64, 49-59.

Talwani, M. and M. Ewing, 1960, Rapid computation of gravitational attraction of three-dimensional bodies of arbitrary shape, Geophysics, 25, 203-225.

TASC, 1987, Preliminary results of GGSS flight test data analysis for eleven selected tracks, TASC Report SP-5362-6, The Analytic Sciences Corp., Reading, MA.

Vigneresse, J. L., 1977, Linear inverse problem in gravity profile interpretation: J. Geophys., 43, 193-213.

Widess, M. B. and G. L. Taylor, 1959, Seismic reflections from layering within the pre-cambrian basement complex, Oklahome, Geophysics, 24, 417-425.

Figures

Figure 1. View of the gravity gradiometer. Three sets of accelerometers can be seen in the figure. Each set consists of two accelerometer pairs which are differenced to determine a gradient.

Figure 2. Vertical gravity gradient (T_{zz}) data from the Gravity Gradient Survey System (GGSS). Plotted with it is the regional gravity field for this area of southwestern Oklahoma. Note the coherent features of both the gravity and gradient fields.

Figure 3. Component T_{zz} of the gravity gradient tensor used in this study. The size of each square is proportional to its value, positive values are solid, negative values are open. The regional vertical gravity field, in milligals, is denoted by the contours.

Figure 4. Resolution matrices for the vertical gravity and gravity gradient data sets. The maximum resolution of the density of the prisms is 1.0.

Figure 5. Density parameter standard errors for the vertical gravity and gravity gradient operators.

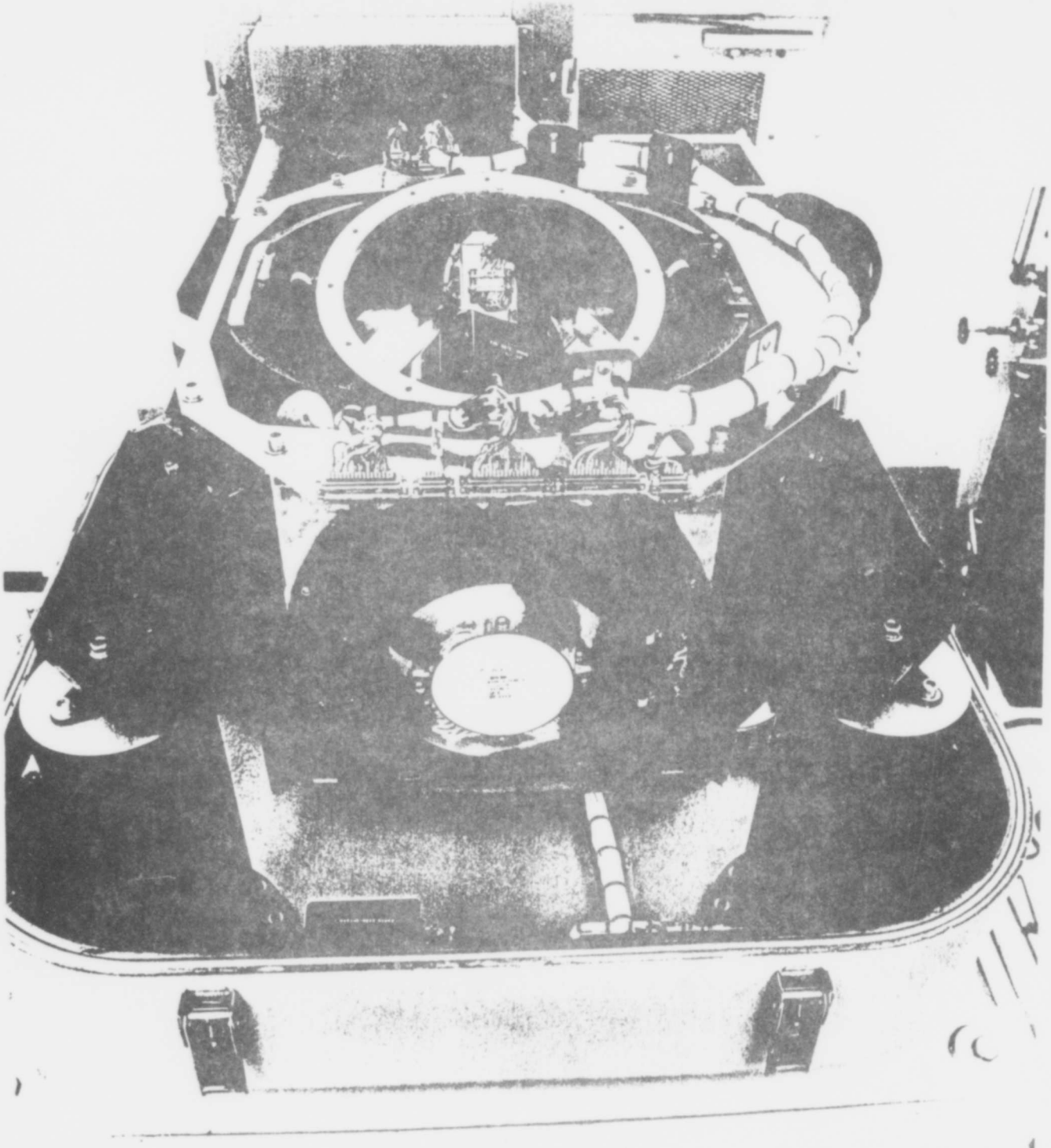

Figure 1

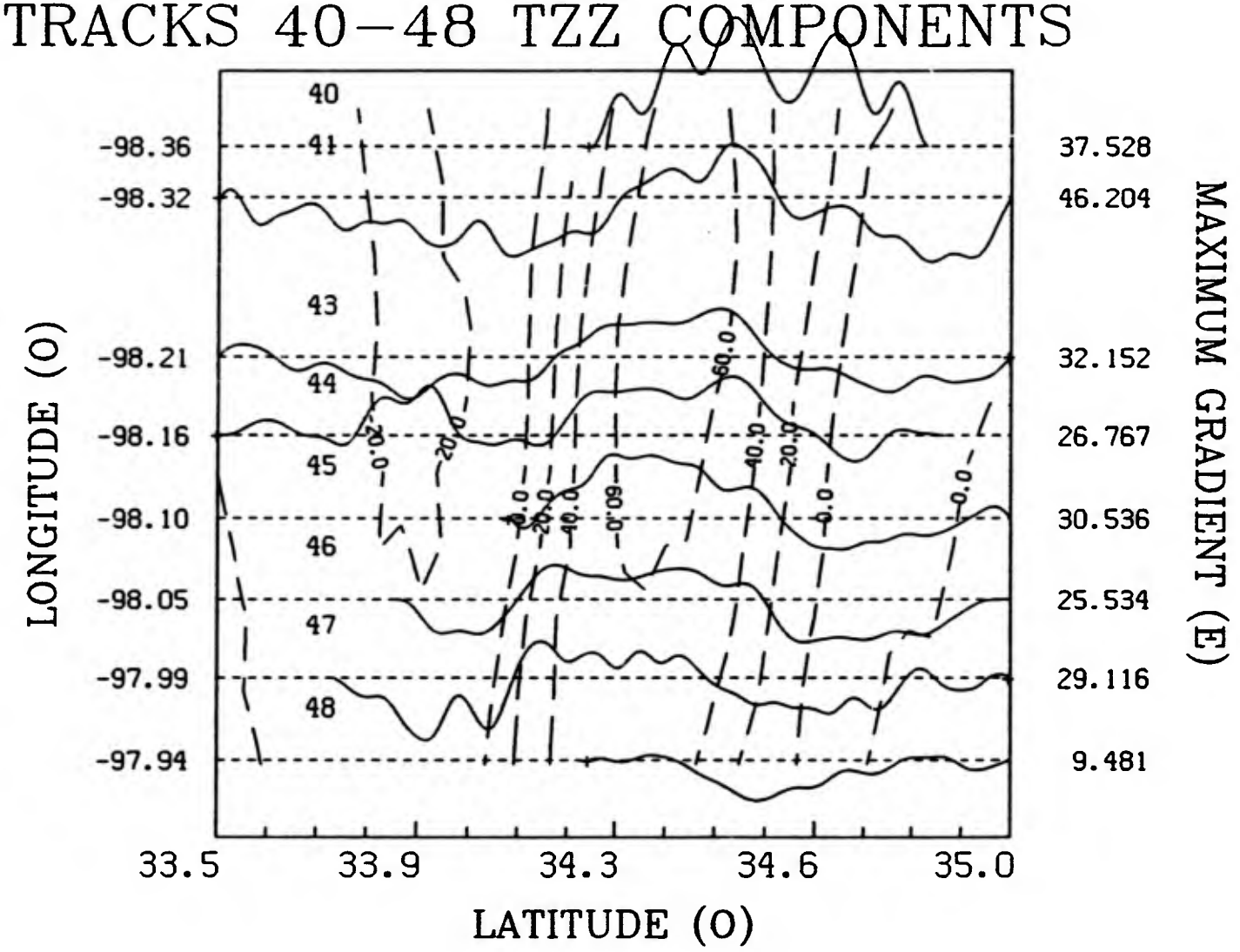
TRACKS 40-48 TZZ COMPONENTS
40
41
43
44
45
46
47
48
-98.36
-98.32
-98.21
-98.16
-98.10
-98.05
-97.99
-97.94
37.528
46.204
32.152
26.767
30.536
25.534
29.116
9.481
MAXIMUM GRADIENT (E)
LONGITUDE (O)
33.5
33.9
34.3
34.6
35.0
LATITUDE (O)

Figure 2

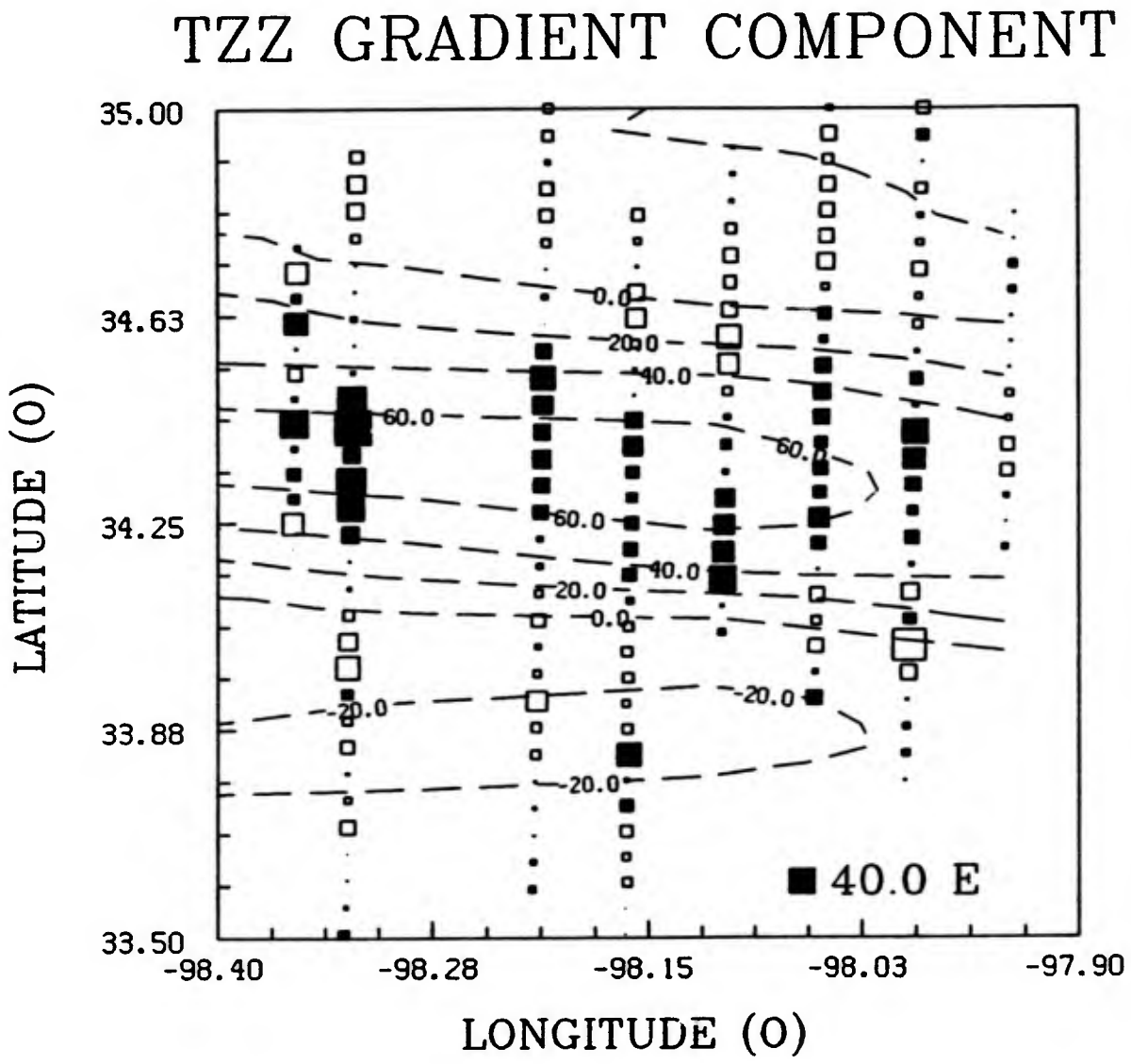
TZZ GRADIENT COMPONENT
35.00
34.63
34.25
33.88
33.50
LATITUDE (O)
-98.40
-98.28
-98.15
-98.03
-97.90
LONGITUDE (O)
0.0
20.0
40.0
60.0
60.0
60.0
40.0
20.0
0.0
-20.0
-20.0
-20.0
40.0 E

Figure 3

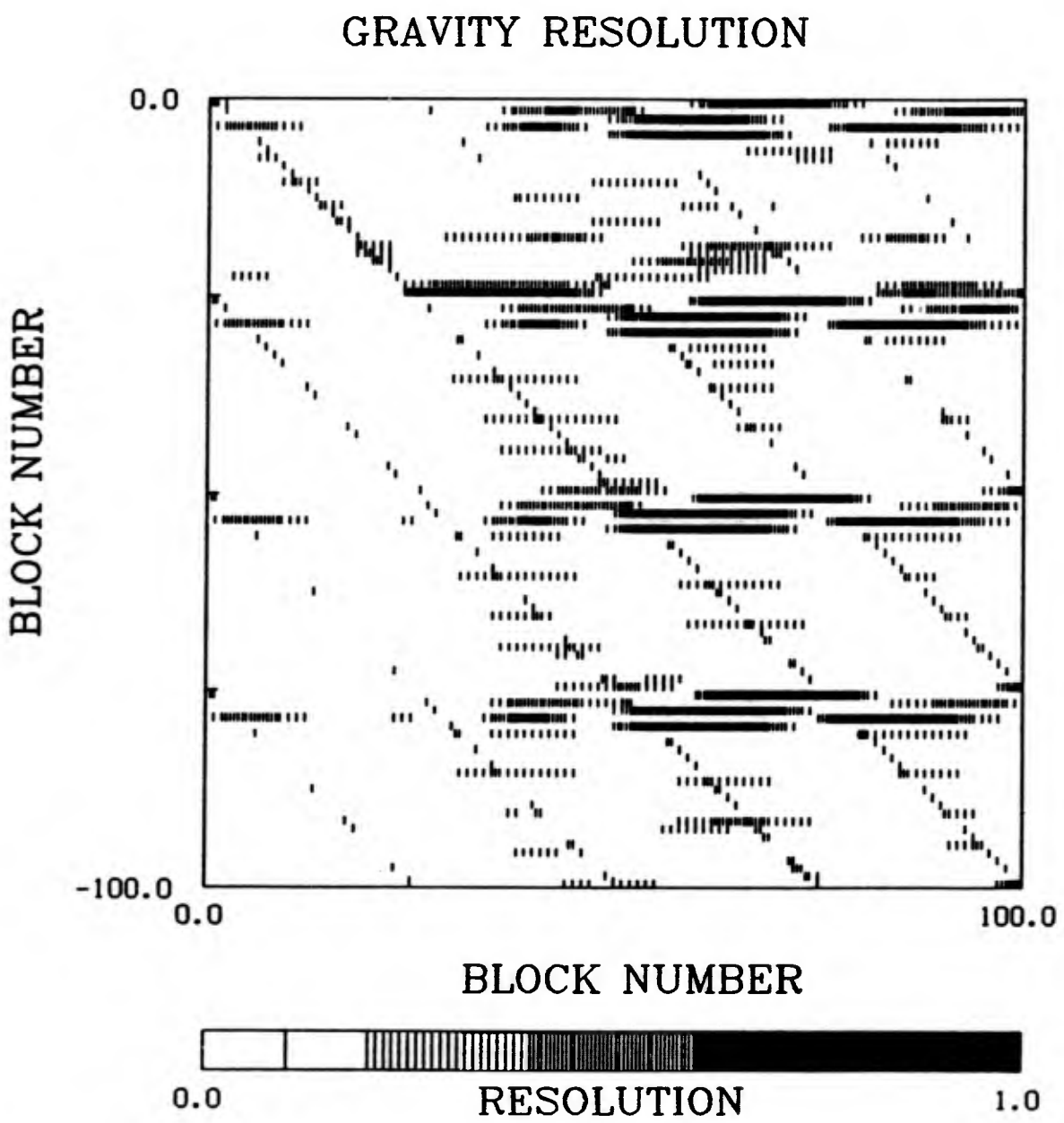
GRAVITY RESOLUTION
0.0
BLOCK NUMBER
-100.0
0.0
100.0
BLOCK NUMBER
0.0
RESOLUTION
1.0

Figure 4a

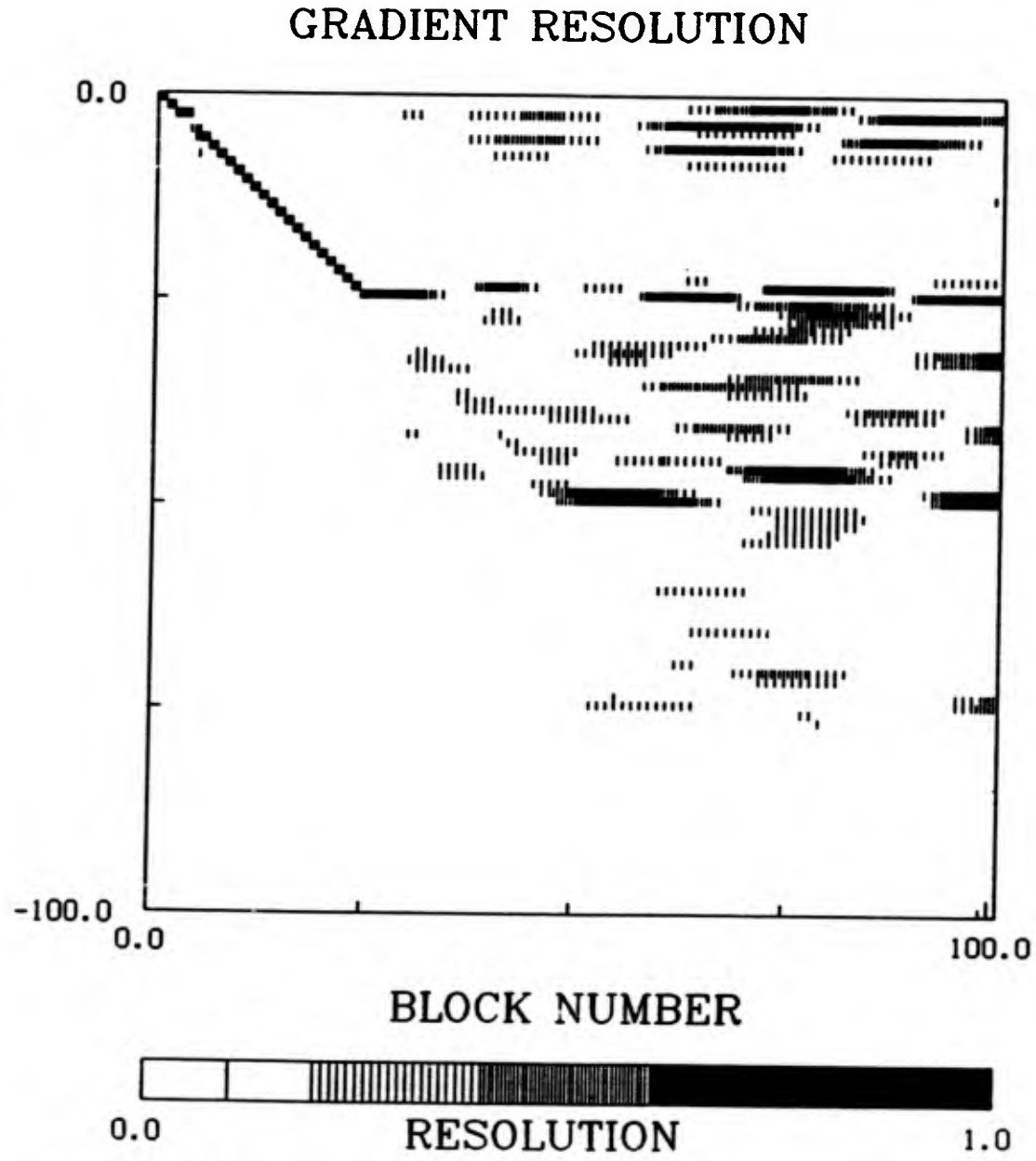
GRADIENT RESOLUTION
0.0
-100.0
0.0
100.0
BLOCK NUMBER
BLOCK NUMBER
0.0
RESOLUTION
1.0

Figure 4b

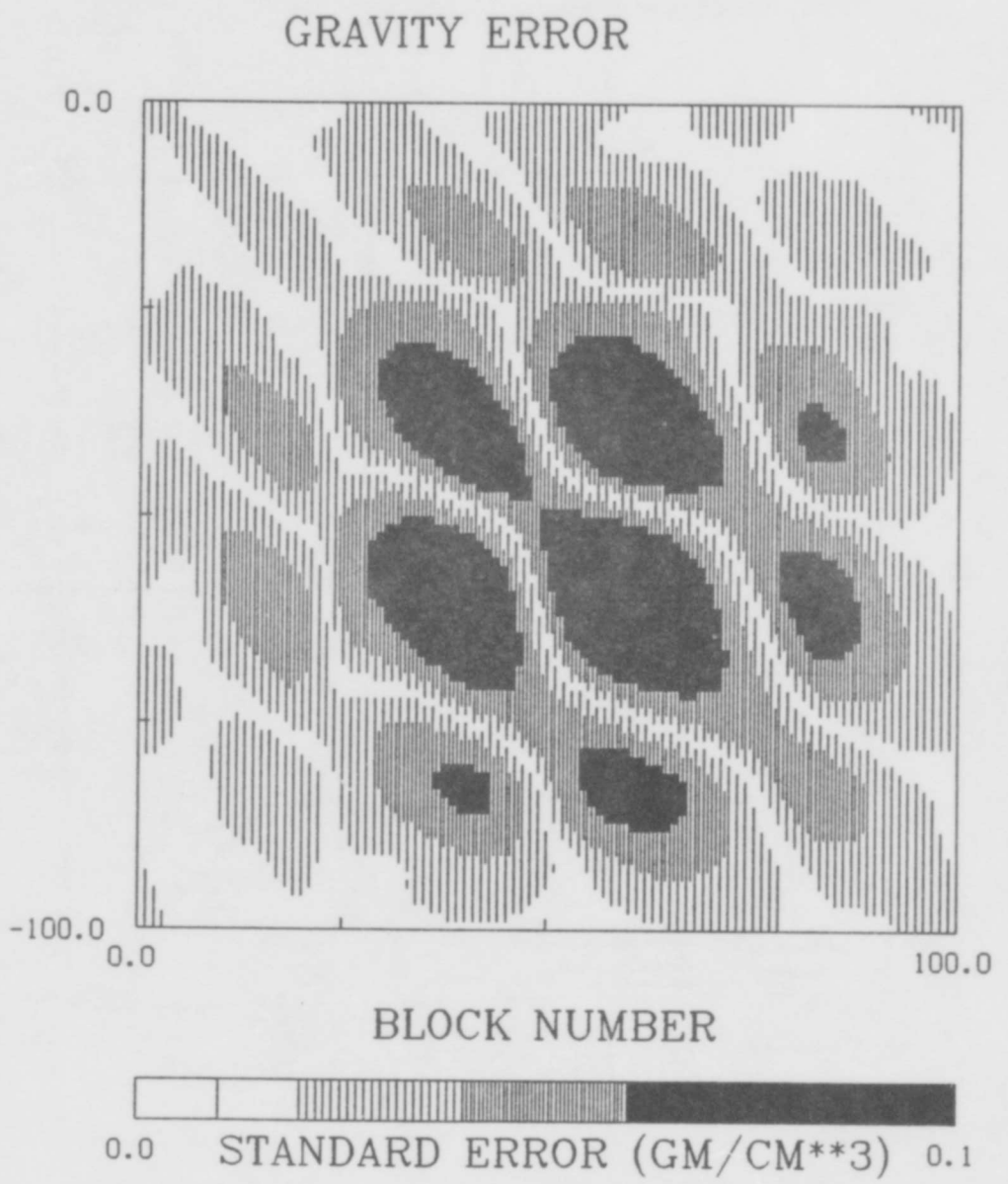
GRAVITY ERROR
0.0
-100.0
0.0
100.0
BLOCK NUMBER
BLOCK NUMBER
0.0
STANDARD ERROR (GM/CM**3)
0.1

Figure 5a

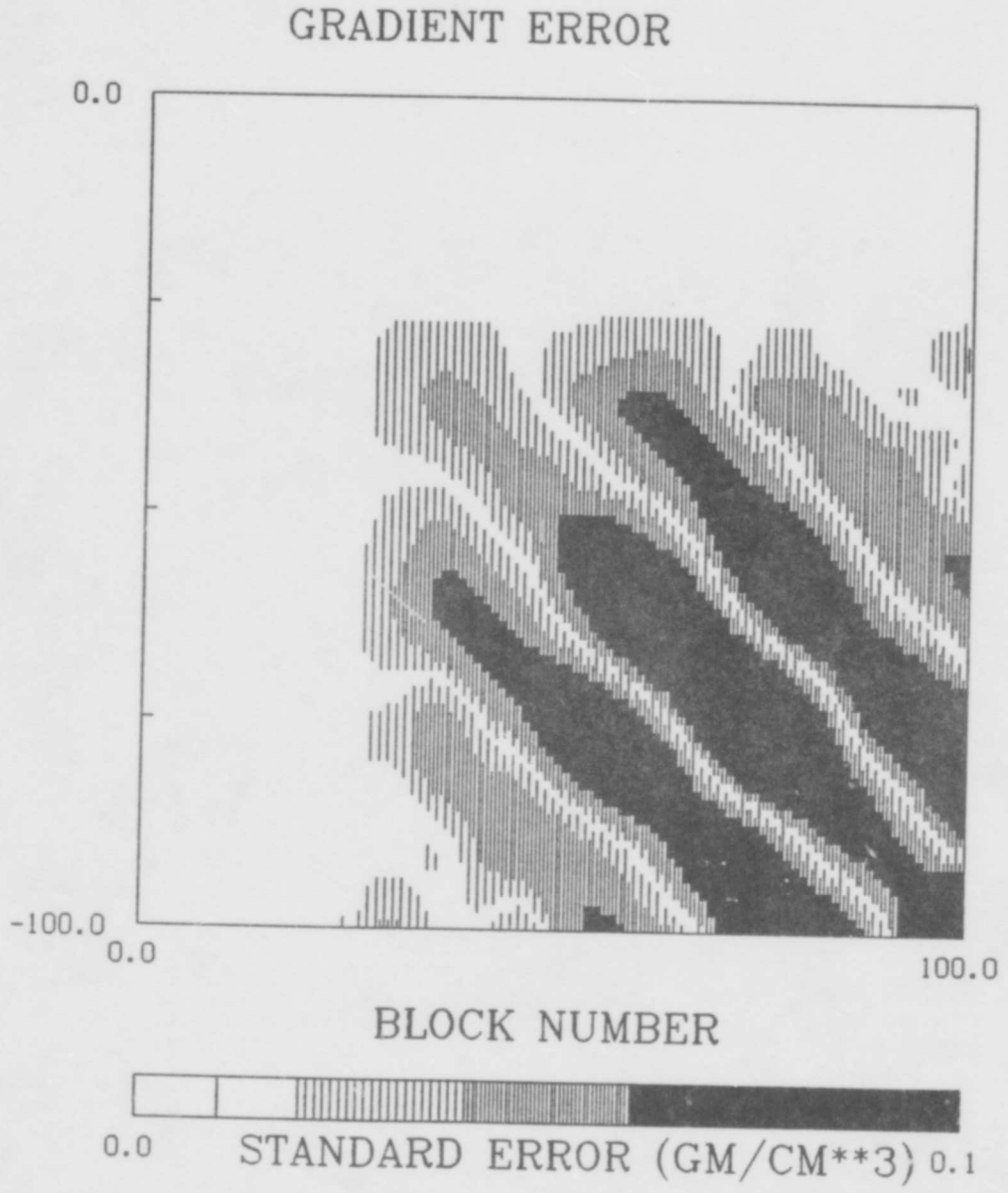
GRADIENT ERROR
0.0
BLOCK NUMBER
-100.0
0.0
100.0
BLOCK NUMBER
0.0
STANDARD ERROR (GM/CM**3)
0.1

Figure 5b

16th GRAVITY GRADIOMETRY CONFERENCE
10-11 FEBRUARY 1988

SPONSORED BY:
AIR FORCE GEOPHYSICS LABORATORY
EARTH SCIENCES DIVISION

TITLE OF PAPER: Linear Inversion of Gravity and Gravity Gradiometry: A Tale of Two Operators

SPEAKER: Don Vasco

QUESTIONS AND COMMENTS:

1. Question: Don Benson

   Have you looked at combining both gravity and gradient measurements?

   Response:

   Yes. It improved the results significantly.

2. Question: Alan Zorn

   Do you have any feel for the sensitivity of your inversion method to the norm used in the SVD?

   Response:

   Yes, it is quite sensitive. I currently use a norm which minimizes the Laplacian. I plan to try other norms and investigate this sensitivity.

THE AIRBORNE GRAVITY MEASUREMENT PROGRAM AT THE NAVAL RESEARCH LABORATORY

by

John M. Brozena

Naval Research Laboratory
Code 5110
Washington, D.C. 20375-5000

In 1979 we began the preliminary design studies for an airborne gravity measurement system (AGMS) at the Naval Research Laboratory. The initial prototype was installed aboard one of NRL's P3-A Orion aircraft and the first tests completed in mid-1981. The system was based on a LaCoste-Romberg air/sea gravity meter, a high precision radar altimeter, and a prototype Texas Instruments Global Positioning System (GPS). The success of these initial tests encouraged further development of the AGMS. In 1984 pressure altimetry was added to extend the operation of the system to coastal and sea-ice covered regions. A test of the updated system performed over eastern North Carolina and the Outer Banks for the Defense Mapping Agency proved the feasibility of operation in this type of environment by achieving an rms error of 2.8 mgals. Subsequent to this we have flown 2 studies of the Antarctic margins for the National Science Foundation and on the eastern seaboard for the Naval Surface Weapons Center. More than 1000 flight hours experience in aerogravity have been acquired in course of this program.

Our most recent experiment is a joint effort with the National Geodetic Survey to incorporate dynamic GPS interferometry for three dimensional positioning. We are currently reducing the data from a set of flights over the Wallops Island gravity test range using this system. If successful, the current requirement for periodic absolute altitudes (radar altitude above surfaces of known height) may be eliminated or reduced. This would permit worldwide use of the system.

HISTORY OF NRL AIRBORNE GRAVITY PROGRAM

1979	PRELIMINARY DESIGN OF SYSTEM	
JUNE 1980	FIRST TEST OF EARLY PROTOTYPE OFF CALIFORNIA COAST LORAN C NAV RMS ≈ 20 MGALS	8 FLIGHTS
JUNE 1981	INCORPORATION OF GPS NAV & TEST OFF WALLOPS ISLAND, VA. RMS < 6 MGALS	2 FLIGHTS
DEC. 1983	PIGGY BACK GRAVITY ON AIRBORNE MAGNETICS STUDY EAST OF BRAZIL	12 FLIGHTS NO GROUND TRUTH
APRIL 1984	BLIND TEST OVER EASTERN N.C. FOR DMA INCORPORATION OF PRESSURE ALTIMETRY RMS 2.5 MGALS	4 FLIGHTS
MAY 1984	PIGGY BACK GRAVITY ON AIRBORNE STUDY OF THE ANGOLA BASIN	15 FLIGHTS DATA BEING REDUCED
FEB. 1986	NSF FUNDED STUDY OF THE ANTARCTIC MARGIN AIRBORNE GRAVITY OVER ICE	12 FLIGHTS
JUNE 1986	EASTERN SEABOARD TEST FOR NSWC RMS DIFFERENCE WITH NSWC SHIPBOARD DATA < 4 MGALS	6 FLIGHTS
FEB. 1987	NSF STUDY OF ANTARCTIC MARGIN AVERAGE MISS-TIE 2.2 MGALS	10 FLIGHTS
SEPT. 1987	NSWC INTERFEROMETRIC GPS TEST	5 FLIGHTS
OCT. 1987	NSF STUDY OF ANTARCTIC MARGIN	9 FLIGHTS

AIRBORNE GEOPHYSICAL SENSOR SUITE

INTEGRATED SET OF GEOPHYSICAL SENSORS AND PROCESSING TECHNIQUES FOR RAPID ASSESSMENT AND CHARTING OF LARGE OCEAN AREAS

- MAGNETICS
- GRAVITY
- ALTIMETRY
- NAVIGATION
- FULLY EXPANDABLE TO INCLUDE ADDITIONAL SENSORS OR NEW TECHNOLOGICAL ADVANCES

NAVIGATION POINT RELATIVE TO LOCAL VERTICAL

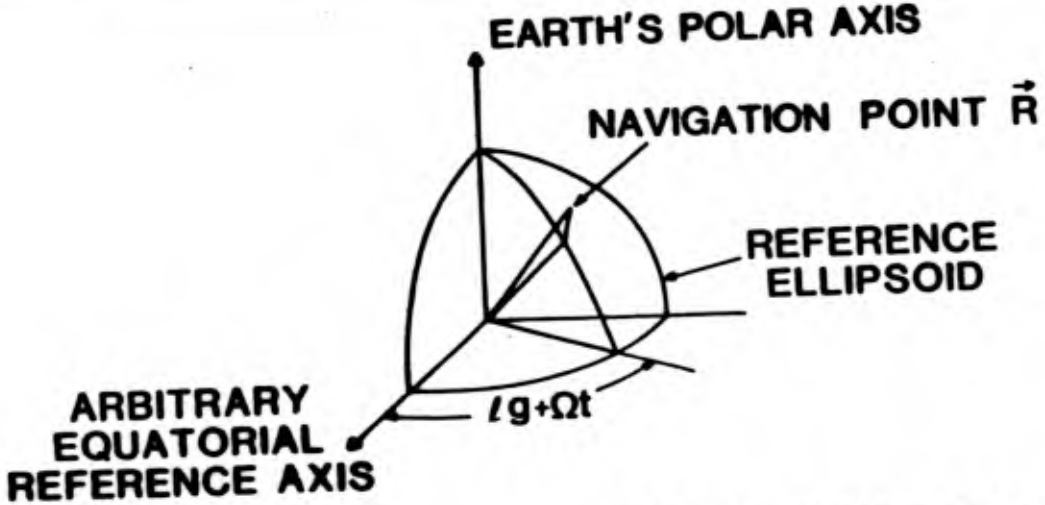

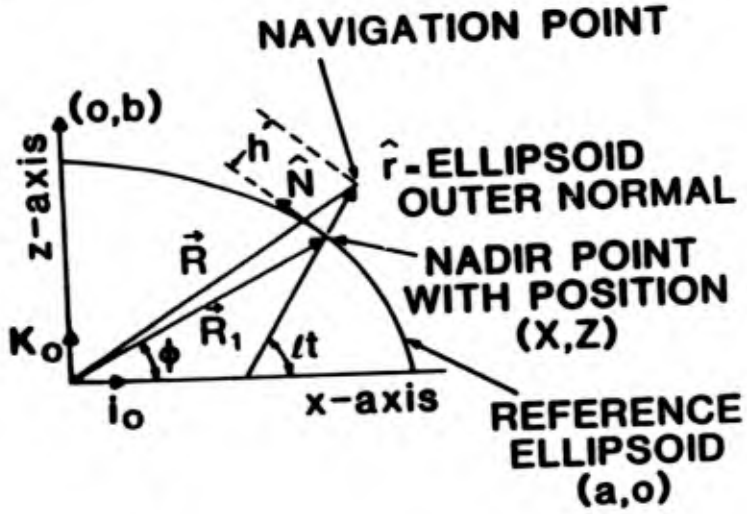

ℓt GEODETIC LATITUDE

ϕ GEOCENTRIC LATITUDE

MEASUREMENT PARAMETERS REQUIRED FOR AIRBORNE GRAVIMETRY

- **ACCELERATION**

  MEASURES GRAVITY FIELD AND VERTICAL ACCELERATION OF AIRCRAFT

- **ALTITUDE**

  MEASURES HEIGHT OR VERTICAL VELOCITY (DOPPLER) OF AIRCRAFT FOR CALCULATION OF VERTICAL ACCELERATION CORRECTION

- **NAVIGATION**

  DETERMINE POSITIONS OF AIRCRAFT FOR CALCULATION OF VELOCITY (EOTVOS) CORRECTION AND LATITUDE CORRECTION

MECHANIZATION EQUATIONS

$$\dot{V}_E = A_E + (\omega_r V_N - \omega_N V_r) - \Omega \dot{R}_X - \delta g_E$$

$$\dot{V}_N = A_N + (\omega_E V_r - \omega_r V_E) - \Omega \dot{\ell g} s\ell t R_X - \delta g_N$$

$$\dot{V}_r = A_r + (\omega_N V_E - \omega_E V_N) + \Omega \dot{\ell g} c\ell t R_X - \delta g_r - \gamma(n)$$

WHERE

- $$\dot{\ell t} = \left[\frac{V_N}{a\sqrt{1-e^2 s^2 \ell t}+h}\right]\left\{1 - \frac{ae^2\left[\cos 2\ell t + \frac{e^2 s^2 \ell t}{4(1-e^2 s^2 \ell t)}\right]}{a(1-e^2 s^2 \ell t)+h\sqrt{1-e^2 s^2 \ell t}}\right\}^{-1}$$

- $$\dot{\ell g} = \frac{V_E}{\left[\frac{a}{\sqrt{1-e^2 s^2 \ell t}}+h\right]\cos \ell t}$$

- $$\dot{R}_X = \dot{h} c\ell t - \left\{h + \frac{a}{\sqrt{1-e^2 s^2 \ell t}}\left[1 - \frac{e^2 c^2 \ell t}{(1-e^2 s^2 \ell t)}\right]\right\} s\ell t \dot{\ell t}$$

- $$R_X = \left[\frac{a}{\sqrt{1+e^2 s^2 \ell t}}+h\right] c\ell t$$

- $$\gamma(h) = 978.049\left[1 + 0.0052884 \sin^2 \ell t - 0.0000059 \sin^2 2\ell t\right]\left[1 - \frac{2h}{a}(1+f+m-2f\sin^2 \ell t) + \frac{3h^2}{a^2}\right]$$

- $$\dot{h} = V_r$$
- $$\omega_N = (\dot{\ell g} + \Omega) c\ell t$$
- $$\omega_E = -\dot{\ell t}$$
- $$\omega_r = (\dot{\ell g} + \Omega) s\ell t$$

EQUIPMENT AND DATA

LACOSTE-ROMBERG AIR/ SEA GRAVITY METER S-93	3-AXIS STABILIZED PLATFORM	< 1 MGAL	2-20 HZ
NRL RADAR ALTIMETER	ALTITUDE ABOVE WATER	2-5 CM	10 KHZ
ROSEMOUNT 1201 PRESSURE TRANSDUCER	PRESSURE ALTITUDE BOOM MOUNTED	≈ 50 CM	20 HZ
TI-HDUE GLOBAL POSITIONING SYSTEM	POSITIONS & VELOCITIES ≈ 14M SEP	.15 M/SEC	2 HZ
LITTON-72 INERTIAL NAV SYSTEM	INTERFACED WITH AUTOPILOT		
HEWLITT-PACKARD 1000 COMPUTER SYSTEM	ANALOG TO DIGITAL CONVERSION DATA ACQUISITION AND MONITORING		

GRAVIMETERS

LACOSTE-ROMBERG	BELL
1mGAL (APPROXIMATE DYNAMIC ACCURACY)	1 mGAL (APPROXIMATE DYNAMIC ACCURACY)
GOOD DC & LOW FREQUENCY DRIFT	GOOD DC & LOW FREQUENCY DRIFT
LIMITED DYNAMIC RANGE FOR LOW FREQUENCY - HIGH AMPLITUDE ACCELERATIONS	LIMITED DYNAMIC RANGE FOR ALL FREQUENCIES
EXCELLENT HIGH FREQUENCY - HIGH AMPLITUDE CHARACTERISTICS	
GOOD STABILIZED PLATFORM FOR AIRCRAFT	STABILIZED PLATFORM MUST BE MODIFIED FOR AIRBORNE USE
TOLERANT OF TEMPERATURE CYCLING	INTOLERANT OF TEMPERATURE CYCLING

AIRBORNE GRAVIMETRY ERROR SOURCES

GRAVIMETER ERRORS

- INSTRUMENTAL
- ALIGNMENT AND MOUNTING

ALTIMETRY ERRORS

- GEOIDAL UNDULATIONS
- ALTIMETRY ABOVE GEOID

NAVIGATION ERRORS

- VELOCITY
- AZIMUTH
- POSITION

ERRORS DUE TO FILTERING

- ANALOG
- DIGITAL

HUMAN ERRORS

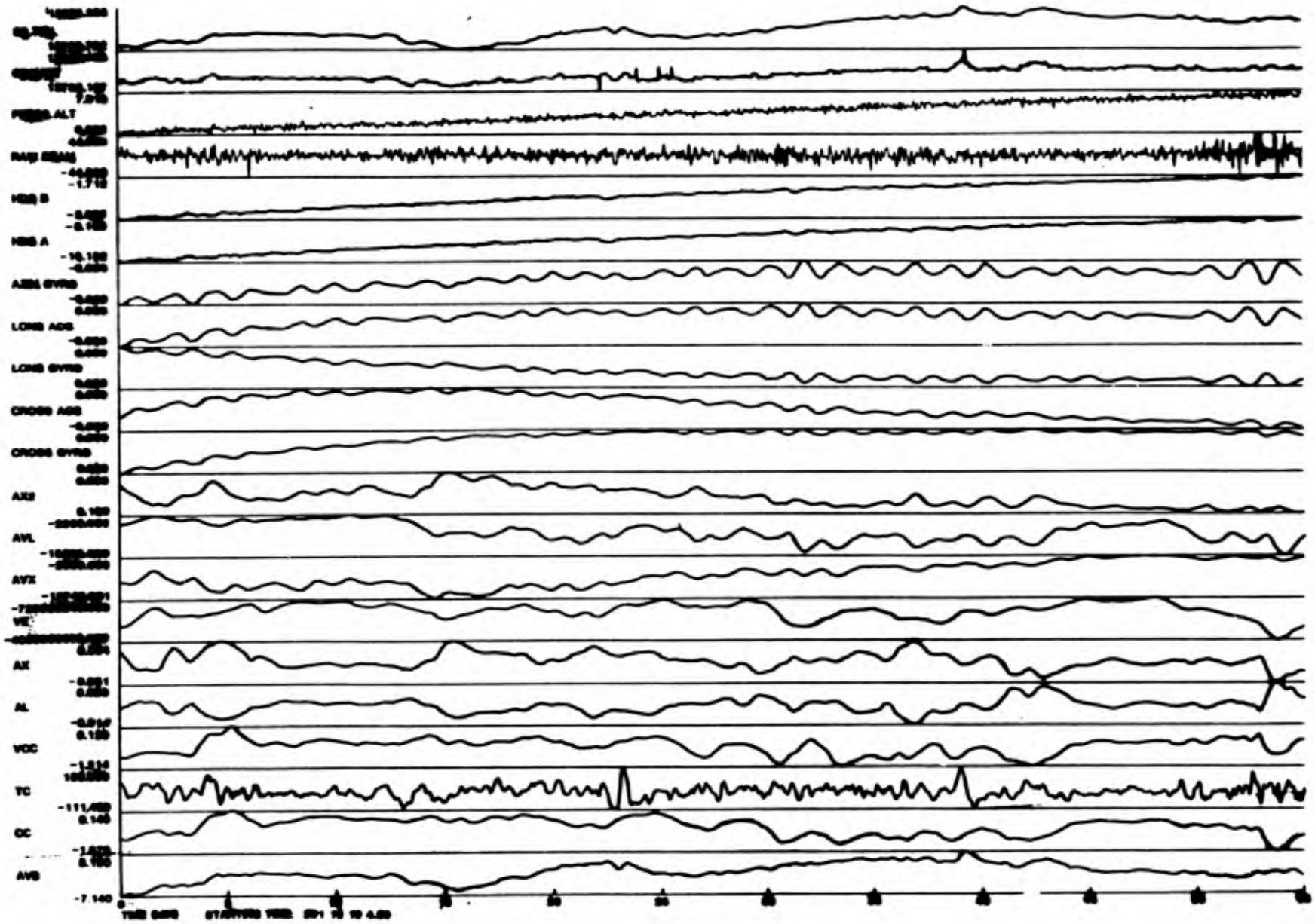
RAD ABAR
HDG B
HDG A
AXIS GYRO
LONG ACC
LONG GYRO
CROSS ACC
CROSS GYRO
AXII
AVL
AVX
VE
AX
AL
VCC
TC
CC
AVB

ALTIMETERS

SENSOR	RESOLUTION	REMARKS
SHORT PULSE (1-2 NS) NRL RADAR	< 2CM	• 40M SQUARE FOOTPRINT AT 600M • MEASUREMENT IS FROM AC TO SURFACE • ALL WX • RANGE = 1 - 10,000M
LASER PROFILER	< 2CM	• FOOTPRINT < $1M^2$ • REQUIRES STABILIZATION OR GEOMETRIC CORRECTION • MEASUREMENT IS FROM AC TO SURFACE • CLEAR WX • RANGE = 1 - 600M
PRESSURE TRANSDUCER	≈50CM	• ISOBARIC SURFACES NOT NECESSARILY PARALLEL TO GEOID • REQUIRES SPECIAL MOUNTING
GPS INTERFEROMETRY	≈10CM	• MEASUREMENT IS ΔX, ΔY, ΔZ FROM BASE STATION - NOT TIED TO ANY SURFACE • SAME 4 SATELLITES MUST BE VISIBLE TO BASE AND MOBILE UNITS

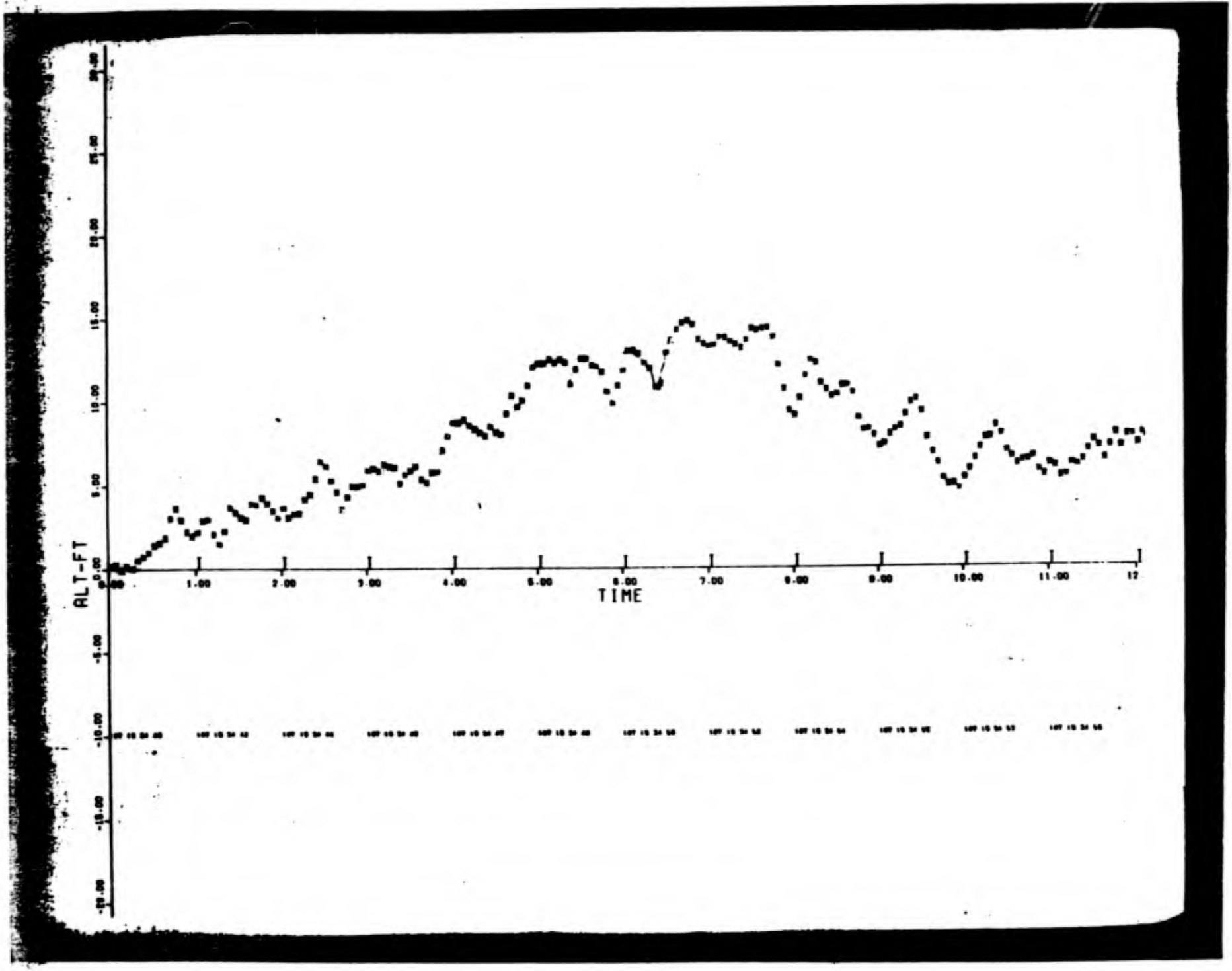
ALT-FT
TIME

POWER SPECTRUM OF RADAR ALTIMETER

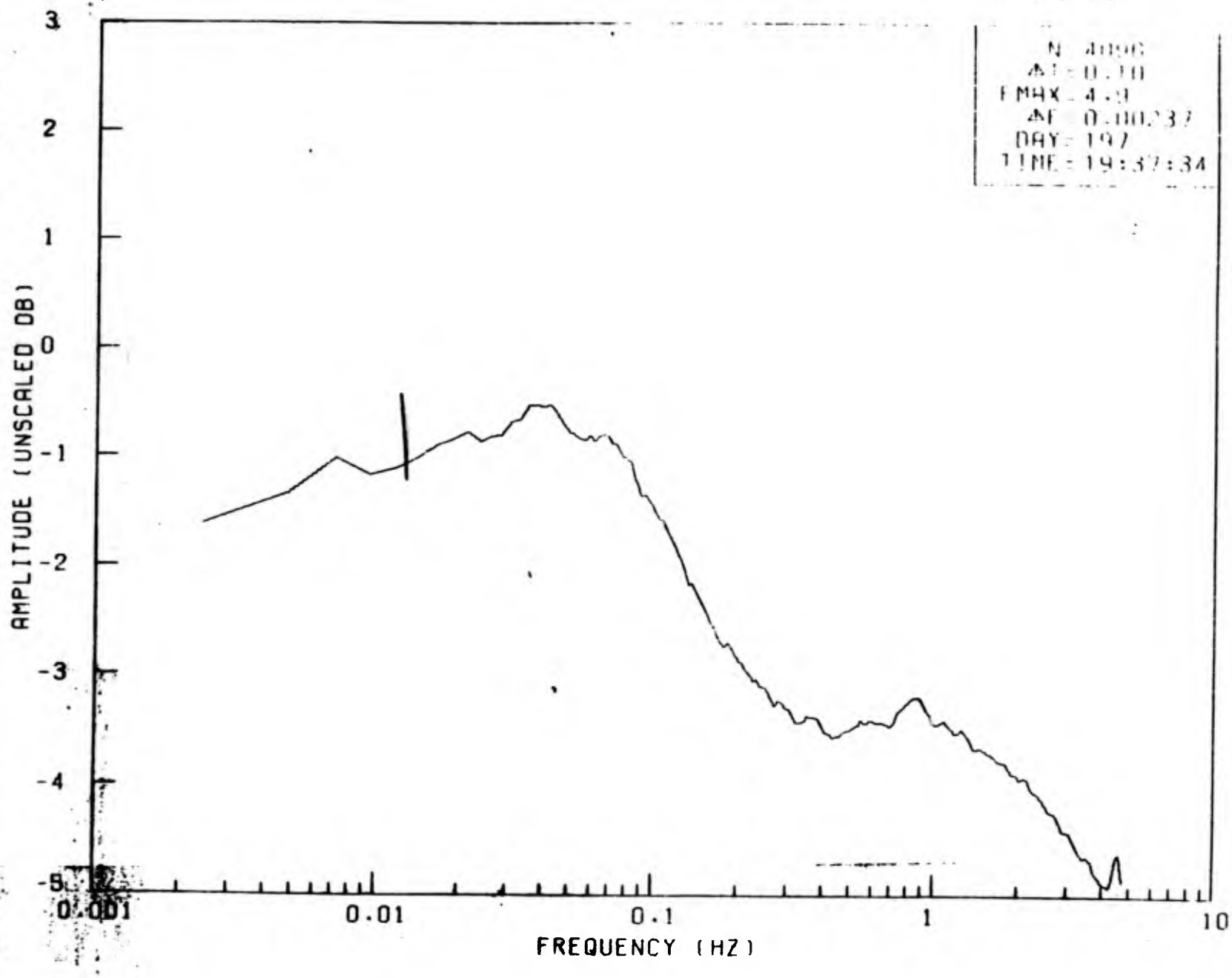

DMA ERROR ANALYSIS

12/86

NORTH CAROLINA DATA

GSR

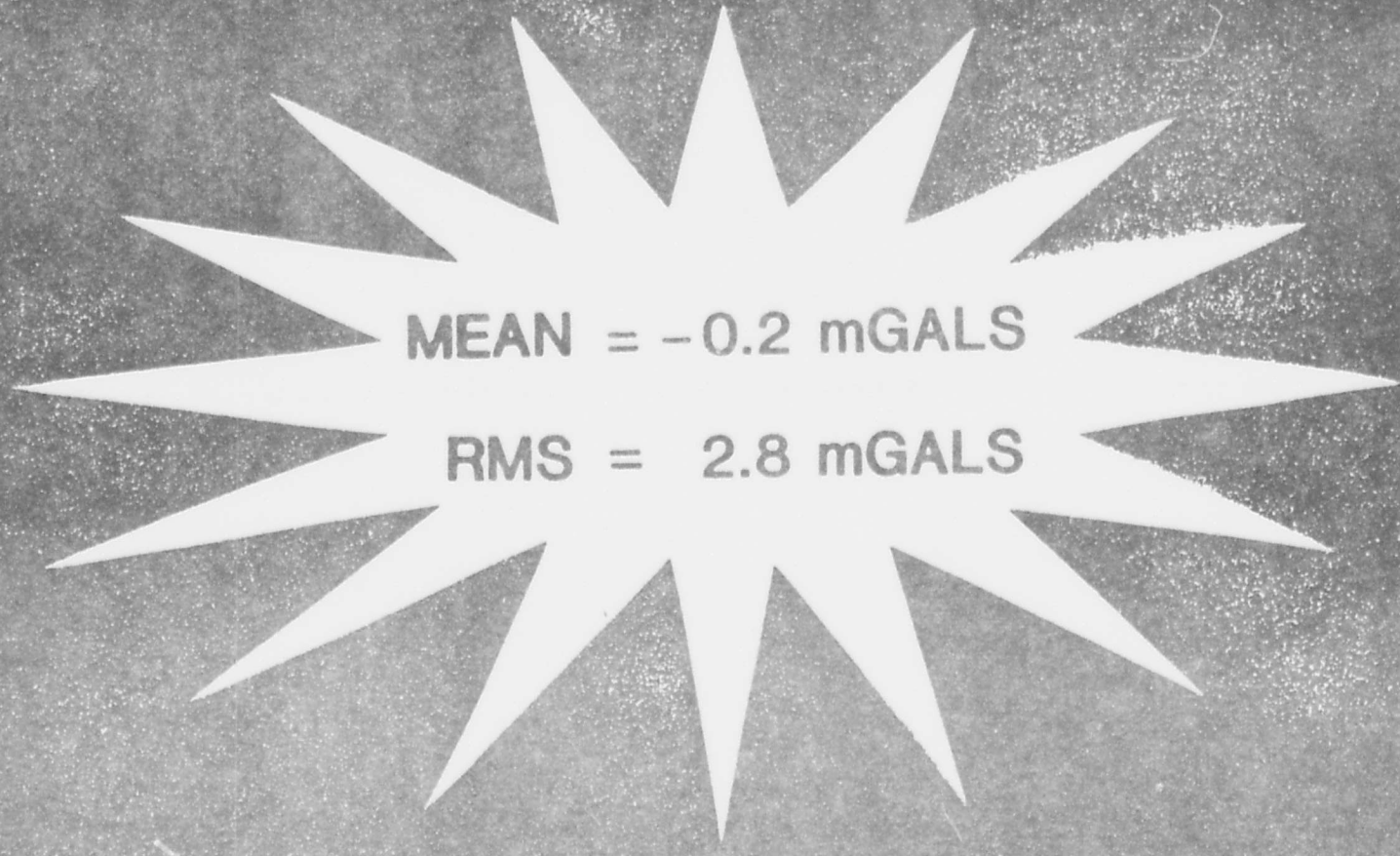

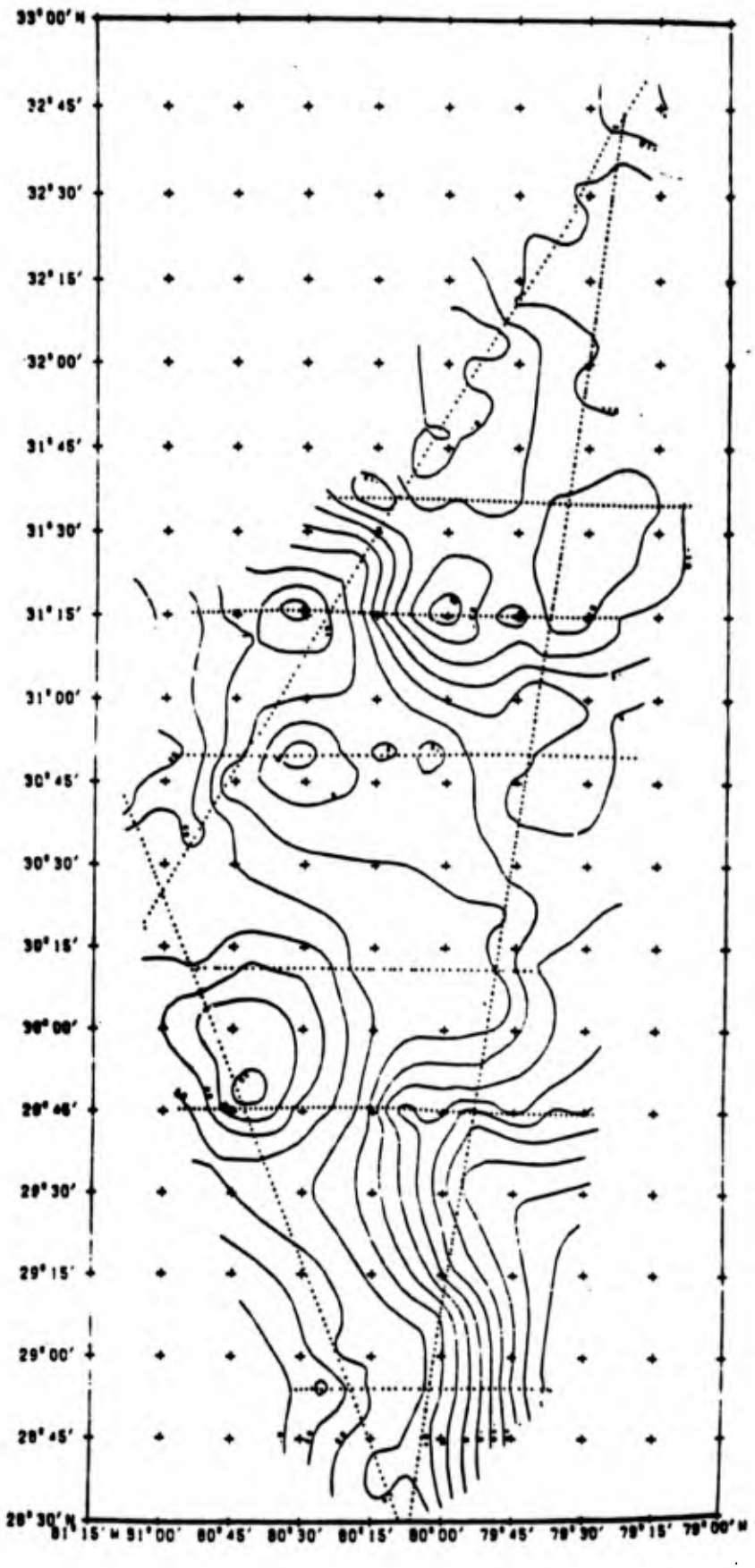
33°00' N
32°45'
32°30'
32°15'
32°00'
31°45'
31°30'
31°15'
31°00'
30°45'
30°30'
30°15'
30°00'
29°45'
29°30'
29°15'
29°00'
28°45'
28°30' N
81°15' W
81°00'
80°45'
80°30'
80°15'
80°00'
79°45'
79°30'
79°15'
79°00' W

EFFECT OF FILTERING ON ANOMALY AMPLITUDE

ANOMALY AMPLITUDE	MINIMUM SPEED (335 km/hr)	MAXIMUM RANGE (465 km/hr)
%	km	km
97	33	46
95	28	39
90	19	27
80	13	18
70	11	15
60	8	11
50	7	10
25	5	7

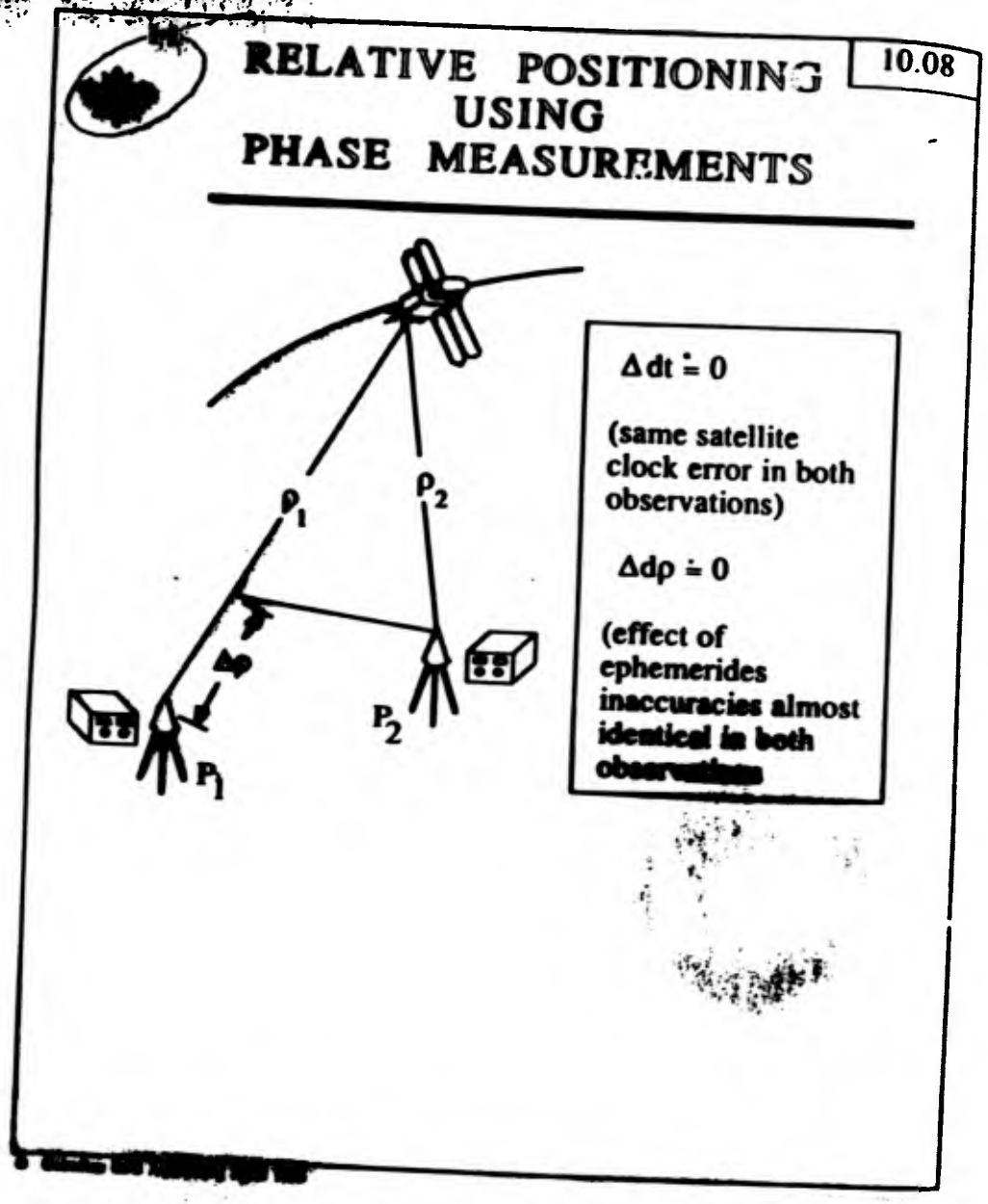

Figure 10.8 from Guide to GPS Positioning, prepared under leadership of David Wells, by Beutler Bock, et al., entitled "Solutions." Copyright 1986 Canadian GPS Associates, used by permission.

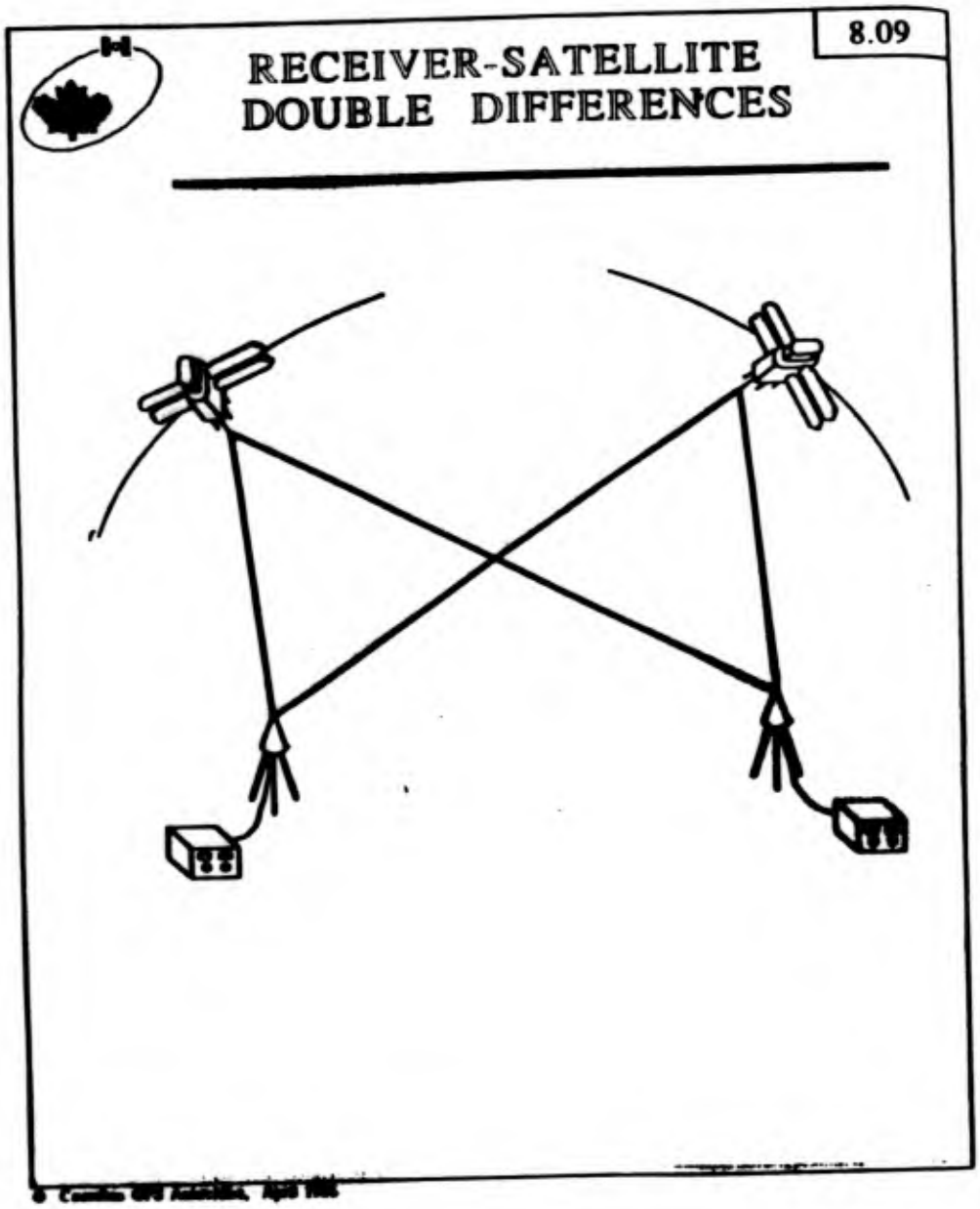

Figure 8.9 from Guide to GPS Positioning, prepared under leadership of David Wells, by Norman Beck, et al., entitled "Observation Equations," Copyright 1986 Canadian GPS Associates, used by permission.

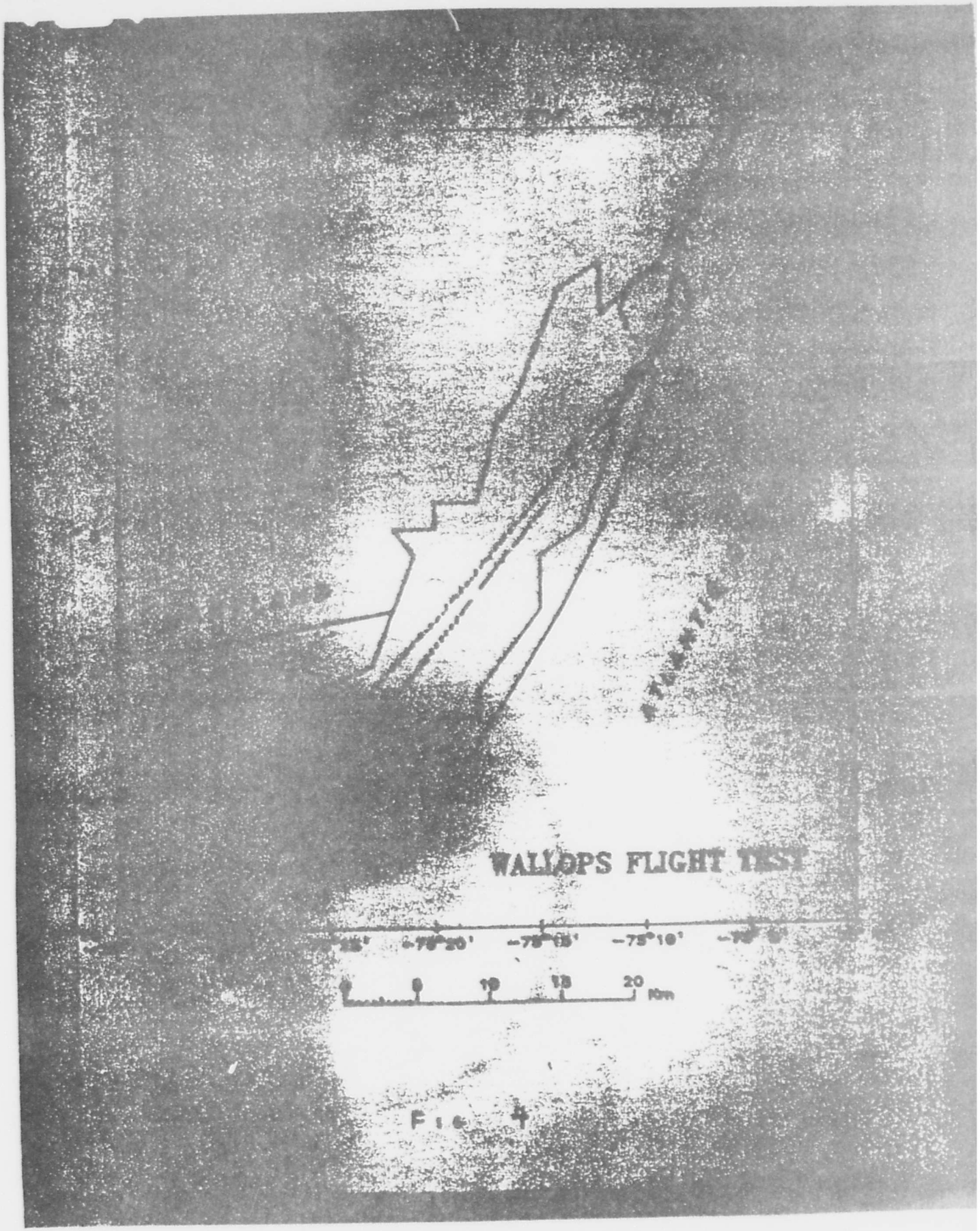

Fig. 4

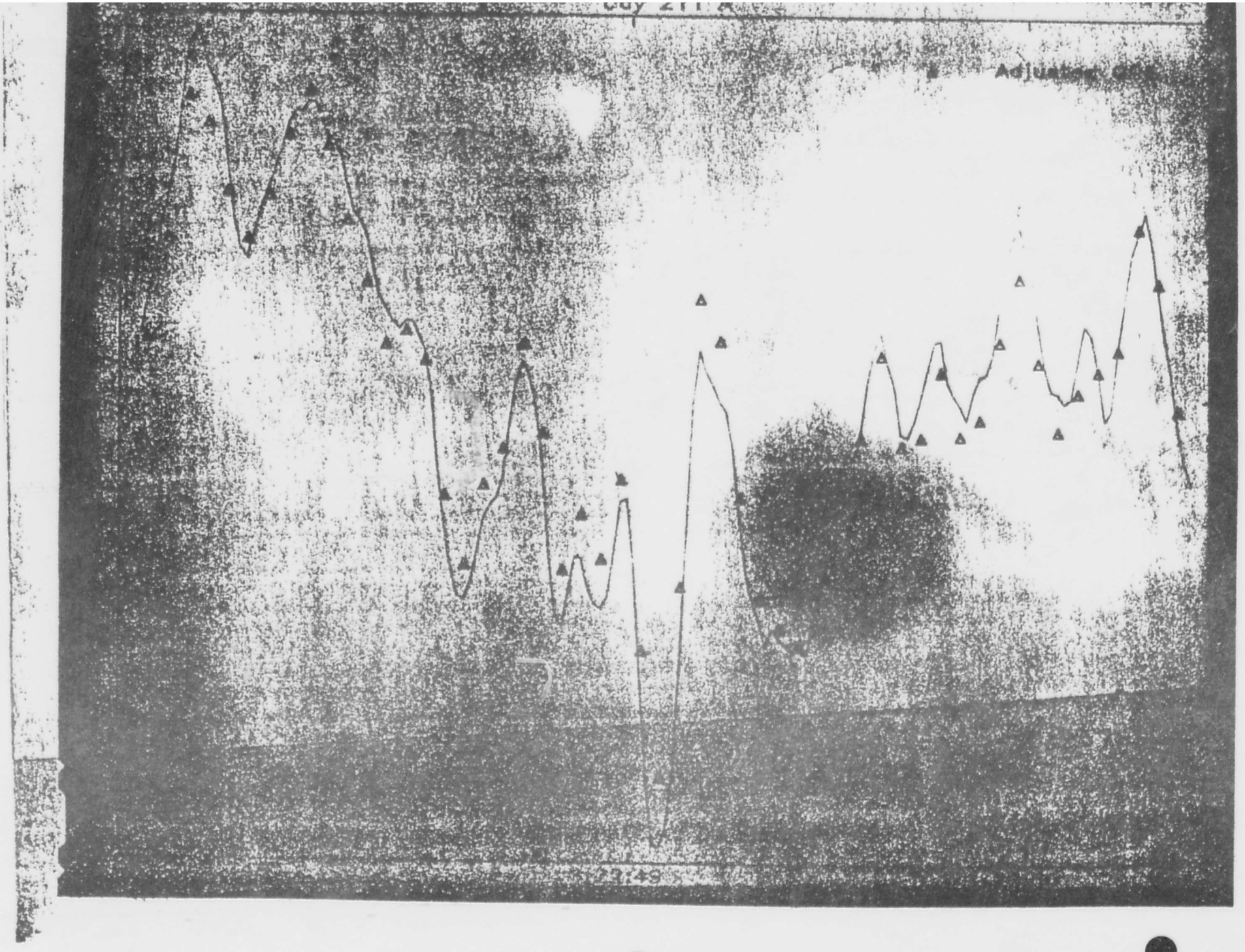

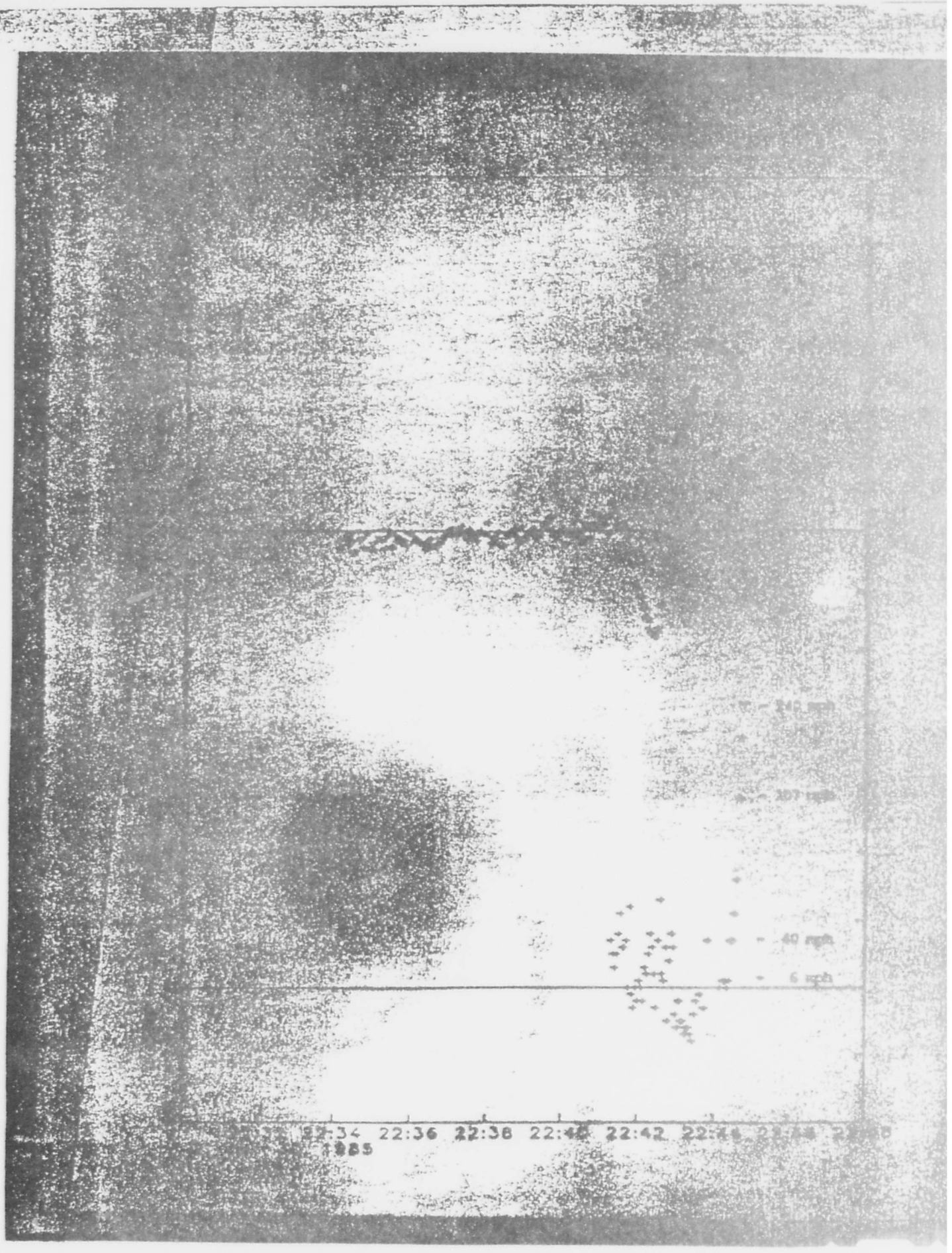
22:34
22:36
22:38
22:42
1985

COMPARISON OF AIRBORNE GRAVITY MEASUREMENT SYSTEMS

GRAVIMETRY

- GOOD LOW FREQUENCY RESPONSE
- INSENSITIVE TO REDISTRIBUTION OF MASS IN AIRCRAFT
- VERY SENSITIVE TO ERRORS IN NAVIGATION AND ALTIMETRY
- RELATIVELY LOW COST SYSTEM

GRAVITY GRADIOMETRY

- GOOD HIGH FREQUENCY RESPONSE
- VERY INSENSITIVE TO REDISTRIBUTION OF MASS ON AIRCRAFT
- RELATIVELY INSENSITIVE TO ERRORS IN NAVIGATION AND ALTIMETRY
- HIGH COST SYSTEM

ESTIMATED SYSTEM DEVELOPMENT COSTS TO PRESENT DATE

	NRL	DMA	AFGL	NSWC	NAVO	NSF
• HARDWARE						
1) L & R GRAVITY METER	155	74				
2) RADAR ALTIMETER	250					40
3) DATA ACQUISITION SYSTEM	200					50
• ENGINEERING DEVELOPMENT	250	25				50
• SOFTWARE DEVELOPMENT	250		35			50
• DOCUMENTATION	100				150	
• TESTING AND EVALUATION	250	30		135	50	50
• AIRCRAFT HOURS	600					
	2,055K	129K	35K	135K	200K	240K

16th GRAVITY GRADIOMETRY CONFERENCE
10-11 FEBRUARY 1988

SPONSORED BY:
AIR FORCE GEOPHYSICS LABORATORY
EARTH SCIENCES DIVISION

TITLE OF PAPER: The Airborne Gravity Measurement Program at NRL

SPEAKER: John Brozena

QUESTIONS AND COMMENTS:

1. Question: B. Louis Decker

   What did you say about the accuracy of the airborne gravity data collected in Antarctica?

   Response:

   The gravity values at profile intersection points were compared. The rms difference from this comparison was $\pm$ 2.2 milligals for gravity field wavelengths longer than 10 km. The true accuracy of the airborne gravity data in Antarctica is, of course, unknown since there is no truth gravity data in that area at this time.

A DETECTION OF NON-NEWTONIAN GRAVITY

by

Anestis J. Romaides
Christopher Jekeli

Earth Sciences Division
Air Force Geophysics Laboratory
Hanscom AFB, MA 01731

An experiment was performed to test Newton's inverse-square law of gravitation. The test compared accurately measured gravity values along a 600 m tower with upward continued gravity estimates calculated from ground measurements using algorithms based on Newtonian potential theory. The tower is the WTVD-TV tower in Garner, North Carolina, with an accessible height of 562 m. A number of sets of gravimetric measurements were made on the tower at intervals of about 90 m using a LaCoste-Romberg Model G gravimeter. The measurement sets have an internal consistency of better than 20 microgal (1 microgal = 10^{-8} m/s^2). The heights of the gravimeter were determined to about 1 cm by using a conventional electronic distance measuring device. Field measurements of gravity and corresponding geodetic positions were performed at 77 points within a radius of 5 km from the tower. These and other gravimetric data within a radius of about 220 km were used to perform the upward continuation using two independent computational techniques. Taking into account such effects as the gravitational attraction of the air surrounding the tower and the attraction of the sun, moon, and tidally deformed earth, this upward continuation is estimated to have an uncertainty comparable to the in situ measurements. Effects such the mass attraction of the tower itself and the actual variations in the water table are insignificant relative to this uncertainty. The gravity measurements along the tower and on the ground were corrected for the proper scale factor of the instrument. Other effects, such as the sway of the tower, changes in atmospheric pressure, and magnetic and RF effects were determined also to be insignificant. The results of the experiment show a substantial departure from the inverse-square law, asymptotically approaching about 500 microgals at the top of the tower, with a standard deviation of better than 40 microgals. This indicates that there is a non-Newtonian attractive force which falls off rapidly with elevation.

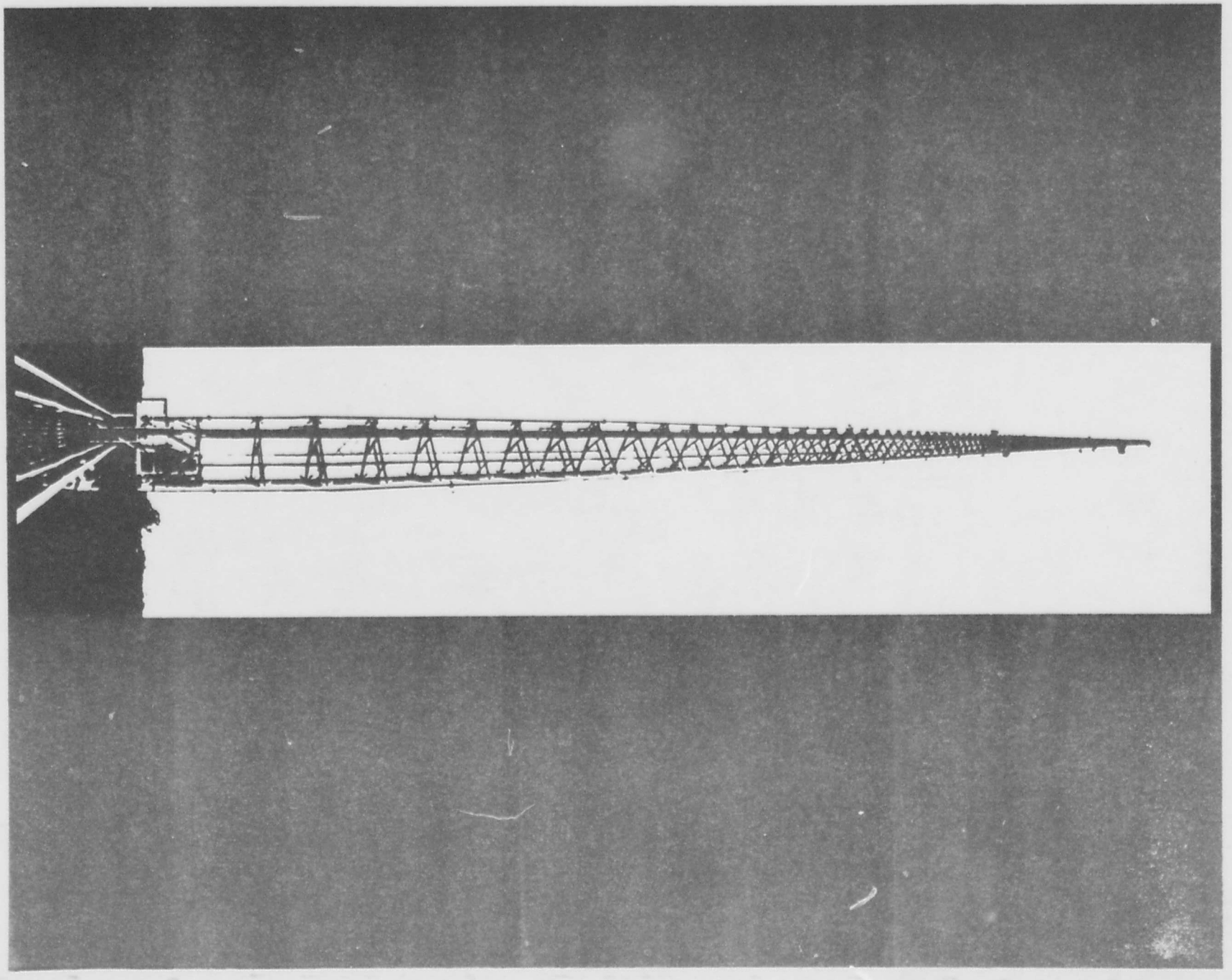

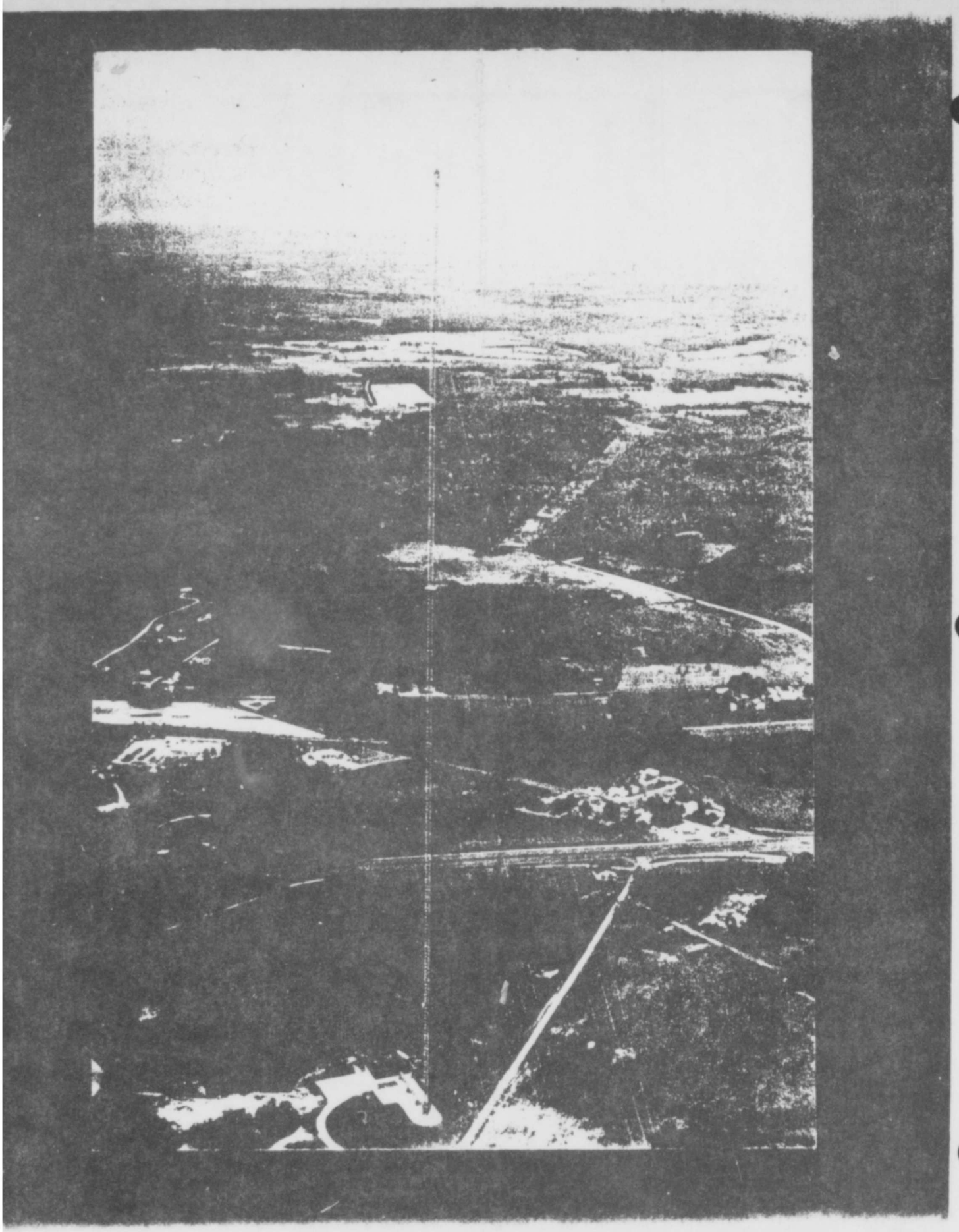

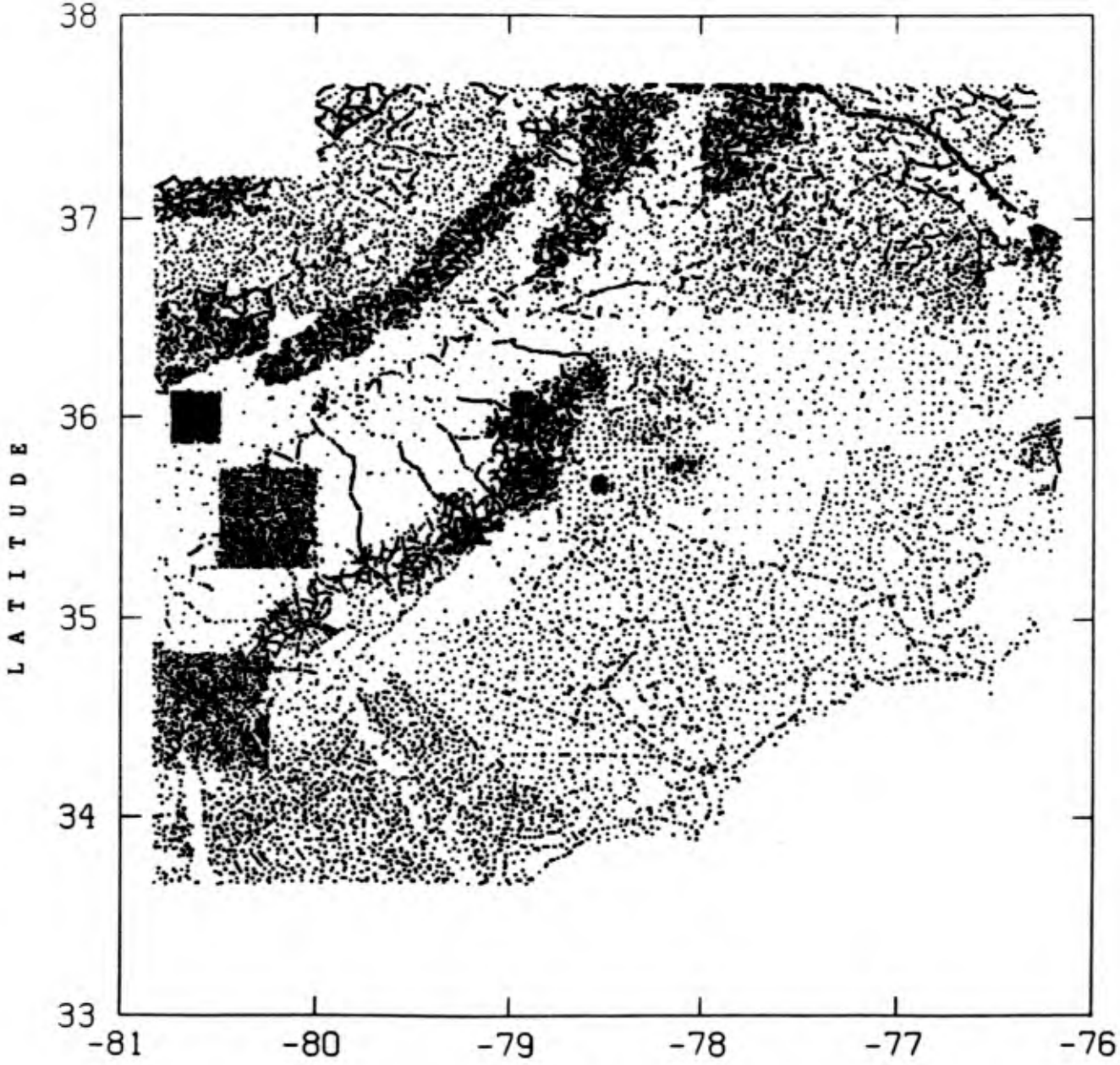

REGIONAL

GRAVITY DATA BASE

AVAILABLE FOR

UPWARD CONTINUATION

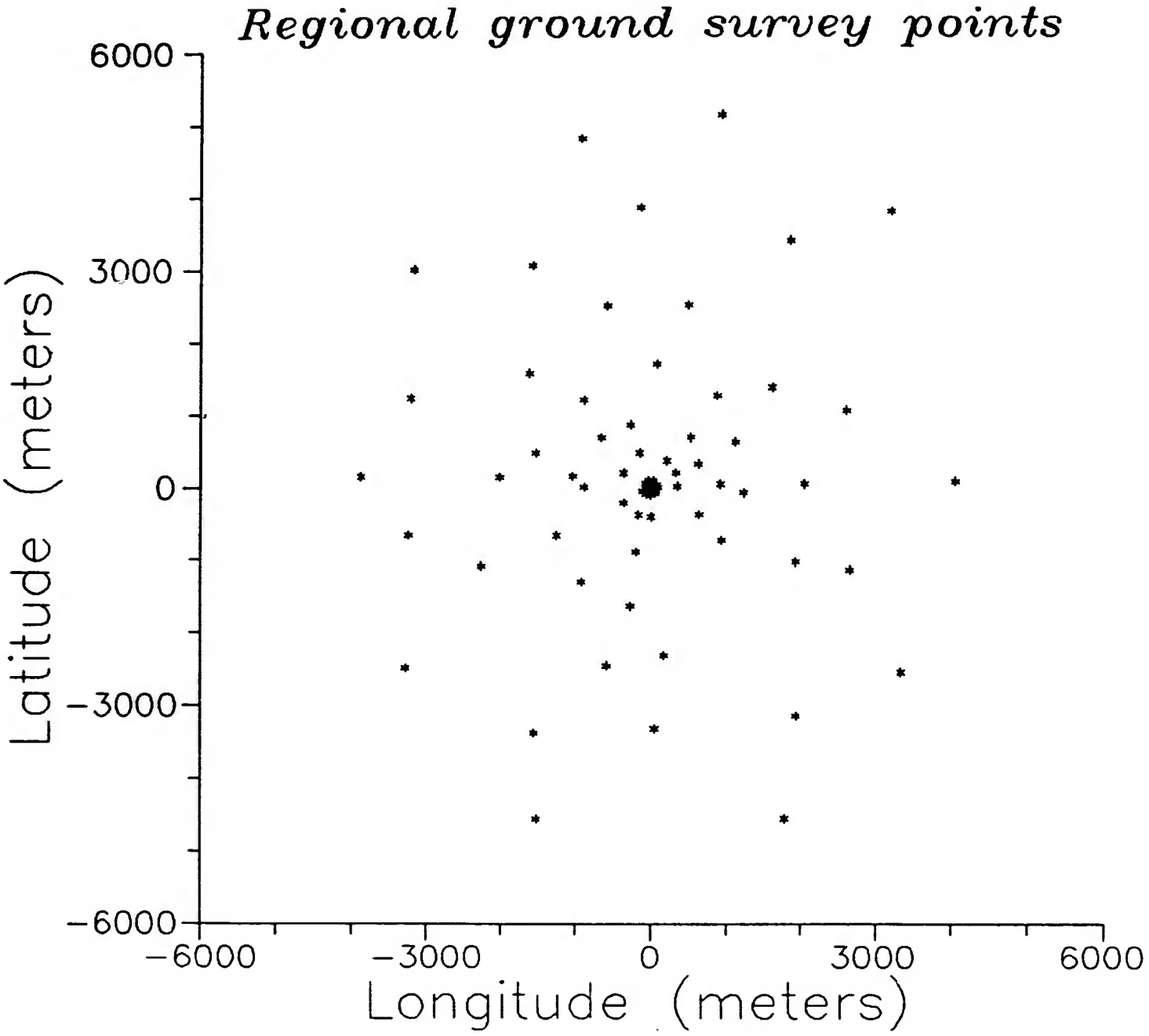
Regional ground survey points
6000
3000
0
−3000
−6000
Latitude (meters)
−6000
−3000
0
3000
6000
Longitude (meters)

PROCESS TO UPWARD-CONTINUE GRAVITY

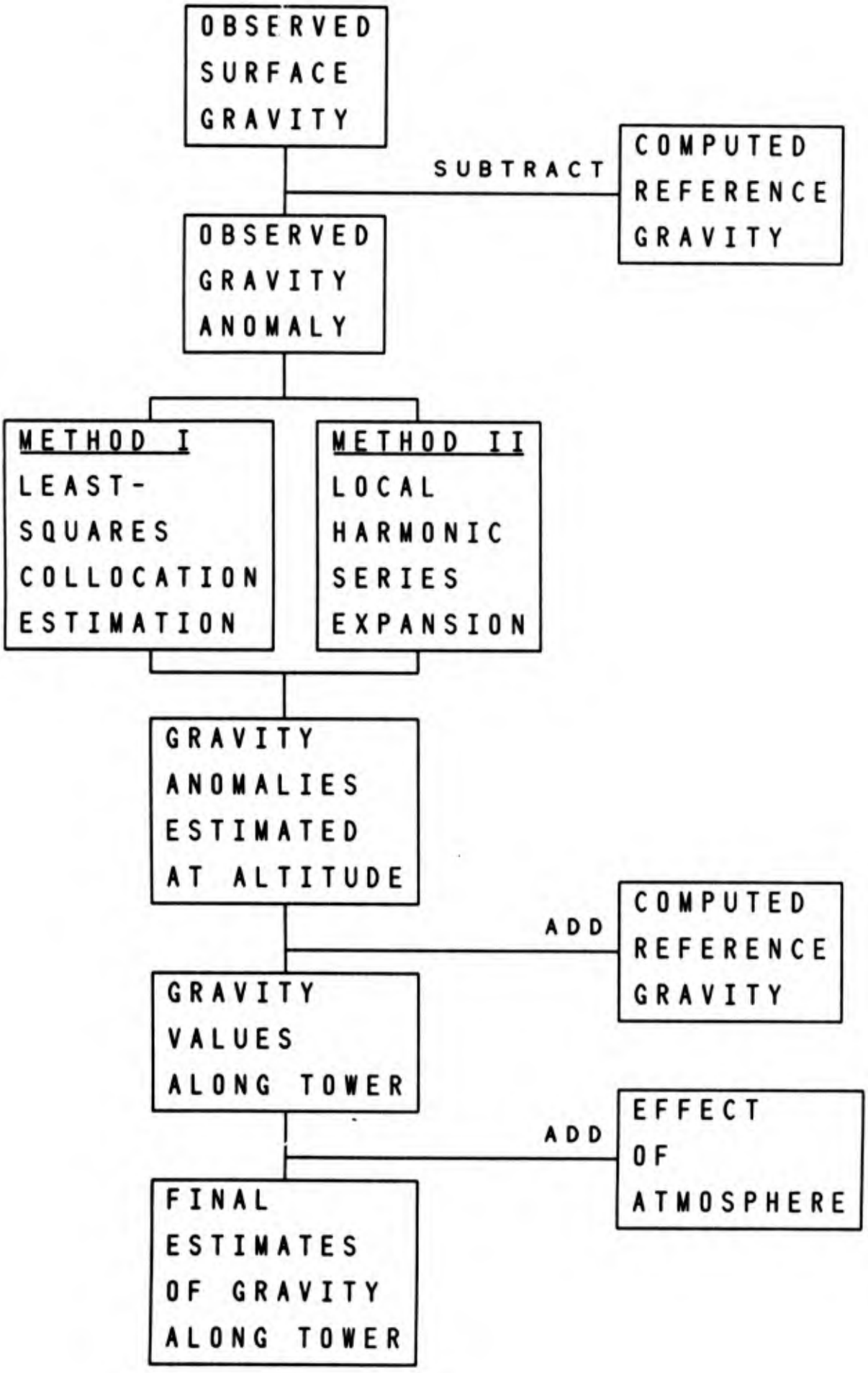

ERROR SOURCE	ERROR (μgal)
GRAVITY MEASUREMENT ERROR (INTERNAL CONSISTENCY)	varies (~ 10 - 20)
INSTRUMENT RANDOM ERROR	7
TABLE-OF-DIAL-FACTOR ERRORS (RANDOM)	5
SCALE FACTOR CORRECTION ERROR (RANDOM)	≤16
SCREW ERROR (RANDOM)	10
DRIFT CORRECTION ERROR (RANDOM)	7
TIDE CORRECTION ERROR (RANDOM)	5
BASE STATION ERROR (BIAS)	10
WATER TABLE ERROR (BIAS)*	~6
RELATIVE ELEVATION MEASUREMENT ERROR (RANDOM)	6
RELATIVE HORIZONTAL POSITION ERROR (RANDOM)	4
ATMOSPHERIC CORRECTION ERROR (RANDOM)*	2
MASS OF TOWER (BIAS)**	~3
TOWER SWAY (BIAS)**	<10
RADIO FREQUENCY INTERFERENCE**	NEGLIGIBLE (?)
OUTER ZONE GRAVITY ANOMALY ERRORS (RANDOM)*	100 - 1000 (GENERALLY)

* - DOES NOT APPLY TO TOWER MEASUREMENTS
** - DOES NOT APPLY TO GROUND MEASUREMENTS

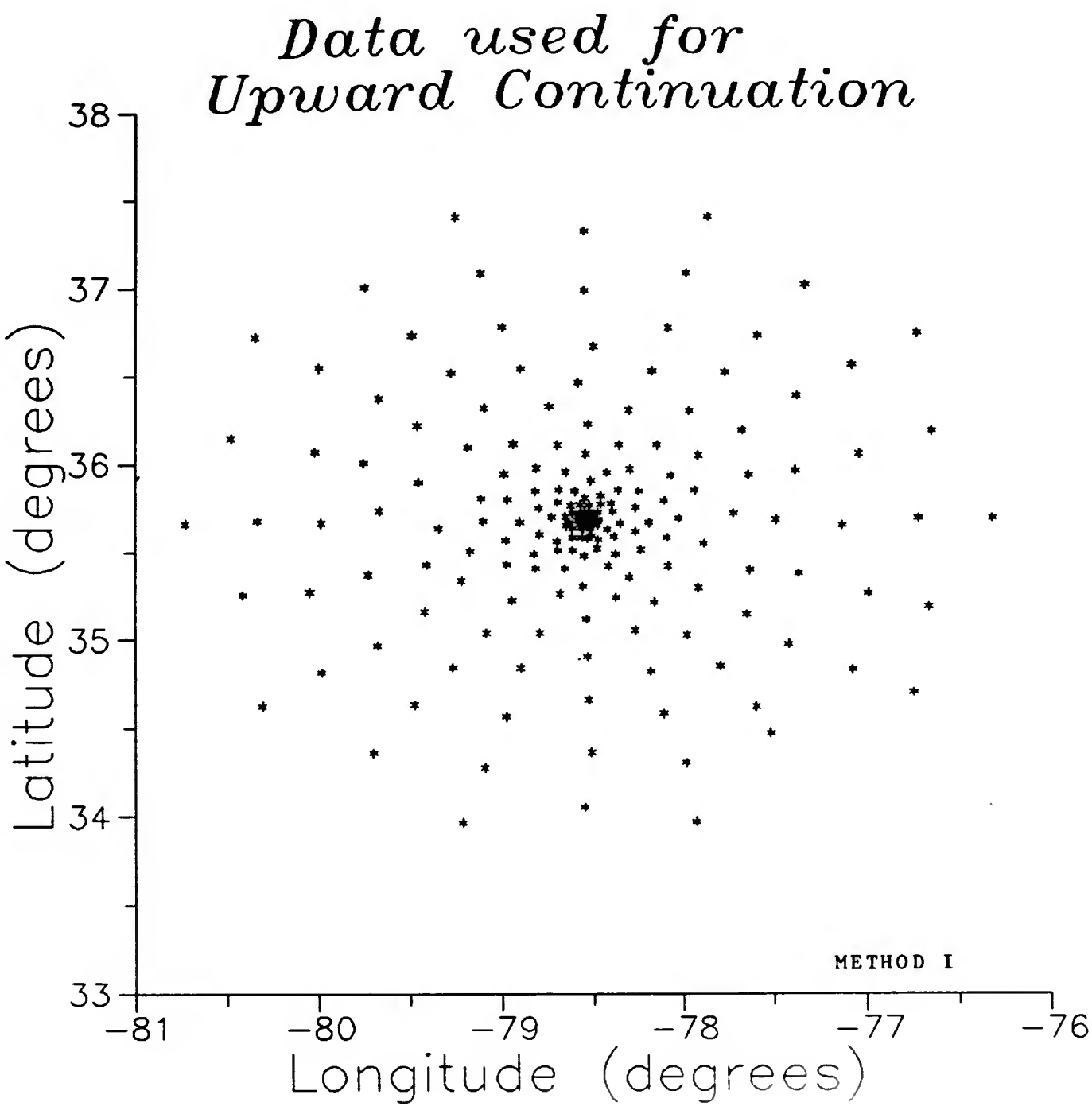
Data used for
Upward Continuation
38
37
36
35
34
33
Latitude (degrees)
−81
−80
−79
−78
−77
−76
Longitude (degrees)
METHOD I

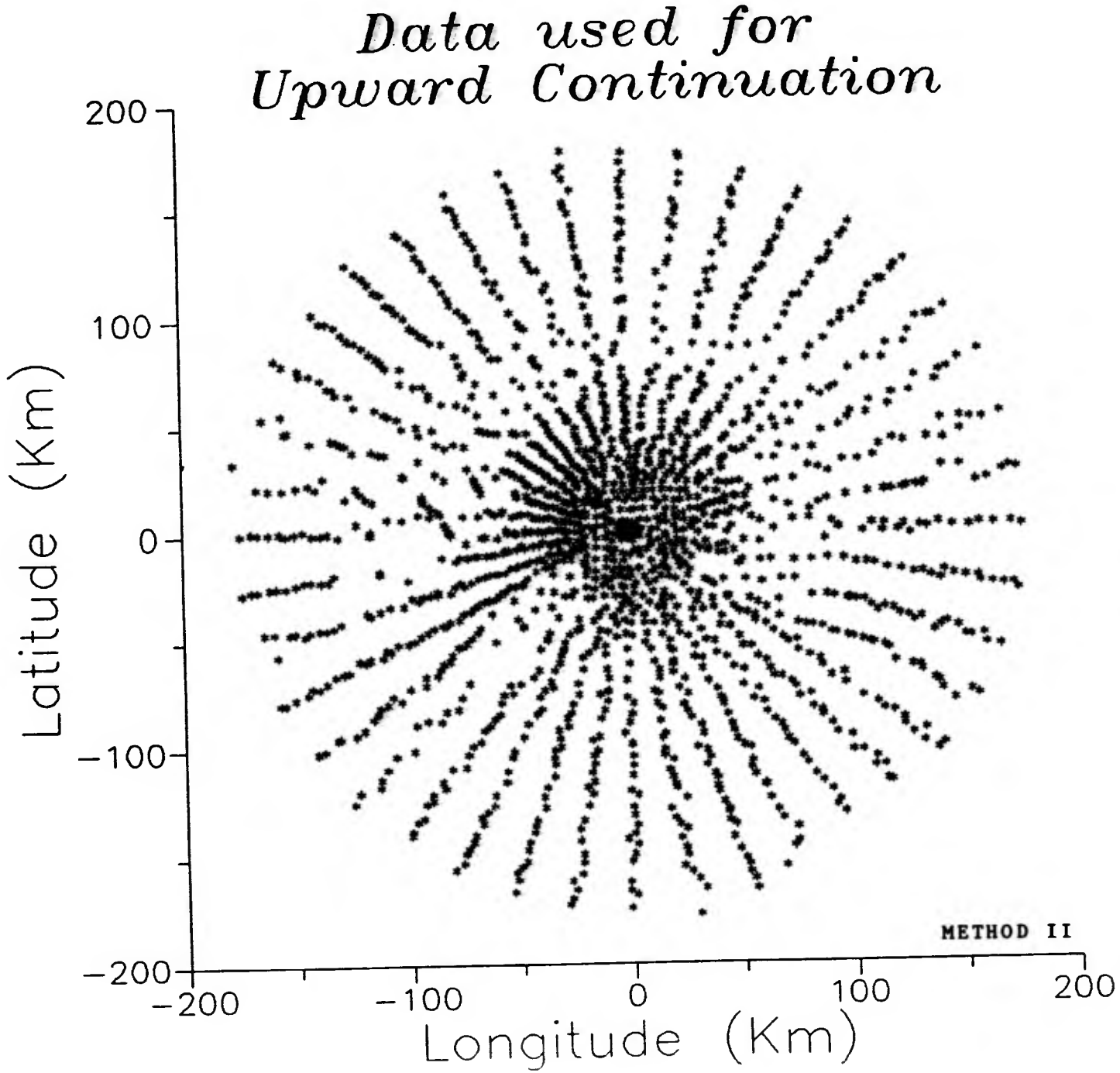
Data used for
Upward Continuation
200
100
0
−100
−200
Latitude (Km)
−200
−100
0
100
200
Longitude (Km)
METHOD II

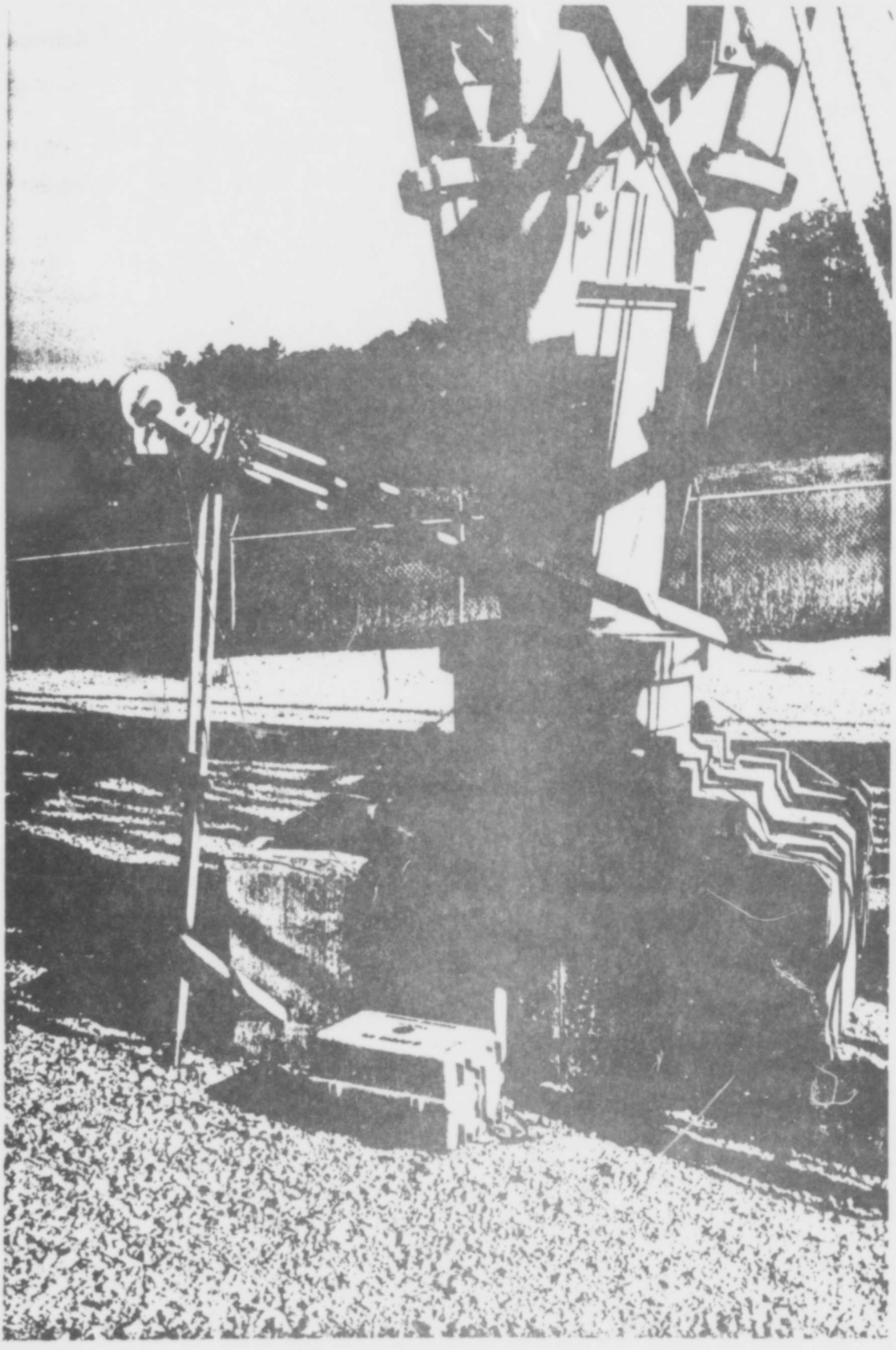

ELEVATIONS FROM ELECTRONIC DISTANCE MEASURING DEVICE ALONG THE TOWER

DATE	TIME	ELEVATION
30 JUL	1115	305.830
30 JUL	1402	305.830
03 AUG	0937	305.805
03 AUG	1038	305.800
05 AUG	1236	305.830
05 AUG	1504	305.835
16 AUG	1151	305.800
16 AUG	1217	305.800

DATE	TIME	ELEVATION
30 JUL	1243	1843.080
05 AUG	1404	1843.195
07 AUG	1536	1842.995
07 AUG	1602	1843.005
07 AUG	1732	1843.005
16 AUG	1326	1843.050
21 SEP	1330	1843.080
21 SEP	1344	1843.100
21 SEP	1413	1843.120

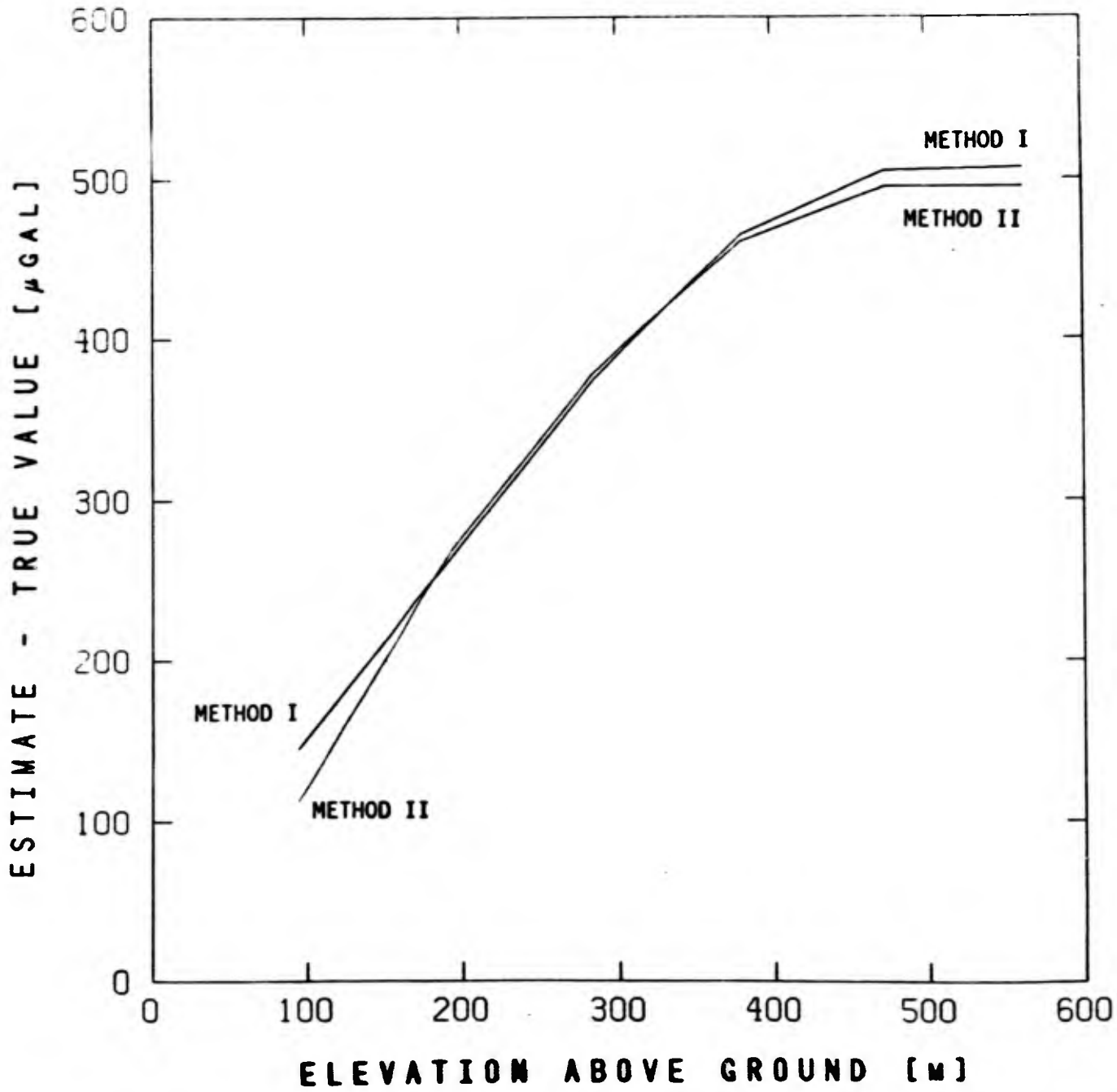
600
500
400
300
200
100
0
0
100
200
300
400
500
600
METHOD I
METHOD II
METHOD I
METHOD II
ESTIMATE - TRUE VALUE [μGAL]
ELEVATION ABOVE GROUND [m]

RESULTS OF TOWER GRAVITY EXPERIMENT

	True Value		Upward Continuation Estimates				Difference Between True Value and Estimates			
Height [m] †	Measurement	Error	Method I	Error *	Method II	Error	Method I - True	Error *	Method II - True	Error
93.90	979711208	22	979711353	19	979711321	50	145	29	113	55
192.14	979681067	24	979681331	24	979681335	43	264	34	268	49
283.56	979653048	26	979653423	23	979653427	37	375	35	379	45
379.51	979623666	24	979624131	22	979624127	31	465	33	461	39
473.21	979595017	26	979595522	21	979595512	26	505	33	495	37
562.24	979567824	27	979568331	21	979568319	22	507	34	495	35

All values (except column 1) in microgal (1 μgal = 10^{-8} m/s^2)

† Height above ground

* Formal standard deviation

Position of Tower:
Elevation above MSL: 96.96 m
Latitude: 35° 40' 06".1
Longitude (east): -78° 31' 58".9

$$V(r) = \frac{-GM}{r}\left[1 + \alpha_0 e^{-r/\lambda_0} - \alpha_1 e^{-r/\lambda_1}\right]$$

2-TERM YUKAWA MODEL FIT TO OBSERVED DISCREPANCY

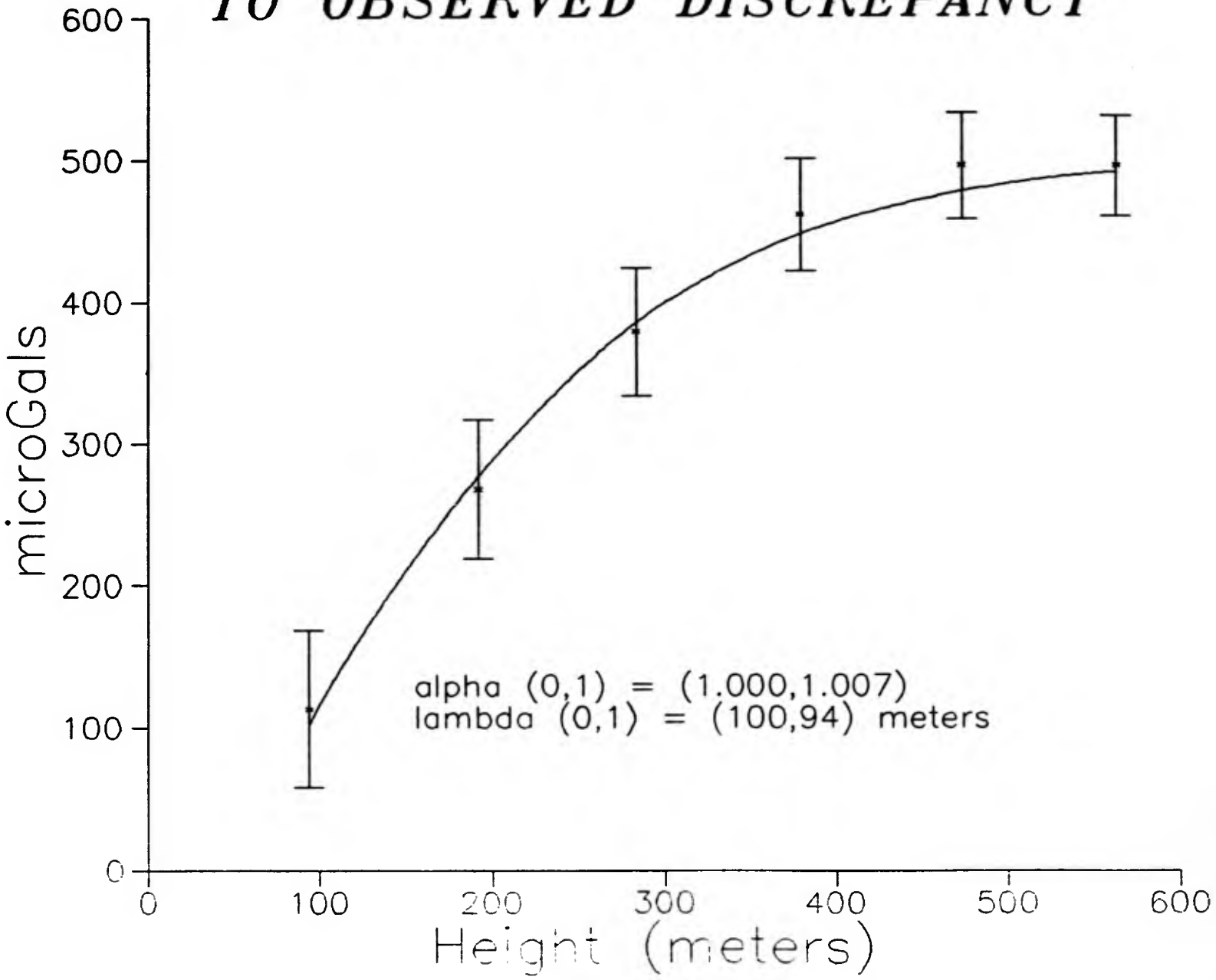

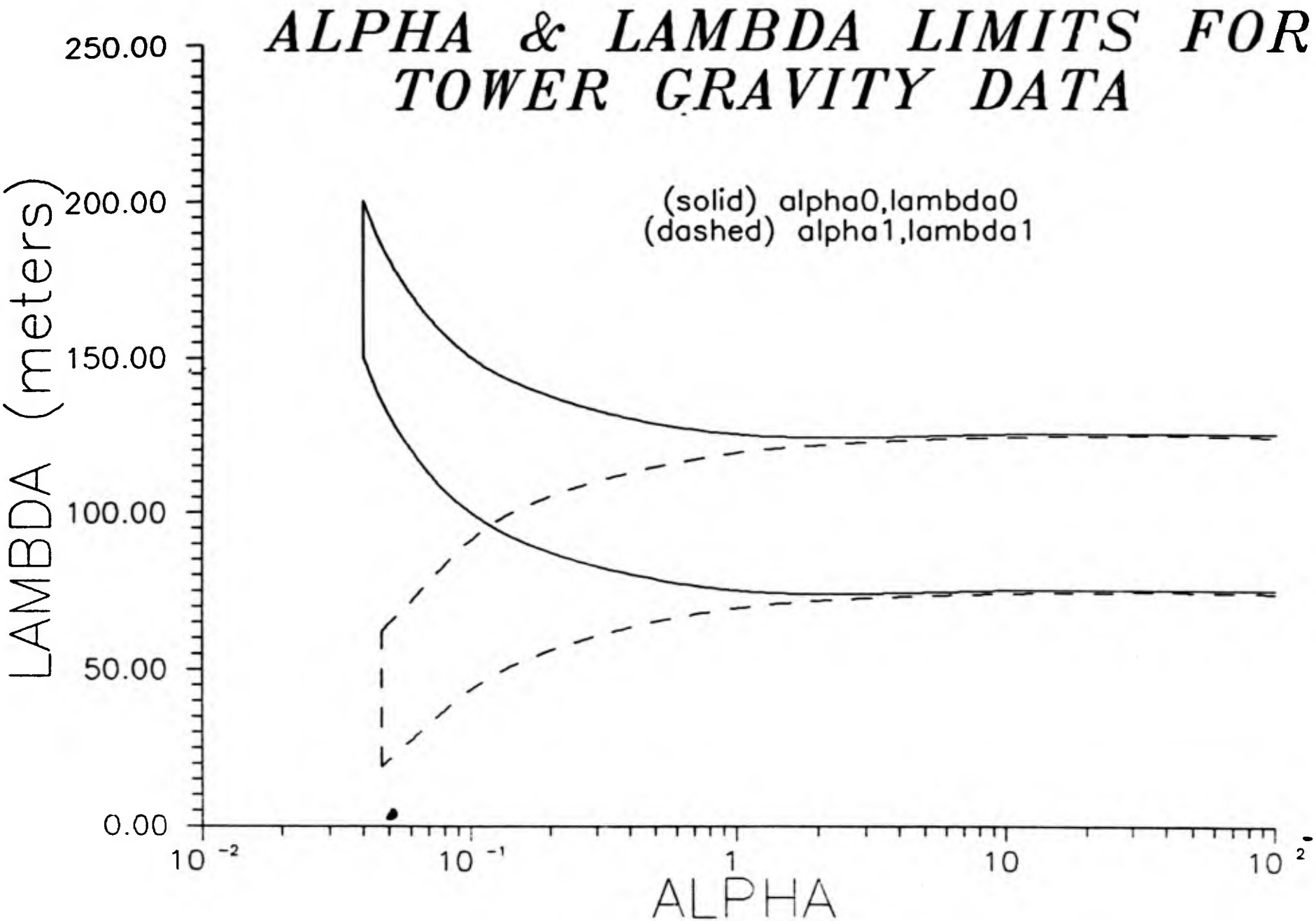
ALPHA & LAMBDA LIMITS FOR
TOWER GRAVITY DATA
(solid) alpha0,lambda0
(dashed) alpha1,lambda1
LAMBDA (meters)
250.00
200.00
150.00
100.00
50.00
0.00
10 -2
10 -1
1
10
10 2
ALPHA

16th GRAVITY GRADIOMETRY CONFERENCE
10-11 FEBRUARY 1988

SPONSORED BY:
AIR FORCE GEOPHYSICS LABORATORY
EARTH SCIENCES DIVISION

TITLE OF PAPER: A Detection of Non-Newtonian Gravity

SPEAKER: Anestis Romaides

QUESTIONS AND COMMENTS:

1. Question: Milton Trageser

   What corrections were made in height measurements?

   Response:

   Small atmospheric corrections.

2. Question: Alan Zorn

   What type of covariance models did you use for your least-squares collocation?

   Response:

   A model which consists of three parts: (a) Rapp spherical harmonic for low frequencies, (b) Texas-Oklahoma model for medium frequencies, and (c) power spectrum determined from North Carolina data for high frequencies.

3. Question: Alan Zorn

   What is the sensitivity of observed discrepancy on the tower to these models?

   Response:

   There is some sensitivity, but I feel there is no doubt that the correct covariance model was used since it was obtained from data near the tower.

4. Question: Don Benson

   How sensitive were your results to horizontal and vertical position errors for the survey around the tower? You didn't include these in your error budget.

   Response:

   Horizontal accuracy to 1.0 m and vertical accuracy to 2.0 cm.

5. Question: Paul Zucker

Did you make corrections for direct tidal effects and earth tides for the ground points and measurements aloft?

Response:

Yes, corrections were made based upon published models. The error budget for these corrections was 5 microgals.

6. Question: Rene Forsberg

Did you try your computations with and without the high-degree and order reference field?

Response:

Only an ellipsoidal normal field was used.

7. Question: Dave Sonnabend

What was the settling time of your gravimeter?

Response:

5 minutes when quiet. It wouldn't settle in strong winds.

8. Question: Ho Jung Paik

Was the data you showed averaged over many runs?

Response:

Yes. The data represents an average over 6 or 7 up-and-down runs.

9. Question: Ho Jung Paik

Have you plotted data taken on calm and windy days separately and compared them?

Response:

Yes. We have compared individual data points obtained during quiet and windy times. They differ by less than 30 microgals. The difference for closure is less than 10 microgals.

STP-GPS TRACKING FOR ANOMALOUS GRAVITATION ESTIMATION - STAGE

by

Triveni N. Upadhyay
Duncan B. Cox, Jr.

Mayflower Communications Company, Inc.
Wakefield, MA

and

Christopher Jekeli

Earth Sciences Division
Air Force Geophysics Laboratory
Hanscom AFB, MA

A technique is investigated to apply high-low satellite-to-satellite tracking for gravitation estimation to the shuttle (low satellite) and the Global Positioning System of satellites (multiple high satellites). The appeal of this type of mission lies in its low cost and the novelty of determining the total rather than just a component of the gravitation vector at altitude. Its feasibility is based on the relatively low altitude of the shuttle, the availability of space qualified GPS receivers and accelerometers, and the possibility of repeated flights of permanently installed hardware. As a minimum, a successful demonstration with the shuttle would support the launch of a dedicated free-flyer carrying the same hardware in a polar orbit for an extended duration.

The gravitational acceleration of the shuttle is measured by accurately tracking it with GPS (thus obtaining the total acceleration) and subtracting the shuttle's non-gravitational acceleration as sensed by on-board accelerometers. An on-board gyroscope is also required to determine the orientation of the GPS antennas with respect to the shuttle's center of mass.

A preliminary hardware configuration consists of a GPS receiver similar to the one planned for NASA's TOPEX mission, the Bell Aerospace three-axis MESA accelerometer, and the Honeywell GG1342 ring laser gyro. Ancillary equipment includes a tape recorder and electronic processor.

The significant error sources of STAGE include GPS clock frequency errors, antenna phase and multipath errors, receiver errors, GPS orbit errors and poor GPS constellation geometry, as well as gyro and accelerometer bias, scale factor, and alignment errors. Techniques are expounded to mitigate the effects of these errors to the extent that each component of the gravitation vector can be estimated to an accuracy of 1 mgal (10^{-5} m/s^2) or better.

STS-GPS TRACKING FOR ANOMALOUS GRAVITATION ESTIMATION* STAGE EXPERIMENT

February 1988

Triveni N. Upadhyay and Duncan B. Cox, Jr.
MAYFLOWER COMMUNICATIONS COMPANY, INC., WAKEFIELD, MA

Christopher Jekeli
AIR FORCE GEOPHYSICS LABORATORY, HANSCOM AFB, MA

Paper to be presented at the 16th Gravity Gradiometry Conference, U.S. Air Force Academy, Colorado Springs, CO, February 10-11, 1988.

* This work is sponsored by the Air Force Geophysics Laboratory, Electronic Systems Division, Air Force Systems Command, Contract No. F19628-86-C-0136.

STS-GPS TRACKING FOR ANOMALOUS GRAVITATION ESTIMATION

Experiment Objective

- Determine the feasibility of a STS-GPS tracking experiment to estimate the perturbations in gravity vector at STS altitude to an accuracy of 1 mgal or better.
  - identify and analyze the significant error sources of GPS and IMU measurements.
  - develop processing techniques to mitigate the effect of primary error sources.
  - identify the experiment payload system requirements for a 1991 flight.
- Imrove local area gravity models by post-flight processing of GPS and IMU data.
  - Polar regions, Regions of Africa and Asia

STS-GPS TRACKING FOR ANOMALOUS GRAVITATION ESTIMATION

Current Knowledge of the Global Gravity Field

- Acceleration error (quadratic sum of radial and horizontal components) at altitude due to uncertainty in the gravitational potential of the earth*

h (km)	Error (mgal)
0	± 14.2
150	2.5
200	1.9
250	1.6
300	1.3

- The error at h = 0 (height given above a sphere of radius 6378.136 km) reflects the assumption in the original coefficient error determination that $1^0 x 1^0$ mean anomalies on the surface of the earth are known, in a global sense, to ± 10 mgal.

Reference: The Representation of the Earth's Gravitational Potential in a Spherical Harmonic Expansion to Degree 250, Richard H. Rapp and Jaime Y. Cruz, Ohio State University, AFGL Report AFGL-TR-86-0191.

* Courtsey of Prof. Richard Rapp, Ohio State University

STS-GPS TRACKING EXPERIMENT FOR GRAVITATION ESTIMATION

- Estimation of STS Acceleration Errors: Geometric Effects

  - For low earth orbit space vehicles (e.g., STS) the line-of-sight LEO user-to-GPS satellite geometry changes rapidly and depends greatly on the look angle.

  - EG&G simulation results were obtained assuming a look angle (angle from the zenith) of 80^0 (or elevation angle of 10^0). The resulting position dilution of precision (PDOP) is higher.

  - Mayflower simulation results were obtained with an assumed look angle of 100^0.

    - indicates 25% improvement in PDOP and avoids the data gap problem (less than 4 SVs)

STS-GPS TRACKING EXPERIMENT FOR GRAVITATION ESTIMATION

- Estimation of STS Acceleration Errors: Error Sources

  - Receiver phase measurement noise and phase bias errors
  - Satellite clock frequency error
  - GPS Orbit Errors: Systematic Errors

    - Geopotential field
    - Solar Radiation Pressure
    - Geocentric Gravitational Constant
    - Tracking Station Location Errors

  - IMU Error Sources

    - Gyro and accelerometer bias (on orbit calibration)
    - Gyro and accelerometer scale factor (on orbit calibration)
    - Misalignment (on orbit transfer alignment)

GRAVITY ANOMALY ESTIMATION USING GPS MEASUREMENTS ONBOARD THE STS

Measurement System Concept

- Estimate total forces (gravitation and non-gravitation) acting on the STS during on-orbit phase using precision GPS carrier phase measurements from four or more GPS satellites.

- Measure non-gravitation forces acting on the STS during on-orbit phase using precision IMU accelerometer measurements.

- Estimate perturbations in gravity vector (i.e., its error covariance) at STS orbit by optimally processing the on-orbit GPS and IMU measurements.

GRAVITY ANOMALY ESTIMATION USING GPS MEASUREMENTS
ONBOARD THE STS

NOVEL FEATURES OF THE EXPERIMENT:

1. Determination of the three components of the gravity acceleration along the STS orbit track.

   - stronger recovery of gravity anomalies at the surface of the earth
   - minimizes potential problems of aliasing of the recovered parameters from errors in geopotential models in regions where data is unavailable

2. Improved measurement sensitivity to short wavelength variations in the geopotential due to lower STS orbit (250 km)

   - improved ability to estimate higher order harmonics

3. Direct ability to precisely measure the non-gravitational disturbances using an IMU instrumentation system.

   - Evaluate shuttle dynamics environment

4. Maximum utilization of the current DoD and NASA investments.

   - possible availability of future STS polar orbit missions.

GRAVITY ANOMALY ESTIMATION USING GPS MEASUREMENTS
ONBOARD THE STS

MEASUREMENT ERROR ANALYSIS

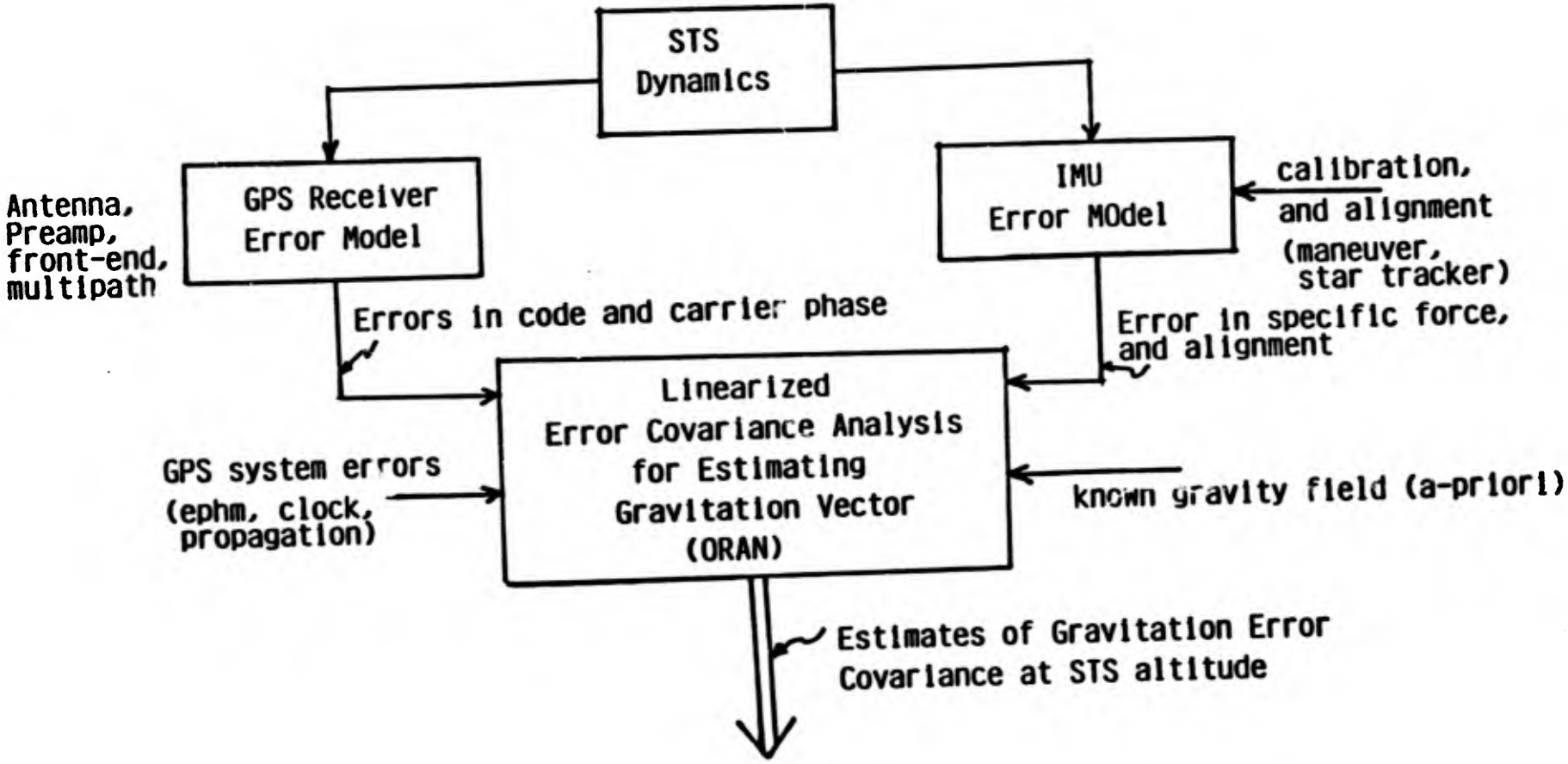

GRAVITY ANOMALY ESTIMATION USING GPS MEASUREMENTS
ONBOARD THE STS

Payload Experiment Subsystems

- A GPS Receiver utilizing existing upper and lower fuselage installed antennas on the STS orbiter
- An experimental IMU consisting of strapdown RLG and accelerometers
- An electronic processing assembly to control the experiment hardware and to integrate the orbiter timing buffer
- A flight recorder with ground support equipment provisions.

GRAVITY ANOMALY ESTIMATION USING GPS MEASUREMENTS
ONBOARD THE STS

Significant Error Sources

- GPS Availability (Geometric effects including antenna look angles)
- GPS Error Sources
  - GPS clock frequency error
  - Antenna phase and multipath
  - Signal propagation
  - Receiver Measurements: phase noise and phase bias
  - GPS orbit errors (geopotential field, solar radiation pressure, gravitational constant, tracking station location): systematic errors
- IMU Error Sources
  - Gyro and accelerometer bias (on orbit calibration)
  - Gyro and accelerometer scale factor (on orbit calibration)
  - Misalignment (on orbit transfer alignment)

STS-GPS TRACKING EXPERIMENT FOR GRAVITATION ESTIMATION

- Estimation of STS Acceleration Errors: Measurement Noise & Clock Error

  - Receiver Phase Measurement Noise

    - 2 mm (1-sigma) phase measurement noise at L_1/L_2
    - dual frequency measurements
    - 5^0 (75 seconds) and 10^0 (150 seconds) averaging intervals analyzed

  - Satellite Clock Frequency Noise

    - short-term variations in satellite clock can be observed from the ground tracking data
    - clock frequency Allan Variance (after post processing)

$$\sigma_{y^2} = \frac{1.2 \times 10^{-23}}{\tau}$$

    - 5^0 (75 seconds) and 10^0 (150 seconds) averaging intervals analyzed

STS Acceleration Error Estimation

Simulation Results

Table 1. GPS Orbit Error Model Components

Error Term	Magnitude
Geopotential Field	0.4 (GEM5 - GEM7)
Solar Radiation Pressure	1% error in C_R
Geocentric Gravitational Constant (GM_e)	0.005 km^3/sec^2
Tracking Station Location Errors	10 cm in each station coordinate

Table 2. GPS Measurement Error Model

Error Term	Value
Phase Noise	2 mm/channel
Phase Bias	0.5 m
GPS Clock Frequency Errors	Allan Variance $= \frac{1.2 \times 10^{-23}}{\tau}$

τ = Averaging Interval

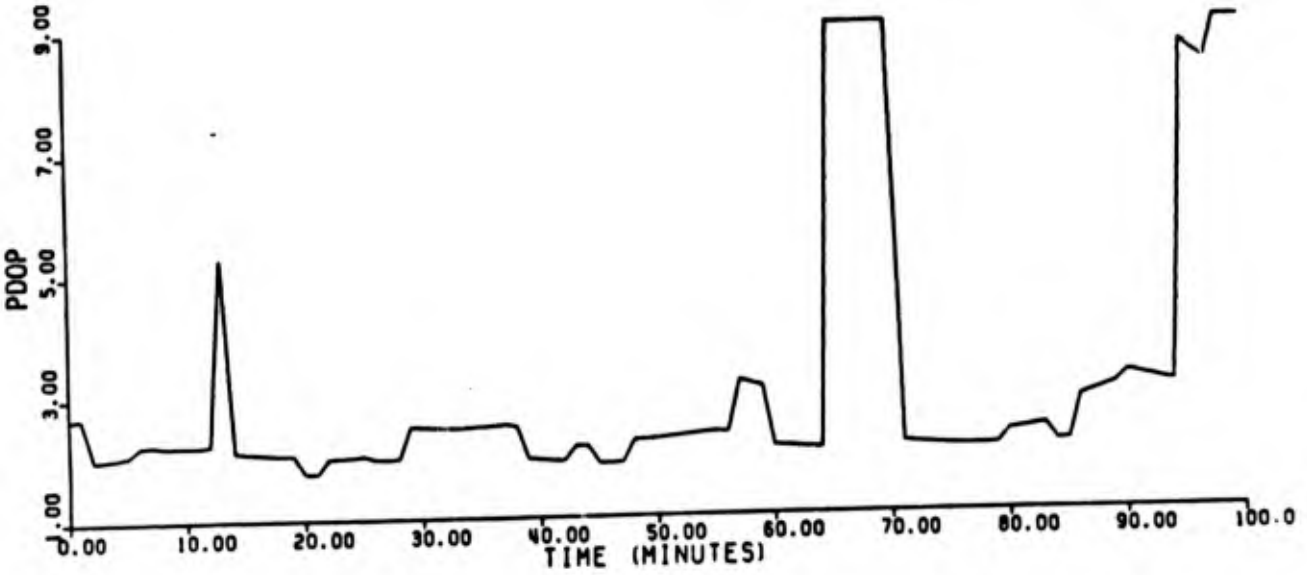

Figure xx: Position Dilution of Precision (PDOP) factor for
STS-GPS Tracking; look angle = 90^{o}
STS Orbit: 250 km
inclination = 27.5^{o}

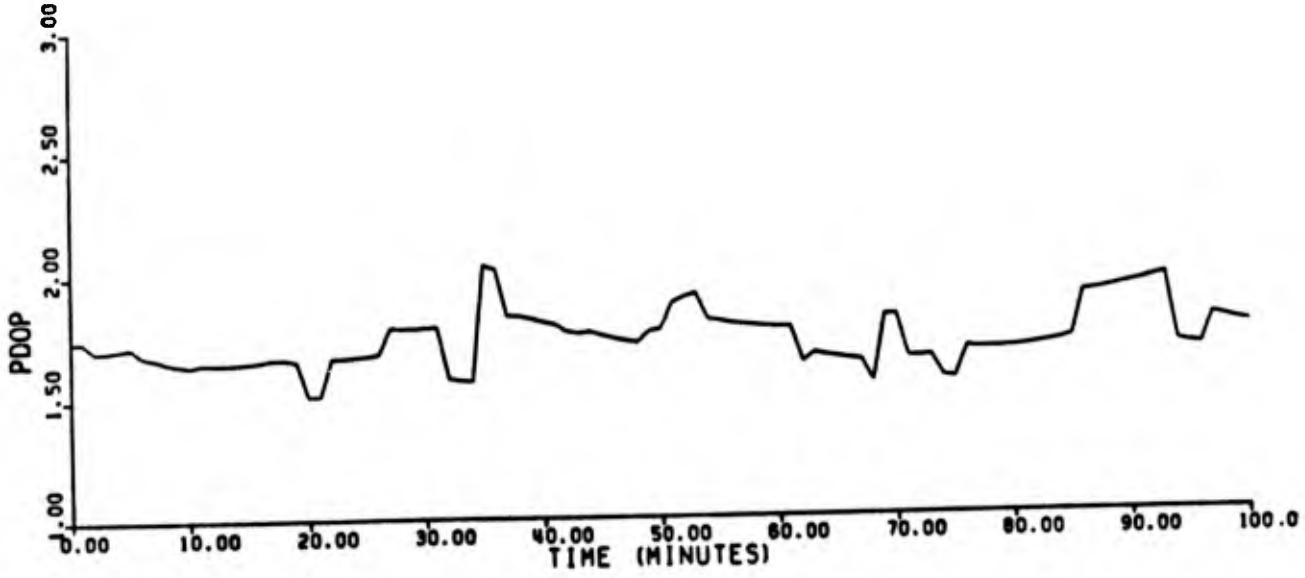

Figure xx: Position Dilution of Precision (PDOP) factor for
STS-GPS Tracking; look angle = 110^{o}
STS Orbit: 250 km
incliniation = 27.5^{o}

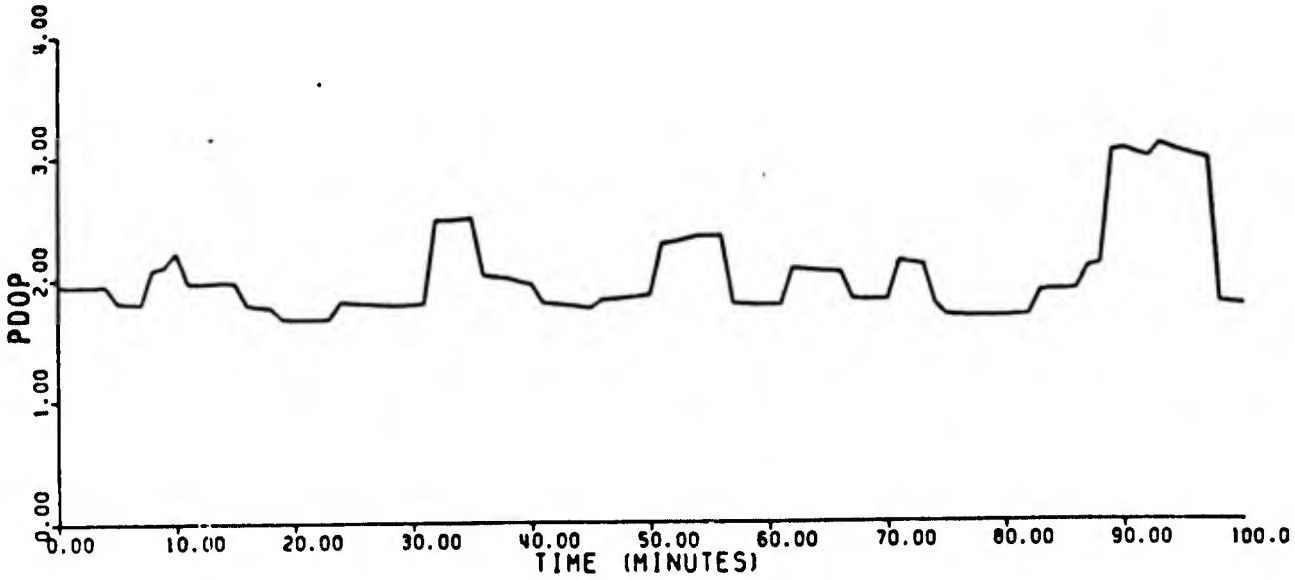

Figure 1: Position Dilution of Precision (PDOP) factor for STS-GPS tracking; look angle = 100^{o}
STS Orbit: 250 km, inclination = 27.5^{o}

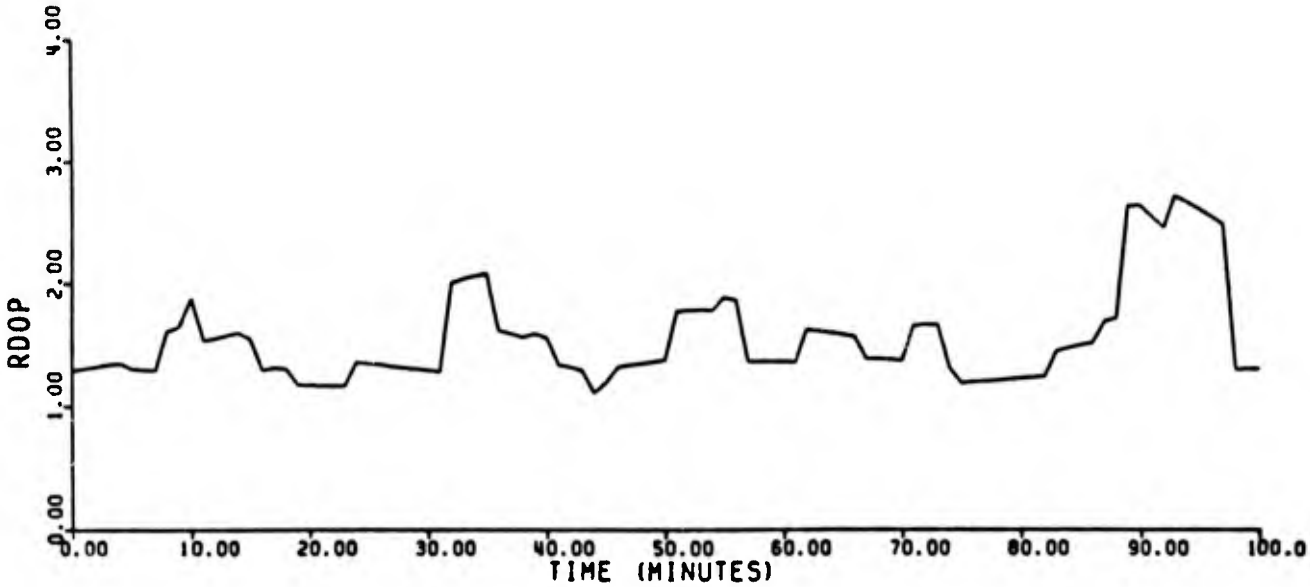

Figure 2a: Radial Dilution of Precision (RDOP) factor for STS-GPS tracking; look angle = 100^{o}

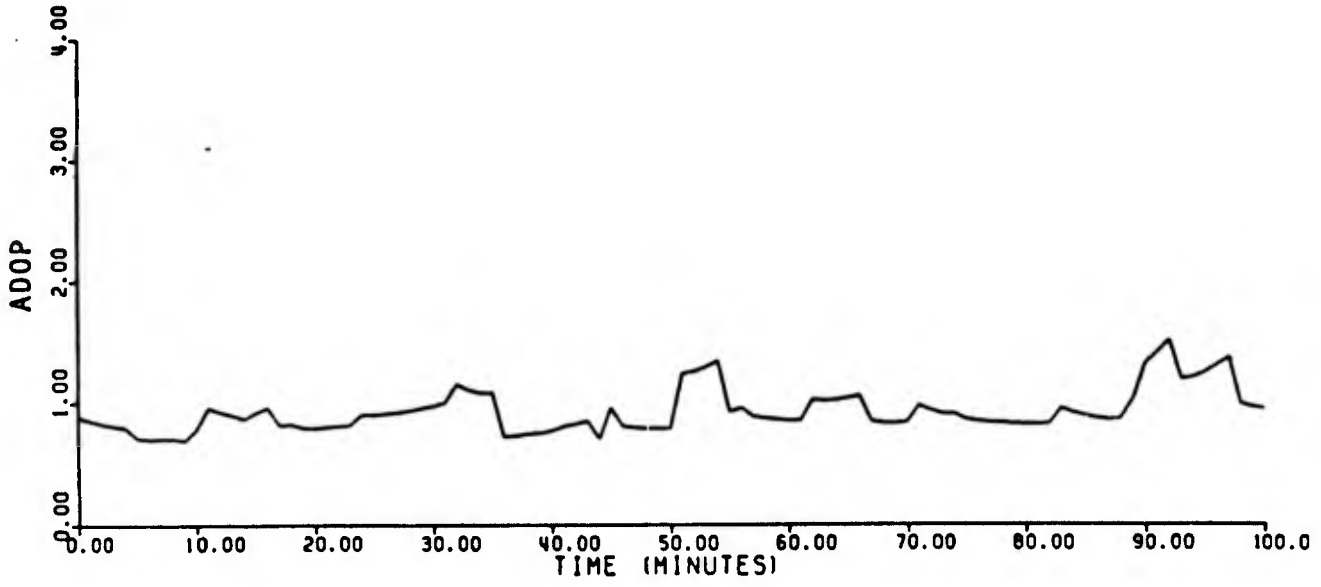

Figure 2b: Alongtrack Dilution of Precision (ADOP) factor for STS-GPS tracking; look angle = 100°

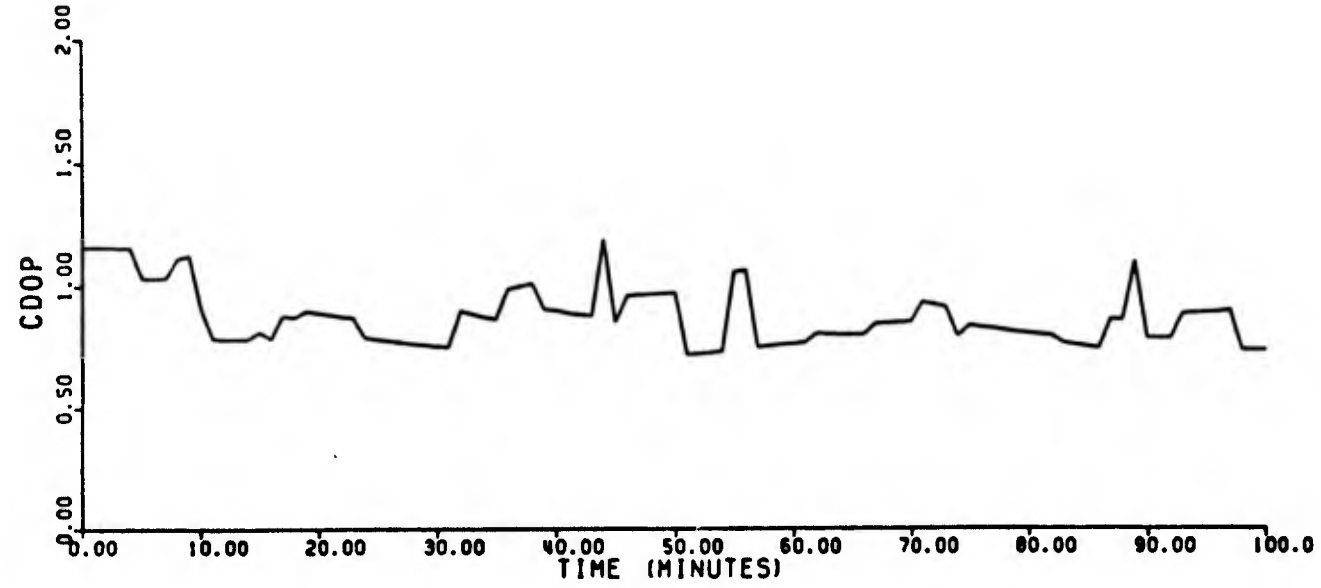

Figure 2c: Crosstrack Dilution of Precision (CDOP) factor for STS-GPS tracking; look angle 100°

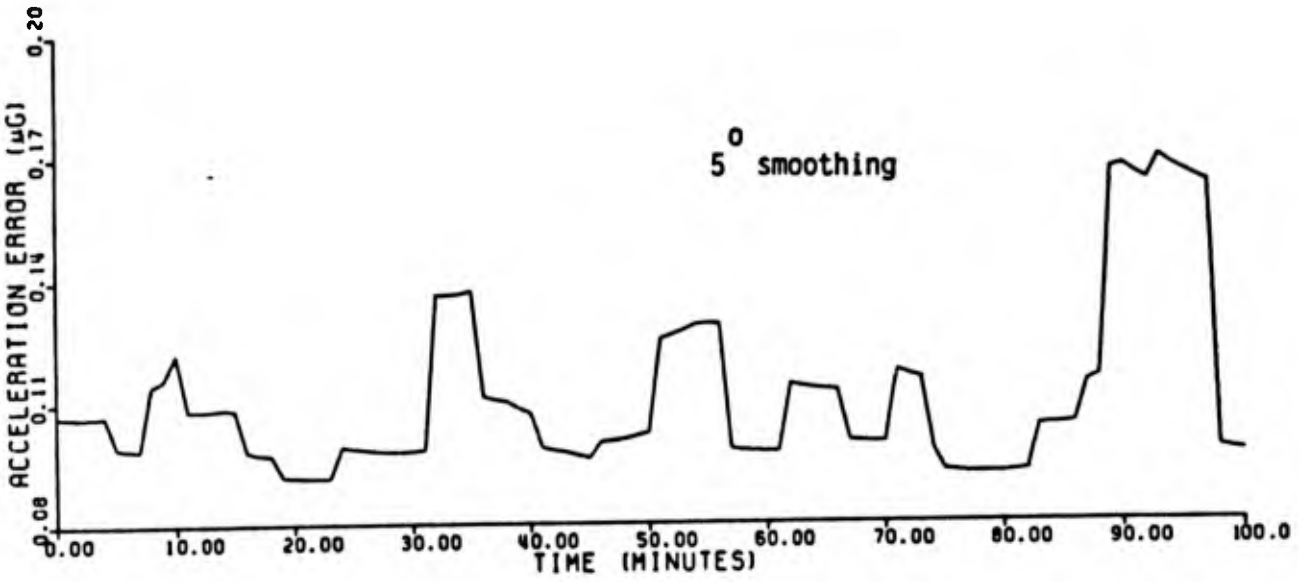

Figure 3a: Effects of GPS Phase measurement noise on estimated STS accelerations. Dual frequency measurements assumed with 2 mm phase noise for each frequency; 5° smoothing interval.

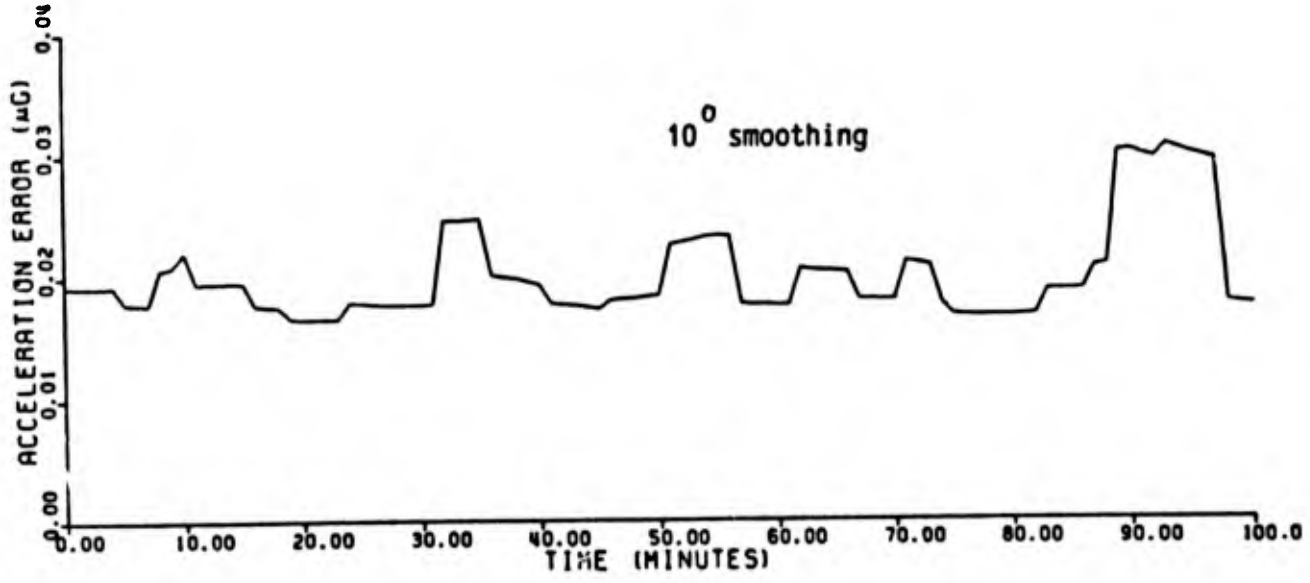

Figure 3b: Effects of GPS Phase measurement noise on estimated STS accelerations. Dual frequency measurements assumed with 2 mm phase noise for each frequency; 10° smoothing interval.

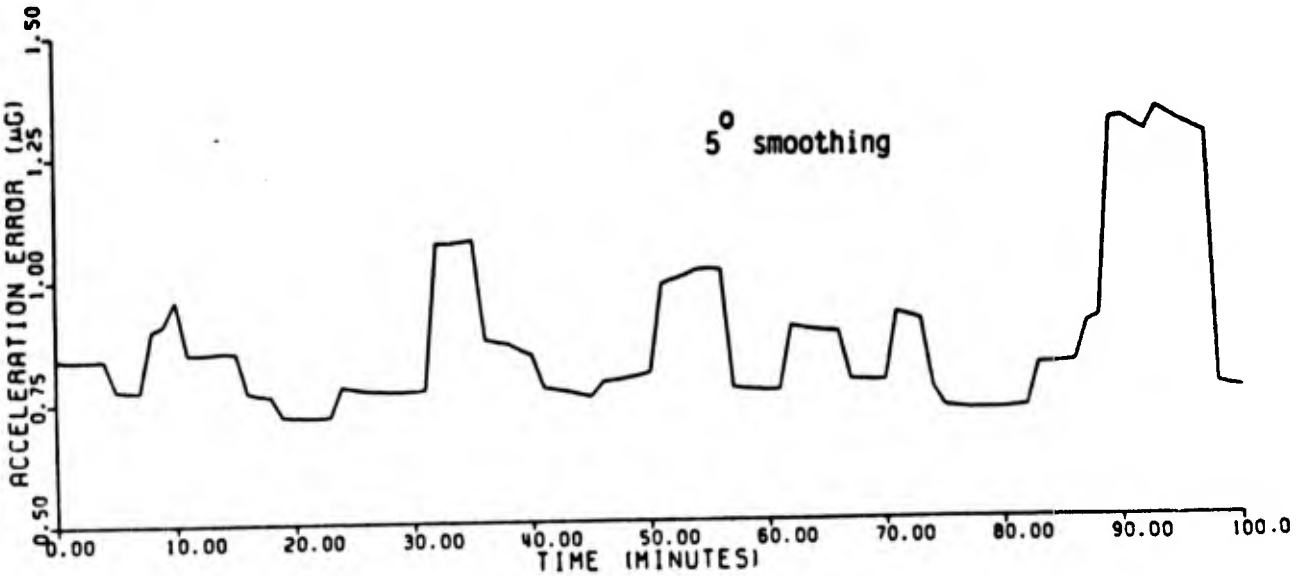

Figure 4a: Effects of GPS satellite clock errors on estimated STS accelerations; 5° smoothing interval

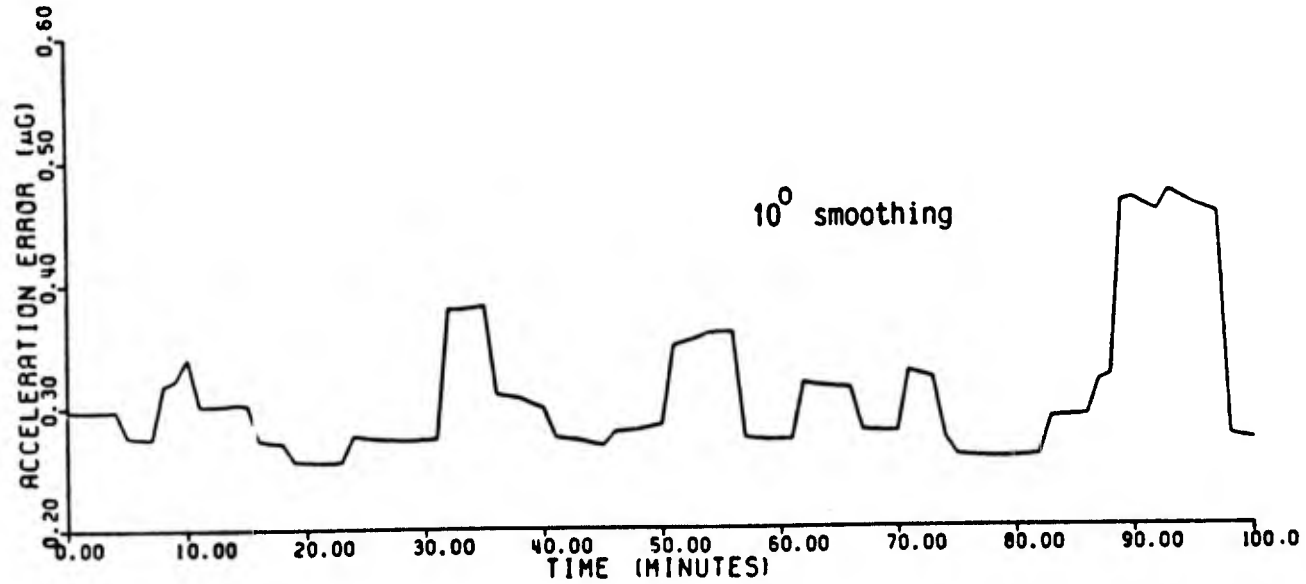

Figure 4b: Effects of GPS satellite clock errors on estimated STS accelerations; 10° smoothing interval

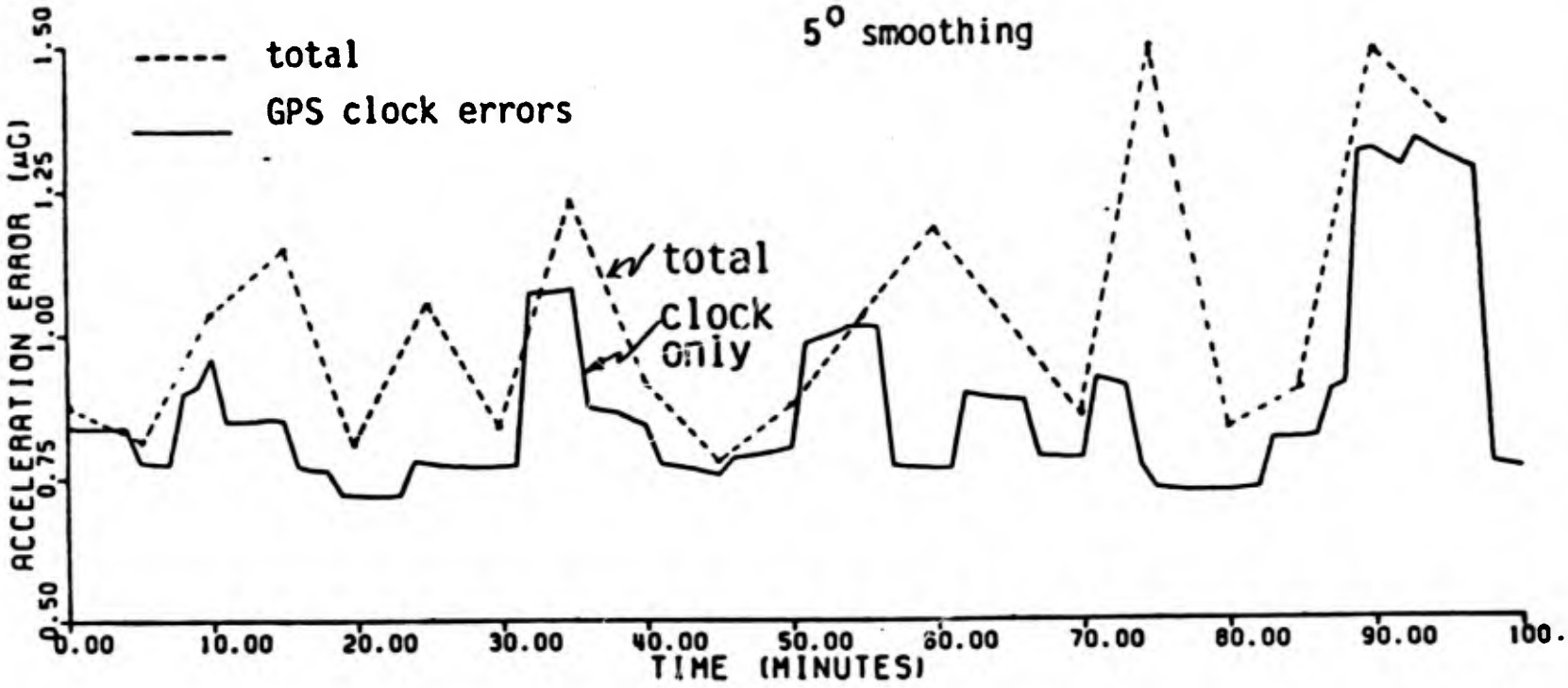

Total estimated STS acceleration error and largest error component (GPS satellite clock errors) assuming 5^{o} (75 second) smoothing interval.

STS-GPS TRACKING FOR ANOMALOUS GRAVITATION ESTIMATION

MEAN ANOMALY ACCURACY VERSUS MEASUREMENT ACCURACY*(h = 0)

Measurement Accuracy (m/s)	Anomaly Estimation Uncertainty (mgal)	
	1^0	2^0
5×10^{-5}	15.7	8.6
4×10^{-5}	15.3	8.0
2×10^{-5}	14.0	6.5
1×10^{-5}	12.8	5.2

Assumptions: STS Orbit = 250 km; Polar Orbit (incl = 90^0)
Data duration = 7 days

- Gravity anomaly uncertainty reduced to 81 % (12.8/15.7) for 1^0 block and to 62 % (5.2/8.6) for 2^0 block when measurement accuracy is improved by a factor of 5.

* Courtsey Prof. Richard H. Rapp, Ohio State University.

GRAVITY ANOMALY ESTIMATION USING GPS MEASUREMENTS
ONBOARD THE STS

- Technique to Mitigate Effects of Satellite Clock on STS Acceleration

  - Short-term fluctuations in GPS satellite clock can be observed from ground tracking data at the GPS monitor stations.

    - Observability limited by the accuracy of the ground monitor station atomic clock. Improvements are possible by the use of Hydrogen Maser as the reference station.

  - Comparison of Clock Allan variance computed from the ground tracking data and from the in-plant test data over several GPS clocks indicates that the monitor station can be used to (partially) eliminate the effect of clock errors on STS acceleration.

    - on an average a factor of 10 improvement is anticipated.

STS-GPS TRACKING FOR ANOMALOUS GRAVITATION ESTIMATION

Short-term Performance of GPS satellite Clocks

- NAVSTAR 10 (Cesium, Serial No. 005)

Data taken on	Allan Variance τ = 10 s	Allan Variance τ = 100 s
5/82 In-plant test data at FTS*	3.99×10^{-12}	3.09×10^{-12}
6/82 Test data at Rockwell*	4.90×10^{-12}	2.81×10^{-12}
4/85 Tracking data at Diego Garcia**	4.30×10^{-12}	2.4×10^{-12}

- Error at 10 s ($0.31 - 0.6 \times 10^{-12}$), at 100 s ($0.41 - 0.69 \times 10^{-12}$)

CLOCK MODEL: Allan Variance = $1.2 \times 10^{-23/\tau}$ (after post-flight processing)

$= 1.09 \times 10^{-12}$ (τ = 10 s) 1-sigma

$= 0.34 \times 10^{-12}$ (τ = 100 s) 1-sigma

* courtsey Phil Tally, Aerospace Corporation

** courtsey Paul Jorgensen, Aerospace Corporation

PAGE 1

TEST DATA SHEET 6. 10

OPERATION AND VERIFICATION TEST

TEST SEQUENCE 10

PART DESCRIPTION: CESIUM FREQUENCY STANDARD SERIAL NO. 0005
ROCKWELL PART NO: MC474-0031-0001 FTS PART NO. 2101
ROCKWELL SPECIFICATION NO: MC474-0031, REVISION A04 TEST PARAGRAPH: 6. 10
FTS ACCEPTANCE TEST PROCEDURE NO. 2101

STABILITY DATA

SPECIFICATION	ALLAN VARIANCE MEASURED	MEASUREMENT INTERVAL (SECONDS)	BASED ON (# OF POINTS)
<=1.0E-11	0.4927357E-11	10	2857
	0.4635679E-11	30	951
<=3.7E-12	0.2810146E-11	100	284
	0.1803254E-11	300	93
<=1.4E-12	0.1163235E-11	1000	26
	0.3635911E-12	3000	7
		10000	
		30000	
		100000	

BEAT PERIOD [illegible]

FREQ [illegible]

with respect to [illegible]
1 sec Data

1s 4.411[illegible]E-12
3 sec 2.[illegible]E-12
10 sec 1.[illegible]E-12
20 sec [illegible]E-12

THIS STABILITY INTERVAL FROM 30-JUN-82 10:02 TO END OF OPERATION AND VERIF
ICATION

FINAL ACCEPTANCE & CERTIFICATION

Summary Test Data

Part Description: Cesium Frequency Standard

Rockwell Part No: MC474-0031-0001

Rockwell Specification No. MC474-0031, Revision A04

FTS Acceptance Test Procedure No. 2101

Serial No. 0005

FTS Part No. 2101

Sheet 4 of 5

TEST PARA.	TEST DESCRIPTION	SPECIFICATION LIMITS	RECORDED MEASUREMENT	TESTED BY	DATE
6.15	LONG TERM STABILITY				
	Accuracy	$\pm$ 1 x 10^{-11}	$+5.9 \times 10^{-12}$	F.T.S. Q.A.T. 12	5/25/82
	Stability				
	1 second	$\leq$ 1 x 10^{-11}	2.69×10^{-12}	F.T.S. Q.A.T. 12	5/25/82
	10 second	$\leq$ 1 x 10^{-11}	3.99×10^{-12}		
	10^2 second	$\leq 3.7 \times 10^{-12}$	3.09×10^{-12}		
	10^3 second	$\leq 1.4 \times 10^{-12}$	0.94×10^{-12}		
	10^4 second	$\leq 5.3 \times 10^{-13}$	2.41×10^{-13}		
	10^5 second	$\leq$ 2 x 10^{-13}	1.77×10^{-13}		
	R.F. Power Output/50Ω	+18.5dBm $\pm$ 1.5dBm	+18.6dBm	F.T.S. Q.A.T. 12	5/25/82
6.16	FREQUENCY vs. TEMPERATURE				
	$\Delta f/f$	$\leq$ 4 x 10^{-12}	2.1×10^{-12}	F.T.S. Q.A.T. 12	5/30/82
	R.F. Power Output/50Ω				
	+20°C	+18.5dBm $\pm$ 1.5dBm	+18.9dBm	F.T.S. Q.A.T. 12	5/30/82
	+45°C	+18.5dBm $\pm$ 1.5dBm	+18.0dBm	F.T.S. Q.A.T. 12	5/30/82

K•E LOGARITHMIC 2 X 3 CYCLES
KEUFFEL & ESSER CO

46 7323

NAVSTAR 10 (Cesium, Serial No. 005)

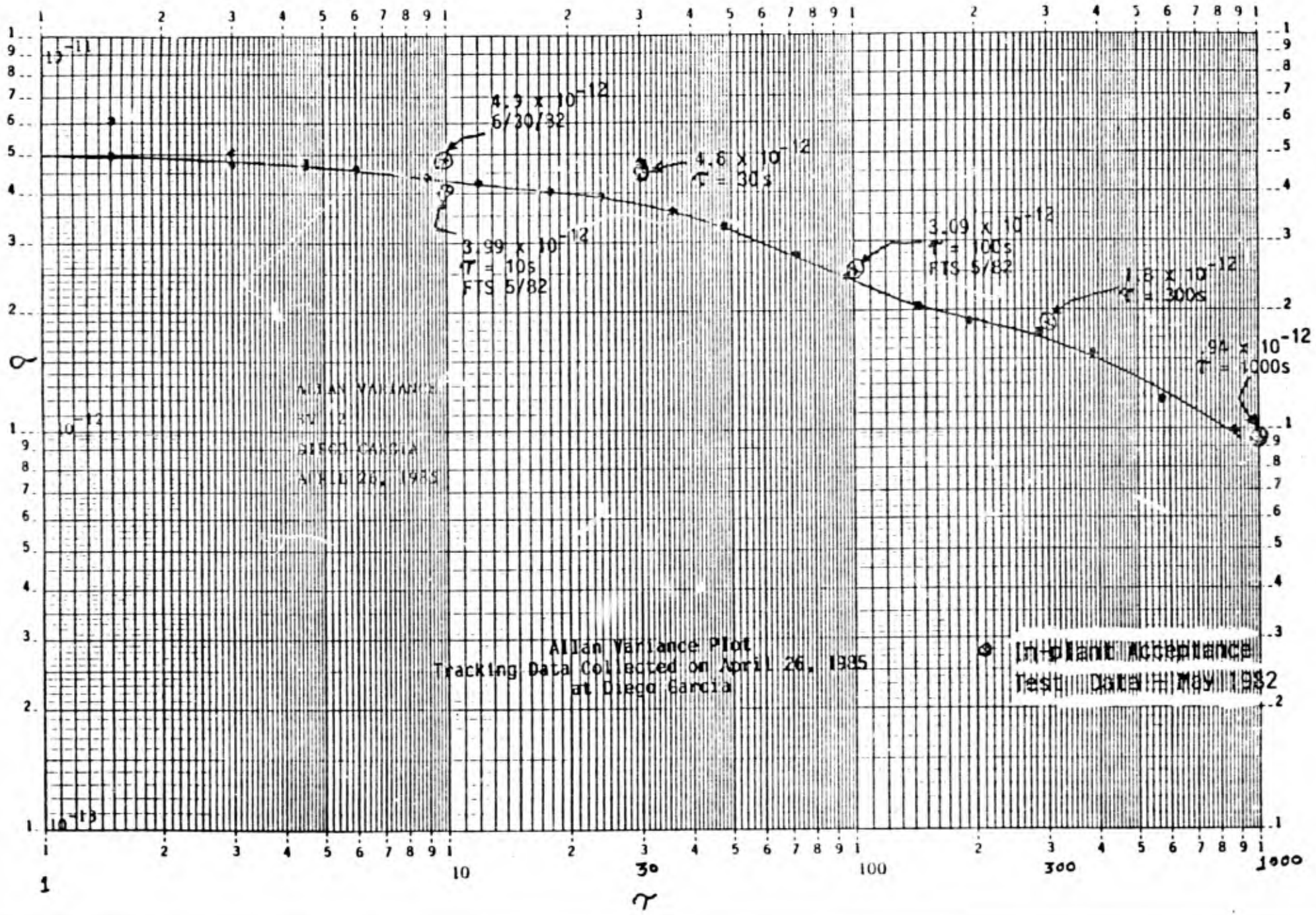

GRAVITY ANOMALY ESTIMATION USING GPS MEASUREMENTS ONBOARD THE STS

Identification of Candidate Hardware Subsystems

- GPS Receiver
  - Modified Motorola GDR (for NASA TOPEX)
- IMU
  - Honeywell LaserRef (strapdown) Gyro
  - Bell MESA Accelerometer
- Recorder
  - Data Tape MARS

GRAVITY ANOMALY ESTIMATION USING GPS MEASUREMENTS
ONBOARD THE STS

Size, Power, Weight Estimates

GPS RECEIVER

-SIZE: 6 X 6 X 12
-POWER: 35 WATTS
-WEIGHT: 14 LBS.
-COOLING: AIR COOLED

EIMU

-SIZE: 17 X 30 X 12
-POWER: 180 W
-WEIGHT: 120 LBS.
-COOLING: HEAT SINK

TAPE RECORDER

-SIZE: 23 X 16.6 X 7.5 W/ISOLATOR
-POWER: 115 W
-WEIGHT: 57 LBS. WITH TAPE
-COOLING: AIR COOLED

PROCESSOR

-SIZE: 18 X 12 X 8
-POWER: 50 W
-WEIGHT: 30 LBS.
-COOLING: AIR COOLED

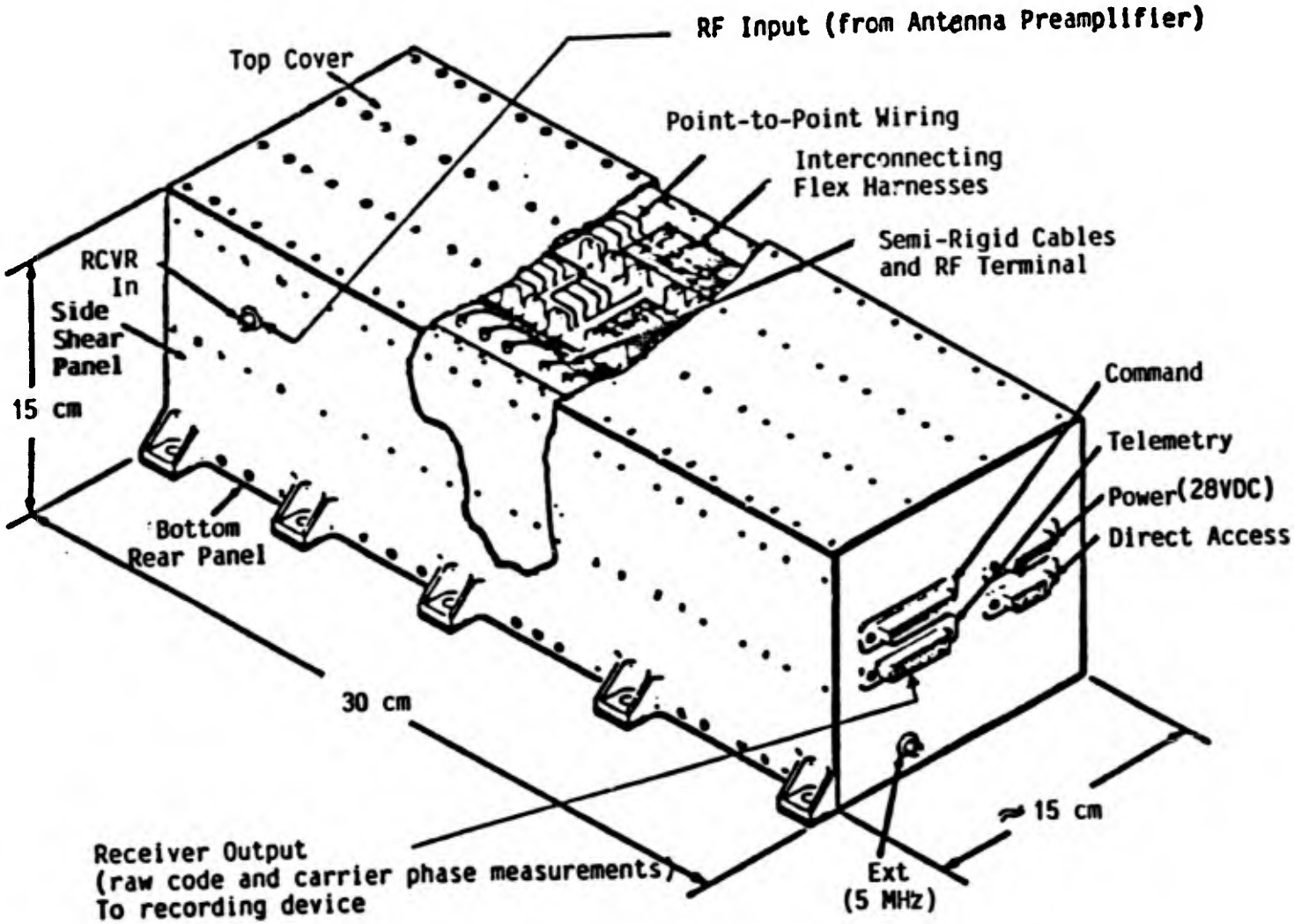

Figure 1: PRELILMINARY PACKAGING CONCEPT FOR EXPERIMENTAL GPS RECEIVER*

* Motorola TOPEX GPS Receiver

IMU With Precision Accelerometer*

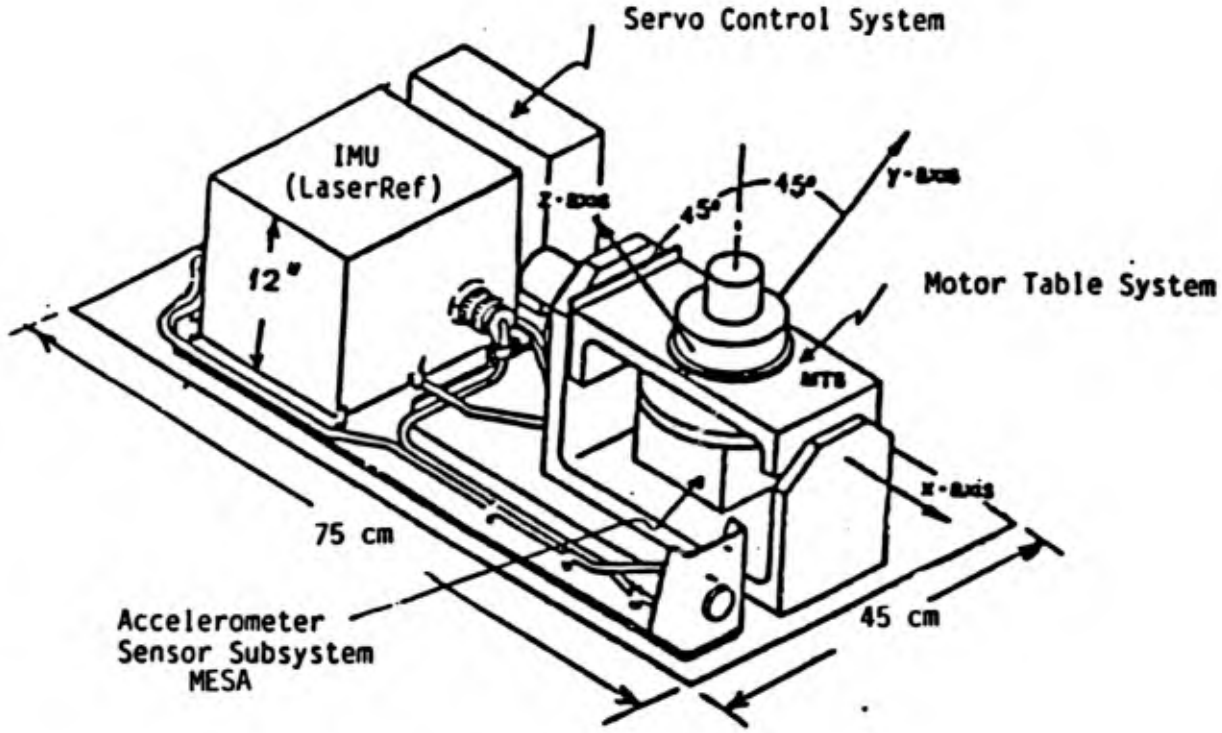

Figure 2: PRELIMINARY PACKAGING CONCEPT FOR EXPERIMENTAL IMU FOR STS-GPS TRACKING EXPERIMENT

* Modified NASA OARE Payload

ORBITER EXPERIMENT INSTALLATION

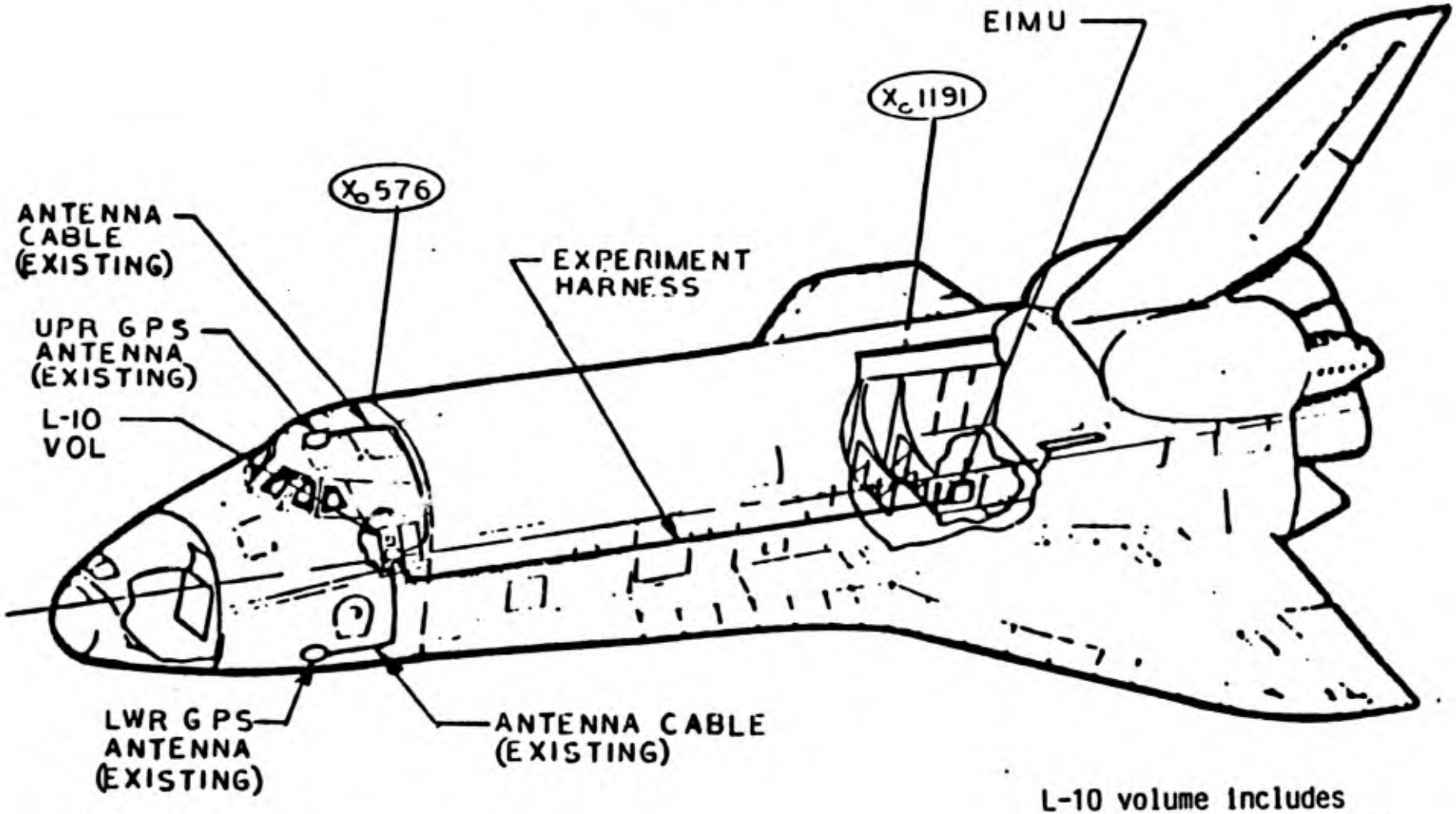

Rockwell International
Space Transportation Systems Division

L-10 volume includes GPS Receiver, Processor and Recorder - Crew Module

ORBITER GPS TRACKING EXPERIMENT
BLOCK DIAGRAM

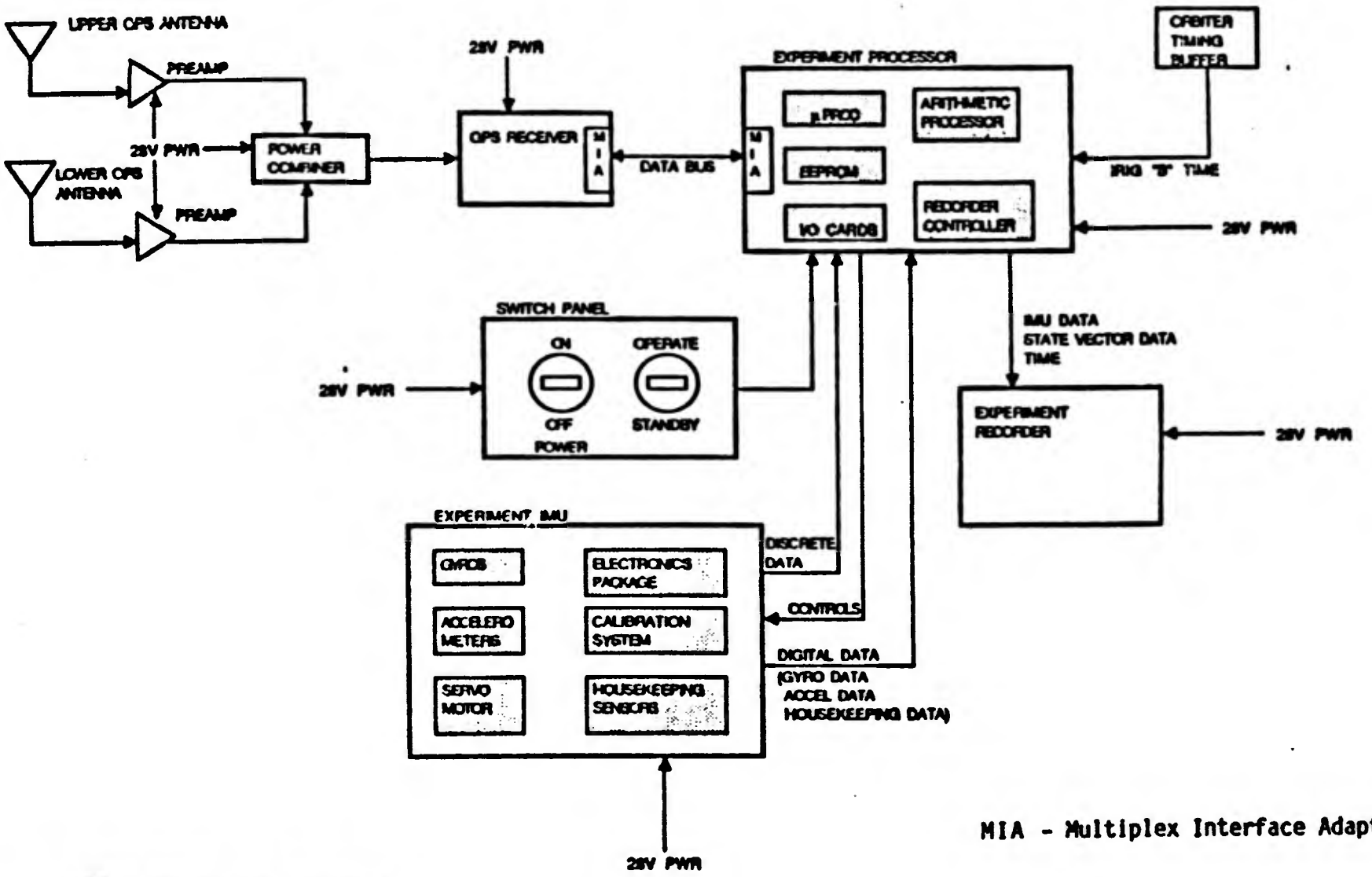

MIA - Multiplex Interface Adapter

Rockwell International
Space Transportation Systems Division

GRAVITY ANOMALY ESTIMATION USING GPS MEASUREMENTS
ONBOARD THE STS

Conclusions

- Error analysis and simulation results indicate that the STS-GPS tracking experiment goals of 1 micro-g can be realized for 5° mean anomaly estimation at the STS orbit provided that certain measures are taken to mitigate the effect of the primary error sources, i.e.,
  - GPS carrier phase data at the monitor stations is processed with the STS GPS carrier phase measurements
  - IMU bias and scale factor errors are calibrated on orbit
  - IMU is aligned with respect to Orbiter IMU on orbit
- Baseline Experiment System Configuration compatible with the Space Transportation System has been developed by Rockwell International

GRAVITY ANOMALY ESTIMATION USING GPS MEASUREMENTS ONBOARD THE STS

Preliminary IMU Sensor Specification

Gyro: (ring laser, e.g., Honeywell GG1342)

Gyro bias drift = 0.004^{o}/hr
Gyro scale factor = 5 ppm
Gyro random walk = $0.001^{o}/\sqrt{hr}$

Accelerometer: (electrostatically suspended, e.g., Bell MESA)

Accelerometer bias = 10 micro-g at full scale,
turn-on to turn-on stability: better than 1 micro-g on-orbit.

Accelerometer bias temperature coefficient = 0.25 micro-g/^{o}F
Accelerometer scale factor $<$ 500 ppm
Accelerometer misalignment = 5 arc sec, on-orbit
Full scale = 100 micro-g to 10 milli-g (3 ranges, selectable)
Resolution = 10^{-8} g

STS-GPS TRACKING FOR ANOMALOUS GRAVITATION ESTIMATION

On-Orbit Accelerometer Bias and Scale Factor Calibration

- Mount the accelerometer package on a precision controlled rotation table
- Technique proven in early 1970's by the Air Force Low-G Accelerometer System (LOGACS) Experiment data
- Record accelerometer output in different opearting modes and solve for the bias and scale factor using the following equations.

Mode	Accelerometer Output
1. No rotation, sensitive axis forward	$A_1 = K (B + A_D)$
2. No rotation, sensitive axis aft	$A_2 = K (B - A_D)$
3. Rotation at fixed angular rate w	$A_3 = K (B + A_D \text{ Cos } w t + R w^2)$
4. Rotation at fixed angular rate 2w	$A_4 = K (B + A_D \text{ Cos } 2w t + 4 R w^2)$

where A_i is the accelerometer output, B is the accelerometer bias. A_D is the atmospheric drag, and K is scale factor.

STS-GPS TRACKING FOR ANOMALOUS GRAVITATION ESTIMATION

On-Orbit Transfer Alignment

- On-orbit transfer alignment accuracy: 1 mrad (goal)
- Payload (experiment) IMU Alignment:
  - Alignment of Orbiter IMU(s) to Orbiter Star Tracker is known.
  - Payload IMU can be aligned to the inertial frame of the Orbiter IMU
    - will require rotation of the shuttle along its body axes
    - rotation rate and duration (TBD)
- Payload IMU to Orbiter GPS Antenna vector baseline is needed
  - lever-arm must be determined

16th GRAVITY GRADIOMETRY CONFERENCE
10-11 FEBRUARY 1988

SPONSORED BY:
AIR FORCE GEOPHYSICS LABORATORY
EARTH SCIENCES DIVISION

TITLE OF PAPER: STS-GPS Tracking for Anomalous Gravitation Estimation (STAGE)

SPEAKER: Triveni Upadhyay

QUESTIONS AND COMMENTS:

1. Question: Don Benson

   Does your requirement for a 1.0 millirad accelerometer alignment include the effects of rotational acceleration?

   Response:

   Yes, it does.

2. Question: Jurn Sun-Leung

   What is your estimate of the contribution of ionospheric and tropospheric error on differential GPS between the receivers on the shuttle and on the ground?

   Response:

   Most of the error is taken care of by using $L_1 + L_2$ correction for the ionospheric effect.

3. Question: B. Louis Decker

   What is your estimate as to when such a gravity experiment might be flown, and what Air Force organization is interested in it?

   Response: Chris Jekeli and Tom Rooney

   The earliest time that such an experiment could be flown would be Fiscal Year 1991. The proposed experiment is not sponsored by any Air Force organization at this time, but such sponsorship is being sought.

THREE-AXIS SUPERCONDUCTING GRAVITY GRADIOMETER - PROGRESS REPORT

by

M.V. Moody
Q. Kong
H.J. Paik
J.W. Parke

Department of Physics and Astronomy
University of Maryland
College Park, Maryland 20742

A single-axis superconducting gravity gradiometer (SGG) Model II has been tested in the laboratory. The instrument has exhibited a noise level of 0.1 E $Hz^{-1/2}$ above 0.5 Hz on a passive platform, suspended from a single point. This "white" noise background comes from the angular acceleration of the platform coupled to the gradiometer through a sensitive-axis misalignment. The noise spectrum deteriorates below 0.1 Hz by $1/f^n$ type noise. This "red" noise has been identified with the centrifugal acceleration noise of the gradiometer. In order to improve the noise spectrum of the instrument, the platform needs to be stabilized against angular motions driven by seismic noise.

A three-axis SGG Model II has been assembled and is undergoing final preparation for a cool-down. It will be cooled on a new passive platform, which has been stiffened against tilts by having a three-point suspension. The tilt angles of the gradiometer axes will be monitored optically in order to detect angular modes and drifts. A single-axis portion of SGG Model III is also under construction. Model III incorporates the "superconducting negative spring" to improve the intrinsic sensitivity of SGG from 3 x 10^{-3} E $Hz^{-1/2}$ of Model II to 10^{-4} E $Hz^{-1/2}$.

THREE-AXIS SGG - PROGRESS REPORT

M.V. Moody, Q. Kong, H.J. Paik and J.W. Parke
Department of Physics and Astronomy
University of Maryland, College Park, MD 20742

1. Single-Axis SGG Model II
2. Six-Axis Accelerometer
3. Three-Point Pendulum Suspension
4. Three-Axis SGG Model II
5. Single-Axis SGG Model III
6. Outlook

2/10/88
Colorado Springs

1. Single-Axis SGG Model II

Has been tested extensively.

a) Common mode frequency $\gtrsim 50$ Hz.
Differential mode frequency $\cong 8.5$ Hz.

$\Rightarrow$ "Push-pull levitation" worked partially.

$\Rightarrow$ Non-linearity in the circuit.
Redesign of the coil form.

b) Differential mode $Q \geq 5.6 \times 10^5$.

$\Rightarrow$ Exceeds requirement for Model III.

$\Rightarrow$ Cold damping is essential.

c) Common axis misalignment $\delta r_{+2} = 2.5 \times 10^{-4}$.

$\Rightarrow$ A factor 2.5 improvement from Model I.

$\Rightarrow$ Active axis alignment is tested.
Easy

d) Sensitivity: $0.1\,E\,Hz^{-1/2}$ at $0.6 \sim 0.9$ Hz.
$0.3\,E\,Hz^{-1/2}$ at $0.1 \sim 0.2$ Hz.

$\Rightarrow$ Low frequency excess noise is from centrifugal acceleration.

$\Rightarrow$ Platform stabilization is essential.

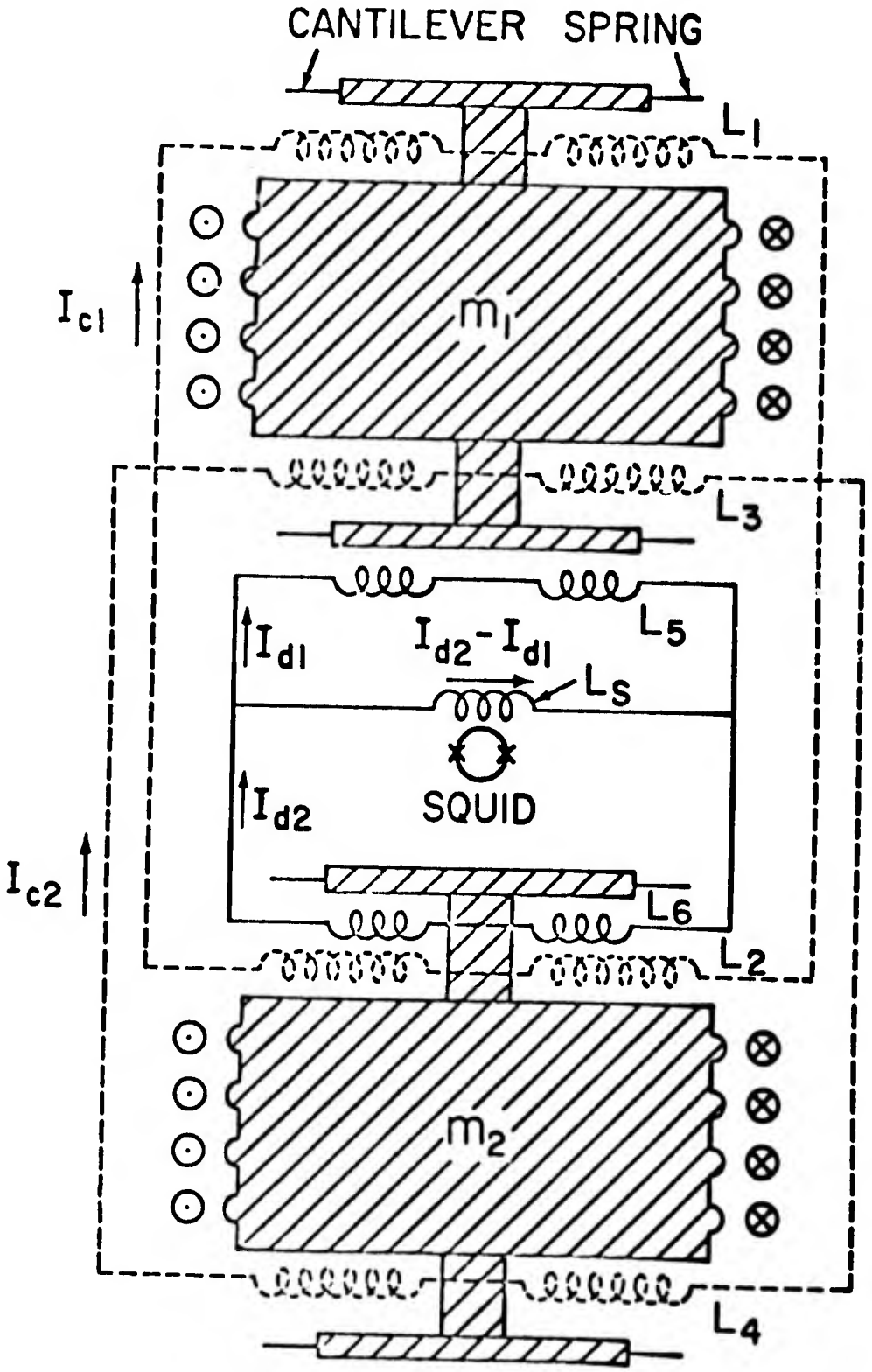

Fig. 2. Circuitry for a superconducting gravity gradiometer.

3-AXIS SUPERCONDUCTING GRAVITY GRADIOMETER
DESIGN FOR ONE OF SIX IDENTICAL UNITS

Model II

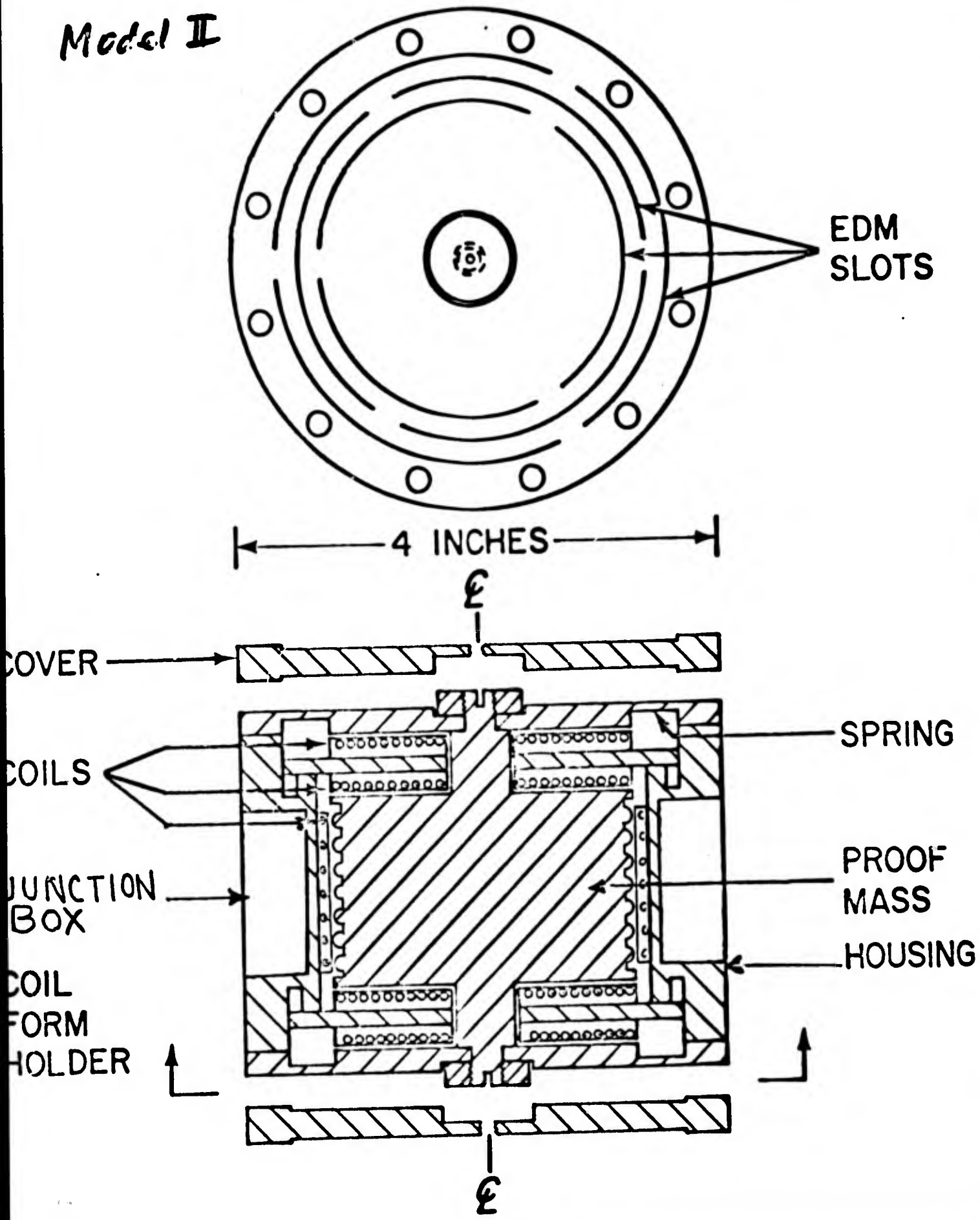

RELAXATION TIME

$\tau_{amp} = 6$ hrs!

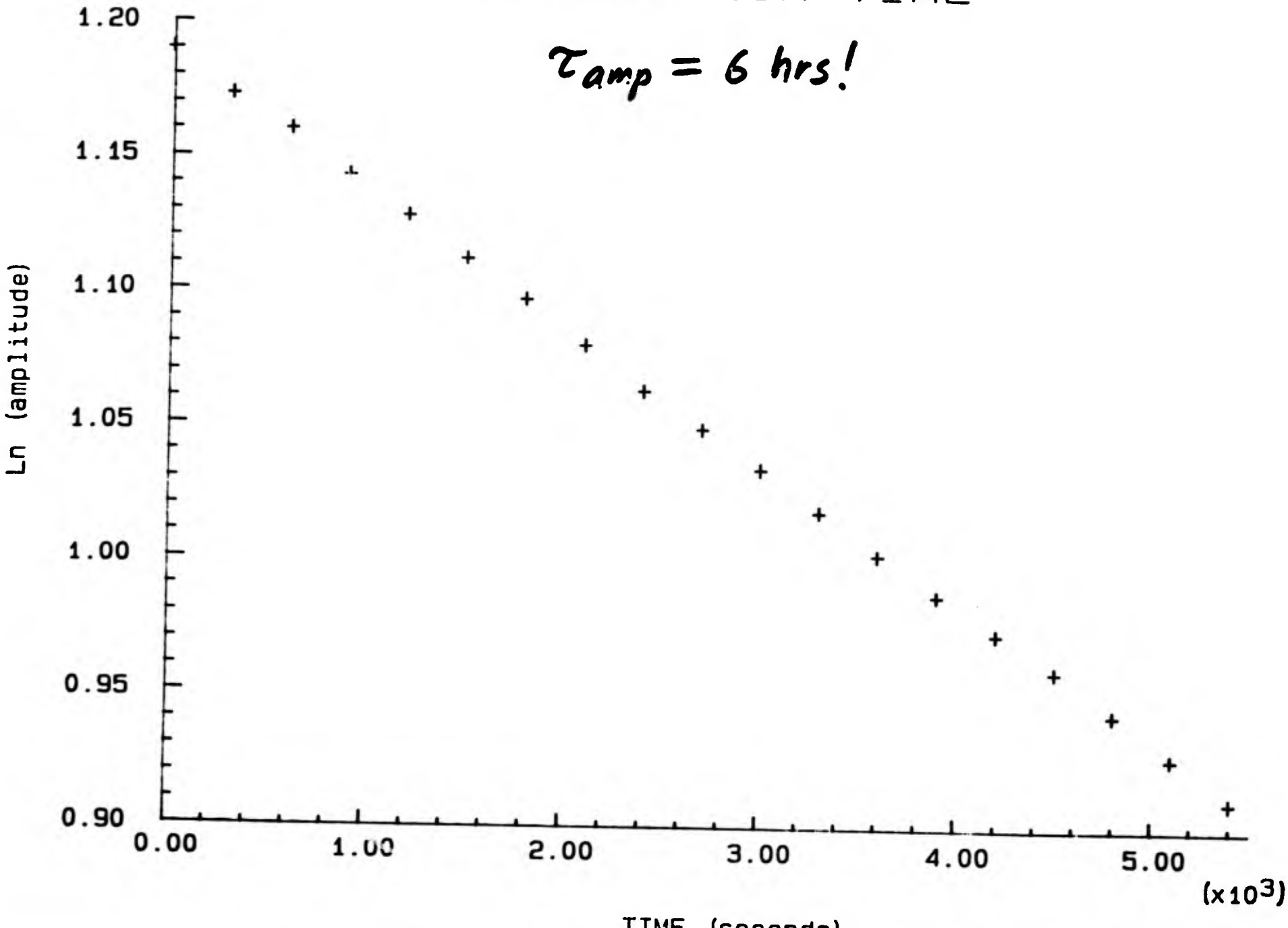

Gradiometer Error due to Angular Motion of Platform

Angular velocity : $\vec{\Omega}_p(t)$.

Angular acceleration : $\vec{\alpha}_p(t) = \dot{\vec{\Omega}}_p(t)$.

a) coupling to angular acceleration:

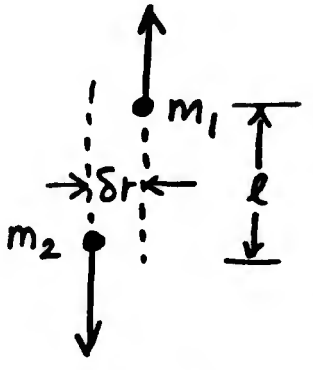

$$\delta\Gamma_{\vec{\alpha}}(t) = -\delta\hat{n}_{+\hat{\ell}} \times \hat{n} \cdot \vec{\alpha}_p(t).$$

$$|\delta\hat{n}_{+\hat{\ell}}| = \delta r/\ell \cong 3\times10^{-4}.$$

b) centrifugal acceleration:

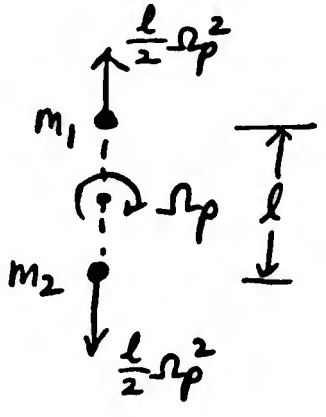

$$\delta\Gamma_C(t) = [1-(\hat{n}\cdot\hat{\Omega})^2]\,\Omega_p^2(t).$$

If $\Omega_p(t) = \Omega_p \cos(\omega_0 t + \theta)$,

$$\Omega_p^2(t) = \frac{\Omega_p^2}{2}[1 + \cos(2\omega_0 t + 2\theta)].$$

Down-converted noise — 2nd harmonic generation

Error model $\Rightarrow$ Eq. (B68) of Paper II :

$$S_{\Gamma,C}^{1/2}(f) = [1-(\hat{n}\cdot\hat{\Omega})^2]\sqrt{\frac{2}{\pi}}\,\frac{1}{\tau}\,\frac{1}{f^{3/2}}\left[\int_0^\infty S_{\vec{\Omega}}(f')\,df'\right]^2.$$

c) modulation of the Earth's gravity:

$$\delta\Gamma_{\vec{\theta}}(t) = +\delta\hat{n}_- \times \vec{g}_E \cdot \vec{\theta}_p(t). \quad \text{in general}$$

Error Sources

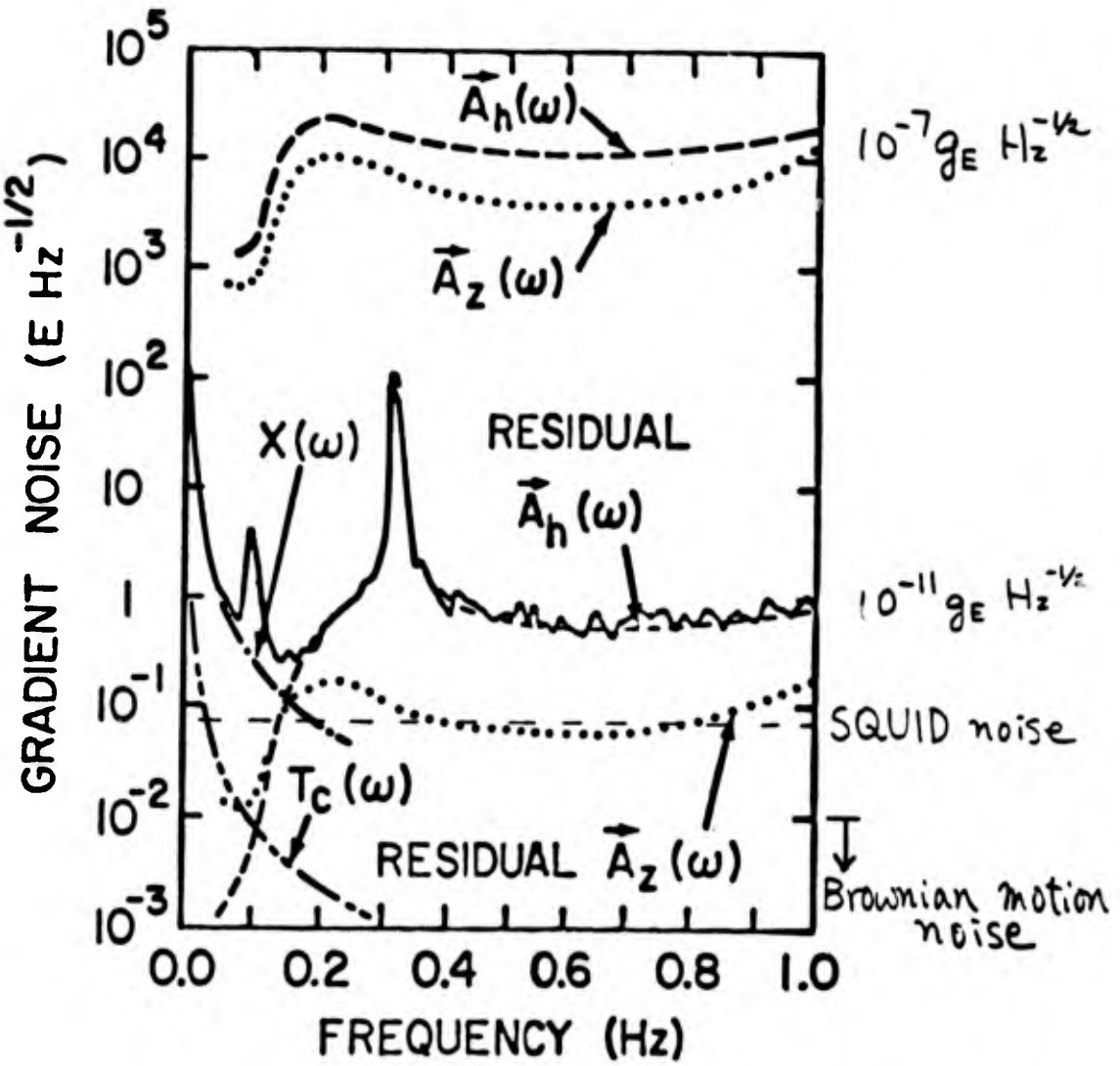

X=887mHz

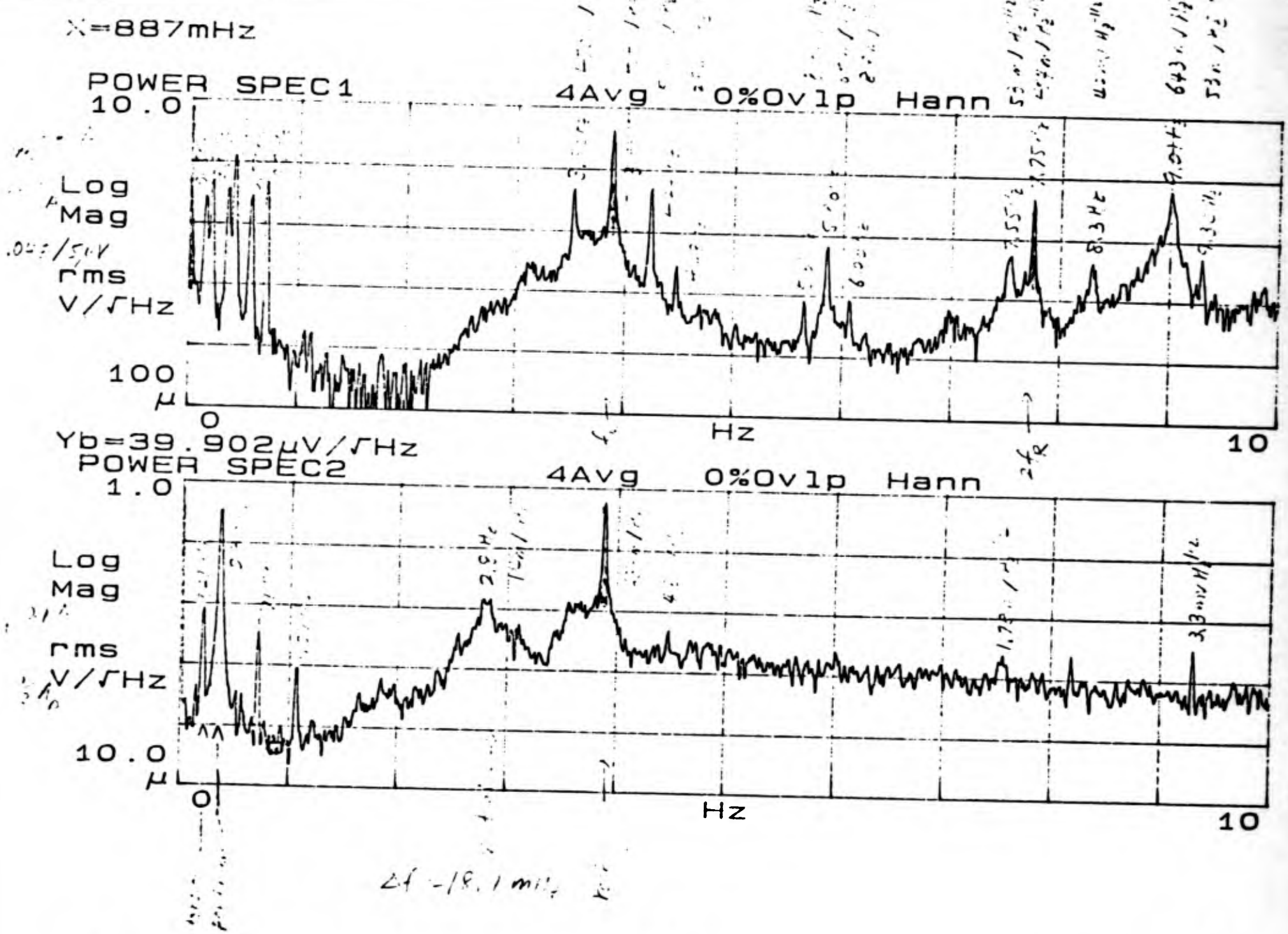
POWER SPEC1
4Avg 0%Ovlp Hann
10.0
Log
Mag
rms
V/√Hz
100
μ
0
Hz
10
Yb=39.902μV/√Hz
POWER SPEC2
4Avg 0%Ovlp Hann
1.0
Log
Mag
rms
V/√Hz
10.0
μ
0
Hz
10

Noise Spectra of the New SGG

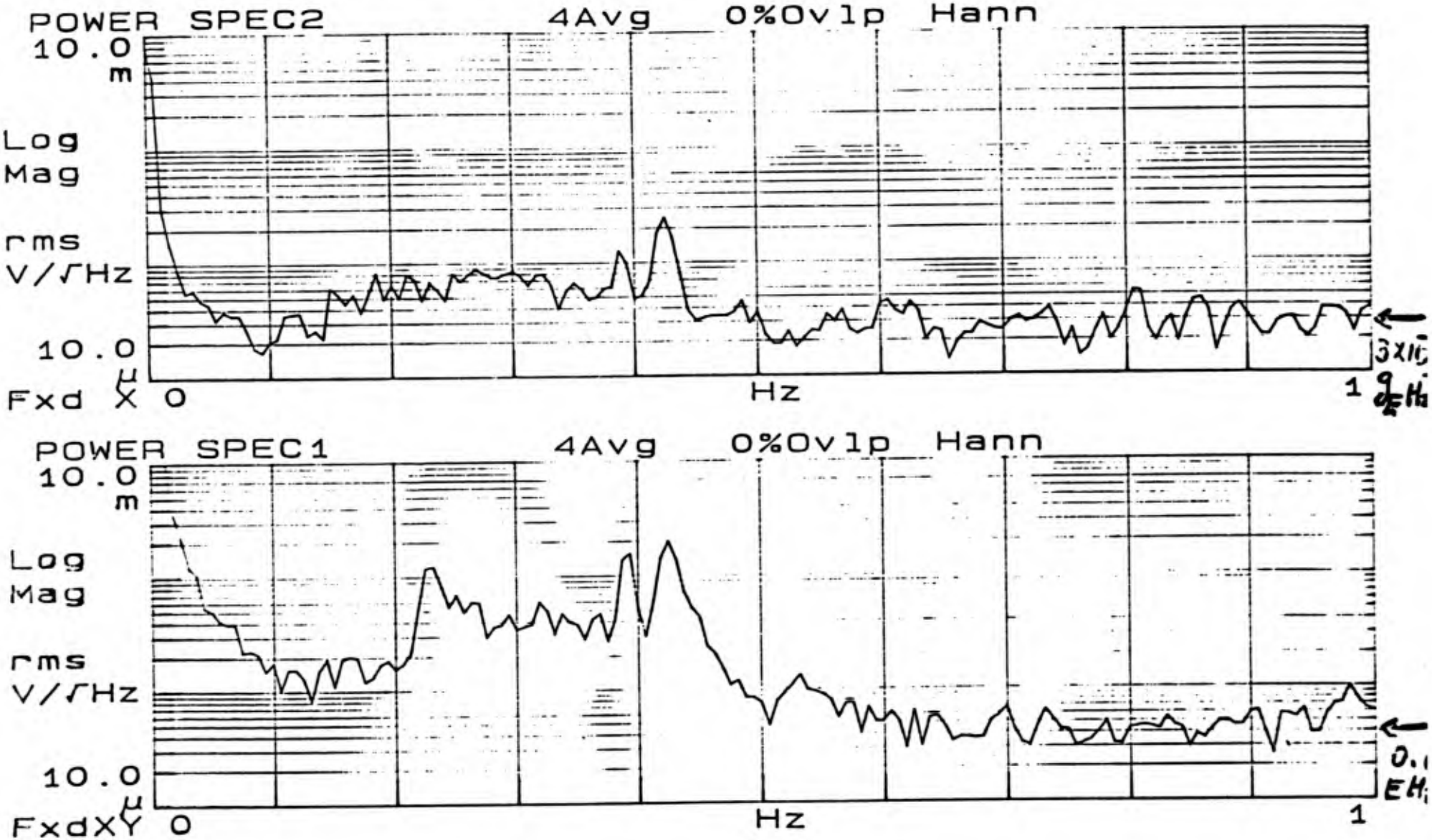

2. Six-Axis Accelerometer Test

a) 1st cool-down of the accelerometer (June, 1987)

1) 4 of 6 levitation/feedback circuits operated.
⇒ levitation in two degrees of freedom demonstrated

2) SQUID did not operate.
⇒ rf interference identified.

b) Partial repair of the accelerometer

1) New S/C joints were made for 2 levitation/feedback coils that did not operate.

2) Shielded transformers were inserted between the osillator signal leads and the inductance bridges.

c) 2nd cool-down of the accelerometer (August, 1987)

1) Same problems as before for levitation/feedback circuitry
⇒ Problems are with the coils.

2) SQUID circuitry operated well.
⇒ No deterioration of noise performance with osillator connected.
⇒ Intial demonstration of multi-frequency sensing.

3) Some sensing circuits had open coils.

d) Complete overhaul and reassembly (March, 1988).

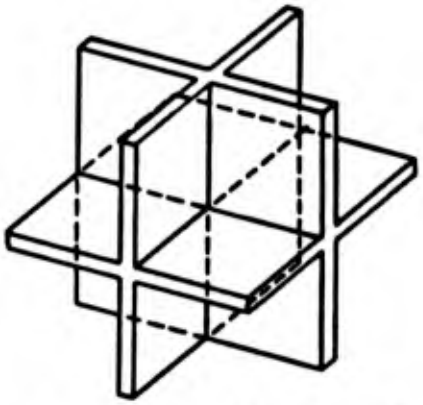

Proof mass (Niobium)
(a)

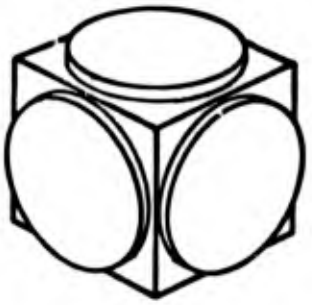

Coil form (Macor ceramic)
(b)

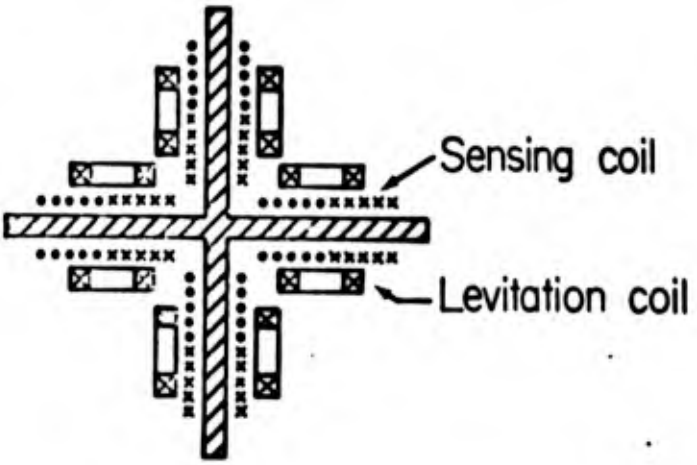

Coils (24 sensing coils + 24 levitation coils)
(c)

Levitation / Feedback Circuit

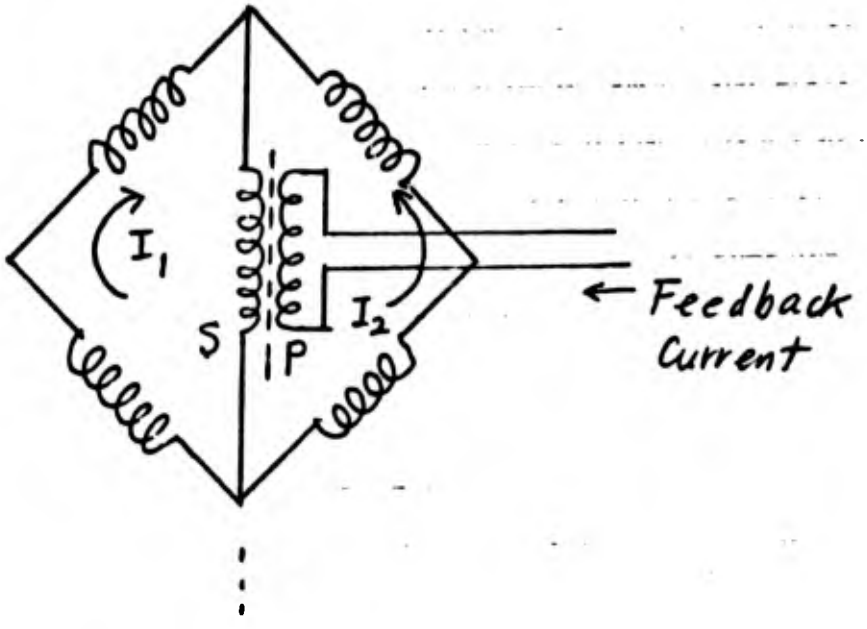

Sensing Circuit

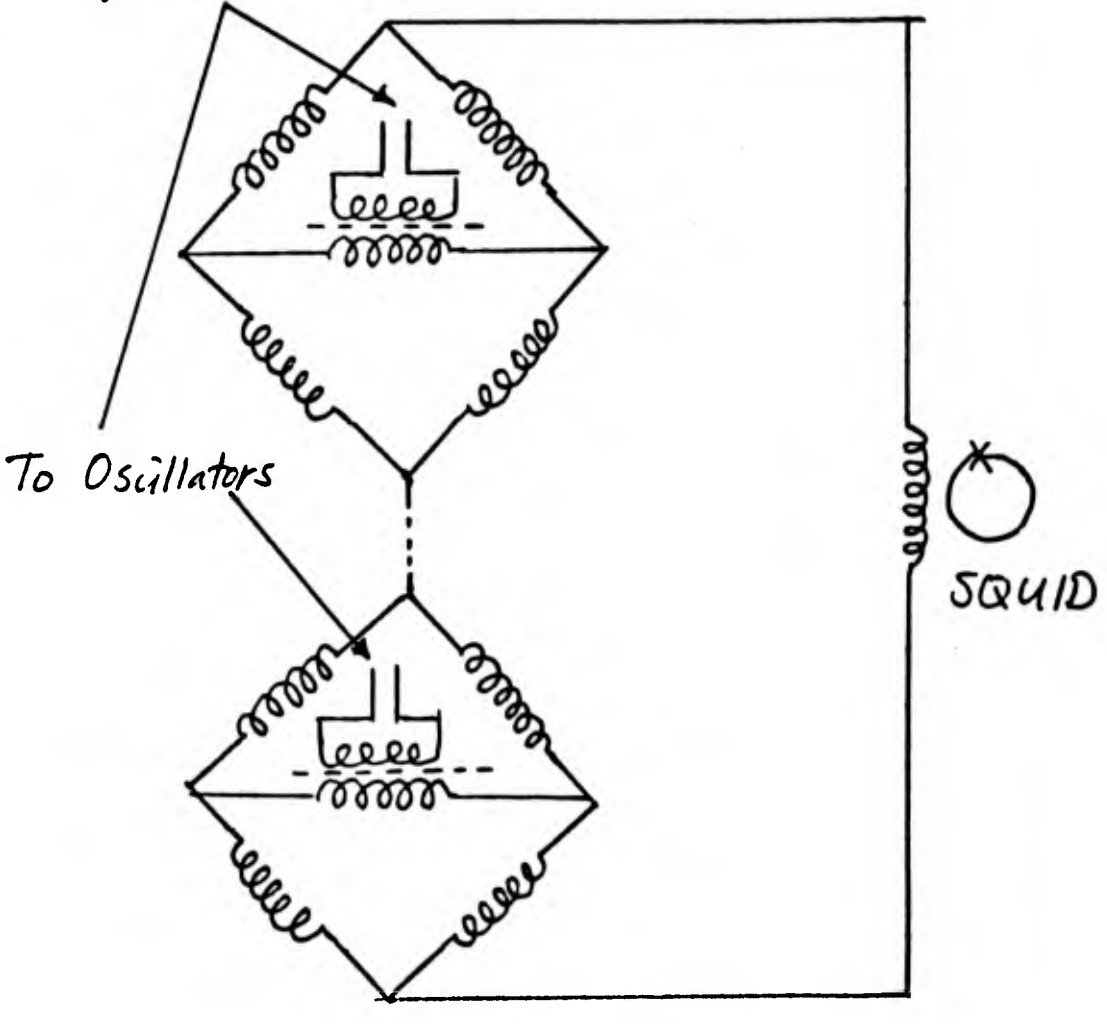

3. Design of 3-Point Adjustable Suspension

Rationale : a) Increased rigidity for angular motions

b) Adjustment of tilt angle for R^{-2} law test.

Features : a) 3-Point adjustable suspension

b) Laser alignment of tilt angle to 10^{-5} rad.

Design :

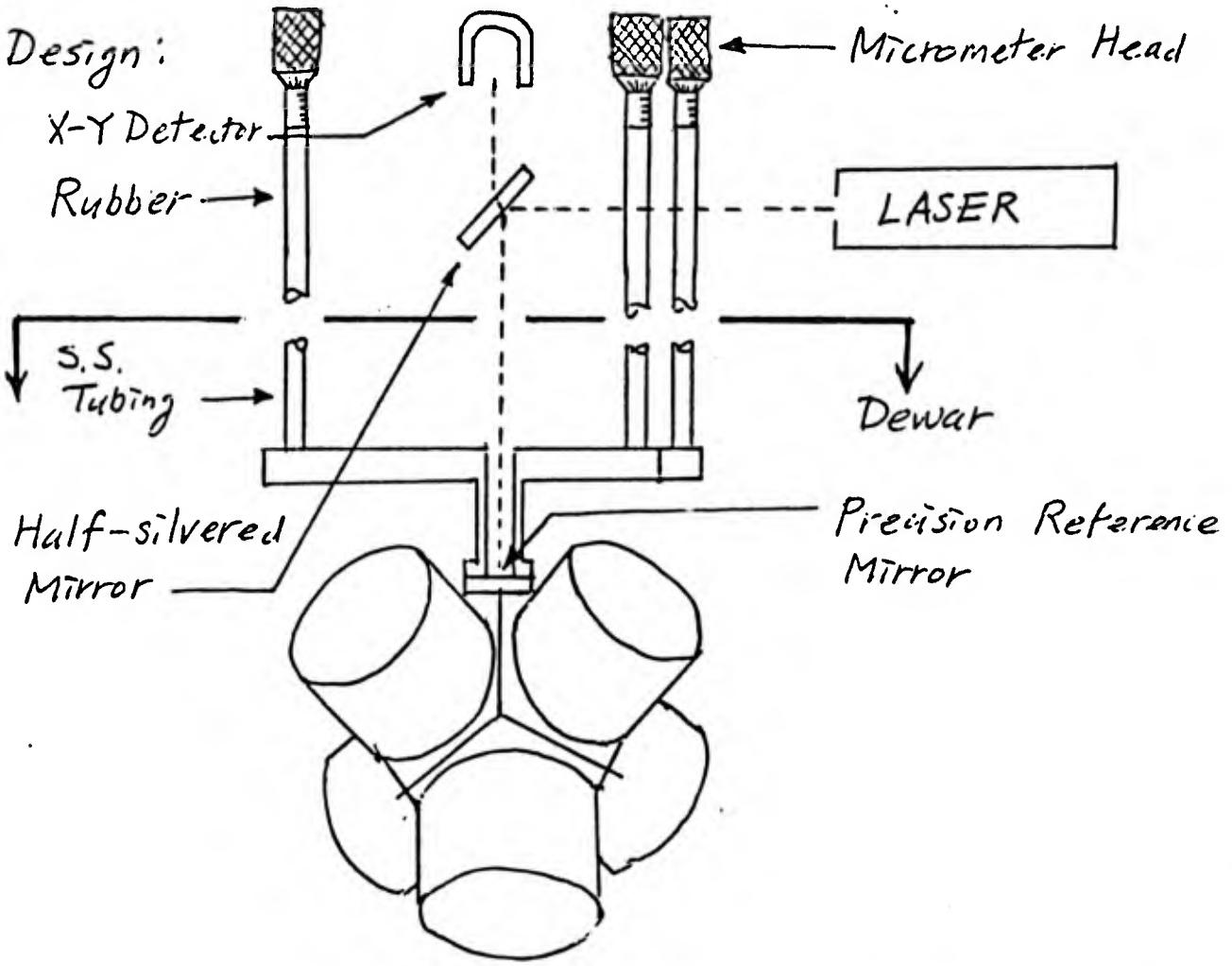

Disadvantages : a) Low frequency tilt noise couples in directly

b) No pendulum isolation for horizontal acceleration $\Rightarrow$ Residual balance

Pendulum Suspension

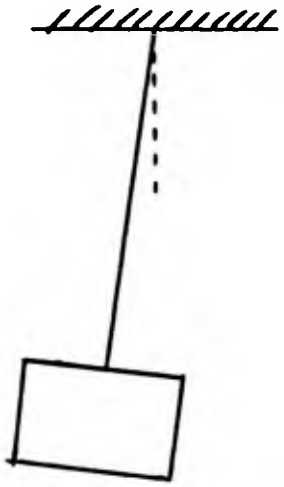

Advantages: 1) Platform decoupled from ground tilt
2) Horizontal acceleration balanced by induced tilt modulation of Earth's gravity

Disadvantage: Horizontal acceleration drives angular acceleration of platform ⇒ centrifugal acceleration

Solutions: 1) Platform stabilization by angular sensing and feedback
2) Axis alignment to reduce angular acceleration sensitivity.

Three-Point Suspension

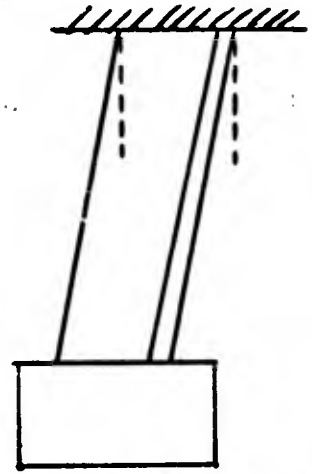

Advantages: 1) Linear acceleration of ground drives linear acceleration of platform only.
2) Torsional mode is stiffened.

Disadvantage: Sensitive to low frequency ground tilt.
⇒ important source of noise for R^{-2} law experiment.

Solutions: 1) Residual balance of common mode
2) Platform stabilization by angular sensing and feedback

Initial Performance of 3-Point Suspension

1. Tilt angle of the gradiometer with respect to the vertical adjusted to 10^{-4} rad.
   (with aid of a mercury pool)

2. Tilt sensitivity of the optical system: 10^{-6} rad $Hz^{-1/2}$.
   Cf. Required sensitivity for platform stabilization

$$\boxed{\frac{1}{\ell}\frac{a_E}{\sqrt{3}}\,\delta n_-\,\delta\theta \le \delta\Gamma}$$

   For $\delta n_- = 10^{-3}$ (worst case),

$$\underline{\delta\theta \le (3\times 10^{-8}\ \text{rad/E})\,\delta\Gamma}$$

   a) Tilt sensitivity could be improved to 10^{-9} rad $Hz^{-1/2}$ by chopping the laser
   $\Rightarrow \delta\Gamma \ge 0.03\,E\ Hz^{-1/2}$.

   b) With 3-D balance, $\delta n_- \to < 3\times 10^{-6}$.
   $\Rightarrow \delta\Gamma \to 10^{-4}\,E\ Hz^{-1/2}$.

3. Low frequency excess noise below 0.05 Hz due to drift in electronics.
   $\Rightarrow$ Laser chopping is required.

4. Three-Axis SGG Model II

Has been assembled and is being tested.

a) Common mode sensing circuit is identical to differential mode sensing circuit.

⇒ Complete decoupling between the two modes. Desired redundancy.

b) 3-dimensional balance circuits incorporated.

⇒ Common mode rejection in 3 dimensions

⇒ Required for 3-point suspension.

c) Failure of both sensing circuits in one axis.

⇒ Only 2-axes tested during 1st cool-down.

d) Differential axis misalignments $\delta n_- = \begin{cases} 3 \times 10^{-4} \\ 5 \times 10^{-4}. \end{cases}$

⇒ Poorer noise spectrum without 3-D balance ($\sim 0.4\,E\,Hz^{-1/2}$ at $1.0 \sim 1.5$ Hz)

e) Coupling of 3-D balance circuit was too weak.

⇒ 10^{-4} while 10^{-3} is required.

⇒ Transformers will be rebuilt.

f) Low frequency excess noise was comparable.

⇒ Active platform stabilization against tilt may be required.

Previous Circuit

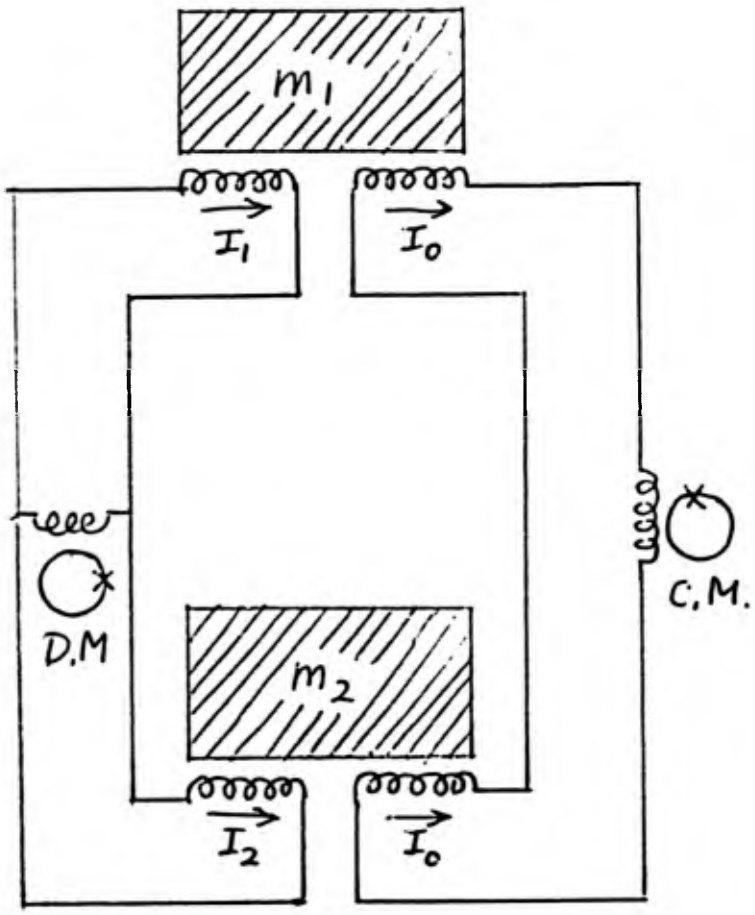

New Circuit

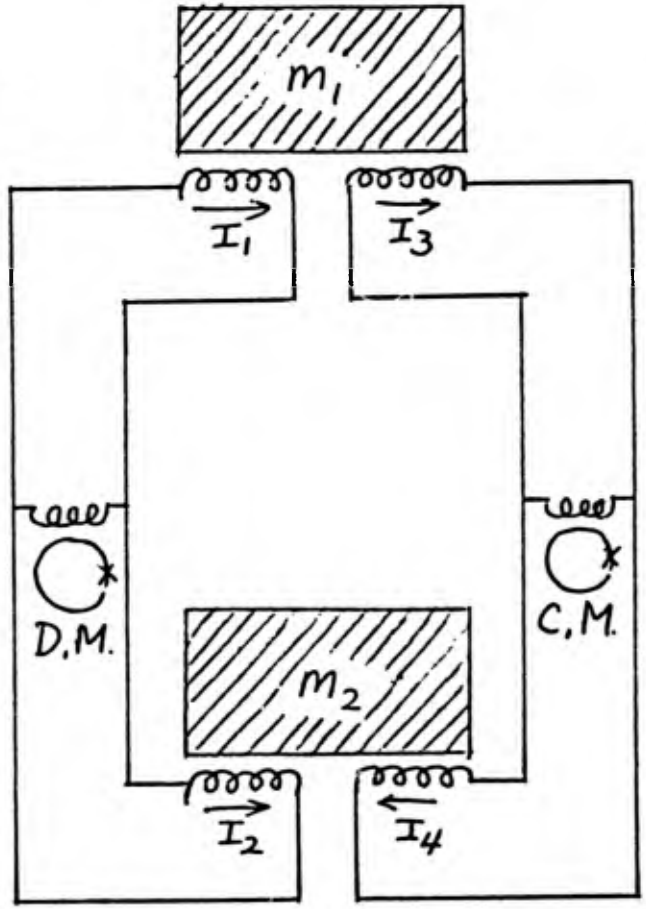

Three-dimensional common mode balance

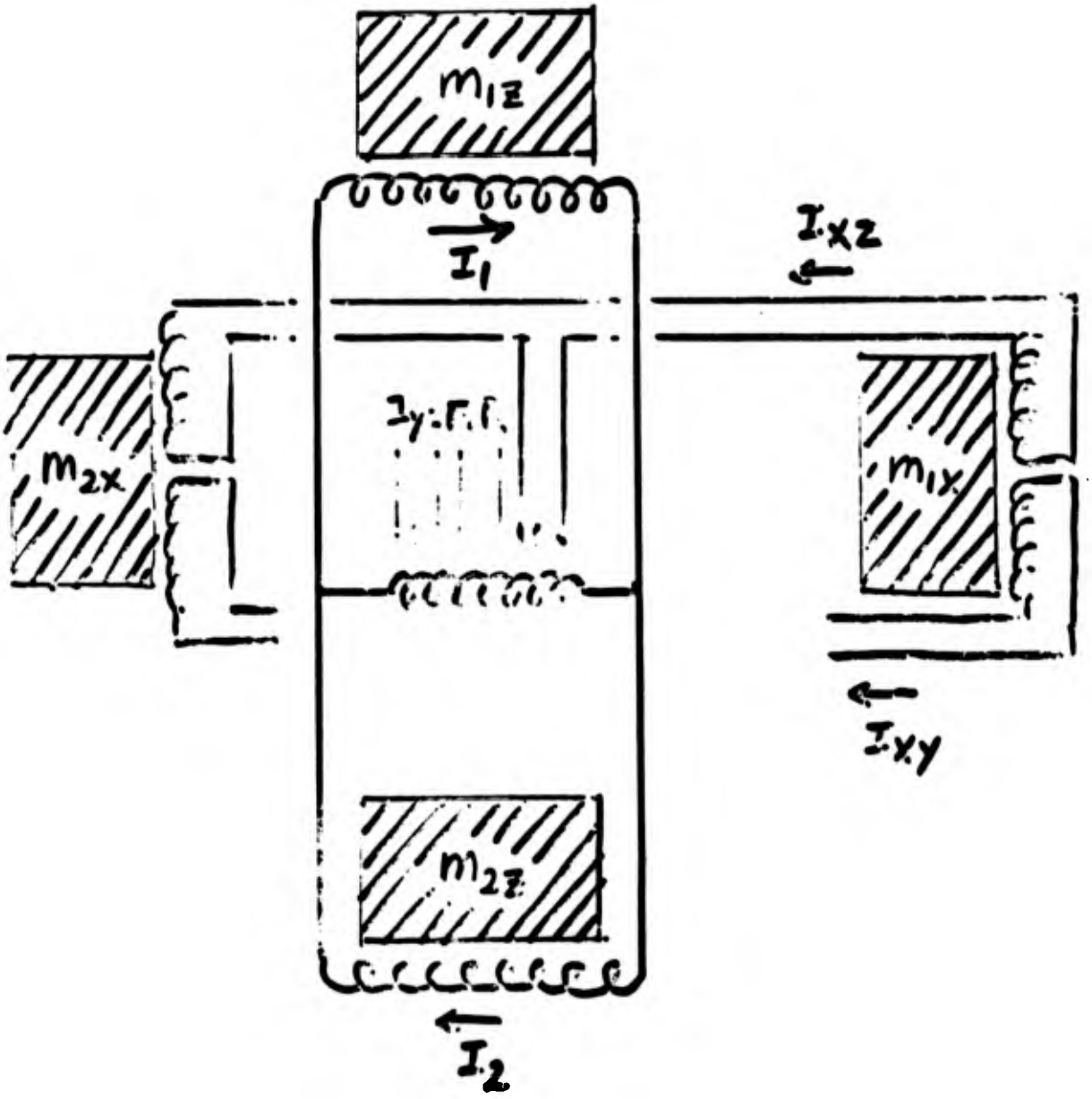

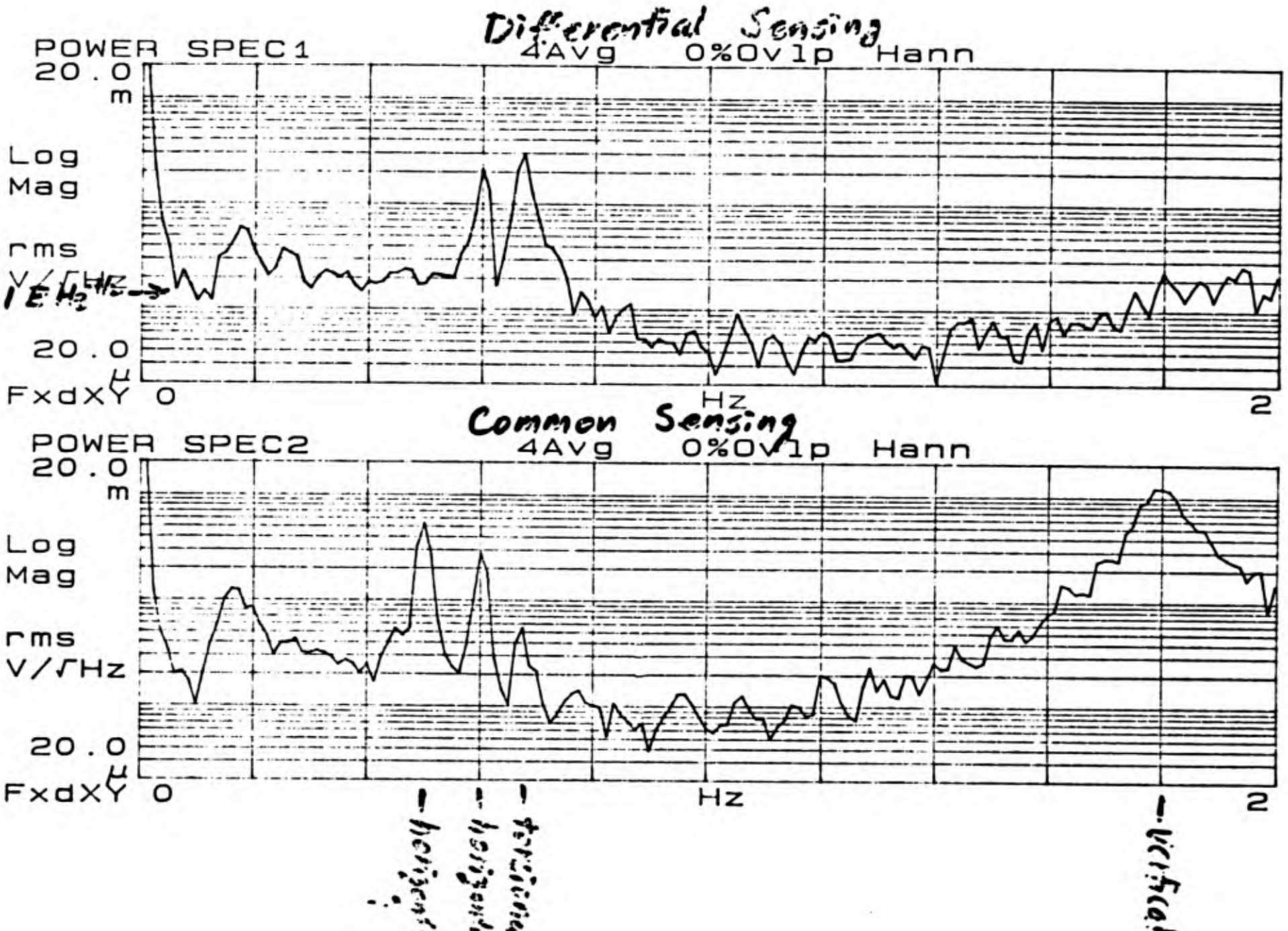
Differential Sensing
POWER SPEC1
4Avg 0%Ovlp Hann
20.0 m
Log Mag
rms V/√Hz
20.0 μ
FxdXY 0
Hz
2
Common Sensing
POWER SPEC2
4Avg 0%Ovlp Hann
20.0 m
Log Mag
rms V/√Hz
20.0 μ
FxdXY 0
Hz
2

5. Single-Axis SGG Model III.

Negative spring is incorporated.

a) A single accelerometer was constructed.

⇒ Redesign of the proof mass and coil forms

b) The accelerometer was tested horizontally.

⇒ Proved that the design allows complete cancellation of differential mode spring.

⇒ Nonlinearity in the negative spring needs to be investigated.

c) A single-axis SGG Model III is being constructed

⇒ Intrinsic sensitivity → 10^{-4} E $Hz^{-1/2}$

Engineering Model for space flight.

d) Piezoelectric alignment flanges are being tested.

⇒ To reduce $\varepsilon_{n_{4L}}$ to $< 10^{-6}$.

⇒ To produce acceleration signals.

Model III

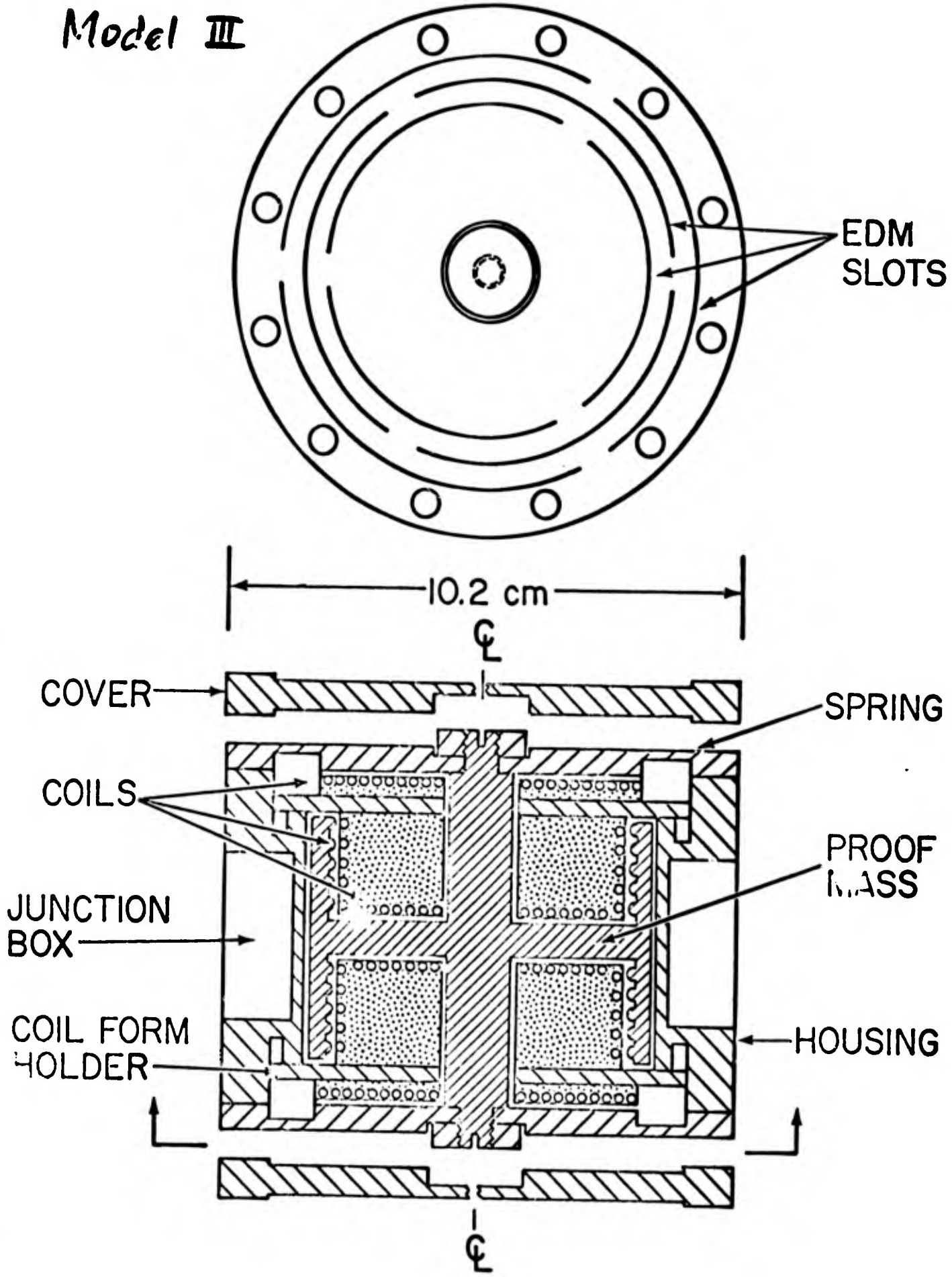
EDM
SLOTS
10.2 cm
COVER
SPRING
COILS
PROOF
MASS
JUNCTION
BOX
COIL FORM
HOLDER
HOUSING

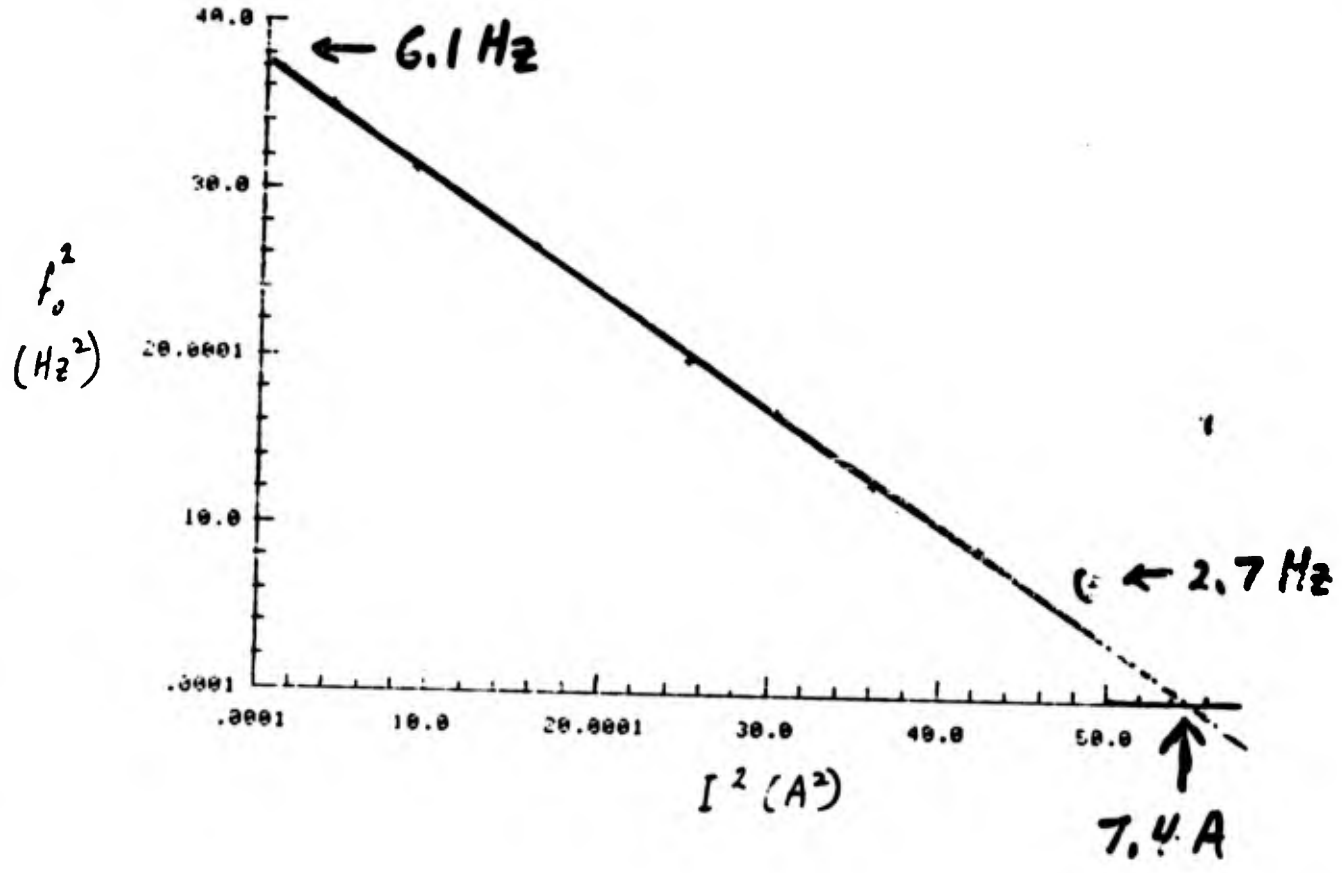

Negative Spring Test.

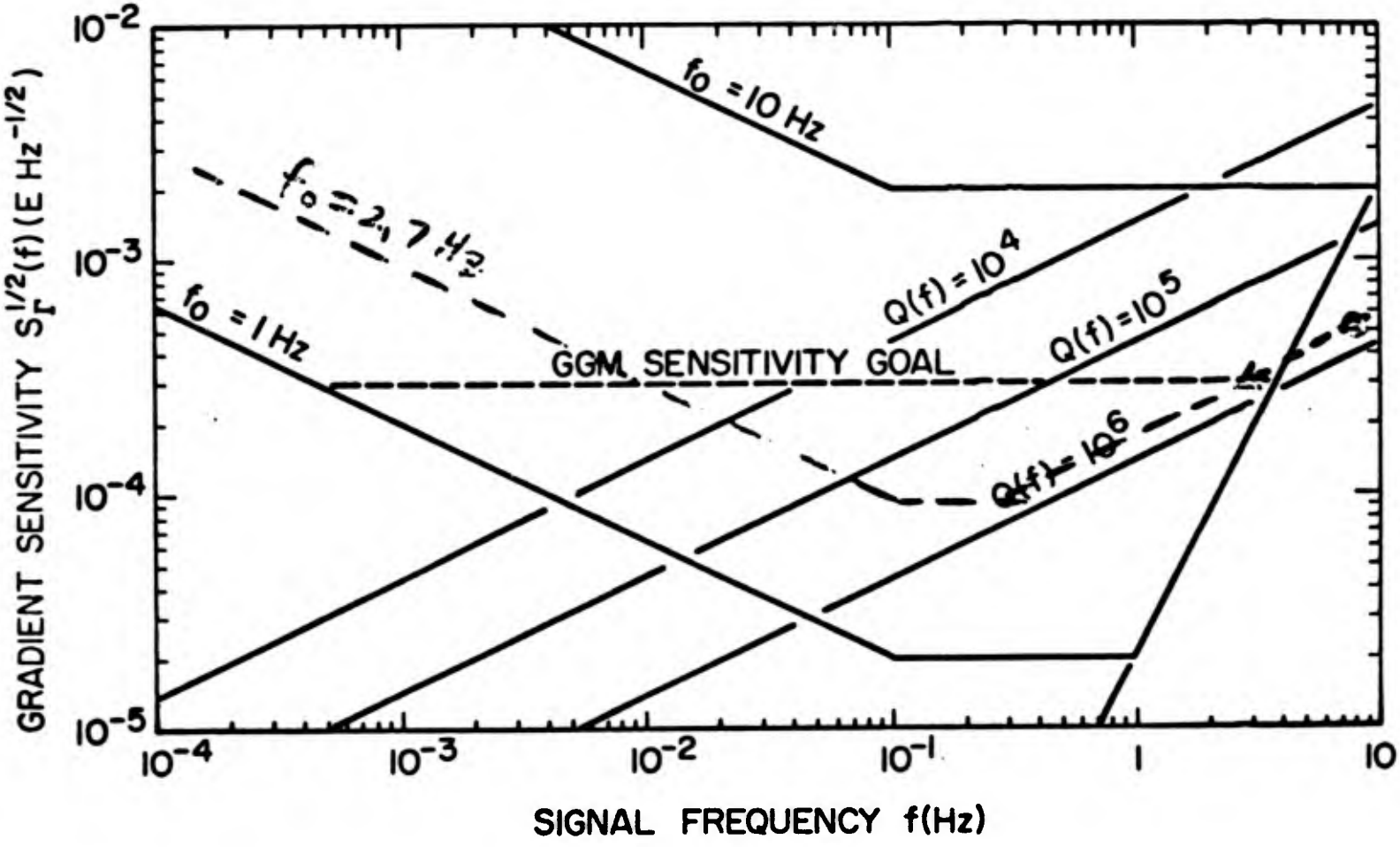
GRADIENT SENSITIVITY $S_\Gamma^{1/2}(f)$ (E Hz$^{-1/2}$)
10^{-2}
10^{-3}
10^{-4}
10^{-5}
f_0 = 10 Hz
f_0 = 2.7 Hz
f_0 = 1 Hz
Q(f) = 10^4
Q(f) = 10^5
Q(f) = 10^6
GGM SENSITIVITY GOAL
10^{-4}
10^{-3}
10^{-2}
10^{-1}
1
10
SIGNAL FREQUENCY f(Hz)

c. Axis Alignment and Platform Stabilization

Common mode balance between 0.5 Hz and 1 Hz

$$3\times10^{-5} = \frac{l}{l_p}\,|\delta\hat{n}_{+\hat{l}}|$$

$$\Rightarrow |\delta\hat{n}_{+\hat{l}}| = 2.5\times10^{-4}.$$

We want $|\delta\hat{n}_{+\hat{l}}| \lesssim 10^{-6}$. $\Rightarrow$ **Active axis aligner**

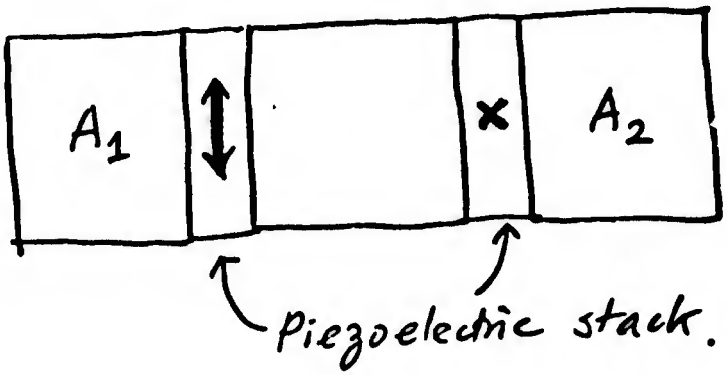

Low frequency excess noise due to centrifugal acceleration $\Rightarrow 0.3\,E\,Hz^{-1/2}$ at 0.1 Hz

We want a factor of 10^2 reduction in angular motion.

$\Rightarrow$ **Active platform stabilization**

6. OUTLOOK

1) Gradiometer Development

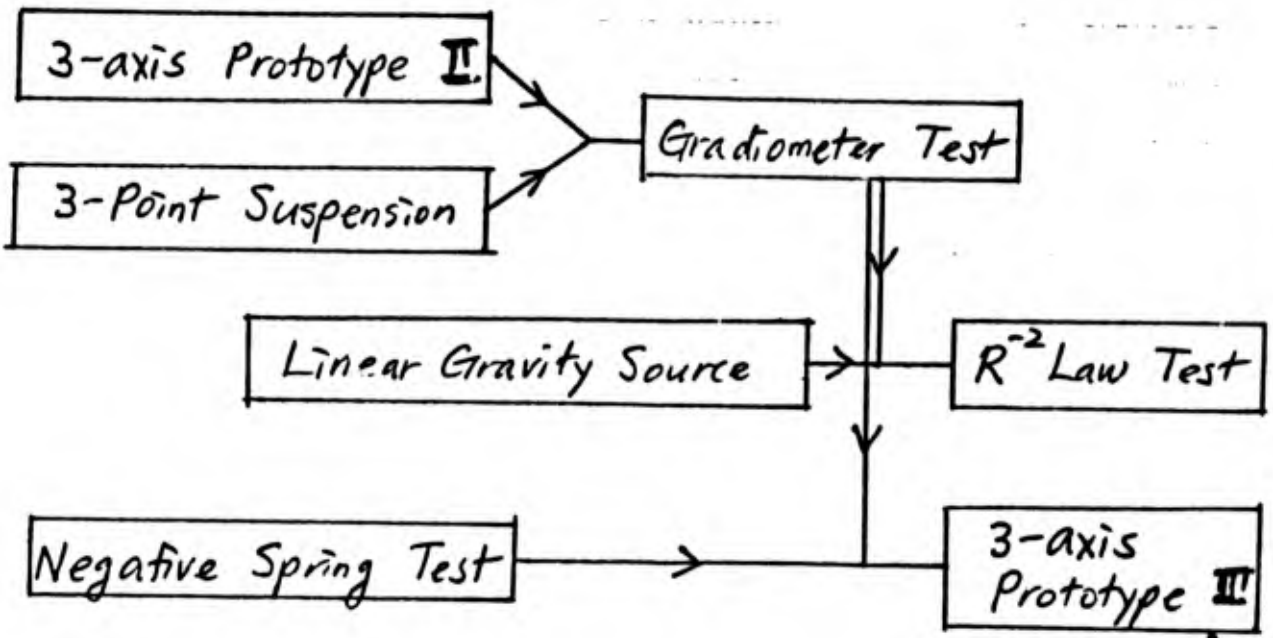

2) Accelerometer Development

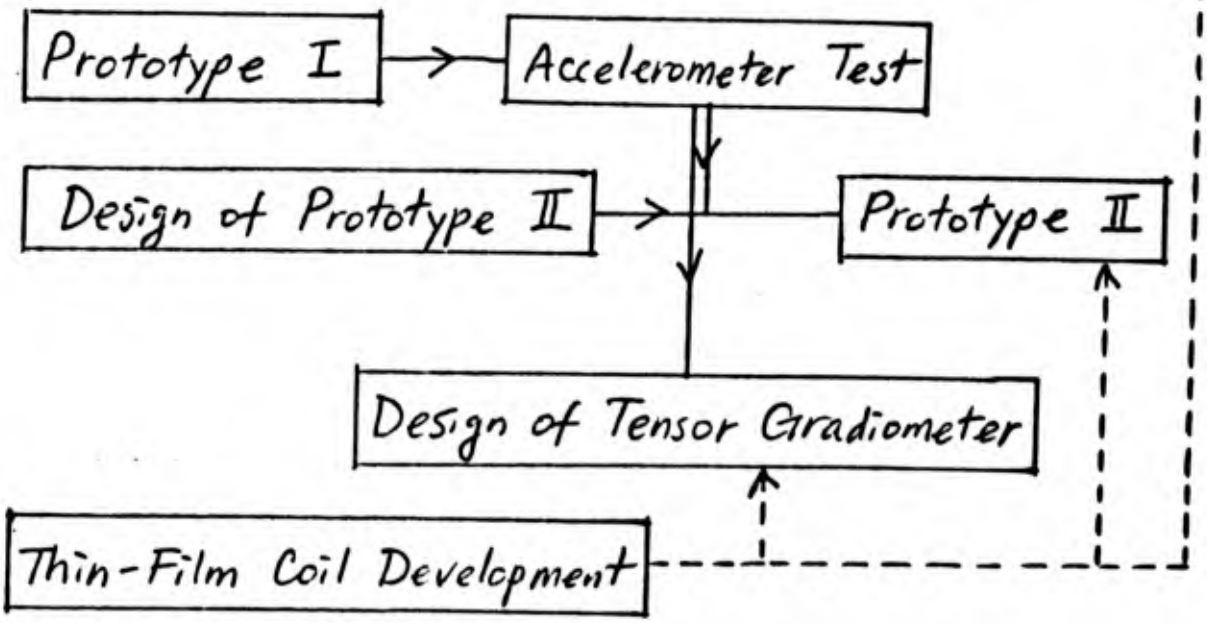

THE GRADIO SPACEBORNE GRAVITY GRADIOMETER: DEVELOPMENT AND ACCOMODATION

by

A. Bernard
P. Touboul

Office National d'Etudes et de Recherches Aerospatiales
BP 72
92322 Chatillon Cedex
France

Ultrasensitive electrostatic accelerometers are being developed in ONERA for satellite gravity gradiometry. The principle of operation, based on a three-axis electrostatic suspension of a cubic proof mass, is well suited for the measurements of accelerations less than 10^{-4} ms^{-2} with a resolution better than 10^{-11} ms^{-2} $Hz^{-1/2}$.

The GRADIO gravity gradiometer is composed of eight accelerometers located at the corners of a cubic structure. The gravity gradient components are determined through differential measurements between these accelerometers. This presentation aims at pointing out the challenging problems to be solved not only for the gradiometer development but also for its accommodation on board a dedicated spacecraft.

To get a resolution of 10^{-2} E $Hz^{-1/2}$ at an altitude of 200 km for the recovery of the Earth gravity field, the gradiometer and the spacecraft must be jointly designed and optimized, step by step, to take advantage of the performances of each one to compensate for the limitations of the other. The spacecraft must insure a peaceful environment for the instrument; the latter must exhibit an outstanding sensitivity and high rejection ratios for the residual disturbances.

According to the principles of Satellite Gravity Gradiometry, the critical areas are identified for two basic options: drag-free and non drag-free spacecrafts. The variations of all disturbances in the measurement bandwidth must be minimized:

- linear and angular accelerations through the altitude and orbit controls,
- vibrations, magnetic and thermal variations, etc... through the on board accomodation.

Even so, variation of the spacecraft self gravity, due to change in mass distribution, is a major item.

Whatever the effort paid for this accommodation, it is necessary to identify the accelerometer misalignments and sensitivity deviations with an accurate on board calibration.

Finally, the differential accelerometric measurements are to be corrected through an on ground data pre-processing to extract the gravity gradient components. All these critical items are studied in parallel with the development of the ultrasensitive electrostatic accelerometers. This development leads to experimental studies performed with laboratory models operating under normal gravity conditions.

Tests in ONERA's drop tower facility will be insured for the engineering and flight models. According to the status of these studies, and to the actual results that are presented, a launch in 1993 is foreseen for the European ARISTOTELES project.

ONERA

GRADIO SPACEBORNE GRAVITY GRADIOMETER: DEVELOPMENT AND ACCOMMODATION

by A. Bernard and P. Touboul

16th Annual Gravity Gradiometry Conf.
Colorado Springs, 10-11/02/1988

OFFICE NATIONAL D'ETUDES ET DE RECHERCHES AEROSPATIALES
29, Avenue de la Division Leclerc, Châtillon-sous-Bagneux (Hauts-de-Seine)

Adresse postale : BP 72, 92322 CHATILLON CEDEX (France)

Téléphone: (1) 46.57.11.60 Télex: ONERA 260907F

GRADIOMETRY THROUGH DIFFERENTIAL ACCELEROMETRY

Gradiometer purpose : → $T_{ij} = \dfrac{\partial^2 U}{\partial x_i \partial x_j}$

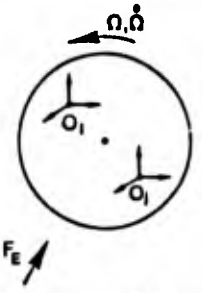

Differential accelerometric measurement :

$$(r_i - r_j) = [M](O_i - O_j)$$

with $[M] = \underbrace{[-T] + [\Omega^2]}_{\text{symmetric}} + \underbrace{[\dot{\Omega}]}_{\text{antisymmetric}}$

By use of sets of differential measurements :

$$1/2\ ([M] - {}^T[M]) = [\dot{\Omega}]$$

$$1/2\ ([M] + {}^T[M]) = [-T] + [\Omega^2]$$

→ ***The attitude control must nullify*** $[\Omega^2]$

GRADIOMETRY THROUGH DIFFERENTIAL ACCELEROMETRY

Earth pointing

$$\vec{\Omega} = [\Delta\Omega_x \quad \Omega_0 + \Delta\Omega_y \quad \Delta\Omega_z]^T \qquad \text{with} \quad \Omega_0 \simeq 10^{-3}\ rad\,s^{-1}$$

$$\Delta\Omega_{x,y,z} < 10^{-6}\ rad\,s^{-1}$$

▷ From the SYMMETRIC part of the accelerometric measurement :

$$[A_S]_L \simeq \underbrace{\hat{M}^T [T]_S \hat{M}}_{[\hat{T}]_L} + \underbrace{\begin{bmatrix} \Omega_0^2 + 2\Omega_0\Delta\Omega_y & -\Omega_0\Delta\Omega_x & 0 \\ -\Omega_0\Delta\Omega_x & 0 & -\Omega_0\Delta\Omega_z \\ 0 & -\Omega_0\Delta\Omega_z & \Omega_0^2 + 2\Omega_0\Delta\Omega_y \end{bmatrix}}_{\text{kinematic acceleration}} + \underbrace{\frac{3GM}{r^4}\begin{bmatrix} \delta r & 0 & r\delta\theta_P \\ 0 & \delta r & -r\delta\theta_R \\ r\delta\theta_P & -r\delta\theta_R & -2\delta r \end{bmatrix}}_{\text{position and orientation}}$$

▷ From the ANTISYMMETRIC part of the accelerometric measurement :

$$[A_{AS}] \simeq -[\dot{\Omega}]$$

▷ From the DIAGONAL components :

Trace free tensor → $\| \vec{\Omega} \|^2$

▷ + independant observations

⟹ ***GRAVITY GRADIENT , ORIENTATION , POSITION***

ORBIT RESTITUTION

■ At first order :

$$[T] = \frac{GM}{r^3}\begin{bmatrix} -1 & 0 & 0 \\ 0 & -1 & 0 \\ 0 & 0 & 2 \end{bmatrix} \qquad [\delta T] = -3\frac{\delta r}{r}[T]$$

radial position $\delta r < 5m$
along- and cross track $\delta x, y < 1km$ } ⇒ $\|[\delta T]\| < 10^{-9}$ E.U.

■ Objective = determination of the high harmonics of the potential : $15 < l < 200$
Gradiometer bandwidth : 5×10^{-3} Hz to 0.25Hz

■ Even if drag is not compensated
(at 200km : $\Gamma_{drag} = 5\times10^{-5}\ ms^{-2}$)
for frequencies $> 5\times10^{-3}$ Hz, orbit variations are acceptable

■ Furthermore, for l=200, a reduction of 1% of the gravity gradient corresponds to δr 150m

CONCLUSION :
for $\|\delta T\| < 10^{-2}$ E.U. $\quad 15 < l < 200$
ORBIT RESTITUTION :
$\delta r < 150m \quad \delta x, \delta y < 1km$

ATTITUDE RESTITUTION

■ Diagonal component measurements
(goal : 10^{-2} E.U.)

– variations of the attitude :
over 200s $\Delta\Omega < 10^{-6}$ rad/s ⇒ $\Delta\theta < 2\times10^{-4}$ rad
⇒ negligible effect

– earth pointing accuracy :
◆ *sensitivity to drag projection*
◆ *coupling of the gradiometer axes*
⇒ attitude restitution accuracy :
5×10^{-3} rad (control to 0.5°)

■ Non diagonal component measurements:
– T_{xy} : idem diagonal components
– T_{xz}, T_{yz} : variations of 1 E.U. correspond to variations of θ_T, θ_R of 2×10^{-4} rad

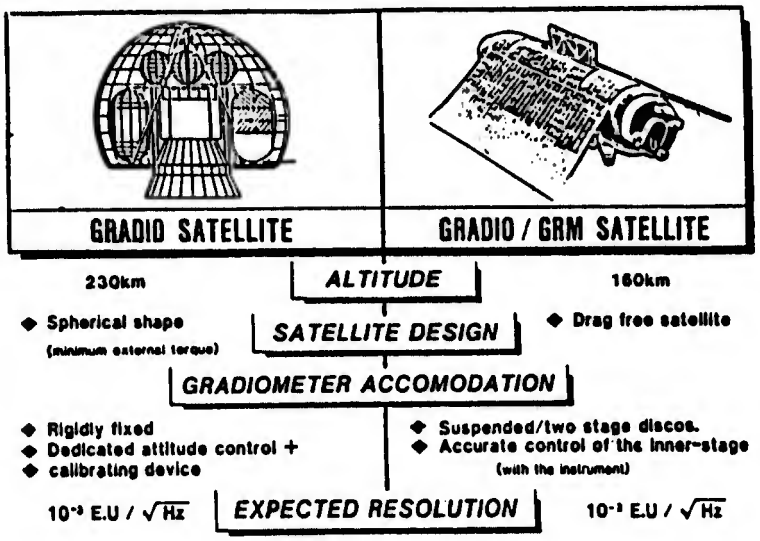

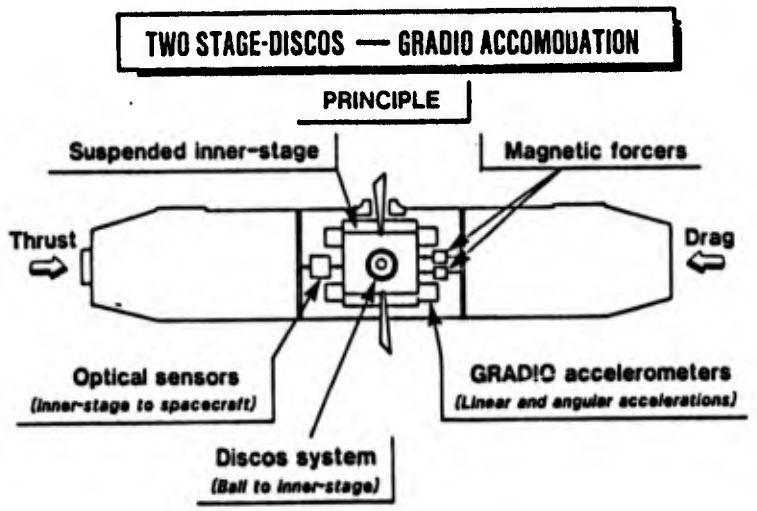

ATTITUDE CONTROL AND DRAG REJECTION

Instrument earth pointed accuracy < 0.5°

Specifications for variations • of :	Non drag free	Drag free
● *Angular acceleration*	10^{-7} rad/s ^{2}	10^{-8} rad/s ^{2}
● *Angular velocity*	10^{-6} rad/s	10^{-6} rad/s
● *Linear acceleration*	1% of the drag	10^{-9} m/s ^{2}
On board calibration performances :		
● *Scale factor matching*	10^{-5}	10^{-3}
● *Alignments*	10^{-5} rad	3×10^{-4} rad
● *Accelerometer locations*	10^{-5} m	10^{-4} m
Goal	10^{-2} E.U. for T_{yy} .T_{zz}	10^{-2} E.U. for T_{xx} .T_{yy} .T_{zz}

• in the measurement bandwidth [5×10^{-3} Hz – 0.25Hz]

GRADIOMETER ACCOMMODATION RIGIDLY FIXED

GRAVITY GRADIOMETER

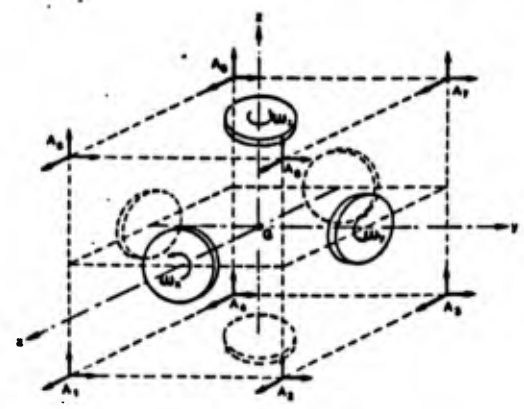

ADVANTAGES :

Simplicity of the instrument interfaces

DRAWBACKS :

High levels of accelerations (DRAG)

Poor resolution in the along track direction
Disturbances at each firing for orbit maintenance
High level of performances required for the gradiometer and its calibration :

- ▲ *Scale factor matching* 10^{-5}
  stability 10^{-6}
- ▲ *Alignments* 10^{-5} *rad*
  stability 10^{-7} *rad*
- ▲ *Accelerometer locations* 10^{-5} *m*
  stability 10^{-6} *m*

with a thermal control to 0.1°C over 200s

ACCELEROMETERS : SENSITIVITY ERRORS

Measurement : $\overrightarrow{\Gamma_i} = ([I]+[\varepsilon])\left\{([-\Gamma]+[\Omega^2]+[\dot{\Omega}])\overrightarrow{OO_1}+\overrightarrow{\Gamma_o}\right\}$

Sensitivity errors : $[\varepsilon] = \begin{bmatrix} \varepsilon_x & 0 & 0 \\ 0 & \varepsilon_y & 0 \\ 0 & 0 & \varepsilon_z \end{bmatrix}$ Diagonal $+ \begin{bmatrix} 0 & \varepsilon_{AS} & 0 \\ -\varepsilon_{AS} & 0 & 0 \\ 0 & 0 & 0 \end{bmatrix}$ Antisymmetric $+ \begin{bmatrix} 0 & 0 & \varepsilon_S \\ 0 & 0 & 0 \\ \varepsilon_S & 0 & 0 \end{bmatrix}$ Symmetric

	SCALE FACTORS	COUPLING	
Errors of :	Calibration $\varepsilon_{x,y,z} < 10^{-2}$	Alignment $\varepsilon_{AS} < 10^{-3}$	Proof-mass geometry —
Requirement : $\varepsilon < 10^{-6}$			
	Scale factor matching	Alignment	Optical cube

Continuous calibration + data processing

ALIGNMENT AND SCALE FACTOR MATCHING : PRINCIPLE

- ***Calibrating acceleration***

(provided by wheels of axis $\overrightarrow{x}$) ⟶ Accelerometer measurement

$$2\frac{\delta m}{M} r\omega_x^2 \begin{pmatrix} 0 \\ \cos\omega_x t \\ \sin\omega_x t \end{pmatrix} \longrightarrow 2\frac{\delta m}{M} r\omega_x^2 \begin{pmatrix} \varepsilon_x^y \cos\omega_x t + \varepsilon_x^z \sin\omega_x t \\ (1+\varepsilon_y)\cos\omega_x t + \varepsilon_y^z \sin\omega_x t \\ (1+\varepsilon_z)\sin\omega_x t + \varepsilon_z^y \cos\omega_x t \end{pmatrix}$$

SYNCHRONOUS DEMODULATION AT ω_x :

For $\overrightarrow{x}$: - in phase (cos) ⟶ ε_x^y
- in quadrature (sin) ⟶ ε_x^z

→ $\overrightarrow{x}$ ALIGNMENT

For $\overrightarrow{y}$: - in phase (cos)
For $\overrightarrow{z}$: - in quadrature (sin)

→ $\dfrac{1+\varepsilon_y}{1+\varepsilon_z}$ → $\overrightarrow{y}$ and $\overrightarrow{z}$ SCALE FACTOR MATCHING

▶ *In these demodulations , phase shifts give second order errors only*

GRADIOMETER ACCOMMODATION SUSPENDED DRAG FREE

ADVANTAGES :

- Low level of accelerations at low altitude
  (D.C. component of the gravity gradient)

Relaxed requirements for the gradiometer:

- *Scale factor matching* 10^{-3}
  stability 10^{-6}
- *Alignments* 3×10^{-4} *rad*
  stability 10^{-6} *rad*
- *Accelerometer locations* 10^{-4} *m*
  stability 10^{-6} *m*

with a thermal control to 0.1°C over 200s

DRAWBACKS :

- Increased complexity of the accommodation
  inner stage suspension and thermal controls
- Self gravity variations

CALIBRATING DEVICE : SUSPENDED GRADIOMETER

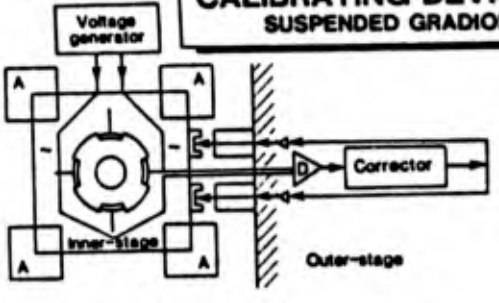

- Inner-stage : controlled to follow the proof-mass of the drag-free sensor (D.F.S.)
- Periodic voltages on D.F.S. electrodes
- I/S calibrated accelerations

CALIBRATING DEVICE : SUSPENDED GRADIOMETER

Electrical arrangment of the drag-free sensor

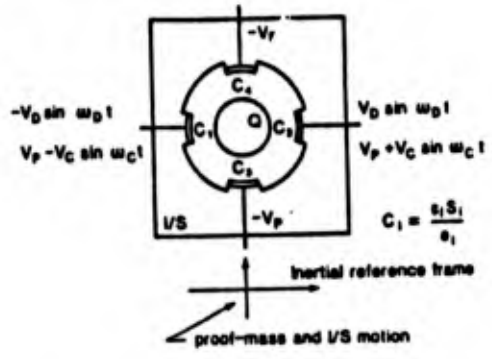

- $Q = \Sigma C_i V_i \simeq 0 \Rightarrow F_Q \simeq 0$
- $\Gamma_{calibration} = \frac{\varepsilon S}{me^2} V_P V_C \sin \omega_C t$

CHANGE IN MASS DISTRIBUTION
(Instrument/Spacecraft relative motions)

Symmetrical distributions :

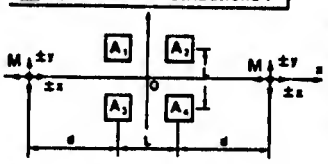

$$\hat{\Gamma}_{xx} = \frac{1}{2L}\left[(\Gamma_{x2} - \Gamma_{x1}) + (\Gamma_{x4} - \Gamma_{x3})\right]$$

For x and y displacements of two masses M : second order variations of $\hat{\Gamma}_{xx}$

M = 300kg L = 50cm d = 1.15m

x = 1cm ⇒ $\delta\hat{\Gamma}_{xx} \simeq 2.10^{-4}$ E.U

$\delta\hat{\Gamma}_{yy} \simeq 6.10^{-4}$ E.U

Lack of symmetry :

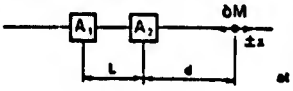

L = 50cm x = ±1cm :

Variations of 10^{-4} E.U correspond to :

δM (kg)	0.11	8.33	21.88
d (m)	0.3	1	1.8

at

CUBIC GRADIOMETER : self gravity effects (1)

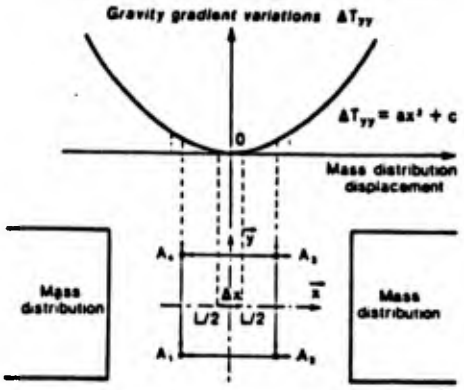

Δx : displacement of the symmetrical distribution of mass

$M_1 = (\Gamma_{3y} - \Gamma_{2y}) \times 1/L \Rightarrow \Delta T_{yy}$

$M_2 = (\Gamma_{4y} - \Gamma_{1y}) \times 1/L \Rightarrow \Delta T_{yy}$

Sensitivity to mass distribution displacement :

M_1, M_2 : first order

1/2 ($M_1 + M_2$) : second order

CUBIC GRADIOMETER : self gravity effects (2)

Effects of the gradiometer off-centering :

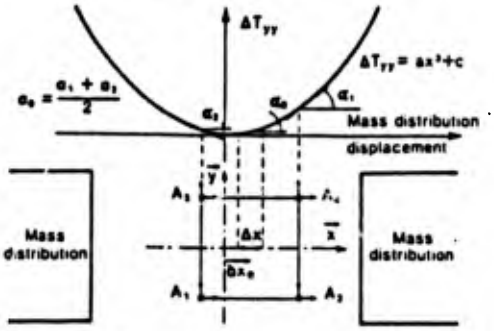

Δx : displacement of the symmetrical distribution of mass

δx_0 : off-centering of the gradiometer

$M_1 = M_{10} + \alpha_1 \Delta x$ $M_2 = M_{20} + \alpha_2 \Delta x$

Sensitivity to Δx : $\frac{1}{2}(M_1 + M_2)$: first order

SELF GRAVITY EFFECTS

For a cylindrical S/C configuration

L = 3.6m Ø = 1.4m M = 1800kg

(Fuel : 2 groups of tanks

m_1, m_2 = 500kg, d = 1.25m)

ΔT (E.U.) $\simeq 10^3 \Delta x^2 + 10^2$

Δx_{max} = 1mm

ΔT = 10^{-2} E.U. ⇒ $\delta x_0 < 5$mm

The estimation of the linear sensitivity to displacement of M_1 and M_2 provides :

. curvature of $\Delta T = F(\Delta x)$

. off-centering δx_0

Accuracy of the data processing to correct for the self gravity variations ?

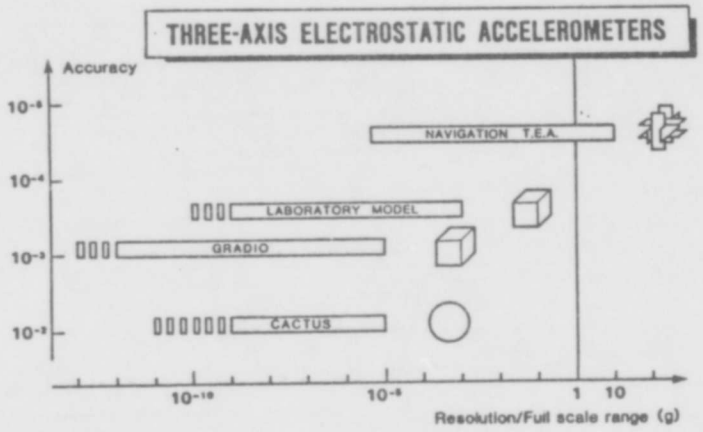
THREE-AXIS ELECTROSTATIC ACCELEROMETERS
Accuracy
10^{-5}
10^{-4}
10^{-3}
10^{-2}
NAVIGATION T.E.A.
LABORATORY MODEL
GRADIO
CACTUS
10^{-10}
10^{-5}
1
10
Resolution/Full scale range (g)

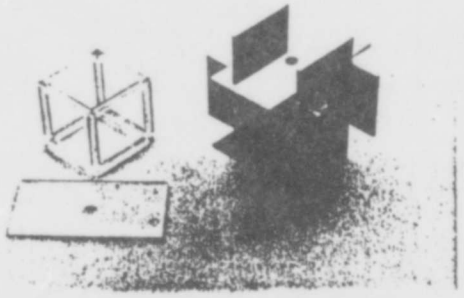

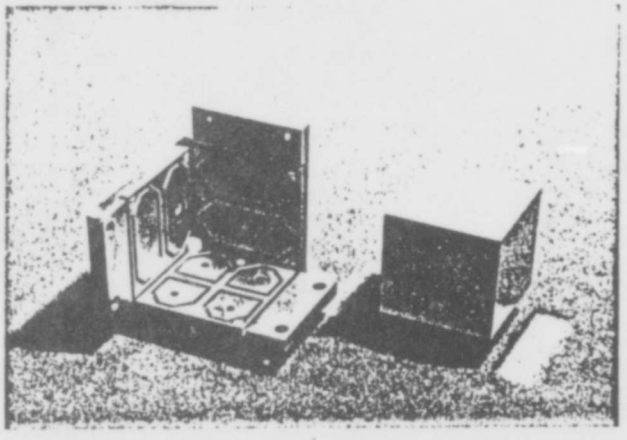

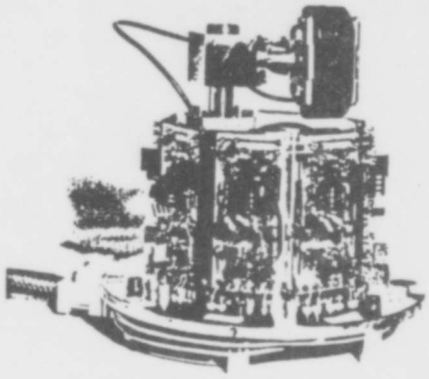

GRADIO ACCELEROMETER : SPECIFICATIONS

△ $T_{ij} \leq 3000$ Eötvös (3×10^{-9} ms^{-2} for 1m base line)

△ Atmospheric drag : 10^{-8} ms^{-2} (200 km)

⇨ ***Range :*** 10^{-4} ms^{-2}. full scale

△ T_{ij} variations 10^{-2} Eötvös / 10 sec

⇨ ***Resolution :*** 10^{-11} ms^{-2} for a bandwidth < 1Hz

△ Use of a set of differential measurements :

- ○ *linearity*
- ○ *low coupling*
- ○ *scale factors matching*

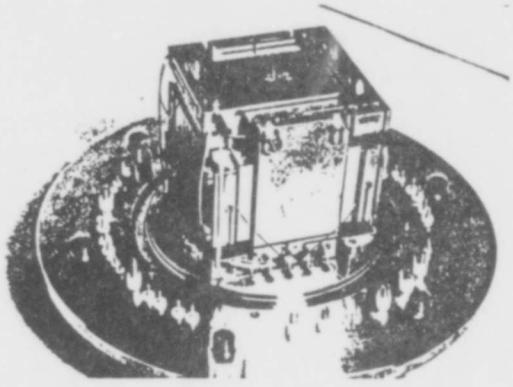

ACCELEROMETER ERROR BUDGET

[1] Parasitic accelerations due to

- ◆ *Thermo-molecular forces*
- ◆ *Magnetic forces*
- ◆ *Random damping*
- ◆ *Stiffness of electrical wires*
- ◆ *Electrical dissymmetries*

[2] Electrical noise of the servoloop

[3] Mechanical assembly stability

Very stable material (electrodes in silica)
Heavy proof-mass
Low magnetic susceptibility

Thermal environment stability 0.1℃
Internal thermal gradient 0.01℃

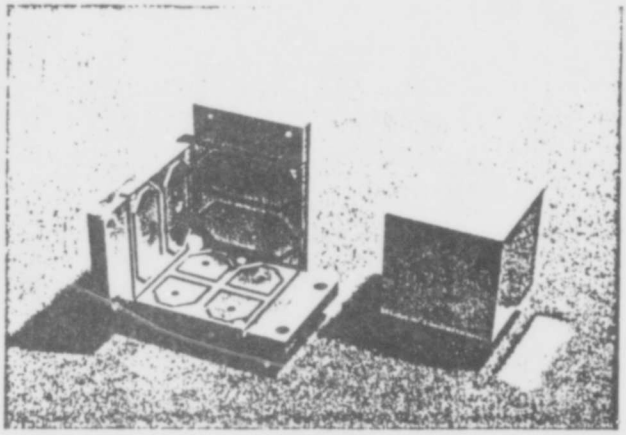

PENDULUM BENCH TEST
PRINCIPLE

$g\alpha - l\ddot{\alpha} \simeq 0 \quad \Rightarrow \quad \Gamma_{x1} \simeq 0$

Seismic vibrations rejected by

- elastic suspension
- pendulum effect
- differential tests

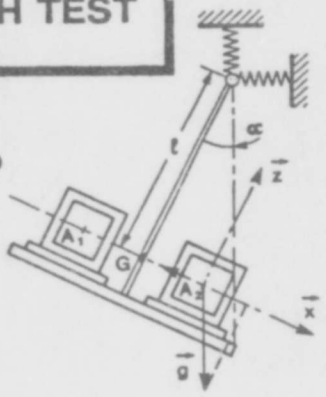

PENDULUM BENCH

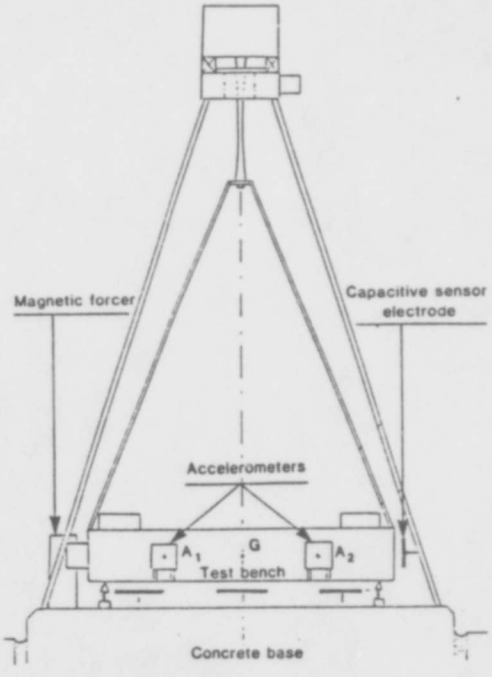

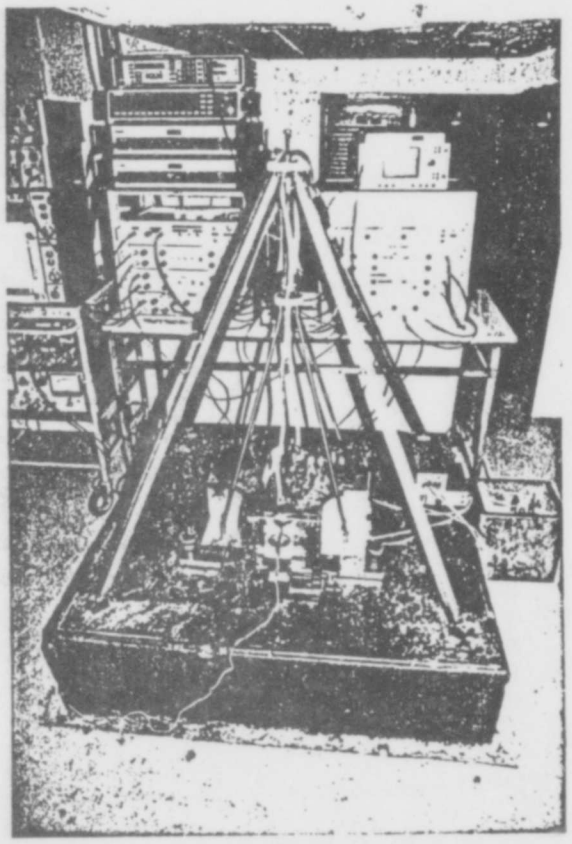

THERMAL TEST
CAPACITIVE POSITION SENSOR STABILITY

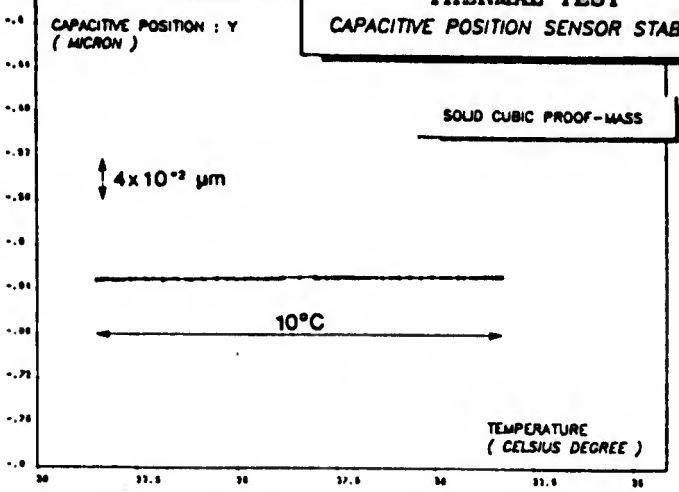

ELECTRICAL STIFFNESS MEASUREMENT
(SENSITIVE AXIS Y)

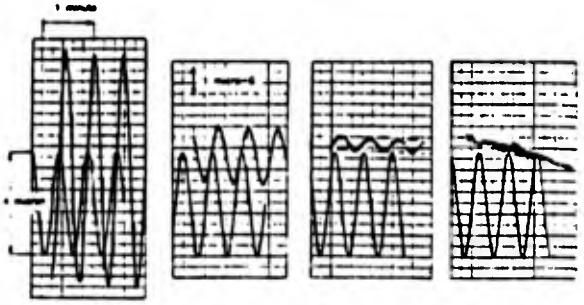

Vp = 100 V Vp = 50 V Vp = 25 V Vp = 10 V

K = 1.648 N/m K = 0.424 N/m K = 0.094 N/m K = 0.016 N/m

ELECTRICAL STIFFNESS :
COMPARISON BETWEEN MEASURED AND THEORICAL VALUES

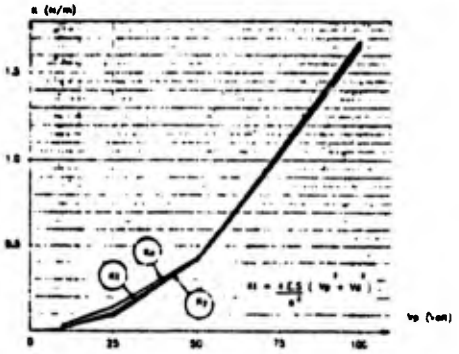

COMPARED OUTPUTS

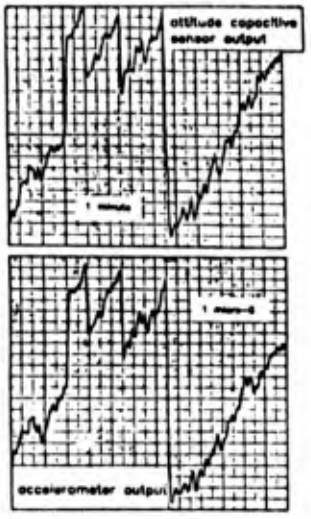

PENDULUM TEST

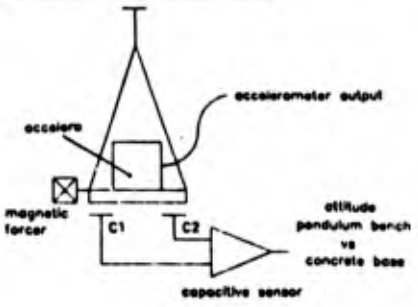

PENDULUM BENCH INCLINATION CONTROLLED THROUGH CAPACITIVE SENSOR OUTPUTS

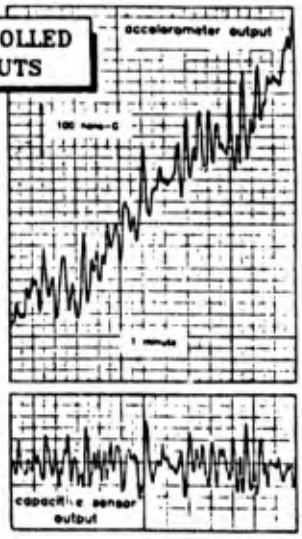

PENDULUM TEST

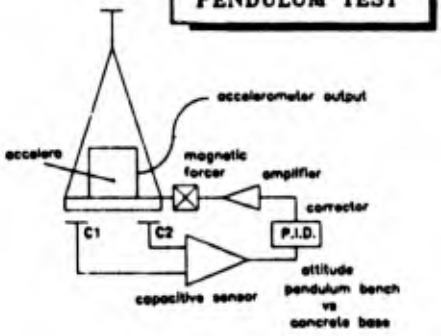

A3 AND A4 LABORATORY MODEL DIFFERENTIAL TEST ON PENDULUN (Y AXIS)

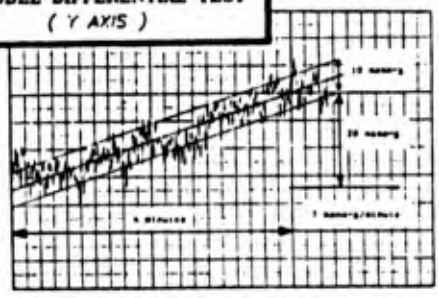

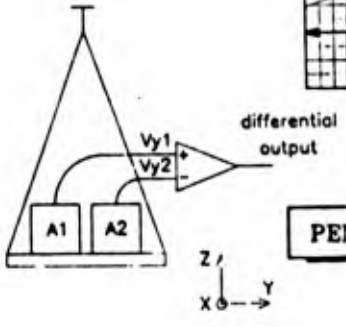

PENDULUM DIFFERENTIAL TEST

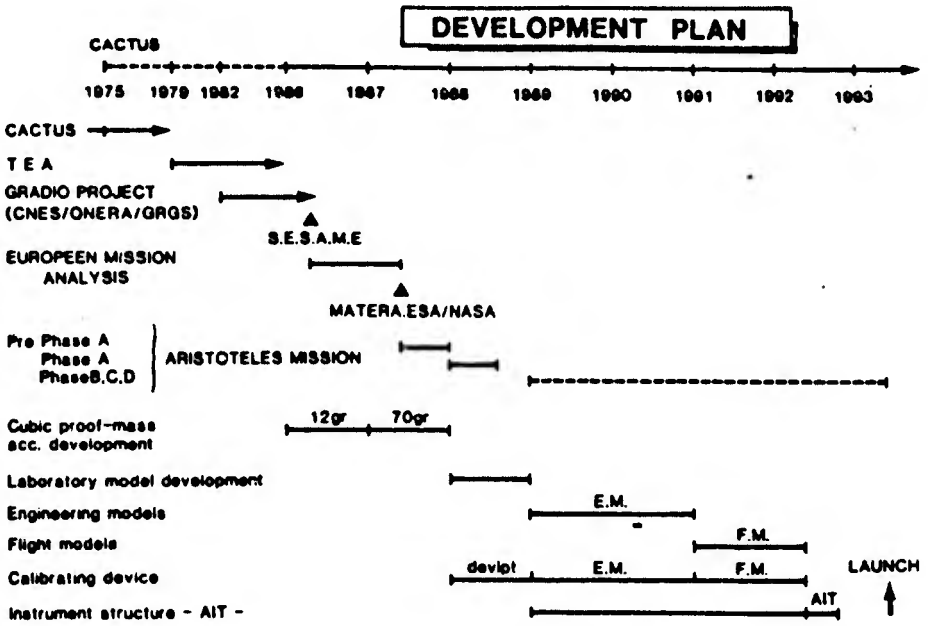
DEVELOPMENT PLAN
CACTUS
1975 1979 1982 1986 1987 1988 1989 1990 1991 1992 1993
CACTUS
T E A
GRADIO PROJECT
(CNES/ONERA/GRGS)
S.E.S.A.M.E
EUROPEEN MISSION
ANALYSIS
MATERA.ESA/NASA
Pre Phase A
Phase A
PhaseB.C.D
ARISTOTELES MISSION
Cubic proof-mass
acc. development
12gr
70gr
Laboratory model development
Engineering models
E.M.
Flight models
F.M.
Calibrating device
devlpt
E.M.
F.M.
LAUNCH
Instrument structure - AIT -
AIT

ONERA

GLOBAL GRAVITY SURVEY AND PRECISION GRAVITY EXPERIMENTS BY AN EARTH-ORBITING GRAVITY GRADIOMETER

by

Ho Jung Paik
Jurn-Sun Leung

Department of Physics and Astronomy
University of Maryland
College Park, Maryland 20742

and

Samuel H. Morgan
Joseph Parker

Marshall Space Flight Center
Huntsville, Alabama 35812

A global gravity map of $0.5^{o} \times 0.5^{o}$ grid with 2 to 3 mgal gravity anomaly error is desired for many geophysical applications. A Superconducting Gravity Gradiometer Mission (SGGM), which could meet this science objective, has been under study. The present concept of this mission involves putting a three-axis superconducting gravity gradiomter of approximately 10^{-4} E $Hz^{-1/2}$ sensitivity in a 200 km altitude polar orbit for six months. A preliminary study of such a mission has identified the attitude control of the gradiometer platform as the most challenging technical problem outside the development of the gradiometer sensor itself. A few approaches to meeting this demanding attitude control requirement are under investigation.

With a gravity gradiometer of 10^{-5} E $Hz^{-1/2}$ orbiting around the earth, one could perform important new tests of general relativity. Two such tests are a null test of the tracelessness of the Riemann tensor and a detection of the Lense-Thirring component of the gravity field. The first experiment tests a relativistic limit of the inverse square law and the second experiment searches for the gravitomagnetic field predicted by general relativity. The attitude control requirements for these physics experiments are comparable to that of Gravity Probe-B (GP-B) mission. This and other additional engineering requirements will necessitate a dedicated physics mission as a follow-on to SGGM and GP-B, which will utilize the technologies developed for these precursor missions.

Global Gravity Survey & Precision Gravity Experiments by an Earth-Orbiting Gravity Gradiometer

Ho-Jung Paik
Jurn Sun Leung — U. of Maryland

Sam Morgan
Joseph Parker — Marshall Space Flight Center

OUTLINE

- Global gravity survey missions of the 1990's
- Science objectives.
- SGGM Requirements
- Orbit
- Space Craft
- Instrument
- Schedule.

SGGM = Superconducting gravity gradiometer mission.

- Spacecraft become convenient probes of planetary gravity field with the advent of space age.

- GEM (Goddard Earth Model)
  - satellite tracking.
  - Radar altimeter
  - surface gravity data
  - 8 - 10 mgal accuracy
  - 1° x 1° resolution.

Missions of the 1990's

- Accuracy · 1 mgal.
- resolution 50 km.
- continuity ⟹ global data

- Relatively long mission duration
  0.5 - 1 year.
- Drag free satellites.
  pair of inner & outer satellite

Alternative Approaches to Global Gravity Survey

1. Satellite-to-Satellite Tracking

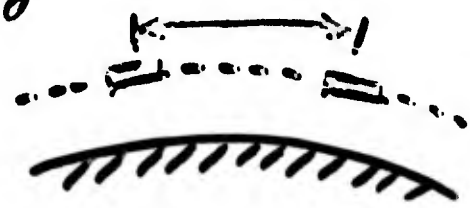

a) Low-low (NASA)

GRM (Geopotential Research Mission)

- 160 km altitude, polar orbit
- Doppler tracking
- Drag-free

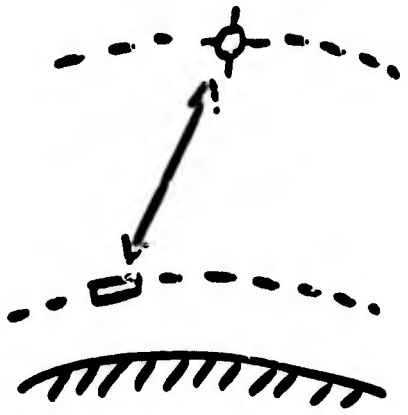

b) High-low (NASA)

Modified GRM

- 1 low spacecraft
- GPS receiver

2. Gravity Gradiometer

a) Room temperature (ESA)

GRADIO

- 8 floated cubes ⇒ tensor gradiometer
- 250 km polar orbit

b) Cryogenic (NASA)

SGGM (Superconducting Gravity Gradiometer Mission)

- 3-axis diagonal components
- 200 km polar orbit

Science Objectives

1. Earth's gravity field mapping
   - 50 km resolution (0.5° x 0.5°)
   - 0.2 mgal gravity anomaly error for 1° x 1°
2. Tests of fundamental laws of gravity
   - 10^{-10} resolution for inverse square law
   - Einstein's field equation for general relativity
   - "Magnetic" component of gravity
3. Technology development
   - Moving-base gravity survey
   - Precision inertial guidance
   - Stable platforms

⇒ Gravity Gradiometer with 10^{-4} E Hz$^{-1/2}$ sensitivity is required

⇒ Superconducting technology is required.

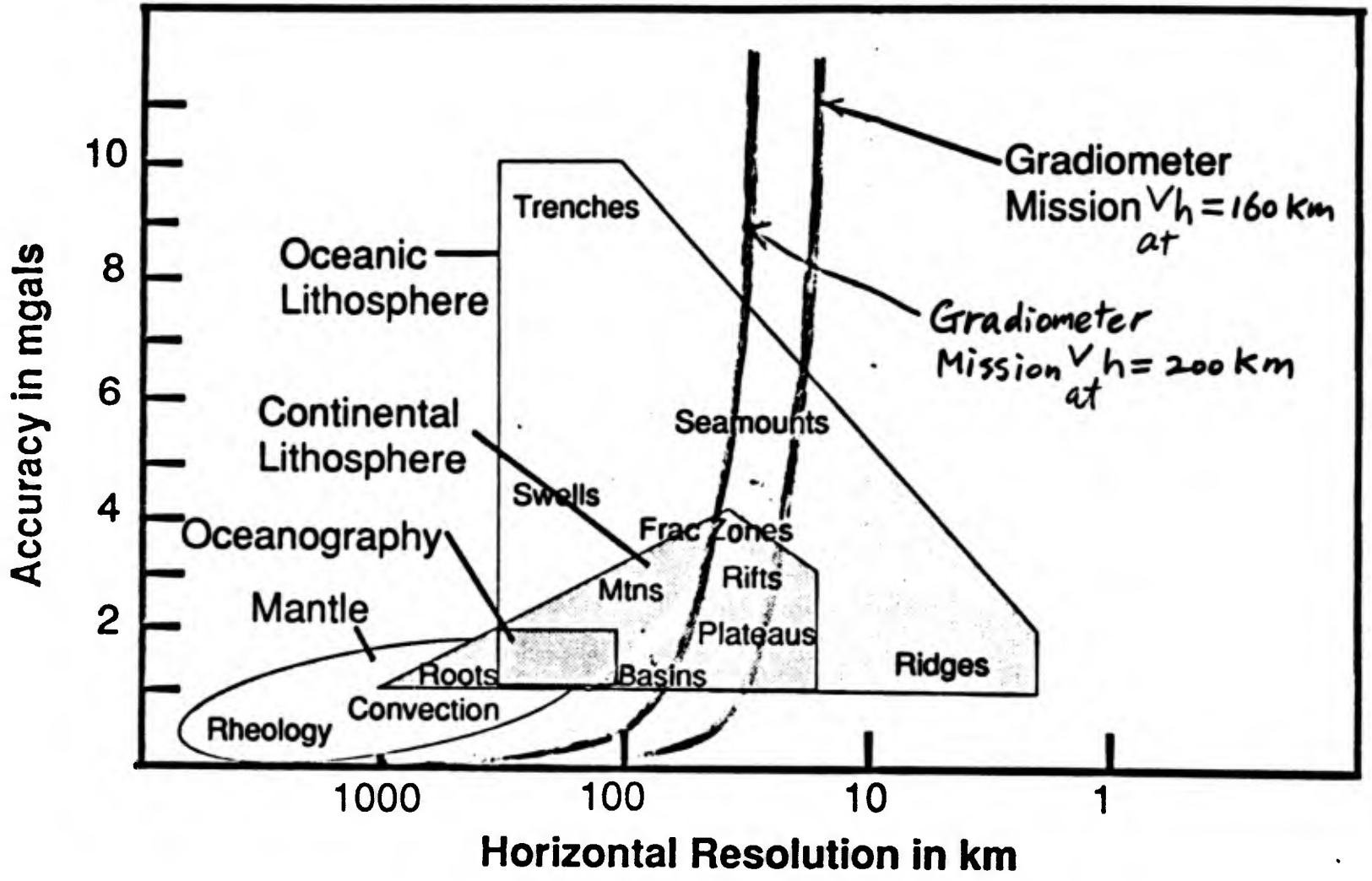
Accuracy in mgals
10
8
6
4
2
Trenches
Oceanic Lithosphere
Continental Lithosphere
Oceanography
Mantle
Seamounts
Swells
Frac Zones
Mtns
Rifts
Plateaus
Roots
Basins
Ridges
Rheology
Convection
Gradiometer Mission V_h = 160 km at
Gradiometer Mission V_h = 200 km at
1000
100
10
1
Horizontal Resolution in km

SPECTRUM OF THE VERTICAL GRAVITY GRADIENT (EU PER COEFFICIENT)

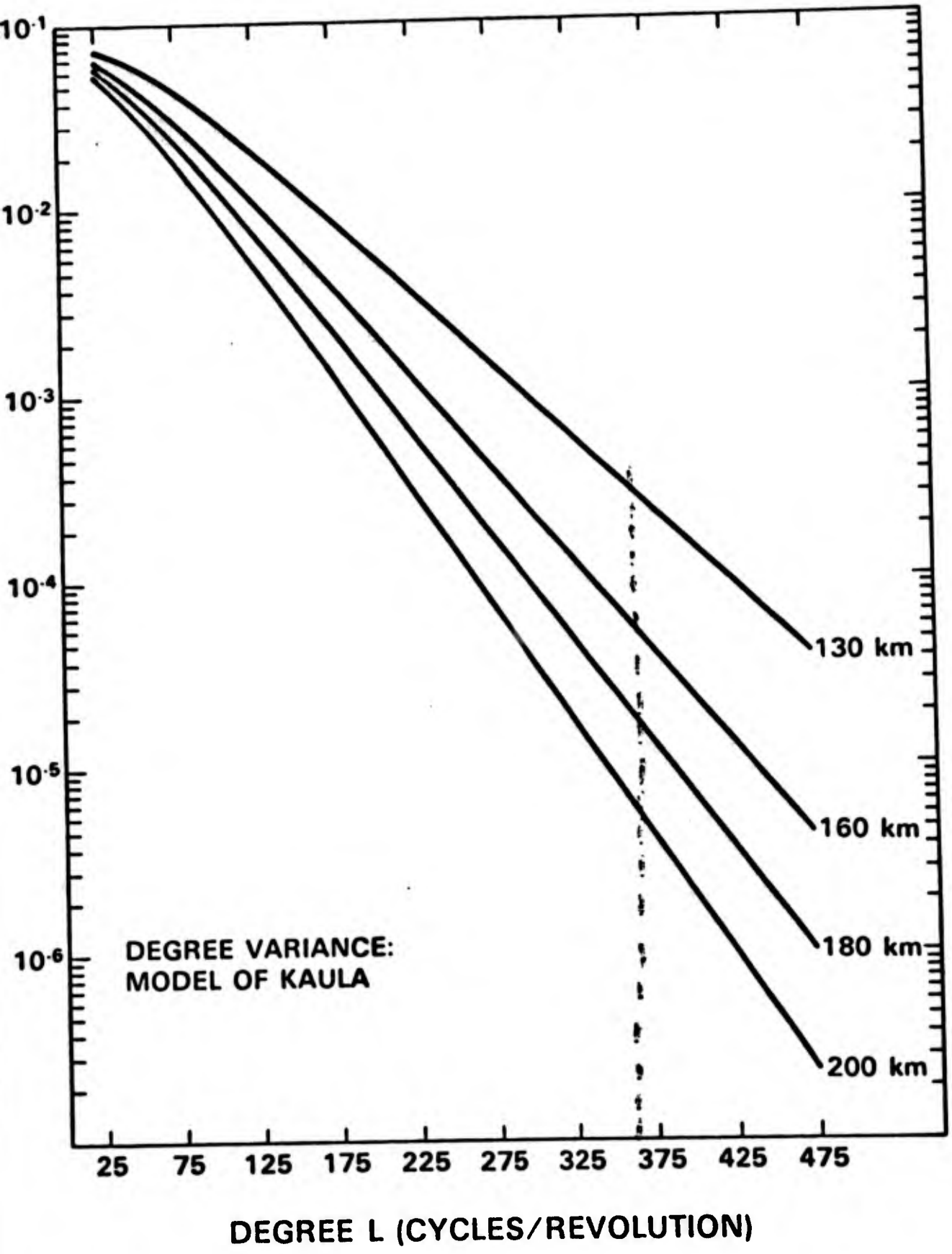

- Inverse square law

  $10^{-4}\,\mathrm{EH_z^{-\frac{1}{2}}}$ Resolve α to $\bar{0}^{10}$, circular orbit *

- Null test of Einstein's field equation.

  $10^{-\frac{1}{2}} - 10^{-4}\,\mathrm{EH_z^{-\frac{1}{2}}}$ elliptic orbit

  $10^{-5}\,\mathrm{EH_z^{-\frac{1}{2}}}$ circular orbit *.

- Lens Thirring

  $10^{-5}\,\mathrm{EH_z^{-\frac{1}{2}}}$ SNR ~100 with 1 year mission.

---

* Make use of the quadrupole moment due to Earth's oblateness.

SGGM Requirements for Geodesy

Parameters	Noise spectral density
a, linear acceleration	$2\times10^{-8}\ g_E\ Hz^{-\frac{1}{2}}$
α, angular acceleration	1×10^{-8} rad $sec^{-2}\ Hz^{-\frac{1}{2}}$
Ω, attitude rate	3×10^{-7} rad $sec^{-1}\ Hz^{-\frac{1}{2}}$
θ, pointing accuracy	6×10^{-6} rad $Hz^{-\frac{1}{2}}$
h, altitude error	0.07 m $Hz^{-\frac{1}{2}}$

gradiometer sensitivity: $10^{-4}\ E\ Hz^{-\frac{1}{2}}$

misalignment: 10^{-5} rad.

ORBIT

- Altitude 200km — Compromise between atmospheric disturbance and gravity gradient signal

- Inclination 96.3° — Sun synchronous, to reduce thermal fluctuation.

- Ground tracks — separation at 53.5 km at equator, repeat every 46 days.

SPACECRAFT

- Two stage drag free spacecraft
- Inner satellite — Experiment Module.
  - A specially designed dewar
    - 180 day helium supply.
    - Management of helium boiloff
    - Prevention of liquid helium sloshing.
- Outer satellite
  - Minimize problem of self gravity
- Command, control, telemetry, power & data links between inner & outer satellites.
- Data rate 45K/sec.
- Power 750 watts.
- Weight 4000Kg.
- Size. 2m diameter X 8m in length

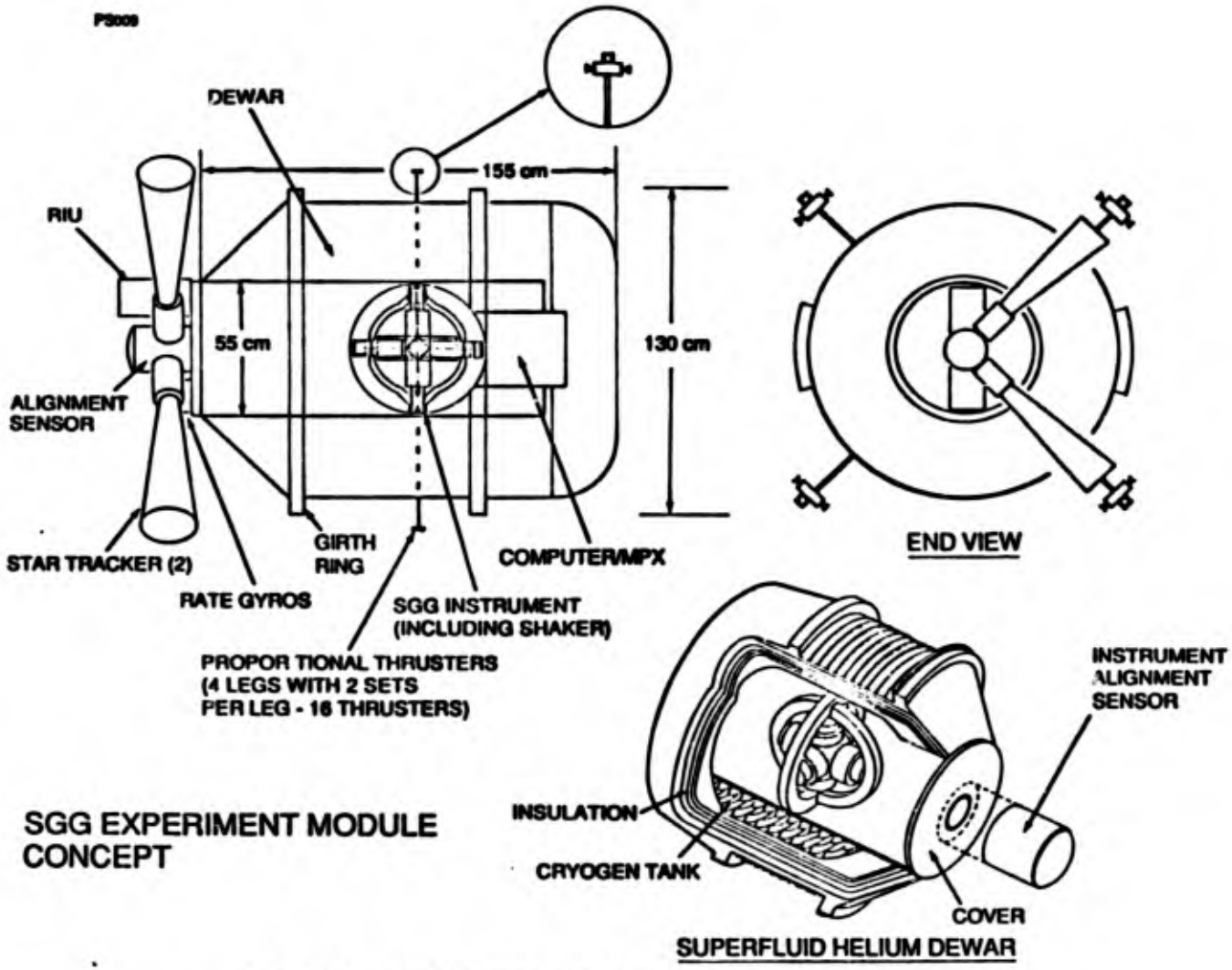

Fig. 7. Experiment Module Layout and Dewar Design

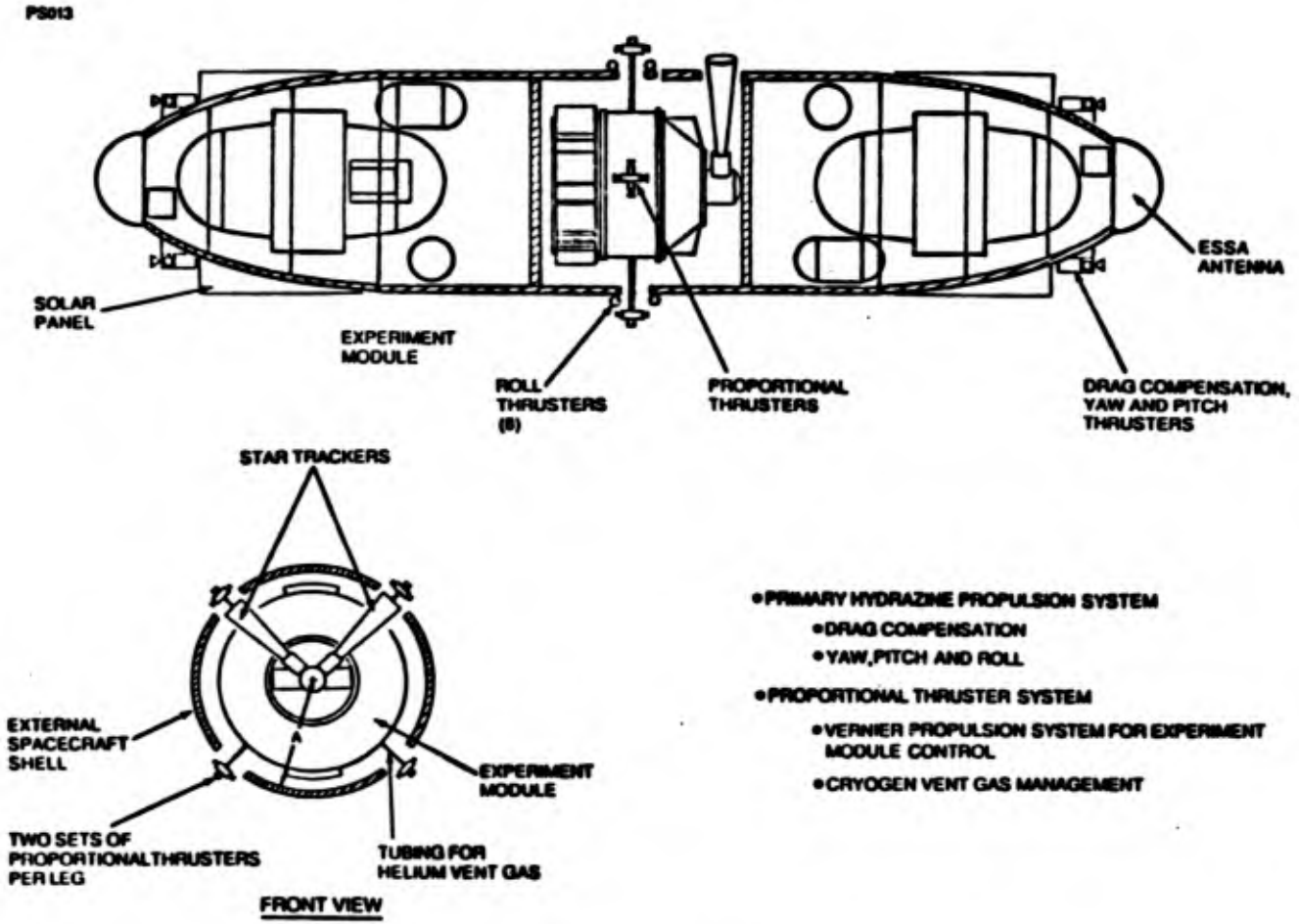

Fig. 8. SGGM Spacecraft

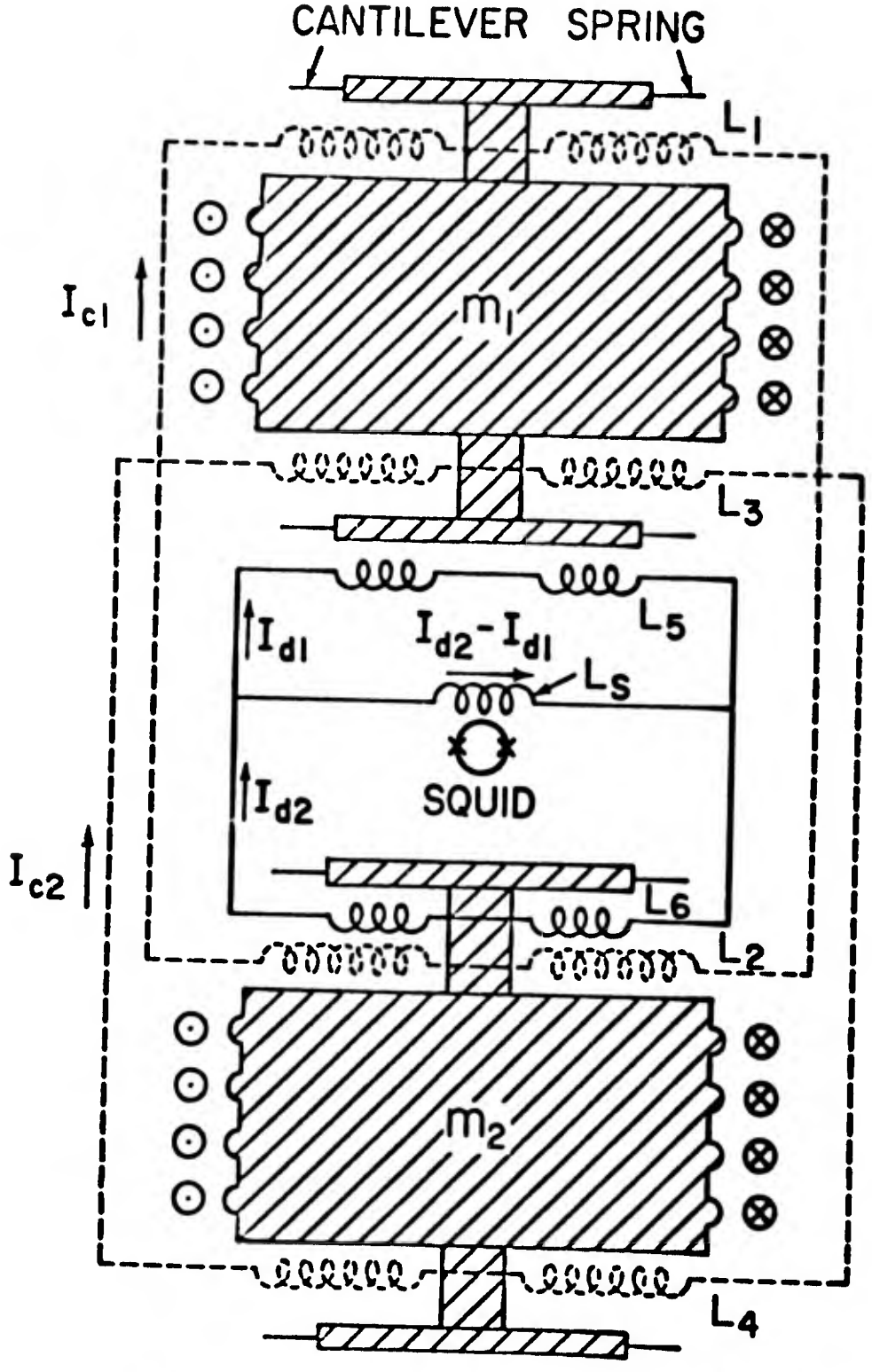

Fig. 2. Circuitry for a superconducting gravity gradiometer.

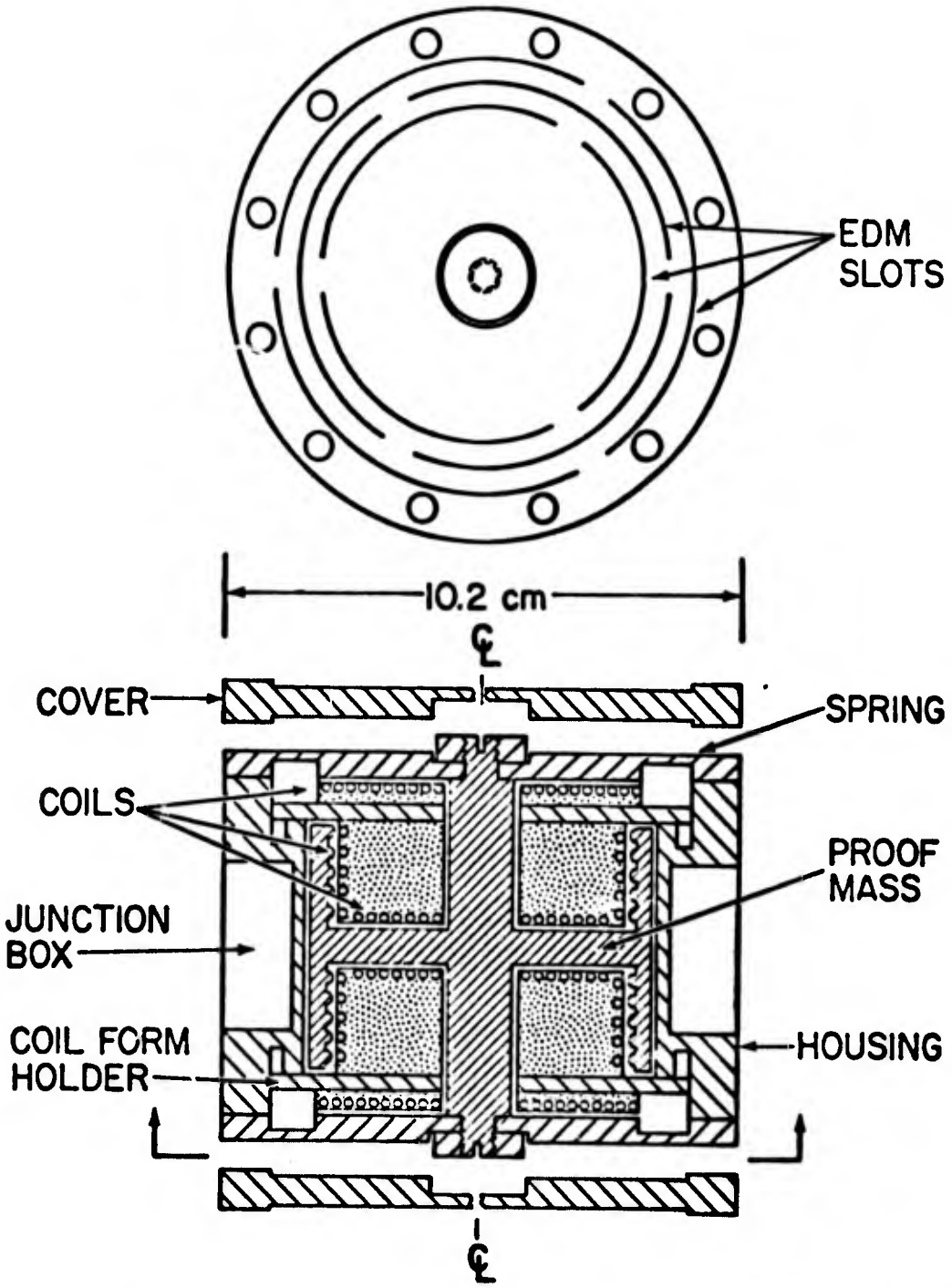

Fig. 3. Mechanical design of the acceleration transducer for the three-axis superconducting gradiometer.

Instrument

- 3-axis superconducting gradiometer
  - measures the in line gradients Γ_{rr}, $\Gamma_{\theta\theta}$, $\Gamma_{\phi\phi}$
  - elimination of 1st order effect due to angular rate error
  - 3-D rebalance.
- 6-axis superconducting accelerometer
  For instrument platform ~~control~~ feedback control sensing.
- 6-axis shaker.
  Mechanization of instrument platform isolation.
- Feedback electronics.

Instrument

- 3-axis superconducting gradiometer
  - in-line gradients, Γ_{rr}, $\Gamma_{\theta\theta}$, $\Gamma_{\phi\phi}$
  - elimination of 1st order effect due to angular rate error
  - 3-D rebalance

- 6-axis superconducting accelerometer

$a = 10^{-12}$ g/$\sqrt{\text{Hz}}$, $\alpha = 10^{-10}$ rad/s^2/$\sqrt{\text{Hz}}$

- 6-axis shaker

- Feedback electronics

3-axis gradiometer elimination of first order effect of error in attitude rate.

In general, $\bar{\Omega} = (\Omega_r, \Omega_\theta, \Omega_\phi)$.

$$\Gamma'_{ij} = \begin{bmatrix} \Gamma_{rr} + (\Omega_\theta^2 + \Omega_\phi^2) & \Gamma_{r\theta} - \Omega_r\Omega_\theta & \Gamma_{r\phi} - \Omega_r\Omega_\phi \\ \Gamma_{r\theta} - \Omega_r\Omega_\theta & \Gamma_{\theta\theta} + (\Omega_\phi^2 + \Omega_r^2) & \Gamma_{r\theta} - \Omega_\theta\Omega_\phi \\ \Gamma_{r\phi} - \Omega_r\Omega_\phi & \Gamma_{\theta\phi} - \Omega_\theta\Omega_\phi & \Gamma_{\phi\phi} + (\Omega_r^2 + \Omega_\theta^2) \end{bmatrix}$$

For Earth fixed spacecraft orientation.

$\bar{\Omega}_0 = (0, 0, \Omega_0)$

Error in rotation rate: $\bar{\Omega} \Longrightarrow (\delta\Omega_r, \delta\Omega_\theta, \Omega_0 + \delta\Omega)$

$$\Gamma'_{ij} = \begin{bmatrix} \Gamma_{rr} + (\Omega_0^2 + 2\Omega_0\delta\Omega) & \Gamma_{r\theta} & \Gamma_{r\phi} - \Omega_0\delta\Omega_r \\ \Gamma_{r\theta} & \Gamma_{\theta\theta} + (\Omega_0^2 + 2\Omega_0\delta\Omega) & \Gamma_{\theta\phi} - \Omega_0\delta\Omega_\theta \\ \Gamma_{r\phi} - \Omega_0\delta\Omega_r & \Gamma_{\theta\phi} - \Omega_0\delta\Omega_\theta & \Gamma_{\phi\phi} \end{bmatrix}.$$

Since $\sum_i \Gamma_{ii} = 0$, $\sum_i \Gamma'_{ii} = 2(\Omega_0^2 + 2\Omega_0\delta\Omega)$.

To recover the in-line components $\Gamma_{rr}, \Gamma_{\theta\theta}, \Gamma_{\phi\phi}$, make substitutions.

$$\Gamma_{rr} = \Gamma'_{rr} - \tfrac{1}{2}\sum_i \Gamma'_{ii}$$

$$\Gamma_{\theta\theta} = \Gamma'_{\theta\theta} - \tfrac{1}{2}\sum_i \Gamma'_{ii}$$

$$\Gamma_{\phi\phi} = \Gamma'_{\phi\phi}$$

In general $\bar{\Omega} = (\Omega_r, \Omega_\theta, \Omega_\phi)$

$$\Gamma'_{ij} = \begin{bmatrix} \Gamma_{rr} + \Omega_\theta^2 + \Omega_\phi^2 & \Gamma_{r\theta} - \Omega_r\Omega_\theta & \Gamma_{r\phi} - \Omega_r\Omega_\phi \\ \Gamma_{r\theta} - \Omega_r\Omega_\theta & \Gamma_{\theta\theta} + \Omega_r^2 + \Omega_\phi^2 & \Gamma_{r\theta} - \Omega_\theta\Omega_\phi \\ \Gamma_{r\phi} - \Omega_r\Omega_\phi & \Gamma_{\theta\phi} - \Omega_\theta\Omega_\phi & \Gamma_{\phi\phi} + \Omega_r^2 + \Omega_\theta^2 \end{bmatrix}$$

For Earth fixed orientation

$$\bar{\Omega}_0 = (0, 0, \Omega_\theta)$$

Error in rotation vector: $\bar{\Omega} \Rightarrow (\delta\Omega_r, \delta\Omega_\theta, \Omega_0 + \delta\Omega)$

$$\Gamma'_{ij} = \begin{bmatrix} \Gamma_{rr} + \Omega_0^2 + 2\Omega_0\delta\Omega & \Gamma_{r\theta} & \Gamma_{r\phi} - \Omega_0\delta\Omega_r \\ \Gamma_{r\theta} & \Gamma_{\theta\theta} + \Omega_0^2 + 2\Omega_0\delta\Omega & \Gamma_{\theta\phi} - \Omega_0\delta\Omega_\theta \\ \Gamma_{r\phi} - \Omega_0\delta\Omega_r & \Gamma_{\theta\phi} - \Omega_0\delta\Omega & \Gamma_{\phi\phi} \end{bmatrix}$$

$$\sum \Gamma_{ii} = 0 \qquad \sum \Gamma_{ii}' = 2(\Omega_0^2 + 2\Omega_0\delta\Omega)$$

$$\therefore \Gamma_{rr} = \Gamma'_{rr} - \frac{1}{2}\sum \Gamma_{ii}'$$

$$\Gamma_{\theta\theta} = \Gamma'_{\theta\theta} - \frac{1}{2}\sum \Gamma_{ii}'$$

$$\Gamma_{\phi\phi} = \Gamma'_{\phi\phi}$$

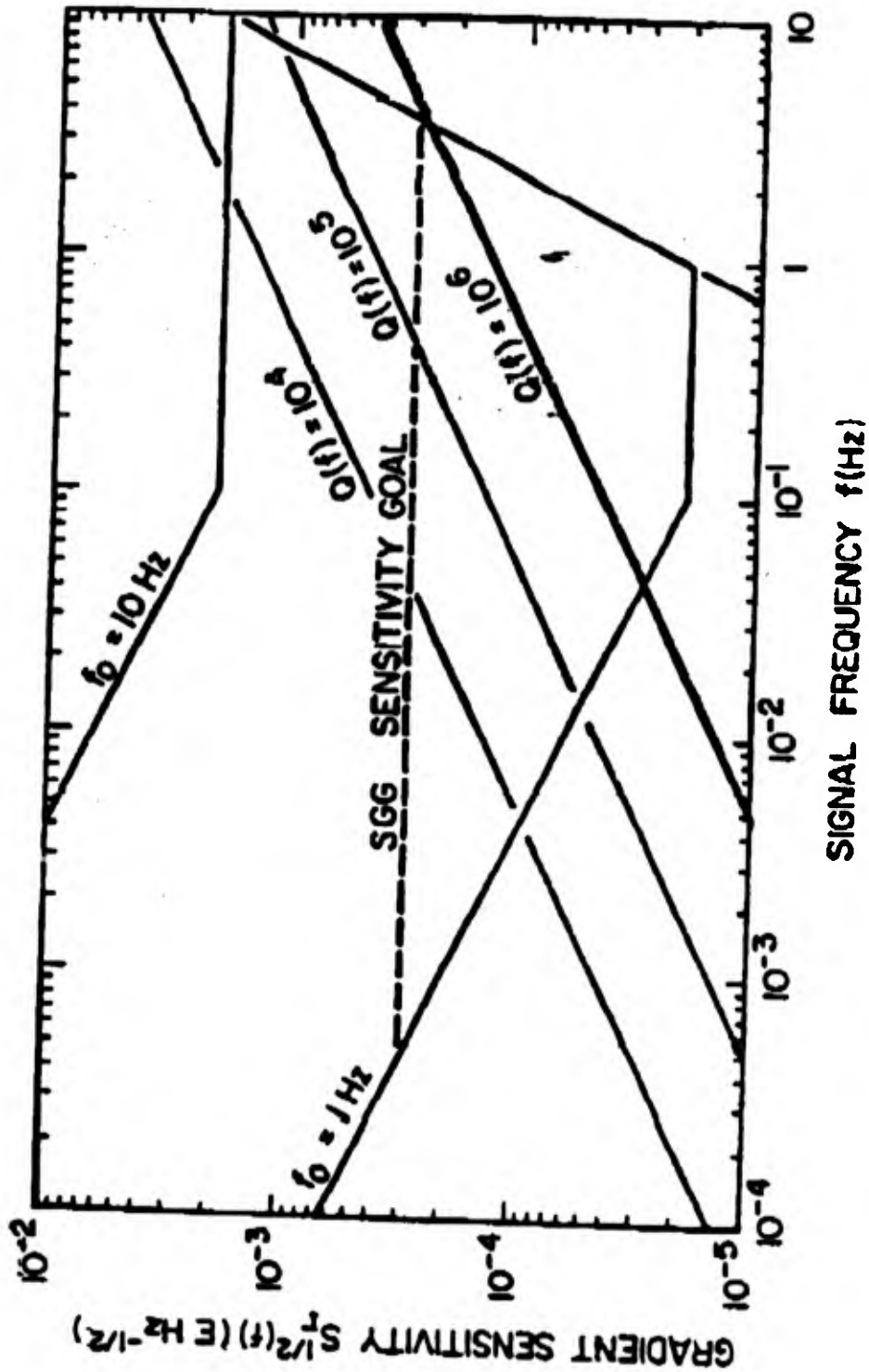

Fig. 4. Expected gradiometer sensitivity as a function of signal frequency.

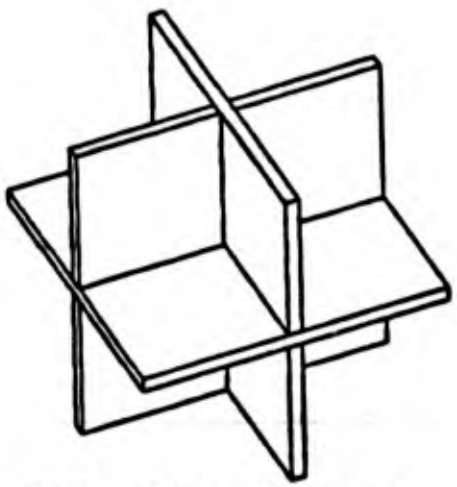

(a) Proof Mass (Niobium)

(b) Coil Form (Titanium)

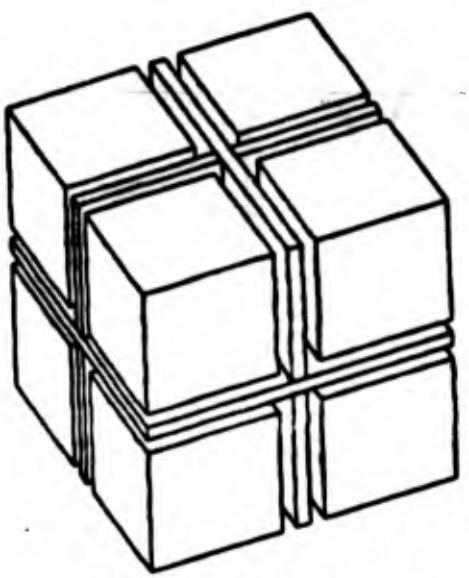

(c) Assembly Drawing

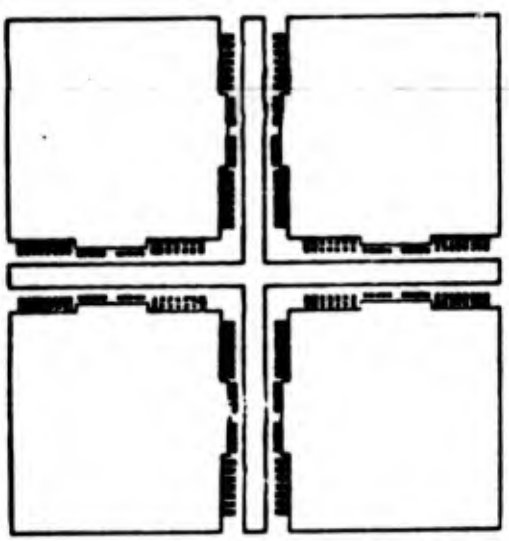

(d) Cross Section View

Fig. 5. Six-Axis Superconducting Accelerometer

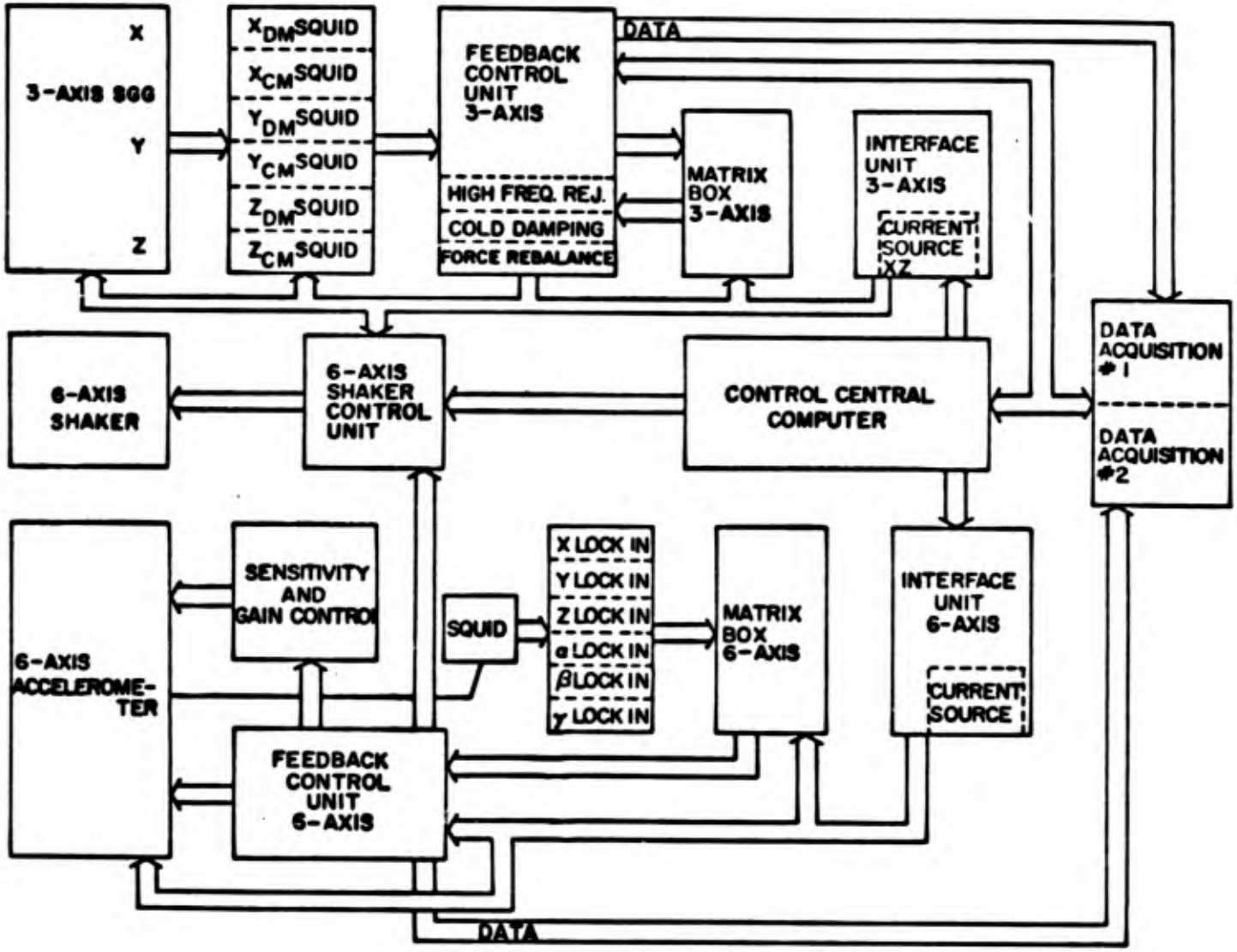

Fig. 6. Block diagram of the integrated SGGM instrument package.

Past Progress (Milestones Achieved)

1. Demonstration of a prototype gradiometer
   - Principle confirmed
   - Performance up to the design
   - Dynamic error analysis
2. Development of ancillary technologies
   - Temperature compensation
   - Superconducting negative spring
   - "6-axis" accelerometer assembly
   - "6-axis" shaker design
   - Cold damping
   - Superconducting magnetic switch
3. Construction of 3-axis gradiometer/6-axis accelerometer system
   - All mechanical components completed
   - Most electrical components completed
   - Computer interface and partial feedback electronics completed
   - 1st single-axis of the new gradiometer assembled and under test

Future Tasks

1. Laboratory test of 3-axis gradiometer
   - Assembly of 3-axis gradiometer
   - Force rebalance feedback
   - Common mode balance and calibration
   - Axis alignment
   - R^{-2} law experiment
2. Integration with 6-axis accelerometer
   - Test of 6-axis accelerometer
   - Assembly of 6-axis shaker
   - Analysis of integrated system
     Calibration, alignment errors
   - Error compensation
3. Electronic automation
   - Software development
   - Hardware development
4. Study of flight test
   - Vibration isolation
   - Attitude control
   - Spacecraft/test platform design

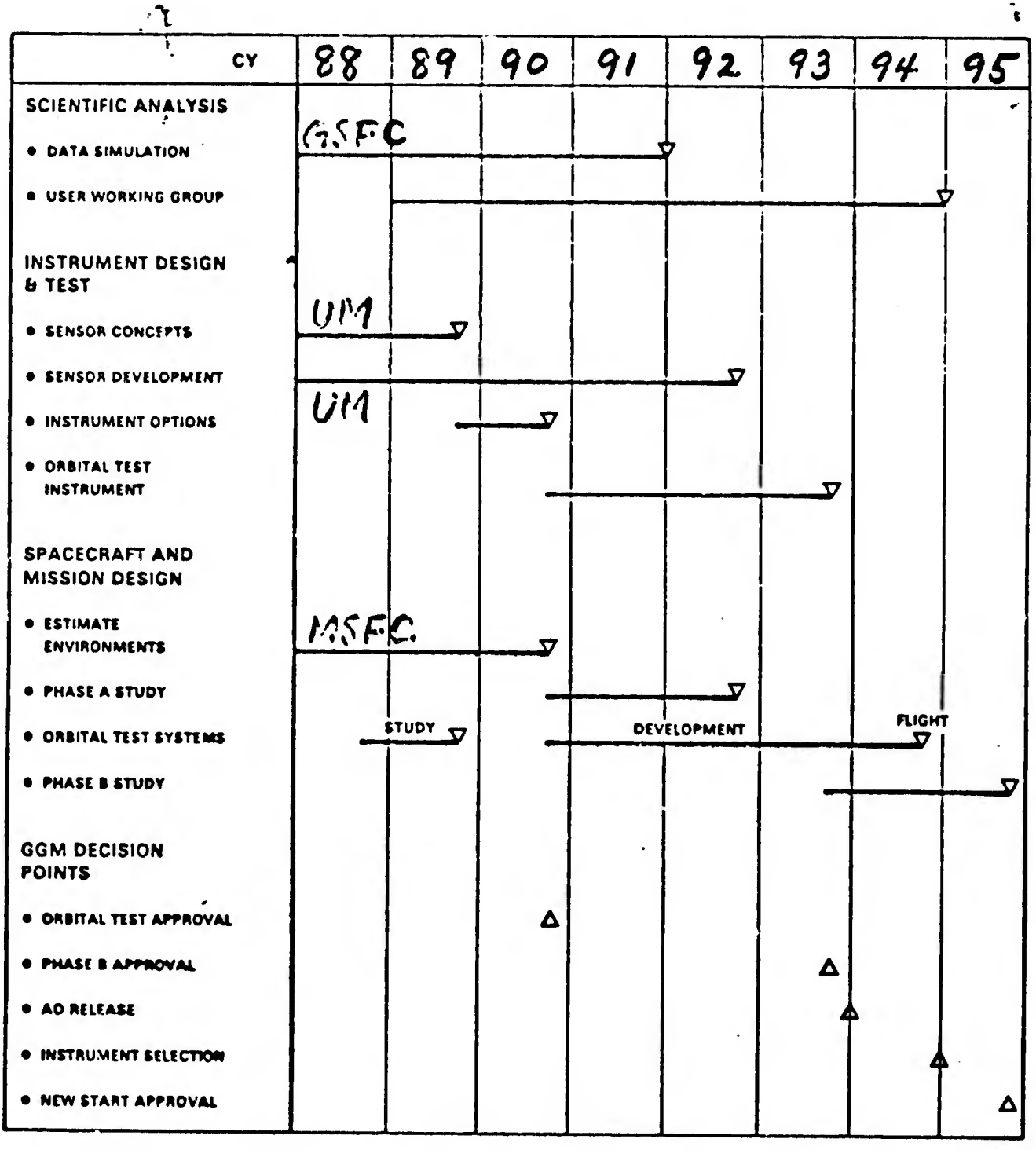

FIGURE 5-1. GRAVITY GRADIOMETER DEVELOPMENT SCHEDULE.

16th GRAVITY GRADIOMETRY CONFERENCE
10-11 FEBRUARY 1988

SPONSORED BY:
AIR FORCE GEOPHYSICS LABORATORY
EARTH SCIENCES DIVISION

TITLE OF PAPER: Global Gravity Survey and Precision Gravity Experiments by an Earth-Orbiting Gravity Gradiometer

SPEAKER: Jurn Sun-Leung

QUESTIONS AND COMMENTS:

1. Question: Warner Miller

   Could you make use of the new high-temperature superconductor physics?

   Response:

   The gradiometer depends on both the SQUID and the temperature gradient. Therefore, we require liquid Helium temperatures to maintain the temperature gradient.

   Comment: Jean-Paul Richard

   A high temperature SQUID does already exist. Also, while there is a linear dependance of sensitivity on temperature, the influence may be more complicated.

2. Question: Wayne Castleman

   What is the reduction in sensitivity of the superconducting gradiometer if high-temperature superconductors are used at 77K instead of low-temperature superconductors at liquid Helium temperatures?

   Response:

   Sensitivity is proportional to temperature.

   Comment: From another attendee

   Rms sensitivity is proportional to $T^{1/2}$.

LASER INSTRUMENTATION FOR GRAVITY MEASUREMENTS IN SPACE

by

Jean-Paul Richard

Department of Physics
University of Maryland
College Park, Maryland 20742

1 to 100 metre base line laser interferometers are considered for gravity measurements in space. A shot noise limited 1m long delay line interferometer operating at a power level of the order of 1 mW would have a sensitivity to gravity gradients at the level of 10^{-4}E $Hz^{-1/2}$. Shot noise limited 1 to 30 metre long Fabry-Perot interferometers operating at a power level of the order of 5 to 35 W would have a sensitivity to gravitational radiation induced deviations in h at the level of 10^{-19} $Hz^{-1/2}$ to 10^{-21} $Hz^{-1/2}$.

Laser Instrumentation
For Gravity Measurements in Space

Jean-Paul Richard
University of MarylandCollege Park, Maryland 20742

16th Gravity Gradiometry Conference
Colorado Spring, Colorado

February 10, 1988

1.-INTRODUCTION

A very important research effort has been made in the last decade in the field of high precision position measurement with laser instrumentation. Significant effort is currently in progress in Munich and Glasgow and at MIT and Caltech with the goal of developing very sensitive kilometre-base-line gravitational radiation antennae. The purpose of our present effort is to develop a space borne gradiometer using laser measurements of the distance between proof masses over a base line of the order of one meter and operating at a sensitivity level of 10^{-4} Eötvös/$\sqrt{Hz}$. Two aspects of laser technology make it a promising tool for gradiometry measurements:

1- QUANTUM LIMITED ACCURACY. Laser technology has already reached the level of accuracy where quantum limited measurements can be performed. This aspect of laser instrumentation is discussed in section 2.4.

2- ABSOLUTE DISTANCE MEASUREMENTS. Distances as measured with a laser are referenced to the speed of light which in vacuum is independent of any parameter of the environment. Thus the potential for high accuracy is outstanding since, in principle, no other potentially unstable reference unit, such as a support for proof-mass position sensors, is needed.

2.-DEVELOPMENTS RELATED TO THE LASER INSTRUMENTED GRADIOMETER CONCEPT

In this section we review the present concept of the laser instrumented gradiometer (section 2.1 and 2.2) and discuss the requirements on the laser instrumentation (sections 2.3 to 2.5). We also discuss in some detail the concepts and advantages of the "zero-derivative force" and light beam "side-injection" (sections 2.6 and 2.7).

2.1.-CONCEPT OF LASER INSTRUMENTED GRADIOMETER

The present conceptual status of the laser instrumented gradiometer is shown schematically in fig. 1. It consists of a laser driven double-delay line sensing the differential distance between two pairs of freely-falling

proof masses. It provides a measurement of the difference in the gravity gradient along the directions of the two delay-line cavities. An other version of the gradiometer which is closely related to this one is also under study: in that version, the frequency of the laser is highly stable. Then, a single cavity is adequate. The laser beam interferes with itself and a gravity gradient along the axis of the single cavity is obtained.

Low frequency drift of the proof masses is prevented by electromagnetic forces. Along the direction of the delay-line cavities, these forces should operate in the frequency band dc to ≈ 0.01 Hz. The signal bandwidth could extend to kHz frequencies where the gradiometer would become (in its present design) a low sensitivity gravitational radiation detector.

2.2.-SENSITIVITY GOALS

The design goal is for the noise power density in the gradient measurement to be at the level of $\Gamma(\omega) = 10^{-4} E/\sqrt{Hz}$. The corresponding proof-mass displacement resolution is $x(\omega) \cong 5 \times 10^{-13} / |\omega_o^2 - \omega^2|$ $m/\sqrt{Hz}$ where the average distance (baseline) between two proof masses is assumed to be 1/2 meter. ω is the signal angular frequency and ω_o is the effective resonant frequency of the suspension. The force associated with such a resolution in the gravity gradient is $f(\omega) = M\,\Gamma(\omega)/2 = 2.5\ 10^{-13}$ $N/\sqrt{Hz}$ for M=10 kg.

In sections 2.3 to 2.5, quantum and classical noise contributions will be evaluated. Where needed, it will be assumed that the laser wavelength is 632 nm and that the number of round trips in the cavities is 50 (100 reflections).

2.3.-QUANTUM NOISE AND LASER POWER REQUIREMENT

The shot noise associated with fluctuations in the arrival rate of individual photons at the photodetector is a fundamental source of noise in interferometer instrumentation. In the best case, this shot noise exhibits a Poisson distribution. This leads to an error in the fringe phase measurement and to a corresponding error in the position measurement which for a two-arm interferometer measurement, is given by:

$$\delta x_{sn}(\omega) = \frac{1}{8\pi\, n_t} \sqrt{\frac{2\, hc\lambda}{\eta P}} \quad , \qquad (1)$$

where n_t is the number of light-round-trips in each cavity, h is Plank's constant, c is the speed of light, λ is the light wave length, η is the photodetector quantum efficiency and P is the power at the photodetector.

If the laser beam is bounced off mirrors attached to the proof masses 100 times, the laser power required to overcome the noise associated with the Poisson shot noise is 1 mW for frequencies up to ~ 10 Hz. Such power level are easily achieved with stable lasers.

In addition to shot noise, the laser interferometric measurement also exhibits a quantum back-action effect. The fluctuations in the arrival rate of photons at the surface of the proof-mass mirrors result in fluctuations in the radiation pressure and in the appearance of a radiation noise force which drive the proof-masses and introduce noise in the gradiometer. For a laser which displays Poisson noise, the spectral density of that force is:

$$f_{qp}^2(\omega) = 8\, n_t^2\, Ph/\lambda c \quad . \qquad (2)$$

This quantum back action is negligible in our case. With 100 reflections and 1 mW laser power, $f_{qp}(\omega)$ is of the order of $10^{-17} N/\sqrt{Hz}$, and 3 orders below the signal.

The considerations in this section indicate that the quantum noise associated with a laser power level of 1 mW would permit operation at the sensitivity goal of $\Gamma(\omega) = 10^{-4} E/\sqrt{Hz}$.

2.4.-QUANTUM LIMIT.

The two expressions given in the preceding sections can be used to derive the quantum uncertainty relationship associated with laser measurements. Eqs. (1) and (2) can be expressed in the following way:

$$\delta x_{sn}(\omega)\ f_{qp}(\omega) = \frac{\hbar}{\sqrt{\eta}} \quad . \qquad (3)$$

$f_{qp}(\omega)$ results in momentum inaccuracies $\delta p_{qp}(\omega)$ of an equal value. If double-sided quantities are used and represented by Δ, then:

$$\Delta x_{sn}(\omega)\ \Delta p_{qp}(\omega) = \frac{\hbar}{2\sqrt{\eta}} \quad , \qquad (4)$$

which, in the limiting case $\eta = 1$ reduces to the known uncertainty relationship.

2.5.-CLASSICAL NOISE AND INTERFEROMETER REQUIREMENTS

2.5.1.-POWER STABILITY REQUIREMENT

Fluctuations in the laser power produce a change in the average pressure on the proof masses. With 100 reflections and 1 mW average power, the average pressure is of the order 10^{-19}N. Thus, the spectral density of the fractional power fluctuations should be less than $10^{-4}/\sqrt{Hz}$. Control of laser power to $10^{-5}/\sqrt{Hz}$ or better can be achieved and will ensure that the laser back action can be neglected in one and two-arm gradiometers.

2.5.2.-FREQUENCY STABILITY REQUIREMENT

Here, we consider two possible instrumental approaches: one and two-arm interferometry.

One-arm interferometry:

In a one-arm interferometer, any change in the frequency is indistinguishable from a change in the measured distance between the proof masses. In such a case, the frequency stability requirement is $60/|\omega_o^2-\omega^2|$ $Hz/\sqrt{Hz}$. The highest stability commercially available is 5000 $Hz/\sqrt{Hz}$. With such lasers, two-arm interferometry would be needed. Laboratory lasers with stability of $100Hz/\sqrt{Hz}$ have been built and extension of their stability to millihertz levels is anticipated in the future. Thus, one-arm interferometry appears as a potentially practical approach to space gradiometry.

Two-arm interferometry:

If the two arms of an interferometer have the same length, frequency instabilities in the laser light can be neglected. In practice, some difference in length ΔL will exist. For $\Delta L/L = 10^{-3}$ and $\delta\nu = 5000Hz/\sqrt{Hz}$, the error in the proof-mass position will be $\cong 4x10^{-15}m/\sqrt{Hz}$ and adequately low for measurements up to $\omega \cong 10$. A lower value for $\Delta L/L$ would permit same sensitivity at higher frequencies. Thus, the required frequency stability required for two-arm gradient interferometry can already be found in some commercial lasers.

2.6.-SIDE INJECTION FOR COMMON MODE BALANCING

As shown in fig. 1, the laser light is injected into the delay line from a point located between the two mirrors associated with that line. For that particular configuration, there is no change in the delay-line optical length if the two proof masses associated with it are subjected to the same

acceleration along the delay-line axis. Thus, side injection confers common mode rejection to the laser readout of the gradiometer. This common mode rejection is performed before any signal transformation or processing. This is an extremely important feature which considerably reduces the demands on the slew rate and linearity of the processing electronics.

2.7.-ZERO DERIVATIVE LOW FREQUENCY RESTORING FORCE FOR THE REDUCTION OF TEMPERATURE CONTROL REQUIREMENTS.

Restoring forces acting in the frequency range dc to ≈ 0.01 Hz and acting on each proof mass are needed to prevent drift of the proof masses with respect to the satellite and to compensate for the quasi-dc component of the earth field gradient. The force discussed in this section is the one acting on each proof mass along the axis of the delay-line cavity or along the axis of the measurement. The restoring forces needed in directions normal to that axis are referred to as lateral restoring forces or suspensions and will not be discussed here.

Mechanical or electromagnetic restoring forces are applied to a proof masses from a reference point or point of support attached to a base which experiences temperature fluctuations. Resulting changes in the dimensions of the base can produce changes and corresponding errors in the restoring force applied to the proof mass. Such errors will not arise, however, if the derivative of that force with respect to the relative position of the proof mass and the base is zero (to first order). Voice-coil type magnetic restoring forces can be made to satisfy such a requirement. We are considering magnetic systems which would provide zero-derivative restoring force and would be sensitive to high order derivatives of the magnetic field only. This latter property would reduce the gradiometer sensitivity to locally generated and residual Earth magnetic field in a satellite environment. Such zero-derivative suspensions sensitive to high order derivatives of the magnetic field are very desirable since they would dramatically reduce the related temperature control and residual magnetic field requirements.

DESIGN CONSIDERATIONS

Q values for aluminum and silicon suspensions have been measured. The purpose was to estimate the noise introduced into a gradiometer if such suspensions were used to provide the required restoring forces. Q of 1000 have been measured for a 0.5 kg mass resonating at 10 Hz. A similar Q at 1 Hz

for a 10 kg mass would correspond to a noise level of $\Gamma \cong 10^{-2}E$. We plan to use such suspensions for earth bound tests of the prototype gradiometer and "voice-coil" type restoring force for fine longitudinal positioning of the test masses.

Electromagnetic restoring forces are now considered for a space version of the laser gradiometer. Such restoring forces can exhibit a zero derivative and are easily made to operate at very low effective frequencies. No fundamental difficulties are expected in maintaining at a satisfactory level the noise contributions from such electromagnetic suspension since the ratio of the maximum gradient ($\approx$ 2000 E) to the desired noise level (10^{-4} E) is less than the ratio between a voltage and the minimum noise level that voltage will exhibit ($\approx 10^{8}$).

FIGURE CAPTION

Fig. 1. Double delay line interferometer with side injection scheme. The laser output passes through a Bragg cell to provide isolation for the laser from reflections from the interferometer input which would worsen the frequency stability. The Bragg cell also provides a means of controlling the laser amplitude. The beam then is injected into a single mode fiber, which removes any side bands and feeds the light into the vacuum chamber. After the initial beam splitter, the beam passes through the Pockel cells. One Pockel cell is used to phase modulate the laser beam for the AC readout scheme in a frequency regime where the laser noise is shot limited. The other Pockel cell is used to keep the optical paths of the two arms balanced. The steering mirrors reflect the beam to the double-sided injection mirrors to the delay lines. The outputs from the multiple-pass delay lines reflect off the back side of the injection mirrors to the second beam splitter/combiner. One beam then goes to the photodiode to provide the output for the interferometer. The photodiode output is amplified and mixed with the phase modulation reference signal to convert the interferometer output to DC. The other beam from the second beam splitter/combiner is trapped, but can be used in future designs as an amplitude stabilizing reference.

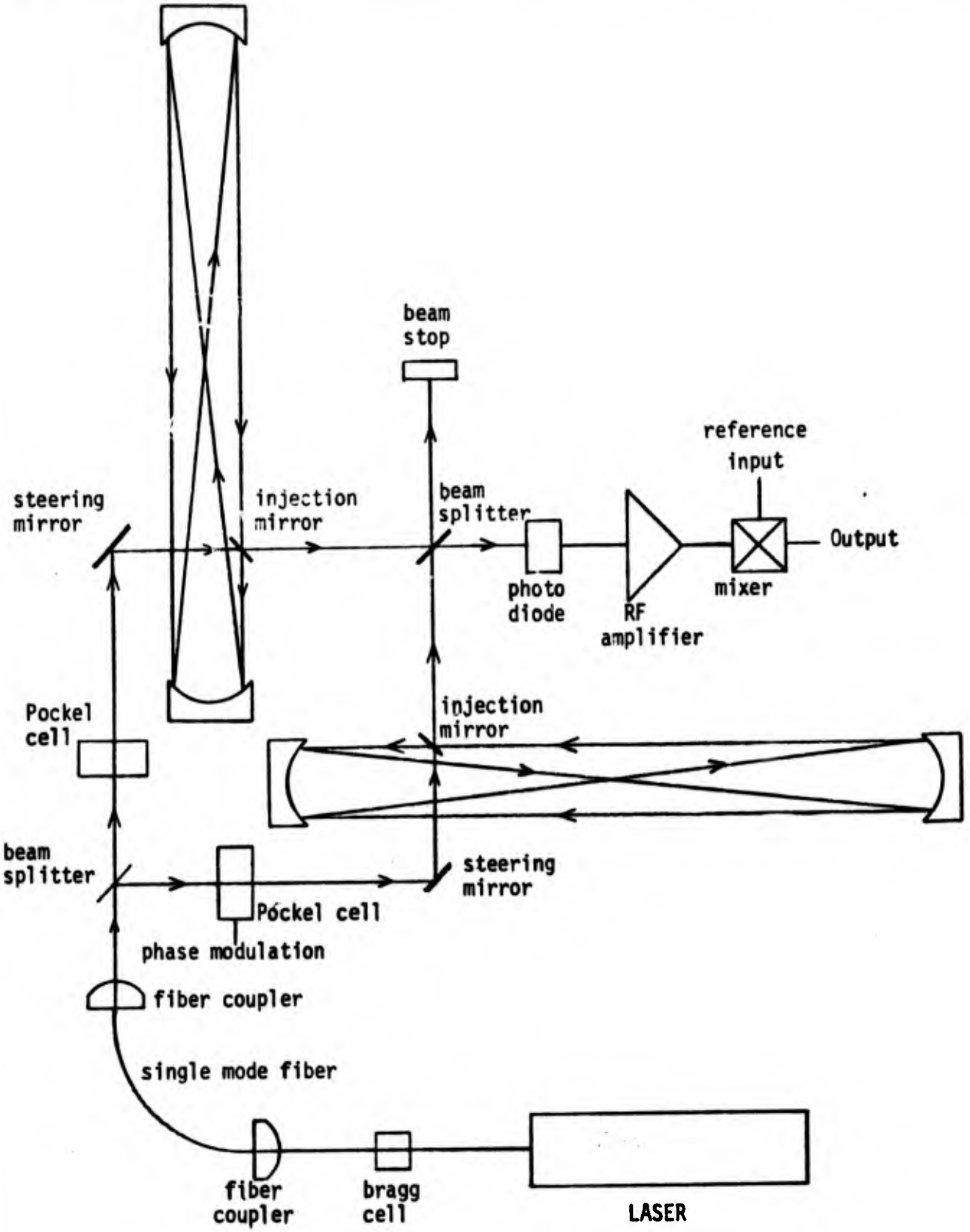
beam
stop
reference
input
steering
mirror
injection
mirror
beam
splitter
Output
photo
diode
RF
amplifier
mixer
Pockel
cell
injection
mirror
beam
splitter
steering
mirror
Póckel cell
phase modulation
fiber coupler
single mode fiber
fiber
coupler
bragg
cell
LASER

Fig. 1

16th GRAVITY GRADIOMETRY CONFERENCE
10-11 FEBRUARY 1988

SPONSORED BY:
AIR FORCE GEOPHYSICS LABORATORY
EARTH SCIENCES DIVISION

TITLE OF PAPER: Laser Instrumentation for Gravity Measurements in Space

SPEAKER: Jean-Paul Richard

QUESTIONS AND COMMENTS:

1. Comment: Warner Miller

   If you use (i) back-action evasion techniques of C. Caves, and (ii) the squeezed state light research of Kimble et al, you can overcome the limits stated in your presentation.

   Response:

   A gain in sensitivity is not needed in current gravity gradiometry technology.

MAGNETIC ISOLATION - AN UPDATE

by

A. Miguel San Martin
D. Sonnabend

Jet Propulsion Laboratory
California Institute of Technology

This paper is a follow up on our paper at last year's Conference, where our early work on eddy current isolation of gradiometers was covered. Since then, closed loop control has been demonstrated, using very simple control laws. Several practical problems have been uncovered, and largely surmounted. These include sampling lags, whose effect has been minimized by discrete control synthesis; nonlinearities in the sensors and forcers, dealt with by placement changes and mapping in the software; and erratic behavior, eventually traced to a software peculiarity. The paper will recap the earlier work, discuss the recent progress in some detail, and touch on our plans for the current year.

16th Gravity Gradiometry Conference

U. S. Air Force Academy

MAGNETIC ISOLATION – an Update

A. Miguel San Martín and D. Sonnabend

Jet Propulsion Laboratory
California Institute of Technology

11 February 1988

Abstract

This paper is a follow up to our paper at last year's conference, where our early work on eddy current isolation of gradiometers was covered. Since then, closed loop control has been demonstrated, using very simple control laws. Several practical problems have been uncovered, and largely surmounted. These include sampling lags, whose effect has been minimized by discrete control synthesis, and nonlinearities in the sensors and forcers, dealt with primarily by calibration and mapping in the software. The paper will recap the earlier work, discuss the recent progress in some detail, and touch on our plans for the current year.

1 Introduction

Our earlier work, reported in Refs. 1 and 2, showed how a torsion pendulum arrangement could be used to simulate one axis of a magnetic isolation system. Ref. 1 discussed the design, construction, and initial testing of the facility. Ref. 2, presented here last year, covered the addition of closed loop controls, including a digital computer, so that the control laws could easily be changed or modified. Stable, but admittedly sloppy control resulted from our first efforts.

The main improvements came from tracking down and correcting for the nonlinearities in the sensors and actuators. Much of this paper is devoted to that effort. Another source of erratic behavior was traced to a peculiarity of the software; and was fixed by rewriting an input-output routine directly in assembly language. Finally, the effect of sampling lags could be minimized by using z-plane control synthesis; but, at least for the simple, low bandwidth controllers studied so far, not much improvement could be expected.

The main control law studied is a proportional-integral-derivative (PID) law, chosen to eliminate offsets due to fixed torque inputs. Other possibilities are mentioned in Section 5. The paper will review the hardware, with emphasis on changes since Ref. 2; elaborate on our success in linearizing the sensors and actuators; discuss the derivation of the control law; and mention our future plans.

2 Hardware Description

2.1 The Plant

The plant comprises the torsion pendulum, four eddy current actuators, and two sensors. A photo, from Ref. 1, is shown in Fig. 1. The actuators are mounted externally, on brackets, positioned at opposite faces of the box (where the gradiometer would reside), two on each side. The coil axes are normal to the box faces, along the direction of the box motion. The design and implementation of the torsion pendulum and actuators are described in Ref. 1. A condensed theoretical treatment of eddy current forcing is given in Ref. 1; and a substantial generalization in Ref. 3.

The force applied by an eddy current actuator to the box is proportional to the square of the amplitude of the sinusoidal voltage supplied by the power amplifier to the actuator coil. This force is always repelling and its magnitude is also a function of the frequency of the sinusoidal voltage, and

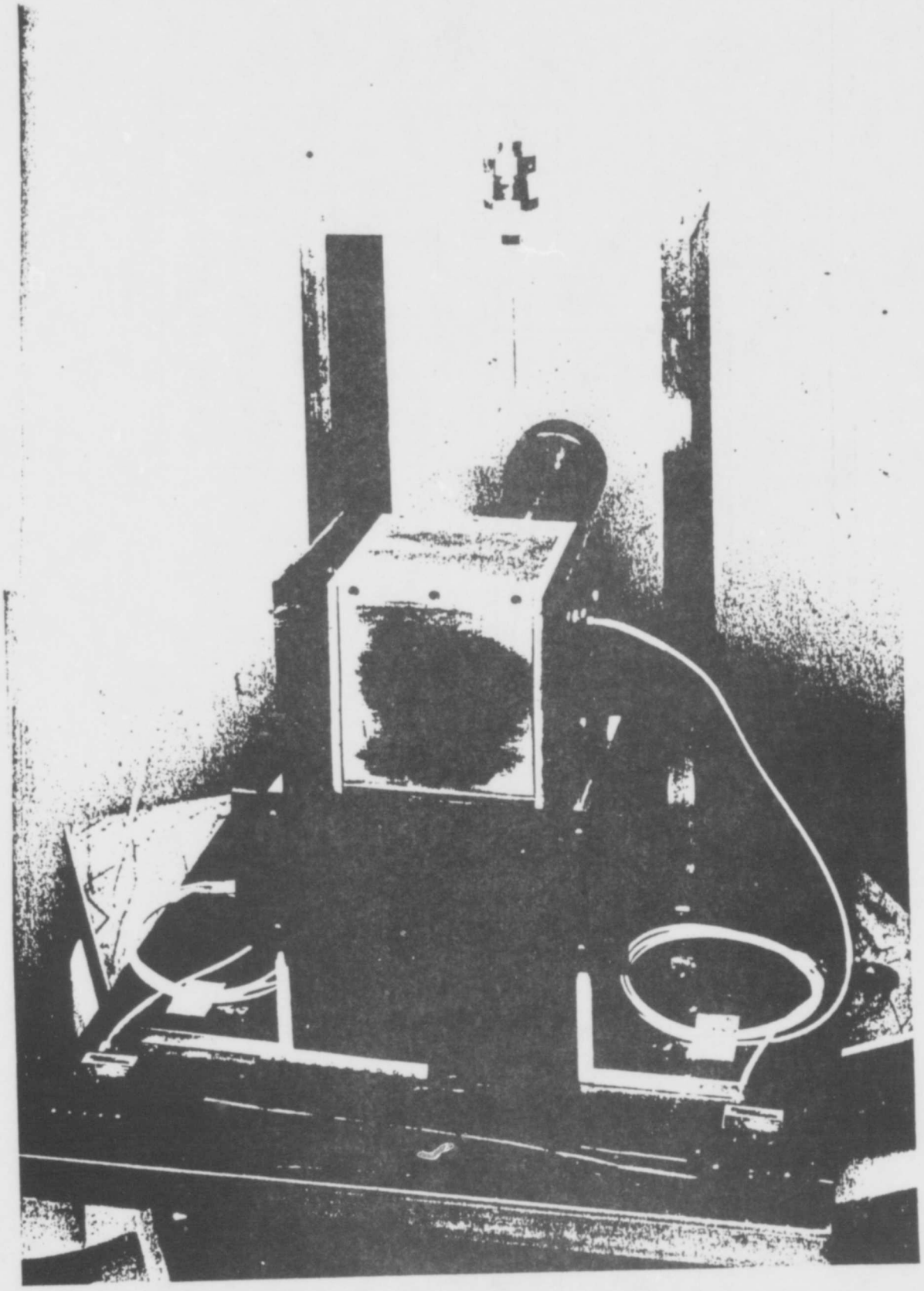

Fig. 1. Magnetic Isolation Test Facility

Figure 2. Controller Block Diagram

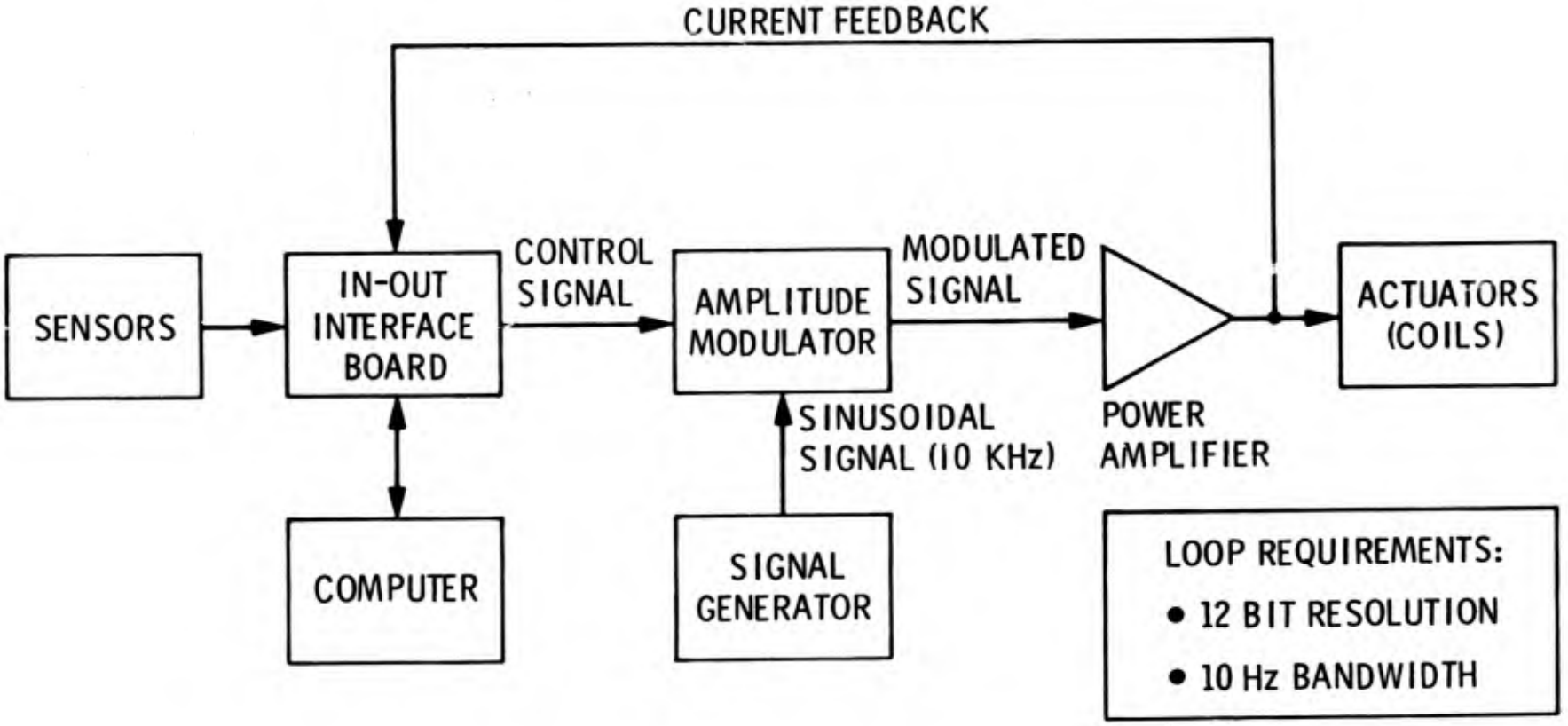

a much weaker function of the distance between the coil and the box. The magnitude of the actuator sinusoidal input voltage is the parameter that is used to control the force applied by the actuator, while the frequency is kept constant at an optimal value. The optimal frequency is the frequency at which, given a constant amplitude voltage, the force is the largest. This frequency was empirically found to be 1 kHz.

The two sensors measure the displacement between the box and the brackets. They are Kaman Instruments Co. eddy current sensors, Model KD-2400. Each sensor consists of two subassemblies: the sensor head and a signal conditioning module. The proximity of the sensor to the box controls a variable gain oscillator within the conditioning module. The oscillator amplitude is detected to provide an analog signal proportional to the displacement. Among the sensor features are low cost, no contact, 10 kHz frequency response, adjustable gauge factor, and 0.25 micrometer resolution.

2.2 The Controller

The function of the controller is to execute a control law, designed to achieve certain performance objectives. The controller samples analog data from the sensors, converts these to digital form, computes actuator commands according to the trial control law, converts back to analog, and finally doles out power to the actuators. All these operations are carried out periodically, in real time. The hardware implementation of the controller allows 12 bit resolution and a sampling frequency of at least 10 Hz.

Fig. 2 shows the block diagram of the controller, and Fig. 3 shows a picture of the torsion pendulum and the digital controller. The computer is a PC's Limited IBM AT compatible with an 80287 math co-processor, and a clock speed of 8 MHz. The function of the computer is to command the operation of the input/output interface board, receive digital sensor data and issue digital actuator commands to the same board, carry out the calculations dictated by the control law, control the overall timing of the loop, and generate test evaluation data.

The input/output interface board is located in one of the expansion slots of the computer, connected to the computer data bus. The operation of the board is controlled by the PC. Its function is to sample the analog data from the sensor specified by the computer, and convert to 12 bit digital words, which are then sent to the computer via the computer data bus. It also receives 12 bit digital actuator commands from the computer, and converts them to analog signals that are fed to the amplitude modulator,

Figure 3. Torsion Pendulum and Digital Controller

corresponding to the actuator specified by the computer. It has the capacity for 8 differential analog inputs and two analog outputs of the sample and hold type. Two analog inputs are connected to the two position sensors, and the two analog outputs are connected to the two amplitude modulators driving the left and right actuator channels (each channel consists of two eddy current actuators connected in parallel). The board consists of a multiplexer, one A/D and two D/A converters, a clock, and a microprocessor that controls the operation of these elements and, with the aid of four registers, communicates with and receives orders from the computer in a high level command language.

The four registers located on the interface board, used in the communication between the board and the computer, are: the command register (write only), the status register (read only), data-in register (write only), and the data-out register (read only). These registers are connected to the computer bus, and are I/O mapped. The command and status registers are located at the same address in the computer I/O address space. This address is the board's Base address. The data-in and data-out registers are both located in the Base+1 address. The board's Base address is jumper-selectable to any even address within the PC 10-bit address space. The computer communicates with (and controls) the interface board by writing and reading bytes of information from these four registers. The computer language used to implement the control loop program must be able to access the I/O address space (e.g. the INP and OUT commands in BASIC).

The signal generator provides an analog, sinusoidal, constant amplitude and frequency signal. We are presently operating at 1 kHz (see eddy current actuators in plant description). The amplitude modulator regulates the amplitude of the voltage sinusoid supplied by the signal generator, according to the analog voltage control signal from the interface board. The result is an analog voltage sinusoid of constant frequency (1 kHz), whose amplitude can be commanded by the computer software.

Finally, the function of the power amplifier is to amplify the signal from the amplitude modulator, in order to drive the actuators. It is a standard stereo amplifier, a Phase Linear Model 400, Series Two. It can put out 205 watts rms into an 8 Ω load, and has a bandwidth of 50 kHz. Each amplifier channel drives the two actuators on each side of the box, connected in parallel.

3 Plant Model

A model that can accurately describe the transfer characteristics of the plant is required for control law synthesis and analysis. This section will develop the models corresponding to the three elements that make up the plant: the torsion pendulum, the sensors, and the actuators.

3.1 The Torsion Pendulum Model

The torsion pendulum, shown in Fig. 1, has two translational and two rotational modes, in addition to the rotational mode present in the ideal single degree of freedom torsion pendulum. All these modes are second order.

One of the "undesirable" rotational modes produces an up and down motion of the box, which is normal to the direction of the actuator forces, and therefore can not be excited by the actuators. The other undesirable rotational mode is a twist motion along the longitudinal axis of the beam, connecting the box to the counterweight through their centers of mass. The excitation of this mode is reduced to a negligible level by placing the two actuators on each side such that the resulting force intersects the twist axis. One of the undesirable translational modes produces a back and forth motion of the box, which is normal to the direction of the actuator forces. Therefore, this mode is also uncontrollable by the actuators. Finally, the last of the undesirable modes is a translational mode characterized by a right/left motion of the box. This mode is controllable by the actuators, but since its natural frequency (2.4 Hz) is much higher than the bandwidth of the control loops to be initially implemented, the dynamics of this mode will be left out of the torsion pendulum model.

This leaves the rotational mode about the vertical wire as the dominant dynamics, and the experimental pendulum approaches an ideal one. The mathematical model of the torsion pendulum is then:

$$I\ddot{\theta} + K\theta = \tau \tag{1}$$

3.2 Sensor Model

The bandwidth of the sensors, as specified by the manufacturer, is DC to 10 kHz. Since we will be operating at frequencies that are down by two orders of magnitude from this, it is reasonable to assume no dynamics in the sensor model. The sensor model will then consist of a DC input/output mapping, and a characterization of the output noise.

In order to generate the input/output mapping, a position reference was needed. For this purpose, a micrometer was installed on the right bracket to measure the distance between the box and the right actuators. The face of one of the right actuators was defined as the reference. Note that the motion of the box describes an arc, but it is constrained to such a small angle that, for practical purposes, the motion of the box can be considered rectilinear.

The output voltage from a sensor is zero when the box is against the sensor, and increases linearly with distance, until it starts to saturate at 2 mm. Since the gap is 5.9 mm wide, the position measurement is constructed by subtracting the two sensor outputs, in order to have a measurement that covers the entire gap. However, the resulting position measurement is a nonlinear function of the box position, due to the sensor saturation. The purpose of the input/output mapping is to determine this nonlinear function, so it can be compensated in software by the inverse mapping. This technique can be successful only if the sensors are not completely saturated when the box is in the middle of the gap.

The procedure used to generate the input/output mapping was the following. First, the torsion pendulum null was preset, such that the resulting torque pushed the box firmly against the micrometer tip, to prevent air currents from moving the box. Then, a computer program was run in real time. This program consists of a loop that outputs the "filtered" box position. The filtered position measurement is constructed by subtracting the output of the two sensors, averaging the result over 5 samples, in order to reduce sensor noise, and finally scaling the result from volts to millimeters. After the micrometer is adjusted to the next setting, one waits until the filtered sensor measurement, also displayed, settles to a steady value. Then one hits any key and the computer registers in a mapping table both the real position of the box, and the position as measured by the sensors. The program then increments the desired micrometer setting displayed on the screen by 0.25 mm and starts the loop again. The process is repeated until the entire 5.9 mm gap is mapped.

The result of the mapping is shown in Fig. 4. The strong nonlinearity due to sensor saturation is clearly visible. Note, however, that when the box is in the middle of the gap, the slope of the function seems large enough to allow a linearization with a respectable signal to noise ratio.

Figure 4. Averaged Position Measurement vs Real Position

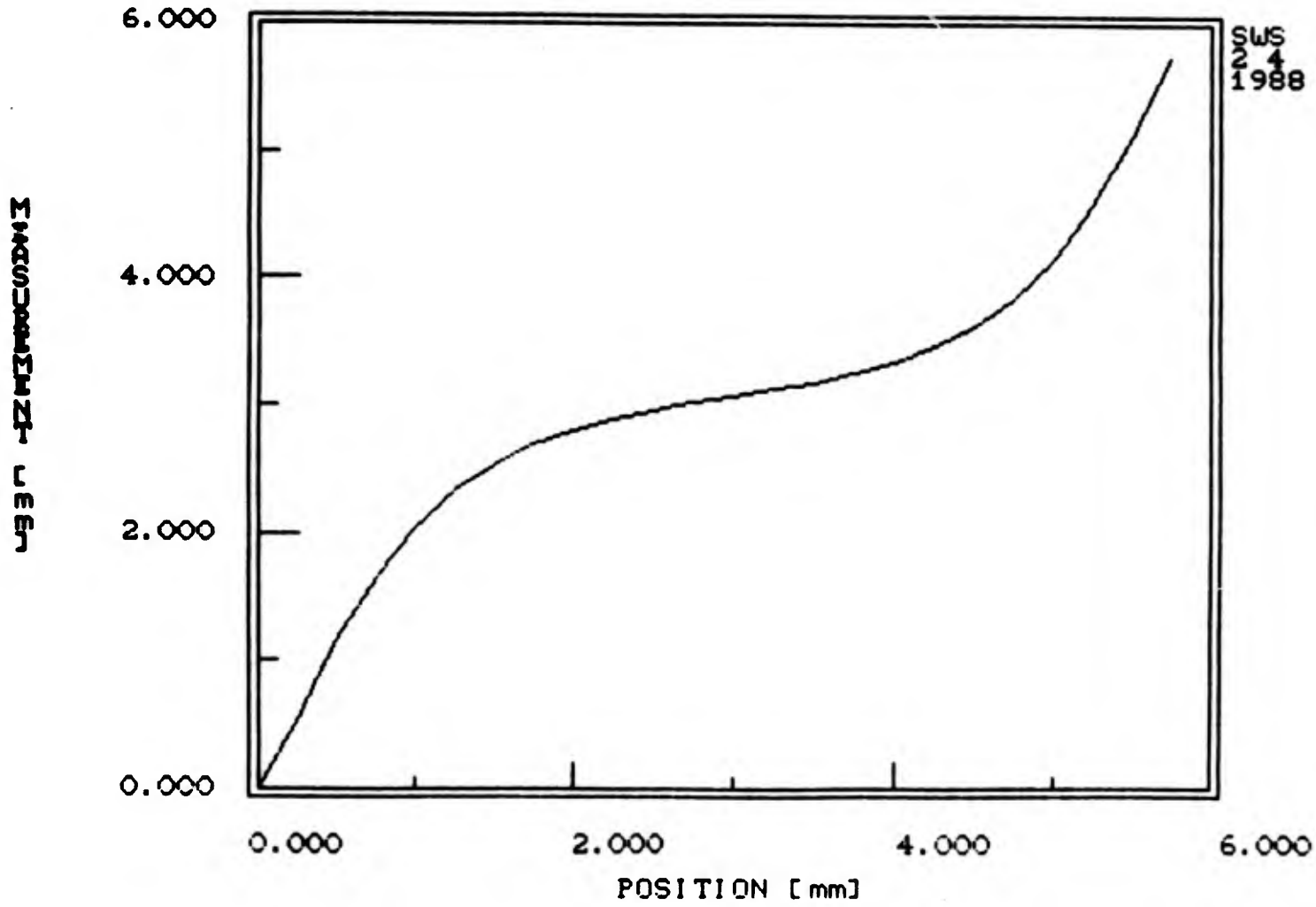

3.3 Actuator Model

Given the high bandwidth of the power amplifier, the amplitude modulator, and the actuators themselves, it is reasonable to assume no dynamics in the model of the actuator (including its electronic drivers). Accordingly, the model of the actuator consists of a function that predicts the force applied by the actuator on the box, given the actuator's input peak voltage, and the distance between the box and the actuator coil face.

In order to determine this function, a measurement procedure was implemented using the experimental apparatus. The procedure consisted first of calibrating the torsion spring to apply a known "constant" torque on the pendulum, and second of measuring the actuator input voltage required to cancel the spring torque at five equally spaced positions of the box in the gap. The procedure was then repeated for a total of five equally spaced spring torques. The torques were then converted into actuator force by dividing the torques by the force moment arm.

The measurement procedure consists of the following steps:

1) Move the torsion pendulum null position 90 deg away from the middle of the gap.

2) Use an HP counter to measure the time it takes the box to travel from one end of the gap to the other, as the result of the torsion spring torque.

3) Assuming constant torque, use the time measurement from step 2, the pendulum moment of inertia (theoretically calculated), and the gap angular size to calculate the torsion spring torque. Since the gap angular distance is such a small fraction of the 90 deg null offset, the constant torque assumption is very reasonable.

4) Command an empirically derived PID control law to place the box at a distance of 0.4 mm from the actuator. This control law uses a sensor rectification function based on the model of the sensor obtained in Section 3.2. This sensor rectification function will be explained in Section 4. In addition, an actuator rectification function was used that compensated only for the theoretically predicted quadratic relation between force and input current. The PID gains were adjusted empirically until stability and a respectable step response was obtained.

5) When the system settles, read the actuator peak input voltage.

6) Repeat steps 4 and 5 for 1.7, 2.9, 4.3, and 5.6 mm.

7) Repeat steps 2 through 6 for torsion spring null settings of 135, 180, 225, and 270 deg.

8) Convert torques to forces by dividing the torques by the actuator

moment arm.

The data obtained from this measurement procedure is plotted in Figs. 5 and 6, together with the data from the actuator mathematical model (below). Fig. 5 shows the plots of normalized input voltage vs force for five different distances between the box and the actuator. A normalized input voltage of 1 is equivalent to a peak input of 15 volts. Note the quadratic nature of the curves, as predicted by theory.

Fig. 6 shows the plots of normalized input voltage vs distance for five different actuator forces. A quadratic fit was performed on these curves which showed that they were actually straight lines that intersected the x axis at the same point D_0 = -4.831 mm. In addition, it was noted that the slopes of the lines were directly proportional to the square root of the force.

From these observations the following actuator mathematical model was constructed to fit the experimental data:

$$F = K\left(\frac{V^*}{D + D_0}\right)^2 \tag{2}$$

Here, V^* is the normalized input (V^* = 1 implies 15 volts), D is the box position in mm, and $K = 1.409 mm^2 N$. Figs. 5 and 6 show how well the mathematical model matches the experimental data. The model error is smaller than 2%.

4 Control Law

In order to use the design and analysis tools of linear control theory, the plant must first be linearized. As shown in the previous section, while the model of the torsion pendulum is linear, the models of the sensors and actuators are not. Therefore, the control law must rectify the outputs from the sensors, and the inputs to the actuators, so the PID compensator will see the resulting plant as a linear system.

4.1 Sensor Rectification

The sensor rectification function, implemented in the control law, consists of a look-up table made up of the input/output mapping points obtained in Section 3.2 (Fig. 4), and a linear interpolation between these points. Fig. 7 shows the result of repeating the sensor input/output mapping of Section 3.2, but with the sensor rectification included. The straight line indicates

Figure 5. Actuator Input vs Force
(experimental and model data)

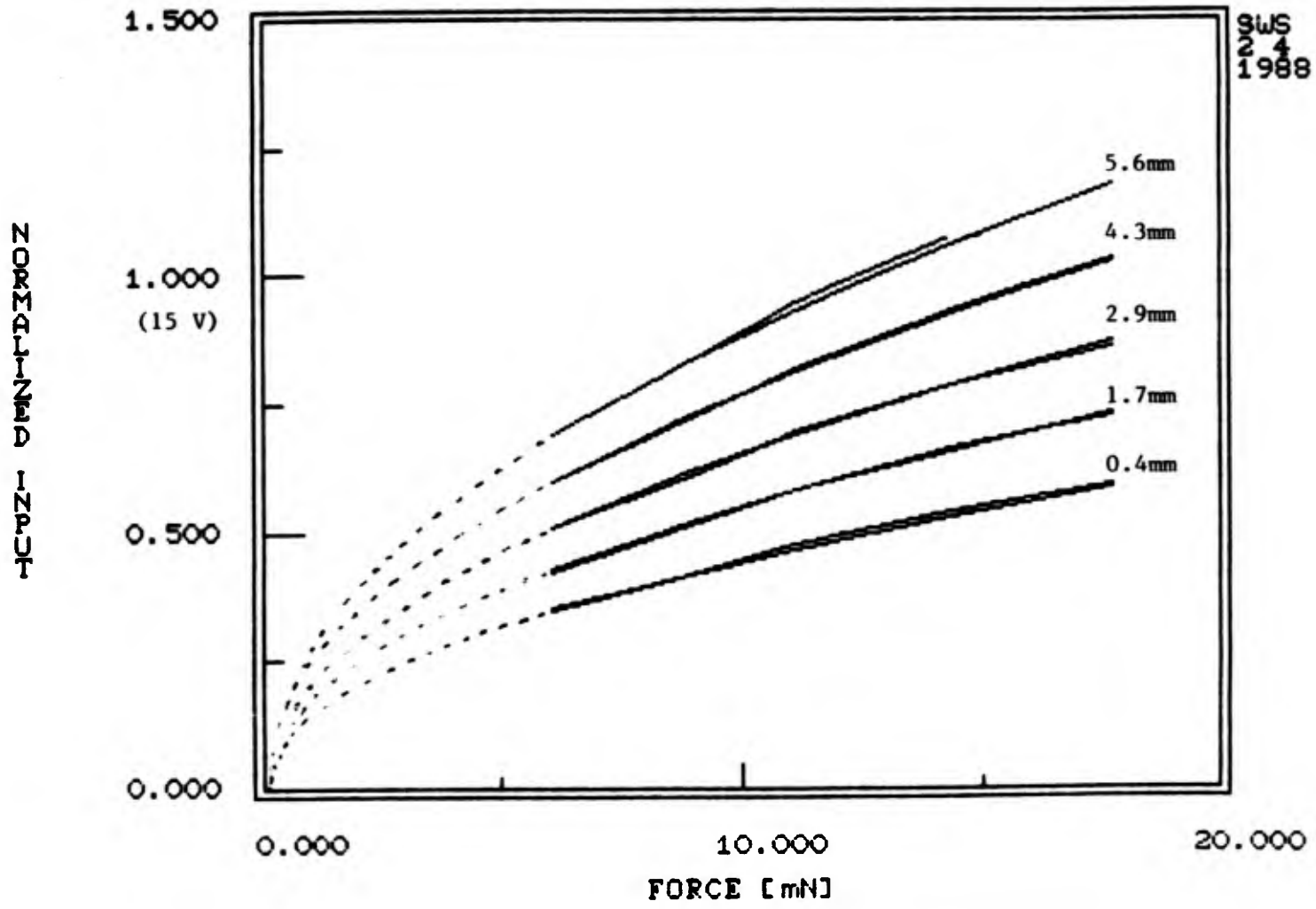

Figure 6. Actuator Input vs Distance
(experimental and model data)

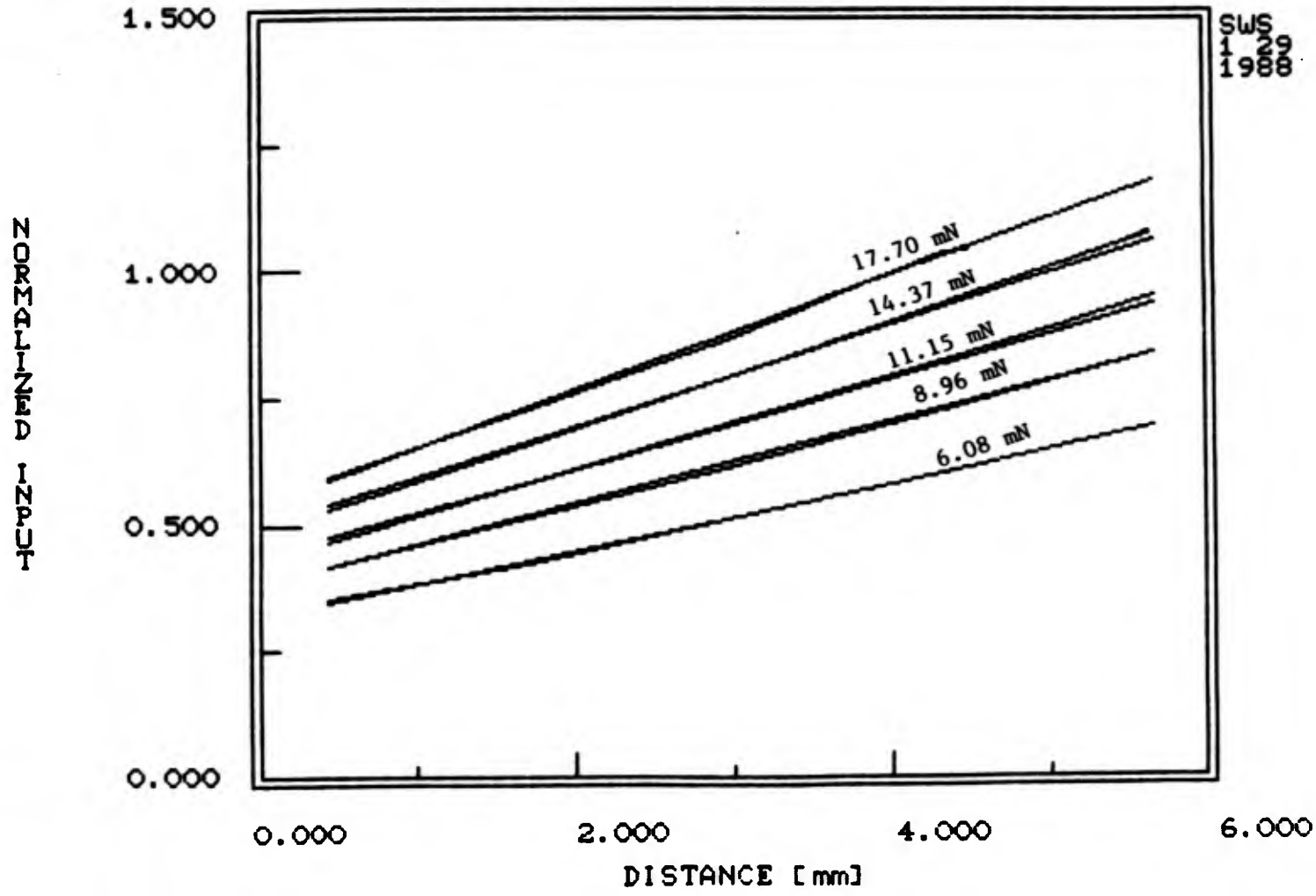

Figure 7. Averaged Rectified Position Measurement vs Real Position

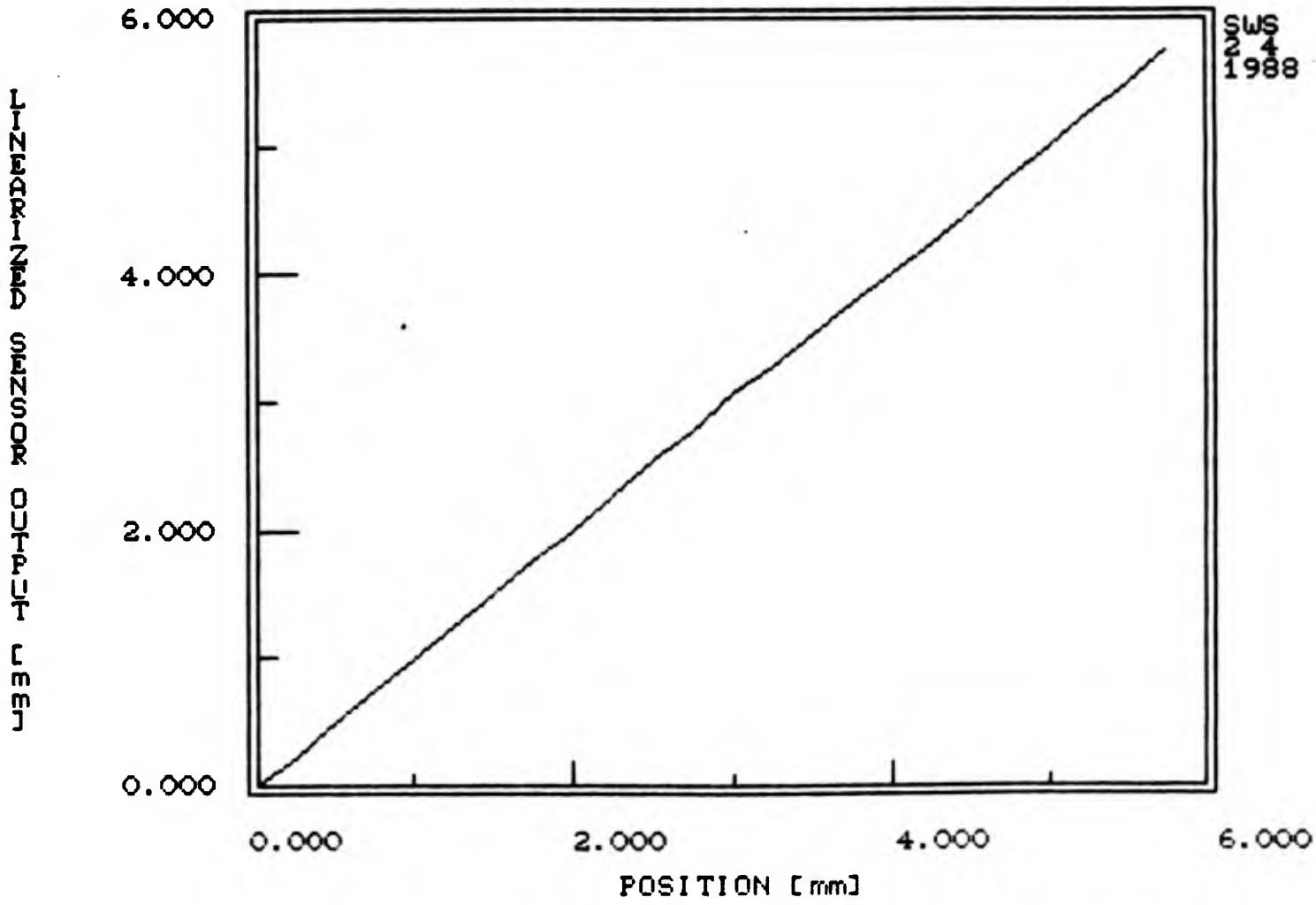

that the sensor rectification function has been successful in linearizing the sensors. The maximum DC error is smaller than 20 micrometers.

The effect of the sensor rectification on the sensor noise was also evaluated. For this purpose the box was held fixed at the 1 and 3 mm positions, and the rectified position measurement was plotted as a function of time. The results are shown in Figs. 8 and 9, for the box positioned at 1 and 3 mm respectively. The peak to peak noise is 7 micrometers, when the box is at 1 mm, and 100 micrometers, when the box is at 3 mm. The factor of 14 difference, between the rectified position measurement noise for these two cases, is because both sensors are saturated when the box is at the 3 mm position (which corresponds to the middle of the gap), while only one is saturated when the box is at the 1 mm position.

4.2 Actuator Rectification

The actuator rectification element of the control law uses the mathematical model of the actuator explained in Section 3.3. Given the force that must be applied by the actuator to the box (which is calculated by the PID controller) and the distance between the box and the actuator provided by the sensor rectifier (Fig. 10), Eq. 2 is solved for the voltage that must be commanded to the actuator.

4.3 PID Controller

The goal in the design of the Proportional, Integral, and Derivative (PID) controller is to achieve a closed loop step response with less than 10% overshoot, a settling time of 2 seconds, and a large low frequency disturbance rejection (actually, due to the integral term in the controller, the closed loop system has "perfect" disturbance rejection at DC).

The gains of the PID controller were first calculated in the continuous time domain. The linearized plant is a second order system, and the proportional and derivative gains were calculated to achieve a damping ratio of 0.707 and an undamped natural frequency of 0.11 Hz. This pole location results in low overshoot and a settling time of 2 seconds. The integral gain was chosen as large as possible, without changing the second order pole locations by much.

Since the sampling frequency (3.5 Hz) is more than an order of magnitude larger than the control bandwidth (0.11 Hz), the PID gains calculated in the continuous time domain can be used without any modifications in the sample data domain. The velocity (derivative term) was estimated using

Figure 8. Rectified Position Measurement vs Time
(@ D = 1 mm)

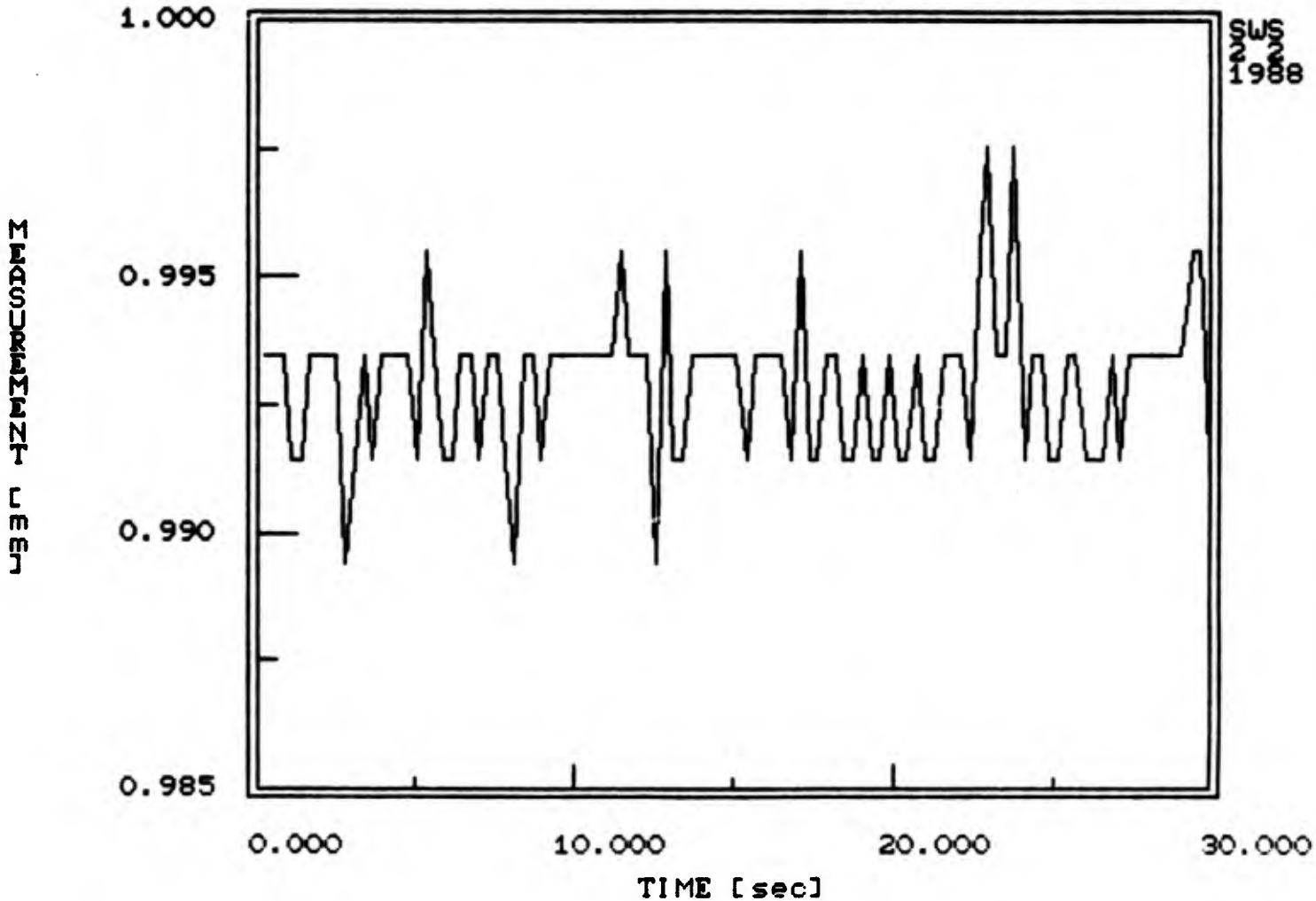

Figure 9. Rectified Position Measurement vs Time
(@ D = 3 mm)

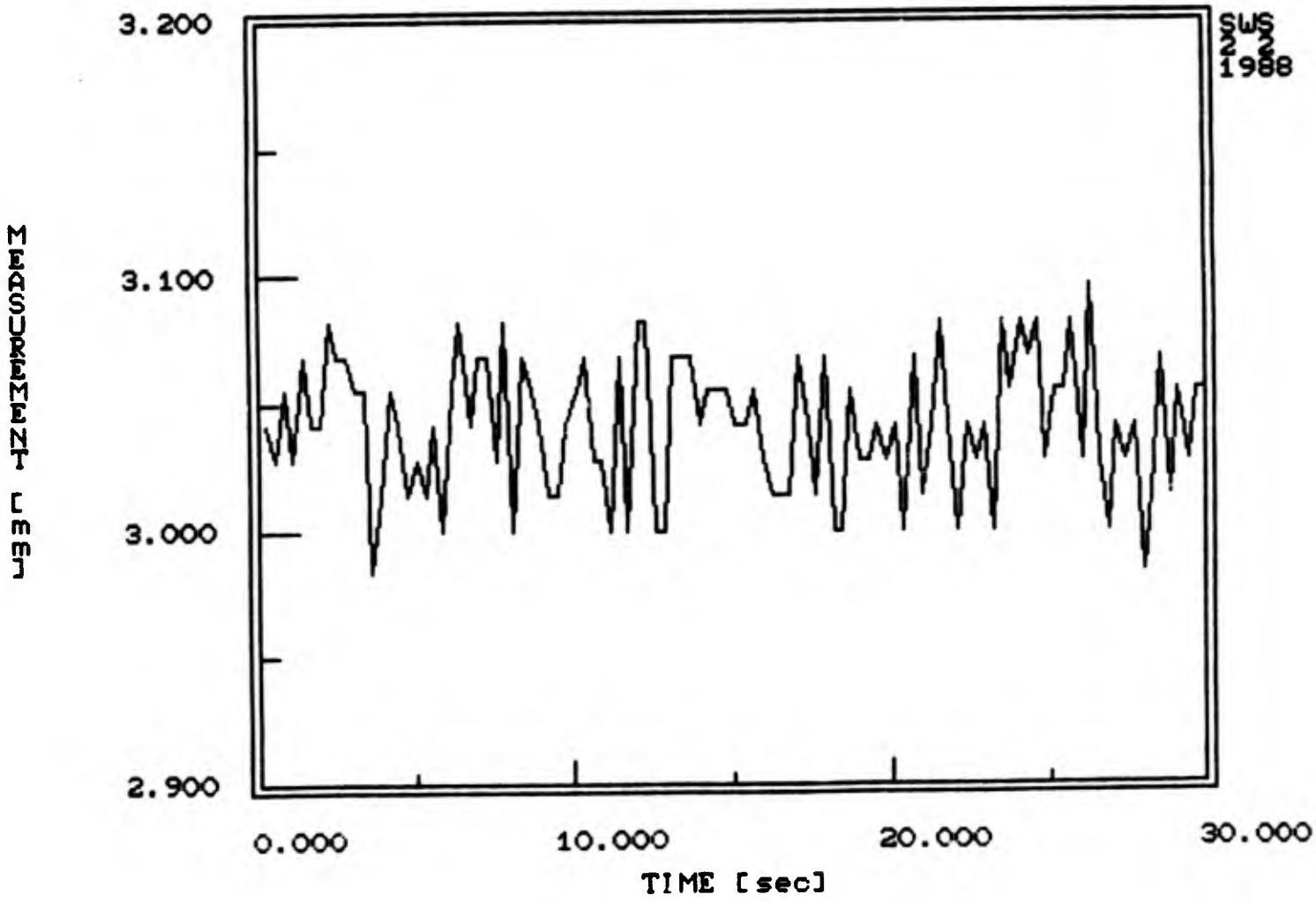

Figure 10. Plant and Control Law Block Diagram

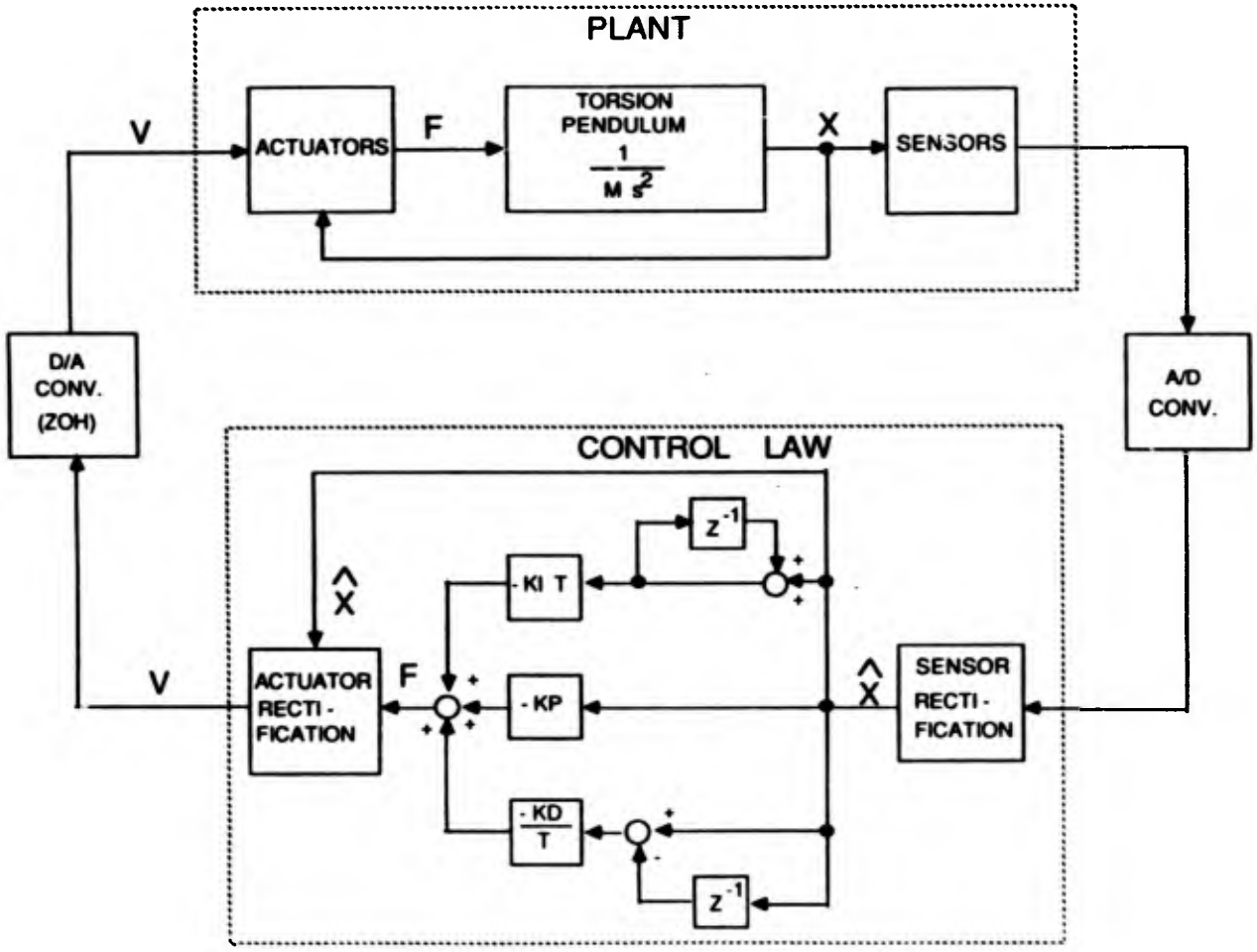

Figure 11. Step Response (set point = 3 mm)

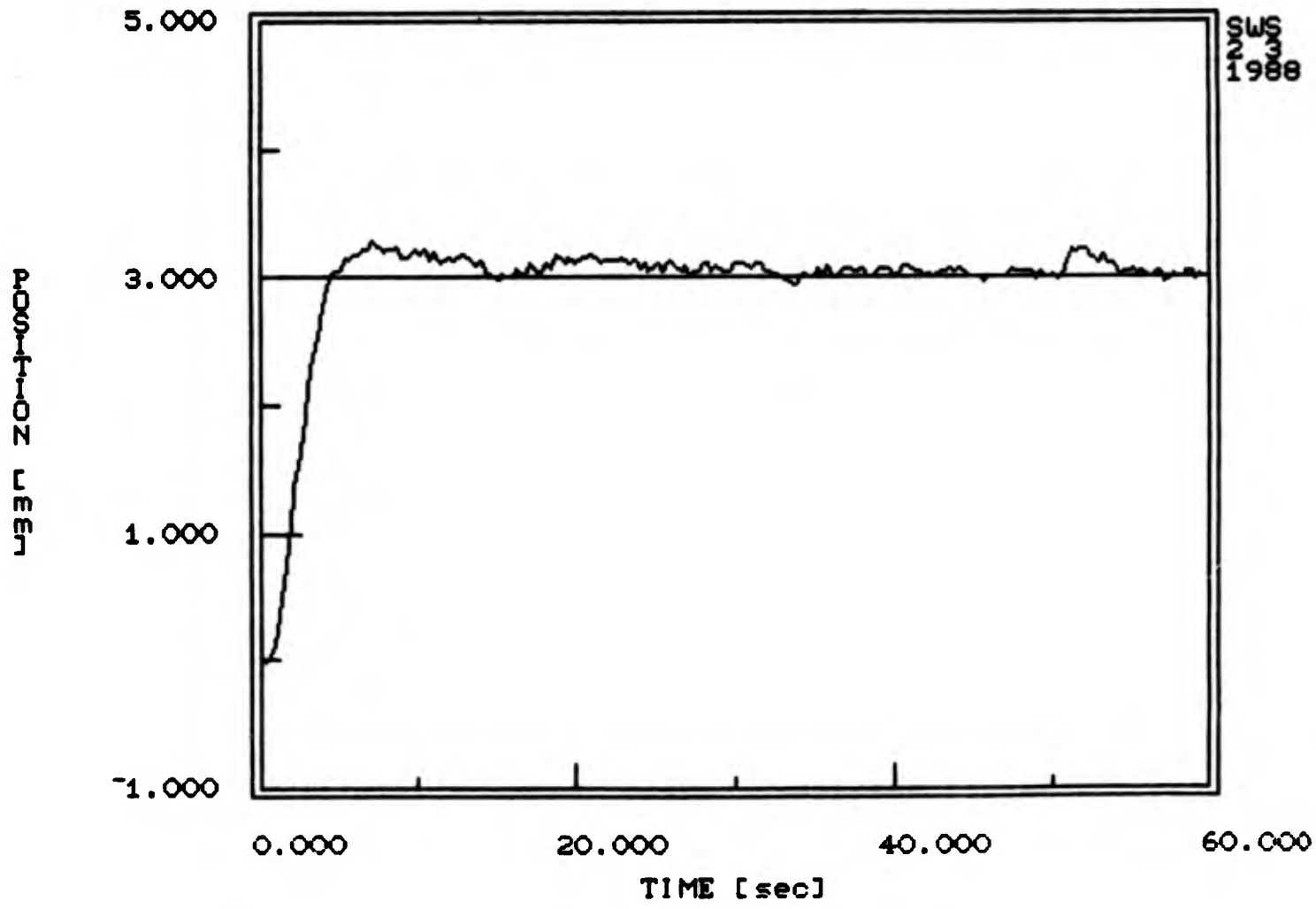

Figure 12. Step Response (set point = 5 mm)

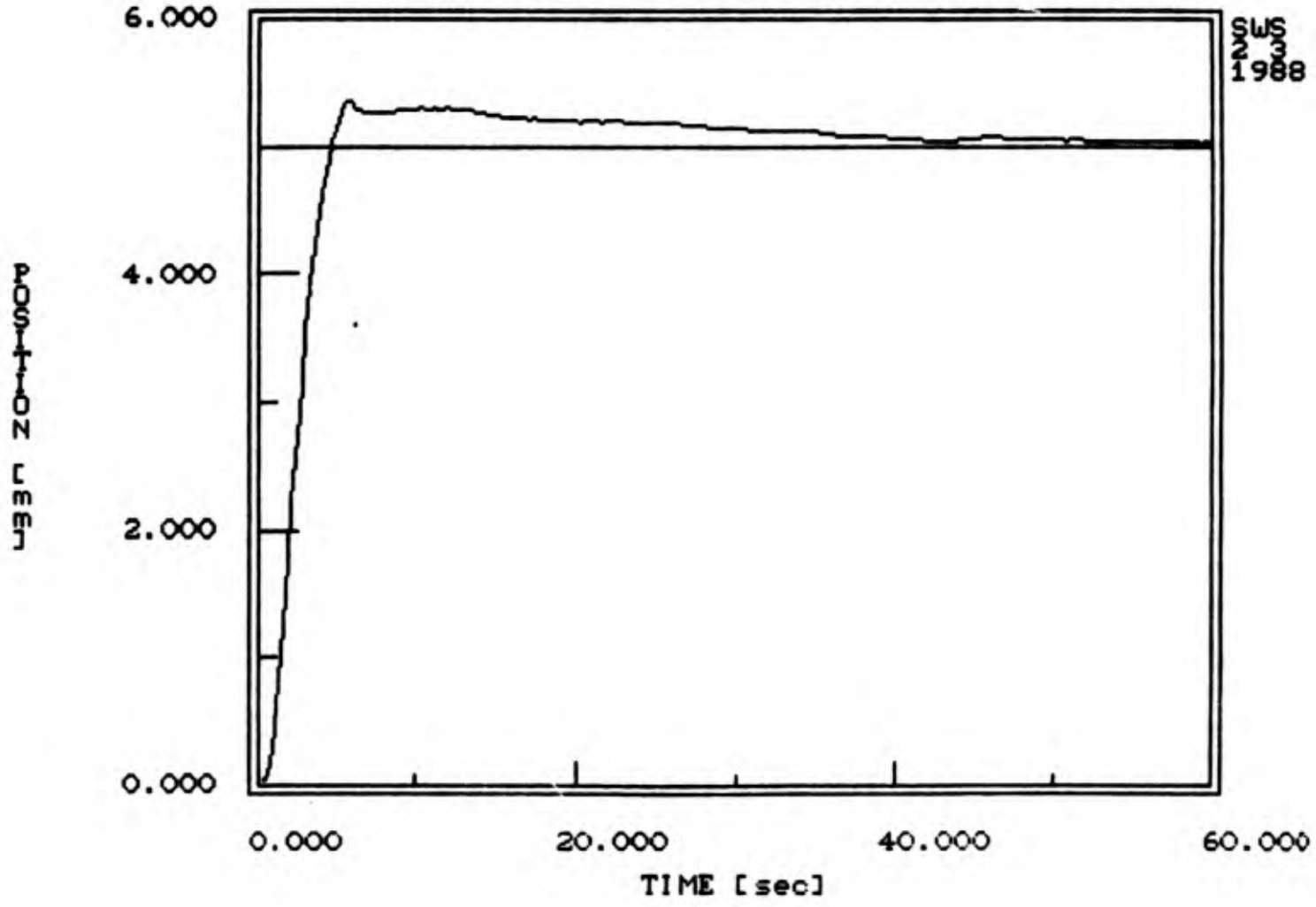

both a first order and second order position curve fit. The second order fit had a better signal to noise ratio and was ultimately used. Fig. 10 shows a block diagram of both the plant model and the control law (the controller has the first order velocity estimator).

4.4 Results

Figs. 11 and 12 show the step response of the system, as measured by the sensors, from the initial 0 mm position to the commanded 3 and 5 mm positions respectively. We can see that the overshoot and settling time requirements have been met with zero steady state DC error. The high frequency noise at steady state is due to the sensor noise, which is larger for the 3 mm case than for the 5 mm case, due to the saturation of both sensors (see Section 4.1). The low frequency steady state error is believed to be caused by air disturbing forces in both cases.

5 Future Plans

In the near future, it is planned to extend the controls work to the design and testing of semi drag free and vibration isolation control laws. In addition, it is intended to continue the eddy current theory effort at Arizona State University (Ref. 3) to provide an electrical model of the combined amplifier-coil-box system, suitable for future practical isolator design. It should then be possible to verify the theory on the existing one axis laboratory simulator. Two axis testing, on the Stanford University ground effect facility is also an attractive possibility.

6 References

1. Seaman, C.H.; and Sonnabend, D.; "A Laboratory Single Axis Magnetic Isolator"; JPL EM 343-1004; 3-21-86.

2. Sonnabend, D.; and San Martin, A.M.; "Magnetic Isolation - Closing the Loop"; 15th Grav. Grad. Conf.; 2-11-87.

3. Bergman, J.; and Hestenes, D.; "Eddy Currents in a Conducting Sphere"; Dept. of Physics; Arizona St. Univ.; 10-86.

FROM GEODETIC TRIANGULATION TO SPACETIME GEODESY

by

Captain Warner A. Miller, USAF

USAF Weapons Laboratory
Kirtland Air Force Base, New Mexico 87117

This paper describes an extension of the 2-dimensional triangulation of the earth to the 4-dimensional triangulation of spacetime geometry. Whereas ordinary triangulation makes use of a known baseline to construct a network of internally flat triangles to reveal the geometry of the surface of the earth, the spacetime triangulation described here makes use of a known base tetrahedron to construct a network of internally flat simplexes (4-dimensional triangles). The edgelengths of these simplexes are then used to reveal the geometry of spacetime. The trigonometry of spacetime triangulation was introduced by Tullio Regge in 1961 and is commonly referred to as Regge Calculus. However, this paper describes a modification of Regge Calculus (Null-Strut Calculus) that includes the maximal use of null struts (laser rays) to interconnect the events in the spacetime triangulation. The trigonometry of Null-Strut Calculus will be introduced in this manuscript.

From Geodetic Triangulation To Spacetime Geodesy: Second Order GPS Time Transfer Effects

ARKADY KHEYFETS† , NORMAN J. LAFAVE‡, AND WARNER A. MILLER*

24 June 1988

Abstract. We have evolved from an era of ordinary geodesy to the era of *spacetime geodesy*. Navigation must – and nowadays does – include both global time transfer and a relativistic-based navigational network (a Global Positioning System *spacetime common grid*). In this paper we (1) motivate spacetime geodesy, (2) use, for the first time, a newly-developed geometric tool for relativity (*null-strut calculus*) to both solve and illuminate the Doppler shift in GPS, and (3) introduce a general relativistic approach to the problem of frequency shift between a signal sent from a GPS satellite to an earth observer so that we may analyze and understand the null-strut calculus approach and the three approaches of N. Ashby, R. Matzner, and J. L. Synge. In particular, we show that N. Ashby's special relativistic analysis of frequency shift, when augmented by the standard red-shift correction yields, to 2^{nd} order, the general relativistic treatment of Matzner, Synge and null-strut calculus.

1. GRAVITATION, TIME TRANSFER, AND SPACETIME GEODESY

No longer can we discuss navigation in space, rather we must define, document and direct all navigation in space plus time (spacetime). Today the Global Positioning System (GPS)[1], which meets the 110ns requirement levied upon it, stands as an anchor point for future communication and navigation needs. Almost every facet of navigation and time transfer, from recreation, to ships, and from planes to satellites, will rely on this spacetime common grid[2]. For example, GPS measurements can determine the sensor velocity needed for the Eötvös reduction of the gravity data in airborne gravity and gravity gradiometry.

The analogies between ordinary geodetic triangulation and the up-and-coming GPS based spacetime common grid [3] are striking. In particular, we see an extension of the 2-dimensional triangulation of the surface of the earth to the 4-dimensional triangulation of the spacetime geometry enveloping the earth. We have evolved from an era of ordinary geodesy to the era of "spacetime geodesy." [4] Whereas ordinary triangulation makes use of a known baseline to construct a network of internally-flat triangles to reveal the geometry of the surface of the earth, modern day triangulations of spacetime makes use of a base tetrahedron (e.g. 4 GPS satellites, Fig. 1) to construct a network of internally-flat simplexes (4-dimensional triangles, Fig. 1). A spacetime geodesist can then use the edgelengths of such simplexes to reveal the curved geometry of spacetime. This entire procedure is in direct analogy with the trigonometric approach used by geodesists to model a terrain via a network of triangles. However, the trigonometry of a spacetime geodesist

---

This paper is dedicated to AFWL Chief Scientist Arthur H. Guenther on the occasion of his retirement. This work was supported in part by AFOSR and AFGL. We wish to thank C. O. Alley, G. M. R. Winkler, H. Fliegel, R. A. Nelson for many stimulating discussions and for introducing this issue to us. We especially extend our gratitude to R. A. Matzner for many stimulating discussions on time transfer in GPS.

is not 2–dimensional Euclidean trigonometry but rather it is 4–dimensional Minkowskian trigonometry. The mathematical machinery that underlies spacetime triangulation was introduced in 1961 by T. Regge and is referred to as Regge calculus [5] [6]. Recently, a working version of Regge calculus (*null-strut calculus*) that includes the maximal use of null struts (laser beams, radio signals etc...) to interconnect events in the spacetime triangulation was introduced [7]. This calculus provides a description of a spacetime lattice network that can be constructed solely from the tools available to spacetime geodesists (clocks, measuring rods, and laser beams). We see every indication that null–strut calculus will become a useful mathematical tool to understand the cohesive ensemble of the full GPS constellation including, in particular, the second generation cross–link ranged GPS satellites. In particular, Sec. 4 uses null–strut calculus to solve for the Doppler shift in GPS.

Just as there are many facets of ordinary geodesy, so too there are many facets of spacetime geodesy. Triangulations of ordinary geodesy range from maps of the rugged terrain of a mountain range, to the analysis of the shape of the geoid. In spacetime geodesy one can map the local gradients of the tide–producing gravitational field using gravity gradiometers, and on the other end of the spectrum, one can analyze the global Schwarzschild–like geometry of the spacetime surrounding the earth. Both arenas of endeavor (the local and global) seek an understanding of the gravitational field. Both seek a deeper understanding of communication and navigation within this field. This can best be encapsulated by the single Wheelerian sentence summarizing Einstein's 1915 theory of gravitation — "The curvature of spacetime tells matter (satellites) how to move, and in turn matter (the earth) tells spacetime how to curve". Einstein's mass–producing curvature model of gravitation forms the basis of spacetime geodesy, and of modern–day navigation.

Much of what we already do is spacetime geodesy. We (1) measure the rotation of perigee of the 1976 NASA launched LAGEOS–I satellite [8] (general relativistic effect, when modeled, corrected a ~25 arcsec linear drift in the perigee residual during the period of 1977 - 1983), (2) determine the distance to the moon to less than 10 cm via lunar laser ranging [9], (3) establish a network of transmitting space clocks (GPS system) for which we globally synchronize time to within 110 ns, and (4) we are now embarking on a measurement of the Lense–Thirring frame dragging effect via laser ranging to the tandem configuration of LAGEOS satellites (LAGEOS–I, LAGEOS–III) (~32 arc msec/year over 4 years) [10]. This paper cannot hope to cover this vast arena of emerging science, but it can hope to analyze an interesting new subject at the heart of GPS–based spacetime triangulations — the second order effects of global time transfer from GPS to a receiver. Along this line, we introduce,in Sec. 2, a general relativistic approach to the problem of frequency shift in order to analyze and understand the three approaches of N. Ashby [11], R. Matzner [12], and J. L. Synge [13]. We show that they are consistent. In particular, N. Ashby's special relativistic analysis of frequency shifts, when augmented by the standard red–shift correction yields the general relativistic second order approximation of Synge, Matzner and the null–strut calculus calculation of Sec. 4. We analyze this particular problem because we believe it to be at the heart of tomorrows navigation (cross–link ranging in GPS).

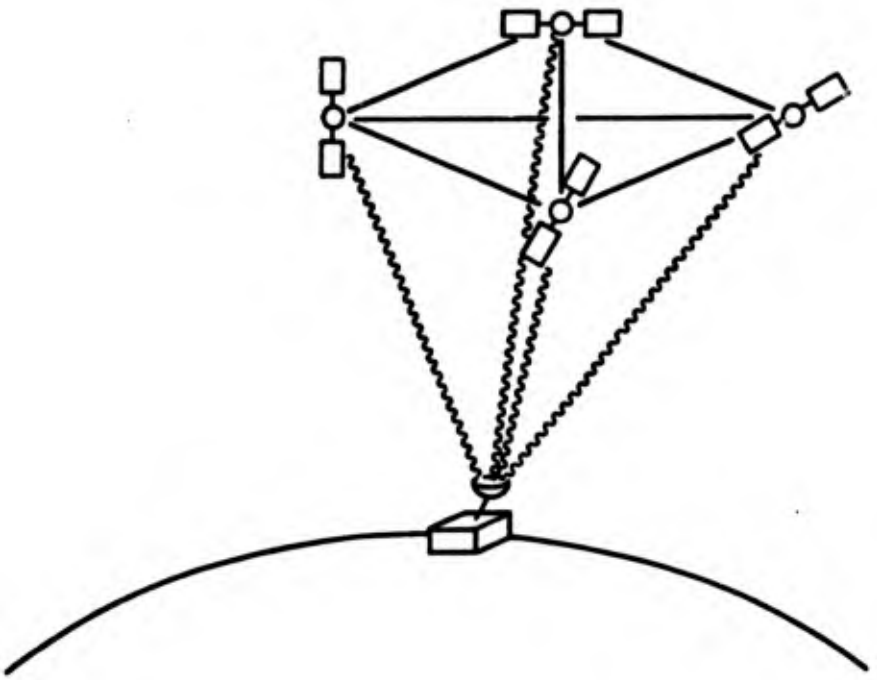

Fig. 1. A GPS–defined spacetime simplex. This is the spacetime geodesist's 4–dimensional analogue of the 2–dimensional triangle of geodetic triangulation. A simplex (4–dimensional triangle) has 5 vertices. Four of these vertices are represented by the satellites, the remaining vertex is represented by the observer's receiving antenna. Whereas the satellites are interconnected to each other by 6 spacelike struts (solid lines interconnecting the observer and obtained by cross–link ranging or modelling), the observer is connected to the satellites by 4 null struts. The 4 null struts or radio signals give the observer information on his relative position in spacetime to the satellites. In other words, the observer can triangulate using the spacelike tetrahedron formed by the 4 satellites.

2. GPS AND CLOCK SYNCHRONIZATION

The requirements on global clock synchronization are becoming increasingly demanding — it is in this sense that spacetime geodesy is an integral part of the GPS operations. Furthermore, when more satellites are added to the GPS constellation to form a *spacetime common grid* (esp. with cross–link ranging between satellites), we believe that these

precision requirements will become crucial. In other words, the problem of precise clock synchronization in a multi–satellite common grid rests on the coherence of the system as a whole.

The GPS constellation will someday contain 18 clocks (with 3 active spares) moving with respect to each other. Such GPS satellites will have almost circular orbits of 4 earth radii, with 12–hour periods, which means that the satellite velocity is ~8 times the velocity of the surface station originating from earth rotation. All the activity of GPS occurs in earth's gravitational field and some clocks and/or receivers are attached to non inertial frames of reference (clocks of surface stations, planes etc...). One is thereby lead to the conclusion that, sooner or later, we will encounter the problem of taking into account relativistic effects on the rate of clocks. Such relativistic effects originate from (1) the difference in the rates of clocks moving with respect to each other (special relativistic effects), (2) from general relativistic effects due to the difference in rate of clocks placed in positions with different gravitational potentials from the earth gravitational field, and (3) the influence on the rate of clocks due to the noninertiality of their system of reference.

It is well known [14] [13] (cf. also below from the formula relating the Doppler shift and the rates of clocks) that the difference in the clocks rates can be treated as a Doppler correction. The first order Doppler corrections are dominant. They are well known and taken into account in the GPS system. The second order corrections are presently under discussion. There is considerable difference in opinions,[15], particularly on the issue of observability of one of the terms in the second order Doppler expansion. The issue is important because, if the term in question were observable, it would provide the maximal contribution to the second order Doppler correction (being proportional to the product of the satellite velocity and the surface station velocity it would be much greater than other second order terms).

Calculation of the second order corrections to the Doppler shift have been represented in wide spectrum ranging from explicitly special relativistic [11], to the explicitly general relativistic [12], and mixtures of both. The results of all approaches are different, although sometimes the difference is insignificant.

A word of caution is in order here: relativistic calculations accurate to a given order demand a consistent treatment of all terms [12]. Such calculations (both in special and general relativity) ordinarily contain an abundance of compensational terms that cancel [16]. Furthermore, depending on ones choice of observers, geometric quantities expanded to a given order (e. g. Doppler effect) can lead to different physical interpretations and even the possibly of different terms in the expansion.

At least two possibilities should be therefore considered. The difference in the results of alternative approaches can be explained either by (1) an inconsistency in treatment of different terms of the second order in one (or more) of the approaches or, (2) it is possible that the authors of the approaches were calculating and considering different things as observable. The last situation would mean that the only matter to be discussed would be the matter of interpretation.

We know of no better approach to estimate the Doppler correction up to the second order than to formulate a general relativistic model of signal transmission from the satellite to the surface station and, then, introduce appropriate approximations explicitly, taking into

account the model symmetries and numerical values of the model parameters.

It seems to be reasonable to use Schwarzschild geometry as the model of the earth's gravitational field. Obviously, in doing so one neglects contribution of the earth rotation into the gravitational field. An enhanced model would no doubt involve the Kerr metric. However, the evaluation of the Kerr model parameters shows that the produced effect of the dragging of the inertial frames would be of higher order than the effects caused by the parameters coming from the Schwarzschild model [10]. Meanwhile, an estimate of the Schwarzschild geometry parameters shows that the effect of $\frac{M}{r}$ (cf. below explanation of notation) is of the same order as effects of the squares of the relevant velocities. Thus, to discuss the second order Doppler corrections, one can use Schwarzschild geometry as a model of the earth gravitational field and, provided that in all approximation terms proportional to $\frac{M}{r}$ (neglecting higher powers of $\frac{M}{r}$) are retained, one will obtain a satisfactory expression for the Doppler corrections up to the second order with respect to the velocities involved in the picture.

The Schwarzschild geometry is a static spherically symmetric geometry. Its metric in Schwarzschild coordinates is given by the expression[1]

$$ds^2 = -\left(1 - \frac{2M_\otimes}{r}\right) dt^2 + \frac{1}{1 - \frac{2M_\otimes}{r}} dr^2 + r^2(d\theta^2 + \sin(\theta) d\phi^2), \tag{1}$$

where t,r,θ, and ϕ are Schwarzschild coordinates, and $M_\otimes$ is the earth mass.

In the geometric picture (cf. Fig. 2) describing the Doppler shift of an electromagnetic signal sent from the transmitting satellite to the surface station (called an observer from now on), the free–falling satellite has a geodesic world line, whereas the observer, being attached to the earth, has a world line with all three of its curvatures not equal to zero. It is clear [13] that the first curvature of the observer world line (called also in common language the acceleration of free fall at the earth surface) is $\sim \frac{M_\otimes}{R_\mathcal{O}^2}$ (here $R_\mathcal{O}$ is the earth radius) and the second and third curvatures are proportional to the angular velocity of the earth (they depend also on the latitude of the observer placement, the second curvature being equal to the earth angular velocity and the third being equal to zero on the equator, and the other way around on the polls).

A Doppler shift arises since the 4–velocity of satellite (at the moment of signal transmission), and the observer (at the moment of receiving) are not parallel. More precisely, the result of parallel transport of the satellite 4–velocity along the null geodesic connecting the event of transmitting to the event of receiving does not coincide with the 4–velocity of the observer.

The relation between the Doppler shift and the rates of clocks is given by the formula (cf. Fig. 3)

$$\frac{\nu_\mathcal{S} - \nu_\mathcal{O}}{\nu_\mathcal{S}} = 1 - \frac{d\tau_\mathcal{S}}{d\tau_\mathcal{O}}, \tag{2}$$

where $\tau_\mathcal{S}$ is the proper time of the satellite, $\tau_\mathcal{O}$ is the proper time of the observer, and $\nu_\mathcal{S}$, $\nu_\mathcal{O}$ are transmitted and received frequencies of the signal.

[1] We use throughout this paper the system of units commonly accepted in general relativity with both the velocity of light and the gravitational constant equal to unity

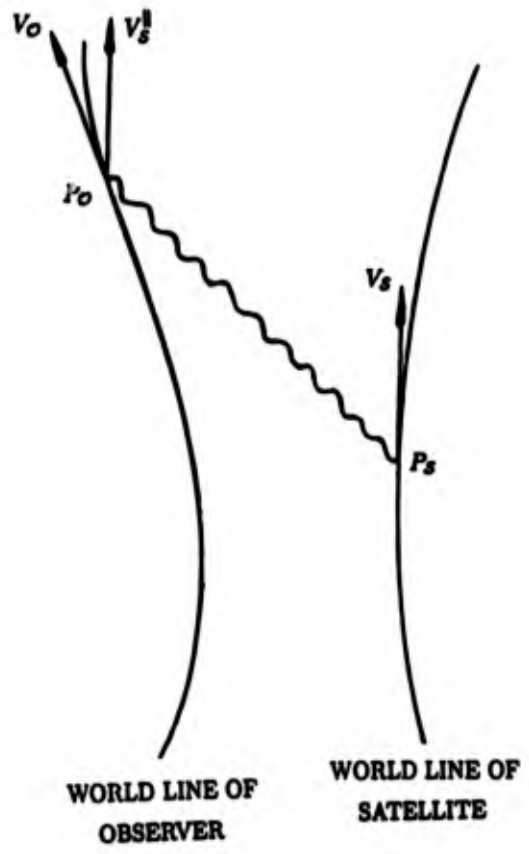

Fig. 2. Geometry of the Doppler shift. Vector $V_S^{\parallel}$ is the result of parallel transport of V_S along null geodesic $P_S P_O$. Doppler shift is caused by $V_O \neq V_S^{\parallel}$.

The frequency shift can be expressed in terms of the 4–velocities of the satellite and the observer and the 4–momentum of the photon traveling from the satellite to the observer as

$$\frac{\nu_S - \nu_O}{\nu_S} = \frac{{}_S p_\mu V_S^\mu - {}_O p_\mu V_O^\mu}{{}_S p_\mu V_S^\mu}, \tag{3}$$

where V_S^μ, V_O^μ are the 4–velocities of the satellite and the observer and ${}_S p_\mu$, ${}_O p_\mu$ are the photon 4–momentum at the event of transmitting and the event of receiving, respectively. The 4–momentum of the photon is parallel transported along the null geodesic connecting the events of transmitting and receiving and is tangent to the null geodesic at all times.

One has to keep in mind that, since the world line of the observer is not a geodesic, the 4–velocity of the observer is not transported parallel to itself along its world line and can be expressed in terms of some initial 4–velocity, the three curvatures of its world line and the spacetime geometry (depending on $M_\otimes$, and r).

Calculation of the Doppler shift up to the second order, i.e. retaining the squares of the velocities and the first power of $\frac{M_\otimes}{r}$ is not very complicated but refined. It has been

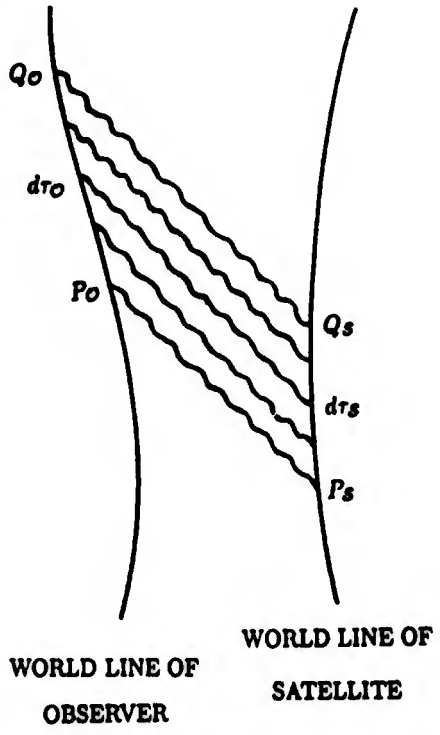

Fig. 3. Relation between the Doppler shift and the rates of the moving clocks. Shown is the set of null geodesics joining the world lines of the satellite and the observer. Each geodesic represents a wave crest. If there are n such crests and $d\tau_S$, $d\tau_O$ are the clock–measures of P_SQ_S and P_OQ_O respectively, then $n = \nu_S d\tau_S = \nu_O d\tau_O$.

performed by J. L. Synge using the techniques developed by him of tensor series expansion of the world function. [13] We will only introduce notations and give enough explanations to make the results comprehensible. Following J. L. Synge, we introduce new coordinates $(x^\mu)_{\mu=0,1,2,3}$ related to the Schwarzschild coordinates in the following way

$$x^0 = t, \quad x^1 = r\sin(\theta)\cos(\phi), \quad x^2 = r\sin(\theta)\sin(\phi), \text{ and } \quad x^3 = r\cos(\theta). \tag{4}$$

The metric in these coordinates takes the form

$$ds^2 = g_{\mu\nu}dx^\mu dx^\nu \tag{5}$$

with

$$g_{\mu\nu} = \eta_{\mu\nu} + \gamma_{\mu\nu} \tag{6}$$

where

$$\eta_{\mu\nu} = \text{diag}(-1, 1, 1, 1)$$

and the components of $\gamma_{\mu\nu}$ are small and static ($\gamma_{\mu\nu,0} = 0$). Of course, if one uses (x^μ) the coordinates of a Euclidean space, the geodesics of the original Schwarzschild spacetime are not going to be the straight lines of the Euclidean space. However, this Euclidean space proves to be convenient for making pictures. One such picture which helps one to understand the Doppler shift and the factors that influence is given in Fig. 4. Both the world lines of the satellite and the observer look curved. The curvature of the satellite world line is due to the gravitational field (spacetime curvature) only, whereas the curvature of the observer world line is due to both its nongeodesity and spacetime curvature. The 4–velocities of the satellite and the observer are not parallel even at the moment of transmission of the photon. The effect of the spacetime curvature and the curvature the observer's world line also has to be taken into account. The resulting Doppler shift, consequently, depends on all of these factors.

The vertical straight lines in the picture are the lines defined by the equations

$$x^i = \text{const}, \quad i = 1, 2, 3, \tag{7}$$

i.e. integral lines of the timelike Killing vector field of the Schwarzschild metric. Both the satellite and the observer have nonzero orbiting velocities and are not at rest with respect to Schwarzschild coordinates. Therefore, V_S as well as V_O are not parallel to the Killing vector $\frac{\partial}{\partial t} = \frac{\partial}{\partial x^0}$. The angles between V_S, V_O and the timelike Killing vectors at corresponding points are different, due to the difference in the orbiting velocities of the satellite and the observer. If the observer and the satellite were at rest with respect to Schwarzschild coordinates, i. e. if their world lines were the integral lines of the timelike Killing vector field, then we would get the well known expression for the Doppler shift

$$\frac{\nu_S - \nu_O}{\nu_S} = \frac{M_\otimes}{R_S} - \frac{M_\otimes}{R_O} \tag{8}$$

The right hand side of this equation is often called the gravitational Doppler shift. It is equivalent to a second order term in magnitude, and we can expect that it will appear as one of the terms in the final result of our estimate. In addition,we expect to obtain both the first order and the second order terms caused by the different inclinations of V_O, V_S with respect to the Killing vectors.

The detailed calculation can be carried out using the techniques of the tensor series expansion of the world function [13]. The calculation is rather straightforward. The only fine point in this calculation is to figure out the exact moment of receiving. The fact that the event of transmitting and the event of receiving are separated by the null geodesic world line of the photon, and are not simultaneous (in Schwarzschild coordinate time) is responsible for the structure of the first order term and, as we shall see, one of the second order terms.

The final result of the calculations gives the expression for the Doppler shift up to the second order.

$$\frac{\nu_S - \nu_O}{\nu_S} = (V_O^i - V_S^i)\frac{\Delta x^i}{\Delta t} + \left(\frac{M_\otimes}{R_S} - \frac{M_\otimes}{R_O}\right) + \frac{\Delta x^i \Delta x^k}{\Delta t^2}(V_O^i - V_S^i)V_S^k + \frac{1}{2}(V_S^i V_S^i - V_O^i V_O^i), \tag{9}$$

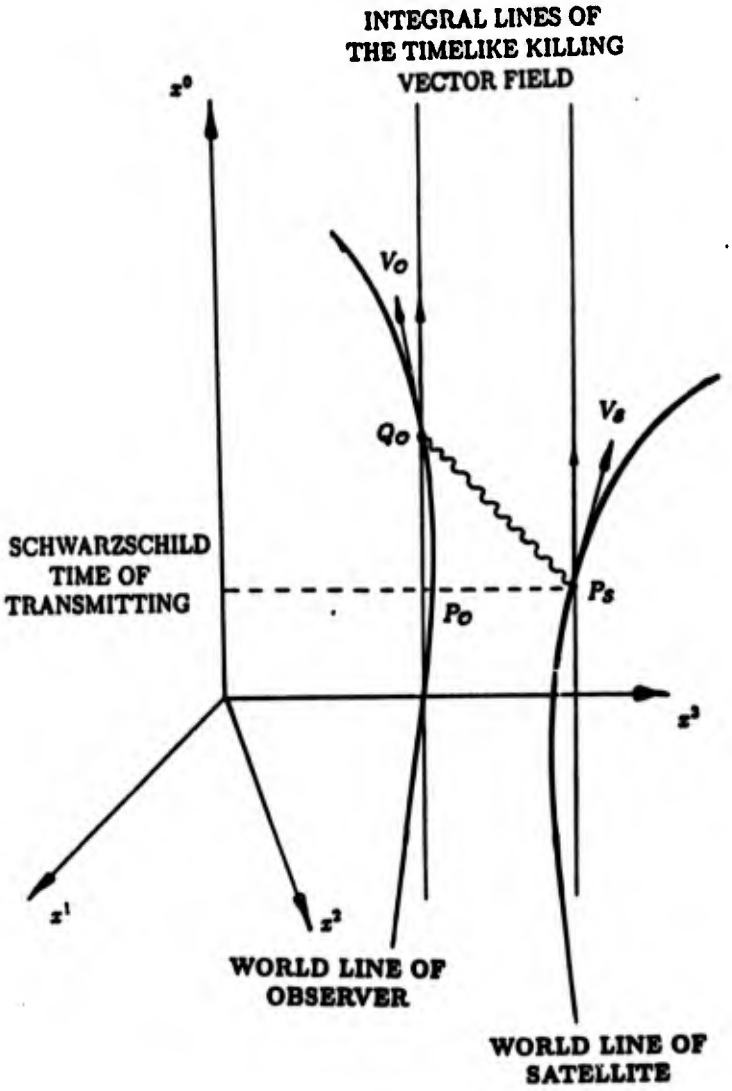

Fig. 4. The Doppler shift and its main contributing factors as viewed by observers resting with respect to Schwarzschild coordinates.

where $i,k = 1,2,3$, $\Delta x^i = x^i_O - x^i_S$, Δt is the time interval between transmitting and receiving and the summation over repeating indices is assumed.

The expression deserves some discussion. We see in it the first order Doppler correction

$$(V^i_S - V^i_O)\frac{\Delta x^i}{\Delta t}, \tag{10}$$

the second order correction term to the first order term

$$\frac{\Delta x^i \Delta x^k}{\Delta t^2}(V^i_O - V^i_S)V^k_S = \frac{\Delta x^i}{\Delta t}(V^i_O - V^i_S)\frac{\Delta x^k}{\Delta t}V^k_S, \tag{11}$$

the gravitational term of the Doppler correction

$$\frac{M_\otimes}{R_S} - \frac{M_\otimes}{R_O}, \tag{12}$$

and the term

$$\frac{1}{2}(V_S^i V_S^i - V_O^i V_O^i), \tag{13}$$

which is natural to call the centrifugal correction term, because, in a classical picture, in a case when the trajectories of both the satellite and the observer are circular, the term can be thought of as the difference of potentials of centrifugal forces arising due to the angular velocities of orbital motion of the satellite and the observer. The second order correction to the first order correction is not symmetric with respect to V_O^i, V_S^i because we are using as the measure of the Doppler shift the ratio $\frac{\nu_S - \nu_O}{\nu_S}$ (it would contain V_O^k instead of V_S^k if we took $\frac{\nu_S - \nu_O}{\nu_O}$ instead).

Eq. 9 for the Doppler shift coincides (up to the second order) with the expression given by Ashby (excluding the gravitational term) but does not contain anywhere the term proportional to the scalar product of the satellite and observer velocities, $\vec{v}_O \cdot \vec{v}_S$. Such a non-local term cannot admit any physical interpretation within the classification of the second-order terms given above. It could appear in the final result only as a consequence of an inconsistency of approximations. The detailed explanation of the cancellation mechanism of such terms can be found in Ashby's paper. Although calculations in Ashby's paper have been performed within the framework of special relativity (and therefore the pure gravitational contribution does not show up), it has been shown convincingly by Ashby that the consistent treatment of all contributions leads to a cancellation of the product term and leaves only the terms admitting a transparent physical interpretation consistent with both Synge, Matzner and our null-strut calculation presented in Sec. 4.

The growing demand for precise global synchronization of the clocks in GPS requires the general relativistic approach to become the everyday language for formulating GPS problems. But this approach, once accepted, makes the presently used concept of an earth centered, inertial reference frame (ECI) unmotivated. Of course, one could try to get rid of the ECI altogether, considering instead the frame of reference of the surface station or, for the sake of comparison new results with old ones, to introduce an observer with the frame of reference at the same point as the surface station but resting with respect to the Schwarzschild coordinate system. This possibility was explored by R. Matzner[12] and in Sec. 4. By means of very simple and brilliant analysis, making use of the Schwarzschild field symmetries and the integrals of motion of the photon moving in the field, he has shown that the difference between the second order Doppler corrections for the surface station observer and the observer resting with respect to the Schwarzschild coordinate system (considered as an analog of ECI) is of the order of V_O^2. The result is quite easily understandable from our point of view (the centrifugal contribution caused by noninertial motion of the receiver disappears), and leaving aside insignificant details, is correct.

However the observer resting with respect to Schwarzschild coordinates does not seem to be an appropriate choice to replace the ECI because its world line has nonzero first curvature and, moreover, this first curvature depends on position of the observer.

One way out, in the spirit of general relativity, is to use the whole congruence of imaginary observers with their 4–velocities parallel to the timelike Killing vectors. It is the closest possible general relativistic analogue of the ECI. Actually, this is the system we have used to obtain our expression for the Doppler shift. Such a system is heavily based on the symmetry properties of the model gravitational field. Ordinarily it looses its meaning and, quite possibly, a better choice can be made.

The problem of choosing the new frame of reference, or any other system of data ordering replacing the ECI frame, which will be meaningful within the framework of general relativity is therefore in order. What is really needed is a satellite–based *Spacetime Common Grid* (SCG). Research having as its focus the defining of such a SCG system, so that it can be made a working tool in GPS should be undertaken in the near future.

3. Null–Strut Calculus: A Mathematics of Spacetime Geodesy

The GPS constellation provides an extension of the 2–dimensional geodetic triangulation of the surface of the earth to the 4–dimensional triangulation of the curved spacetime geometry enveloping the earth. Whereas ordinary triangulation makes use of a known baseline to construct atop a network of internally flat triangles to reveal the geometry of the surface of the earth, the spacetime triangulation discussed here makes use of a known base tetrahedron to construct atop a network of internally flat simplexes (4–dimensional triangle). Just as the edgelengths ($\Delta L = \sqrt{\Delta x^2 + \Delta y^2 + \Delta z^2}$, Euclidean interval in 3–space) of the triangulated lattice in ordinary geodesy are used via trigonometry to reveal the geometry of the terrain, so too the edgelengths or intervals, not in Euclidean space but rather in Minkowski space($\Delta L = \sqrt{\Delta x^2 + \Delta y^2 + \Delta z^2 - \Delta t^2}$) of the simplicial lattice, are used to reveal the geometry of spacetime.

The spacetime geodesist has among his arsenal of tools (1) clocks to form time–directed struts ($\Delta L^2 < 0$) and, (2) lasers to form null struts ($\Delta L^2 = 0$). How fortunate we are that the indefinite metric of spacetime allows null struts (spacetime permits a maximum of 6 of 10 edgelengths of a simplex to be null [4]), for zeros placed in complex trigonometric formulae provide great simplification. Clocks together with lasers can be used in and by themselves (of course with encoders to measure angles of incoming light beams etc.) to construct a spacetime triangulation. The GPS constellation is such a system. In particular, 4 GPS satellites in communication with a receiver form a 4–dimensional triangle or simplex (Fig. 5). Such a simplex has 5 vertices (4 satellites plus receiver), 10 edges (6 spacelike, $\Delta L^2 > 0$, interconnecting the 4 satellites, and 4 null, $\Delta L^2 = 0$, connecting the observer to the 4 satellites), 10 triangles (4 spacelike $Area^2 > 0$, with satellites as its vertices, and 6 timelike, $Area^2 < 0$ each with two satellites and an observer as its vertices), and 5 tetrahedral faces (1 spacelike base tetrahedron, $Volume^2 > 0$, with the 4 satellites as its vertices, and 4 timelike tetrahedrons, $Volume^2 < 0$, each with 3 satellites and an observer as its vertices). The 4 satellites form a spacelike tetrahedron, which we refer to as the base of the simplex. Such a base tetrahedron is the starting point for a spacetime triangulation of the geometry surrounding the earth. Emanating from the 4 vertices of the base are 4 null struts that focus at the observer, forming a wigwam–like simplex. For this reason we refer to such a simplex as a wigwam (the geometry of such a spacetime building block is given by the standard trigonometric formulae as modified by the indefinite metric of spacetime).

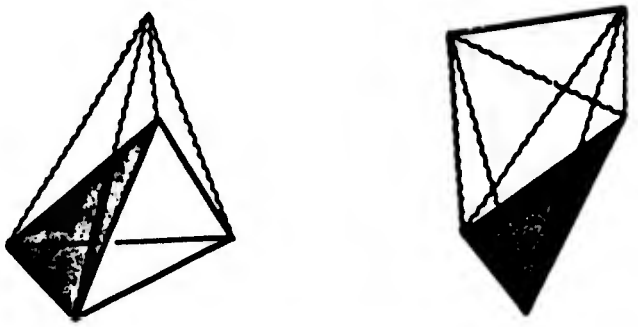

Fig. 5. Wigwam (left) and Wedge simplex (right). These two simplexes, and copies of them, when fitted together can triangulate spacetime. They provide a triangulation of spacetime that contains the maximal use of null struts; and therefore, they provide the most economic triangulation of spacetime.

In addition to the wigwam simplex, the only other simplex needed to construct a complete spacetime triangulation is a "wedge" simplex (shown in Fig. 5). It is referred to as wedge because it fits nicely (or wedges) in between two adjacent wigwams. Both these simplexes, both wigwam and wedge, are formed by the GPS constellation with observers. We can therefore use the GPS satellites to analyze via null–strut calculus (a working version of Regge calculus employing maximal use of null struts or laser beams) the curvature of the spacetime geometry enveloping the earth. We show in Fig. 6 a section of such a triangulation with its 4 wigwams and 2 wedges exploded off of it. The curvature of spacetime in this triangulated region is concentrated in the timelike plane (T^*) perpendicular to the shaded spacelike triangle (T). The curvature at T is a function of the 11 spacelike edges (solid lines). Two particles in T^* that were originally parallel will become boosted toward (or away) from each other. This angle of boost β is referred to in Regge calculus as a *deficit angle*. It is a measure of the disparity of the region bounded by the 6 simplexes away from Minkowski flatness.

$$\beta_T = 2\pi - \sum_{l=1}^{6} {}_T\theta_l, \tag{14}$$

where ${}_T\theta_l$ is the hyperdihedral angle of the simplex l at the triangle hinge T. The curvature $\mathcal{R}$ concentrated at the triangle hinge T is given by,

$$\mathcal{R}_T = \frac{\beta_T}{A_{T^*}}, \tag{15}$$

where A_{T^*} is an appropriate timelike area in the plane perpendicular to T. It can be defined as the set of points in the union of the interiors of the 6 simplexes that is closer

to T than to any other triangle.[17] To present such a calculation in detail is beyond the scope of this paper; however, a (1+1)–dimensional space plus time calculation analogous to this is presented in [4]. We wish to illuminate the striking connection between GPS and a newly developed mathematics of general relativity (null–strut calculus). We have every reason to believe that such a computational tool will be valuable in analyzing GPS in the future. Nevertheless, it does point out the need for cross link ranging to obtain transverse distances, i. e. to obtain directly the spacelike separations between each pair of satellites. It appears to us that such a measurement is a must for (1) the stability of the GPS constellation, and (2) for the accurate measurement of relativistic effects.

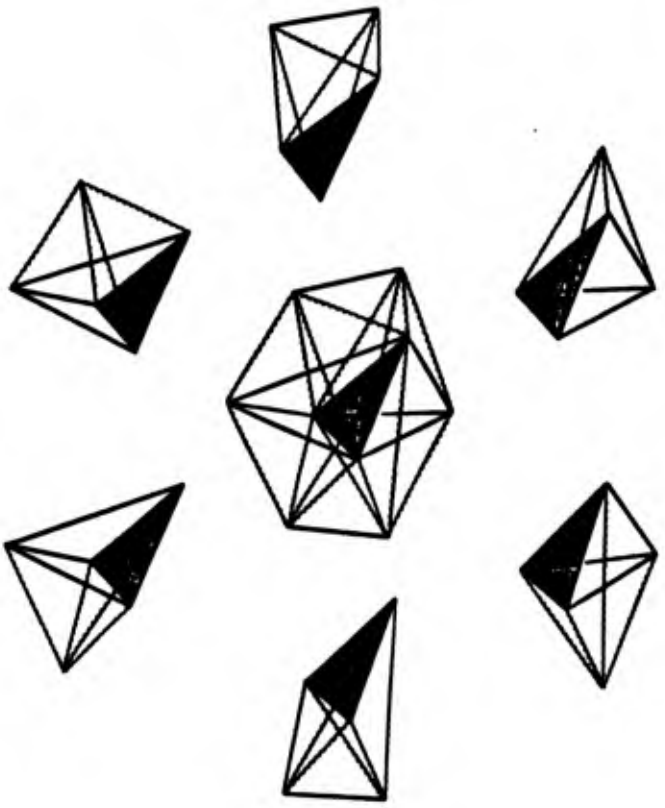

Fig. 6. A section of a triangulation with 4 wigwams and 2 wedges.

4. The Doppler Effect as Viewed Through Null–Strut Calculus

Here for the first time we use *null–strut calculus* to illuminate geometrically the GPS Doppler shift calculations of Ashby [11], Matzner[12], and Synge[13]. Just as Matzner's

and Synge's approaches are fully general relativistic, so too this null–strut calculus calculation is general relativistic. The calculation is coordinate free, and therefore provides a pictorial representation of the Doppler shift. This feature makes clear the interpretation of the terms in Eq. 9.

Let the observer, $\mathcal{O}$, and the satellite transmitter, $\mathcal{S}$, be connected in spacetime by a null strut, N. We can subdivide N into many small segments, and in so doing, form a ladder of triangles reaching from $\mathcal{O}$ to $\mathcal{S}$ (Fig. 7). Each triangle in the ladder has one timelike edge (here we take this edge directed along the Schwarzschild coordinate t of Eq. 1), and two null edges. In particular, we refer to the timelike edge at $\mathcal{O}$ as $\Delta T_{\mathcal{O}}$, and the timelike edge at $\mathcal{S}$ as $\Delta T_{\mathcal{S}}$. We can relate these intervals to the Schwarzschild time coordinate interval ΔT (an observer at spatial infinity).

$$\Delta T_{\mathcal{O}} = \Delta T\left(1 - \frac{2M_{\otimes}}{R_{\mathcal{O}}}\right)^{\frac{1}{2}} \tag{16}$$

$$\Delta T_{\mathcal{S}} = \Delta T\left(1 - \frac{2M_{\otimes}}{R_{\mathcal{S}}}\right)^{\frac{1}{2}} \tag{17}$$

Here $R_{\mathcal{O}}$ is the Schwarzschild radius of $\mathcal{O}$, $R_{\mathcal{S}}$ is the Schwarzschild radius of $\mathcal{S}$, $M_{\otimes}$ is the mass of the earth, and ΔT depends on how finely we subdivide N, the details of this subdivision are not an issue here — we take them as infinitesimal.

Let us consider the two triangles at $\mathcal{O}$ sharing timelike edge $\Delta T_{\mathcal{O}}$ (Fig. 8). The spatial component of the 4–velocity of $\mathcal{O}$ is represented by the boost parameter $\beta_{\mathcal{O}}$ and is given by,

$$V_{\mathcal{O}} = \tanh(\beta_{\mathcal{O}}) \tag{18}$$

To calculate the frequency shift $\frac{\Delta\nu}{\nu}$ of Eq. 2 we need the timelike distance $\Delta\tau_{\mathcal{O}} = \overline{\mathcal{O}N}$ as well as $\Delta T_{\mathcal{O}} = \overline{\mathcal{O}M}$. However, simple Minkowski trigonometry applied to Fig. 8 yields,

$$\Delta\tau_{\mathcal{O}} = \Delta T_{\mathcal{O}} e^{-\beta_{\mathcal{O}}}, \tag{19}$$

Similarly,

$$\Delta\tau_{\mathcal{S}} = \Delta T_{\mathcal{S}} e^{-\beta_{\mathcal{S}}}. \tag{20}$$

Therefore,

$$\frac{\Delta\tau_{\mathcal{S}}}{\Delta\tau_{\mathcal{O}}} = \frac{\Delta T_{\mathcal{S}}}{\Delta T_{\mathcal{O}}} e^{(\beta_{\mathcal{O}} - \beta_{\mathcal{S}})}. \tag{21}$$

This expression, in its infinitesimal form is exact. We now show that it is consistent with Eq. 9 to second order; however, higher order calculations take no more effort.

To expand Eq. 21 to second order we approximate $e^{-\beta} = e^{-V}$ as,

$$e^{-V} = 1 - V + \frac{1}{2}V^2 + O(V^3) \tag{22}$$

This leads to the following:

$$\frac{\Delta\nu}{\nu} = 1 - \frac{\left(1 - \frac{2M_{\otimes}}{R_{\mathcal{S}}}\right)^{\frac{1}{2}}\left(1 - V_{\mathcal{S}} + \frac{1}{2}V_{\mathcal{S}}^2\right)}{\left(1 - \frac{2M_{\otimes}}{R_{\mathcal{O}}}\right)^{\frac{1}{2}}\left(1 - V_{\mathcal{O}} + \frac{1}{2}V_{\mathcal{O}}^2\right)} \tag{23}$$

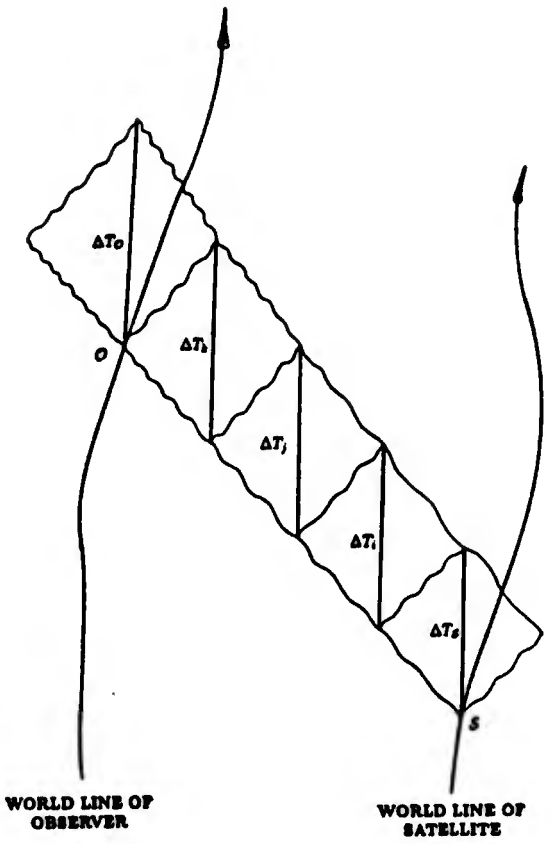

Fig. 7. A null-strut calculus ladder reaching from the world line of the satellite $\mathcal{S}$ to the world line of the observer $\mathcal{O}$. The wavy lines represent null geodesics (null struts). The timelike struts (vertical solid lines) are directed along the Schwarzschild coordinate t (the timelike Killing vector field $\frac{\partial}{\partial t}$.

When we expand this expression, keeping second order terms, we arrive at the null-strut expression for the Doppler shift.

$$\frac{\Delta\nu}{\nu} \sim (V_O - V_S) + \left(\frac{M_\otimes}{R_S} - \frac{M_\otimes}{R_O}\right) + V_O V_S - V_S^2 + \frac{1}{2}\left(V_S^2 - V_O^2\right) \qquad (24)$$

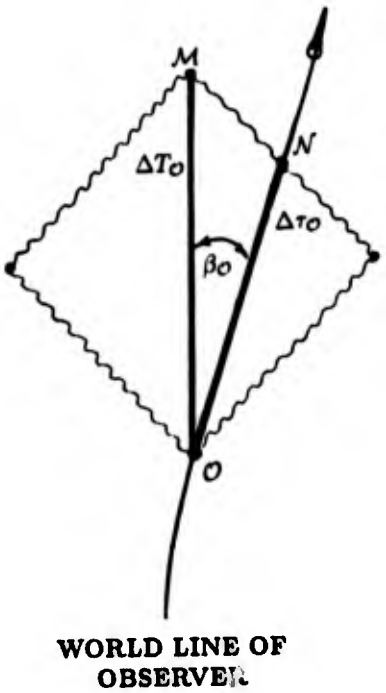

Fig. 8. The section of the null–strut calculus ladder at the observer of Fig. 7 is shown. The 4–velocity of the observer is represented by the Lorentz boost parameterβ_O. It is the angle between the Schwarzschild time directed vertical line and the world line at O. The length $\Delta\tau_O$ is needed to calculate the Doppler shift.

This equation is identical to Eq. 9 if the observer and the satellite are moving along the same radial direction. Furthermore, if one neglects the $\frac{M_\oplus}{R}$ terms and simply identifies ΔT_O and ΔT_S with ΔT, one obtains the special relativistic calculation of Ashby, and Eq. 24 can be recovered by augmenting the special relativistic calculation with the gravitational red–shift term.

We use this example to demonstrate the potential impact that null–strut calculus will have in the arena of accurate time transfer to satellite systems. Null–Strut calculus is based on (1) laser beams, and (2) clocks — the very tools of spacetime geodesy. It provides a geometric, and pictorial avenue to greater understanding of relativistic chronometry, and will no doubt have its place in the future definition of an SCG reference frame.

References

1. P. M. Janiczek, "Global Positioning System," papers in Navigation, The Institute of Navigation,

Washington D.C., 1980.
2. D. Wells ed., "Guide to GPS Positioning," Canadian GPS Associates, University of New Brunswick Graphics Services, 1986.
3. G. Green, *private communication.*
4. W. A. Miller and J. A. Wheeler, *4-Geodesy*, Nuovo Cimento 8 (1985), 418–34.
5. T. Regge, *General Relativity Without Coordinates*, Nuovo Cimento 19 (1961), 558–71.
6. J. A. Wheeler, *Geometrodynamics and the issue of the final state*, in "Relativity Groups and Topology," eds. C. DeWitt and B. DeWitt, Gordon and Breach, New York, 1964, pp. 463–500.
7. W. A. Miller, *Geometric Computation: Null-Strut Geometrodynamics and the Inchworm Algorithm*, in "Dynamical Spacetimes and Numerical Relativity," ed. J. Centrella, Cambridge University Press, 1985, pp. 256–303.
8. I. Ciufolini, R. E. Eanes, R. A. Matzner, J. C. Ries, and B. D. Tapley, *Private communication.*
9. C. O. Alley, *Laser ranging to retro reflectors on the moon as a test of theories of gravity*, in "Quantum Optics, Experimental Gravity, and Measurement Theory," eds. P. Meystre and M. O. Scully, Plenum Publishing Co., 1983, pp. 429–495.
10. I. Ciufolini, *Measurement of the Lense–Thirring drag on high–altitude, laser–ranged artificial satellites*, Phys. Rev. Lett. 56 (1986), 278–281.
11. N. Ashby, *Private communication, presented at the January 1988 PAWG meeting.*
12. R. Matzner, *Private communication/letter.*
13. Synge J. L., "Relativity: The General Theory," North-Holland Publishing Co..
14. C. W. Misner, K. S. Thorne, J. A. Wheeler, "Gravitation," W. H. Freeman and Co., San Francisco, 1971.
15. "Performance Analysis Working Group (PAWG)," chaired by B. Winn, Aerospace Corporation, El Segundo, California, January, 1988.
16. G. Ellis, "Lectures in Relativistic Cosmology," The University of Texas, Austin, Texas, 1984.
17. R. Friedberg and T. D. Lee, *Derivation of Regge's action from Einstein's theory of general relativity*, Nucl. Phys. B242 (1984), 145–166.

Keywords. Global Positioning System, Doppler Effect, Precise Time and Time Interval, and Null-Strut Calculus

†Mathematics Department, North Carolina State University, Raleigh, North Carolina 27695–8205
‡Center for Relativity, Department of Physics, The University of Texas, Austin, Texas 78712
*Advanced Concepts Branch, Air Force Weapons Laboratory, Kirtland AFB, NM 87117–6008

PAPERS APPEARING ON THE AGENDA

THAT COULD NOT BE PRESENTED (10-11 FEBRUARY 1988)

BUT HAVE SINCE BEEN APPROVED

FOR OPEN RELEASE

A PRELIMINARY COMPARISON AT FLIGHT TEST ALTITUDE OF AIRBORNE GGSS SECOND ORDER GRAVITY GRADIENTS WITH SIMILAR DATA COMPUTED AT THE SAME PROFILE POINTS USING SURFACE INTEGRAL FORMULAS AND SURFACE MEAN GRAVITY ANOMALIES

By

John J. Graham/DMASC/WG

And

Joseph L. Toohey/DMAAC/DSG

Presented To

Sixteenth Annual Gravity Gradiometry Conference
United States Air Force Academy
Colorado Springs, Colorado
10-11 February 1988

Defense Mapping Agency Aerospace Center and
Systems Center/West Resources/Career Group
3200 South Second Street
St. Louis, Missouri 63118-3399

ABSTRACT

Flight tests of the Airborne Gravity Gradiometer Survey System (GGSS) developed by Bell Aerospace TEXTRON under an Air Force Geophysics Laboratory (AFGL)/Defense Mapping Agency (DMA) Contract were conducted in Oklahoma during the Spring of 1987. Approximately 120 airborne profiles of second order gravity gradients, of varying quality, were obtained during the flight test period. Eleven profiles of the Airborne GGSS data (6 north/south, 5 east/west) were selected for evaluation. These second order gravity gradients, after processing (filtering, etc.), were compared with another set of second order gravity gradients computed at the same locations along the 11 profiles using surface integral formulas and surface mean gravity anomalies. The graphical and statistical data resulting from this initial analysis provide some insight into the performance of the Airborne GGSS at this point in its development.

1. INTRODUCTION

Field tests of the Airborne Gravity Gradiometer Survey System (GGSS), developed by Bell Aerospace TEXTRON for the Defense Mapping Agency (DMA)*, were conducted during the Spring of 1987 over Oklahoma (Figure 1). Approximately 120 airborne profiles of second order gravity gradients, of varying quality, were obtained during the flight test period. Eleven profiles of the Airborne GGSS data (6 north/south, 5 east/west) were selected for evaluation. The location of these profiles in the GGSS Flight Test Area is indicated in Figures 2 and 3.

2. DISCUSSION

After editing and despiking the raw data, a low-pass filter [1, p 113] was used to eliminate high frequency noise of wavelengths less than 11 kilometers. Since the Airborne GGSS data was collected at one second intervals of time, the 131-point filter eliminated 65 data points at both ends of each profile. After filtering, the inline and cross channel gradients were rotated into a north-east-down (NED) Coordinate System, and their linear trends removed. Any data gap resulting from the despiking process was closed in by using an average of the gradients at the gap end points. Completion of the data processing activities provided the 11-track set of airborne second order gradients to be analyzed from the flight test.

To evaluate this 11-track set of GGSS second order gravity gradients, a similar set of elevated data was calculated at every ninth GGSS profile point in the set using surface integral formulas and surface mean gravity anomalies. The surface integral formulas for calculating this "truth" set of second order gravity gradients were obtained by differentiating Pizetti's Equation [2, p 233]. The surface data used in the formulas consisted of a worldwide set of surface mean gravity anomalies referenced to the World Geodetic System 1984 (WGS 84) Ellipsoid Gravity Formula. Mean gravity anomalies of 1'x1' size were used near the nadir of the computation points. Moving radially away from the nadir point, mean gravity anomalies of progressively larger size (5'x5', 15'x15', $1^{\circ}x1^{\circ}$, and $5^{\circ}x5^{\circ}$) were used. This data formed the "truth" set of second order gravity gradients for comparison against the GGSS-derived gradients.

The GGSS-derived second order gravity gradients are graphically compared in Figures 4-14 with similar values from the "truth" data set. In the figure titles, the term "direct integration" refers to the "truth" gradients. The figures depict all six of the second order gradients found at their appropriate intervals along each of the selected profiles. In general, for the east/west tracks, the north-east and east-east gradients appear to be the best defined of the six GGSS-derived second order gravity gradients. The east-down gradient also appears to be reasonably well defined, with the exception of Track 22.

---

* The Air Force Geophysics Laboratory (AFGL) performed technical and administrative monitorship of the AFGL/DMA Contract with Bell Aerospace TEXTRON.

For the north/south tracks, the north-down and east-east gradients are by far the best defined of the six GGSS-derived second order gravity gradients. The north-north gradient is relatively well defined for Tracks 42, 43, and 45. In general, the root-mean-square (RMS) differences indicate a poorer match for the other second order gravity gradients along the north/south tracks.

Tables 1-6 contain statistical results from a comparison of the GGSS-derived gradients against the aloft "truth" (direct integration) gradients. Differences were formed using the sense, "truth" gradients minus GGSS-derived gradients. Each table lists pertinent statistical data (mean, standard deviation, and RMS) for the differences occurring along each track for a particular gradient.

Due to the lack of 1'x1' mean gravity anomaly data when the "truth" calculations were made, only a portion of the GGSS-derived east/west gradients could be compared with the "truth" gradients. If attempting gravity disturbance component estimation along the east/west tracks by the line integral method [3, p 6], the principal gradients are the north-east, east-east, and east-down gradients as the aircraft flight path deviates little from its intended horizontal direction with negligible vertical motion. With respect to east/west tracks, the RMS differences for the north-east gradient are best for Track 19 and worst for Track 25. The RMS differences for the east-east gradient appear best for Track 22 and worst for Track 19. For the east-down gradient, the smallest and largest RMS differences occurred for Tracks 19 and 22, respectively. Both the north-north and down-down gradients have RMS differences exceeeding 10 Eotvos for Tracks 24-27.

The most important gradient used in the line integral method for estimating the down gravity disturbance components along north/south tracks is the north-down gradient. In the case of horizontal gravity disturbance components, either the north-north or north-east gradient is primary. The RMS gradient differences are the least or second smallest for Track 39 in the set of north/south tracks. The RMS differences indicate that gradient matching was poorest for Tracks 41 and 42 in the north/south set.

3. CONCLUSION

The RMS second order gravity gradient differences for the five east/west tracks ranged from 4.2 to 17.4 Eotvos. The RMS differences ranged from 4.0 to 11.5 Eotvos for the six north/south tracks. In general, the north/south tracks tend to yield better quality north-north, north-down, east-down, and down-down gradients while the east/west tracks gave better results for the remaining two gradients. Several improvements in data processing would have been investigated further, if not prevented by time limitations. These include imposing a zero summation of inline gradients, a better spike gap closure method, determining the onset of the noise floor for the GGSS gradients, a sharper low-pass filter design, a better understanding and compensation for unmodeled error sources, and definition of the spectral band for the GGSS gradients. The recovery of gravity disturbance vectors along these same 11 tracks from the Airborne GGSS second order gradients is discussed in a separate conference paper [4].

REFERENCES

1. Hamming, R. W.; Digital Filters, Second Edition; Prentice-Hall; Englewood Cliffs, New Jersey; 1983.

2. Heiskanen, W. A. and H. Moritz; Physical Geodesy; W. H. Freeman and Company; San Francisco, California; 1967.

3. Moritz, H.; Kinematical Geodesy; Department of Geodetic Science and Surveying Report No. 92; The Ohio State University; Columbus, Ohio; November 1967.

4. Toohey, J. L. and R. W. Valska; A Preliminary Comparison at Flight Test Altitude of Gravity Disturbance Components Derived From Airborne GGSS Second Order Gravity Gradients With Similar Data Computed at the Same Profile Points Using Surface Integral Formulas and Surface Mean Gravity Anomalies; Defense Mapping Agency Aerospace Center and Systems Center/West Group; St. Louis, Missouri; February 1988. [Paper Presented at Sixteenth Annual Gravity Gradiometry Conference; United States Air Force Academy; Colorado Springs, Colorado; 10-11 February 1988.]

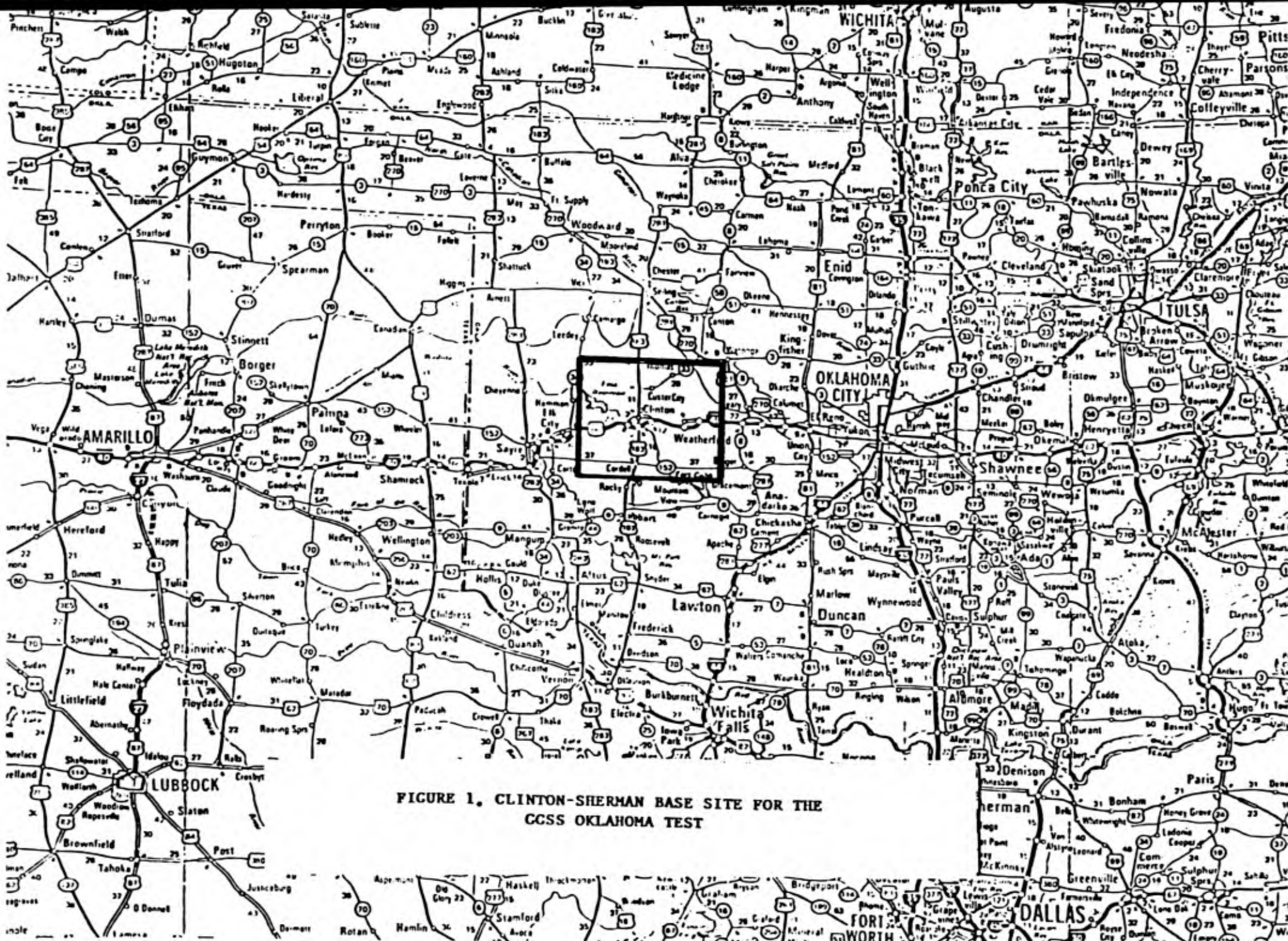

FIGURE 1. CLINTON-SHERMAN BASE SITE FOR THE CCSS OKLAHOMA TEST

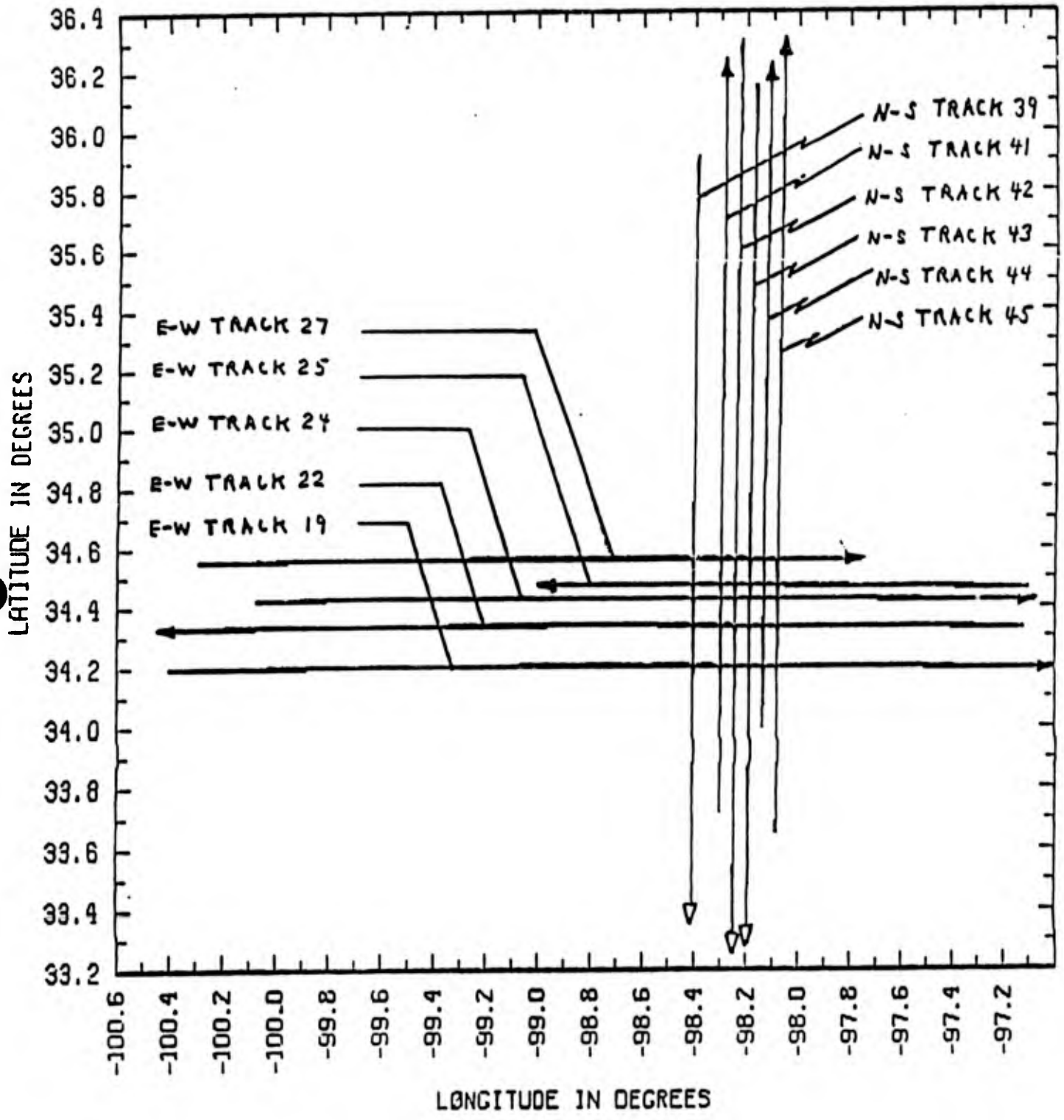

FIGURE 2. THE ELEVEN SELECTED GGSS TRACKS AFTER EDITING

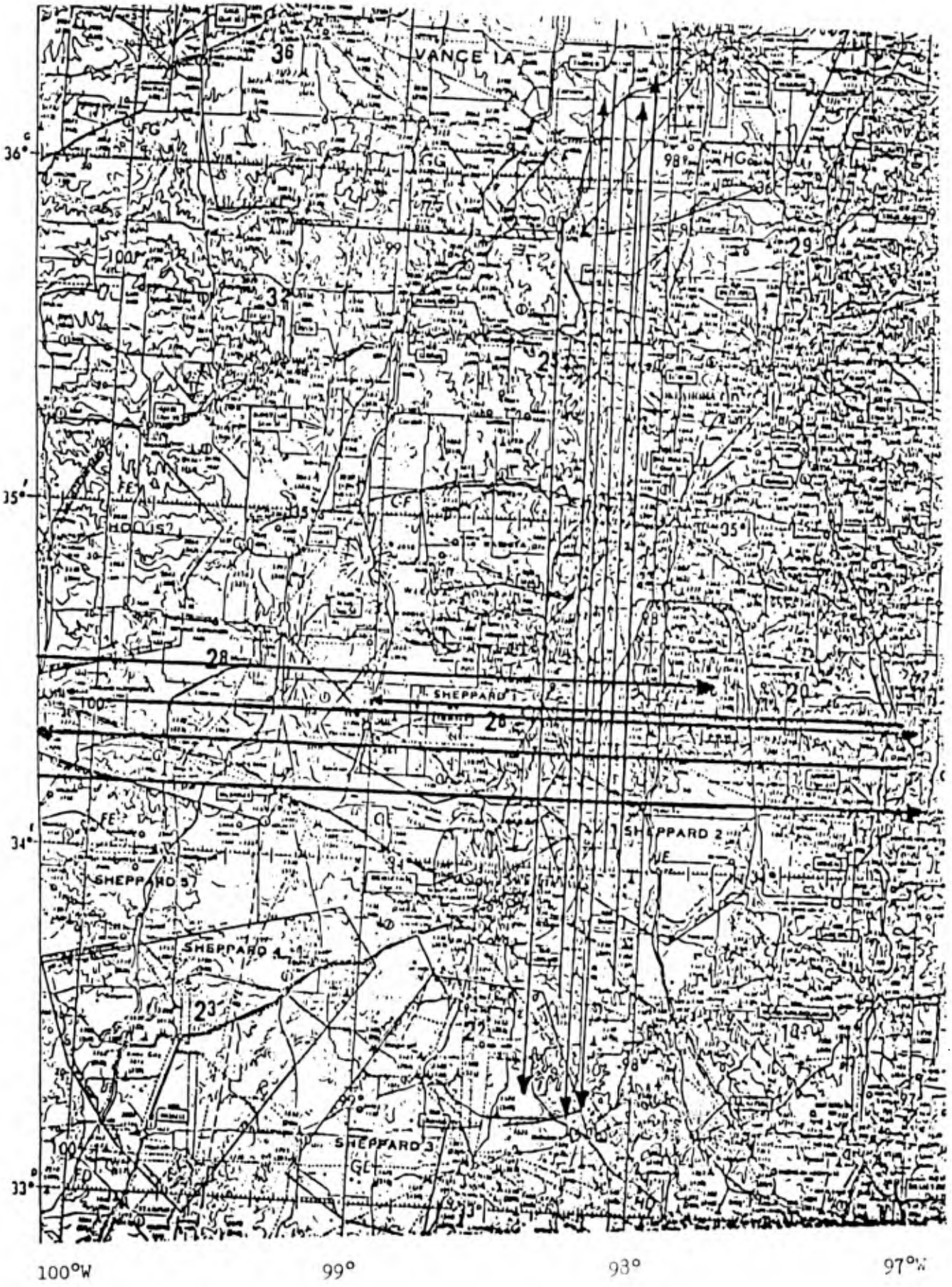

FIGURE 3. THE ELEVEN EDITED GGSS TRACKS ON AN ONC CHART

FIGUR

GGSS GRADIENTS VERSUS DIRECT INTEGRATION GRADIENTS

(RMS OF DIFFERENCES)

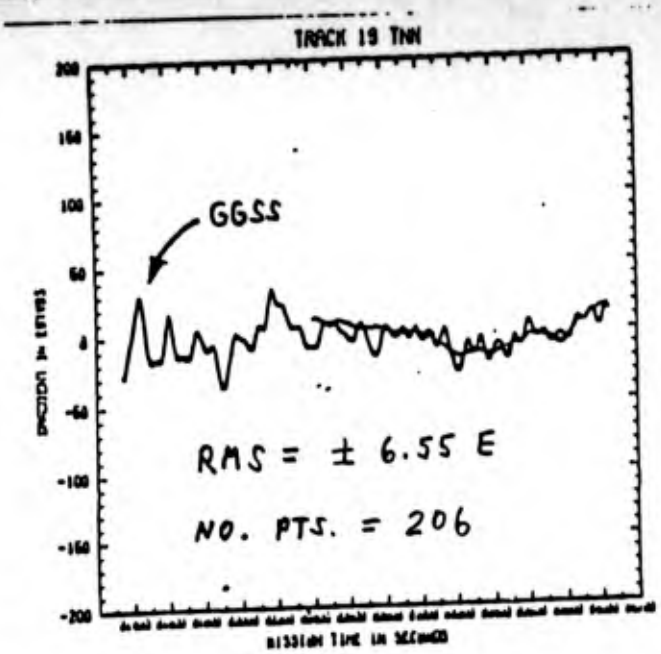

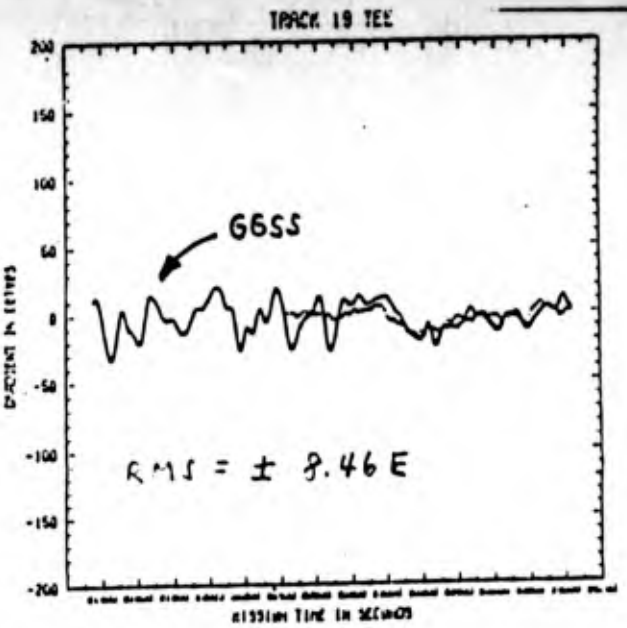

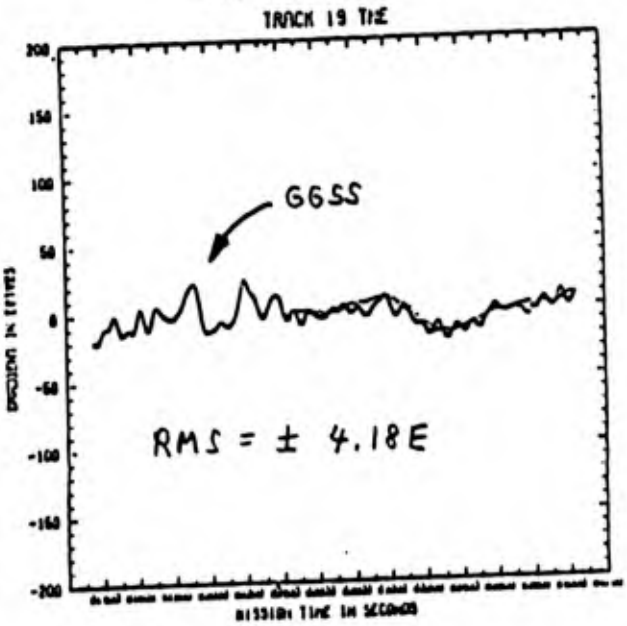

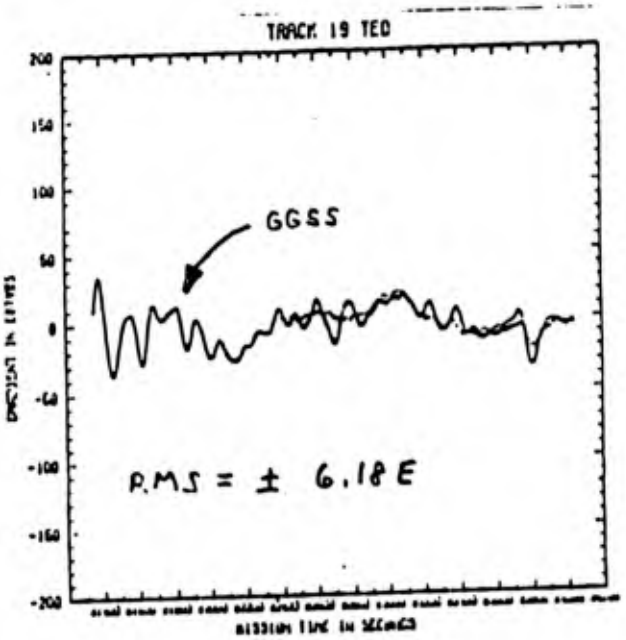

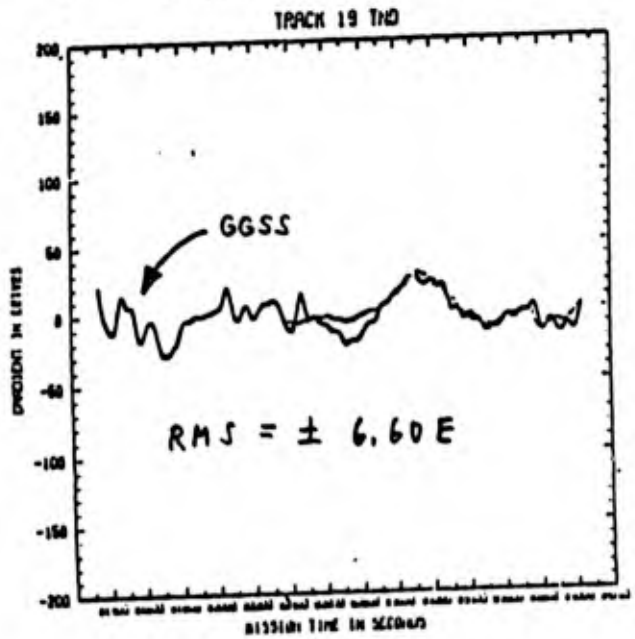

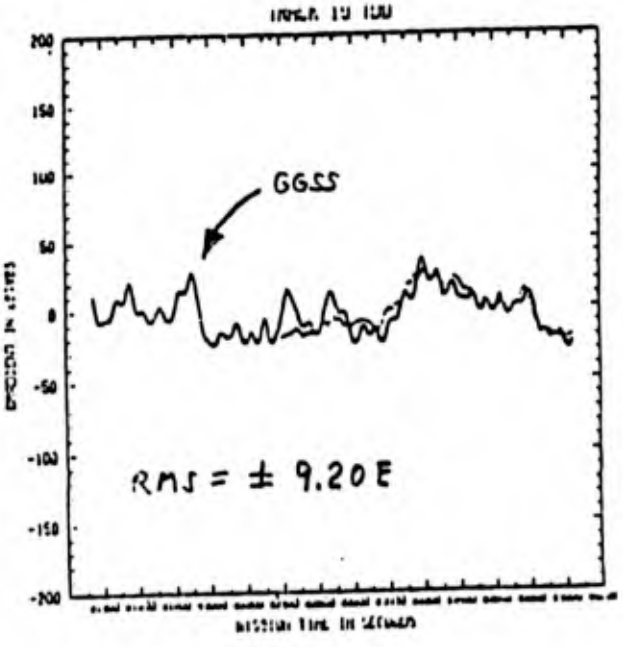

GGSS GRADIENTS VERSUS DIRECT INTEGRATION GRADIENTS

(RMS OF DIFFERENCES)

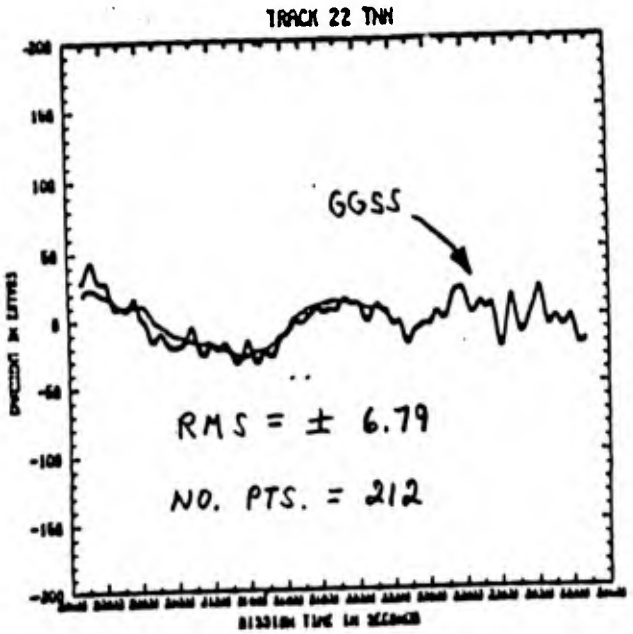

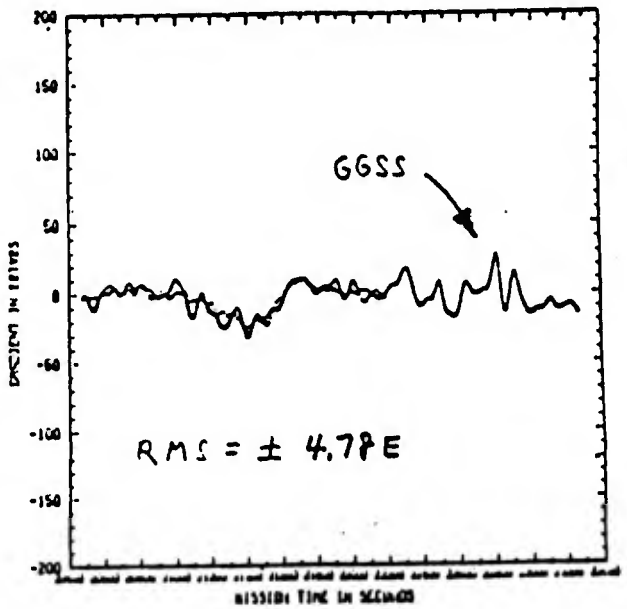

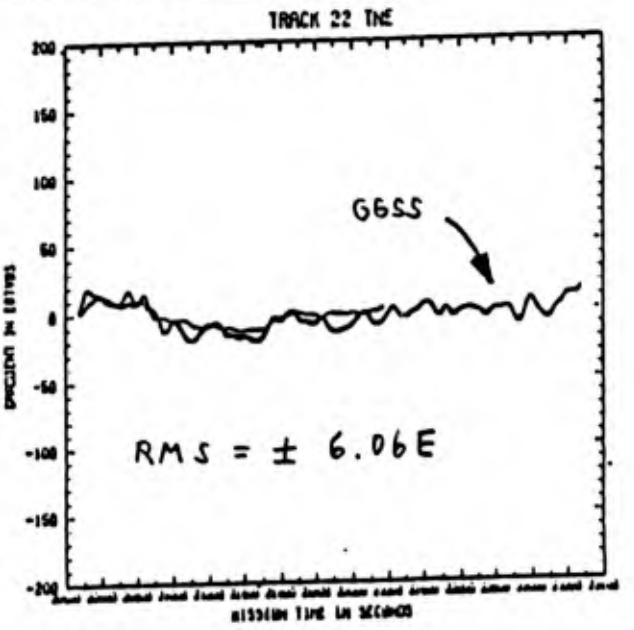

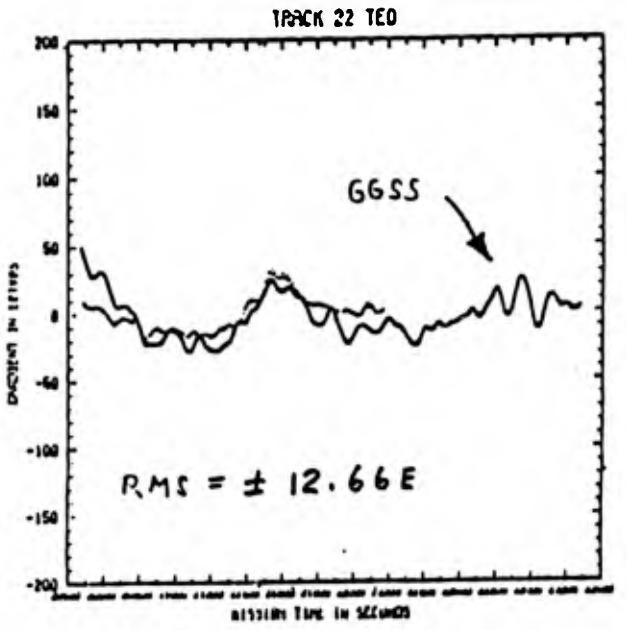

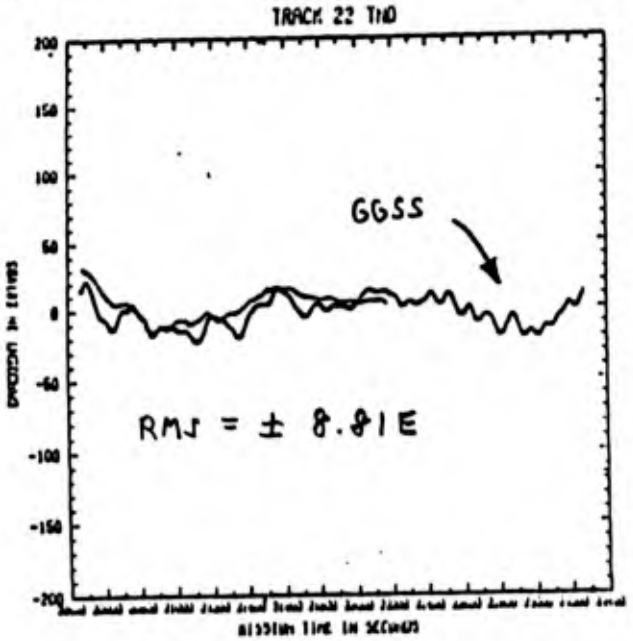

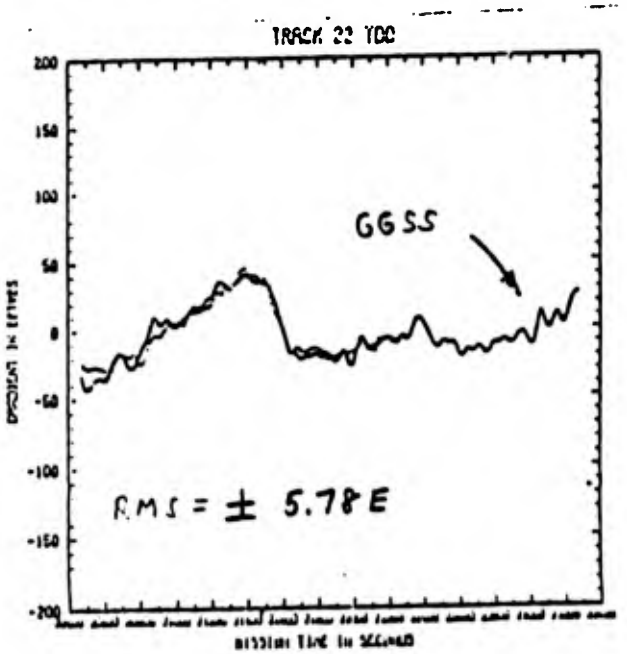

FIGURE

GGSS GRADIENTS VERSUS DIRECT INTEGRATION GRADIENTS
(RMS OF DIFFERENCES)

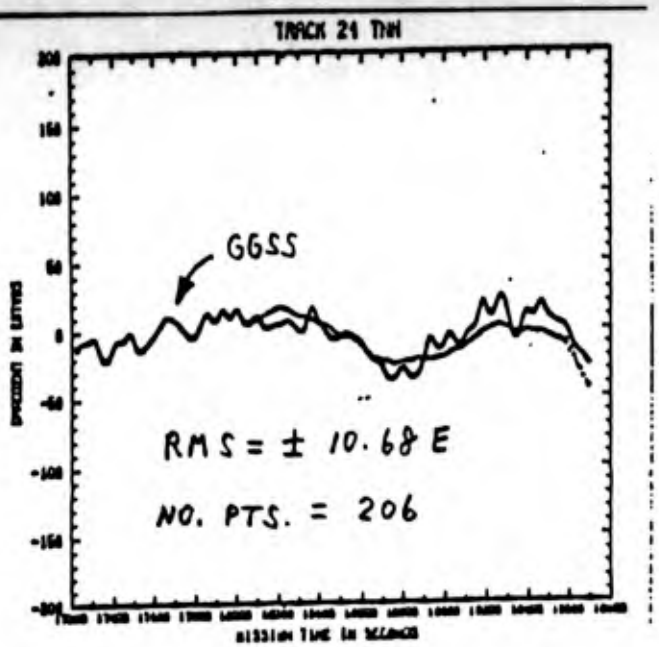

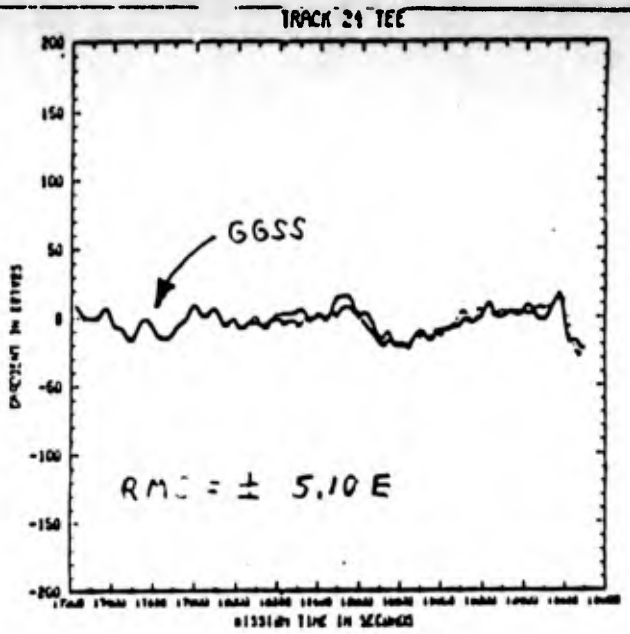

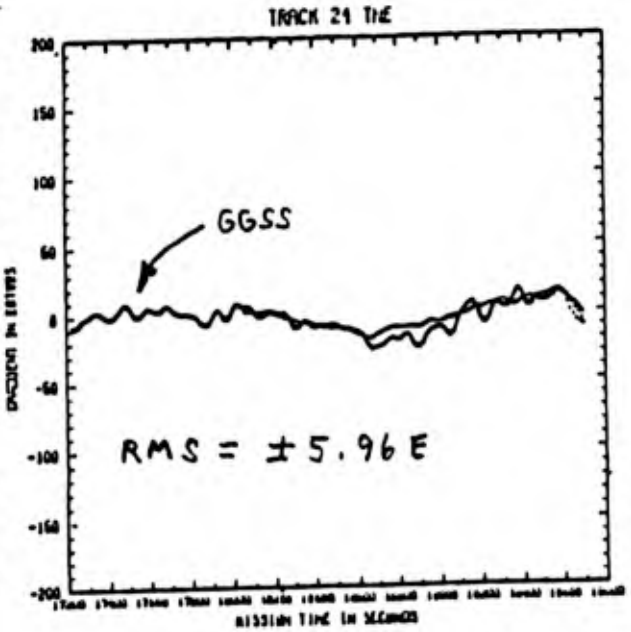

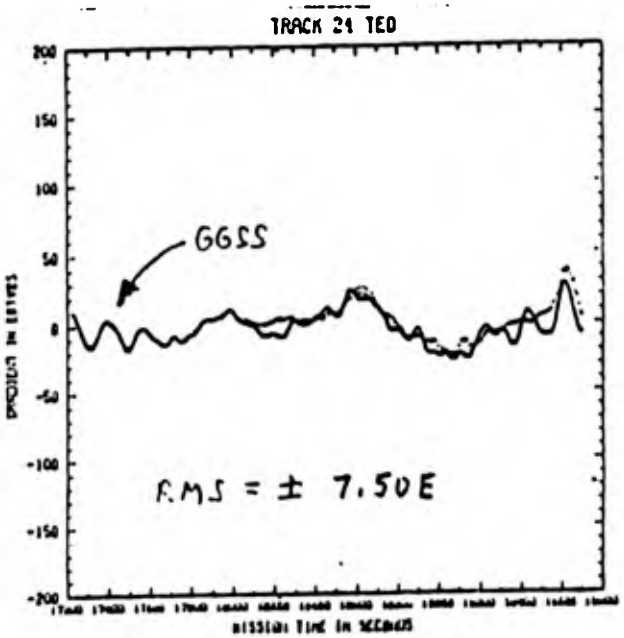

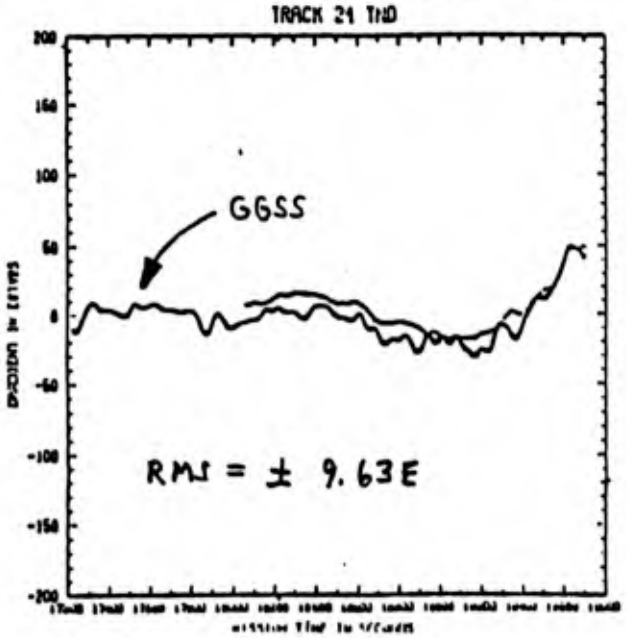

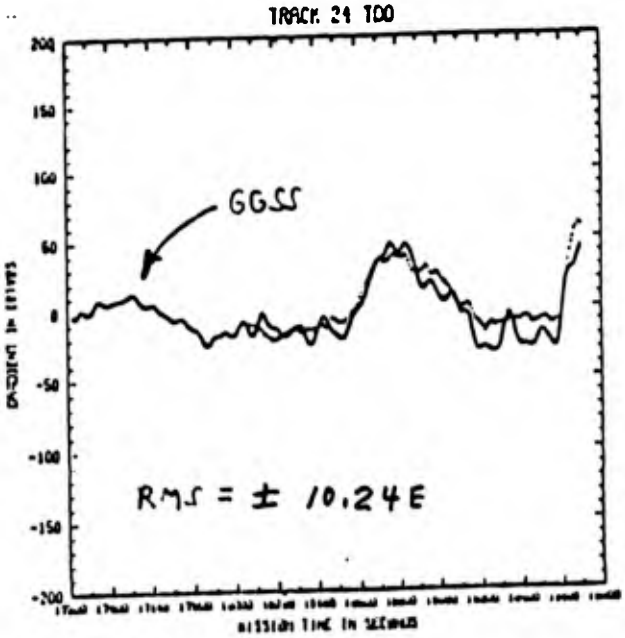

FIGURE 7.

GGSS GRADIENTS VERSUS DIRECT INTEGRATION GRADIENTS

(RMS OF DIFFERENCES)

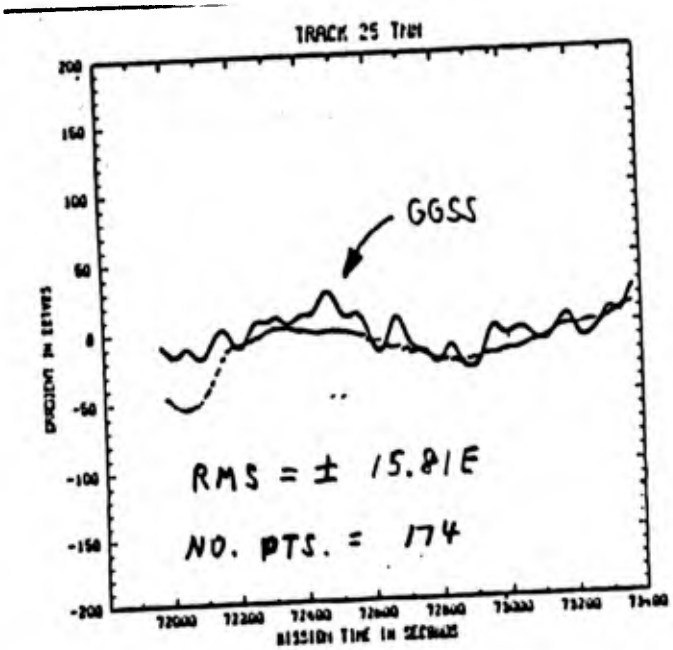

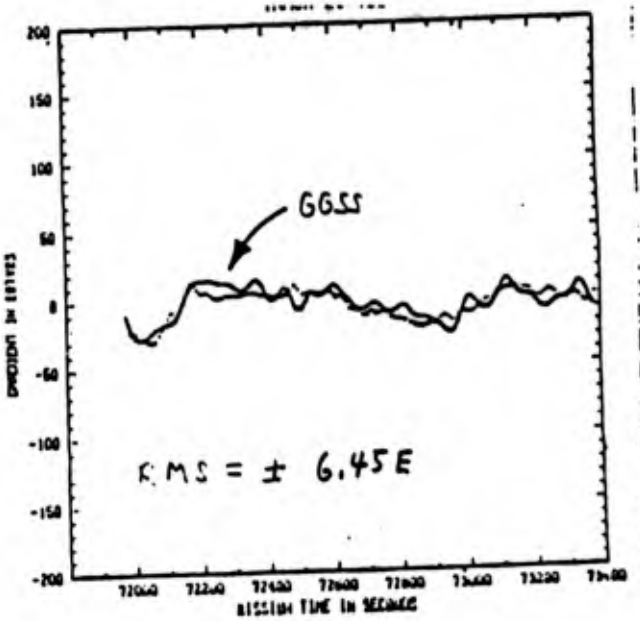

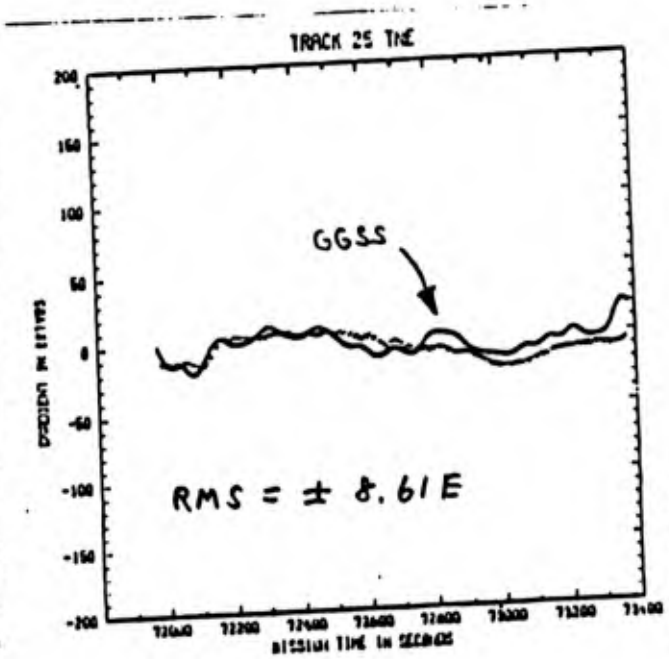

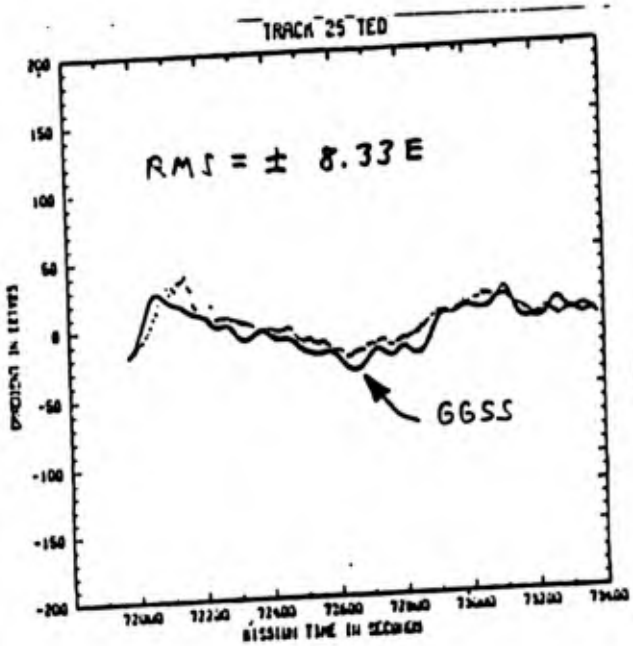

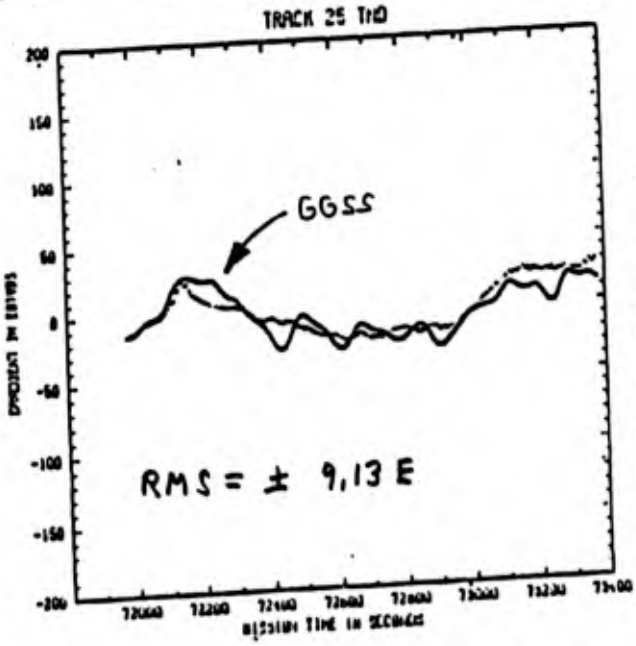

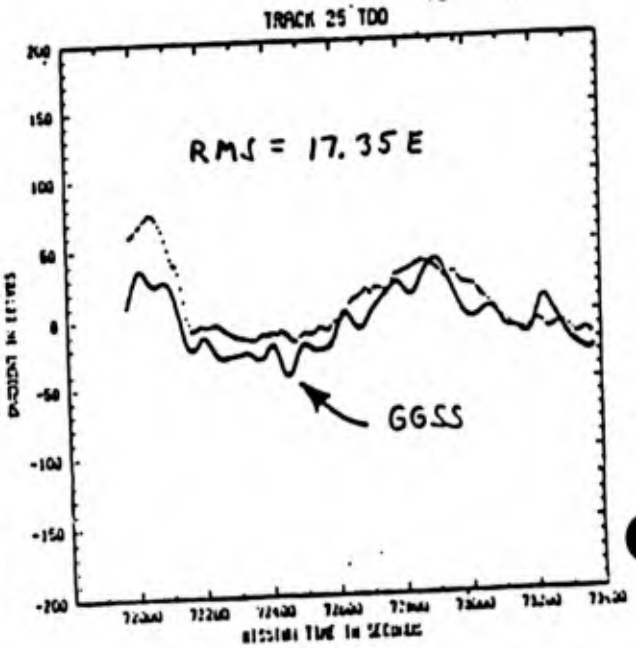

FIG. 8.

GGSS GRADIENTS VERSUS DIRECT INTEGRATION GRADIENTS
(RMS OF DIFFERENCES)

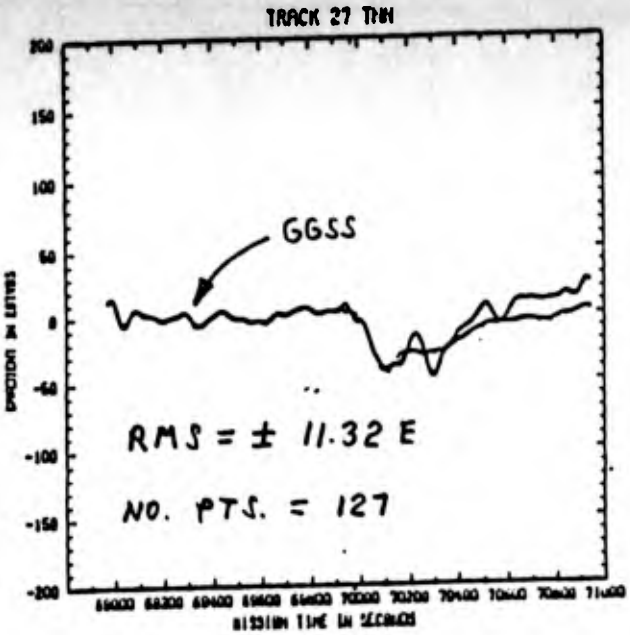

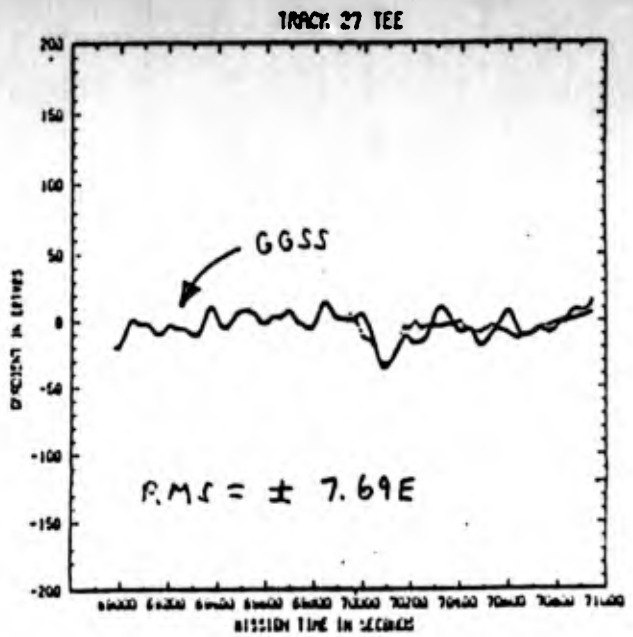

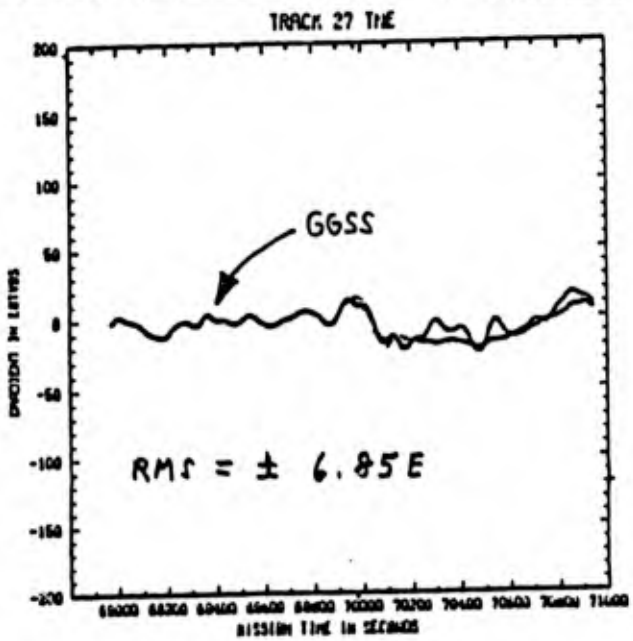

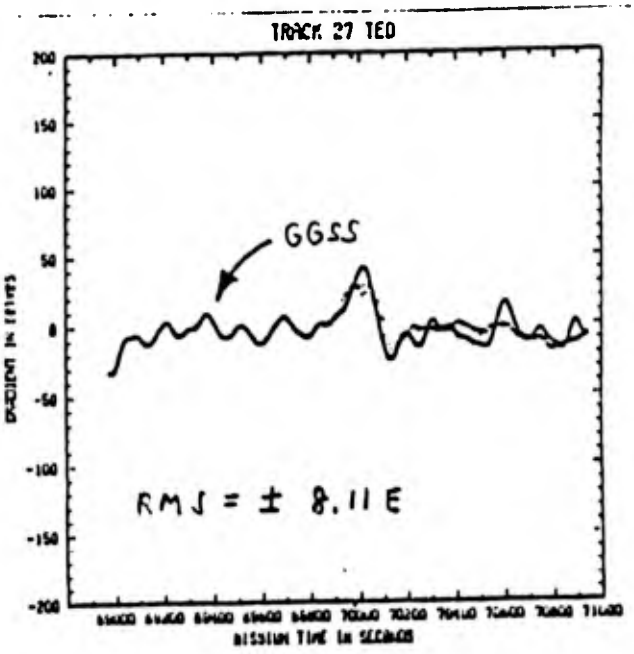

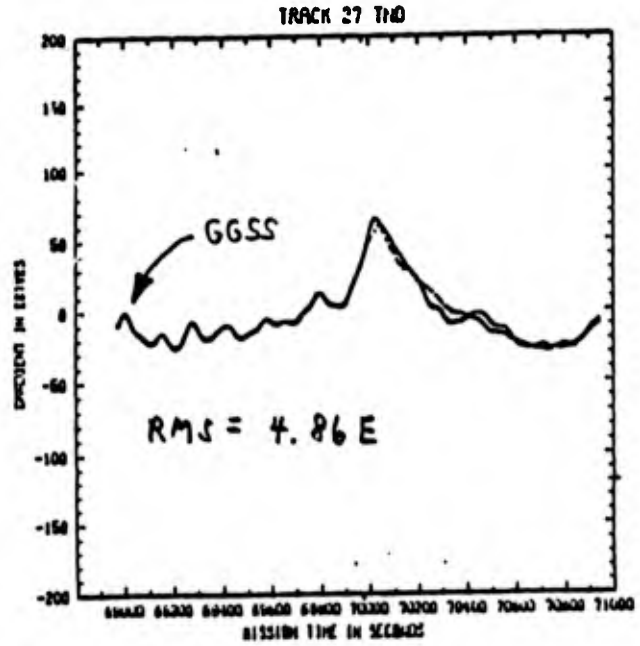

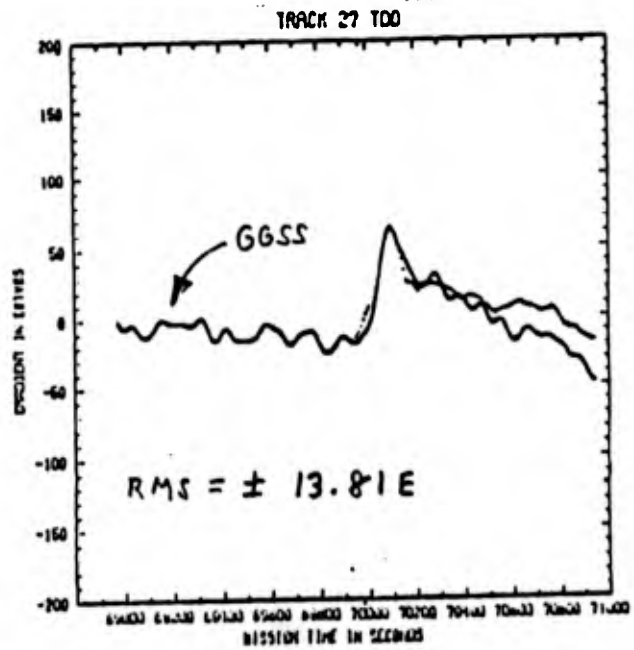

GGSS GRADIENTS VERSUS DIRECT INTEGRATION GRADIENTS
(RMS OF DIFFERENCES)

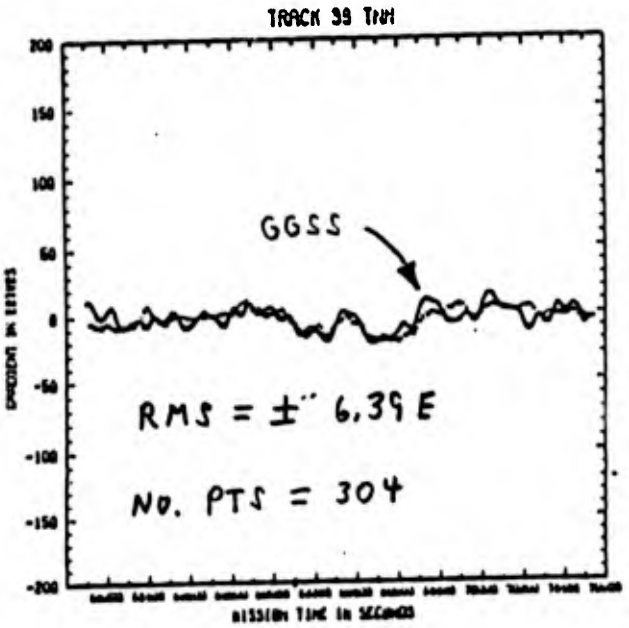

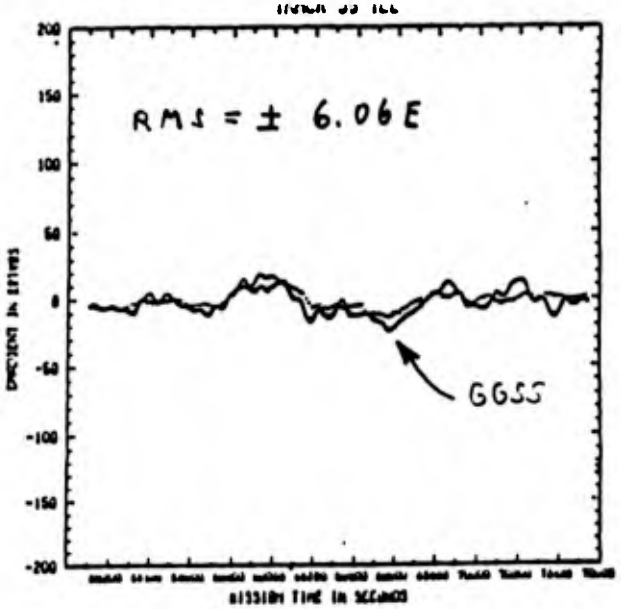

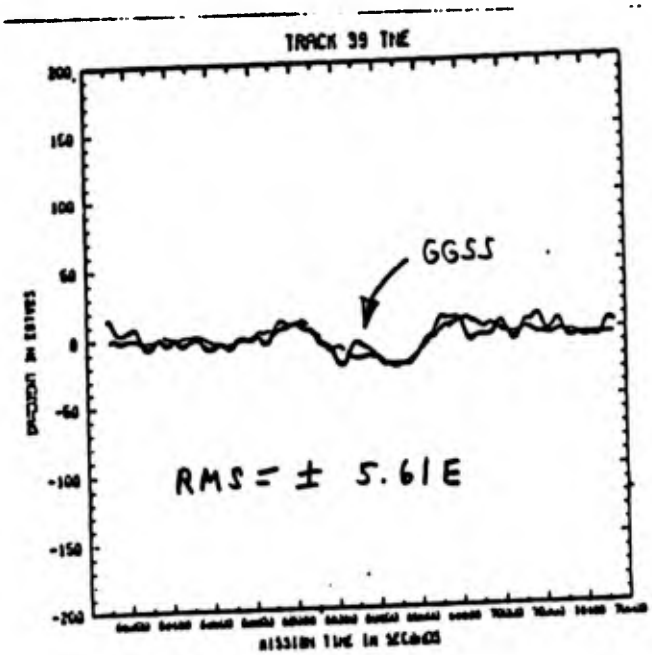

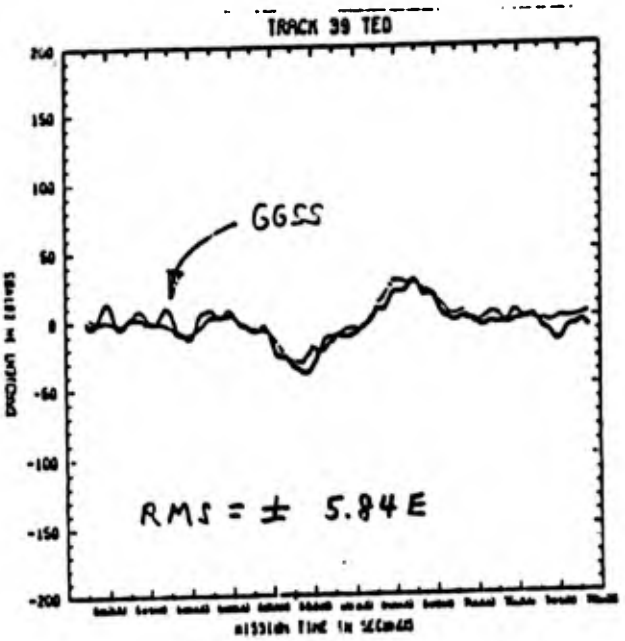

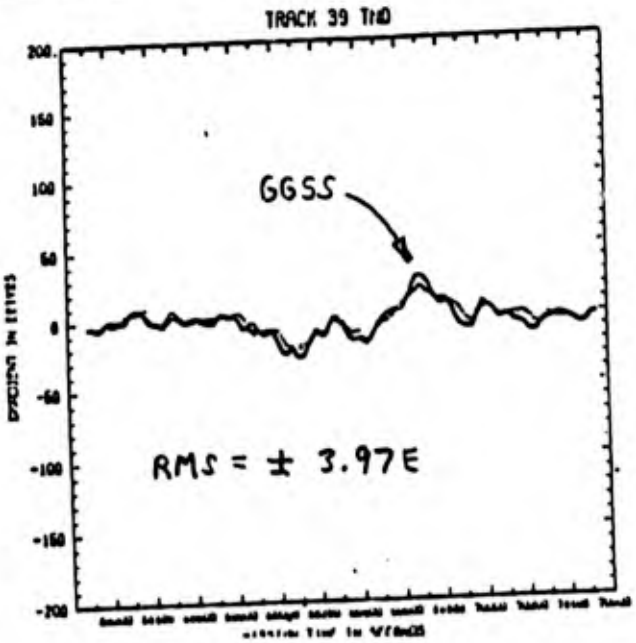

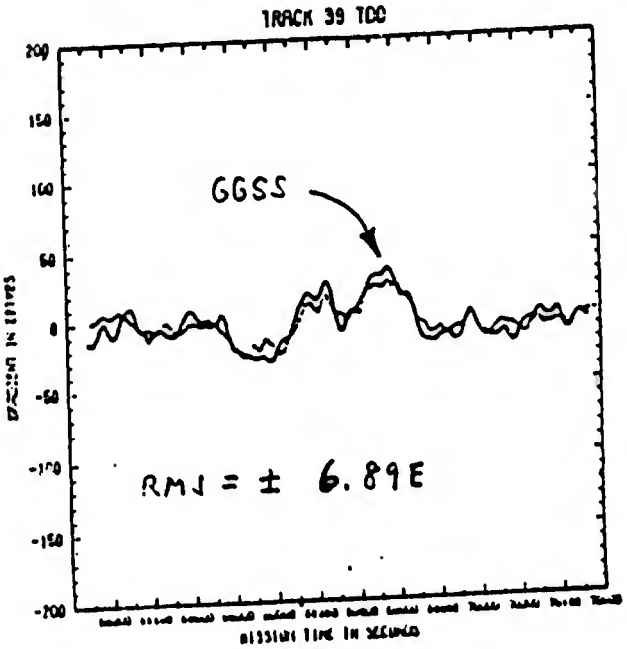

FIGURE

GGSS GRADIENTS VERSUS DIRECT INTEGRATION GRADIENTS

(RMS OF DIFFERENCES)

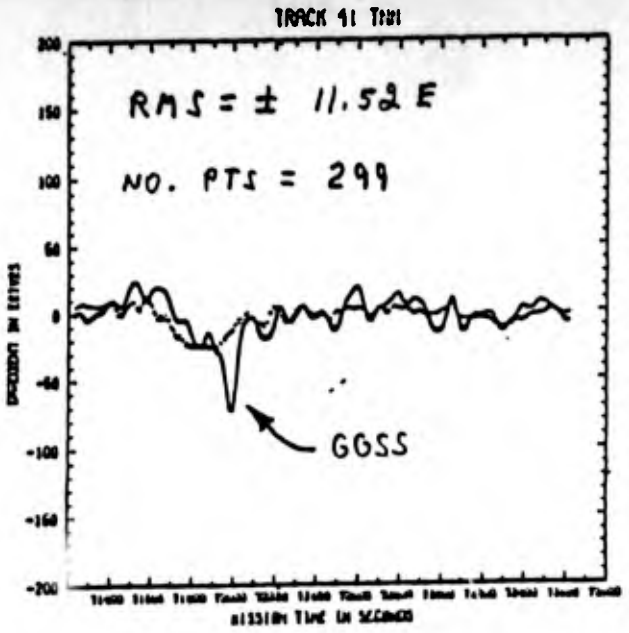

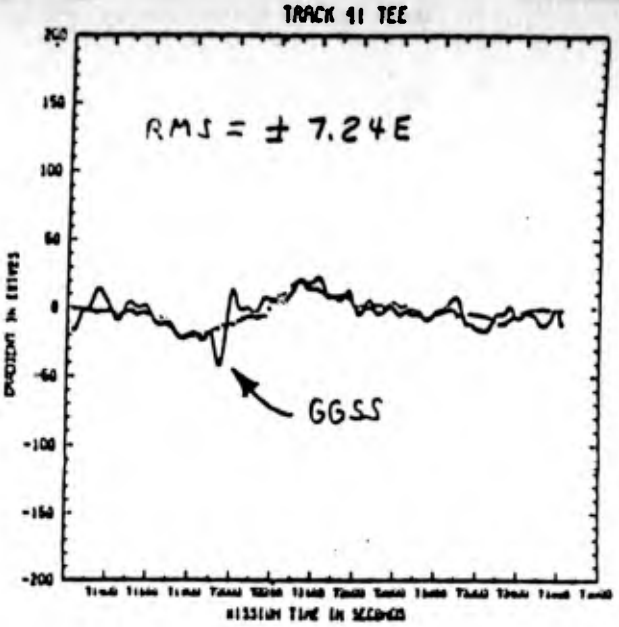

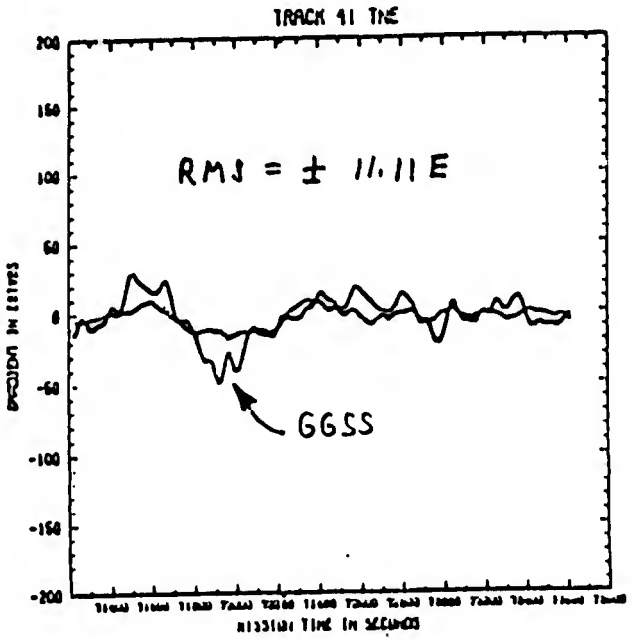

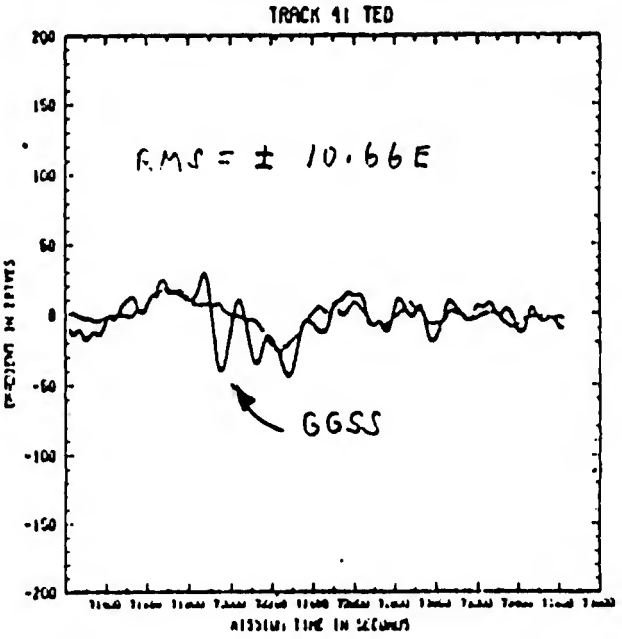

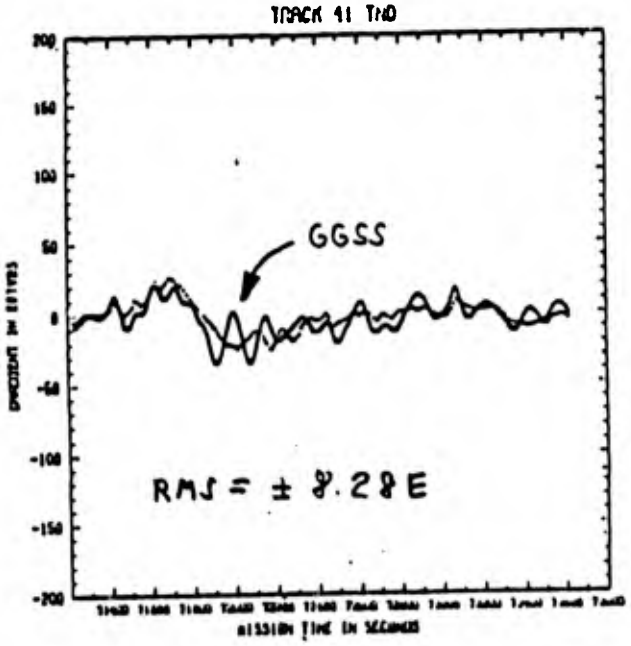

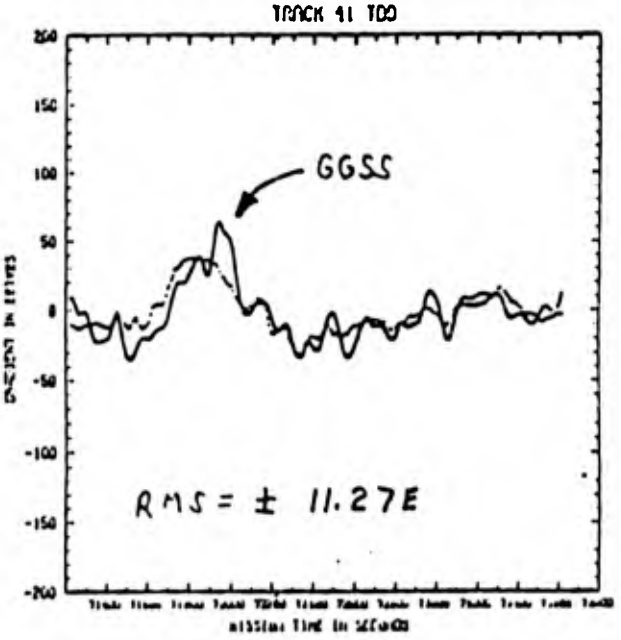

FIGURE 11.

GGSS GRADIENTS VERSUS DIRECT INTEGRATION GRADIENTS

(RMS OF DIFFERENCES)

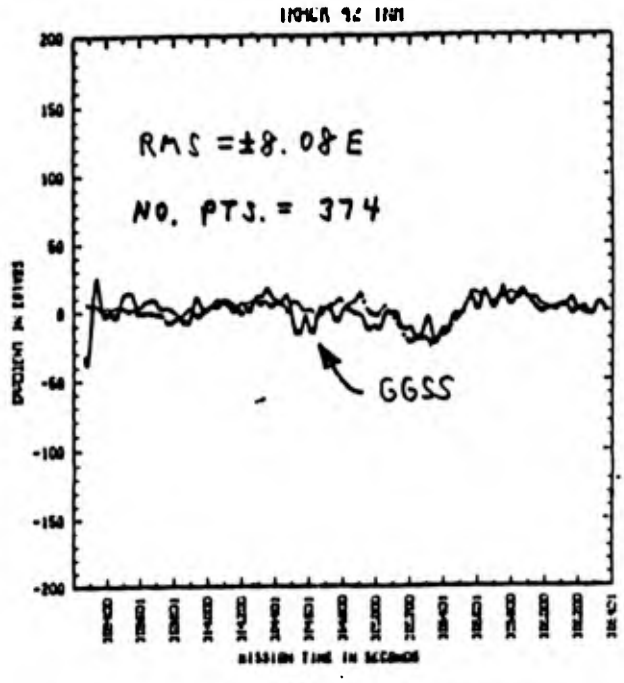

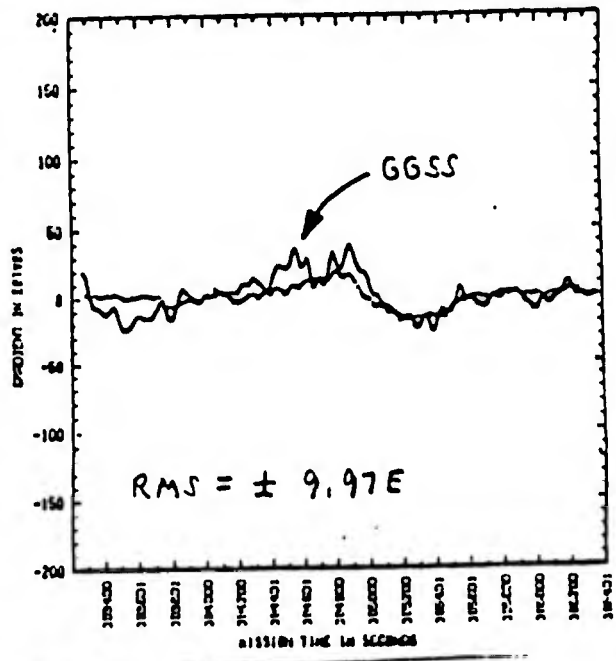

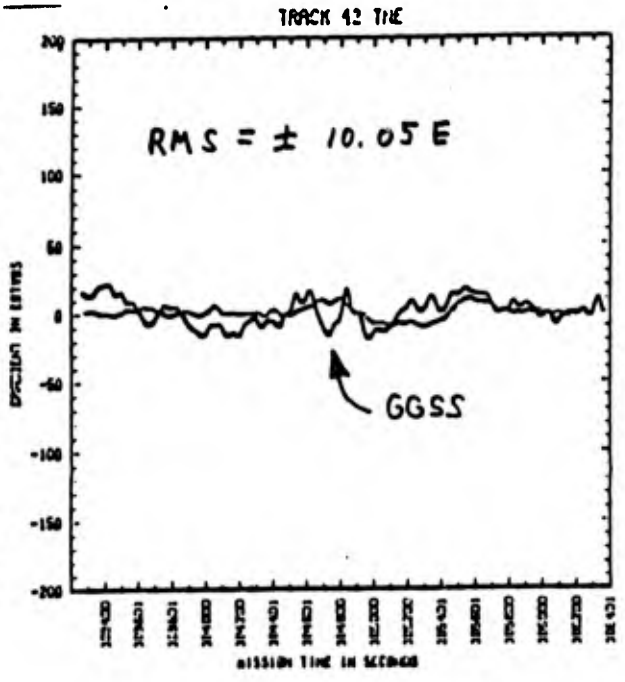

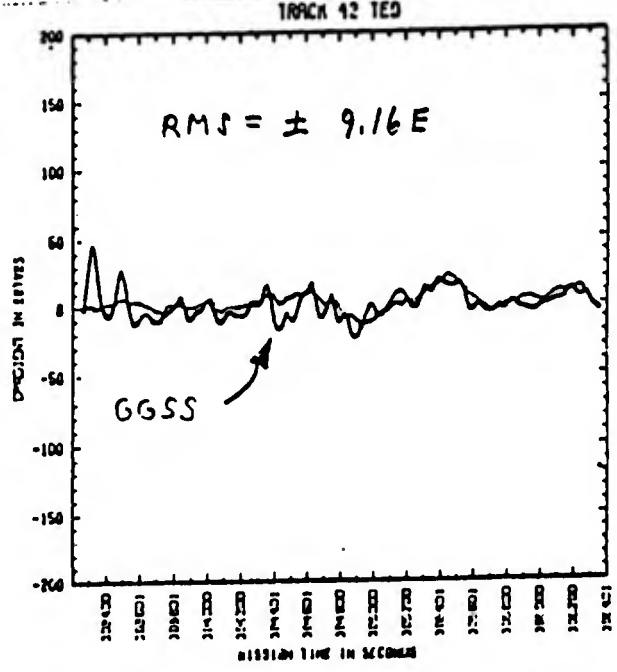

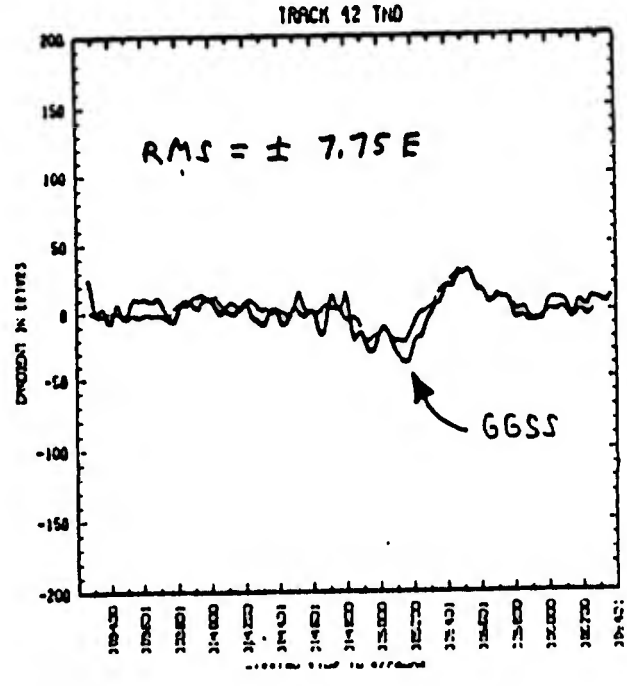

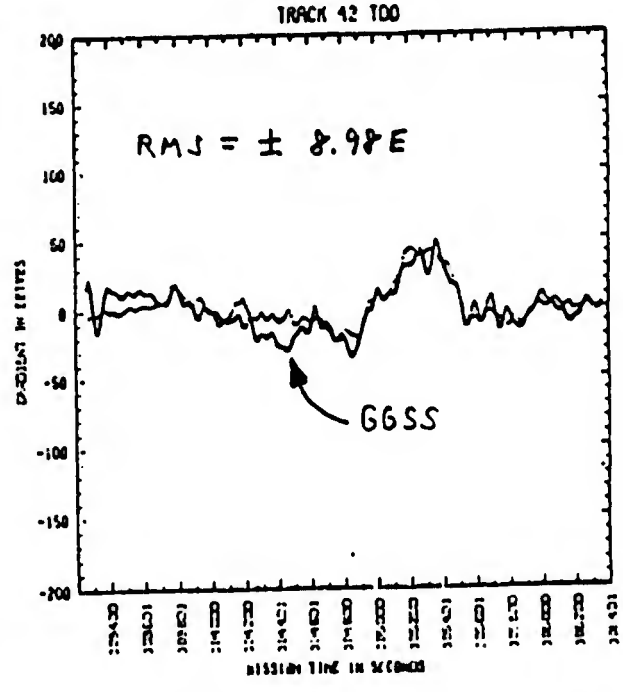

GGSS GRADIENTS VERSUS DIRECT INTEGRATION GRADIENTS
(RMS OF DIFFERENCES)

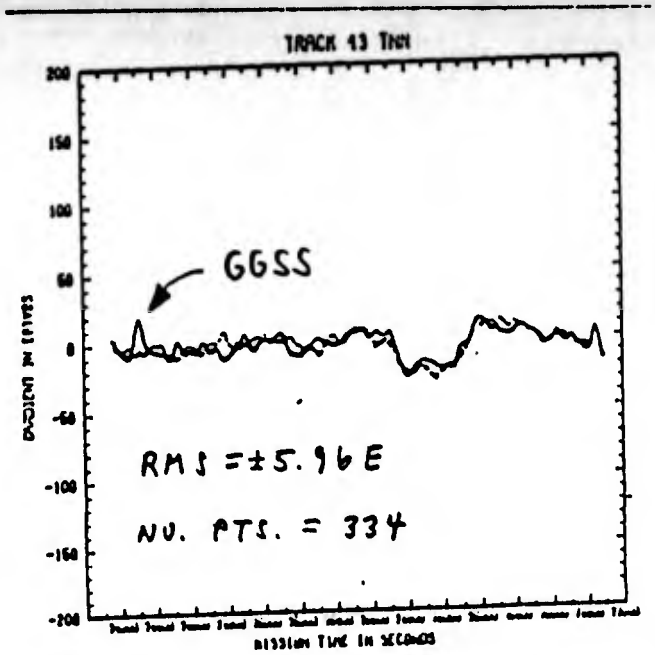

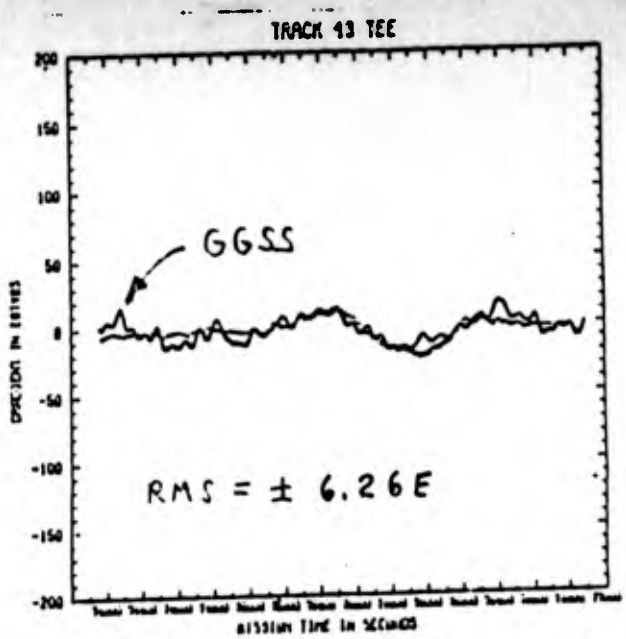

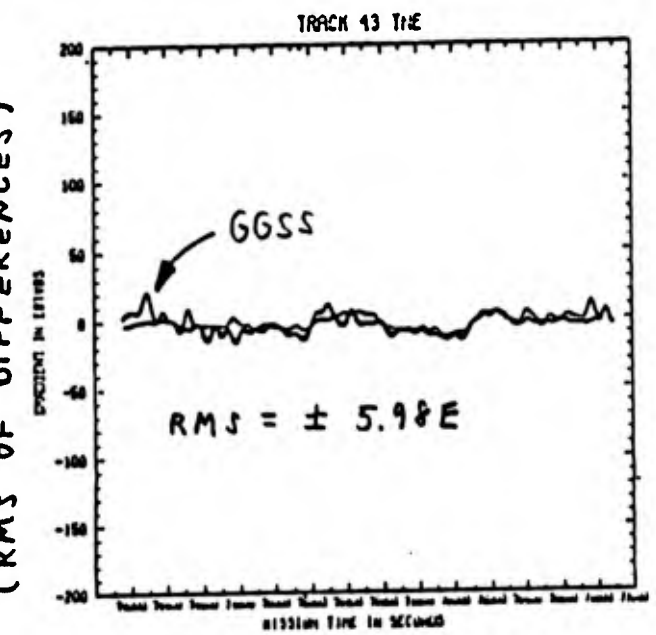

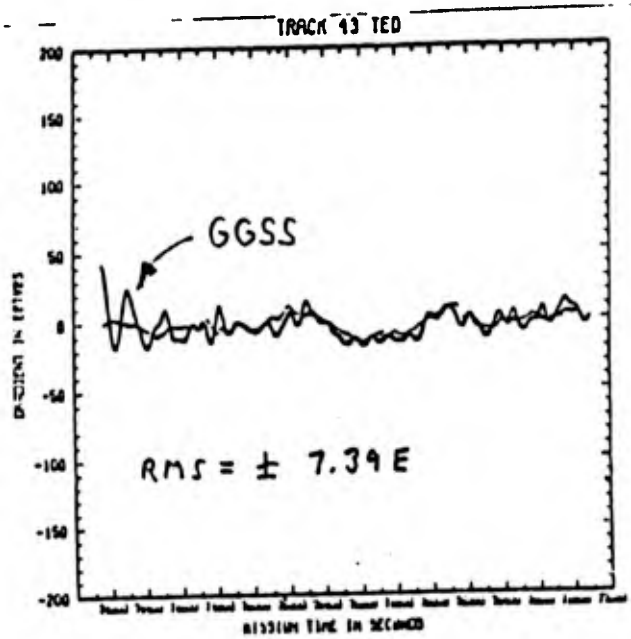

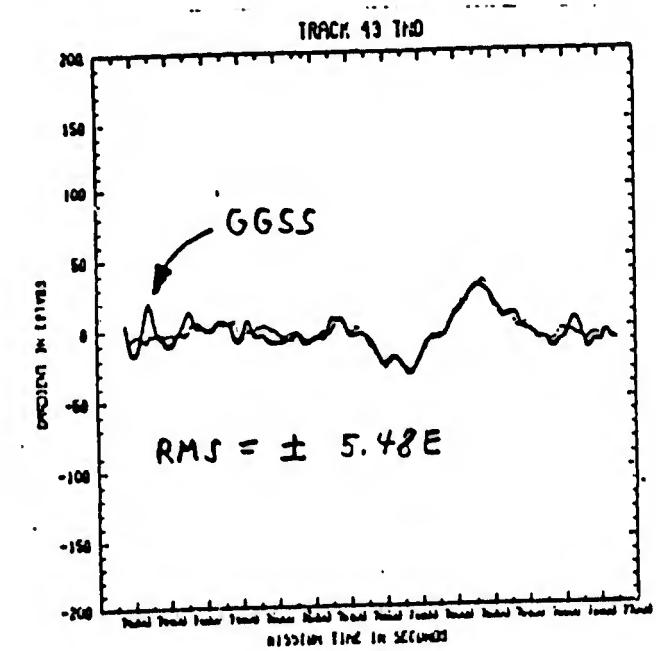

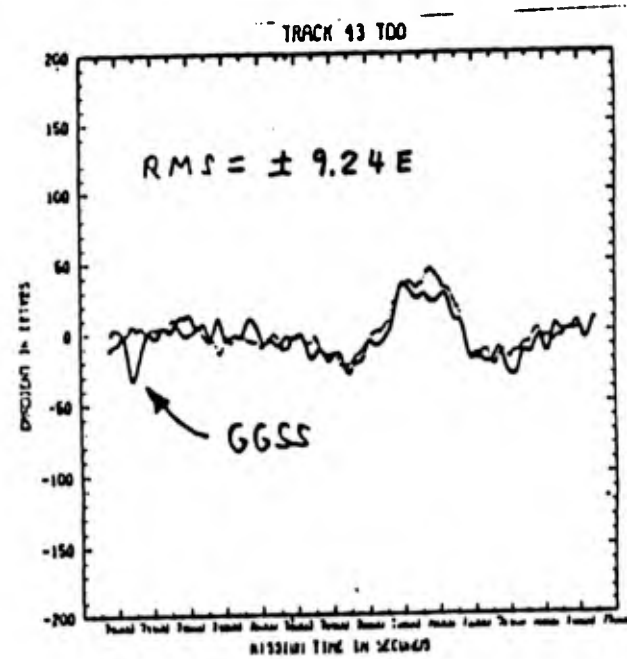

FIGURE 12.

GGSS GRADIENTS VERSUS DIRECT INTEGRATION GRADIENTS

(RMS OF DIFFERENCES)

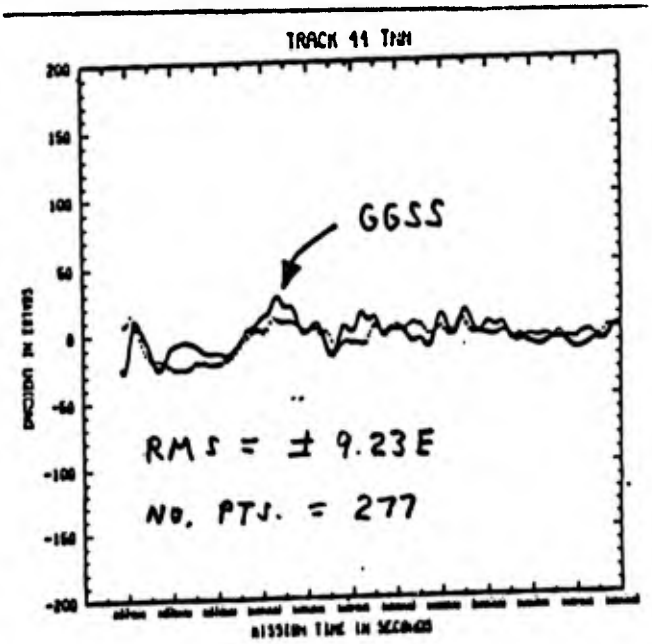

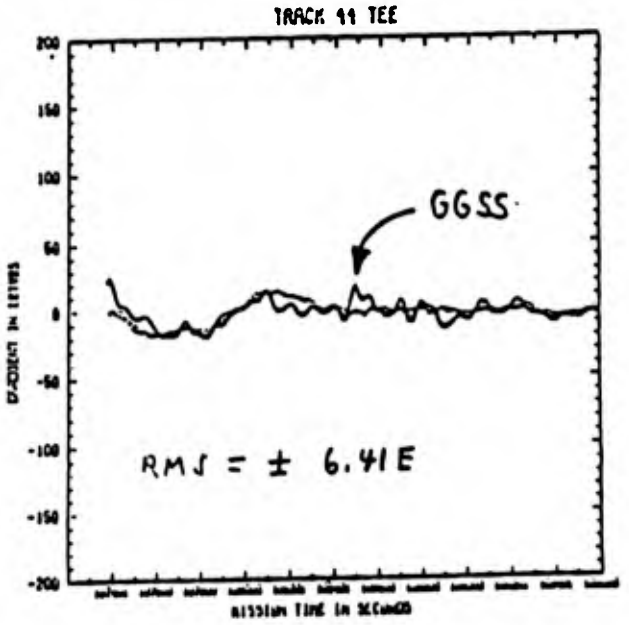

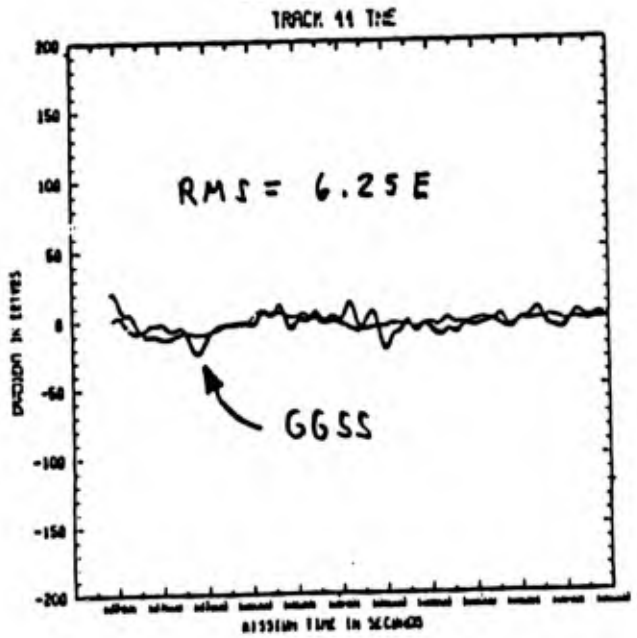

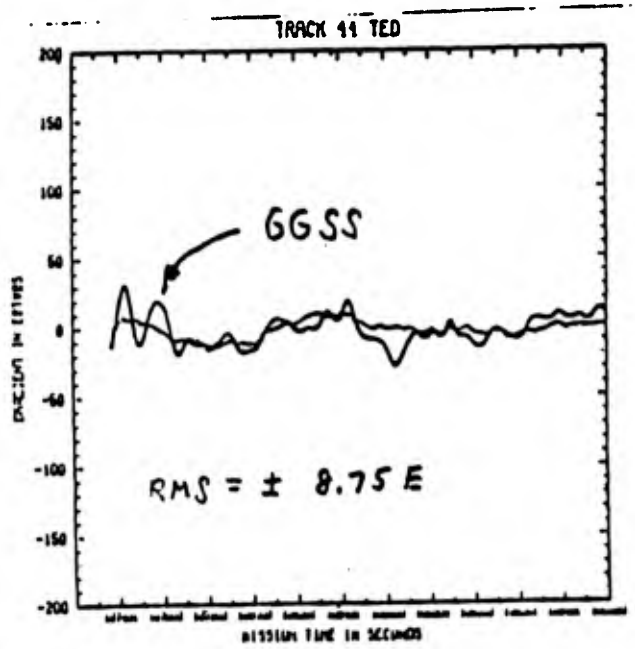

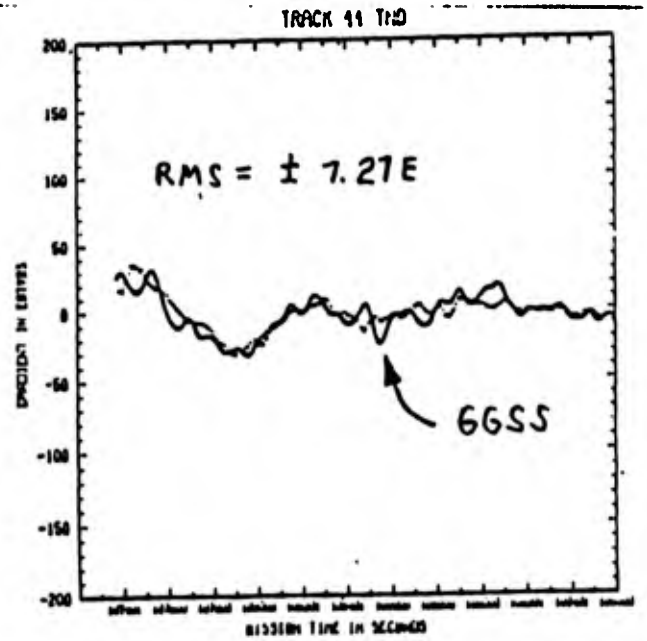

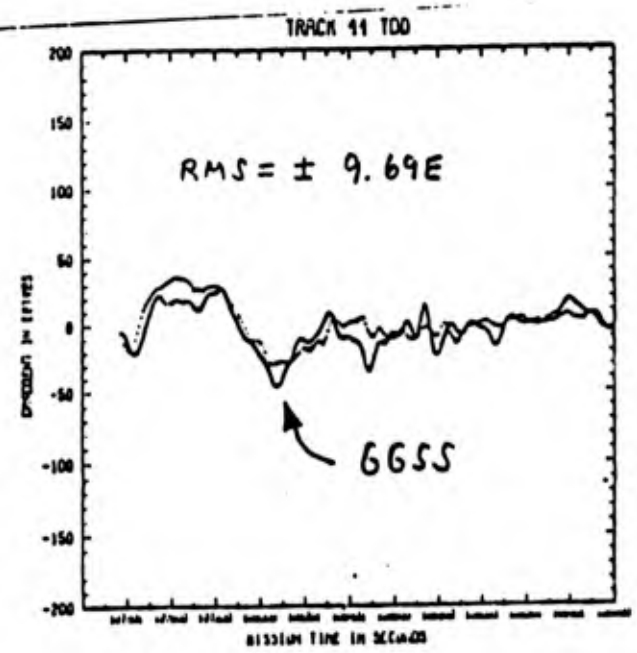

GGSS GRADIENTS VERSUS DIRECT INTEGRATION GRADIENTS
(RMS OF DIFFERENCES)

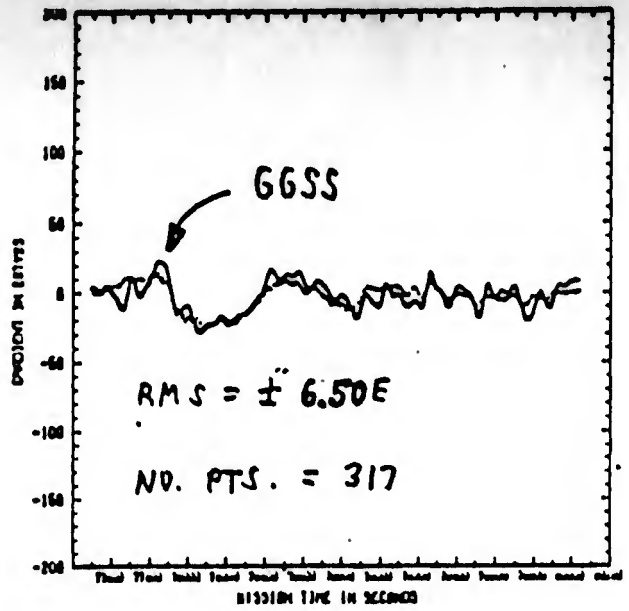

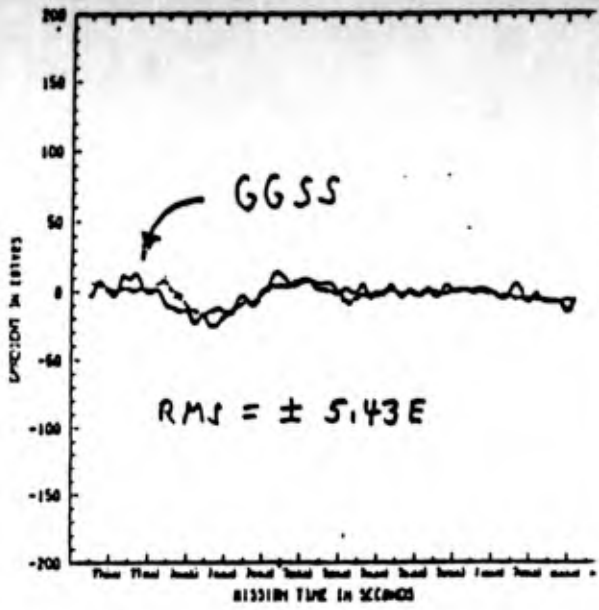

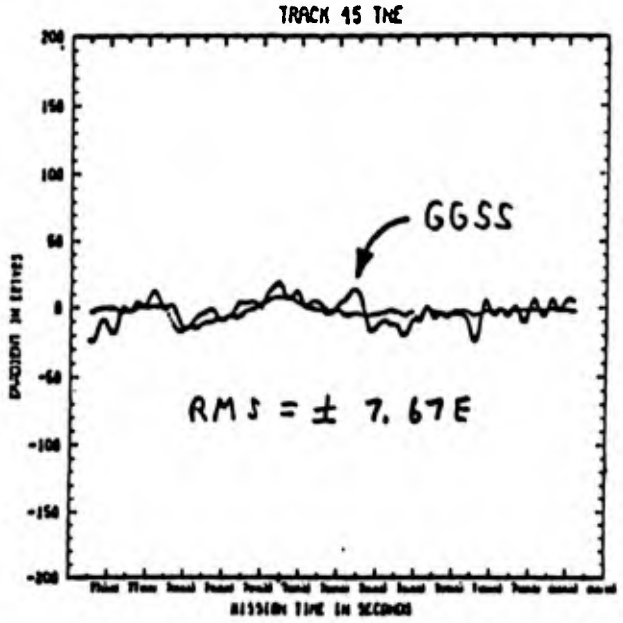

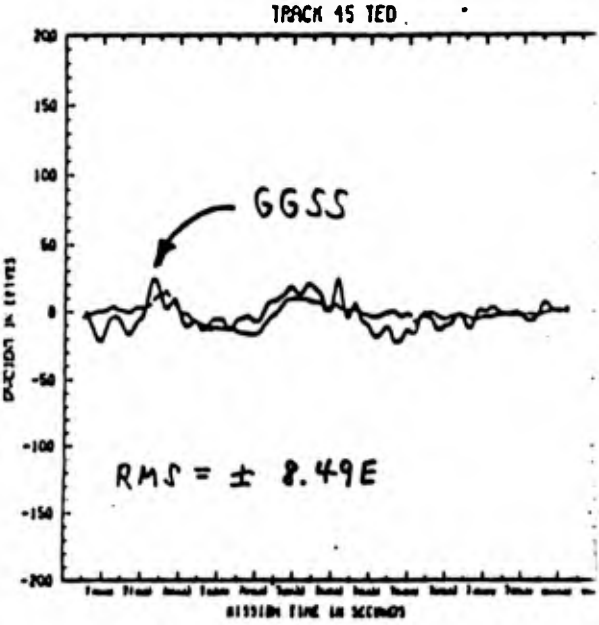

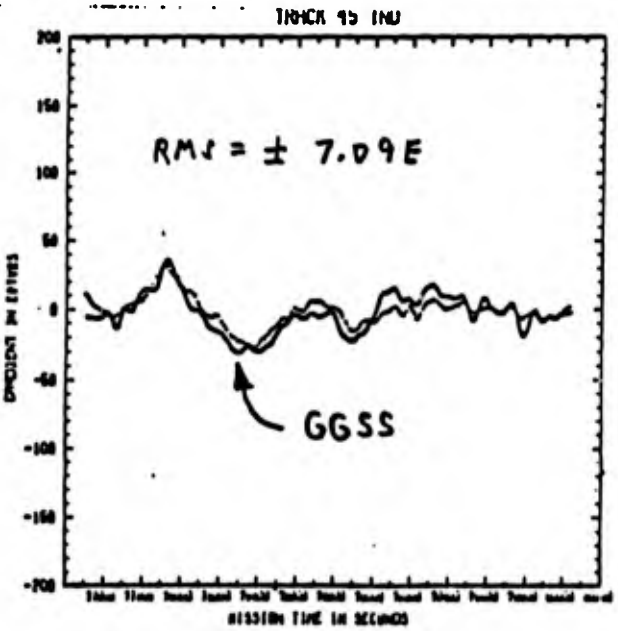

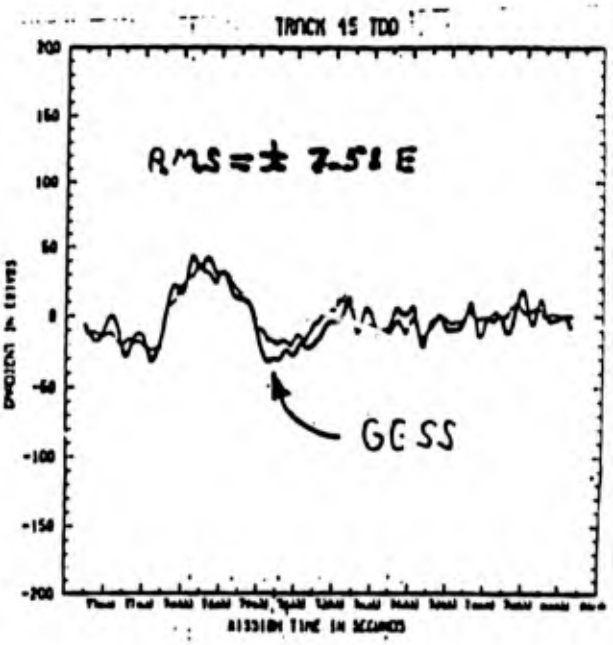

FIGURE 14.

TABLE 1

A STATISTICAL COMPARISON OF DIRECT INTEGRATION MINUS GGSS DERIVED GRADIENT DIFFERENCES

NORTH-NORTH GRADIENT (TNN)

TRACK NO.	MEAN Eotvos	SIGMA Eotvos	RMS Eotvos	NO. PTS
19	1.01	6.49	±6.55	206
22	1.33	6.67	6.79	212
24	-3.64	10.07	10.68	206
25	-10.14	12.17	15.81	174
27	-7.04	8.91	11.32	127
39	-0.61	6.37	6.39	304
41	-0.79	11.51	11.52	299
42	-0.56	8.07	8.08	374
43	-0.76	5.92	5.96	334
44	-2.44	8.92	9.23	277
45	-0.58	6.49	6.50	317

X_i = i-th Difference

$\bar{X}$ = Mean Difference

$$\sigma = \sqrt{\sum_{i=1}^{N} (X_i - \bar{X})^2 / (N-1)}$$

$$RMS = \pm \sqrt{\left(\sum_{i=1}^{N} X_i^2\right) / N}$$

TABLE 2

A STATISTICAL COMPARISON OF DIRECT INTEGRATION MINUS GGSS DERIVED GRADIENT DIFFERENCES

NORTH-EAST GRADIENT (TNE)

TRACK NO.	MEAN Eotvos	SIGMA Eotvos	RMS Eotvos	NO. PTS
19	1.13	4.03	±4.18	206
22	2.58	5.50	6.06	212
24	1.84	5.68	5.96	206
25	-3.30	7.97	8.61	174
27	-4.28	5.37	6.85	127
39	-0.33	5.61	5.61	304
41	-0.68	11.10	11.11	299
42	-0.61	10.04	10.05	374
43	-0.61	5.96	5.98	334
44	-0.90	6.20	6.25	277
45	-0.88	7.63	7.67	317

X_i = i-th Difference

$\bar{X}$ = Mean Difference

$$\sigma = \sqrt{\sum_{i=1}^{N} (X_i - \bar{X})^2 / (N-1)}$$

$$RMS = \pm\sqrt{\left(\sum_{i=1}^{N} X_i^2\right) / N}$$

TABLE 3

A STATISTICAL COMPARISON OF DIRECT INTEGRATION MINUS GGSS DERIVED GRADIENT DIFFERENCES

NORTH-DOWN GRADIENT (TND)

TRACK NO.	MEAN Eotvos	SIGMA Eotvos	RMS Eotvos	NO. PTS
19	2.10	6.27	±6.60	206
22	5.64	6.79	8.81	212
24	7.89	5.54	9.63	206
25	1.93	8.95	9.13	174
27	-1.03	4.77	4.86	127
39	0.95	3.86	3.97	304
41	0.75	8.26	8.28	299
42	0.42	7.75	7.75	374
43	0.17	5.48	5.48	334
44	0.27	7.27	7.27	277
45	0.60	7.07	7.09	317

x_i = i-th Difference

$\bar{x}$ = Mean Difference

$$\sigma = \sqrt{\sum_{i=1}^{N} (x_i - \bar{x})^2 / (N-1)}$$

$$RMS = \pm\sqrt{\left(\sum_{i=1}^{N} x_i^2\right) / N}$$

TABLE 4

A STATISTICAL COMPARISON OF DIRECT INTEGRATION MINUS GGSS DERIVED GRADIENT DIFFERENCES

EAST-EAST GRADIENT (TEE)

TRACK NO.	MEAN Eotvos	SIGMA Eotvos	RMS Eotvos	NO. PTS
19	-0.55	8.46	±8.46	206
22	-0.20	4.79	4.78	212
24	-1.29	4.95	5.10	206
25	-1.87	6.19	6.45	174
27	-1.71	7.52	7.69	127
39	1.42	5.90	6.06	304
41	-0.26	7.25	7.24	299
42	-1.05	9.93	9.97	374
43	-1.28	6.13	6.26	334
44	-0.63	6.39	6.41	277
45	-0.18	5.43	5.43	317

X_i = i-th Difference

$\bar{X}$ = Mean Difference

$$\sigma = \sqrt{\sum_{i=1}^{N} (X_i - \bar{X})^2 / (N-1)}$$

$$RMS = \pm\sqrt{\left(\sum_{i=1}^{N} X_i^2\right) / N}$$

TABLE 5

A STATISTICAL COMPARISON OF DIRECT INTEGRATION MINUS GGSS DERIVED GRADIENT DIFFERENCES

EAST-DOWN GRADIENT (TED)

TRACK NO.	MEAN Eotvos	SIGMA Eotvos	RMS Eotvos	NO. PTS
19	-0.57	6.16	±6.18	206
22	3.06	12.31	12.66	212
24	4.27	6.18	7.50	206
25	4.13	7.26	8.33	174
27	-0.32	8.13	8.11	127
39	1.23	5.71	5.84	304
41	1.48	10.57	10.66	299
42	1.83	8.99	9.16	374
43	0.37	7.40	7.39	334
44	0.04	8.76	8.75	277
45	0.60	8.48	8.49	317

x_i = i-th Difference

$\bar{x}$ = Mean Difference

$$\sigma = \sqrt{\sum_{i=1}^{N} (x_i - \bar{x})^2/(N-1)}$$

$$RMS = \pm\sqrt{\left(\sum_{i=1}^{N} x_i^2\right)/N}$$

TABLE 6

A STATISTICAL COMPARISON OF DIRECT INTEGRATION MINUS GGSS DERIVED GRADIENT DIFFERENCES

DOWN-DOWN GRADIENT (TDD)

TRACK NO.	MEAN Eotvos	SIGMA Eotvos	RMS Eotvos	NO. PTS
19	-0.45	9.21	±9.20	206
22	-1.04	5.70	5.78	212
24	4.98	8.97	10.24	206
25	12.01	12.55	17.35	174
27	8.68	10.79	13.81	127
39	-0.82	6.85	6.89	304
41	1.05	11.24	11.27	299
42	1.59	8.85	8.98	374
43	2.01	9.04	9.24	334
44	3.05	9.21	9.69	277
45	0.75	7.49	7.51	317

x_i = i-th Difference

$\bar{x}$ = Mean Difference

$$\sigma = \sqrt{\sum_{i=1}^{N} (x_i - \bar{x})^2 / (N-1)}$$

$$RMS = \pm\sqrt{\left(\sum_{i=1}^{N} x_i^2\right) / N}$$

A PRELIMINARY COMPARISON AT FLIGHT TEST ALTITUDE OF GRAVITY DISTURBANCE COMPONENTS DERIVED FROM AIRBORNE GGSS SECOND ORDER GRAVITY GRADIENTS WITH SIMILAR DATA COMPUTED AT THE SAME PROFILE POINTS USING SURFACE INTEGRAL FORMULAS AND SURFACE MEAN GRAVITY ANOMALIES

By

Joseph L. Toohey/DMAAC/DSG

And

Robert W. Valska/DMASC/WG

Presented To

Sixteenth Annual Gravity Gradiometry Conference
United States Air Force Academy
Colorado Springs, Colorado
10-11 February 1988

Defense Mapping Agency Aerospace Center and
Systems Center/West Resources/Career Group
3200 South Second Street
St. Louis, Missouri 63118-3399

ABSTRACT

Flight tests of the Airborne Gravity Gradiometer Survey System (GGSS) developed by Bell Aerospace TEXTRON under an Air Force Geophysics Laboratory (AFGL)/Defense Mapping Agency (DMA) Contract were conducted in Oklahoma during the Spring of 1987. Approximately 120 airborne profiles of second order gravity gradients, of varying quality, were obtained during the flight test period. Eleven profiles of the Airborne GGSS data (6 north/south, 5 east/west) were selected for evaluation. Line integration was performed along these GGSS-acquired gravity gradient profiles to obtain gravity disturbance components. These GGSS-derived gravity disturbance components were then compared with another set of gravity disturbance components computed at the same points along the 11 profiles using surface integral formulas and surface mean gravity anomalies. The graphical and statistical data resulting from this initial analysis provide some insight into the performance of the Airborne GGSS at this point in its development.

1. INTRODUCTION

Field tests of the Airborne Gravity Gradiometer Survey System (GGSS), developed by Bell Aerospace TEXTRON for the Defense Mapping Agency (DMA)*, were conducted during the Spring of 1987 over Oklahoma (Figure 1). Approximately 120 airborne profiles of second order gravity gradients, of varying quality, were obtained during the flight test period. Eleven profiles of the Airborne GGSS data (6 north/south, 5 east/west) were selected for evaluation. The location of these profiles in the GGSS Flight Test Area is indicated in Figures 2 and 3.

2. DISCUSSION

After editing and despiking the raw data, a low-pass filter [1, p 113] was used to eliminate high frequency noise of wavelengths less than 11 kilometers. Since the Airborne GGSS data was collected at one second intervals of time, the 131-point filter eliminated 65 data points at both ends of each profile. After filtering, the inline and cross channel gradients were rotated into a north-east-down (NED) Coordinate System, and their linear trends removed. Any data gap resulting from the despiking process was closed in by using an average of the gradients at the gap end points. Completion of the data processing activities provided the 11-track set of airborne second order gradients to be analyzed from the flight test.

As part of the evaluation process for this 11-track set of GGSS second order gravity gradients, gravity disturbance components were calculated at every ninth GGSS profile point in the set using surface integral formulas [2, p 233] and surface mean gravity anomalies. The surface data used in the formulas consisted of a worldwide set of surface mean gravity anomalies referenced to the World Geodetic System 1984 (WGS 84) Ellipsoid Gravity Formula. Mean gravity anomalies of 1'x1' size were used near the nadir of the computation points. Moving radially away from the nadir point, mean gravity anomalies of progressively larger size (5'x5',15'x15', $1^{o}x1^{o}$, and $5^{o}x5^{o}$) were used. This computed data formed a "truth" set of gravity disturbance components for comparison against a similar set to be computed from the GGSS-derived gradients.

Gravity disturbance components from the "truth" data set, previously calculated at profile points, were used at a beginning (selected) point of each data track to initiate a line integration [3]. The line integration proceeded with a summation along each of the six north/south profiles and the five east/west gravity gradient profiles. Results from this line integration effort formed the test set of GGSS-related gravity disturbance components to be evaluated. To check the validity of the calculation procedure that provided the gravity disturbance component test set, a set

---

* The Air Force Geophysics Laboratory (AFGL) performed technical and administrative monitorship of the AFGL/DMA Contract with Bell Aerospace TEXTRON.

of second order gravity gradients, previously calculated using a differential form of Pizetti's Equation [2, p 233] and surface mean gravity anomalies [4], was subjected to the same line integration. The line integration gave gravity disturbance components that agreed with similar values in the "truth" data set.

The GGSS-related gravity disturbance components are graphically compared in Figures 4-14 with similar values from the "truth" data set. In the figure titles, the term "direct integration" refers to the "truth" disturbances. These figures depict all three of the gravity disturbance components found at their appropriate intervals along each of the 11 selected profiles. In addition, these figures show the comparison of "truth" data against GGSS-related gravity disturbance components using one tie (known) point and an adjusted comparison using three tie points for each profile. In the three tie point case, tie points were used at both ends and in the middle of each profile, resulting in a tie-point spacing of approximately 100 kilometers.

Tables 1-3 contain statistical results from a comparison of the GGSS-related gravity disturbance components against the aloft "truth" (direct integration) gravity disturbance components. Differences were formed using the sense, "truth" gravity disturbance components minus GGSS-related gravity disturbance components. Each table lists pertinent statistical data (mean, standard deviation, and RMS) for the gravity disturbance component differences occurring along each track.

It is apparent from the figures and tables that the agreement between the GGSS-related gravity disturbance components and the "truth" gravity disturbance components is better when an adjustment is made using three tie points, as opposed to just using the line integration process with one tie point as the initial gravity disturbance value. For example, the RMS difference decreased from 63.5 to 8.0 milligals (mgals) for the north gravity disturbance component of Track 44, after the one tie point line integration solution was adjusted with three tie points.

Of the east/west tracks, Track 27 has the smallest RMS difference, approximately 5 mgals for each of the three components. For east/west tracks, the "truth" gravity disturbance components and the GGSS-related gravity disturbance components agree much better when an adjustment is made using three tie points.

With respect to the north/south tracks, Track 39 has the smallest RMS differences, the values ranging from 5.5 mgals to 9.5 mgals. After Track 39, Tracks 43 and 44 are the next best north/south tracks with respect to agreement between "truth" and GGSS-related gravity disturbance components. The three remaining north/south tracks (41,42,45) do not exhibit good agreement between "truth" and GGSS-related data in any component. Also, with the exception of Track 39, the north/south tracks do not exhibit very good agreement between "truth" and GGSS-related data for the east gravity disturbance component. The RMS differences for the east gravity disturbance components range from 10 mgals to 30 mgals.

3. CONCLUSION

For the five Airborne GGSS east/west profiles analyzed, the RMS differences ("truth" minus GGSS-related gravity disturbance components) ranged from 3.6 mgals to 23.7 mgals. If the down gravity disturbance component for Track 22 is ignored, the range of the RMS differences improves, becoming 3.6 mgals to 12.5 mgals.

For the six Airborne GGSS north/south profiles analyzed, the RMS differences ranged from 5.5 mgals to 30.1 mgals. Only Track 39 of the north/south tracks had a good recovery of all three gravity disturbance components from the GGSS-derived second order gravity gradients.

The results in the two preceding paragraphs reflect GGSS-related gravity disturbance components determined via a line integration process with an adjustment using three tie points.

The results discussed here are preliminary, representing the findings from an initial, brief analysis of a small set of second order gravity gradients from the first flight test of an Airborne Gravity Gradiometer Survey System. The comparison of "truth" data with GGSS-derived second order gravity gradients along these same 11 tracks is discussed in a separate conference paper [4]. Although much remains to be learned about the GGSS and its capabilities as the data analysis continues, the findings to date are encouraging.

REFERENCES

1. Hamming, R. W.; Digital Filters, Second Edition; Prentice-Hall; Englewood Cliffs, New Jersey; 1983.

2. Heiskanen, W. A. and H. Moritz; Physical Geodesy; W. H. Freeman and Company; San Francisco, California; 1967.

3. Moritz, H.; Kinematical Geodesy; Department of Geodetic Science and Surveying Report No. 92; The Ohio State University; Columbus, Ohio; November 1967.

4. Graham, J. J. and J. L. Toohey; A Preliminary Comparison at Flight Test Altitude of Airborne GGSS Second Order Gravity Gradients With Similar Data Computed at the Same Profile Points Using Surface Integral Formulas and Surface Mean Gravity Anomalies; Defense Mapping Agency Aerospace Center and Systems Center/West Group; St. Louis, Missouri; February 1988. [Paper Presented at Sixteenth Annual Gravity Gradiometry Conference; United States Air Force Academy; Colorado Springs, Colorado; 10-11 February 1988.]

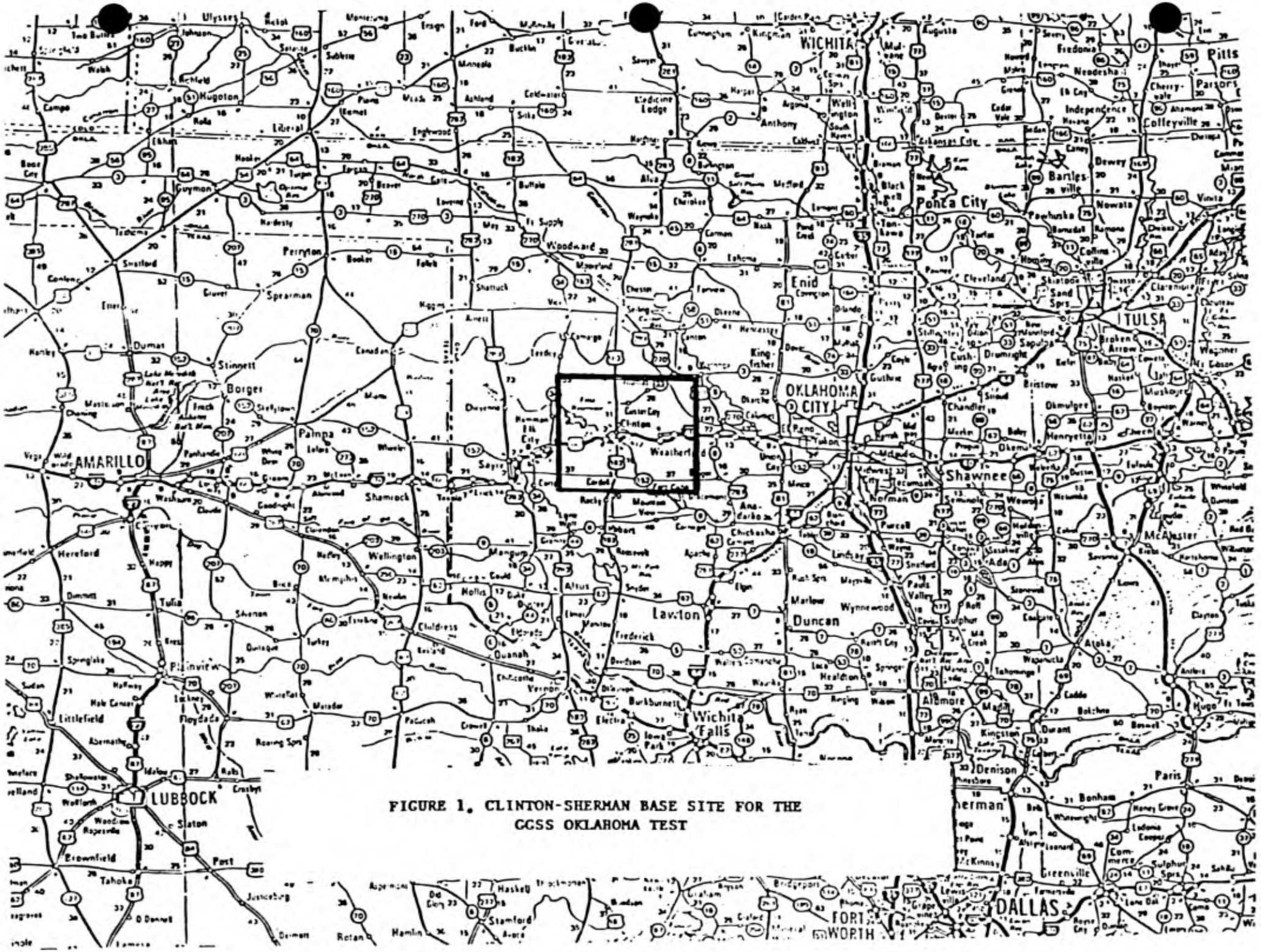

FIGURE 1. CLINTON-SHERMAN BASE SITE FOR THE CGSS OKLAHOMA TEST

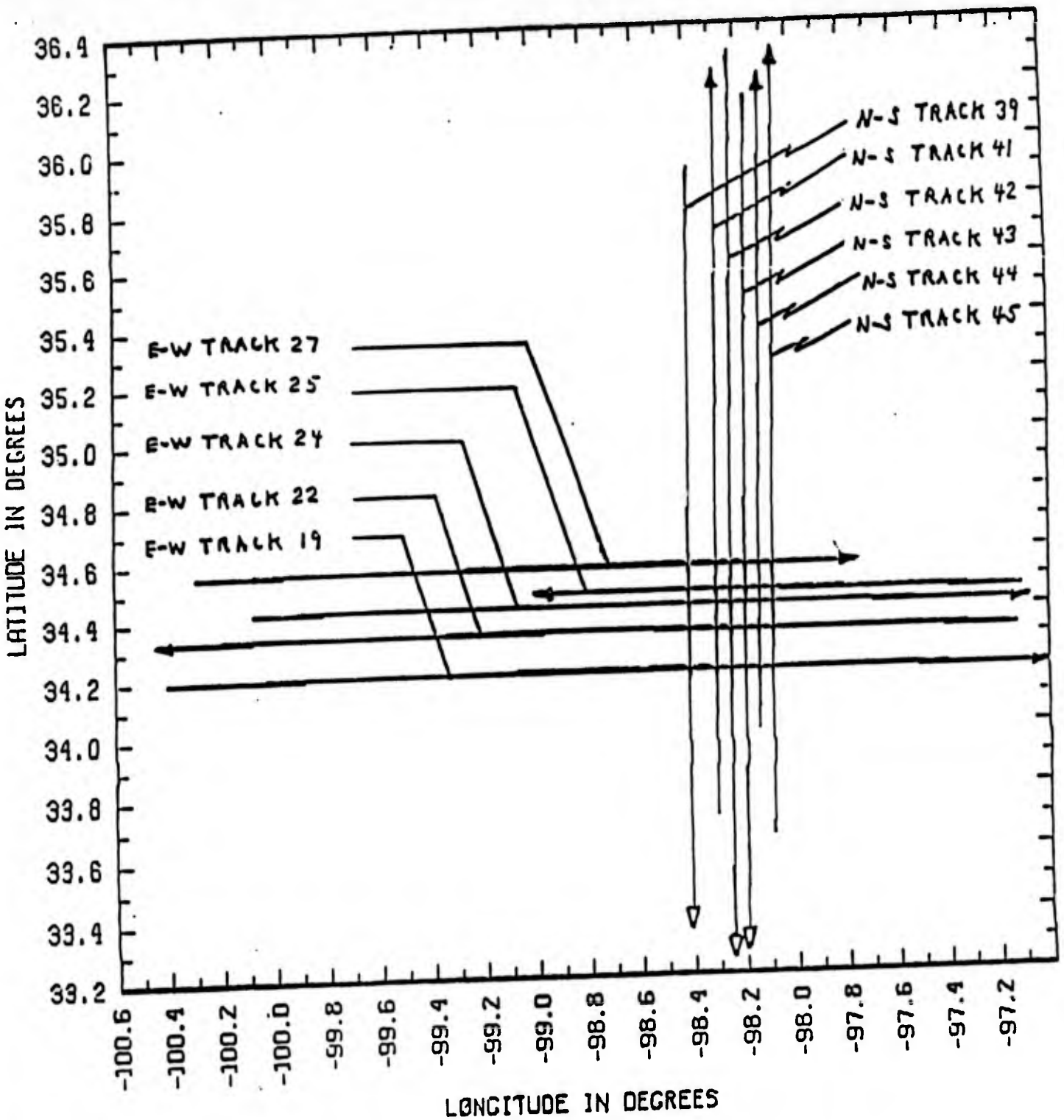

FIGURE 2. THE ELEVEN SELECTED GGSS TRACKS AFTER EDITING

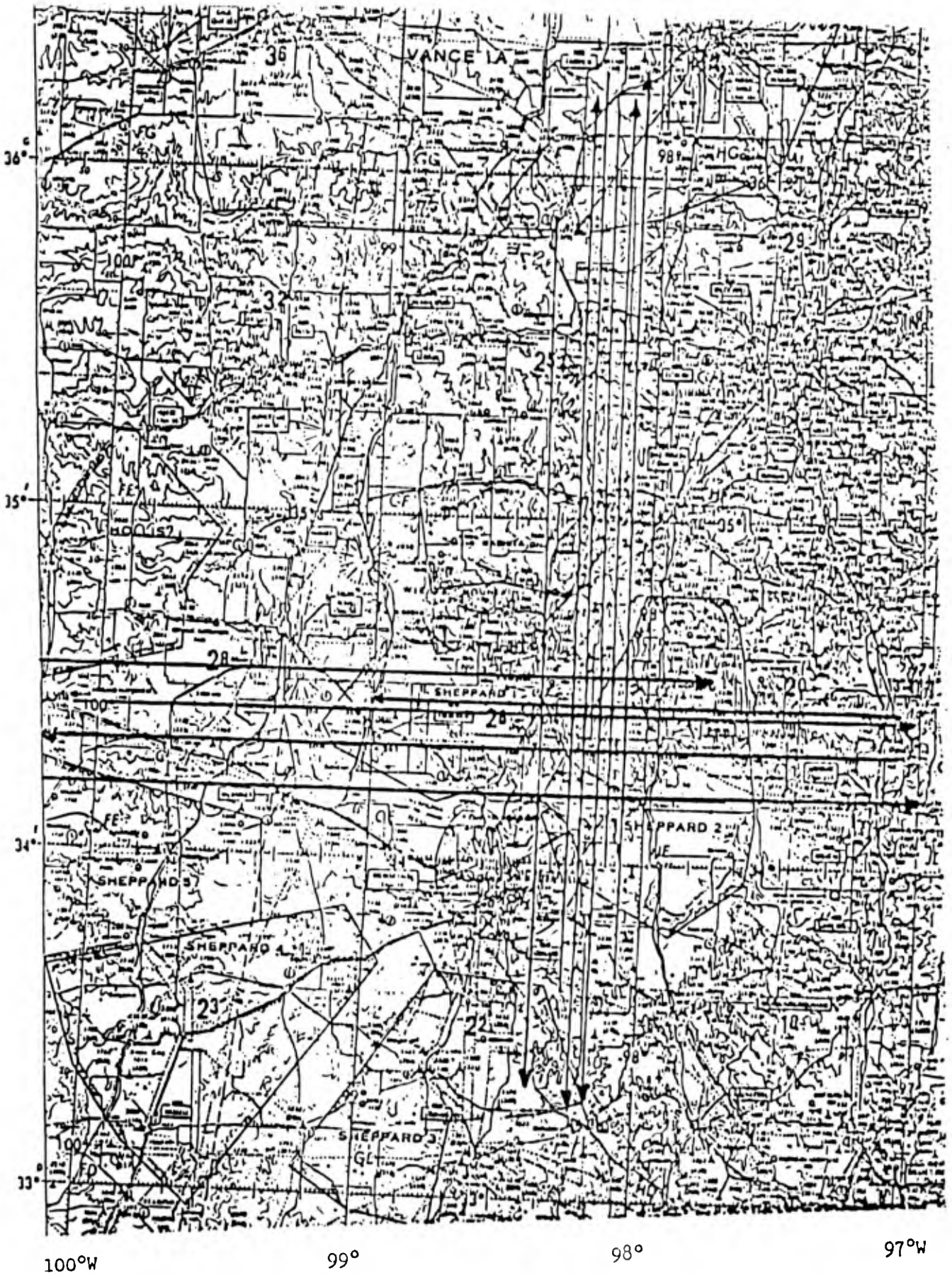

FIGURE 3. THE ELEVEN EDITED GOSS TRACKS ON AN ONC CHART

FIGURE 4.

GGSS DISTURBANCES VERSUS DIRECT INTEGRATION DISTURBANCES

(RMS OF DIFFERENCES)

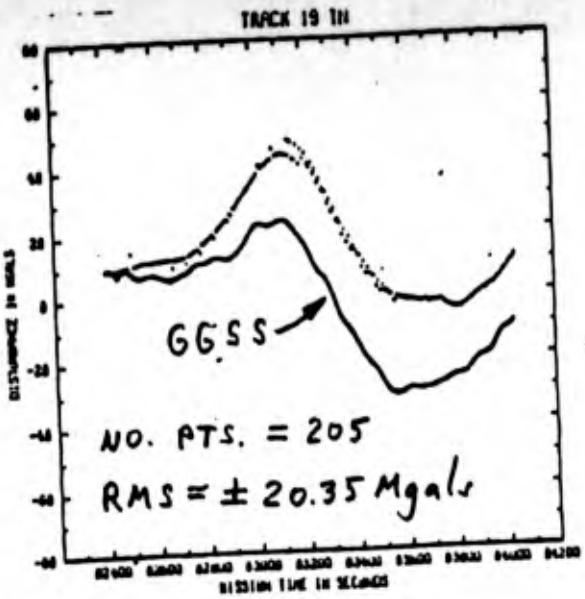

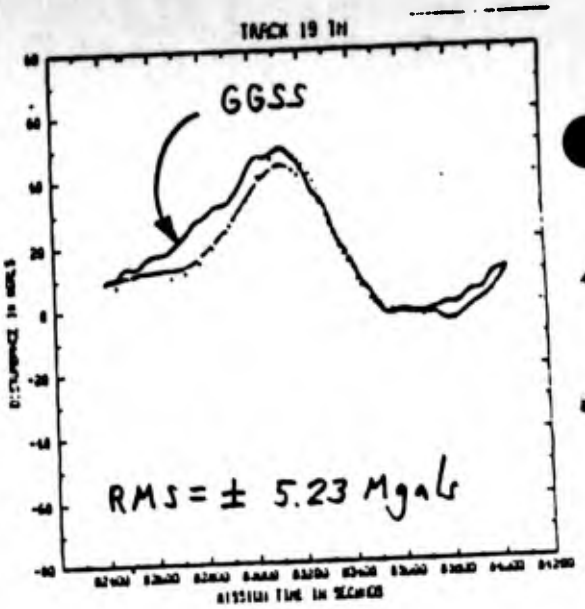

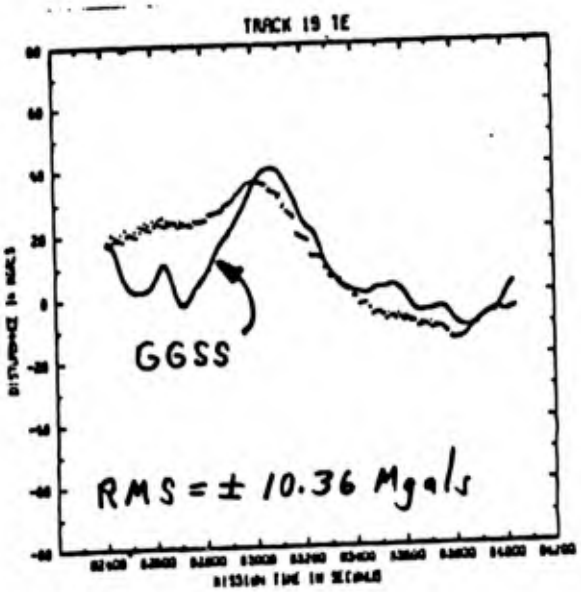

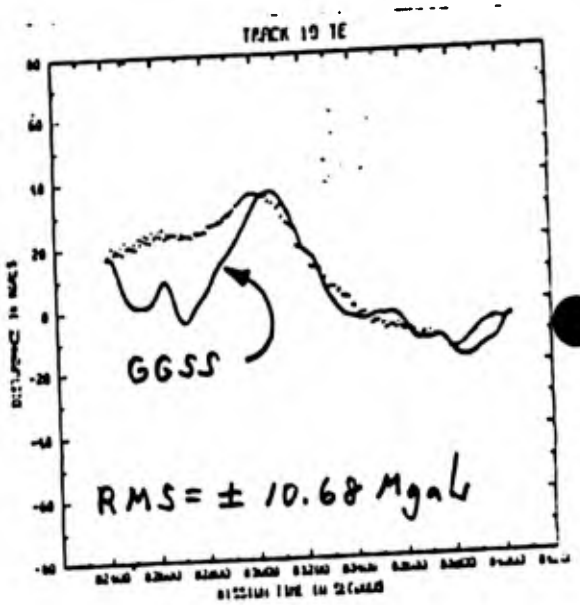

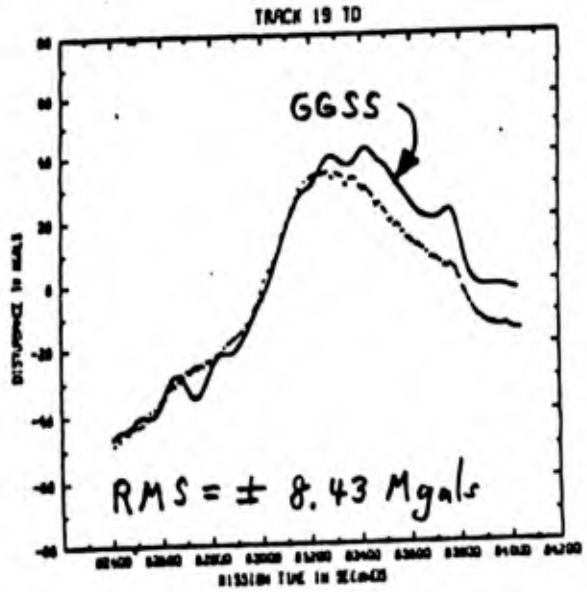

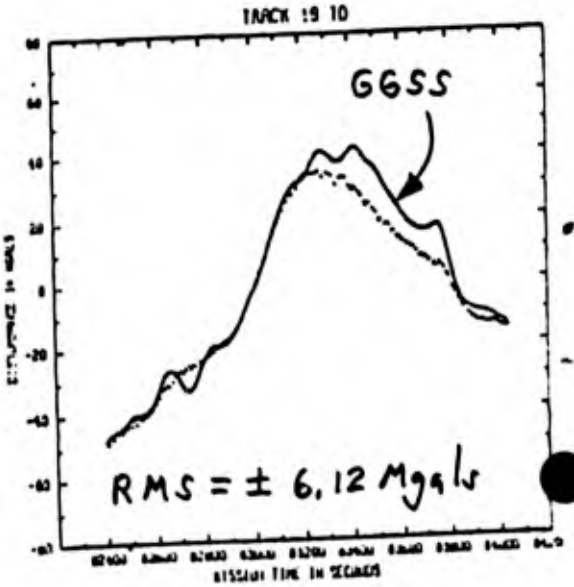

FIGURE 5.

GGSS DISTURBANCES VERSUS DIRECT INTEGRATION DISTURBANCES

(RMS OF DIFFERENCES)

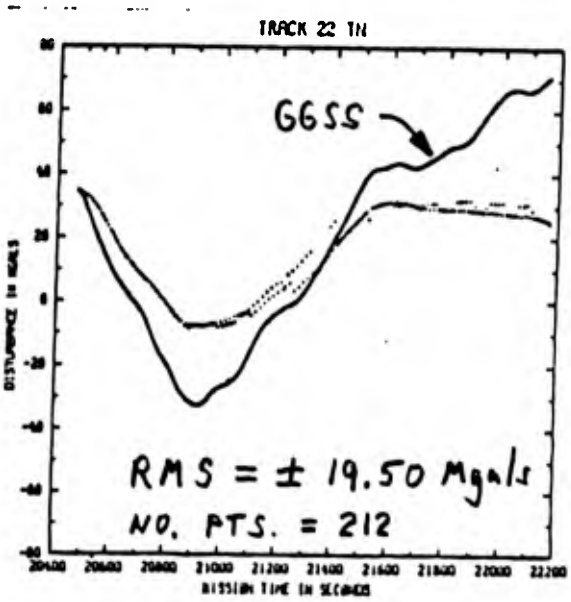

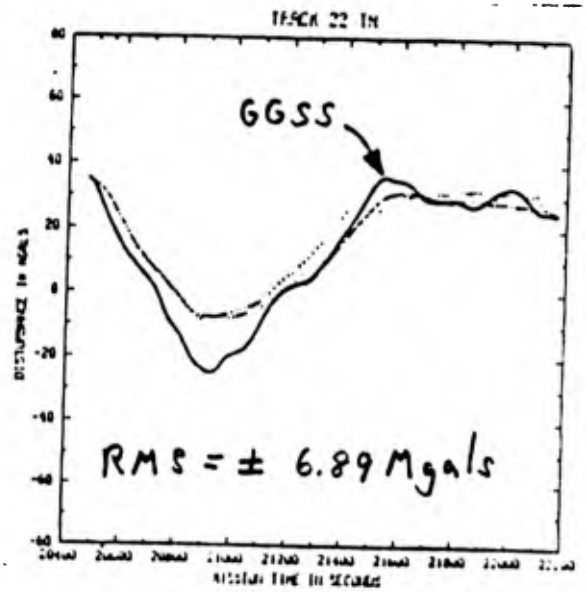

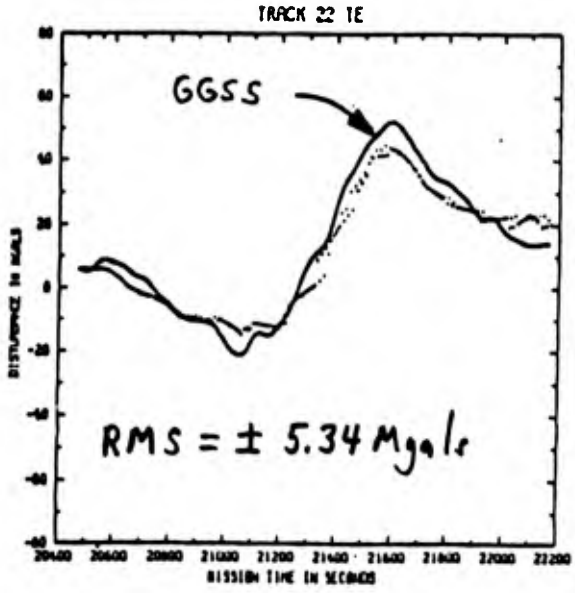

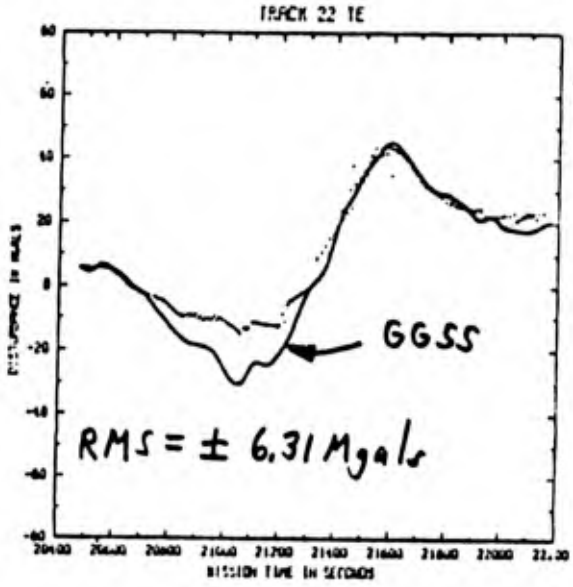

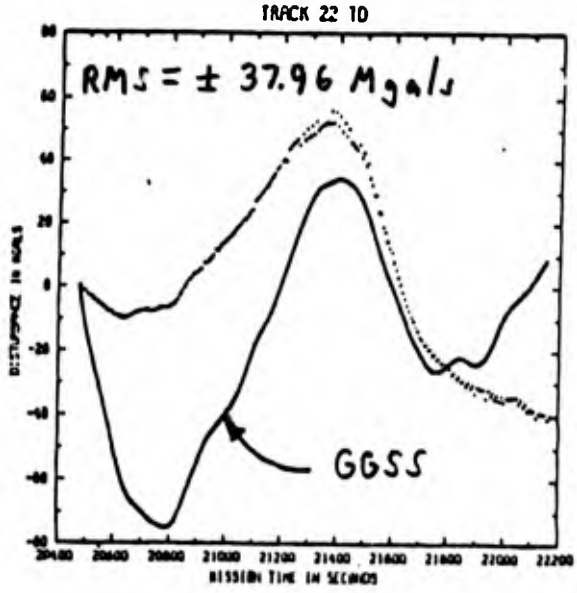

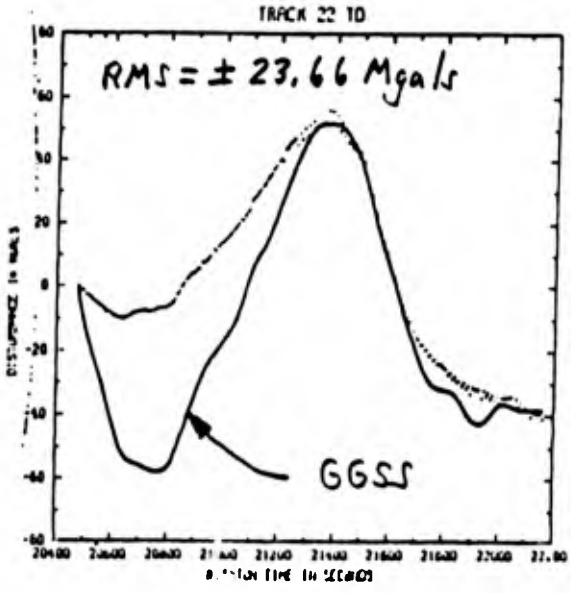

FIGURE 6.

GGSS DISTURBANCES VERSUS DIRECT INTEGRATION DISTURBANCES

(RMS OF DIFFERENCES)

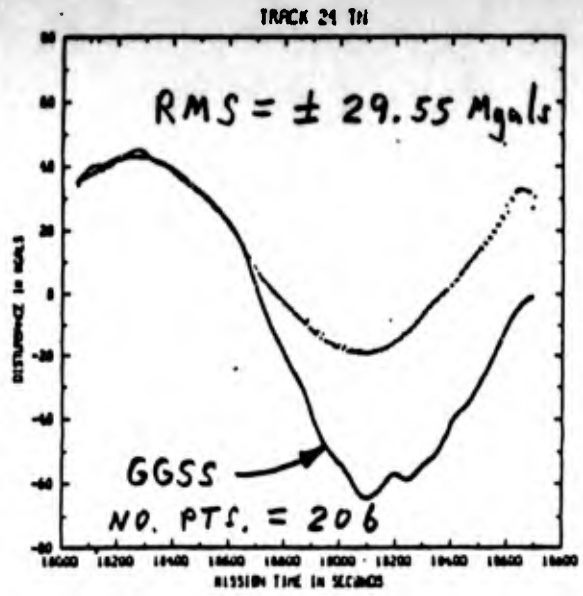

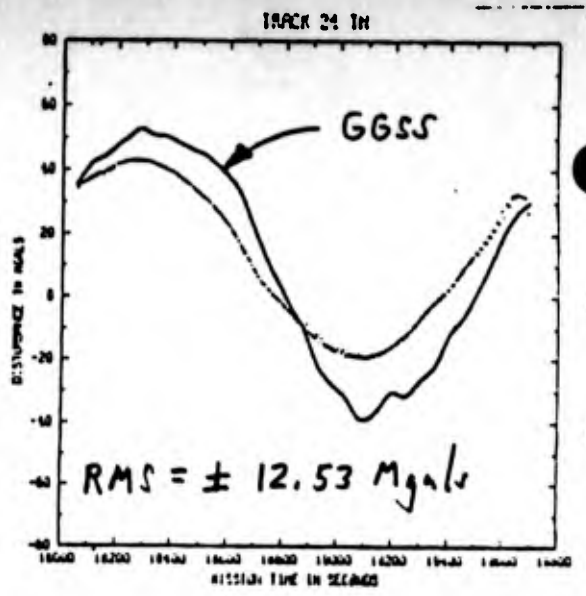

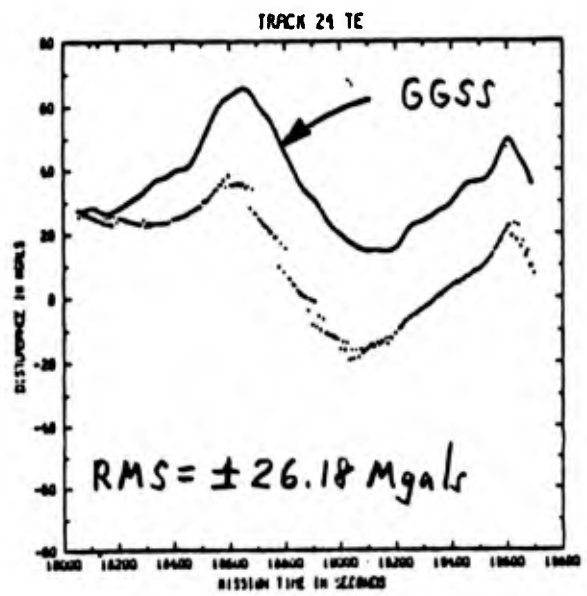

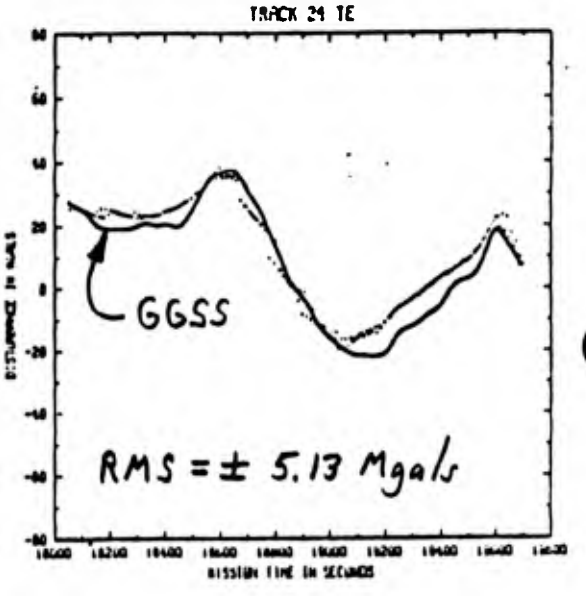

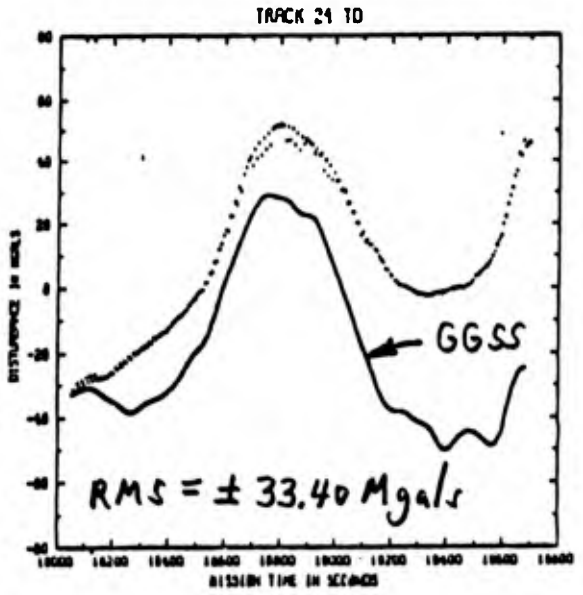

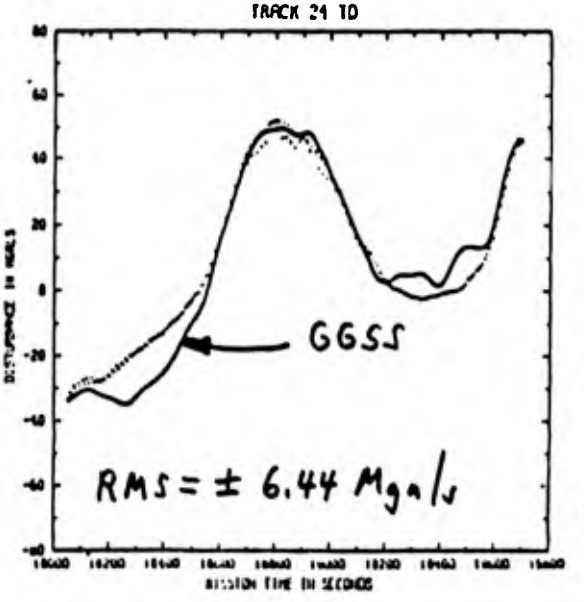

FIGURE 8.

GOSS DISTURBANCES VERSUS DIRECT INTEGRATION DISTURBANCES

(RMS OF DIFFERENCES)

FIGURE 10.

GGSS DISTURBANCES VERSUS DIRECT INTEGRATION DISTURBANCES

(RMS OF DIFFERENCES)

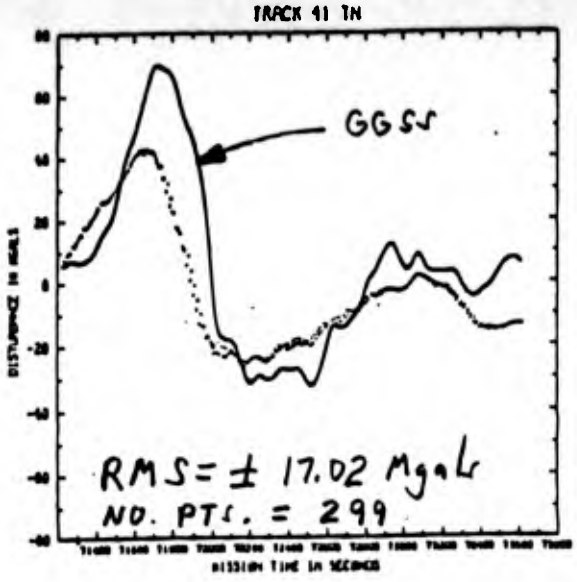

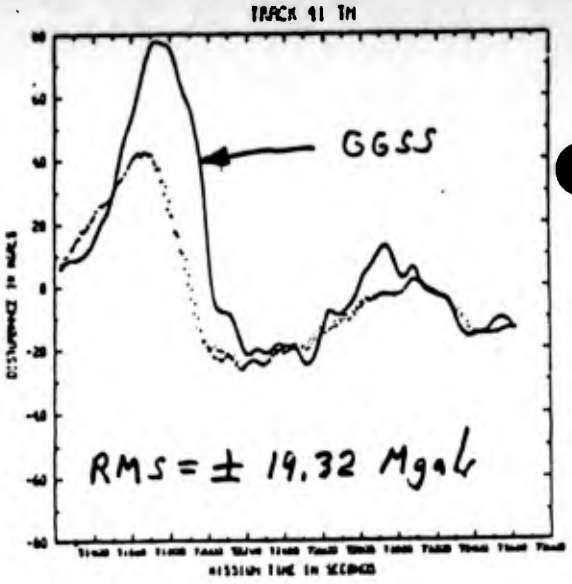

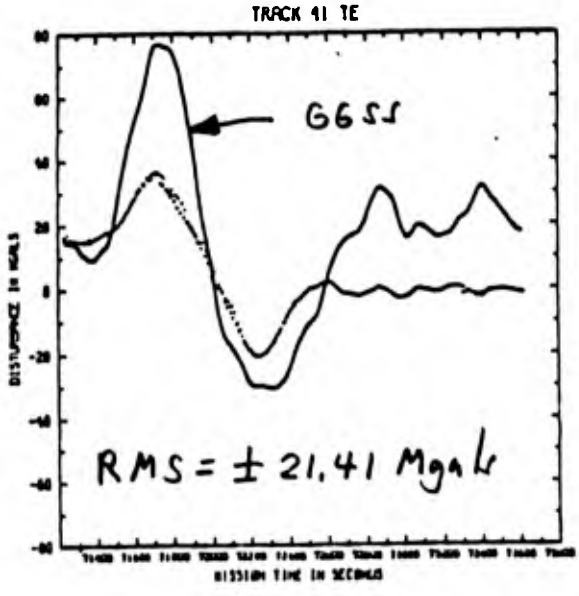

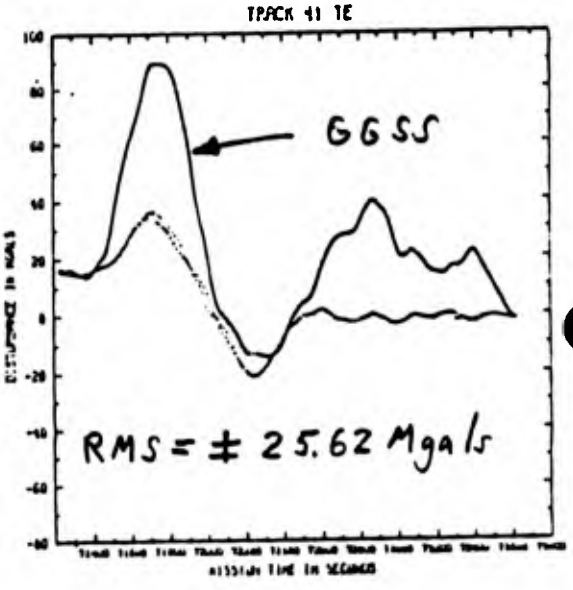

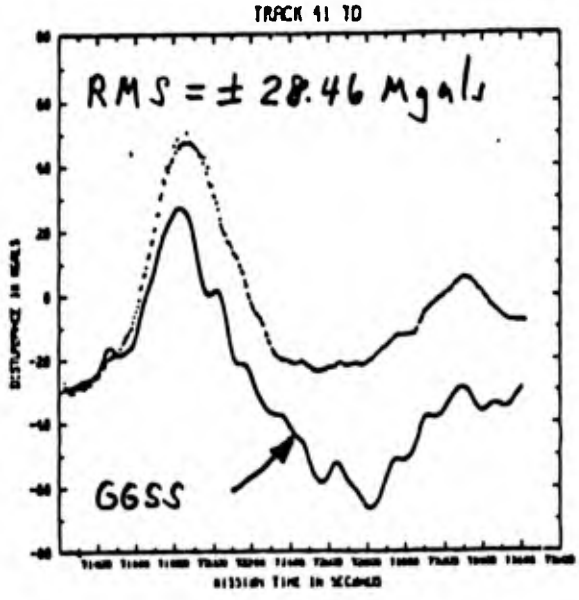

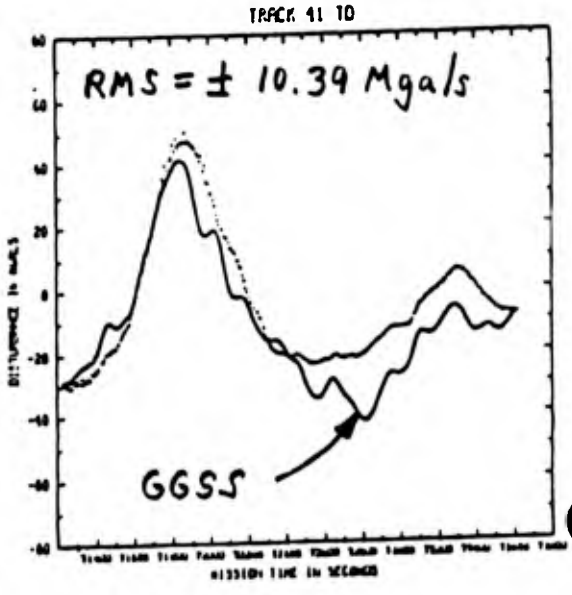

FIGURE 9.

GGSS DISTURBANCES VERSUS DIRECT INTEGRATION DISTURBANCES

(RMS OF DIFFERENCES)

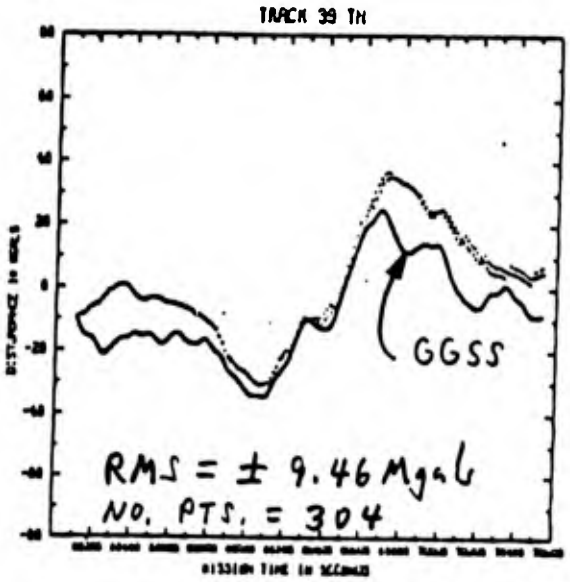

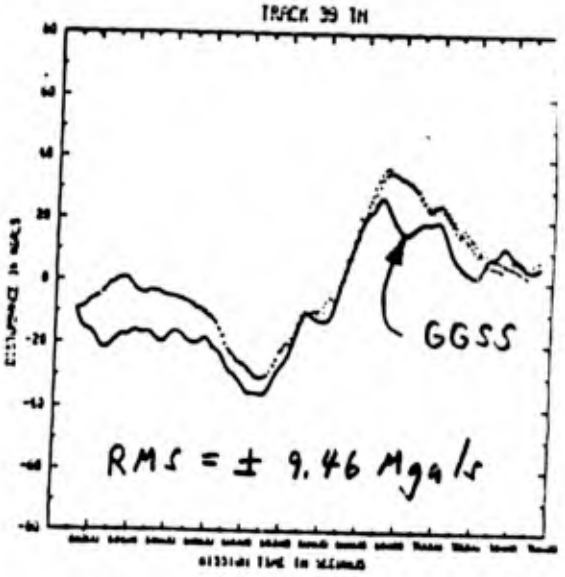

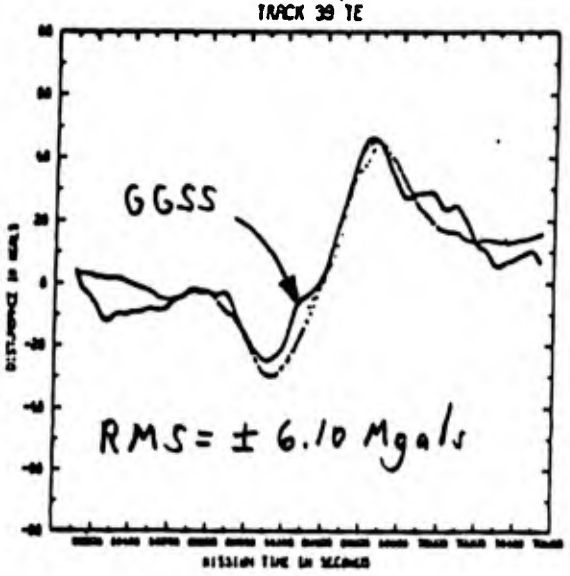

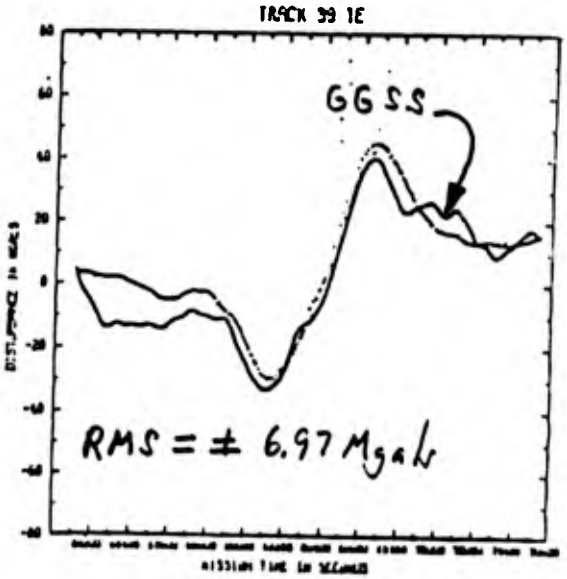

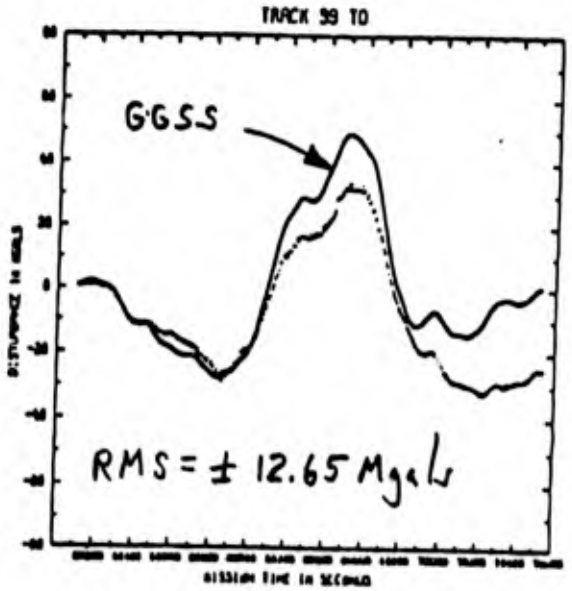

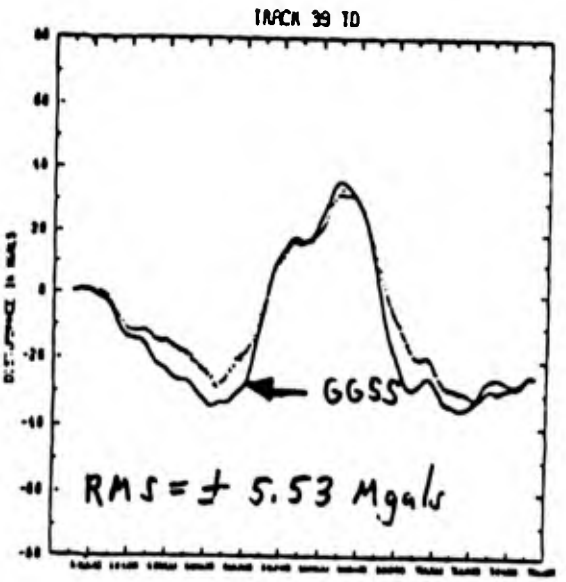

FIGURE 11.

GGSS DISTURBANCES VERSUS DIRECT INTEGRATION DISTURBANCES

(RMS OF DIFFERENCES)

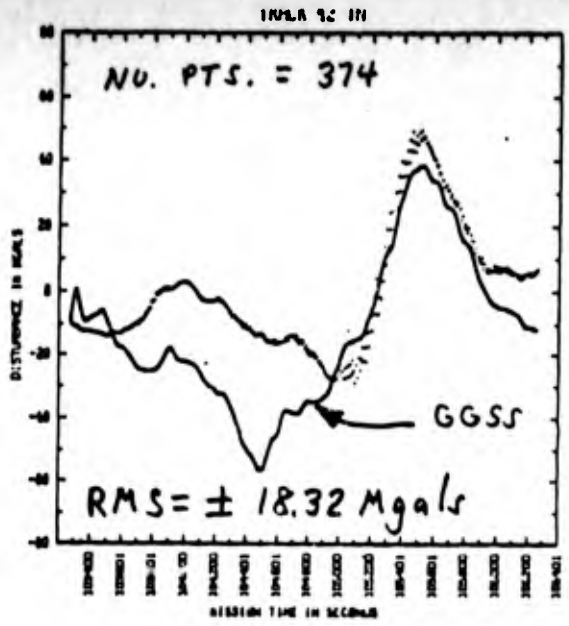

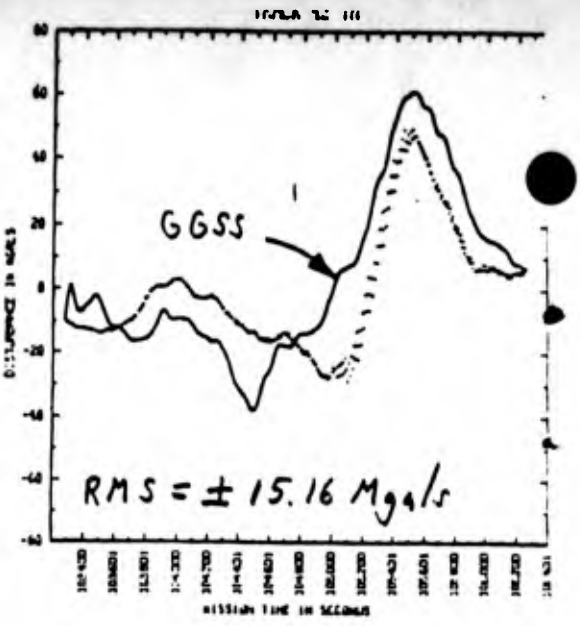

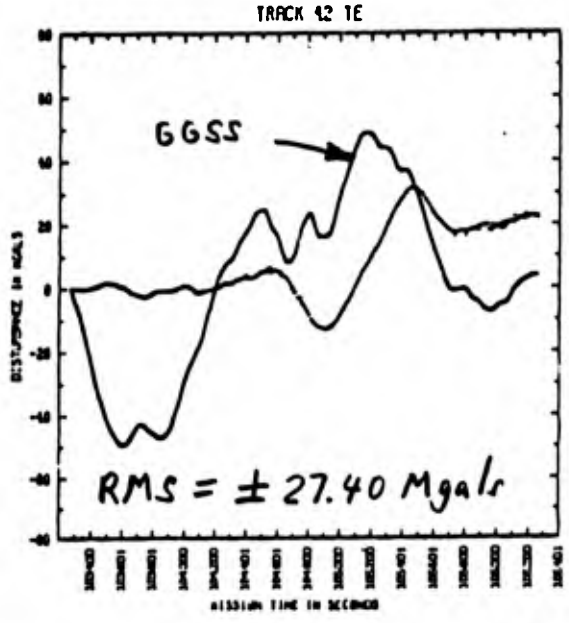

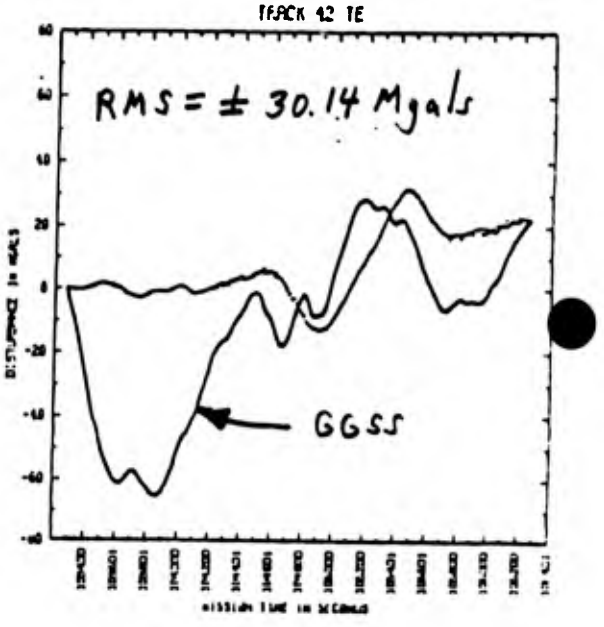

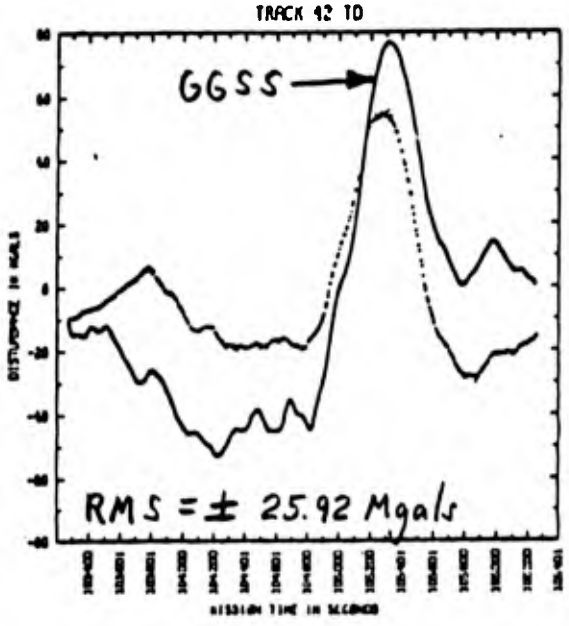

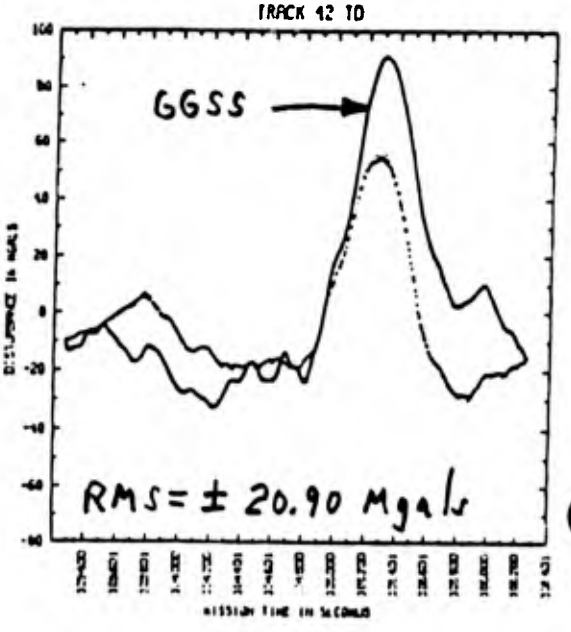

FIGURE 12.

GGSS DISTURBANCES VERSUS DIRECT INTEGRATION DISTURBANCES

(RMS OF DIFFERENCES)

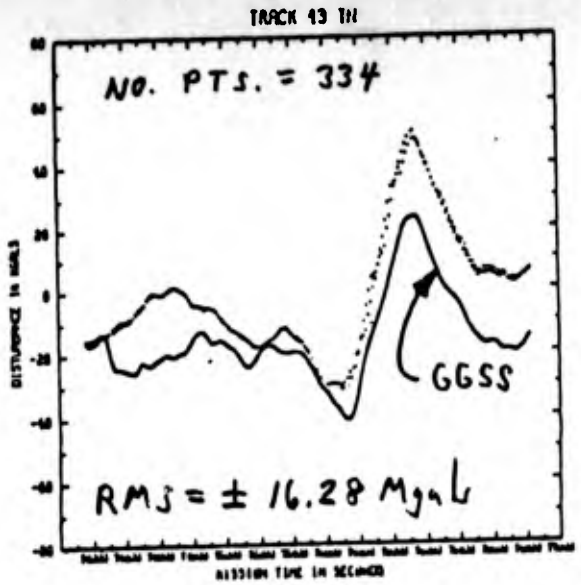

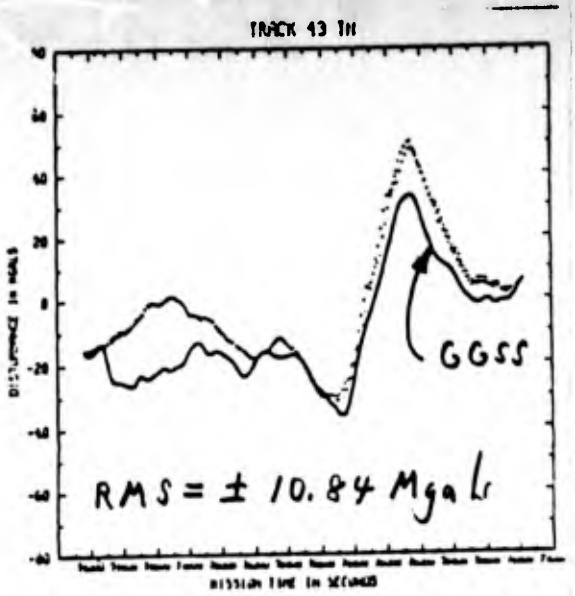

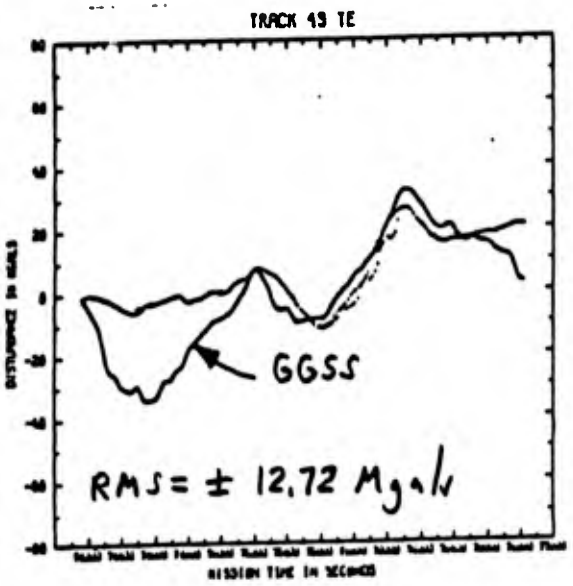

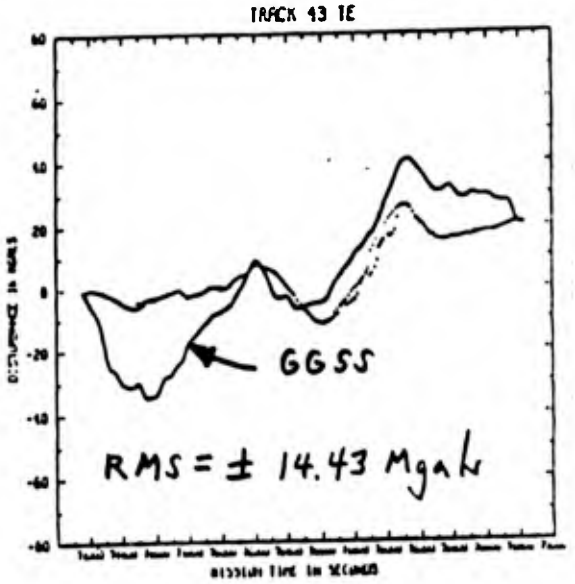

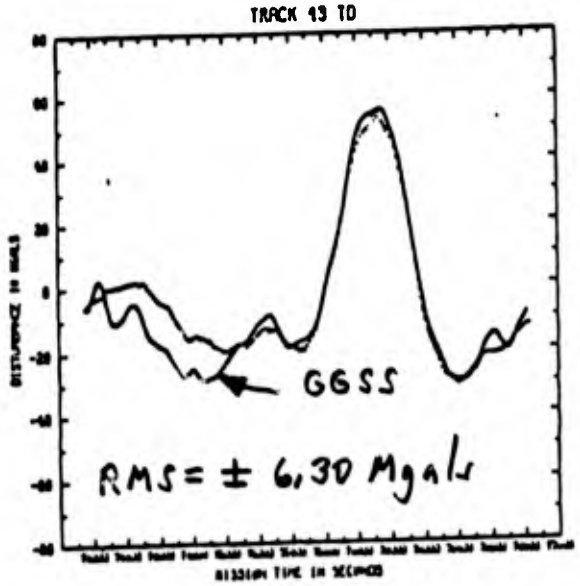

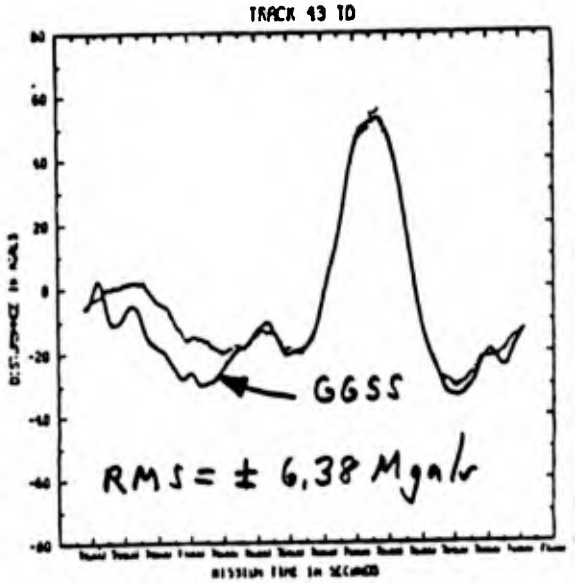

FIGURE 13.

GGSS DISTURBANCES VERSUS DIRECT INTEGRATION DISTURBANCES

(RMS OF DIFFERENCES)

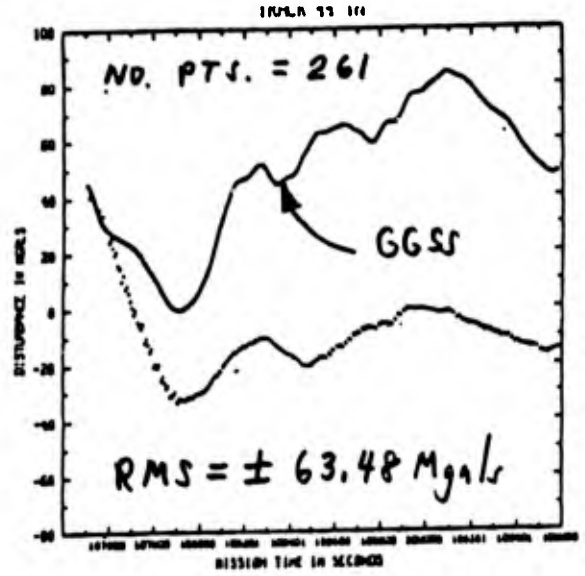

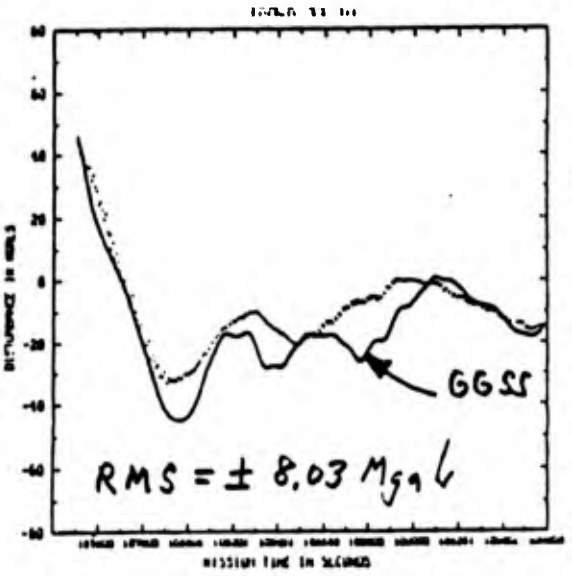

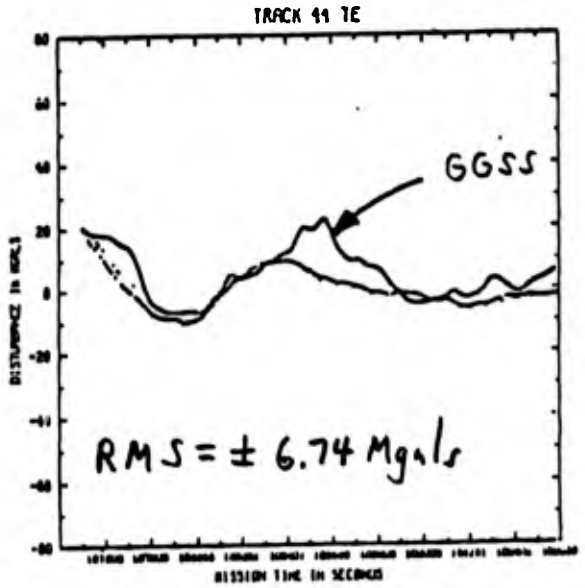

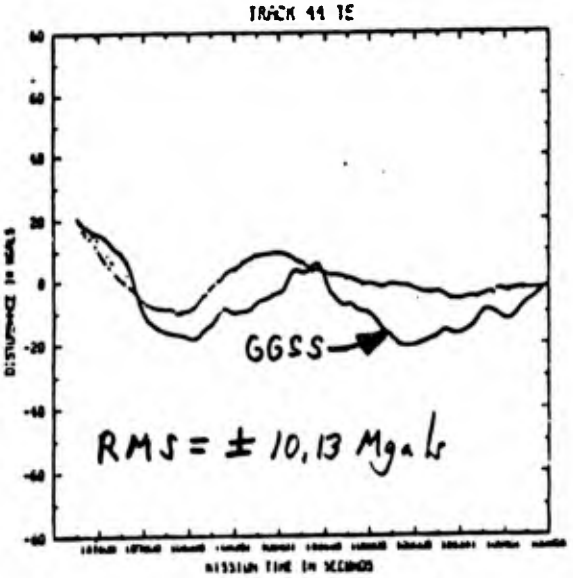

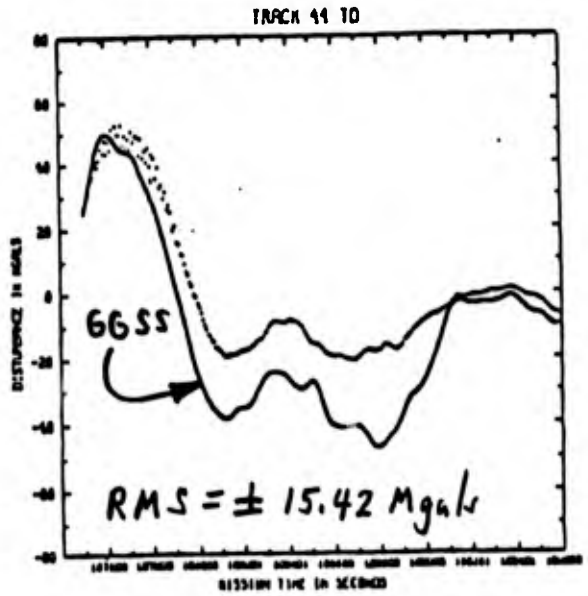

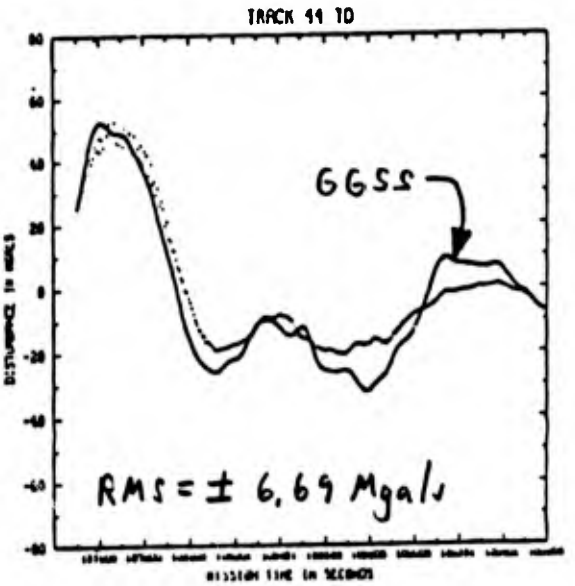

FIGURE 14.

GGSS DISTURBANCES VERSUS DIRECT INTEGRATION DISTURBANCES

(RMS OF DIFFERENCES)

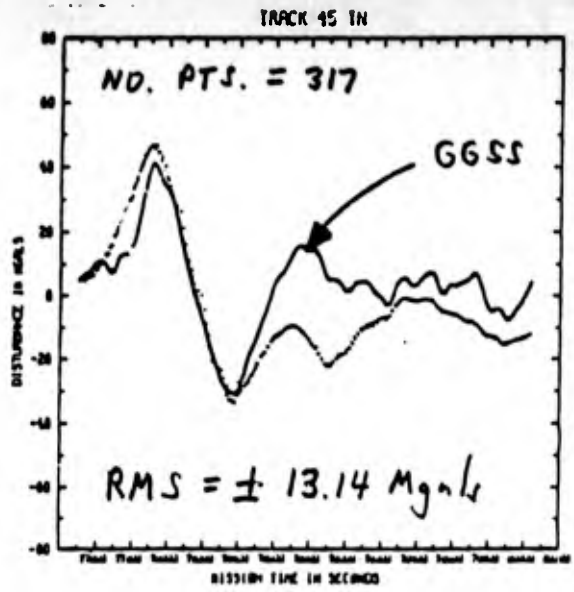

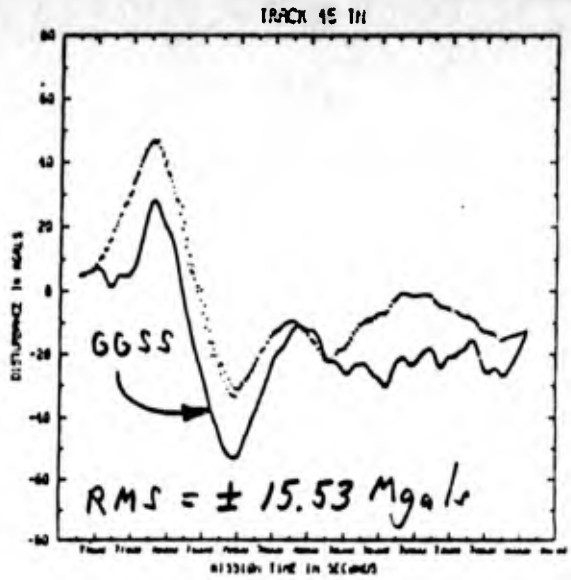

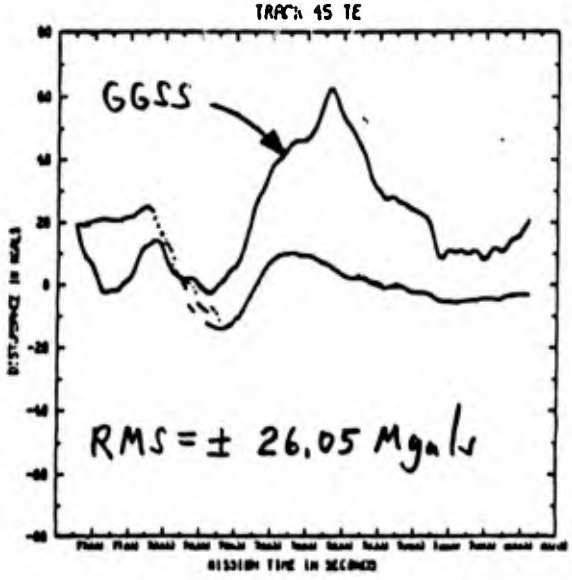

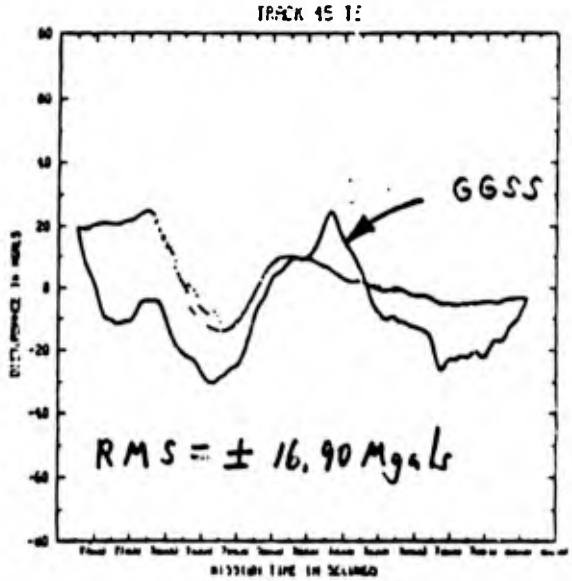

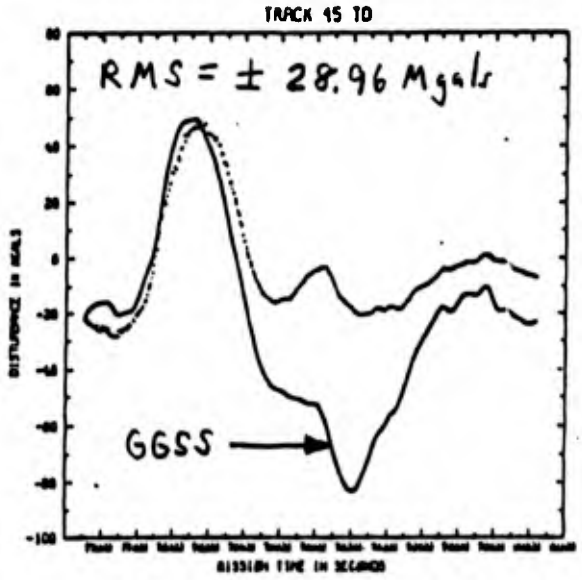

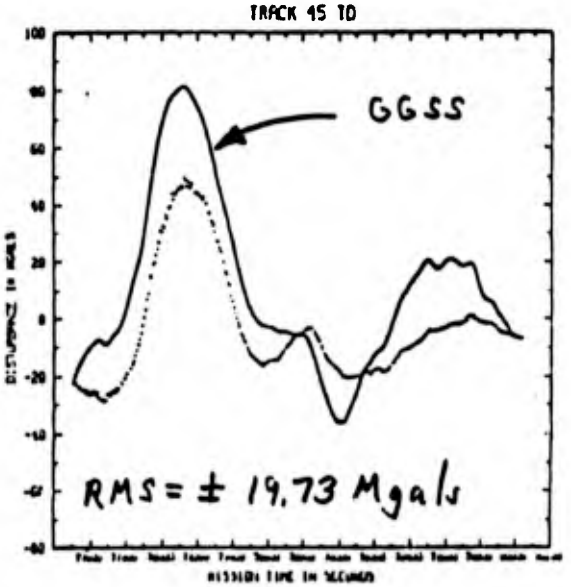

TABLE 1

A STATISTICAL COMPARISON OF DIRECT INTEGRATON MINUS GGSS DERIVED DISTURBANCE COMPONENT DIFFERENCES
(Only one tie point used in GGSS line summation)

TRACK NO.	NORTH DISTURBANCE (TN) MEAN mgals	SIGMA mgals	RMS mgals	NO. PTS
19	17.81	9.80	±20.35	205
22	-2.79	19.34	19.50	212
24	21.90	19.83	29.55	206
25	1.29	14.31	14.33	174
27	-16.92	15.98	23.23	127
39	7.23	6.10	9.46	304
41	-7.16	15.46	17.02	299
42	12.48	13.41	18.32	374
43	13.99	8.31	16.28	334
44	-58.61	24.15	63.48	261
45	-7.20	11.01	13.14	317

A STATISTICAL COMPARISON OF DIRECT INTEGRATON MINUS GGSS DERIVED DISTURBANCE COMPONENT DIFFERENCES
(Three tie points, at middle and ends of comparison)

TRACK NO.	NORTH DISTURBANCE (TN) MEAN mgals	SIGMA mgals	RMS mgals	NO. PTS
19	-3.71	3.69	±5.23	205
22	3.35	6.03	6.89	212
24	2.22	12.36	12.53	206
25	2.98	8.35	8.84	174
27	2.57	3.71	4.50	127
39	7.23	6.10	9.46	304
41	-9.54	16.82	19.32	299
42	-4.42	14.52	15.16	374
43	8.53	6.67	10.84	334
44	5.57	5.78	8.03	261
45	13.33	7.98	15.53	317

A STATISTICAL COMPARISON OF DIRECT INTEGRATON MINUS GGSS DERIVED DISTURBANCE COMPONENT DIFFERENCES

(Only one tie point used in GGSS line summation)

EAST DISTURBANCE (TE)

TRACK NO.	MEAN mgals	SIGMA mgals	RMS mgals	NO. PTS
19	2.10	10.17	±10.36	205
22	-1.53	5.13	5.34	212
24	-23.99	10.37	26.18	206
25	17.43	10.01	20.13	174
27	-0.57	6.66	6.66	127
39	0.13	6.11	6.10	304
41	-12.20	17.61	21.41	299
42	5.51	26.87	27.40	374
43	6.27	11.08	12.72	334
44	-4.72	4.81	6.74	261
45	-16.48	20.20	26.05	317

A STATISTICAL COMPARISON OF DIRECT INTEGRATON MINUS GGSS DERIVED DISTURBANCE COMPONENT DIFFERENCES

(Three tie points, at middle and ends of comparison)

EAST DISTURBANCE (TE)

TRACK NO.	MEAN mgals	SIGMA mgals	RMS mgals	NO. PTS
19	6.21	8.70	±10.68	205
22	3.62	5.18	6.31	212
24	3.03	4.14	5.13	206
25	-0.51	3.56	3.59	174
27	0.69	4.95	4.97	127
39	3.99	5.71	6.97	304
41	-19.65	16.43	25.62	299
42	19.26	23.20	30.14	374
43	1.16	14.41	14.43	334
44	7.64	6.65	10.13	261
45	11.90	12.03	16.90	317

TABLE 3

A STATISTICAL COMPARISON OF DIRECT INTEGRATON MINUS GGSS DERIVED DISTURBANCE COMPONENT DIFFERENCES
(Only one tie point used in GGSS line summation)

DOWN DISTURBANCE (TD)

TRACK NO.	MEAN mgals	SIGMA mgals	RMS mgals	NO. PTS
19	-4.59	7.08	±8.43	205
22	21.77	31.14	37.96	212
24	28.82	16.81	33.40	206
25	-34.39	26.51	43.45	174
27	5.50	6.62	8.58	127
39	-8.56	9.31	12.65	304
41	25.00	13.55	28.46	299
42	4.57	25.55	25.92	374
43	1.35	6.16	6.30	334
44	12.55	8.95	15.42	261
45	19.52	21.43	28.96	317

A STATISTICAL COMPARISON OF DIRECT INTEGRATON MINUS GGSS DERIVED DISTURBANCE COMPONENT DIFFERENCES
(Three tie points, at middle and ends of comparison)

DOWN DISTURBANCE (TD)

TRACK NO.	MEAN mgals	SIGMA mgals	RMS mgals	NO. PTS
19	-3.68	4.89	±6.12	205
22	16.33	17.12	23.66	212
24	0.91	6.39	6.44	206
25	0.19	9.38	9.36	174
27	-0.11	5.43	5.41	127
39	3.11	4.58	5.53	304
41	6.82	7.83	10.39	299
42	-6.81	19.78	20.90	374
43	3.38	5.41	6.38	334
44	1.86	6.44	6.69	261
45	-14.18	13.75	19.73	317